PART I:

IMPROVEMENTS TO THE SYNTHESIS OF CALCITROIC ACID

PART II:

SYNTHESIS OF NEW IMIDAZODIAZEPINES TO TARGET NON-CENTRAL NERVOUS SYSTEM GABA(A) RECEPTORS

PART III:

IMPROVED 2-PYRIDYL REDUCTIVE HOMOCOUPLING REACTION USING BIORENEWABLE SOLVENT CYRENE™ (DIHYDROLEVOGLUCOSENONE)

by

Daniel Webb

A Dissertation Submitted in

Partial Fulfillment of the

Requirements for the Degree of

Doctor of Philosophy

in Chemistry

at

The University of Wisconsin-Milwaukee

December 2023

ABSTRACT

PART I: IMPROVEMENTS TO THE SYNTHESIS OF CALCITROIC ACID

PART II: SYNTHESIS OF NEW IMIDAZODIAZEPINES TO TARGET NON-CENTRAL NERVOUS SYSTEM GABA(A) RECEPTORS

PART III: IMPROVED 2-PYRIDYL REDUCTIVE HOMOCOUPLING REACTION USING BIORENEWABLE SOLVENT CYRENE™ (DIHYDROLEVOGLUCOSENONE)

by

Daniel Webb

The University of Wisconsin-Milwaukee, 2023
Under the Supervision of Professor Alexander Arnold

Abstract Part I:

Calcitroic acid (CTA) was first isolated and characterized over four decades ago.[6] At that time, radiolabeled calcitriol (1,25-dihydroxyvitamin D3) was utilized to facilitate the detection of radioactive CTA generated *in vivo*. Subsequently, researchers extracted and characterized CTA through derivatization.[7] Notably, CTA was predominantly formed in the liver and transported to the gut through the bile duct via enterohepatic circulation, resulting in significant concentrations of this vitamin D metabolite in the intestines.[8] However, since it was initially regarded as merely a breakdown product of calcitriol, it remained largely overlooked.

Recent groundbreaking experiments have unveiled a new dimension to CTA's biological role. It has been revealed that CTA can bind to the vitamin D receptor (VDR) and initiate the regulation of specific metabolic enzymes.[9] VDR, a nuclear hormone receptor found in various tissues, is capable of binding to several endogenous ligands. While calcitriol exhibits the highest affinity for VDR and has undergone extensive investigation, our knowledge regarding the principal end-stage metabolite of vitamin D, calcitroic acid, remains limited. Initially considered

biologically inactive due to its weaker binding to VDR compared to calcitriol, recent findings challenge this assumption.

Recent research has demonstrated gene regulation in the presence of CTA in epithelial cells, keratinocytes, and prostate cancer cells.[8] One proposed role of VDR in the intestine is the regulation of P450 enzymes, critical for detoxification processes, especially concerning the accumulation of harmful endogenous molecules such as lithocholic acid. Our hypothesis states that CTA interacts with VDR to regulate this process, potentially safeguarding against the development of inflammation-related gastrointestinal disorders, including irritable bowel syndrome and colorectal cancer. Here is presented a detailed report of the 12-step synthesis to obtain CTA.

Abstract Part II:

Novel gamma-aminobutyric acid receptor ($GABA_AR$) ligands structurally related to imidazobenzodiazepine MIDD0301 were synthesized using spiro-amino acid N-carboxyanhydrides (NCAs). These compounds demonstrated increased resistance to phase 2 metabolism and avoided the formation of a 6H isomer. Compound design was guided by molecular docking using the available crystal structure of the $\alpha_1\beta_3\gamma_2$ $GABA_AR$ and correlated with *in vitro* binding data. The carboxylic acid containing $GABA_AR$ ligands have high aqueous solubility, low permeability, and low cell toxicity. The inability of $GABA_AR$ ligands to cross the blood-brain barrier was confirmed *in vivo* by the absence of sensorimotor inhibition. Pharmacological activities at lung $GABA_ARs$ were demonstrated by *ex vivo* relaxation of guinea pig airway smooth muscle and reduction of methacholine induced airway hyperresponsiveness (AHR) in conscious mice. We identified bronchodilator DAW-III-30 with an affinity of 9 nM for $GABA_ARs$ that was metabolically stable in the presence of human and mouse microsomes.

Abstract Part III:

The synthesis of 5,5′-bis(trifluoromethyl)-2,2′-bipyridine using 2-bromo-5-(trifluoromethyl) pyridine was achieved at 50 °C using palladium acetate, tetrabutylammonium iodide (TBAI), potassium carbonate, and isopropanol in Cyrene™ (dihydrolevoglucosenone), a bio-renewable "green" solvent formed by a two-step process from cellulose. Improvements were achieved with 50% of γ-valerolactone (GVL) in Cyrene™ resulting in a 95% yield and 99% product purity without the use of column chromatography or recrystallization. At 80 °C, the reaction was completed within 1 h. Full conversion with 1 mol% instead of 15 mol% of palladium acetate was observed within 10 h. We showed that the formed 2,2′-bipyridine product significantly accelerated the reaction probably due to the stabilization of the catalytic species. The addition of TBAI was essential for the rapid homocoupling, however, 20 mol% of TBAI was sufficient to reach full conversion of 2-bromo-5-(trifluoromethyl) pyridine within 6 h at 80 °C. Another improvement was observed with the substitution of isopropanol by 1,4-butanediol achieving full conversion within 6 h. 2-Bromopyridines with electron withdrawing substituents in the 6, 5, 4 ring position reacted under these conditions. 2-Bromopyridines with an electron donating substituent reacted slower. Overall, we demonstrated that the 50% GVL in Cyrene™ blend is a superior "green" and less toxic alternative to dimethylformamide for the reductive homocoupling reaction. Using a quantitative scoring for twelve principles of green chemistry (DOZN™), we found significant improvements that were mediated by higher yield (atom economy), shorter heating time and lower reaction temperature (energy efficiency), safer solvent (hazardous chemical synthesis), and safer chemistry (accident prevention).

© Copyright by Daniel A. Webb, 2023
All Rights Reserved

TABLE OF CONTENTS

LIST OF FIGURES

LIST OF TABLES

LIST OF SCHEMES

LIST OF ABBREVIATIONS

$1,25(OH)_2D_3$:	1,25-dihydroxyvitamin D_3; calcitriol
$25(OH)D_3$:	25-hydroxyvitamin D_3
2-MeTHF:	2-methyltetrahydrofuran
ACN:	acetonitrile
AcOH:	acetic acid
AHR:	airway hyperresponsiveness
Arg:	arginine
ASM:	airway smooth muscle
BBB:	blood-brain barrier
Boc:	tert-butyloxycarbonyl
BTFFH:	fluoro-N,N,N′,N′-bis(tetramethylene)formamidinium hexapluorophosphate
Bz/$GABA_AR$:	benzodiazepine γ-aminobutyric acid type A receptor
Bz:	benzodiazepine
BZD:	benzodiazepine
CaF:	calcium fluoride
CDC:	Centers for Disease Control and Prevention
$CDCl_3$:	deuterated chloroform
CDI:	carbonyldiimidazole

cEF:	complete *E* factor
$CHCl_3$:	chloroform
ClPO(OEt)2:	diethyl chlorophosphate
CNCH2CO2Et:	ethyl isocyanoacetate
CNS:	central nervous system
CSA:	camphorsulfonic acid
CTA:	calcitroic acid
$CuSO_4$:	copper sulfate
CV:	column volume
CYP:	cytochrome p450
CYP_{450}:	cytochrome P450
D_2O:	deuterium oxide
DBPD:	Drug-Based Peptide Design
DCC:	N,N′-dicyclohexylcarbodiimide
DCM:	dichloromethane
DI:	deionized
DIBAL:	diisobutylaluminum hydride
DMAP:	4-dimethylaminopyridine
DME:	dimethoxyethane

DMF:	dimethyl formamide
DMF:	dimethylformamide
DMSO:	dimethyl sulfoxide
DMSO-d_6:	deuterated dimethyl sulfoxide
DNA:	deoxyribonucleic acid
EC_{50}:	half maximal effective concentration
EDC:	1-ethyl-3-(3-dimethylaminopropyl)carbodiimide
ESI:	electrospray ionization
Et_2O:	diethyl ether
Et_3N:	triethyl amine
EtOAc:	ethyl acetate
EtOH:	ethanol
FBS:	fetal bovine serum
FDA:	Food and Drug Administration
GABA:	γ-aminobutyric acid
$GABA_AR$:	γ-aminobutyric acid type A receptor
GAD:	glutamate decarboxylase
GAT:	GABA transporter
GVL:	γ-valerolactone
H_2O:	water

H_2SO_4:	sulfuric acid
HATU:	hexafluorophosphate Azabenzotriazole Tetramethyl Uronium
HBTU:	hexafluorophosphate Benzotriazole Tetramethyl Uronium
HCl:	hydrochloric acid
HEK:	human embryonic kidney cells
Hep:	heptane
Hex:	hexanes
His:	histidine
HPLC:	high-performance liquid chromatography
HRMS:	high-resolution mass spectrometry
IACUC:	Institutional Animal Care & Use Committee
IC_{50}:	half maximal inhibitory concentration
IP:	intraperitoneal
IPA:	isopropyl alcohol
IS:	internal standard
IT-TOF:	ion trap time-of-flight
IV:	intravenous
K_2CO_3:	potassium carbonate
KCN:	potassium cyanide
$KHCO_3$:	potassium bicarbonate

KOH:	potassium hydroxide
LBD:	ligand binding domain
LBP:	ligand-binding pocket
LC:	liquid chromatography
LCMS:	liquid chromatography-mass spectrometry
LCMS-IT-TOF:	liquid chromatography-mass spectrometry ion trap time-of flight
$LiAlH_4$:	lithium aluminum hydride
LiOH:	lithium hydroxide
Log P_e:	relative apparent permeability
MCh:	methacholine
MeOD:	deuterated methanol
MeOH:	methanol
$MgSO_4$:	magnesium sulfate
MOE:	Molecular Operating Environment
MS:	mass spectrometry
MTBE:	*tert*-butyl methyl ether
MW:	molecular weight
$NaBH_4$:	sodium borohydride
NaCl:	sodium chloride
$NaClO_2$:	sodium chlorite

NaH:	sodium hydride
$NaHCO_3$:	sodium bicarbonate
NaOH:	sodium hydroxide
n-BuLi:	*n*-butyl lithium
NCA:	amino acid N-carboxyanhydride
NH_4Ac:	ammonium acetate
NH_4Cl:	ammonium chloride
NH_4OH:	ammonium hydroxide
NMM:	*n*-methyl morpholine
NMP:	N-Methyl-2-pyrrolidone
NMR:	nuclear magnetic resonance
Noopept:	N-phenylacetyl-L-prolylglycine ethyl ester
NR:	nuclear receptor
O_3:	ozone
PAMPA:	parallel artificial membrane permeability assay
PBR:	peripheral benzodiazepine receptor
PBS:	phosphate buffered saline
$Pd(dppf)Cl_2$:	[1,1′-Bis(diphenylphosphino)ferrocene]dichloropalladium(II)
$Pd(OAc)_2$:	palladium acetate
Pd/C:	palladium on activated carbon

PDA:	photodiode array
PDC:	pyridinium dichromate
PDSP:	Psychoactive Drug Screening Program
PEG:	polyethylene glycol
PK:	pharmacokinetics
PTSA:	*p*-Toluenesulfonic acid
PyBOP:	benzotriazol-1-yloxytripyrrolidinophosphonium hexafluorophosphate
QTOF:	quadrupole time of flight
R&D:	research and development
RB:	round bottom flask
RNA:	ribonucleic acid
RT:	room temperature
RXR:	retinoid X receptor
SAR	structure-activity relationship
SEM:	standard error of the mean
Ser:	serine
SNAr:	nucleophilic aromatic substitution
sRAW:	specific airway resistance
StD:	standard deviation
TBA:	tetrabutyl ammonium

TBAF:	tetrabutylammonium fluoride
TBAI:	tetrabutylammonium iodide
TBS:	*tert*-butyl silyl
TBSOTf:	*t*-butyldimethylsilyl trifluoromethanesulfonate
t-BuOK:	potassium *tert*-butoxide
TEA:	triethylamine
TES-Cl:	triethylsilyl chloride
TES-OTf:	triethylsilyl triflate
TFA:	trifluoroacetic acid
THF:	tetrahydrofuran
TLC:	thin layer chromatography
TSPO:	translocator protein
Tyr:	tyrosine
UV:	ultraviolet
UWM:	University of Wisconsin-Milwaukee
VDR:	vitamin D receptor

ACKNOWLEDGEMENTS

First, I would like to give the biggest thanks to Prof. Alexander (Leggy) Arnold for being by far the best professor I could have asked for during my PhD. Beginning when I was an undergrad and welcoming me into the research group where Dr. Arnold took the time to personally train me on many chemistry techniques that I would use daily throughout my degree. As well as always keeping his door open and having time to talk where I could go to get help with research or bounce around new ideas. I could not have asked for a better research group to join. I would also like to thank Dr. Arnold not only for providing me with the numerous opportunities to take part in multiple internships, complete multiple projects for startup companies, and work on other projects for various collaborators, but I would also like to express my thanks for the continued encouragement to attend and present research at as many conferences as I could. All of the support helped to not only better my chemistry skills but to also made me a better student, presenter, and teacher. I would not be nearly the chemistry that I am today and for that I am incredibly grateful.

Next, I would like to thank everyone in the Arnold Group, for the lifelong friendships I have made and always having the most incredible people around me. Throughout my degree, I could not have asked for a better group of friends to do lab work with, to talk with, and to travel with. The continued support from everyone and the privilege to spend every day with everyone in the Arnold group is something that I would not have though would have made such a big impact, but without, the time I spent during my degree would have been much different. Thank you to all the current members of the Arnold Group, as well as the past members, undergrad students, and other friends. I truly hope that I was able to pass on some of my knowledge and teach everyone even a small portion of what everyone has taught me.

I would like to give a big thanks to my committee members; Drs. Shama Mirza, Nicholas Silvaggi, Xiaohua Peng, Chris Cunningham, and Alan Schwabacher. I have very much enjoyed being able to share my progress with everyone during my degree. I would like to thank every committee member for making every milestone meeting as stress free as possible, while at the same time providing me with encouragement and advice for the next steps in my degree. I would also like to thank Dr. Anna Benko and Dr. Holger Foersterling for their extensive help, training, and expertise with mass spectrometry and NMR respectively. I would also like to thank the outstanding teams of people at MilliporeSigma who I had the opportunity to work with during my internships.

Lastly, I would like to give a huge thank you to my family. My mom Lynda, my dad David, and my sister Ellyn. Thank you for giving me everything I needed to succeed and always being around for anything I needed. Your support and constant interest in my work only encouraged me to work harder and I would not be anywhere close to where I am today without you. I would also like to thank all the other family members around me, especially my grandparents Ken and Susan Webb, and Larry and Joanne Jackowiak. Everyone around me has given me nothing but encouragement and always wanted to hear about my work. Thank you to everyone who has been a part of my degree from start to finish.

CHAPTER 1: IMPROVEMENTS TO THE SYNTHESIS OF CALCITROIC ACID

1.1 A Brief History of Vitamin D:

The recognition of vitamins as a vital component of a well-rounded diet is a relatively recent revelation, emerging in the wake of the 20th century. While specific illnesses stemming from vitamin deficiencies had already been identified and could be resolved through dietary supplements.[10] The underlying causes remained a mystery or were misunderstood during that era. It was during the early 1900s that the inaugural "vital amines," or vitamins, were unveiled, with Elmer McCollum playing a significant role in this breakthrough.

In 1910, both Hopkins[11] and Funk's[12] demonstrations highlighted the inadequacy of diets composed solely of purified proteins, fats, salts, and carbohydrates in promoting animal growth. McCollum's pivotal work, conducted in the same period, isolated a lipophilic, non-saponifiable compound from butter fat. This compound was identified as essential for growth and effective in preventing xerophthalmia in rats[13]. This substance, initially identified as "factor A," soon was given the name vitamin A, paving the way for the subsequent identification of vitamin B by McCollum and others merely four years later[14].

Simultaneously, during the early 20th-century Industrial Revolution in England, rickets cases, particularly among children, reached epidemic proportions. This was attributed to polluted air blocking sunlight and individuals in poverty laboring long hours in factories[15]. The discovery of the initial vitamins led to the widespread use of cod liver oil, which proved to be a rich source of vitamin A, vitamin D, and vitamin E, though the latter two were initially unknown. While cod

liver oil effectively treated rickets, McCollum harbored doubts about whether vitamin A alone was responsible for this action. To address this uncertainty, he conducted a groundbreaking study, oxidizing vitamin A within cod liver oil to nullify its activity. Surprisingly, even in this altered state, it continued to cure rickets (though not xerophthalmia). McCollum thus concluded that another vital vitamin present in cod liver oil was responsible for curing rickets, which he subsequently named vitamin D,[16] making it the fourth vitamin to be identified.

In Europe, an entirely different approach to rickets treatment was discovered by Huldschinsky and Chick[17], among others. They independently demonstrated that exposing ricketic children to UV light could also cure the condition. This therapeutic sunlight exposure was as effective as administering cod liver oil, offering a unique insight into vitamin D's dual properties being both vitamin-like and hormone-like[18]. In 1924, Steenbock at the University of Wisconsin confirmed this by using UV light to induce vitamin D activity, effectively curing rickets in lactating goats. This experiment showcased the presence of an inactive substance that could be converted into an active form of vitamin D.

The initial isolation of vitamin D was somewhat accidental, as Windaus in Germany inadvertently discovered a tachysterol/ergocalciferol adduct that effectively combated rickets, naming it vitamin D_1. Later, Askew in Britain successfully conducted the true isolation and structure determination of ergocalciferol, known as vitamin D_2, a discovery subsequently confirmed by Windaus' group. In 1936, Windaus and Bock isolated 7-dehydrocholesterol from the skin, a precursor to vitamin D3, and converted it into cholecalciferol, thereby identifying the two nutritional forms of vitamin D.

The realization that radiolabeled vitamin D was not the active form only emerged in 1967,[19] thanks to Hector DeLuca's work. He demonstrated that polar metabolites in target tissues were

responsible for the physiological response and possessed greater biological activity than unmetabolized vitamin D. In 1968, DeLuca's team isolated the primary circulating form of vitamin D, 25-hydroxyvitamin D_3 ($25(OH)D_3$), initially thought to be the most active form. However, subsequent research by DeLuca's group conclusively established that the even more polar molecule, 1,25-dihydroxyvitamin D_3 ($1,25(OH)_2D_3$, also known as calcitriol), was the primary active form of vitamin D.[20]

1.2 Structure and Function of the Vitamin D Receptor:

The Vitamin D Receptor (VDR) is a member of the nuclear receptor superfamily and serves as a transcriptional regulator. Its primary role involves governing the expression of genes responsible for maintaining calcium levels, regulating cell growth, and guiding cell differentiation.[21] Although vitamin D was first isolated in 1930, it took the scientific community almost four decades to grasp that the conversion of vitamin D was essential to generate biologically active compounds.[19] This complexity arises from their interactions with VDR. While VDR binds to vitamin D metabolites and various molecules, the vitamin D_2 and D_3 molecules themselves do not directly interact with the receptor.

VDR was initially identified in 1973[22] and subsequently cloned fourteen years later. In the year 2000, the three-dimensional structure of a crucial part of VDR, known as the ligand binding domain (LBD) responsible for binding small molecules, was unveiled using X-ray crystallography. This domain consists of three β-sheets and three layers with 12 α-helices, resembling a sandwich-like structure as seen in Figure 1a. It undergoes a significant conformational shift upon binding to a ligand. Helix 11 shifts to align with helix 10, closing off the binding pocket. Helix 12, often referred to as the "activating domain," contributes to stabilizing the structure by establishing

additional contacts with the ligand, thus creating a more hydrophobic environment within the binding pocket. Interestingly, within this pocket, VDR's native ligand calcitriol occupies only 56% of the space. Key hydrogen bonds anchoring $1,25(OH)_2D_3$ (calcitriol) in the binding cavity are formed by residues such as R274, S278 from Helix 5, S237 from Helix 3, γ143 from loop H1-H2, H305 from loop H6-H7, and H397 from Helix 11.[23]

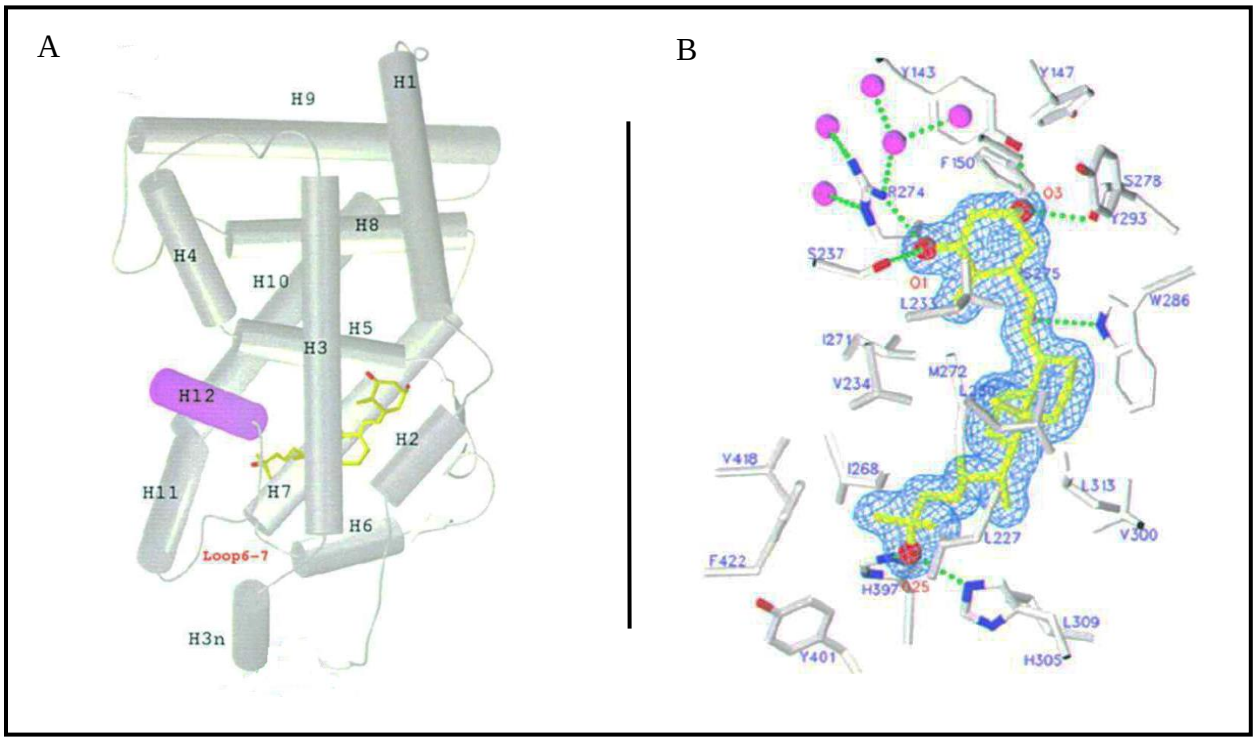

Figure 1: (a) The 12 α-helices of VDR represented as cylinders, with the activating domain helix shown in its closed position (pink) and its native ligand bound (yellow ball-and-stick). (b) The binding pocket cavity (blue mesh) and the anchoring interactions with surrounding residues that hold $1,25(OH)_2D_3$ in the binding cavity.

To function as a transcription factor, VDR must interact not only with small molecules but also with cofactors, bind to specific DNA sequences, and form heterodimers with the retinoid X receptor (RXR). Because of this, VDR comprises multiple domains. The A/B domain, located at the N-terminus, is unique among nuclear receptors, as it is responsible for binding various cofactors and enzymes.[24] In VDR, this domain contains activating function 1 (AF-1), which exhibits some weak transcriptional activity in the absence of a ligand.

The C domain as shown in Figure 2, known as the DNA binding domain, is highly conserved among nuclear receptors.[25] It comprises 66 residues forming two structures, both containing zinc finger motifs. The amino-terminal zinc finger region interacts with the major groove of DNA at specific sequences called hormone response elements. The second zinc finger region facilitates heterodimerization with other proteins. A typical hormone response element for the VDR-RXR heterodimer consists of two hexameric half-sites with the sequence 5'-AGGTCA-3' in a direct repeat, separated by three neutral base pairs. This differs from other nuclear receptors, which may involve inverted, everted, and mirror repeats in their half-site combinations. VDR response elements encompass numerous gene targets, including CYP24A1, CYP3A4, SULT2A1, ABCB1, CYP2B6, CDKN1A, SPP1, OC, OPN, and many others.

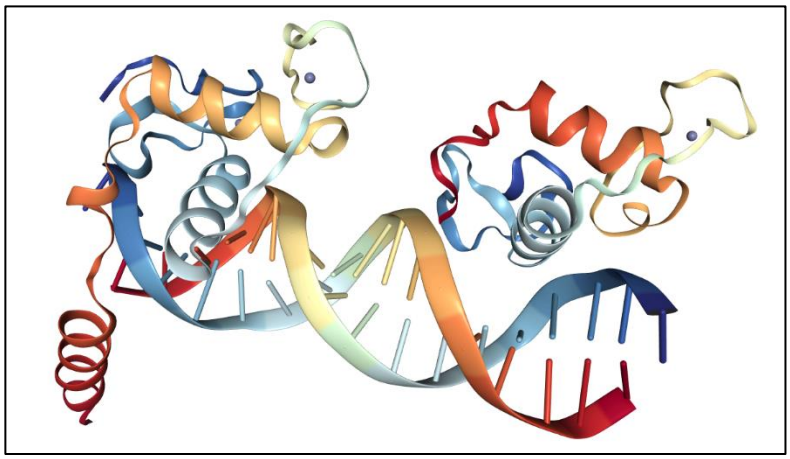

Figure 2: Crystal structure of the DBDs of both VDR (left) and its typical heterodimer partner RXR (right) bound to their respective DNA hexameric half-sites.[5] The light blue alpha helices in both structures bind to the major groove of the DNA. The Zn^{2+} ions taking part in coordination with cysteine residues are shown in gray. (PDB: 1YNW)

The D domain serves as the highly flexible hinge region connecting the DNA binding domain (DBD) and the ligand binding domain (LBD), which is situated in the E domain. The E domain is well-preserved and, as the name implies, is responsible for ligand binding. It comprises three β-sheets and 12 α-helices in three layers of sandwich folds. This domain also interacts with

coregulators (both corepressors and coactivators) in a ligand-dependent manner.[26] Upon ligand binding, a significant conformational shift occurs, with Helix 12 closing over the binding pocket, stabilizing the structure via additional interactions with the ligand, and creating a more hydrophobic environment within the pocket. Helix 12 also provides a new exterior surface with a hydrophobic cleft and features two charged residues, K246 and E420, at either end, forming a "charge clamp" that interacts with coregulators and heterodimers.

The ability to modulate activity based on the presence of ligands, cofactors, and corepressors is referred to as the activating function 2 (AF-2) of the nuclear receptor, representing ligand-dependent activity in contrast to the ligand-independent activity of AF-1. The ligand-binding domain thus serves as the central hub of VDR, regulating both DNA binding and transcriptional modifications. Within the LBD, there exists a crucial ligand "cave" known as activating function 2 (AF-2), where interactions with VDR's various ligands occur. Once a ligand is bound, AF-2 also finalizes the interface for binding with the retinoid X receptor, as well as other coactivators and corepressors as seen in Figure 3. When VDR forms a heterodimer with the retinoid X receptor (its most common dimeric partner), the two bind to DNA sequences known as "vitamin D-responsive elements" (VDRE) on target genes, thereby recruiting additional coactivators.[27]

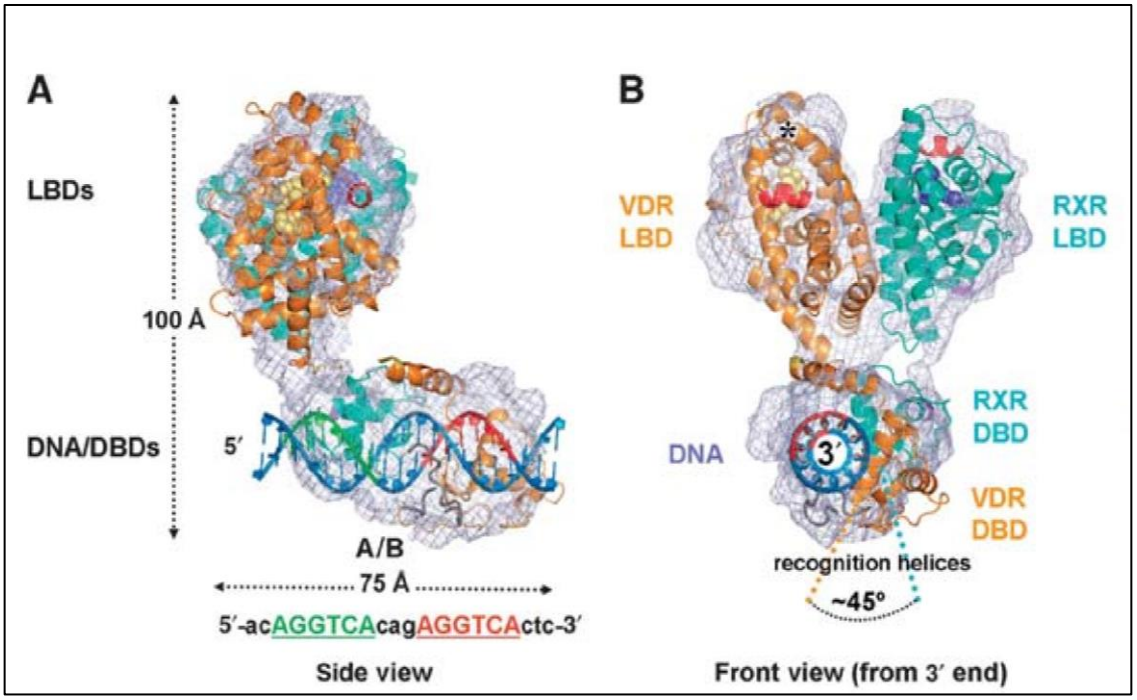

Figure 3: The flash-frozen RXR-VDR structure in complex with a DNA response element, as imaged by electron microscopy and overlaid with individual crystal structures.[1] A) Side view shows the ligand binding domains of VDR (orange, facing) and RXR (green, far side) at ~90° angle from where they are bound to DNA. B) The DBDs encapsulate the response element DNA, the two recognition helices positioned at about 45° from each other due to the 3 base-pair spacer between the half-sites. Helix 12 is shown on VDR in red, in its closed position with ligands bound (shown in yellow for VDR; blue for RXR).

The specificity of these target binding sequences allows for selective gene transcription from promoters, ultimately determining the rate of protein production through RNA polymerase II transcription. Once the VDR-RXR heterodimer is bound, additional coactivators are recruited, including RNA polymerase II and other transcriptional proteins with histone acetyl transferase activity. These coactivators mediate the priming and subsequent transcription of DNA.[28]

Lastly, the F domain, which exhibits significant variability across nuclear receptors, is notably absent in VDR.[29]

1.3 Phase I Metabolism of Vitamin D and Calcitroic Acid:

As previously mentioned, scientists took some time to determine that it wasn't vitamin D_2 or D_3 directly interacting with the vitamin D receptor, but rather their metabolites. This groundbreaking research began in 1961 when Kodicek and Chalk pioneered the use of ^{14}C-labeled vitamin D_2 in live subjects, revealing signs of metabolic activity.[30] However, it wasn't until the 1960s when ^{3}H-labeled vitamin analogs were administered that the first vitamin D analog with significant biological activity, $25(OH)D_3$, was identified. In 1971, this same group discovered the most potent vitamin D analog, $1,25(OH)_2D_3$. These findings sparked extensive research in various fields such as medicine, biochemistry, physiology, chemistry, and pharmacology, especially after the identification and eventual cloning of the vitamin D receptor.[31]

A close opportunity to uncover CTA arose in 1965 when significant radioactivity was detected in the aqueous extracts of bile and intestines from rats dosed with 1α-^{3}H-D_3. Unfortunately, further analysis of these radioactive substances was not pursued at that time.[32] Subsequently, with improved techniques involving rat bile duct cannulation, the same group collected bile over 24 hours and separated it into five fractions, including "fraction D." After acid hydrolysis, this fraction divided into polar and less polar components, and a glucuronide conjugate of a vitamin D analog emerged as a major component, masking CTA's presence.[33] However, methods for isolating acidic metabolites, such as anion-exchange chromatography and derivatization with diazomethane, were established. Although researchers consistently reported high radioactivity levels in aqueous liver and intestine extracts from animals treated with ^{3}H-$25(OH)D_3$, it took another decade to finally isolate CTA.[34] In this study, rats were treated with a combination of ^{14}C- and ^{3}H-labeled $1,25(OH)_2D_3$. After four hours, the soluble contents of the liver and intestine were separated into chloroform and methanol/water fractions. The aqueous

layers from both tissues were enriched in ^{3}H relative to ^{14}C, indicating that the side chain of $1,25(OH)_2D_3$ underwent shortening during metabolism which was a critical discovery. Notably, fractions containing negatively charged compounds after diethylaminoethyl cellulose separation (anion exchange) displayed significant radioactivity. Subsequently, ^{3}H-CTA was isolated as a methyl ester following esterification with diazomethane and characterized through mass spectrometry. While a small amount of ^{3}H-CTA was found in the blood, significantly larger quantities were present in the liver and, notably, the intestine with its contents. Thus, the hypothesis that CTA participates in the enterohepatic circulation was confirmed through the identification of ^{3}H-CTA in the bile duct.[35] A more detailed tissue distribution analysis of CTA, utilizing the techniques mentioned earlier, demonstrated a complex metabolism.[36] Notably, other acidic metabolites, potentially polar CTA conjugates, were identified. Additionally, CTA was found in the intestine of bile duct-cannulated rats, suggesting endogenous mucosal CTA synthesis. Furthermore, only up to 50% of the radioactive material could be extracted from dried liver, indicating the formation of complex metabolites.

Despite CTA initially escaping detection, attention to organ chloroform extracts led to the identification of several less abundant metabolites, shedding light on one of the most prominent vitamin D metabolic pathways. The first evidence of vitamin D 24-hydroxylation was observed in $[1,2\text{-}^{3}H]D_3$-treated chicks' blood, initially believed to be $21,25(OH)_2D_3$ but later identified as $24,25(OH)_2D_3$ in chick kidney homogenates.[37] It was also discovered that $1,25(OH)_2D_3$ promotes the production of $24,25(OH)_2D_3$, suggesting the upregulation of 24-hydroxylase (CYP24A1) by $1,25(OH)_2D_3$. CYP24A1 was first identified in chick kidneys,[38] with further characterization of

the purified enzyme found in kidney mitochondria achieved by multiple research groups, ultimately leading to the cloning and expression of mitochondrial kidney CYP24A1.[39]

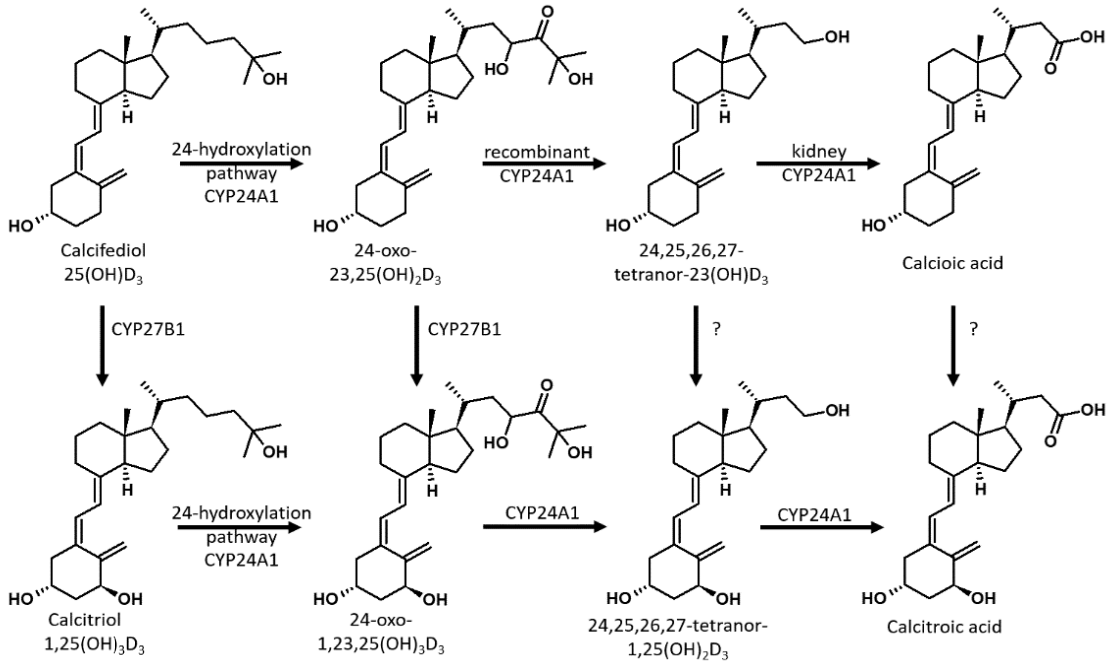

The metabolism of various vitamin D metabolites and analogues to CTA.

Simultaneously, several new vitamin D metabolites were identified *in vivo* or through perfused rat kidney studies,[40] including 24,25,26,27-tetranor-23(OH)D_3 and 24,25,26,27-tetranor-1,23$(OH)_2D_3$, believed to be the likely precursors for CTA as seen in Scheme 1. The conversion of 24,25,26,27-tetranor-1,23$(OH)_2D_3$ into CTA was subsequently reported by two separate groups in the same year using perfused rat kidney models.[41] It had already been demonstrated that cultured bone cells mediated the same metabolic conversion, in addition to the previously reported conversion of 25-(OH)D_3 to 24,25$(OH)_2D_3$. This indicated that the expression of CYP24A1 extended beyond the kidney. The analysis of recombinant human CYP24A1 confirmed that a single P450 enzyme catalyzed the six-step pathway from 1,25$(OH)_2D_3$ to CTA,[42] reaffirming the importance of the C-24 hydroxylation pathway in CTA production. Furthermore, it was shown that CYP24A1 also mediated the alternative C-23 hydroxylation pathway, a four-step

monooxygenation process from 25-(OH)D_3 to 25(OH)D_3-26,23-lactone, which was notably absent in rat CYP24A1. Human recombinant CYP24A1 could also convert 25(OH)D_3 to 24,25,26,27-tetranor-23(OH)D_3, although complete oxidation to calcitroic acid was only observed in perfused rat kidney models.[43] CTA was also identified in perfused kidney models when treated with supplement-derived 1,25$(OH)_2D_2$, although it appeared that CYP24A1 was not the sole enzyme involved in this process. Additionally, CTA was identified in the bile of rats treated with 1,25$(OH)_2D_4$.[44]

Vitamin D analogs with an α1 hydroxyl group, such as 1,25$(OH)_2D_3$, exhibit higher binding affinity to the vitamin D receptor (VDR) compared to their non-1α-hydroxylated counterparts like 25(OH)D_3. As a result, they demonstrate greater biological activity at equivalent concentrations. The ongoing research into the identification, purification, and characterization of the enzyme responsible for this hydroxylation, 25-hydroxyvitamin D3 1α-hydroxylase (CYP27B1), has spanned five decades.[45] Similar to CYP24A1, CYP27B1 expression is not confined to kidney mitochondria. Recent studies have revealed that CYP27B1 can convert most vitamin D metabolites from the 24-hydroxylation pathway into their corresponding 1α-hydroxylated.[46]

1.4 Ligand Design for the Vitamin D Receptor:

1.4.1 Introduction

The vitamin D receptor (VDR) takes a special place among nuclear receptors because the biosynthesis of its endogenous ligand, 1α,25-dihydroxyvitamin D_3 (1α,25$(OH)_2D_3$), is dependent on sun exposure. Poor living conditions during the industrial revolution when people were destined to work and live inside with minimal light exposure caused bone deformations and skin diseases

that improved with light therapy. Once irradiated food was found to have the same medicinal effect,[47] isolation of vitamin D was rapidly accomplished.[48] Identification of the corresponding receptor turned out to be difficult because vitamin D does not bind VDR at physiological concentrations. However, once radiolabeled vitamin D was generated,[49] $25(OH)D_3$ and $1\alpha,25(OH)_2D_3$ were identified,[20, 50] which in turn enabled the identification and cloning of VDR.[31, 51] The genomic function of VDR regulates genes involved in calcium homeostasis, cell proliferation, and cell differentiation. The endocrine receptor is expressed in the epithelia of endocrine organs, digestive tract, kidneys, and thymus,[52] but is also found in leukocytes and bone cells. VDR can be found in the cytosol or membrane-bound.[53] In the nucleus, VDR is liganded and binds DNA and the retinoid X receptor (RXR).[54] VDR-specific gene promoter sequences have been identified.[55] The transcriptional complex includes, among other proteins, nuclear receptor coactivators and corepressors that interact with RNA polymerase II,[56] changing chromatin packing and enabling specific gene transcription.[57]

1.4.2 Secosteroid VDR Ligands

$1\alpha,25(OH)_2D_3$ has the highest affinity for VDR among all vitamin D metabolites. The competitive VDR binding of $1\alpha,25(OH)_2D_3$ using $[^3H]$-$1\alpha,25(OH)_2D_3$ as a probe has been reported in the range of 0.04-0.16 nM with protein isolated from tissue and cells or recombinantly expressed VDR as full-length receptor or ligand binding domain.[58, 59] Other assays such as biochemical coactivator recruitment assays reported EC_{50} of 1.2 nM for $1\alpha,25(OH)_2D_3$.[60] For most cases, the affinities of new compounds in comparison to $1\alpha,25(OH)_2D_3$ are reported as percent affinity in this chapter.

Calcitriol or 1α,25(OH)$_2$D$_3$ has six chiral centers and two trisubstituted double bonds that can adopt an E or Z configuration. First, we will compare VDR binding of 1α,25(OH)$_2$D$_3$ epimers and stereoisomers depicted in Figures 1-4.

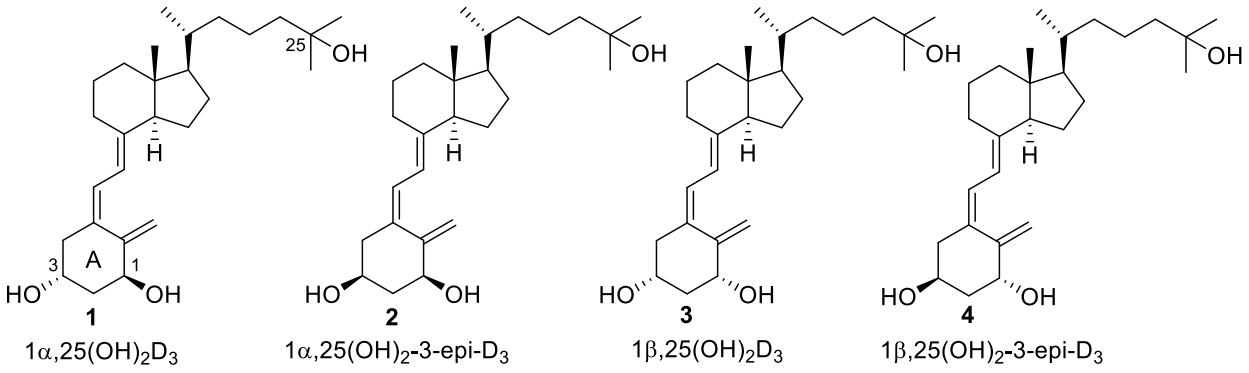

Figure 4. A-ring diastereomers of 1α,25(OH)$_2$D$_3$.

1α,25(OH)$_2$D$_3$ is the metabolic product of vitamin D$_3$, which lacks a hydroxyl group in the C1 and C25 positions (Figure 4). 25-Hydroxyvitamin D-1α hydroxylase mainly in the kidneys but also in other tissues stereospecifically introduces a C1α-hydroxyl group.[61] The 3-OH group is part of vitamin D$_3$ and its precursor 7-dehydrocholersterol. The evaluation of A-ring diastereomers of 1α,25(OH)$_2$D$_3$ demonstrated that binding to VDR is more impacted by the stereochemistry of the C1-position than the C3-position.[62] VDR affinity for **2** was 24% in comparison to 1α,25(OH)$_2$D$_3$ but only 0.2% and 0.8% for **3** and **4**, respectively. 1α,25(OH)$_2$-3-epi-D$_3$ has been identified as a natural metabolite of 1α,25(OH)$_2$D$_3$[63] and intensively studied *in vivo*. 1β,25(OH)$_2$D$_3$ was first synthesized in 1977[64] and has also recently been identified as a natural metabolite of vitamin D.[65] 1β,25(OH)$_2$D$_3$ has been reported as a non-genomic antagonist of 1α,25(OH)$_2$D$_3$.[62]

Secosteroids in contrast to steroids have a "broken" B ring resulting in a triene system with 5(Z),7(E) configuration (Figure 5). The formation of secosteroids occurs via a retro Diels-Alder reaction in the presence of light followed by a [1,7] sigmatropic rearrangement. In the skin, this conversion occurs with high stereoselectivity.

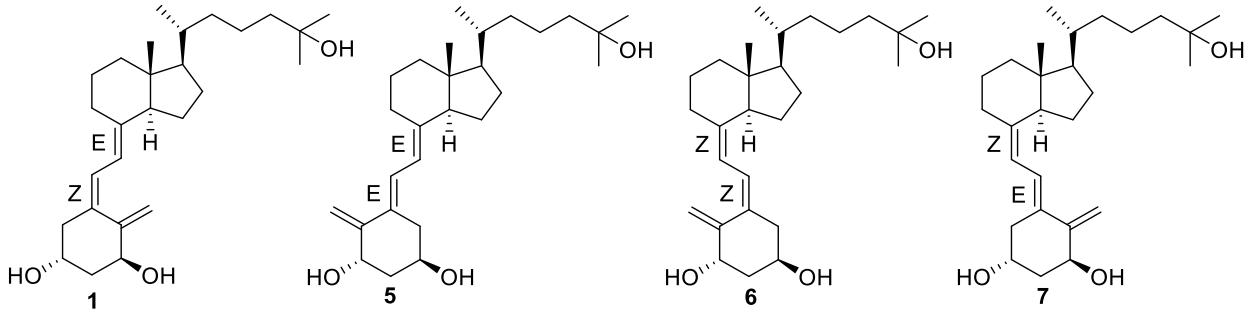

Figure 5. Diene stereochemistry of 1α,25(OH)$_2$D$_3$.

Isomer **5** retains a good affinity towards VDR, which is 13% in comparison to 1α,25(OH)$_2$D$_3$.[66] The E,E stereochemistry can be generated by light in the presence of iodine,[67] or by a cheleotropic addition-elimination with sulfur dioxide.[68] In contrast, isomers **6** and **7** were not observed for photochemical reactions but synthesized using a chromium (0) mediated isomerization reaction with a vinylallene precursor.[68] The affinity towards VDR was 0.82 % for **6** and 1.6% for **7** in comparison to 1α,25(OH)$_2$D$_3$. Thus, the position of the A-ring with respect to the B and C ring is more important for VDR binding than the location of the terminal alkene.

The stereochemistry of the fused B,C ring system of 1α,25(OH)$_2$D$_3$ originated from 7-dehydrocholersterol. Interestingly, the configuration of the fused system has a direct influence on the equilibrium of the thermal [1,7] sigmatropic rearrangement reaction (Figure 6). When 1α,25(OH)$_2$D$_3$ was heated at 80 °C, only 12% of the pre-1α,25(OH)$_2$D$_3$ was detected.[69] However, when epimer 8 was heated at 80 °C, a 95:5 ratio in favor of the pre-structure was formed.

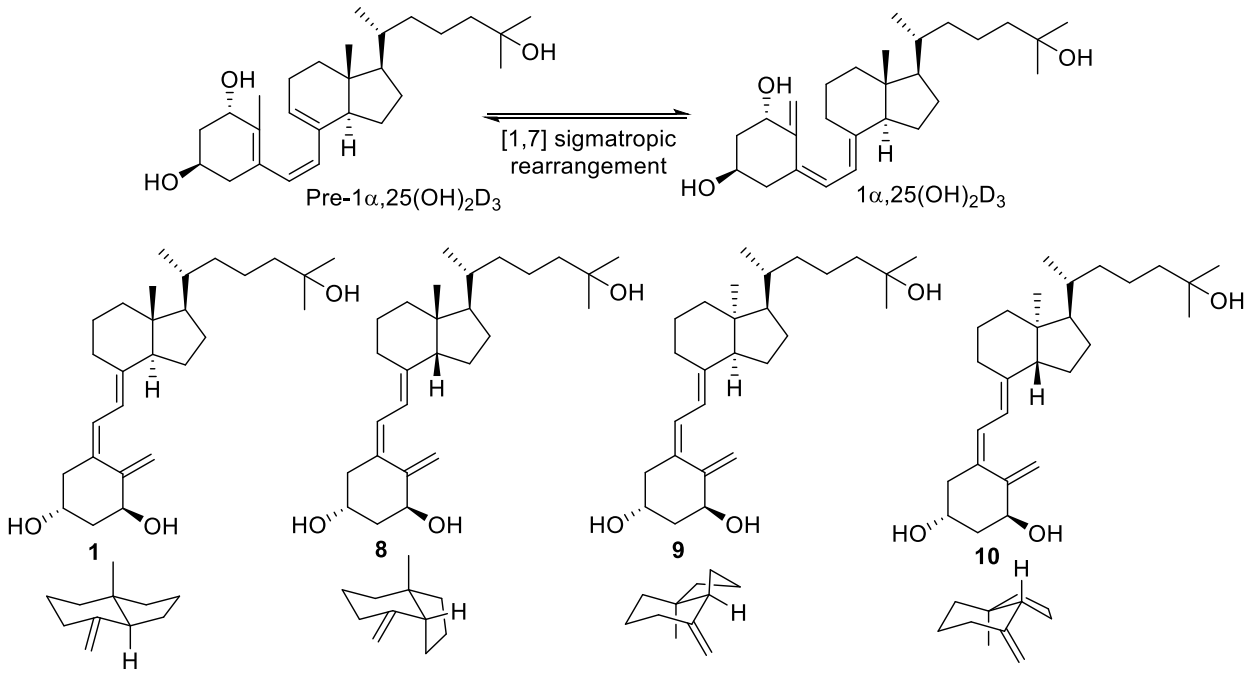

Figure 6. Diene stereochemistry of $1\alpha,25(OH)_2D_3$.

Pure **8** was synthesized by epimerization of Grundmann's ketone and retained a VDR affinity of 15% in comparison with $1\alpha,25(OH)_2D_3$.[69] Interestingly, no reports were found for compound **9** and **10**.

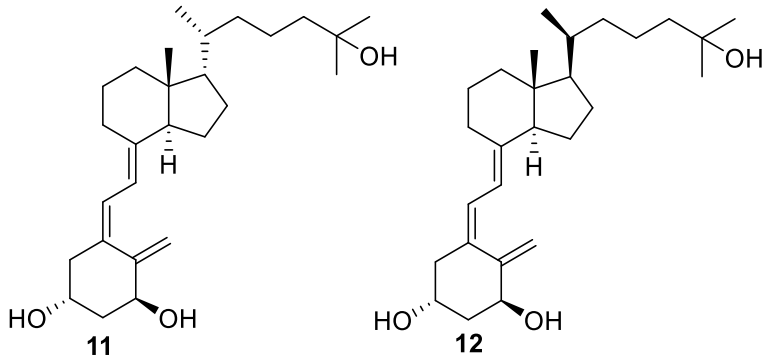

Figure 7. C17 and C20 epimers.

The synthesis of **11** has been reported (Figure 7).[70] Later, an improved route was developed but VDR binding was not reported.[71] However, inhibition of human breast cancer cell (MCF-7) proliferation was more pronounced in the presence of **11** than $1\alpha,25(OH)_2D_3$. Epimer **12**

demonstrated inhibition of T cell proliferation at picomolar concentrations.[72] The VDR binding was 88% in comparison to 1α,25(OH)$_2$D$_3$.[73]

Next, the importance of functional groups and substituents with respect to VDR binding is discussed. Analogs that lack certain structural elements are compared to 1α,25(OH)$_2$D$_3$ (Figure 8).

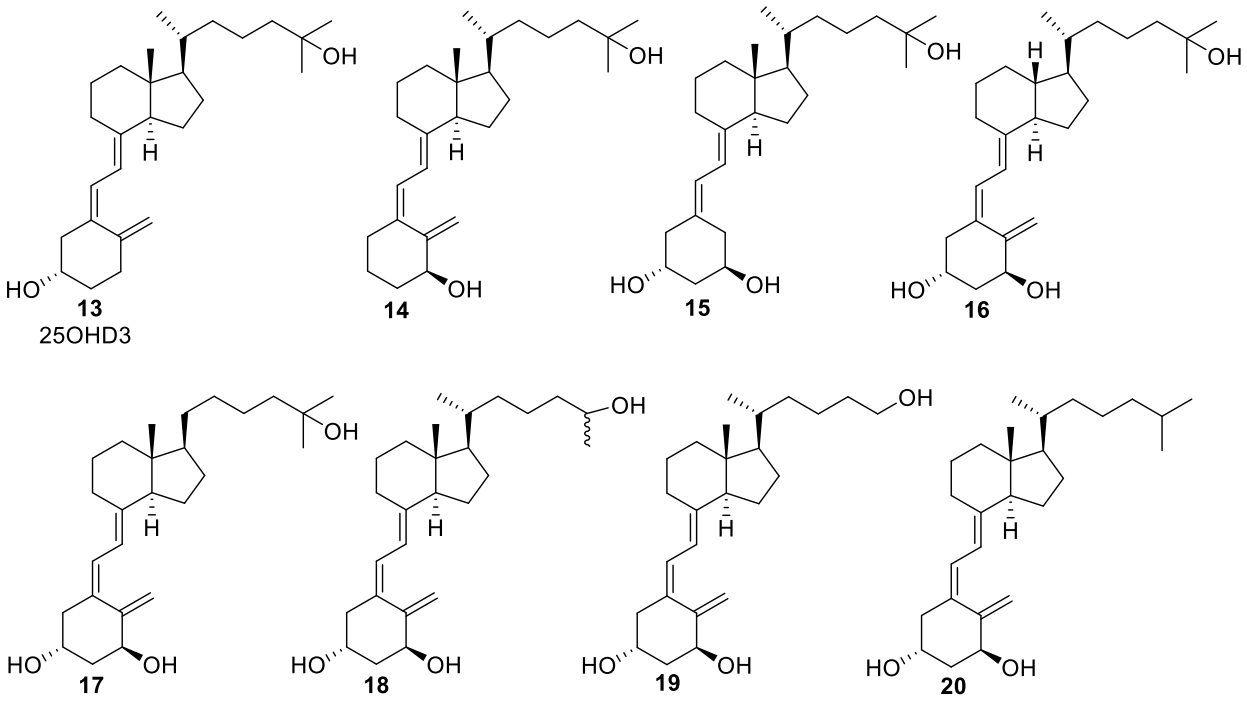

Figure 8. 1α,25(OH)$_2$D$_3$ analogs that lack certain structural elements.

25OHD$_3$ is a metabolic product of vitamin D$_3$ and was identified in 1968 (Figure 8).[50] It is abundant in blood and used to determine the vitamin D status in humans.[74] The binding towards VDR is 900 fold less than 1α,25(OH)$_2$D$_3$.[75] In contrast to **13**, the affinity of **14** was only 1/8 less effective than 1α,25(OH)$_2$D$_3$ making the 1α-OH group significantly more important for VDR binding than the 3-OH group.[75] Compound **15** lacking the methylene group was first synthesized in 1990 and has been shown to induce the differentiation of HL-60 cells at the same concentration of 1α,25(OH)$_2$D$_3$.[76] The VDR binding was 30% in comparison to 1α,25(OH)$_2$D$_3$.[77] Compound **16** was reported to be three times more potent than 1,25(OH)$_2$D$_3$ with respect to porcine VDR

binding.[78] Thus the presence of C18 impaired VDR binding in contrast to C21, which reduced affinity towards chick VDR to 10% in comparison to 1α,25(OH)$_2$D$_3$ (**17**).[79] Interestingly, substitution of C20 by oxygen reduced VDR affinity to 0.1% in comparison to 1α,25(OH)$_2$D$_3$,[79] emphasizing the importance of hydrophobicity for good receptor binding. **18** with possible (R) and (S) configurations have not been reported. VDR binding of **19** has not been investigated, however, the ability to differentiate HL-60 cells compared to 1α,25(OH)$_2$D$_3$ was 1% at the same concentration.[80] For a similar molecule with a terminal alkene in the 2-position a 1.9% VDR affinity was reported in comparison the parent compound.[81] **20** also known as alfacalcidiol, was first reported in 1973.[82] Alfacalcidiol is converted to 1α,25(OH)$_2$D$_3$ *in vivo* and therefor exhibit similar activities. The VDR affinity was 900-fold less than 1α,25(OH)$_2$D$_3$.[75] Thus, it can be concluded that hydroxyl groups in the C1 and C25 positions are the most important substituents to promote VDR binding.

Further investigations into the significance of the bicyclic structure of 1α,25(OH)$_2$D$_3$ with respect to VDR binding is represented by compounds depicted in Figure 9.

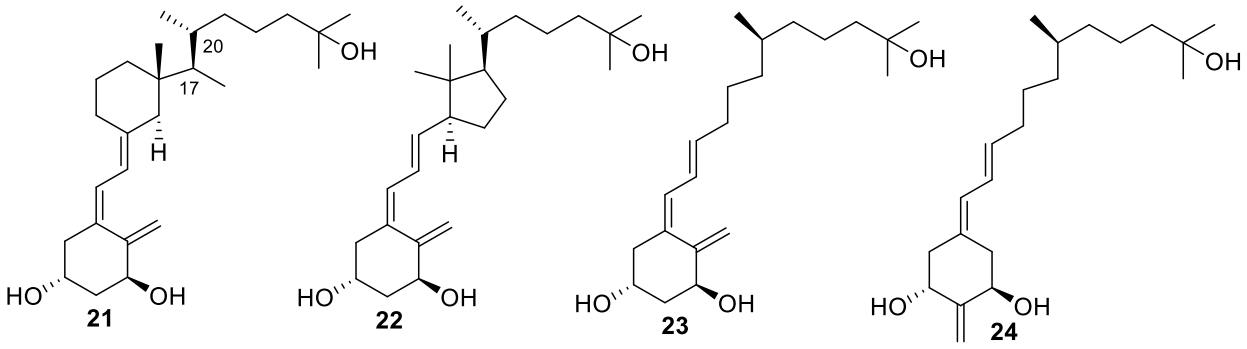

Figure 9. VDR ligands without a fused ring system.

Removal of the five membered ring of 1α,25(OH)$_2$D$_3$ was investigated with **21** and analogs thereof.[83] The relative stereochemistry of C17 marginally influenced VDR binding, however, large differences between these epimers were observed for anti-proliferation and calcium homeostasis.

VDR binding of **21** was 60% in comparison to 1α,25(OH)$_2$D$_3$. The VDR affinity of the C20 epimer of **21** was 70%. The same report characterized compounds like **22** with a VDR affinity of 80% in comparison to 1α,25(OH)$_2$D$_3$. The synthesis of **23** was reported but VDR binding was not determined.[84] However, **24** with the terminal alkene in the 2 position exhibited a 80 times lower affinity towards VDR than 1α,25(OH)$_2$D$_3$.[58]

Overall, it can be concluded that structural changes to the hydrophobic core of 1α,25(OH)$_2$D$_3$ can still result in high affinity ligands for VDR. The ligand binding domain of VDR consists of 12 helixes when bound to 1α,25(OH)$_2$D$_3$. Most essential features of 1α,25(OH)$_2$D$_3$ are the C1 and C25 hydroxyl groups, which have been shown to form canonical hydrogen bonds with VDR (Figure 10).

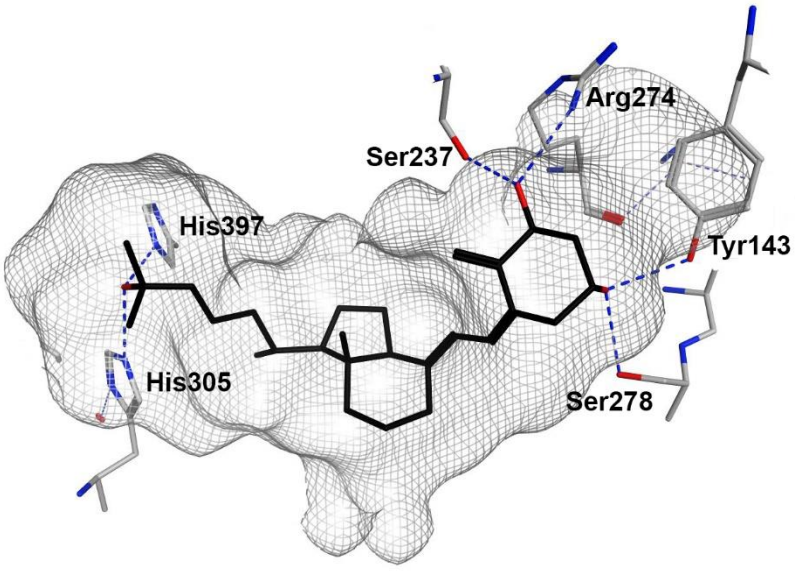

Figure 10. Crystal structure of 1α,25(OH)$_2$D$_3$ bound to human VDR [PDB ID:1DB1].[23]

25-OH interacts with His305 (loop H6-H7) and His 397 (H11), which is important for the conformational change of VDR to interact with coregulatory proteins. 1-OH interacts with Ser237 (H3) and Arg273 (H5), anchoring the ligand in the binding pocket. 3-OH interacts with Ser278 (H5) and Tyr143 (loop H1-H2) but compounds like **2** and **14** have shown that these contacts merely

further stabilize the complex. 1α,25(OH)$_2$D$_3$ only fills 56% of the VDR binding pocket, which explains the great variety of high affinity ligands that have been developed for VDR. Important however is the spacing and orientation of the hydroxyl groups, which is supported by ring structures, a diene moiety, and chiral carbon centers. The majority of the central VDR ligand pocket surface is hydrophobic and assembled by leucine, isoleucine, and valine side chains.

1.4.2 Non-secosteroid VDR Ligands

The first non-secosteroid ligands with a diarylmethane moiety were reported by Ligand Pharmaceuticals (Figure 11). The quaternary carbon center bearing two ethyl substituents was superior to other alkyl substituents and aligned well with the fused ring system of VDR bound 1α,25(OH)$_2$D$_3$.[85]

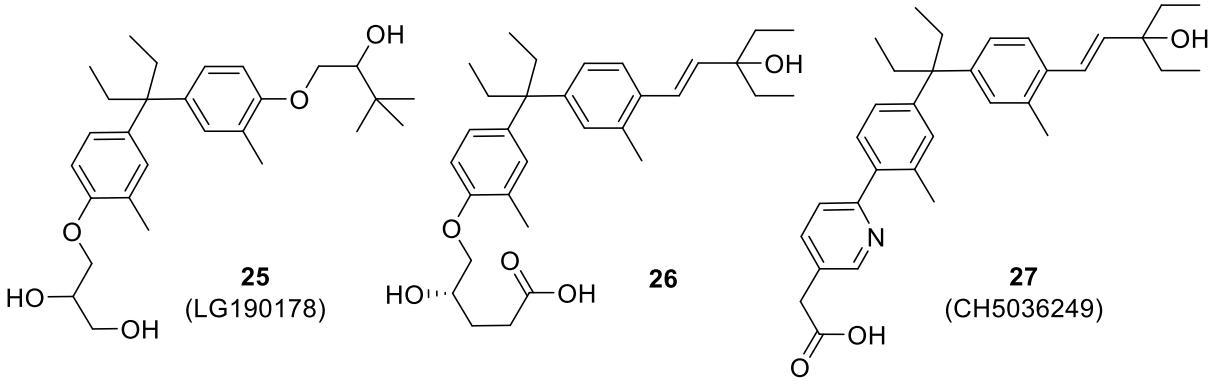

Figure 11. VDR ligands with a diarylmethane moiety.

The racemic mixture of LG190178 exhibited a VDR affinity of 0.3% in comparison to 1α,25(OH)$_2$D$_3$.[86] The synthesis of individual LG190178 stereoisomers identified the (2S, 2'R) isomer as the most active compound with a 28.3% VDR affinity in comparison to 1α,25(OH)$_2$D$_3$.[87] The systematic development of these ligands resulted in **26**, which was equally active as 1α,25(OH)$_2$D$_3$ in a cell-based transcription assay.[88] An analog of **26** with CF_3 groups instead of

ethyl groups adjacent to the tertiary alcohol showed a five-fold improvement in the transcription assay.[89] In recent years, many similar compounds were developed with thiophene, pyrrol,[90] and other heterocycles, however **27** with a pyridine substituent exhibited the highest affinity towards VDR, which as 37% of the VDR-1α,25$(OH)_2D_3$ interaction.[91]

Another successful approach for a non-steroidal VDR ligand design was the incorporation of a dicarba-closo-dodecaborane as a hydrophobic moiety instead of the fused ring system of natural VDR ligands (Figure 12).

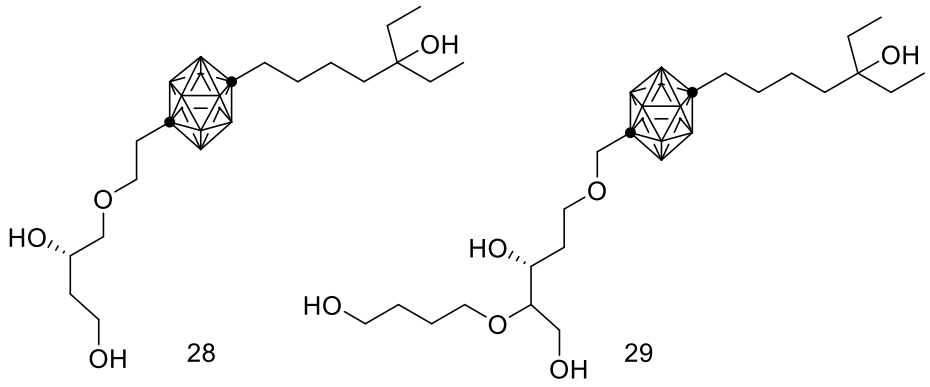

Figure 12. VDR ligand with a carborane structure.

The development of carborane-based VDR ligands with different side chains resulted in **28**, which exhibited an affinity of 640 nM (IC_{50}).[92] The (R) isomer was one-fifth as active. Subsequent research identified compound **29** being twice as potent as **28** in a HL60 differentiation assay.[93]

Other approaches for VDR ligands included the use of aromatic ring structures, which are absent for natural VDR ligand 1α,25$(OH)_2D_3$. The earliest examples were identified from a library of bis-aromatic compounds (Figure 13).

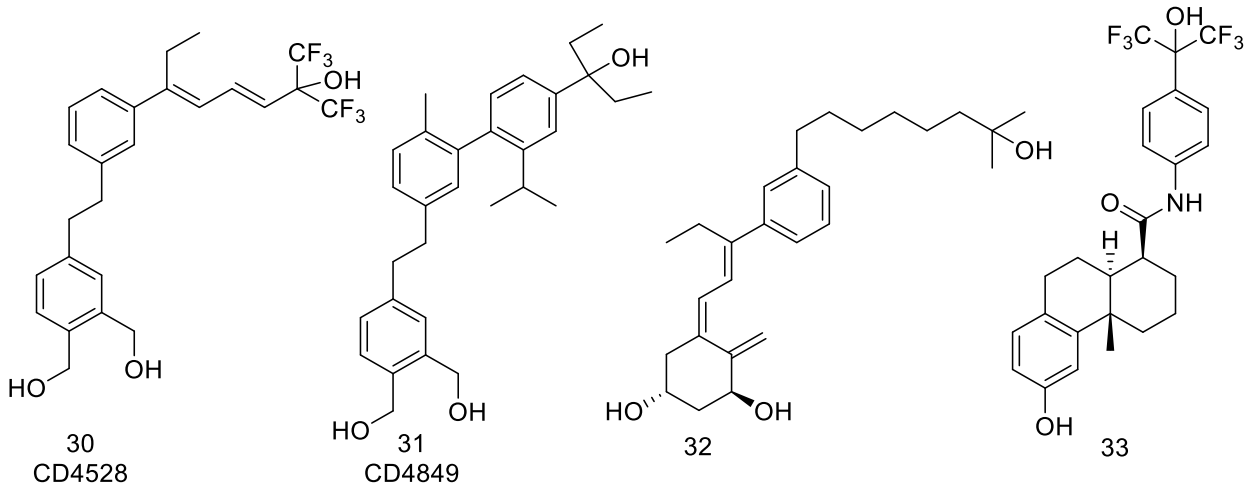

Figure 13. Bis- and trisaromatic VDR ligands.

CD4528 was characterized with a CYP24A1 reporter assay demonstrating an EC_{50} of 1.7 nM.[94] For the same assay, the EC_{50} of 1α,25$(OH)_2D_3$ was 1.0 nM. Other related VDR ligands exhibited similar low nanomolar activities, for example CD4849 (0.5 nM).[95] A recent study employing the A-ring structure of 1α,25$(OH)_2D_3$ resulted in **32** with a VDR affinity of 24% in comparison to 1α,25$(OH)_2D_3$.[96] Less active was **33**, exhibiting a 0.01% VDR affinity in comparison to 1α,25$(OH)_2D_3$.[97] Other nutritional ligands with low VDR affinities were reported by Haussler et al..[98]

VDR is highly expressed in the intestine and has been described as a bile acid sensor due to its ability to bind lithocholic acid (Figure 14).[99]

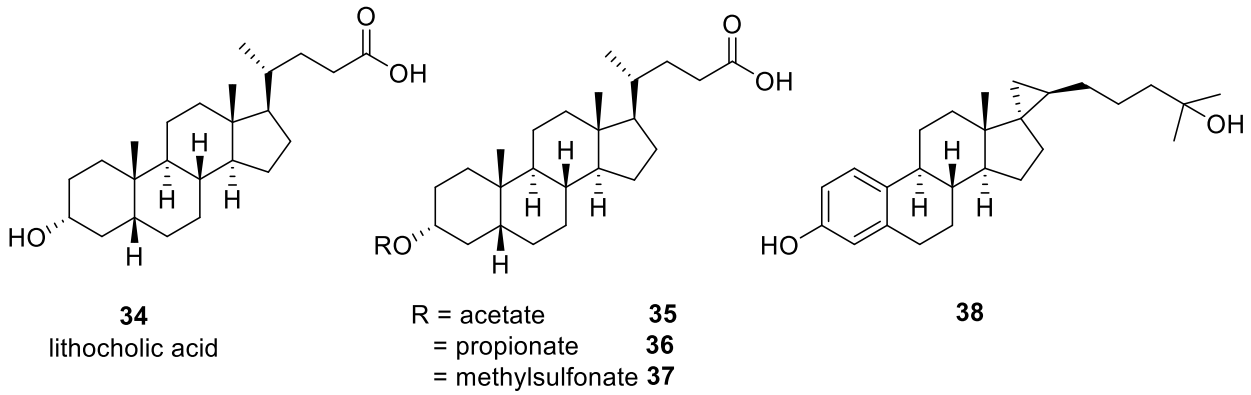

Figure 14. Steroid VDR ligands.

The affinity of VDR for lithocholic acid was less than 0.005% in comparison to 1α,25(OH)$_2$D$_3$. The corresponding acetate was more potent with a 0.01% VDR affinity in comparison to 1α,25(OH)$_2$D$_3$.[100] A later VDR binding study reported an IC$_{50}$ of 30 μM for **35** and **36**.[101] Recently, a methylsulfonate analog of lithocholic acid showed an IC$_{50}$ of 1.2 μM.[102] For estrone analog **38** an EC$_{50}$ of 850 nM was reported in a VDR transactivation assay.[103]

The first Y shaped VDR ligand called Gemini was introduced in 2000 by Norman et al.[104] (Figure 15)

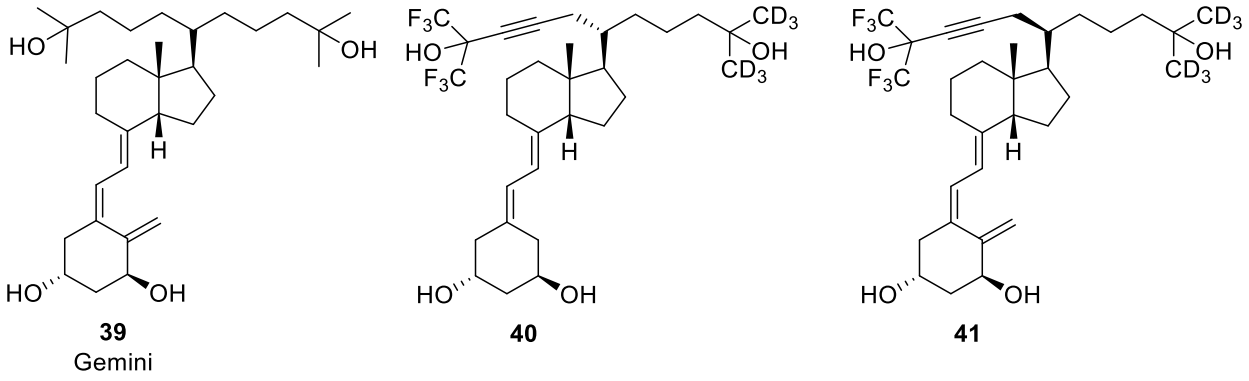

Figure 15. Gemini ligands.

Gemini exhibited a VDR affinity of 38% in comparison to 1α,25(OH)$_2$D$_3$. Based on an available crystal structure of VDR bound to 1α,25(OH)$_2$D$_3$, it was hypothesized that VDR might accommodate this second site chain in a so called A pocket (alternative pocket).[105] The later reported crystal structure of VDR bound to Gemini confirmed the adaptability of VDR to accommodate Y-shaped ligands.[106] Further development resulted in **40** and its C20 epimer **41**, which were 36 and 22- fold more active in a gene reporter assay than 1α,25(OH)$_2$D$_3$.[107]

1.4.3 VDR Antagonists

During the last two decades many different antagonists with strong VDR affinities have been reported.[108] The earliest disclosed antagonists were derivatives from natural occurring vitamin D metabolite (23S,25R)-1α,25$(OH)_2D_3$-26,23-lactone,[109] like compound TEI-9647 and its C23 epimer TEI-9648 (Figure 16).

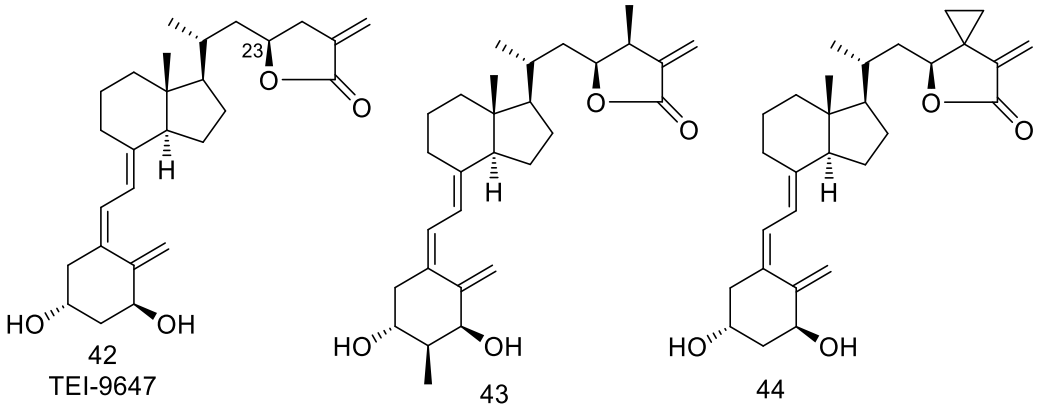

Figure 16. Electrophilic VDR ligands

The VDR affinity of TEI-9647 was 10% compared to 1α,25$(OH)_2D_3$. Its C23 epimer TEI-9648 bound VDR with a 8% affinity.[110] Further research confirmed that these unsaturated esters underwent a conjugate addition reaction with cysteine residues in the human VDR ligand pocket.[111] 2-Methyl substitution (**43**) significantly increased VDR affinity (63% in comparison to 1α,25$(OH)_2D_3$).[112] The introduction of a cyclopropyl group resulted in **44** that surpassed the VDR affinity of 1α,25$(OH)_2D_3$ (166%).[113]

Based on structure of calcipotriol (**45**), an approved treatment for psoriasis and high affinity VDR ligand, other related ligands were synthesized by Schering (Figure 17).

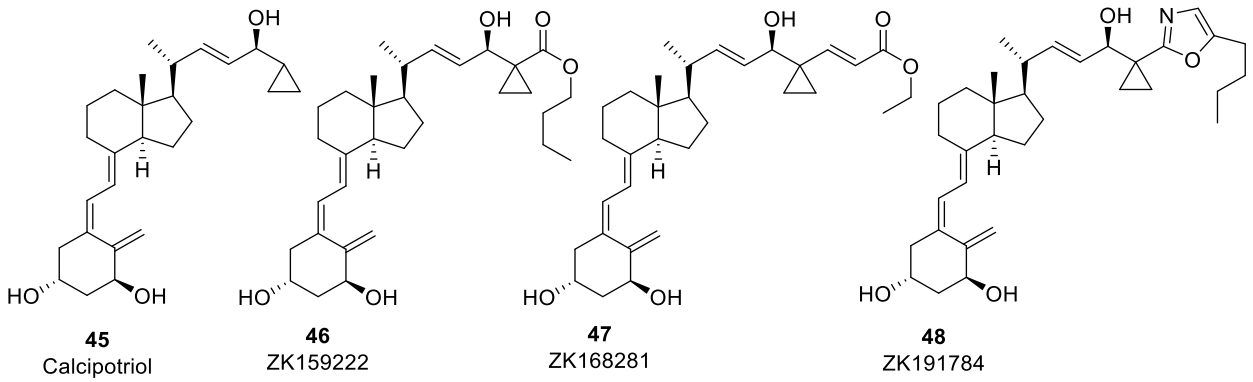

Figure 17. ZK series of VDR antagonists

In contrast to agonist calcipotriol, ZK159222 and ZK168281 were poor inducers of VDR transcription and reduced 1α,25$(OH)_2D_3$ meditated transcription.[114] For ZK191784, a VDR affinity of 33% in comparison to 1,25-$(OH)_2D_3$ was reported. [115] Thus, the VDR affinities of these ligands are strong but they induced an antagonistic VDR conformation. In addition, these antagonists were investigated *in vivo* demonstrating promising anti-inflammatory properties.[108]

Amide-based VDR antagonists were introduced in 2004 inspired by calcitriol lactone (Figure 18).

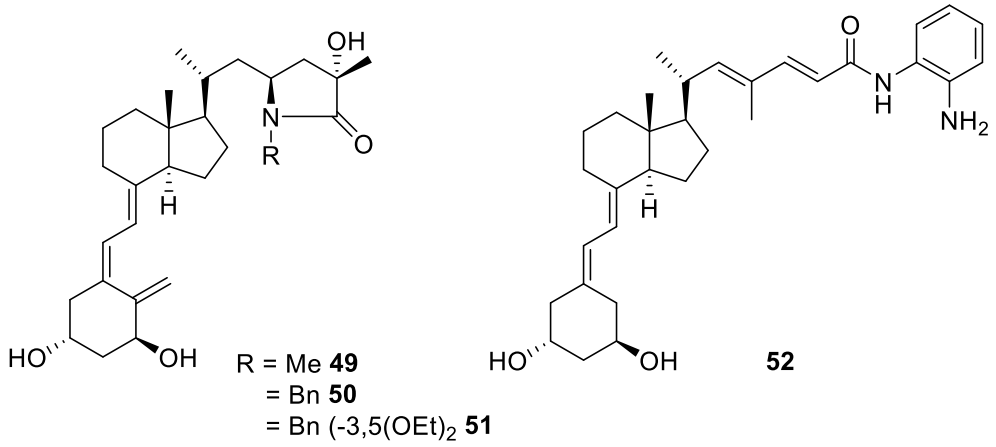

Figure 18. Amide series of VDR antagonists.

The corresponding lactam **49** exhibited a VDR affinity of 10.2 nM in comparison to 1α,25$(OH)_2D_3$ with 0.5 nM.[116] The measured VDR binding of **50** was 1.9 nM (IC_{50}). Importantly, **50** inhibited VDR-mediated transcription at nanomolar concentrations without showing any agonist activity in

the absence of 1α,25-$(OH)_2D_3$.[117] Further improvement was achieved with **51** exhibiting a 52% VDR binding in comparison to 1α,25$(OH)_2D_3$ and inhibited 1α,25$(OH)_2D_3$ mediated transcription with an IC_{50} of 90 nM.[118] For ortho-aniline compound **52** an IC_{50} of 107 nM was reported.[119]

Another approach to introduce a bulky group to change the conformation of VDR was realized with the introduction of an adamantane group (Figure 19).

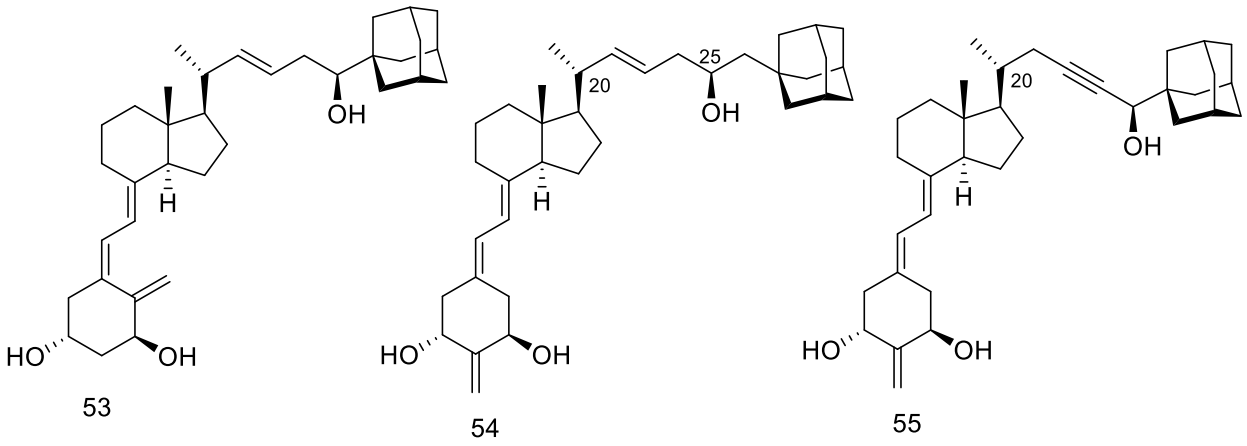

Figure 19. Adamantyl derived VDR antagonists.

53 exhibited a 2% VDR affinity in comparison to 1α,25$(OH)_2D_3$.[120] In the presence of 1α,25$(OH)_2D_3$, VDR-mediated transcription was inhibited at 100 nM. Among a series of diastereomeric analogs, **54** exhibited the highest affinity towards VDR with 17% affinity in comparison to 1α,25$(OH)_2D_3$.[121] Further improvements resulted in ligands with an internal triple bond named ADTK1-4.[122] The compound with the highest VDR affinity among this group was **55** reaching 90% of the VDR-1α,25$(OH)_2D_3$ interaction. This compound behaved like partial agonists. Finally, a library of VDR ligands with a diyne system was synthesized and evaluated achieving a 7% VDR affinity in comparison to 1α,25$(OH)_2D_3$.[123]

Inspired by Gemini, a series of Y-shape VDR ligands were developed that depending on the substitution pattern were antagonists, partial agonists, or superagonists (Figure 20).

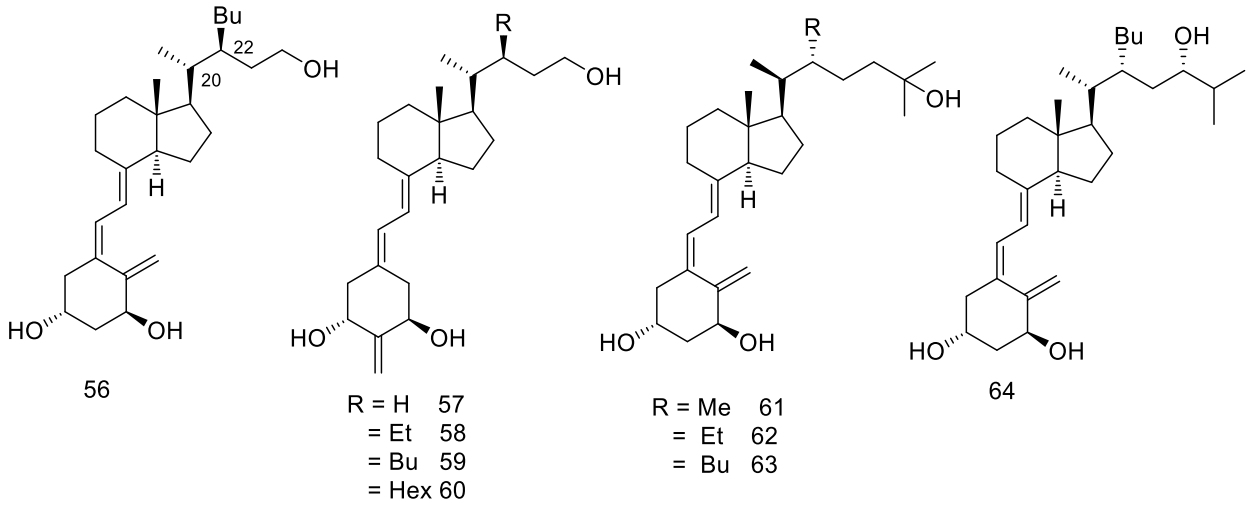

Figure 20. VDR ligand with C22 substitution.

Among a series of diastereomers with a butyl substituent in the C22 position, **56** was identified as a VDR antagonist.[124] The VDR affinity was 4.1% in comparison to 1α,25-$(OH)_2D_3$.[124] Interestingly, the C20 epimer of **58** was identified as an agonist with a 2.5% affinity towards VDR in comparison to 1α,25-$(OH)_2D_3$. For very similar compounds with a methylene group in C2 position, the influence of the alkyl chain length with respect to VDR binding was investigated (**57-60**).[81, 125] Also in this case, a butyl substituent resulted in antagonist **59** with a VDR affinity of 61% in comparison to 1α,25$(OH)_2D_3$. The partial agonists **60**, **58** and **57** exhibited lower VDR affinity. Further structural changes of **59** achieved by introducing two methyl substituents in the C24 position or elongating the hydroxyl bearing carbon chain by one carbon still produced antagonists. However, implementing the carbon chain inherent to 1α,25$(OH)_2D_3$ resulted in a superagonist with higher VDR affinity than 1α,25$(OH)_2D_3$.[81] Other superagonists were produced with the introduction of C22 substituents for 20-epi-1α,25-$(OH)_2D_3$ (**12**).[126] **63** exhibited the highest affinity for VDR (797%) followed by **62** and **61**. Finally, antagonists were produced with an isopropyl group (**64**).[124] Among different diastereomers, **64** exhibited the highest VDR affinity of 1.4% in comparison to 1α,25$(OH)_2D_3$.

A high throughput screen of 390,000 compounds identified PPARδ agonist GW0742 as novel VDR antagonist (Figure 21).[127]

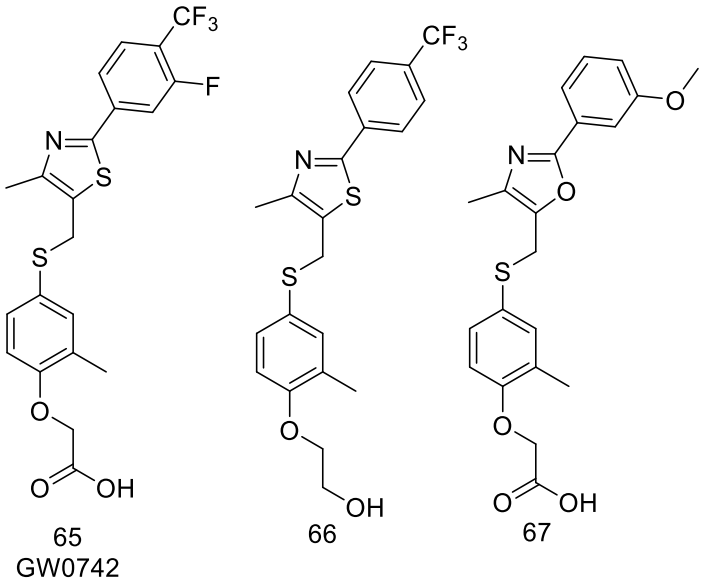

Figure 21. GW0742 based VDR ligands.

The VDR affinity of **65** was 8.7 μM. The structural change of the acid function into an hydroxyl group resulted in partial VDR agonist **66** with an EC_{50} of 120 nM.[128] The evaluation of a library of compounds related to **65** demonstrated that CF_3 substituents in the meta and ortho position reduced the affinity towards PPARδ without influencing the affinity for VDR.[129] Recently VDR antagonist **67** was reported with activity of 660 nM.[130] This compound did not bind PPARδ. Virtual screening of known nuclear receptor ligands for VDR binding identified several compounds possible candidates. VDR binding was demonstrated for several compounds including H6036.[131]

1.4.4 Discussion.

New VDR ligand design and synthesis is still a very active research area with many international research groups working together to develop new drug candidates for disorders caused by vitamin D deficiency, cancer, and inflammatory diseases. Newly discovered VDR ligands are being investigated in clinical trials reflecting the need for new medications in those disease areas. A great number of ligands have been elucidated in complex with VDR using X-ray crystallography. The structural information has guided new ligand design but has also demonstrated that the VDR ligand pocket is amendable to very different ligand shapes. However, as highlighted in this chapter, hydrogen bonding on opposite ends is essential for high VDR affinity. Another important feature is distinct spacing of these groups by a flexible hydrophobic spacer. Recently, endogenous VDR ligands for VDR such as lithocholic acid and fatty acids have been identified but their biological function is still unclear. Furthermore, new vitamin D metabolites have been identified in the last decades, which offer new areas of research in the field of vitamin D.

1.5 Calcitroic Acid Synthetic History

As these discoveries have revealed, calcitroic acid stands out as the primary end product of vitamin D metabolism. When CTA was initially identified by DeLuca in 974, it underwent swift characterization, yet it remained relatively obscure for four decades due to the belief that it had no specific biological function. Recently, a study conducted in our laboratory unexpectedly unveiled CTA's activity within cells. In a VDR-mediated transcription assay, our research group observed an upregulation of the VDR target gene CYP24A1 in DU145 cells when exposed to CTA.[132] Unfortunately, CTA is not readily available for commercial purchase in the quantities required for extensive research, and even in small amounts, it commands a very high price of approximately $4000 per milligram. This high cost is primarily attributed to the extremely low overall yields achieved through both synthetic and enzymatic isolation methods.

The initial synthesis of CTA was documented in 1981 as seen in Scheme 1.[133]

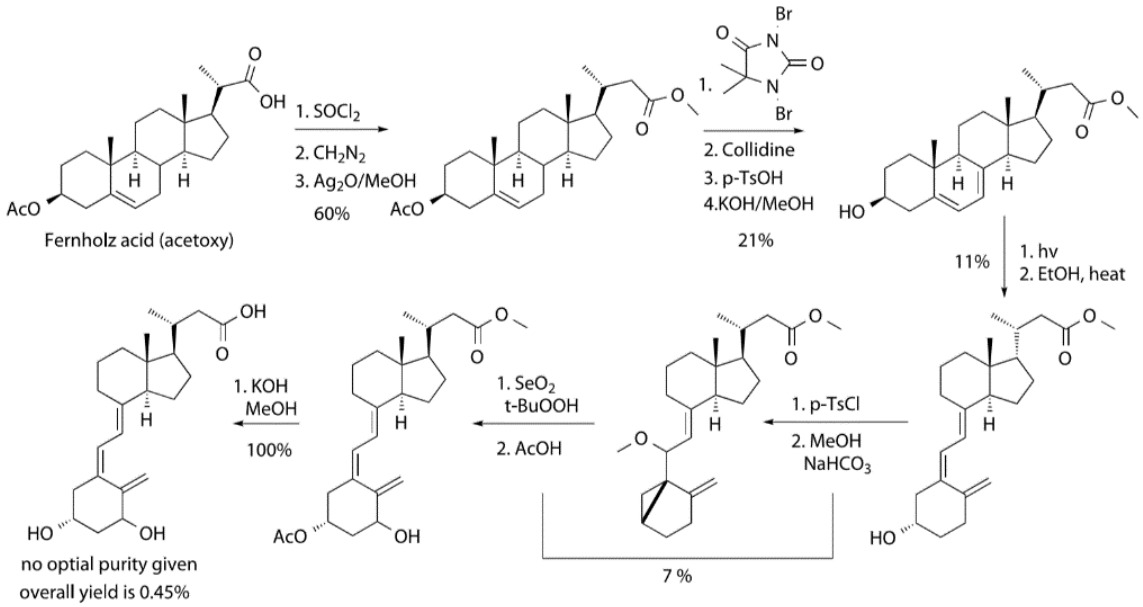

Scheme 1: Synthesis of CTA starting from a cholesterol analogue precursor

It commenced with the acetoxy derivative of Fernholz acid, a compound commercially available from Steraloids, which served as the starting material. This compound underwent an Arndt-Eistert reaction to yield the corresponding higher carboxy homologue. Subsequent steps involved allylic bromination, followed by elimination to introduce the diene moiety, which was then converted to the methyl ester of calcitroic acid, albeit in low yield, using photochemical and thermal conditions. 1α-hydroxylation was achieved through the synthesis of a cyclovitamin D derivative, followed by allylic oxidation and cycloreversion with acetic acid. Hydrolysis finally yielded CTA, albeit with an overall yield of just 0.09%. Although the optical rotation data were not provided, the corresponding methyl ester coeluted with the derivatized material isolated from rat livers. Subsequent refinements to this route managed to raise the overall yield to 0.28%.[134]

Two years later, a different approach based on a prior synthesis of vitamin D analogs was reported as seen in Scheme 2, which achieved an improved overall yield of 0.36%.[135]

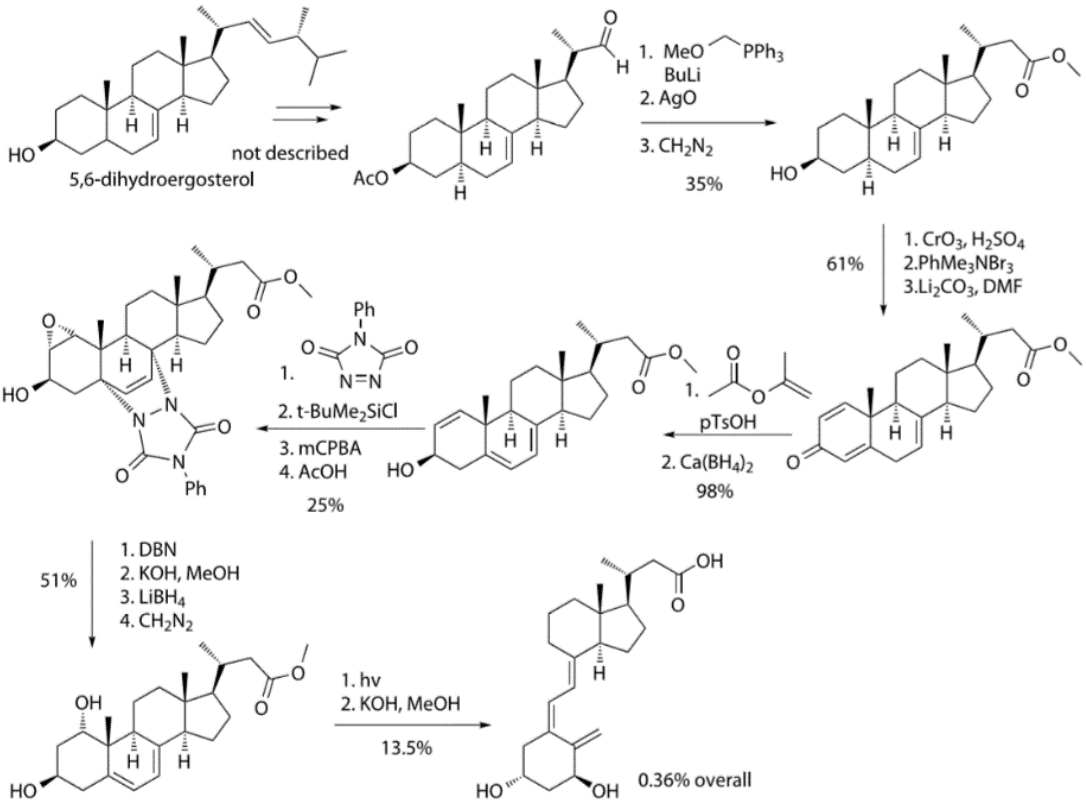

Scheme 2: Synthesis of CTA using a provitamin D precursor

This alternative synthesis began with 5,6-dihydroergosterol, leading to the preparation of the corresponding aldehyde. A Wittig reaction elongated the carbon chain, followed by demethylation, oxidation, and esterification steps. An oxidation process generated a quinone-like structure through α-carbon bromination and elimination, which was subsequently isomerized and reduced to form the allylic alcohol. Protective measures were applied to both the diene and alcohol functionalities, followed by oxidation and deprotection steps. The retro Diels−Alder reaction recreated the diene, and conversion of the ester to the acid enabled a selective reduction of the epoxide, concluding with esterification. Finally, the seco-steroid scaffold was generated through a light-induced ring opening reaction and subsequent saponification, achieving CTA with an overall yield of 0.36%. It's worth noting that the light-induced ring opening reaction significantly impacted the overall yield in both described methods.

During the 1980s and 1990s, various synthetic strategies were explored to create other vitamin D analogs, leading to the development of several new building blocks for their synthesis.

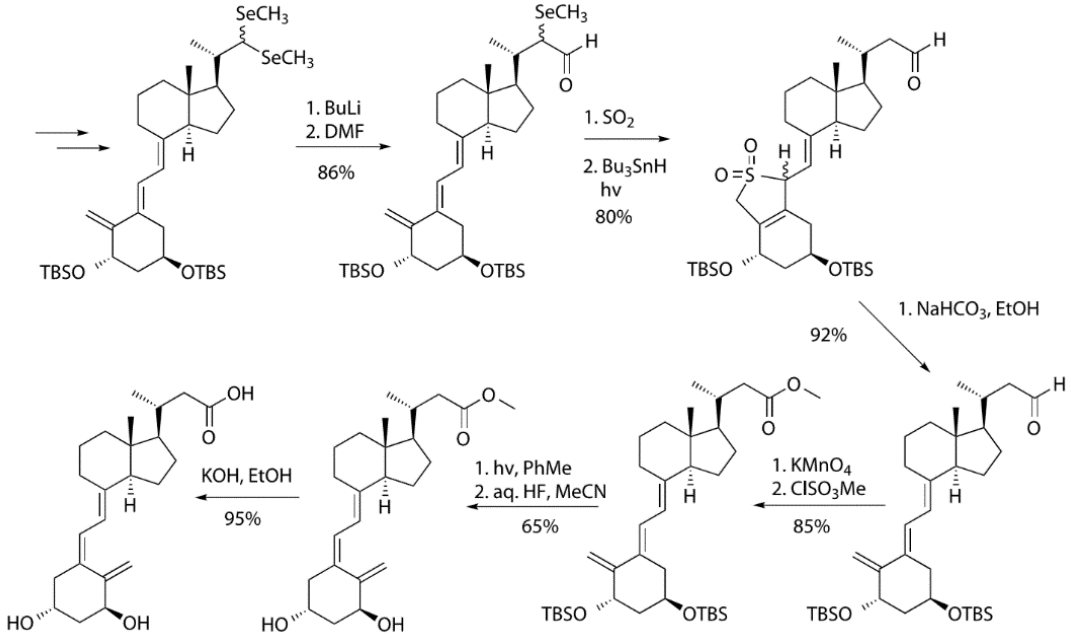

Scheme 3: Synthesis of CTA starting from a seco-steroid precursor

In 1990, a method employing a seco-steroid as a starting material to produce CTA was introduced as seen in Scheme 3.[136]

This approach starts with a seleno acetal, generated from the corresponding 1α-hydroxy vitamin D aldehyde derivative. A series of reactions, including formylation, lithio-demethylseleno derivative formation, hetero Diels−Alder protection with sulfur dioxide, radical deselenation under light, retro Diels−Alder reaction, oxidation, and esterification, ultimately resulted in the methyl ester of protected CTA. Photoisomerization was employed to establish the natural Z-configuration, followed by deprotection and hydrolysis to obtain CTA. While this route achieved high yields, it involved numerous steps, particularly when considering precursor synthesis.

More recently, a synthesis method employing readily available chemicals was developed, enabling, for the first time, the production of gram quantities of CTA as seen in Scheme 4.[137]

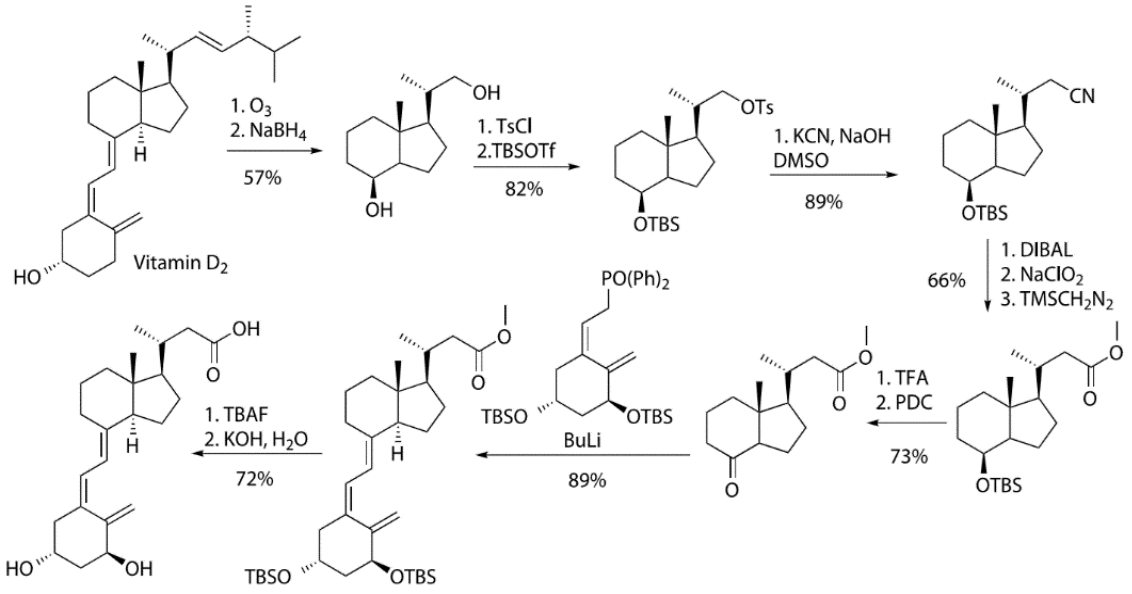

Scheme 4: Synthesis of CTA starting from vitamin D_2 using a Ring A phosphine oxide synthon

Originally designed to produce ^{13}C-labeled CTA for metabolic research, this synthesis utilized Inhoffen Lythgoe diol, which can be either commercially procured or readily synthesized

from vitamin D_2.[138] Our CTA production is founded on this new route, which has been modified in several ways to enhance reaction yields.

1.6 Synthetic Strategy for Calcitroic Acid (Scheme 4)

Synthesis of Inhoffen Lythgoe Diol

Due to the relatively cheap price of ergocalciferol (vitamin D_2), we began our synthesis with this compound that was reacted via an ozonolysis reaction followed by a reduction with sodium borohydride to convert the resulting aldehydes to alcohols. This proved to be successful as a one-pot two-step reaction to generate the Inhoffen Lythgoe diol. The amount of methanol used in this reaction was necessary to have enough solvent to completely dissolve all of the reagents, however, too much methanol would result in a lack of ozone saturation and cause the reaction to fail. A bubbler proved to be necessary to ensure the ozone was saturating the solvent upon which the solution would turn a deep blue signaling sufficient ozone saturation. Furthermore, it was determined that this reaction needed to be run at -78 °C with a dry ice acetone bath. It proved to be most effective to crush the dry ice to supply sufficient cooling. The reaction could be scaled to 3 g, however, it is not recommended to scale the reaction to larger quantities without the proper equipment as this resulted in the reaction failing. To ensure all double bonds of the starting material were broken, it was found most successful to run the reaction for a full 7 h before allowing the reaction to warm up and the sodium borohydride was added portion wise to prevent overheating.

During the work-up, evaporation of the methanol resulted in a significant amount of residual pyridine. The solution to removing the excess pyridine came with a single wash with 10% aqueous copper sulfate which successfully removed the pyridine. Once the crude product was obtained, pure product could be obtained via column chromatography.

It was observed that during evaporation of the methanol, if the solution was concentrated until approximately 1/3 the volume remained, and the solution was then allowed to sit for 18 h, a significant amount of crystals formed. It was determined by NMR that these crystals were structurally related to the desired product however, after analysis via ^{11}B NMR, it is our belief that these crystals are the desired product as a boronate form of the alcohol. Initial attempts were made to protonate the alcohols with small amounts of HCl, however all initial attempts failed. To obtain enough material to continue forward with the synthesis, column chromatography was used to purify material from subsequent reactions, however, future work could be conducted to look for a successful recrystallization procedure.

Synthesis of O-silylated C,D-ring tosylate

A Meyer synthesis was used to add protecting groups to the two alcohols on the diol. The first group to be protected was the primary alcohol due to its greater accessibility. This protection was successfully achieved with one equivalent of tosyl chloride to install a tosylate group. This procedure was followed by the protection of the secondary alcohol via t-butyldimethylsilyl trifluoromethanesulfonate (TBSOTf) which successfully installed a TBS protecting group. A silyl group was chosen for the protection of this alcohol due to the stability under basic conditions and lability with fluoride ions.

Synthesis of O-silylated C,D-ring nitrile

In this step, the installed tosylate functionality was utilized as a good leaving group for a substitution reaction with potassium cyanide. To achieve the best yields possible, it was determined that it was necessary to quench the reaction as soon as all the staring material was

consumed. Previous attempts carried out this reaction in DMSO, however, removing the DMSO proved challenging and resulted in extremely low yields. Therefore, the solvent was changed to ACN which was successful in dissolving the staring material, but unsuccessful in dissolving the salts. It is known that crown ethers such as 18-crown-6 solubilize potassium ions and therefore, the addition of this crown ether allowed for a better CN^- nucleophile despite the lack of a counter ion. When the reaction was run with these conditions at 75 °C, the yield was greatly improved.

Synthesis of O-silylated C,D-ring aldehyde

A reduction of the nitrile to an aldehyde was accomplished with DIBAL in anhydrous dichloroethane at 0 °C. Importantly, this reaction should be kept at 0 °C for the extent of the reaction as well as the work-up due to the exothermic nature of the quenching step with aqueous ammonium chloride. The addition of the aqueous ammonium chloride should be added very slowly initially due to the risk of the reaction bubbling over. Upon the complete addition of the aqueous ammonium chloride, it was necessary to stir the reaction for 30 min to break up the viscous solution. *Tert*-butyl methyl ether could be added to assist with breaking up the solution, and stirring of the reaction should be continued at 0 °C until a more thorough separation of the aqueous layer was achieved. The aqueous later could then be dried by the addition of a significant amount of anhydrous magnesium sulfate directly into the reaction flask. The reaction could then be filtered, and the organic layer concentrated before purification by column chromatography.

Synthesis of O-silylated C,D-ring acid

A Pinnick oxidation was utilized to convert the aldehyde to a carboxylic acid. This reaction forms chlorous acid from the chlorite under acidic conditions which is then used by the reaction as an

oxidant. Being a biphasic reaction, the starting material is dissolved in tert-butanol with the addition of 2-methyl-2-butene. Sodium hypochlorite was then dissolved in water and added to the reaction. Upon completion of the reaction, all salt byproducts could be easily removed via extraction into the aqueous layer, and the desired product could be obtained by evaporation of the organic layer. It was determined that higher yields could be obtained if the crude product was carried forward to the next reaction without purification.

Synthesis of O-silylated C,D-ring ester

To convert the starting carboxylic acid to the desired methyl ester, trimethylsilyldiazomethane was used as the methylating agent. The reaction was run in a mixture of anhydrous toluene and methanol where the methylating agent was added dropwise which resulted in a yellow color indication the formation of the diazo compound. Once complete, the reaction was quenched with acetic acid and purified via column chromatography.

Synthesis of C,D-ring alcohol

Trifluoroacetic acid (TFA) was used to deprotect the silyl group. The TFA was successful in removing the TBS group, however, a significant byproduct was observed which greatly limited the yield out of the reaction. This byproduct was determined to be a molecule of TFA bound to the freed alcohol. Initial procedures simply concentrated the reaction with no work-up which likely caused the TFA byproduct to remain unaffected in the crude material. This crude material could be re-reacted with TBAF to convert all of the byproduct to desired product, however, it would be recommended that for future reactions, a work-up be implemented that would break the byproduct

into desired product. This will likely result in good yields without the use of re-reacting crude material.

Synthesis of C,D-ring ketone

The now free alcohol was oxidized to the corresponding ketone with PDC as the oxidizing agent. Running this reaction under a nitrogen atmosphere, in anhydrous DCM, and running the reaction for at least 18 h proved to give the best yields. The PDC is insoluble in DCM, however the reaction will turn black as it progresses signaling a successful reaction. Despite however, similar retention factors between the starting material and product via TLC, the product could be confirmed by NMR. Furthermore, if the reaction was stopped before all of the starting material had been consumed, the material could be re-reacted with fresh PDC in order to ensure full conversion.

Synthesis of O-Bis-silylated calcitroic acid methyl ester

A Wittig-Horner-Emmons reaction was used to couple the A-ring to the C,D-ring of the calcitroic acid. This reaction was extremely water sensitive and all glassware including the stir bar and any other pieces of the reaction apparatus needed to be oven dried overnight. The A-ring ligand was commercially available, however, to ensure the dryness of this material, the A-ring was dissolved in THF with the addition of molecular sieves and left to dry overnight the day before the reaction was conducted. Upon conducting the reaction, all glassware needed to be set up while hot and purged with vacuum and nitrogen while hot. Once set up, the reaction apparatus needed to remain under a nitrogen atmosphere for the extent of the reaction.

It was necessary to cool the reaction to -78 °C using a dry ice acetone bath before the addition of n-butyl lithium, which was added dropwise via syringe. At this point, the reaction

turned a vibrant red color which lasted until the reaction was quenched. If a red color was not observed or if the red color did not persist, the reaction was wet and would not be successful. It is recommended that the ratio of *n*-BuLi to ketone be 1:1.5 to prevent 1,2 addition of the *n*-BuLi attacking the ketone rather than deprotonating the phosphine oxide.

If the reaction proceeds successfully, the reaction could be removed briefly from the ice bath after one hour has elapsed to ensure full deprotonation. This would be evident by the deepening of the red color. During the addition of the ketone, the reaction was again suspended in the ice bath and the ketone was added slowly enough to prevent the reaction from warming significantly. Once the addition was complete, the reaction was allowed to proceed for 5 h until no further conversion was observed via TLC. The reaction was then quenched with water before being allowed to warm to room temperature for the work-up.

Synthesis of calcitroic acid methyl ester

The two TBS protecting groups found on the A-ring were deprotected using TBAF. It was determined that 10 equivalents of TBAF afforded excellent yields for the reaction, however, the highest yields were obtained for smaller scale reactions. When scaled up, the removal of tetrabutylammonium became challenging despite multiple water washes. It has been proven that this reaction could also be run with camphorsulfonic acid (CSA) as the deprotecting agent, however, TBAF always afforded the highest yields.

Synthesis of calcitroic acid

The removal of the methyl group yielded the final calcitroic acid product. This synthesis was accomplished using sodium hydroxide at room temperature. Multiple hydrolysis procedures for

this conversion have also been reported, however, the use of potassium hydroxide at 60 °C proved to be difficult, and procedures utilizing elevated temperatures caused product degradation.

1.7 Synthetic Methods and Characterization of Synthesized Calcitroic Acid Compounds

Ergocalciferol was purchased from various commercial sources including (Alfa Aesar J62163, AstaTech 44109, Research Products International C20300, Sigma-Aldrich 95220, VWR 101172-472). The phosphine oxide used to attach the A-ring was purchased from ChemScene (CS-M1835, CS-M0003). All moisture or oxygen-sensitive reactions were carried out in oven dried glassware and under a nitrogen atmosphere. Reaction temperatures refer to the containing bath temperatures. Reactions were monitored by thin-layer chromatography (TLC) using Merck 60 UV254 silica gel plates (Sigma-Aldrich). Visualization was performed with UV light, cerium molybdate general stain followed by heating, and other methods as noted. Synthesized compounds were purified by normal phase flash chromatography (SPI Biotage, silica gel 230-400 mesh) except where noted. Compound characterization was performed via NMR. Spectra were recorded on a Bruker Avance 500MHz instrument with compounds dissolved in the specified deuterated solvent.

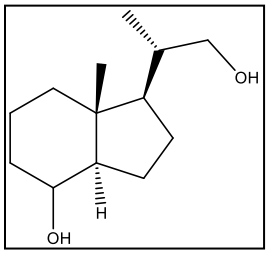

Inhoffen-Lythgoe diol: Ergocalciferol (3.08 g, 7.76 mmol) was dissolved in anhydrous pyridine (7 mL) before being diluted in anhydrous MeOH (250 mL). A single neck RB flask was used and a bubbler was attached and inserted into the reaction for the addition of the ozone. A small outlet was left for excess gas to be vented out of the reaction. The reaction was cooled to -78 °C and ozone was bubbled through for 7 h using an A2Z Ozone A2ZZ-5G 110 V with 38g/m3 O3 output. The

reaction was monitored by TLC with many spots appearing initially, but later showed three main spots. When no more conversion was observed, the reaction was warmed to 0 °C and stirred vigorously. Sodium borohydride (2 g, 53 mmol) was added portion wise and once fully dissolved, the reaction was quenched with 70 mL of H_2O and stirred for 5 min before the mixture was concentrated to dryness. The residue was diluted with 100 mL of H_2O and extracted with DCM (3x100 mL). The organic layers were combined and washed with 5% aqueous $CuSO_4$ (300 mL). The organic layer was then washed with 1M HCl (2x100 mL) and saturated aqueous $NaHCO_3$ (300 mL). The organic layer was then dried with anhydrous $MgSO_4$ and concentrated to dryness. The crude material was purified via column chromatography (EtOAc:Hex 1:3) to yield the Inhoffen Lythgoe diol as a white solid (919 mg, 55.8%). ^{1}H-NMR (500MHz, $CDCl_3$) δ 4.05 (s, 1H), 3.61-3.58 (dd, *J* = 10, 3.0 Hz, 1H), 3.33-3.30 (dd, *J* = 5.0, 3.5 Hz, 1H), 1.97-1.95 (m, 1H), 1.91-1.78 (m, 3H), 1.62-1.54 (m, 2H), 1.53-1.41 (m, 5H), 1.40-1.31 (m, 2H), 1.23-1.14 (m, 2H), 1.00-0.99 (d, *J* = 5.0, 3H), 0.92 (s, 3H).

Figure 22: ^{1}H Spectra of Inhoffen-Lithgoe Diol:

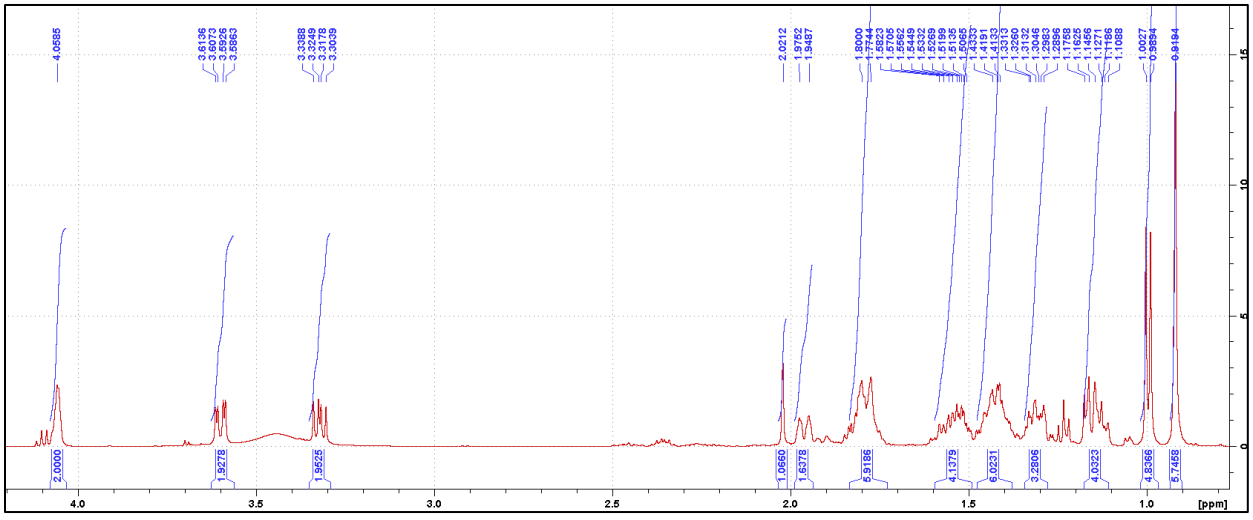

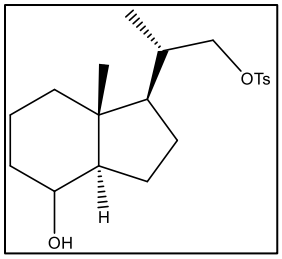

C,D-ring tosylate: Inhoffen-Lythgoe diol (125.6 mg, 0.59 mmol) was dissolved in anhydrous DCM (6.5 mL) before DMAP was added (147 mg, 1.19 mmol), followed by the addition of p-toluenesulfonyl chloride (120 mg, 0.63 mmol). The reaction was then allowed to stir overnight at RT before being quenched with 1M HCl (6.5 mL). The mixture was extracted with DCM (3x15 mL), and the combined organic layers were washed with H_2O (15 mL) before being dried with anhydrous $MgSO_4$. The organic layer was concentrated to dryness and the crude material was purified via column chromatography (EtOAc:Hex 3:7) to yield the product was a crystalline white solid (182 mg, 84.0%). ^{1}H-NMR (500MHz, $CDCl_3$) δ 7.80-7.79 (d, *J* = 8.5 Hz, 2H), 7.33-7.35 (d, *J* = 8.4 Hz, 2H), 4.08 (s, 1H), 7.07-3.995 (dd, *J* = 6.2, 3.0 Hz, 1H), 3.84-3.81 (dd, *J* = 6.5, 3.0 Hz, 1H), 2.48 (s, 3H), 1.98-1.92 (m, 1H), 1.88-1.77 (m, 2H), 1.75-1.66 (m, 2H), 1.62-1.52 (m, 1H), 1.51-1.42 (m, 3H), 1.38-1.31 (m, 1H), 1.26-1.13 (m, 4H), 0.98-0.97 (d, *J* = 5.0 Hz, 3H), 0.92 (s, 3H).

Figure 23: ^{1}H Spectra of C,D ring tosylate:

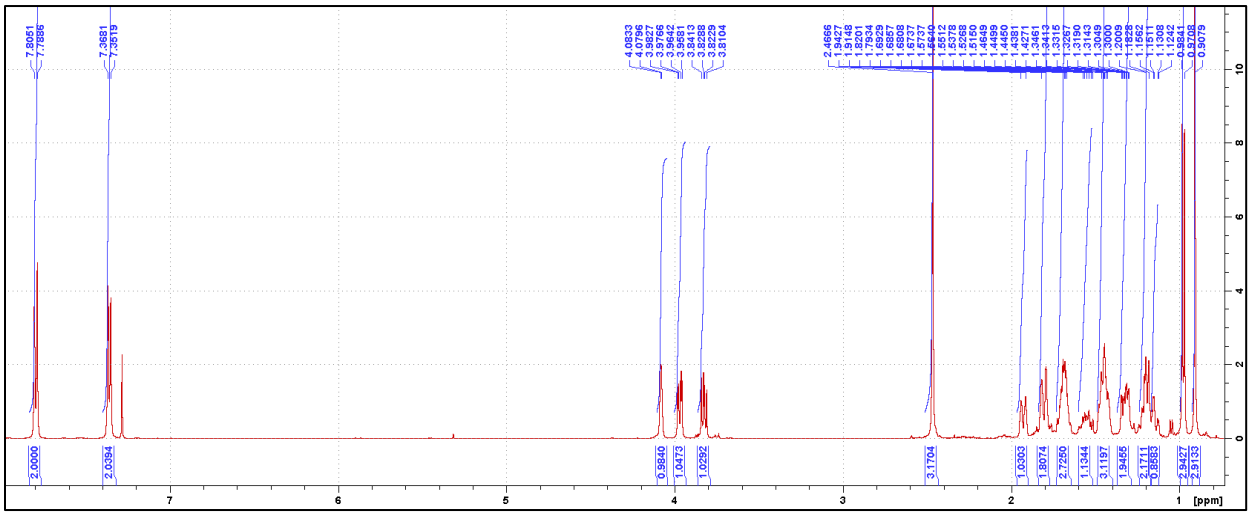

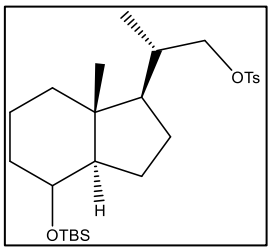

O-silylated C,D-ring tosylate: C,D-ring tosylate (305.1 mg, 0.83 mmol) was dissolved in anhydrous DCM (1.5 mL) and the reaction was cooled to 0 °C before the addition of 2,6-lutidine (115 µL, 1.0 mmol). Tert-butyl dimethylsilyl trifluoromethanesulfonate (270 µL, 1.2 mmol) was then added and the reaction was allowed to stir at 0 °C for 2 h until the reaction was deemed complete by TLC. The reaction was then quenched with H_2O (2 mL) and the mixture was extracted the DCM (3x15 mL). The organic fractions were combined and washed with H_2O (45 mL) and dried over anhydrous $MgSO_4$. The organic layer was concentrated and the crude product was purified via column chromatography (EtOAc:Hex 1:19) to yield the product as a nearly clear oil which solidified over time (333 mg, 83.3%). ^{1}H-NMR (500MHz, $CDCl_3$) δ 7.81-7.79 (d, *J* = 10.2 Hz, 2H), 7.36-7.35 (d, *J* = 8.0 Hz, 2H), 4.00-3.95 (m, 2H), 3.82 (dd, *J* = 6.5, 2.8 Hz, 1H), 2.47 (s, 3H), 1.92-1.86 (m, 1H), 1.84-1.73 (m, 1H), 1.71-1.58 (m, 3H), 1.57-1.49 (m, 1H), 1.42-1.26 (m, 3H), 1.25-1.19 (m, 1H), 1.18-1.08 (m, 3H), 0.97-0.96 (d, *J* = 6.5, 3H), 0.89 (s, 9H), 0.88 (s, 3H), 0.02 (s, 3H), 0.00 (s, 3H).

Figure 24: ^{1}H Spectra of O-silylated C,D ring tosylate:

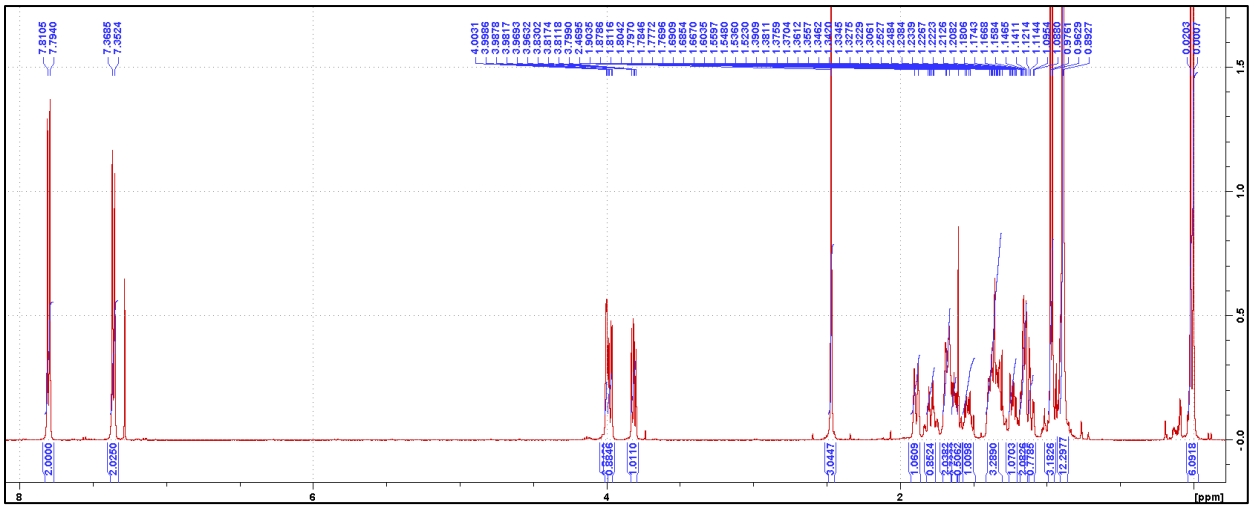

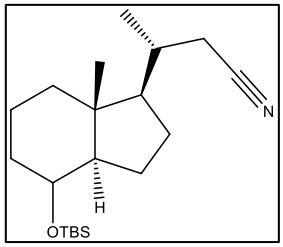

O-silylated C,D-ring nitrile: O-silylated C,D-ring tosylate (248.1 mg, 0.52 mmol) was dissolved in anhydrous ACN (7 mL). Solid NaOH was added (42 mg, 1.0 mmol) before the addition of KCN (67 mg, 1 mmol) and 18-crown-6 (343 mg, 1.3 mmol). The solution was heated to 75 °C and the reaction was allowed to stir for 2.5 h before all the starting material was consumed via TLC. The solvent was removed and the residue was dissolved in H_2O (10 mL) before being extracted with EtOAc (3x10 mL). The organic layers were combined and washed with brine (30 mL) before being dried with anhydrous $MgSO_4$. The organic layer was concentrated and the crude material was purified via column chromatography (EtOAc:Hex 3:97) to yield the product as a clear oil (144 mg, 82.9%). ^{1}H-NMR (500MHz, $CDCl_3$) δ 4.03-4.02 (m, 1H), 2.38-2.37 (dd, *J* = 16.6, 3.8 Hz, 1H), 2.26-2.25 (dd, *J* = 16.6, 7.0 Hz, 1H), 1.97-1.92 (m, 1H), 1.88-1.75 (m, 3H), 1.73-1.67 (m, 1H), 1.66-1.56 (m, 1H), 1.46-1.37 (m, 3H), 1.36-1.30 (m, 1H), 1.29-1.18 (m, 3H), 1.16-1.15 (d, *J* = 6.6Hz, 3H), 0.95 (s, 3H), 0.91 (s, 9H), 0.04 (s, 3H), 0.02 (s, 3H).

Figure 25: ^{1}H Spectra of O-silylated C,D ring nitrile:

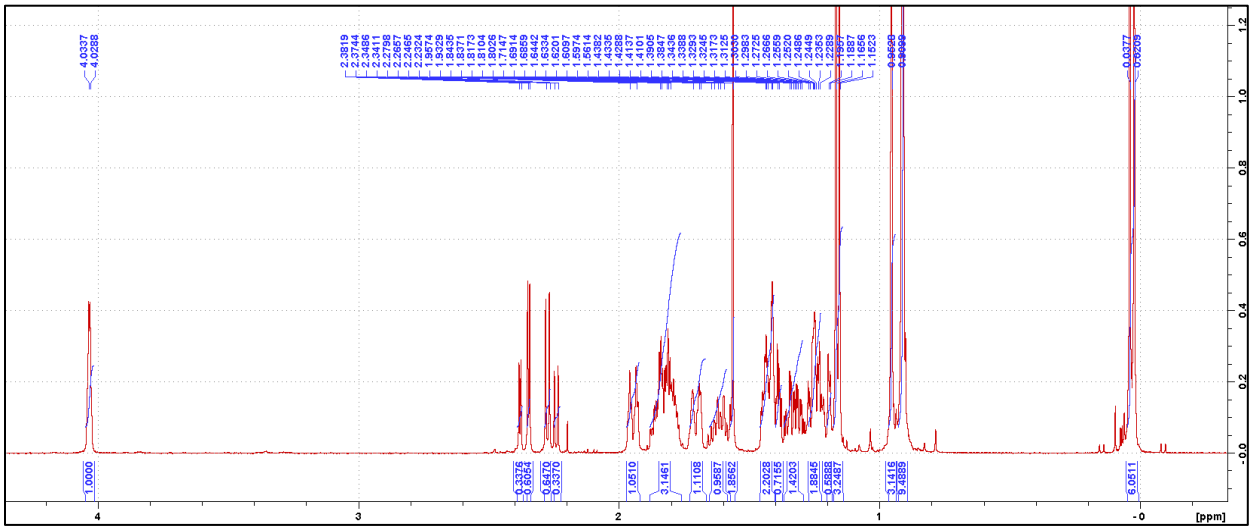

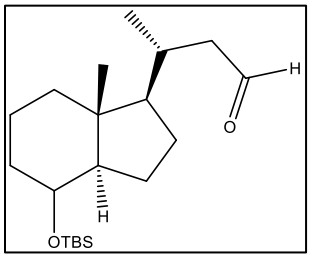

O-silylated C,D-ring aldehyde: O-silylated C,D-ring nitrile (200.9 mg, 0.60 mmol) was dissolved in anhydrous DCM (6 mL) and the solution was cooled to 0 °C. DIBAL (1.5M in toluene, 1.4 mL, 2.05 mmol) was added dropwise and the reaction was allowed to stir at 0 °C. After 45 min, the reaction was deemed complete by TLC and the reaction was slowly quenched with the dropwise addition of aqueous saturated NH_4Cl (5 mL). The mixture was then vigorously stirred at 0°C for 1 h before the addition of MTBE (20 mL) which was still allowed to stir at 0°C for an additional 2 h. The mixture was then allowed to warm up overnight at which point the aqueous later appeared as a fluffy white substance. Anhydrous $MgSO_4$ was added until the aqueous layer was completely dried. The $MgSO_4$ was then filtered and the filtrate was concentrated to dryness before the crude material was purified via column chromatography (EtOAc:Hex 5:95). The product was collected as a clear oil (145 mg, 71.3%). ^{1}H-NMR (500MHz, $CDCl_3$) δ 9.76 (dd, *J* = 3.6, 1.4 Hz, 1H), 4.03-4.02 (m, 1H), 2.48-2.46 (dd, *J* = 15.7, 2.5 Hz, 1H), 2.19-2.13 (m, 1H), 2.09-2.02 (m, 1H), 2.00-1.94 (m, 1H), 1.86-1.76 (m, 2H), 1.73-1.67 (m, 1H), 1.65-1.56 (m, 1H), 1.43-1.36 (m, 3H), 1.30-1.23 (m, 2H), 1.19-1.12 (m, 2H), 1.02-1.01 (d, *J* = 6.5 Hz, 3H), 0.98 (s, 3H), 0.91 (s, 9H), 0.04 (s, 3H), 0.02 (s, 3H).

Figure 26: ^{1}H Spectra of O-silylated C,D ring aldehyde:

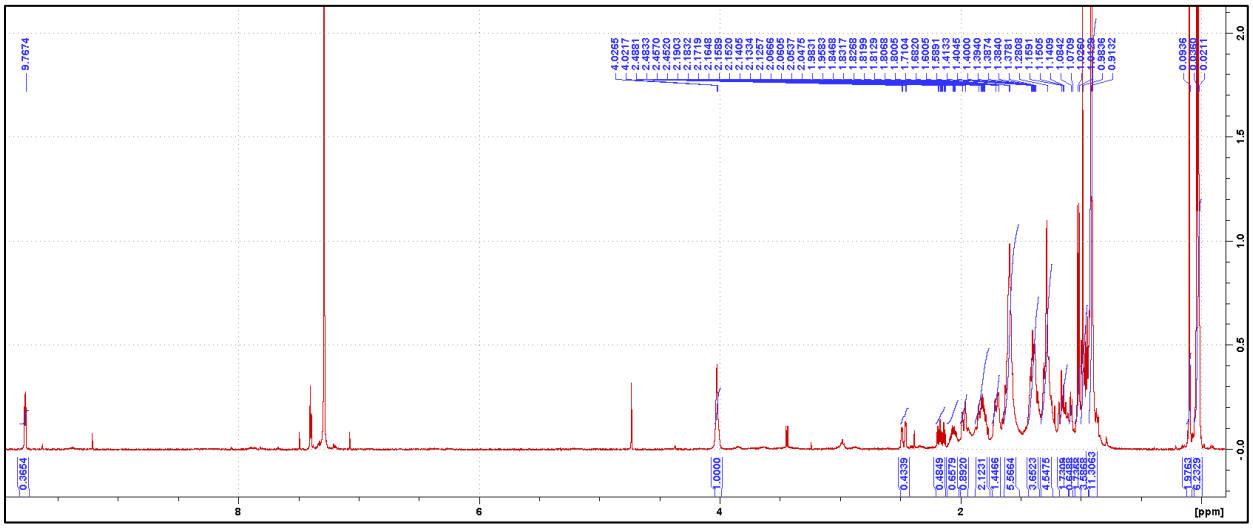

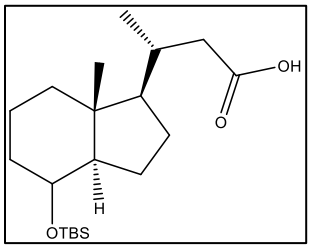

O-silylated C,D-ring acid: Sodium phosphate monobasic monohydride (616 mg, 4.5 mmol) was dissolved in H_2O (6 mL) before the addition of sodium chlorite (620 mg, 6.8 mmol). A separate solution was prepared containing O-silylated C,D-ring aldehyde (245.6 mg, 0.73 mmol) in tert-butanol (15 mL) and 2-methyl-2-butene (3.5 mL). The aqueous solution was then added to the organic solution and the reaction was stirred for 1 h until deemed complete via TLC. The mixture was concentrated and the residue was dissolved in H_2O (25 mL) and extracted with DCM (3x25 mL). The organic layers were combined and washed with H_2O (50 mL) before being dried over anhydrous $MgSO_4$. The organic layer was then concentrated and the crude material which was obtained as w white powder was carried forward to the next reaction (280 mg, 109% crude). ^{1}H-NMR (500MHz, $CDCl_3$) δ 4.02 (m, 1H), 2.51-2.47 (dd, *J* = 14.8, 3.2 Hz, 1H), 2.06-1.96 (m, 3H), 1.84-1.81 (m, 2H), 1.70-1.66 (m, 1H), 1.65-1.58 (m, 1H), 1.39-1.37 (m, 3H), 1.31-1.28 (m, 2H),

1.15-1.11 (m, 2H), 1.03-1.02 (d, *J* = 6.4 Hz, 3H), 0.97 (s, 3H), 0.91 (s, 9H), 0.03 (s, 3H), 0.02 (s, 3H).

Figure 27: ^{1}H Spectra of O-silylated C,D ring acid:

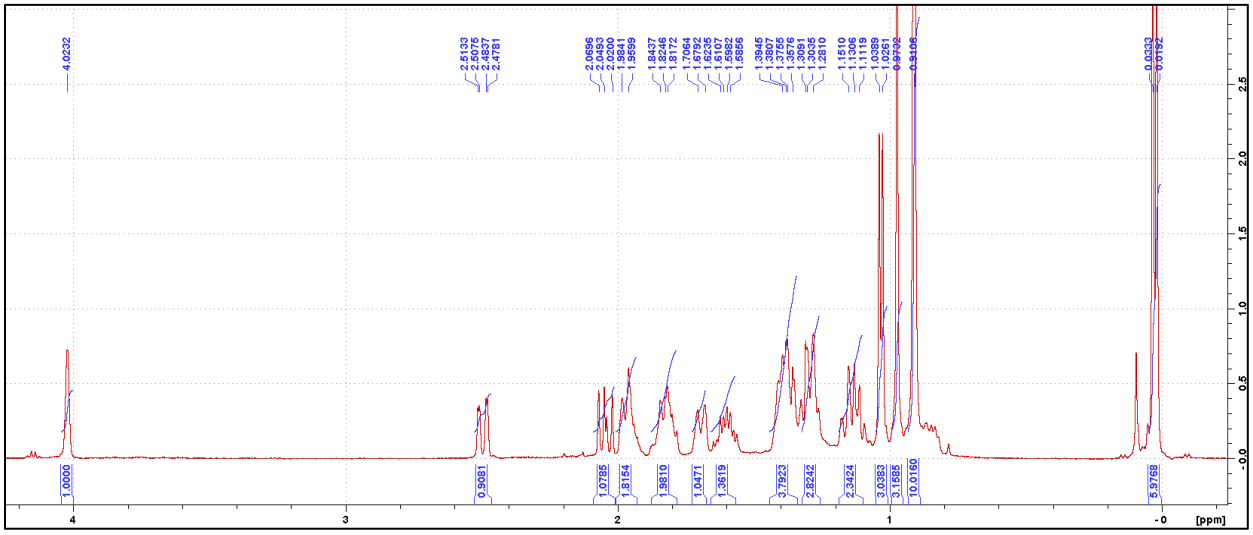

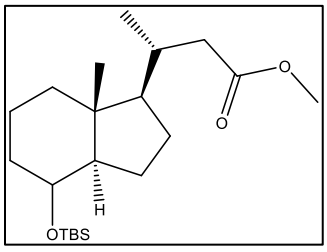

O-silylated C,D-ring methyl ester: O-silylated C,D-ring acid (145.5 mg, 0.41 mmol) was dissolved in a mixture of toluene (2.5 mL) and methanol (1.5 mL). Trimethylsilyl diazomethane (2M in diethyl ether, 300 µL, 0.60 mmol) was added dropwise and the reaction was stirred at RT for 1.5 h until the reaction was deemed complete by TLC. The reaction was then quenched with acetic acid (100 µL) and the mixture was then concentrated to dryness. The crude material was purified via column chromatography (EtOAc:Hex 3:97). The product was obtained as a clear oil (117 mg, 77.4%). ^{1}H-NMR (500MHz, $CDCl_3$) δ 4.02-4.01 (m, 1H), 3.67 (s, 3H), 2.46-2.43 (dd, *J* = 14.2, 3.1 Hz, 1H), 2.03-1.89 (m, 3H), 1.87-1.74 (m, 2H), 1.71-1.65 (m, 1H), 1.64-1.54 (m, 1H), 1.49-1.33 (m, 3H), 1.30-1.24 (m, 2H), 1.17-1.06 (m, 2H), 0.98-0.95 (m, 6H), 0.90 (s, 9H), 0.03 (s, 3H), 0.01 (s, 3H).

Figure 28: ^{1}H Spectra of O-silylated C,D ring methyl ester:

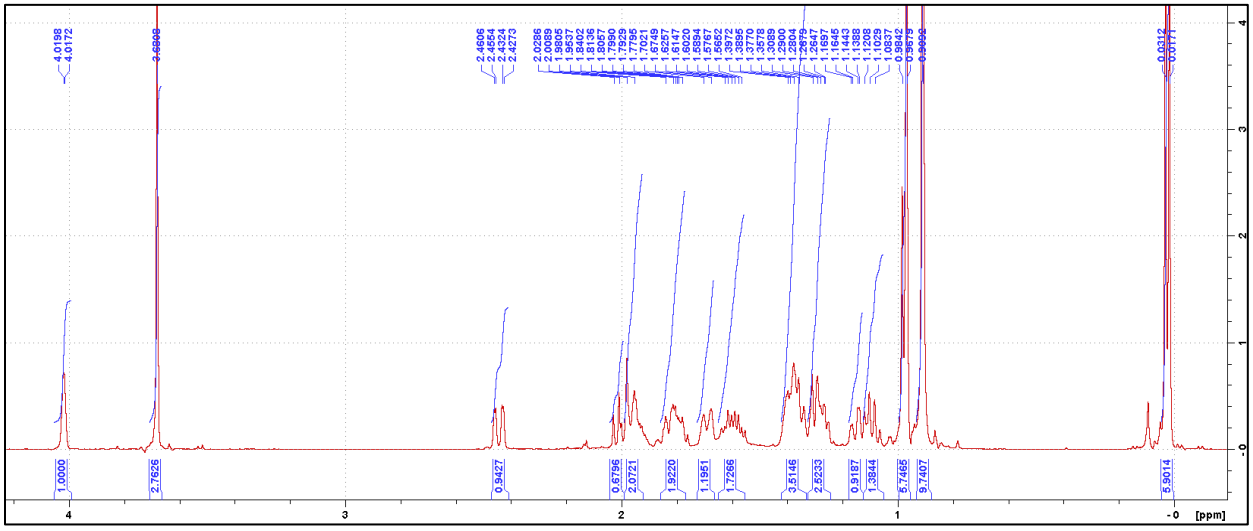

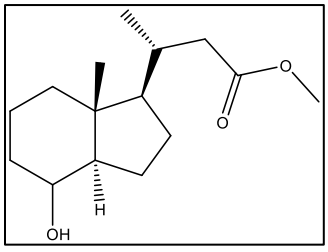

Methyl ester C,D-ring alcohol: O-silylated C,D-ring ester (180.1 mg, 0.449 mmol) was dissolved in anhydrous DCM (6 mL) and the solution was cooled to 0 °C. Trifluoroacetic acid (560 µL, 7.3 mmol) was added dropwise and the reaction was stirred at 0 °C for 1.5 h until it was deemed complete via TLC. The reaction was then concentrated and the crude material was purified via column chromatography (EtOAc:Hex 1:4). The product was obtained as a clear oil (113 mg, 91.0%). ^{1}H-NMR (500MHz, $CDCl_3$) δ 4.12-4.11 (m, 1H), 3.68 (s, 3H), 2.45-2.41 (dd, *J* = 14.2, 3.2 Hz, 1H), 2.05-1.97 (m, 2H), 1.96-1.89 (m, 1H), 1.87-1.78 (m, 3H), 1.65-1.55 (m, 1H), 1.53-1.40 (m, 3H), 1.40-1.29 (m, 3H), 1.21-1.09 (m, 2H), 0.98-0.97 (m, 6H).

Figure 29: ^{1}H Spectra of methyl ester C,D ring alcohol:

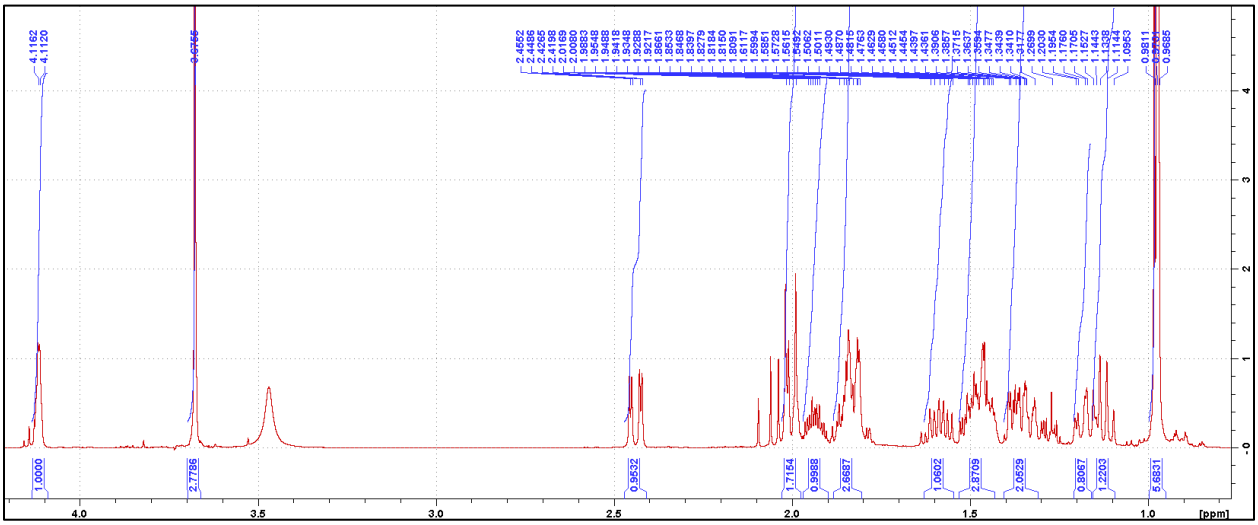

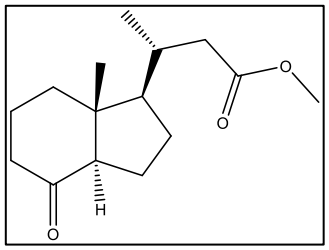

Methyl ester C,D-ring ketone: C,D-ring alcohol (152.5 mg, 0.60 mmol) was dissolved in anhydrous DCM (12 mL) before the addition of freshly ground PDC (450 mg, 1.2 mmol). The reaction was stirred at RT for 2 h before being diluted with MTBE (12 mL) and filtered over celite. The solid collected on the filter was slurried in DCM twice with vigorous stirring before being filtered again to ensure that all of the desired product had dissolved. The filtrated were combined and concentrated. The crude product was purified via column chromatography (EtOAc:Hex 1:4). The product was obtained as a white solid (133 mg, 87.9%). ^{1}H-NMR (500MHz, $CDCl_3$) δ 3.69 (s, 3H), 2.50-2.46 (m, 2H), 2.27-2.14 (m, 2H), 2.09-2.04 (m, 1H), 2.04-1.94 (m, 2H), 1.93-1.78 (m, 3H), 1.76-1.66 (m, 1H), 1.60-1.42 (m, 3H), 1.36-1.26 (m, 1H), 1.05-1.04 (d, *J* = 6.5, 3H), 0.70 (s, 3H).

Figure 30: ^{1}H Spectra of methyl ester C,D ring ketone:

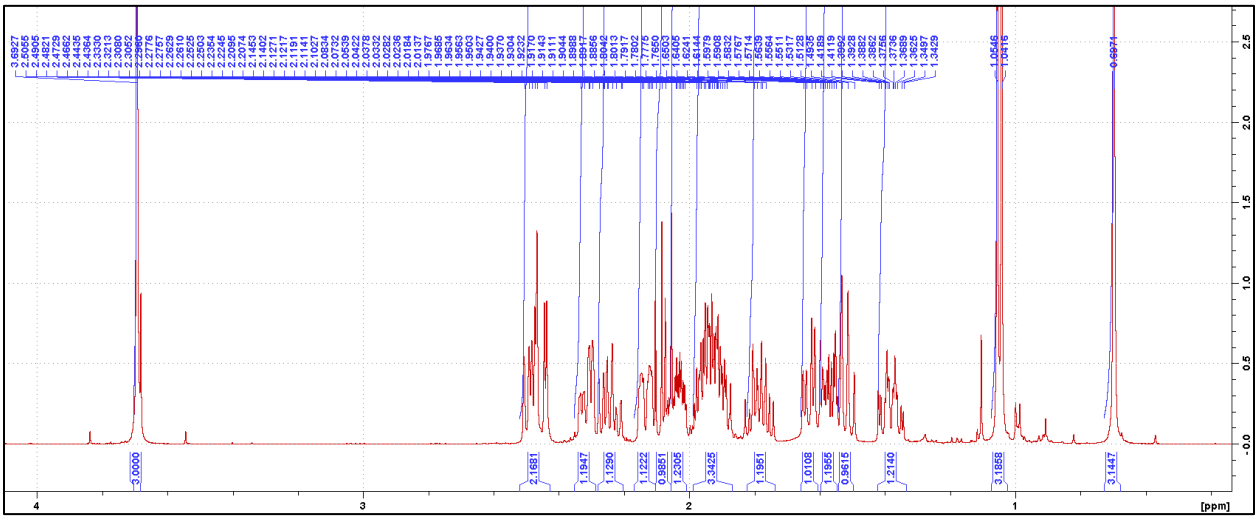

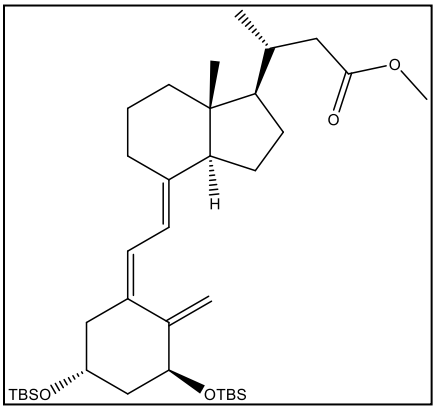

O-Bis-silylated calcitroic acid methyl ester: CTA A-ring phosphine oxide (460 mg, 0.79 mmol), which had been drying overnight in anhydrous THF (3 mL) with 3Å molecular sieves, was added to an oven dried and nitrogen purged flask before being cooled to -78 °C. n-butyllithium (1.6M in hexanes, 390 µL, 0.63 mmol) was added dropwise at which point the reaction turned a deep red color. The solution was stirred at -78 °C before being raised out of the ice bath for approximately 5 min at which point the red color deepened signaling the deprotonation was complete. The mixture was then returned to the ice bath before C,D-ring ketone (96.5 mg, 0.38 mmol) was added dropwise in anhydrous THF (5 mL) via dropper funnel. The reaction was then stirred for 5 h at -78 °C before being allowed to warm up to RT. The reaction was then quenched with H_2O (10 mL) and diluted with MTBE (20 mL). The aqueous layer was then extracted an additional two times with MTBE before the organic fractions were combined and

washed with brine. The organic layer was dried with anhydrous $MgSO_4$ and the organic layer was concentrated. The crude product was purified via column chromatography (EtOAc:Hex 5:95). The product was obtained as a viscous white oil (129 mg, 54.8%). ^{1}H-NMR (500MHz, $CDCl_3$) δ 6.26-6.24 (d, *J* = 11.2 Hz, 1H), 6.05-6.02 (d, *J* = 11.2 Hz, 1H), 5.20-5.19 (m, 1H), 4.88-4.87 (m, 1H), 4.70-4.37 (m, 1H), 4.21-4.20 (m, 1H), 3.67 (s, 3H), 2.86-2.80 (m, 1H), 2.48-2.40 (m, 2H), 2.22-2.20 (dd, *J* = 12.6, 7.6 Hz, 1H), 2.05-1.96 (m, 3H), 1.95-1.81 (m, 3H), 1.80-1.73 (m, 1H), 1.72-1.61 (m, 2H), 1.60-1.46 (m, 3H), 1.36-1.26 (m, 3H), 1.01-1.00 (d, *J* = 6.3 Hz, 3H), 0.89 (s, 18H), 0.58 (s, 3H), 0.08-0.07 (m, 12H).

Figure 31: ^{1}H Spectra of O-Bis-silylated calcitroic acid methyl ester:

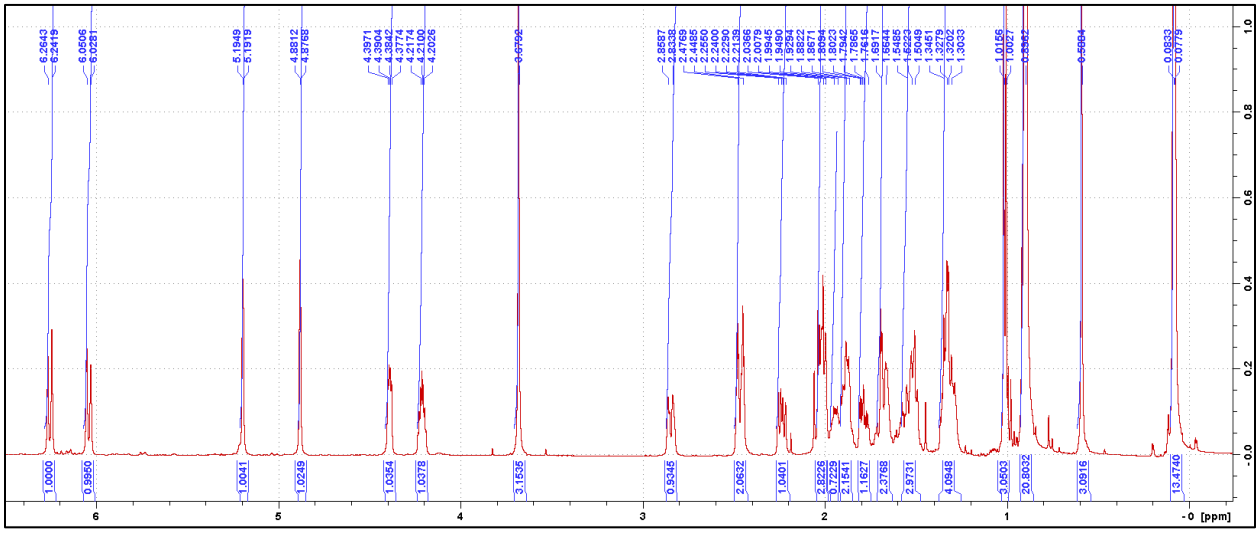

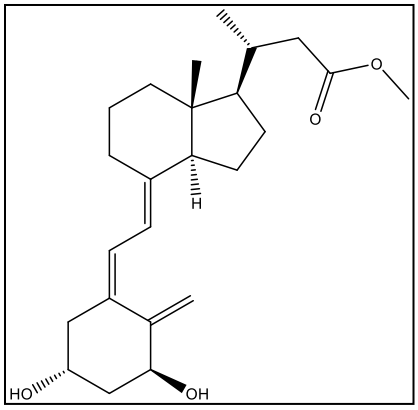

Calcitroic acid methyl ester: O-Bis-silylated CTA methyl ester (151.2 mg, 0.25 mmol) was dissolved in dry THF (5 mL) before tetrabutylammonium fluoride (1M in THF, 3.5 mL, 3.6 mmol) was added dropwise. The reaction was allowed to stir at RT overnight before being quenched with saturated aqueous NH_4Cl (5 mL). The mixture was extracted with EtOAc (3x20 mL) and the organic fractions were combined before being washed with brine (50 mL). The organic layer was dried with anhydrous $MgSO_4$ before being concentrated to dryness. The crude material was purified by column chromatography (EtOAc:Hex 7:3). The product was obtained as a yellow tinted oil (68 mg, 71.4%). ^{1}H-NMR (500MHz, $CDCl_3$) δ 6.37-6.36 (d, *J* = 11.0 Hz, 1H), 6.03-6.01 (d, *J* = 11.0 Hz, 1H), 5.32 (s, 1H), 4.99 (s, 1H), 4.44-4.41 (dd, *J* = 7.6, 4.5 Hz, 1H), 4.23-4.21 (m, 1H), 3.66 (s, 3H), 2.84-2.82 (dd, *J* = 12.6, 4.3 Hz, 1H), 2.57-2.55 (dd, *J* = 13.7, 3.1 Hz, 1H), 2.43-2.42 (dd, *J* = 14.5, 3.5 Hz, 1H), 2.30-2.29 (dd, *J* = 14.0, 8.0 Hz, 1H), 2.03-1.96 (m, 4H), 1.95-1.81 (m, 4H), 1.72-1.63 (m, 2H), 1.59-1.45 (m, 4H), 1.34-1.27 (m, 3H), 1.00-0.99 (d, *J* = 6.4 Hz, 3H), 0.58 (s, 3H).

Figure 32: ^{1}H Spectra of calcitroic acid methyl ester:

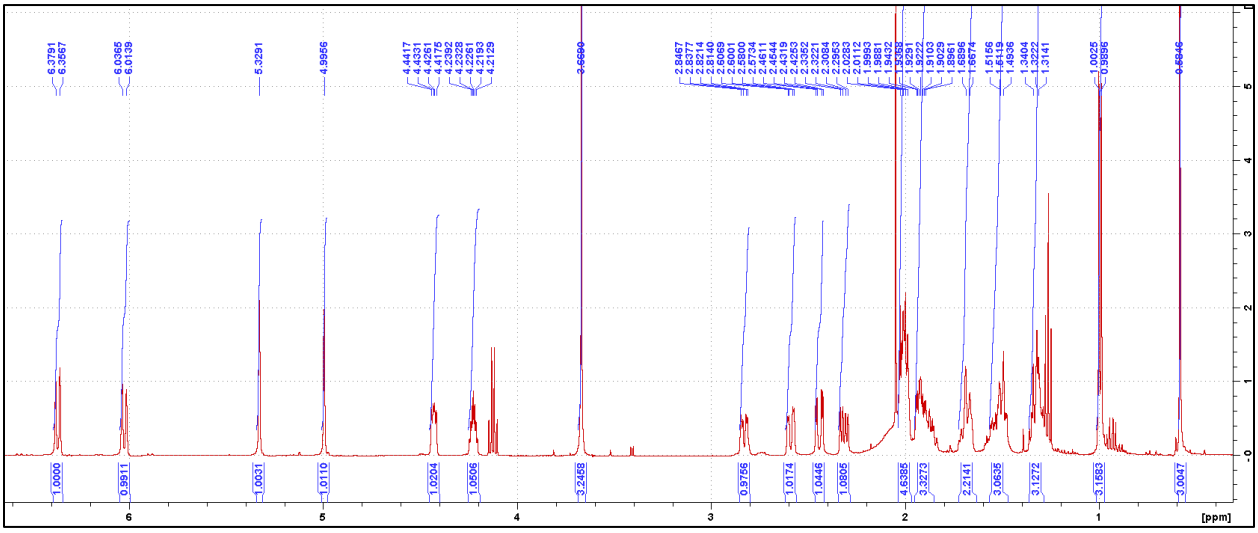

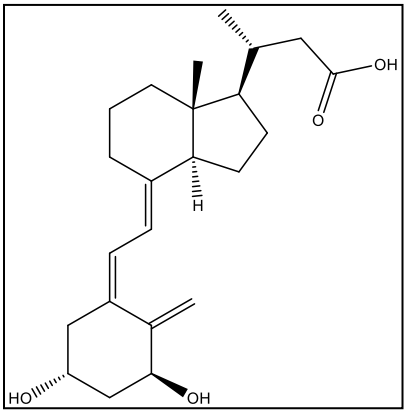

Calcitroic acid: CTA methyl ester (80.4 mg, 0.21 mmol) was dissolved in a solution of 10% NaOH in 9:1 MeOH:H_2O (5 mL). The reaction was allowed to stir at RT for 2 h at which point all of the starting material had dropped to the baseline via TLC. The reaction was neutralized with 3M HCl until a pH of ~7 was reached. The MeOH was evaporated, and the mixture was diluted with H_2O (15 mL). The mixture was then acidified with 3M HCl to a pH of 1 before being extracted with EtOAc (3x20 mL). The organic fractions were combined before being washed with brine (50 mL) and dried with anhydrous $MgSO_4$. The organic layer was concentrated, and the crude material was purified via column chromatography (EtOAc). The product was obtained as a yellow solid (57 mg, 74.2%). ^{1}H-NMR (500MHz, $CDCl_3$) δ 6.40-6.38 (d, *J* = 11.2 Hz, 1H), 6.05-6.03 (d, *J* = 11.2 Hz, 1H), 5.34 (s, 1H), 5.02 (s, 1H), 4.47-4.44 (dd, *J* = 4.2, 7.6, 1H), 4.27-4.24 (m, 1H), 2.86-2.84 (dd, *J* = 13.6, 4.6 Hz, 1H), 2.62-2.60 (dd, *J* = 13.5, 3.2 Hz, 1H), 2.50-2.49 (dd, *J* = 15.0, 3.5

Hz, 1H), 2.34-2.32 (dd, *J* = 13.0, 6.5 Hz, 1H), 2.12-1.98 (m, 4H), 1.97-1.86 (m, 4H), 1.76-1.67 (m, 3H), 1.61-1.48 (m, 3H), 1.41-1.30 (m, 3H), 1.07-1.05 (d, *J* = 6.5 Hz, 3H), 0.60 (s, 3H).

Figure 33: ^{1}H Spectra of calcitroic acid:

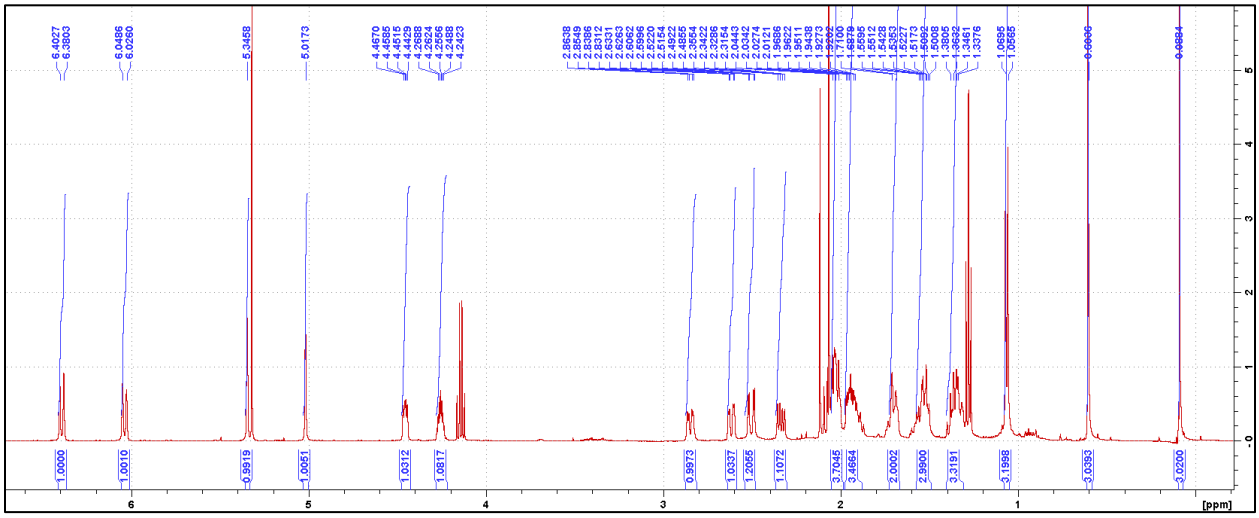

1.8 Conclusion

In summary, calcitroic acid represents a ligand of interest for the vitamin D receptor due to its potential to control the amount of bile acids in the intestine. Due to the interest in CTA but lack of commercial availability at a cheap price, CTA had to be synthesized. Previous synthetic routes resulted in extremely low yields, however, following the synthetic route outlined above, we have been able to produce a significant amount of CTA. The low yield from the current synthetic route can mainly be attributed to the first step, being the ozonolysis reaction. It may be possible to improve this yield with more work looking into the isolation of the product post reaction as described above. Yields and overall reaction scalability may also be possible with increased purification methods throughout the synthesis. Column chromatography was utilized in nearly every step, and while recrystallization or other purification techniques may not be possible due to a number of products being obtained as oils. It may be possible to develop recrystallization techniques for some products including calcitroic acid itself. Overall, the current synthetic route

for CTA is sufficient in producing low gram quantities of product, however, more work would be needed to develop scalable procedures. CTA will likely be used for future irritable bowel disease (IBD) studies as well as others to determine its efficacy as a potential anti-inflammatory.

CHAPTER 2: SYNTHESIS OF NEW IMIDAZODIAZEPINES TO TARGET NON-CENTRAL NERVOUS SYSTEM GABA(A) RECEPTORS

2.1 Discovery of γ-aminobutuyric acid (GABA)

In the 1800s, γ-aminobutuyric acid (GABA) was first discovered in plants and was initially associated with the Kreb's Cycle.[139] However, it wasn't until the 1950s that researchers made the groundbreaking observation that GABA was present in the brain in exceptionally high quantities,[140] surpassing the levels of any other neurotransmitter by up to 1000-fold.[141] This remarkable revelation was credited to Eugene Roberts and Sam Frankel, who employed straightforward paper chromatograms and ninhydrin stains to identify GABA as the predominant amine in the brain.

The true nature of GABA as an inhibitory neurotransmitter emerged a few years later. Initially referred to as "Substance I,"[142] a compound was identified that had the ability to inhibit crayfish neurons, ultimately recognized as GABA.[143] The initial skepticism surrounding GABA's neurotransmitter status stemmed from its lack of rapid inactivation,[144] a characteristic typically associated with neurotransmitters.[145] However, subsequent investigations uncovered that rapid intracellular uptake was responsible for its inactivation mechanism. Additionally, it was found that GABA played a crucial role in hyperpolarizing neocortical neurons. These findings solidified GABA's classification as an inhibitory neurotransmitter.[146]

2.2 Formation of GABA

GABA synthesis occurs via the GABA shunt pathway as seen in Figure 34, commencing with the transformation of succinic semialdehyde into α-ketoglutarate within the Krebs cycle. Initially, the Krebs cycle-associated GABA production led to hypotheses about GABA's involvement in metabolism.[139] Subsequently, GABA-transaminase (GABA-T) converts α-ketoglutarate into glutamate within the mitochondria. In presynaptic terminals, glutamate decarboxylase (GAD) facilitates the conversion of glutamate into GABA,[2] with two identified forms, GAD_{65} and GAD_{67}. GAD_{67} continuously generates GABA, while GAD_{65} becomes active when additional GABA is required for neurotransmission.[147]

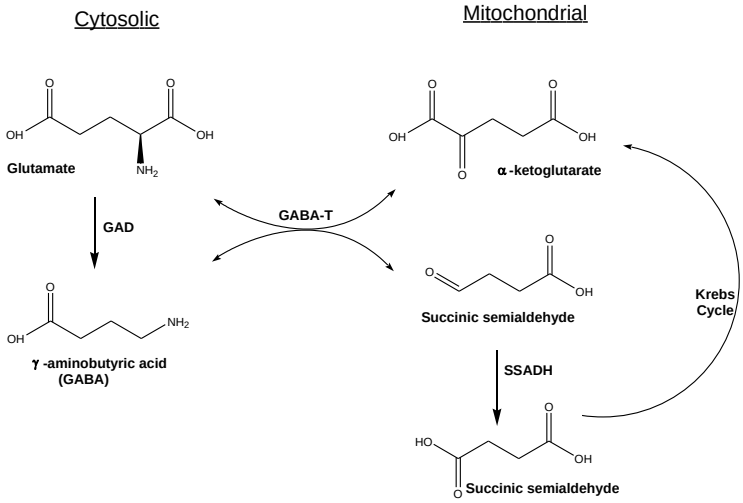

Figure 34. GABA Shunt GABA-T: GABA α-oxoglutarate transaminase, GAD: glutamic acid decarboxylase, SSADH: succinic semialdehyde dehydrogenase[2]

Upon depolarization of presynaptic neurons, GABA is released into the synaptic cleft. It then binds to receptors on the postsynaptic cell surface of recipient cells before being taken up by the GABA transporter (GAT) to prevent overspill to neighboring synapses.[148] This process occurs against a concentration gradient, as the internal GABA concentration is approximately 200 times higher than the external concentration. Subsequently, GABA is either reused by neurons or

converted back to succinic semialdehyde by GABA-T, reentering the Krebs cycle. When glial cells absorb GABA, it is converted through the Krebs cycle into glutamine, which can be utilized for GABA generation.[2]

2.3 Discovery of $GABA_AR$

It took a span of three decades to pinpoint the receptors responsible for GABA. The initial hint at their structure emerged in 1990.[149] In the interim, research unveiled other neurotransmitter receptors, such as nicotinic acetylcholine, glycine, and 5-hydroxytryptamine ($5HT_3$) receptors, which displayed notable similarities in their sequence, particularly within the ligand binding regions,[150] when compared to $GABA_AR$. Collectively, this assembly of receptors was eventually categorized as the Cys loop ligand-gated ion channel superfamily.[151]

Over time, functional and mutagenesis studies provided educated guesses about the possible binding sites for GABA and other modulators. However, these remained unverified until the crystal structure of a $GABA_AR$ was finally determined.[152] This breakthrough occurred in 2018 when high-resolution cryo-electron microscopy unveiled the structure of a heteropentameric $GABA_AR$, ultimately confirming the precise binding locations for GABA and flumazenil, an allosteric modulator.[3]

2.4 Structure of $GABA_AR$

The $GABA_AR$, a receptor anchored in the cell membrane,[153] is a complex composed of five different subunits from a pool of nineteen potential subunits ($\alpha_{1–6}$, $\beta_{1–3}$, $\gamma_{1–3}$, δ, ε, π, θ, ρ_{1-3}).[154]

Analysis through cryo-electron microscopy has unveiled that each subunit shares a similar structural arrangement, featuring an extracellular domain bearing the distinctive cys loop and ten β-strands configured in a β-sandwich motif. This is followed by four α-helices, which collectively form the ion channel embedded within the membrane.[3] The crystal structure of the $GABA_AR$ is shown in Figure 35.

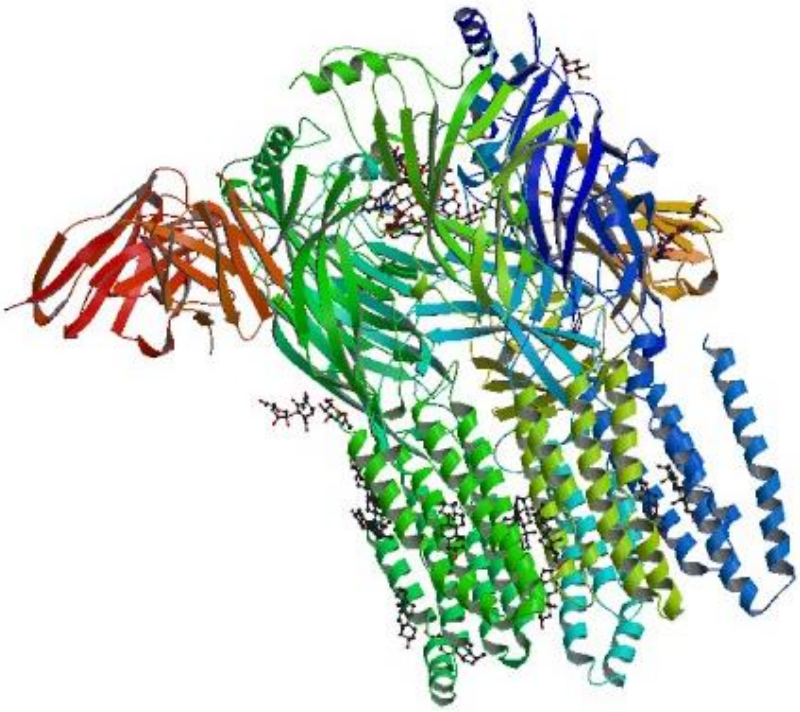

Figure 35. Cryo-electron microscopy structure of $GABA_AR$ composed of α_1, β_2, and γ_2 subunits with GABA and Flumazenil bound as determined by Zhu et al.[3] In red and yellow are antibodies used for isolation of the protein. Accessed from the Protein Data Bank (PDB: 6D6U)

Typically, classical $GABA_ARs$ are comprised of two α, two β, and one tertiary subunit (either γ or δ). The published cryo-electron microscopy structure is the $\alpha_1\beta_2\gamma_2$ receptor, which is one of the most prevalent types found in the brain. The use of monoclonal antibodies allowed the

isolation of this receptor, specifically targeting the extracellular region of the α_1 subunits, denoted in red and yellow.

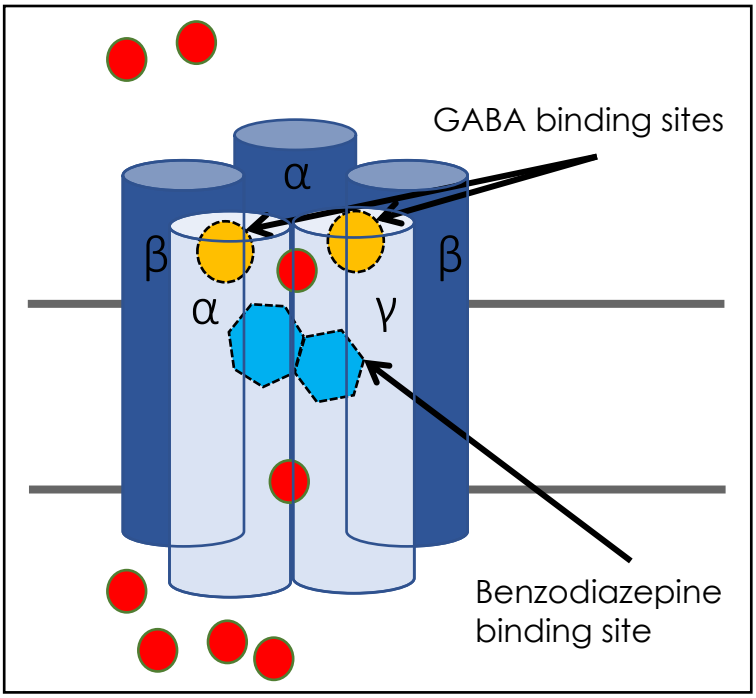

Figure 36. Structure of the $GABA_AR$ A typical $GABA_AR$ contains two α subunits, two β subunits, and one γ subunit, forming two extracellular binding sites between α and β subunits for the endogenous ligand GABA and one extracellular binding site between α and γ subunits for benzodiazepines. Chloride ions are shown in red.

$GABA_ARs$ have a multitude of binding sites, attracting various molecules including GABA itself, pharmaceutical compounds, and substances of abuse. In this discussion, we will focus on three primary binding sites: the GABA site, the chloride channel, and the benzodiazepine site.[2] It's worth noting that there are additional allosteric modulator binding sites within the receptor, such as those for neurosteroids, barbiturates, and ethanol.[155]

Within the receptor, the interfaces between α and β subunits form two binding sites for the endogenous neurotransmitter γ-aminobutyric acid (GABA). The structural analysis confirmed that GABA binds between the α1 and β2 subunits of the isolated receptor.[3] This binding is stabilized by interactions between GABA and three tyrosine residues and one phenylalanine, forming what is referred to as an 'aromatic glove.' Additionally, an interaction between the carboxylate group of

GABA and a threonine group contributes further to the stability of the binding. The benzodiazepine binding site of the $GABA_AR$ is rich in aromatic residues, including one phenylalanine, two tyrosine, two serine, and one threonine residue of the alpha subunit, and one phenylalanine, one tyrosine, and one threonine reside of the gamma subunit. The nature of this binding site allows for the strategic binding of a variety of benzodiazepines to effectively modulate the receptor.

2.5 The Benzodiazepine Binding Site

Benzodiazepines were initially discovered through the innovative manipulation of benzheptoxdiazines, which were originally studied in the quest for new dye materials.[156] However, when these compounds failed to serve their original purpose, they gained interest as potential tranquilizers due to their uncharted territory, easy accessibility, adaptability for chemical modifications, intriguing chemical properties, and a vague resemblance to potential biological activity.[156] After years of experimentation, one particular compound (along with its salt form) emerged from obscurity during a activity analysis and were subsequently subjected to biological testing. These tests confirmed their superior muscle relaxation and anticonvulsant properties compared to chlorpromazine, the prevailing standard at the time.[156]

This compound, to be called Librium,[156] which was eventually approved by the FDA, marked the inception of benzodiazepines in the market. Three years later, diazepam made its market debut under the trade name Valium.[156] This milestone spurred extensive research into benzodiazepines, greatly enhancing our understanding of their structure-activity relationships. This surge in research led to a multitude of compounds flooding the market, including clonazepam in 1975 and lorazepam in 1977. Remarkably, in 2018, alprazolam and clonazepam ranked as the 23rd and 38th most prescribed drugs, respectively.[157]

More recently, scientists have developed knock-in mice with specific mutations in each α subunit,[4] enabling pharmacological and behavioral studies that linked each α subtype to distinct physiological effects (see Figure 37). Targeting α_2 or α_3 subunit-containing $GABA_AR$ has proven effective in achieving clinically relevant effects such as anxiety reduction and muscle relaxation, while avoiding the α_1 subunit-containing $GABA_AR$ can significantly mitigate unwanted side effects like amnesia or addiction.[4]

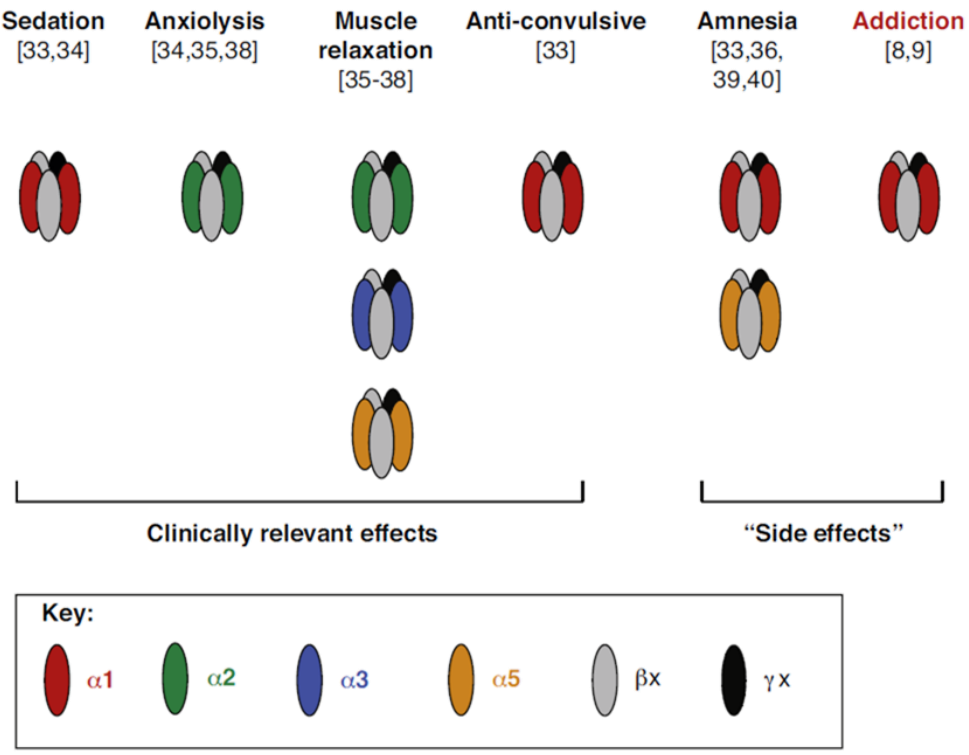

Figure 37. Subtype Specific Benzodiazepine Pharmacology Experiments with knock-in mice have allowed researchers to correlate $GABA_AR$ subunits with pharmacological effects.[4]

In the pursuit of subtype-selective benzodiazepines, Professor James Cook devised a pharmacophore model to guide synthesis towards compounds that selectively bind to specific α subunit-containing $GABA_AR$.[158] This model has been instrumental in producing subtype-selective imidazodiazepines with applications spanning from central nervous system disorders like depression,[159] schizophrenia,[160] and neuropathic pain[161] to pulmonary conditions like asthma.[162]

Flumazenil (see Figure 38), is an imidazodiazepine, functions as an antagonist for $\alpha_{1\text{-}3}$ and α_5-containing $GABA_AR$. Clinically, it is employed to reverse the effects of benzodiazepines, such as diazepam-induced sedation, by competing for the benzodiazepine binding site.[163] Interestingly, flumazenil also acts as a weak partial agonist for $\alpha_{4/6}$-containing receptors.[164]

An analog of flumazenil, known as Ro15-4513 (see figure 38), was initially identified as a behavioral antagonist to alcohol. It reverses ethanol-enhanced $GABA_AR$ currents through $\alpha_{4/6}$ and δ-containing $GABA_AR$.[165] However, flumazenil is incapable of blocking the effects of ethanol. It is believed that the extended nitrogen tail of Ro15-4513 obstructs the ethanol binding site on the δ subunit, a feat that the analogous fluorine on flumazenil cannot achieve.[166]

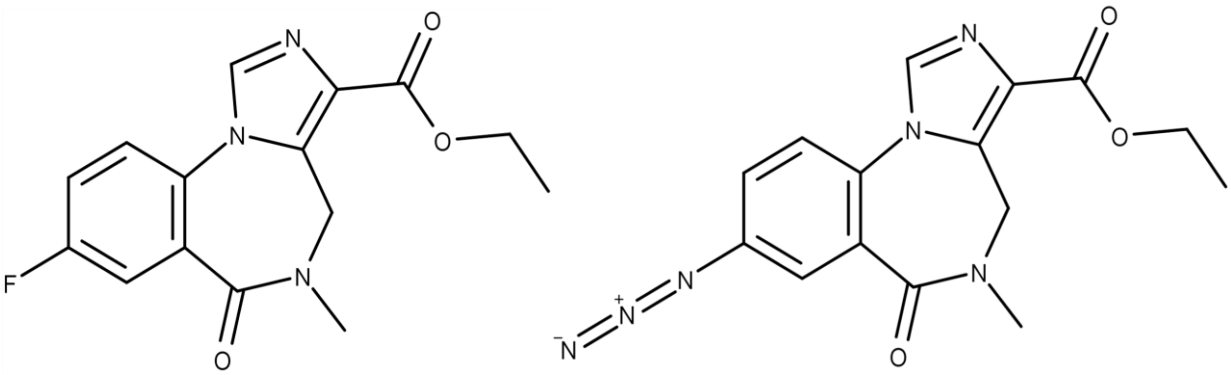

Figure 38: Structure of Flumazenil (left) and Ro15-4513 (right).

2.6 Distribution of $GABA_AR$

$GABA_AR$ receptors exhibit high expression within the brain, predominantly facilitating inhibitory neurotransmission. However, $GABA_AR$ receptors are increasingly being identified in peripheral tissues, including the lungs, endocrine glands, muscle tissues, lymphoid organs, and bone marrow reference.[167] These receptors gather valuable data pertaining to the human proteome, offering insights into protein expression across different tissues, cells, pathologies, and various cellular effects.[168] This initiative amalgamates data from three separate projects: the Human

Protein Atlas, Genotype-Tissue Expression, and the FANTOM5 project. It standardizes the expression data obtained from each project and compiles it into a unified representation, denoted as unitless normalized RNA transcription expression.

The distribution of alpha subunits of $GABA_AR$ receptors exhibits notable variations among different tissue types. Within the brain, the expression of alpha subunits differs significantly by region reference.[169] For instance, the cerebral cortex demonstrates substantially high expression levels of α_{1-3} and α_5 subunits, nearly three times more pronounced than α_4 and fifty times greater than α6 expression. Conversely, α_6 expression predominates in the cerebellum, where it attains a normalized concentration tenfold higher than any other alpha subunit.

In contrast to the brain, where normalized alpha subunit expression can reach as high as 96.4 units, peripheral tissues typically exhibit much lower $GABA_AR$ receptor expression, usually hovering around normalized levels of approximately 1. Various cell types within these peripheral tissues present distinctive $GABA_AR$ expression profiles.

The discovery of $GABA_AR$ expression in extracerebral tissues highlights their potential as innovative and appealing targets for novel pharmaceutical interventions. The well-established class of benzodiazepines in pharmacology can now be customized for these new targets and diverse diseases, all while preserving the safety and effectiveness of proven medications. The research presented here aims to provide support for the utilization of imidazodiazepines in targeting non-neuronal cell types in conditions like asthma and neuropathic pain.

2.7 Design, Synthesis, and Biological Evaluation of Novel Spiro Imidazobenzodiazepines to Identify Improved Inhaled Bronchodilators

2.7.1 Introduction

The CDC reported in 2020 that more than 25 million people in the United States have some form of asthma.[170] Asthma is one of the most common chronic lung inflammatory diseases affecting children and young adults[171] and a very heterogeneous disease with several endotypes and degrees of severity.[172] Asthma symptoms include shortness of breath, wheezing, chest tightness, and severe cough, and can result in severe exacerbations and in some cases can lead to death.[171] Treatments to control asthma symptoms include inhaled β_2- adrenoreceptor agonists, corticosteroids, muscarinic receptor antagonists, orally available leukotriene receptor antagonists, and injectable biologics.[173] Novel therapeutic approaches are needed to improve safety and efficacy for patients with uncontrolled asthma. One new approach is based on pharmacological targeting the gamma-aminobutyric acid receptors ($GABA_AR$s),[174] which include $GABA_AR$ subtypes with α_4 and α_5 subunits present on airway smooth muscle[175] and α_2 and $\alpha3$ subunits present on inflammatory cells.[176] We have investigated imidazodiazepines, including compound 68 with strong preference to $GABA_AR$ subtypes with a α_5 subunit (Figure 39), which relaxed constricted human airway smooth muscle and reduced airway hyperresponsiveness (AHR) in several murine asthma models.[177,178] To avoid adverse central nervous system (CNS) effects, we have engineered pharmacokinetic properties of these compounds to prevent blood-brain barrier transit.[179, 180] MIDD0301 (Figure 39) is a more potent analog of compound 68 and is currently developed for asthma symptom control. MIDD0301 was shown to attenuate AHR and reduced lung inflammation in rodents when administered orally[179] or nebulized.[181]

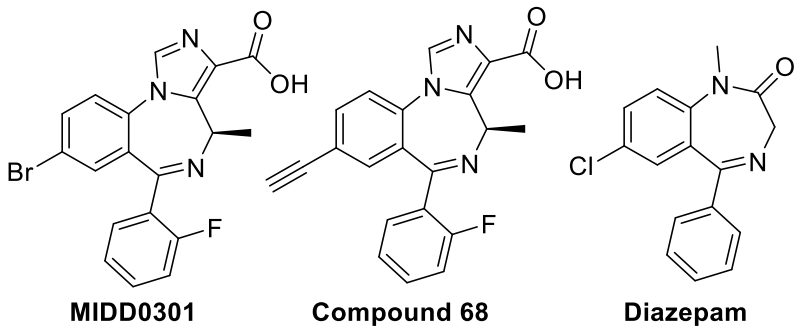

Figure 39: Structure of positive GABA(A) receptor modulators MIDD0301 (also known as PI301), compound 68, and diazepam.

MIDD0301 acts by binding to several $GABA_AR$ subtypes expressed on airway smooth muscle[182] and inflammatory cells.[183] Relaxation of *ex vivo* contracted human airway smooth muscle was shown to occur within minutes following MIDD0301 treatment.[184] In rodents, MIDD0301 did not cause any adverse effects or suppress systemic T-dependent antibody responses following repeated high dose exposure.[185] Herein, we describe the improvements to the phase 2 metabolic stability of MIDD0301,[186,187] by designing, synthesizing, and evaluating analogs DAW-III-10, 30, 40, 50, 60, 70, 31, 32, 35 with a sterically crowded carboxylic acid function to reduce the rate of glucuronidation. In addition, substituents in the 8 position were investigated, which have been shown to increase $GABA_AR$ affinity. Additional compounds DAW-III-20, 80, 51, 52, 53, 55 were also synthesized, however, due to the lack of $GABA_AR$ binding or binding to other receptors, little biological testing was conducted for these compounds.

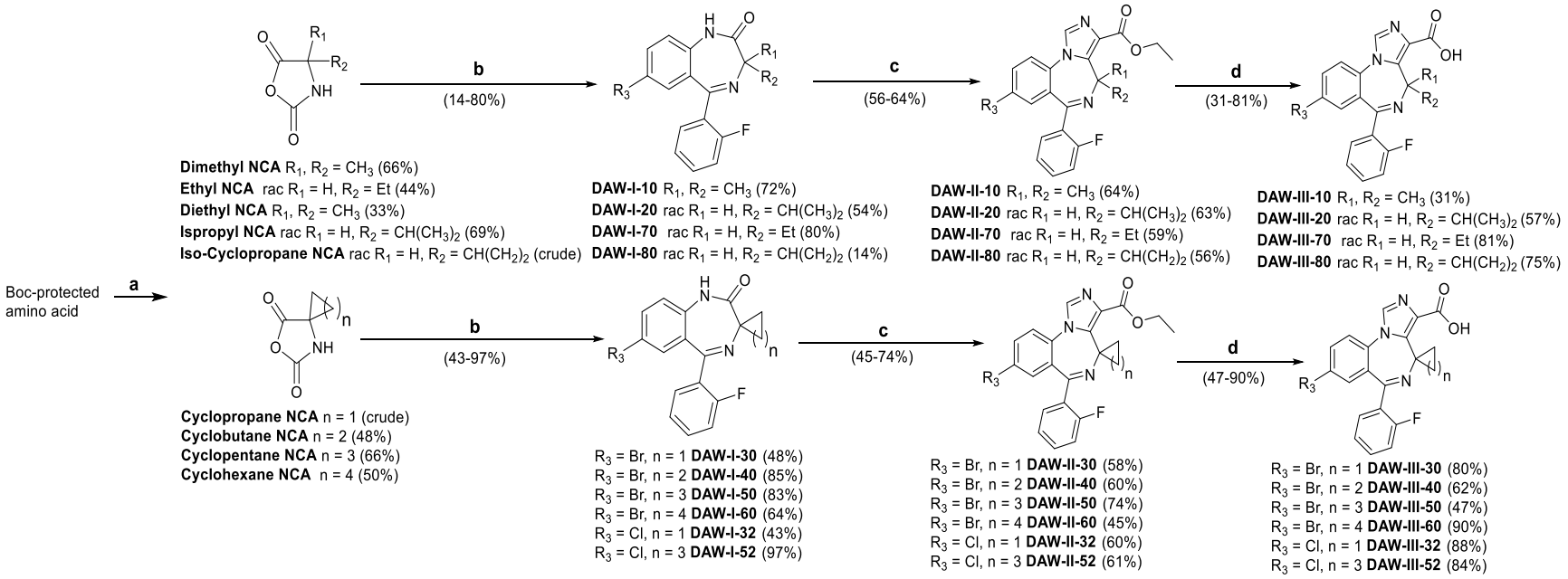

Scheme 5: Imidazobenzodiazepine standard synthetic route: [a] Reagents and conditions: (a) triphosgene 0.4 equiv, EtOAc, triethylamine 1.1 equiv, 70 °C, 20 h. (b) (1) 2-Amino-5-bromo-2′- fluorobenzophenone or 2-amino-5-chloro-2′-fluorobenzophenone 0.67 equiv, trifluoroacetic acid 2 equiv, toluene 50 °C, 24 h; (2) triethylamine 2.1 equiv, 100 °C, 24 h. (c) (1) t-BuOK 1.3 equiv, THF, −20 °C, 1 h, followed by ClPO(OEt)2 1.4 equiv, 2 h; (2) CNCH2CO2Et 1.3 equiv, −20 °C, 15 min followed by t-BuOK 1.3 equiv in THF 2 h, RT. (d) THF/H2O (43:1), NaOH 30 equiv, 80 °C, 24 h; (2) acetic acid until pH = 5, 50 °C, 18 h.

2.7.2 Results and Discussion

2.7.3 Chemical Synthesis

To obtain new compounds DAW-III-10, 20, 30, 40, 50, 60, 70, 80, 31, 32, 33, 35, 51, 52, 53, 55 a previously reported synthesis was followed.[188] Therefore, BOC protected amino acids were converted into amino acid N-carboxyanhydrides (NCAs) using triphosgene and triethylamine (Scheme 5).[189] Due to the high reactivity of spiro NCAs, coupling reactions with 2-amino-5-bromo-2′-fluorobenzophenone and 2-amino-5-chloro-2′-fluorobenzophenone were achieved in good yields. Reactions of disubstituted BOC protected amino acids and 2-amino-5-bromo-2′-fluorobenzophenone using peptide coupling reagent N,N′-dicyclohexylcarbodiimide (DCC) resulted in very low conversion due to the weak nucleophilic character of the aniline function and increased steric hindrance of the unnatural amino acids. Various other coupling agents were attempted such as HBTU, PyBOP, and BTFFH to obtain a better conversion, but with limited success. The conversion into the corresponding acid chlorides and subsequent coupling with 2-amino-5-bromo-2′- fluorobenzophenone in the presence of triethylamine failed.

NCAs (DAW-NCA-10, 20, 30, 40, 50, 60, 70, 80, 90) were obtained in yields ranging from 33 to 69%. Recrystallization with dichloromethane/hexanes mixtures afforded pure material except for the spiro-cyclopropane NCA (DAW-NCA-30) and cyclopropane substituted NCA (DAW-NCA-80). Attempts to purify DAW-NCA-30 with a water wash to remove residual triethylamine were successful and resulted in a solid material, albeit in low yield. We are currently optimizing this process but used crude material for the synthesis of DAW-I-30. NCAs have proven to be moderately stable in water despite their anhydride functionality.[190] Furthermore, NCAs are

stable during flash chromatography using silica gel. All NCAs synthesized were coupled successfully with 2-amino-5-bromo-2′-fluorobenzophenone or 2-amino-5-chloro-2′-fluorobenzophenone in the presence of trifluoroacetic acid, followed by addition of triethylamine to generate the corresponding benzodiazepines. Compounds DAW-I-10, 20, 30, 40, 50, 60, 70, 80, 32, 52 were synthesized in yields ranging from 14 to 97%. The diethyl NCA (DAW-NCA-90) was synthesized successfully, but subsequent coupling with 2- amino-5-bromo-2′-fluorobenzophenone gave no conversion.

The benzodiazepines obtained were converted using a two-step procedure including diethyl chlorophosphate and ethyl isocyanoacetate in the presence of potassium *t*-butoxide to afford the corresponding imidazobenzodiazepines DAW-I-10, 20, 30, 40, 50, 60, 70, 80, 32, 52 in 45-74% yield. Purification of imidazobenzodiazepines was accomplished through a trituration with 50% *t*-butyl methyl ether (MTBE) in hexanes. Earlier work showed that imidazobenzodiazepines purified

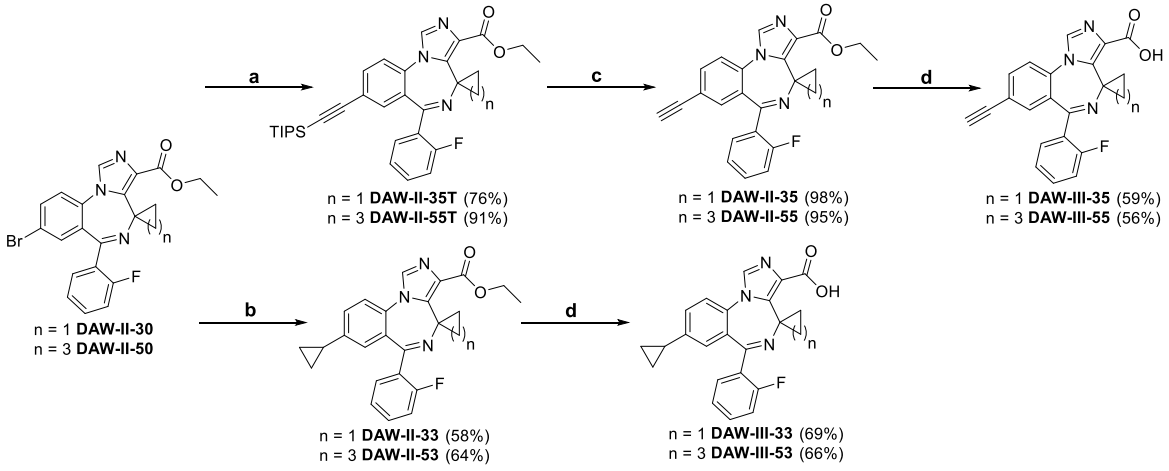

Scheme 6: Br substitution reactions: [a] Reagents and conditions: (a) (1) 4.7 mol % $Pd(OAc)_2$, 9.4 mol % P(o-tolyl)$_3$, triisopropylsilylacetylene 1.2 equiv, triethylamine 2 equiv, acetonitrile, reflux, 75 °C, 4 h; (c) TBAF 1.15 equiv, THF, water, −20 °C to rt, 1.5 h. (b) 10 mol % Pd(OAc)2, 20 mol % P(o-tolyl)3, cyclopropylboronic acid 5 equiv, K_3PO_4 4.3 equiv, toluene/water (1:4), 100 °C, 18 h. (d) THF/H_2O (43:1), NaOH 30 equiv, 80 °C, 24 h; (2) acetic acid until pH = 5, 50 °C, 18 h.

by flash chromatography often coelute with the side product diethyl hydrogen phosphate. This impurity can be removed by the addition of hexanes to the crystalline product (5 mL hexanes/1 g

product) followed by sonication for 2 min. Filtration afforded pure imidazodiazepines. A single trituration of 50% MTBE in hexanes often afforded purity of >95%; however, it was often

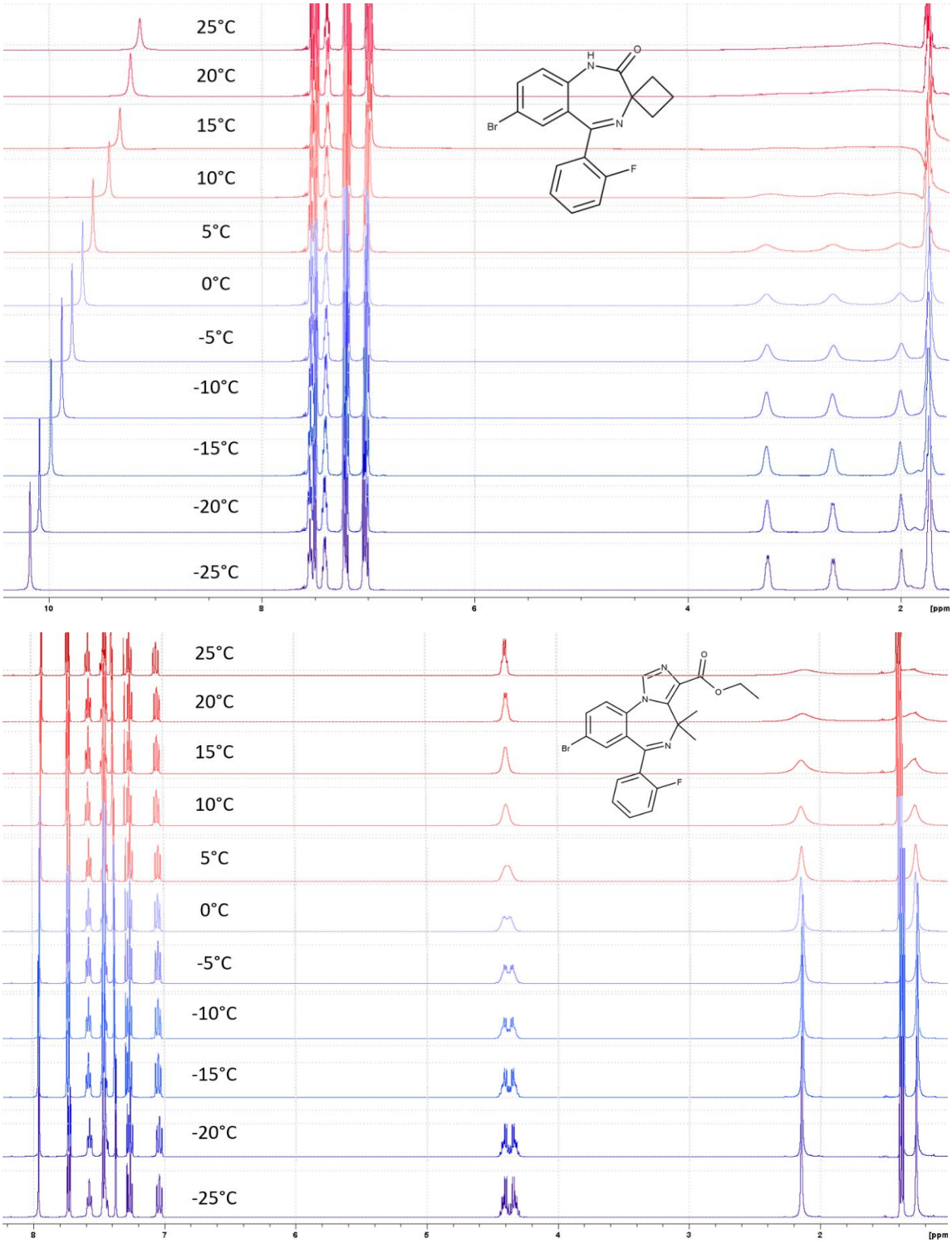

Figure 40: Variable temperature ^{1}H experiment of DAW-I-40 (top) and DAW-II-10 (bottom)

beneficial to purify the imidazobenzodiazepines via flash chromatography in addition to the trituration before the hydrolysis step to obtain high purity acids (>98%) with no further purification. During the analysis of DAW-II-10 by ^{1}H and ^{13}C NMR, signals of the dimethyl group were missing in deuterated chloroform at room temperature. Recording of NMR spectra at −20 °C, however, revealed a reduced line broadening due to rapid interconversion of rotamers (Figure 40).[191] In addition, we observed inequivalence of the methylene hydrogens indicating a hindered rotation of the ethyl ester group at lower temperature.

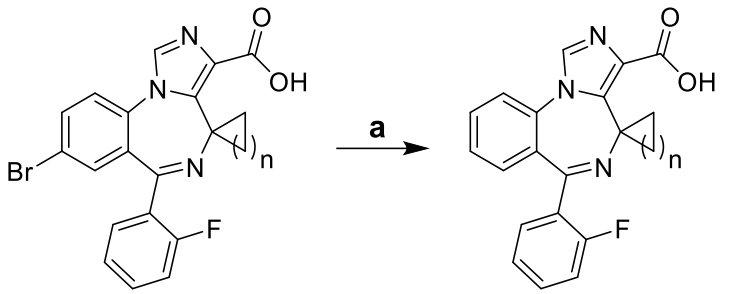

Scheme 7: Hydrogenation reactions: [a] Reagents and conditions: (a) Pd/C methanol, H_2 (1 bar), rt, 5 min.

The use of four equivalents of NaOH at 50 °C was reported for synthesis of enantiomerically pure MIDD0301.[188] However, for compounds with moderate steric hinderance, such as DAW-II-70 and DAW-II-30, 15 equivalents of NaOH at 80 °C were employed to achieve full hydrolysis in 6 h. For compounds with significant steric hinderance such as DAW-II-40, 50, 60, 30 equiv of NaOH at 80 °C for 24 h was deemed necessary. Racemization of imidazobenzodiazepine acids was not a concern due to the use of non-chiral and racemic amino acids. We reported the 6H isomer as an impurity of 1.4% for MIDD0301,[188] which is formed during the addition of the imidazole ring via [1,3] hydrogen shift (Scheme 5). The resulting 6H isomer with an aliphatic imine has nearly identical physical properties, and separation from the product was not achieved by recrystallization. The application of disubstituted amino acids

overcame this problem because these compounds now lack a proton adjacent to the imine nitrogen, affording higher purities for this series of imidazodiazepines. We have previously investigated the energy requirement needed for MIDD0301 to interconvert between rotamers.[187] We repeated this experiment for disubstituted compounds DAW-III-10, 30, 40, 50, 60 and calculated a zero-energy requirement for interconversion. This was supported by the fact that NMR analysis of these compounds showed one set of signals in contrast to the 20:80 ratio of two signals for MIDD0301.[191] Even at -25 °C, the ^{1}H NMR showed only one set of signals confirming rapid interconversion at low temperature.

Isolation of the carboxylic acid containing imidazodiazepines has the potential to be difficult because of an equilibrium that exists between the diazepine form (ring closed) and the acyclic ammonium salt form (ring open).[191] Strong acidic conditions favor the open form. At neutral or basic pH, the amine cyclizes with the ketone to form the corresponding imine diazepine ring. Post hydrolysis, the reaction mixture is strongly basic forming a water-soluble carboxylate. We have reported that imidazobenzodiazepine carboxylate salts form non-crystalline amorphous solids that are difficult to isolate.[191] Isolation of carboxylic acid involves the addition of acetic acid, which is acidic enough to protonate the imidazobenzodiazepine carboxylate but too weak to protonate the imine and create the ammonium salt (open form). Although this process was successful for most products, it was inadequate for DAW-III-10, DAW-III-70, and DAW-III-40, yielding mixtures of open and closed forms. Equivalents of acetic acid and NaOH were changed; however, open/closed form mixtures were still obtained. DAW-III-10 was isolated as ∼30% open, DAW-III-70 as ∼10% open, and DAW-III-40 as ∼50% open after treatment with acetic acid. The open/close mixtures can still be used for biological testing because they will form the imidazobenzodiazepine carboxylate exclusively at neutral pH within 1 h.[191] We successfully

isolated DAW-III-10, DAW-III-70, and DAW-III-40 as pure ammonium salts by heating the mixtures of open and closed form in 5 M HCl at 95 °C for 18 h. The products were collected by filtration, and purification was accomplished by trituration with hot isopropanol.

As described later, DAW-III-30 was shown to be the most promising compound in terms of binding to $GABA_ARs$, muscle relaxation, and reduction of AHR. To create a comprehensive structure-activity relationship (SAR), modifications were made to the bromine functionality of DAW-II-30. Introduction of an acetylene function, which was reported for compound 68 (Figure 39) with $\alpha_5\beta_3\gamma_2$ $GABA_AR$ subtype selectivity,[180] was accomplished with a Sonogashira coupling like reaction using triisopropylsilylacetylene in the presence of a palladium catalyst (Scheme 6). Subsequent deprotection with tetrabutylammonium fluoride and hydrolysis yielded DAW-III-35 in 5 h. A cyclopropyl group was introduced via a Suzuki reaction by adapting a reported procedure.[192] DAW-II-33 was isolated in 58% yield and converted into DAW-III-33 by hydrolysis.

DAW-III-31 was synthesized by hydrogenation of DAW-III-30 in 5 min (Scheme 7). Stopping this reaction once completed was important to prevent reduction of imine functionality.

comp.	aqueous solubility[a] (μM)	permeability[b] (log P_e (cm/s)	cytotoxicity[c] LD_{50} (μM)	$GABA_AR$ binding, % inhibition at 10 μM[d]	$GABA_AR$ binding IC_{50} μM[d]
DAW-I-10	319 ± 24	−5.7 ± 0.01	>150	70	1246
DAW-I-20	57 ± 22	−6.6 ± 0.03	>150	60	2477
DAW-I-30	321 ± 19	−5.6 ± 0.05	>150	97	42
DAW-I-40	109 ± 16	−5.5 ± 0.16	>150	71	2035
DAW-I-50	98 ± 4	−6.8 ± 0.27	>120	13	n.d.
DAW-I-60	94 ± 7	−7.1 ± 0.09	87 ± 7	33	n.d.
DAW-I-70	397 ± 31	−5.7 ± 0.04	>150	95	134
DAW-I-80	155 ± 6	−5.3 ± 0.09	>150	105	158
DAW-I-32	39 ± 3	−5.2 ± 0.15	>150	90	665
DAW-I-52	13 ± 3	−6.7 ± 0.25	>150	-13	n.d.
DAW-II-10	103 ± 5	−6.0 ± 0.12	>150	78	733
DAW-II-20	100 ± 6	−5.6 ± 0.03	>150	32	n.d.
DAW-II-30	141 ± 20	−5.1 ± 0.10	>120	94	87
DAW-II-40	186 ± 17	−5.2 ± 0.03	>120	83	859
DAW-II-50	144 ± 7	−5.8 ± 0.10	106 ± 9	19	n.d.
DAW-II-60	141 ± 19	−6.0 ± 0.06	96 ± 11	74	6222
DAW-II-70	417 ± 17	−5.7 ± 0.01	>300	61	175
DAW-II-80	213 ± 4	−6.7 ± 0.11	>150	97	805
DAW-II-32	54 ± 2	−5.6 ± 0.04	>150	34	n.d.
DAW-II-33	96 ± 1	−4.9 ± 0.01	>120	22	n.d.
DAW-II-35	53 ± 3	−4.6 ± 0.03	>150	56	509
DAW-II-52	114 ± 2	−5.2 ± 0.09	>150	11	n.d.
DAW-II-53	17 ± 3	−5.7 ± 0.04	>150	70	n.d.
DAW-II-55	51 ± 1	−5.5 ± 0.04	>150	-1	n.d.
DAW-III-10	4400 ± 100	−7.0 ± 0.22	>300	74	4053
DAW-III-20	15,250 ± 100	−7.1 ± 0.15	>300	35	n.d.
DAW-III-30	8200 ± 100	−6.8 ± 0.09	>300	97	9
DAW-III-40	58,700 ± 4400	−6.6 ± 0.10	>300	59	1833
DAW-III-50	46,700 ± 600	−6.7 ± 0.04	>300	2	n.d.
DAW-III-60	46,900 ± 1300	−6.6 ± 0.10	>300	24	n.d.
DAW-III-70	77,600 ± 300	−6.6 ± 0.10	>300	102	145
DAW-III-80	32,500 ± 100	−6.3 ± 0.06	>300	89	381
DAW-III-31	15,100 ± 100	−7.0 ± 0.14	>300	74	289
DAW-III-32	36,200 ± 400	−6.6 ± 0.03	>300	18	n.d.
DAW-III-33	12,800 ± 100	−6.4 ± 0.04	>300	58	1832
DAW-III-35	40,300 ± 500	−6.7 ± 0.12	>300	55	59
DAW-III-51	95,900 ± 200	−6.3 ± 0.13	>300	5	n.d.
DAW-III-52	12,000 ± 230	−6.3 ± 0.12	>300	48	n.d.
DAW-III-53	28,100 ± 230	−6.1 ± 0.03	>300	31	n.d.
DAW-III-55	22,500 ± 100	−6.2 ± 0.10	>300	-15	n.d.

Table 1: Physiochemical properties of synthesized imidazobenzodiazepines. a Shake flask, pH 7.2. b Permeability was measured using the parallel artificial membrane permeation assay at pH 7.4. Reference standards (log P_e): ranitidine (−7.0 cm/s) low permeability, naproxen (−5.0 cm/s) medium permeability, and verapamil (−4.0 cm/s) high permeability. c Cytotoxicity was determined using HEK293 cells using CellTiter-Glo. d Competition assay of GABAAR ligand 3 H-flunitrazepam using rat brain extract.

2.7.4 Aqueous Solubility

Aqueous solubility is an important characteristic of any drug and was determined by a "shake flask" method for 24 h at pH 7.4 (Table 1). DAW-I-10, 20, 30, 40, 50, 60, 70, 80, 32, 52 have aqueous solubilities in the range of 13−397 μM. DAW-I-10, 70, 30 have solubilities greater than 300 μM. DAW-I-30 and DAW-I-32 differ only by the halogen substituent at position 8. The chloro-substituent markedly reduced solubility, making DAW-I-32 one of the least soluble compounds. This trend in substituting the bromine for chlorine was further supported with the testing of DAW-I-50 and DAW-I-52. The aqueous solubility of imidazobenzodiazepines DAW-II-10, 20, 30, 40, 50, 60, 70, 80, 32, 52 ranged from 51 to 417 μM. Most compound solubilities were in the range of 100−200 μM, except DAW-II-70 with aqueous solubility of 417 μM bearing an ethyl substituent at position 4 demonstrating the best aqueous solubility. The ethyl substituent also increased the solubility of DAW-I-70.

The trend for lower solubility for chlorine-substituted compounds in comparison to bromine-substitution was observed for DAW-I-32 and DAW-II-32. The introduction of an acetylene function also reduced solubility of DAW-II-35 in comparison to bromine-substituted (DAW-II-30). Acids DAW-III-10, 20, 30, 40, 50, 60, 70, 80, 31, 32, 33, 35, 51, 52, 53, 55 are negatively charged at neutral pH and exhibited mM solubility. The solubility of MIDD0301 was investigated extensively, showing marked solubility changes at different pH values.[191] At strong acidic, neutral, and basic conditions, MIDD0301 has excellent solubility, whereas at pH values between 3 and 6, the solubility is significantly decreased. It was expected that compounds DAW-III-10, 20, 30, 40, 50, 60, 70, 80, 31, 32, 33, 35, 51, 52, 53, 55 would exhibit similar properties. DAW-III-10 was the least soluble acid at 4.4 mM. DAW-III-70 was the most soluble compound

at 77.6 mM. These data are consistent with the trend of compounds containing an ethyl substituent at position 4 being the most soluble in each series. Surprisingly, compounds with different spiro ring sizes have similar aqueous solubility except for DAW-III-30 (8.2 mM). Substitution of the bromine of DAW-III-30 by an acetylene group increased the solubility for DAW-III-35 (40.3 mM).

2.7.5 Permeability

Permeability is an important parameter of small molecules that describes their ability to cross cell membranes. Permeability was determined by a parallel artificial membrane permeability assay (PAMPA).[193] The membrane consisted of a hexane/hexadecane layer, and compounds were added as dimethyl sulfoxide (DMSO) solutions at a final concentration of 5% (v/v). The equilibrium across the membrane was determined after 18 h. Compounds DAW-I-10, 20, 30, 40, 50, 60, 70, 80, 32, 52 exhibited medium permeabilities compared to control compounds ranitidine (log P_e = −7.0 cm/s) low permeability, naproxen (log P_e = −5.0 cm/s) medium permeability, and verapamil (log P_e = −4.0 cm/s) high permeability (Table 1). The five and six-membered spiro analogs DAW-I-50 and DAW-I-60 exhibited the lowest permeabilities of the tested benzodiazepines. The same trend was observed for compounds DAW-II-10, 20, 30, 40, 50, 60, 70, 80, 32, 33, 35, 52, 53, 55 in the imidazodiazepines series with lower-than-average permeabilities for DAW-II-50 and DAW-II-60. The highest permeability was observed for acetylene substituted compound DAW-II-35 (log P_e = −4.6 cm/s). Due to the charged carboxylate function at neutral pH, compounds DAW-III-10, 20, 30, 40, 50, 60, 70, 80, 31, 32, 33, 35, 51, 52, 53, 55 have the lowest permeabilities of all tested compounds. This design feature resulted in excellent tissue

selectivity; thus, restricting of $GABA_AR$s targeting to non-CNS tissue, especially in lung.[179] The observed low permeabilities are in a narrow range between −6.4 and −7.1 cm/s.

2.7.6 Cellular Toxicity

To improve the success in downstream *in vivo* evaluation, cell-based toxicity assays represent an important no-go decision point for drug candidates. Toxicity was determined with embryonic kidney cells (HEK-293) after 18 h using CellTiter-Glo (Promega) (Table 1). Compounds DAW-I-10, 30, 40, 70, 32 were toxic at 300 μM but showed minimal toxicity at 150 μM (see below for dose response curves). DAW-I-50 and DAW-I-60 bearing five- and six-membered spiro substituents were slightly more toxic. A similar trend was observed for DAW-II-50 and DAW-II-60, being slightly more toxic than the small ring spiro imidazobenzodiazepines DAW-II-30 and DAW-II-40. It was noted that after 18 h, crystals formed in the wells with 150

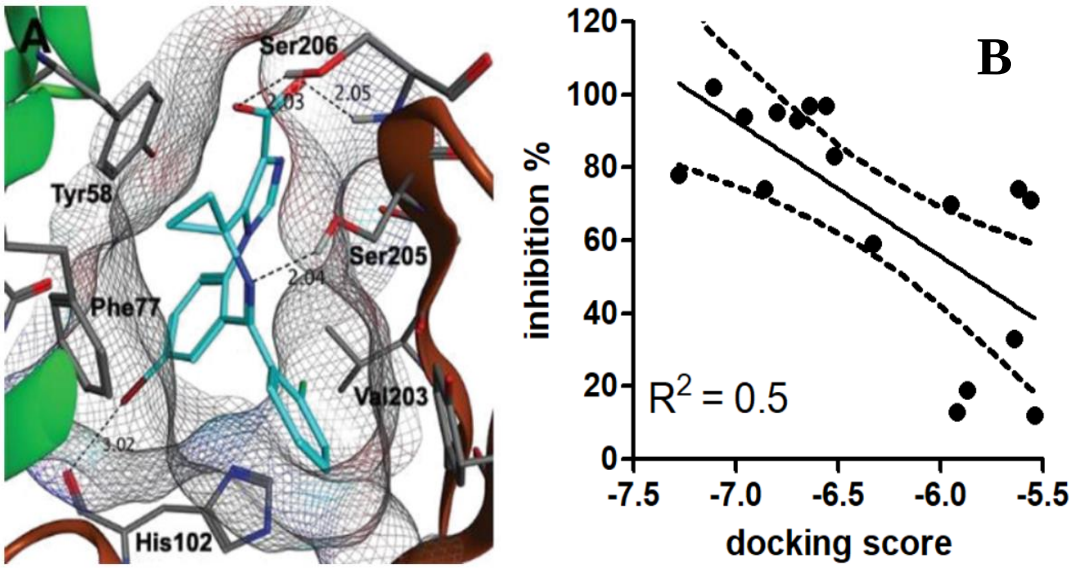

Figure 41: (A) Docking pose of DAW-III-30 in the complex with the $\alpha_1\beta_3\gamma_{21}$ $GABA_AR$ using the structure 6HUO The $\alpha1^+/\gamma2^-$ interface is indicated as α_1 (green) and γ_2 (brown). Hydrogen and halogen bonds are indicated as dashed lines. (B) Correlation plot of docking scores calculated with MOE and % inhibition of bromo-substituted benzodiazepines.

and 300 μM of DAW-II-70. This was surprising, given that DAW-II-70 has by far the greatest aqueous solubility. Nevertheless, the actual LD_{50} of DAW-II-70 might be lower than 300 μM. Finally, compounds DAW-III-10, 20, 30, 40, 50, 60, 70, 80, 31, 32, 33, 35, 51, 52, 53, 55 containing a carboxylic acid showed no toxicity at 300 μM.

2.7.7 $GABA_AR$ Binding

$GABA_AR$ binding was determined by competition of ^{3}H-flunitrazepam using rat brain extract by the PDSP program (University of NC Chapel Hill).[194] All compounds were screened initially at 10 μM, and compounds that achieved more than 50% inhibition were subjected to a dose response analysis (Table 1). Benzodiazepines DAW-I-10, 30, 40, 70, 32 interacted with the $GABA_AR$ subtypes that bind flunitrazepam ($\alpha_{1-3,5,6}\beta_{1-3}\gamma_{1-3}/\delta$).[195] Expression of $GABA_ARs$ in the brain include 43% $\alpha_1\beta_2\gamma_2$, 15% $\alpha_2\beta_3\gamma_2$ plus 8% $\alpha_2\beta\gamma_1$, 10% $\alpha_3\beta_3\gamma_2$, 6% $\alpha_4\beta\gamma/\delta$, 4% $\alpha_5\beta_3\gamma_2$, and 4% $\alpha_6\beta_2\gamma_2/\delta$.[196] DAW-I-50 and DAW-I-60 bearing a five- or six-membered spiro substituent, respectively, showed no significant binding to the mix of brain expressed $GABA_ARs$. The strongest binding in this series was observed for cyclopropyl spiro compound DAW-I-30 with an IC_{50} of 42 nM. The corresponding chloro analog DAW-I-32 showed less binding with an IC_{50} of 665 nM. DAW-I-70 bearing an ethyl substituent instead of the cyclopropyl spiro function interacted well with $GABA_ARs$ (IC_{50} = 134 nM). Among the imidazobenzodiazepines, cyclopropyl spiro compound DAW-II-30 was also the best $GABA_AR$ binder with an IC_{50} of 87 nM. The next best binder in this series was DAW-II-70 with an ethyl substituent. Interestingly, substitution of bromine with chlorine (DAW-II-32) and cyclopropyl (DAW-II-33) generated weak $GABA_AR$ ligands, whereas DAW-II-35 with an acetylene group had an IC_{50} of 509 nM. Some activity was

retained for the cyclobutyl spiro (DAW-II-40) and dimethyl substituted ligands (DAW-II-10), but cyclopentyl (DAW-II-50) and cyclohexyl (DAW-II-60) spiro compounds were not active. Post hydrolysis, DAW-III-30 containing a cyclopropyl spiro group, was the best binder (IC_{50} = 9 nM). Consistent with other compound series, $GABA_AR$ binding diminished with increasing spiro ring size. Other observed trends apply as well, such as substitution of bromine by chlorine (DAW-III-32) and cyclopropyl (DAW-III-33) generated weak $GABA_AR$ ligands. The acetylene substituted compound DAW-III-35 is an excellent $GABA_AR$ binder (IC_{50} = 55 nM) and even removal of the bromine resulted in DAW-III-31 with an IC_{50} of 289 nM. Very good $GABA_AR$ binding was observed for ethyl substituted compounds DAW-III-70 (IC_{50} = 145 nM), whereas dimethyl substituted compound DAW-III-10 did not show strong $GABA_AR$ binding.

2.7.8 $GABA_AR$ Docking Studies

We investigated if molecular docking using crystal structure 6HUO[197] of $\alpha_1\beta_3\gamma_2$ $GABA_AR$ in complex with alprazolam would correspond to the SAR inferred by the empirical in vitro binding assays. First, we docked the best $GABA_AR$ binder DAW-III-30 (IC_{50} = 9 nM) in the $\alpha1^+/\gamma2^-$ interface and identified a halogen bond interaction with His102 (Figure 41A). Furthermore, hydrogen bond interactions between the carboxylate and Ser206 and Ser205 and the imine function were identified. We reported molecular docking poses for MIDD0301 bearing a (R) or (S) methyl substituent instead of the cyclopropyl substituent and observed the almost same docking poses.[198] The stereochemistry of the methyl substituent did not significantly influence $GABA_AR$ binding (MIDD0301 (IC_{50} = 26 nM) and MIDD0301S (IC_{50} = 25 nM)). Based on this

knowledge, we used molecular operating environment (MOE) software to compute binding scores of other synthesized $GABA_AR$ ligands.

For docking, a pharmacophore was created that only scored ligand poses that included halogen bonding with His102 and hydrogen bonding with Ser206. Compounds were docked using both the "rigid receptor" and the "induced fit" model. We found that the "rigid receptor" model yielded the best homogeneity of docking poses. Due to the presence of two stable rotamers for this compound class, rotamers of each compound were docked individually. The rotamer depicted in Figure 41A gave the best docking score for all ligands. When related to the % $GABA_AR$ binding, a moderate correlation between activity and docking score was observed (Figure 41B). Poor correlation was observed for weak binders due to percent $GABA_AR$ binding with high standard deviation. Spiro cyclopropane ring compounds DAW-I-30, DAW-II-30, and DAW-III-30 with high $GABA_AR$ affinities achieved excellent docking scores. Interestingly, we observed a significantly better docking score for the (S) enantiomer of DAW-III-70 than the corresponding (R) enantiomer. Because $GABA_AR$ binding was determined for racemic DAW-III-70, it can be anticipated that (S) DAW-III-70 has a better IC50 than 145 nM.

2.8.9 Microsomal Stability

We reported the phase 1 and phase 2 metabolic stability of structurally related asthma candidate MIDD0301. Although this compound was stable in the presence of NADPH with human, dog, mouse, and rat S9 fractions, some phase 2 conjugation (glucuronidation and glucosidation) occurred in the presence of mouse and human S9 fractions. Accordingly, we designed analogs of MIDD0301, described herein, with more steric hinderance in proximity to the

acid function to suppress phase 2 conjugation. The results of the stability evaluation are summarized in Table 2.

Compounds DAW-III-10, 30, 40, 50, 60, 70, 31, 32, 33, 35 were all stable for 2 h in the presence of mouse and human S9 using a NADPH regeneration system. For glucuronidation, we identified several compounds that exhibited superior stability in comparison to MIDD0301.

For mouse S9 fractions, we found that the change of the methyl substituent of MIDD0301 to an ethyl (DAW-III-70) significantly improved stability. The dimethyl substituted compound DAW-III-10 was also more stable than MIDD0301. For the spiro compounds DAW-III-30, 40, 50, 60, we found all except DAW-III-60 were more stable than MIDD0301. All analogs of DAW-III-30 with replacement of the bromine were equally stable for 2 h. We found that all compounds in this series except DAW-III-30 were more resistant to phase 2 conjugation in the presence of human S9 fractions than MIDD0301. Thus, except for DAW-III-30 for mouse S9 only, it can be concluded

	mouse		human	
comp.	phase 1[a]	phase 2[b]	phase 1[a]	phase 2[b]
MIDD0301	110 ± 14	73 ± 8	98 ± 4	77 ± 3
DAW-III-10	106 ± 4	107 ± 10***	106 ± 7	111 ± 9***
DAW-III-30	120 ± 4	90 ± 6***	104 ± 1	69 ± 7
DAW-III-40	90 ± 2	91 ± 4***	122 ± 7	113 ± 9***
DAW-III-50	117 ± 3	92 ± 3***	114 ± 7	96 ± 7***
DAW-III-60	111 ± 6	78 ± 1	107 ± 11	106 ± 8***
DAW-III-70	108 ± 2	114 ± 7***	119 ± 9	111 ± 6***
DAW-III-31	108 ± 2	99 ± 3***	106 ± 9	96 ± 4***
DAW-III-32	101 ± 8	98 ± 4***	103 ± 4	103 ± 6***
DAW-III-33	102 ± 6	95 ± 4***	107 ± 3	96 ± 4***
DAW-III-35	108 ± 5	113 ± 4***	106 ± 4	93 ± 7***

Table 2: Microsomal Stability: [a] Enzymatic oxidation in the presence of NADPH and liver S9. [b] Glucuronidation in the presence of UDP-glucuronic acid and liver S9. All assays were performed with 10 μM compound in three independent assays in triplicate. The remaining percentage of the parent compound after 2 h is given as averages (n = 6) with StD. A one-way ANOVA analysis was applied to determine significance in respect to MIDD0301 with *, **, and *** equals $p < 0.05$, 0.01, or 0.001, respectively.

that substituents other than the methyl group of MIDD0301 resulted in significantly more stable compounds with regard to phase 2 conjugation.

2.7.10 Sensorimotor Inhibition

Compounds binding $GABA_AR$ in the brain often induce changes in behavior and coordination. We designed compounds DAW-III-10, 30, 40, 50, 60, 70, 31, 32, 33, 35 to not cross the blood−brain barrier and reported for structural analog MIDD0301 the absence of sensorimotor inhibition following oral dosing up to 1000 mg/kg as determined by a rotarod assay.[185] Using the same protocol, we found that none of the imidazodiazepines acids described herein impaired the ability of trained mice to balance on a rotating rod following oral doses of 40 mg/kg (Figure 42).

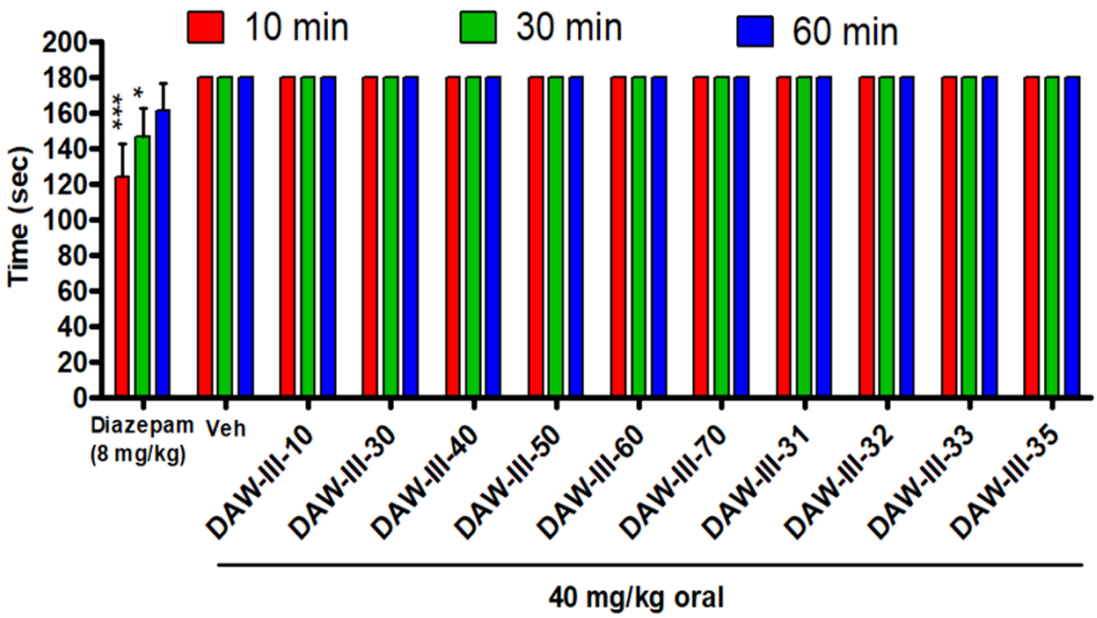

Figure 42: Female Swiss Webster mice were monitored on a rotarod apparatus for 3 min at 10, 30, and 60 min after oral administration. The time of fall was recorded if occurring before 3 min. Data are expressed as means ± SEM (n = 12). * $p < 0.05$ and ***$p < 0.001$ significance were calculated with 2-way ANOVA in

GABA$_A$R ligand diazepam (Figure 39), which has similar affinity to the GABA$_A$R as DAW-III-30 (but in contrast to DAW-III-30 crosses the blood−brain barrier), induced rapid and significant loss of sensorimotor coordination at 8 mg/kg.

2.7.11 Airway Smooth Muscle Relaxation

We previously reported that MIDD0301 potently relaxes constricted airway smooth muscle ex vivo and reduces AHR in vivo.[179,181,184,198] For the ex vivo experiment, guinea pig tracheal rings were suspended in an organ bath, constricted with substance-P, and treated with DAW-III-10, 30, 40, 50, 60, 70, 31, 32, 33, 35 followed by recording of muscle force (Figure 43).

25 μM of DAW-III-30, DAW-III-60, DAW-III-31, and DAW-III-35 caused significant relaxation of constricted airway smooth muscle at 30 min. The contractile force difference

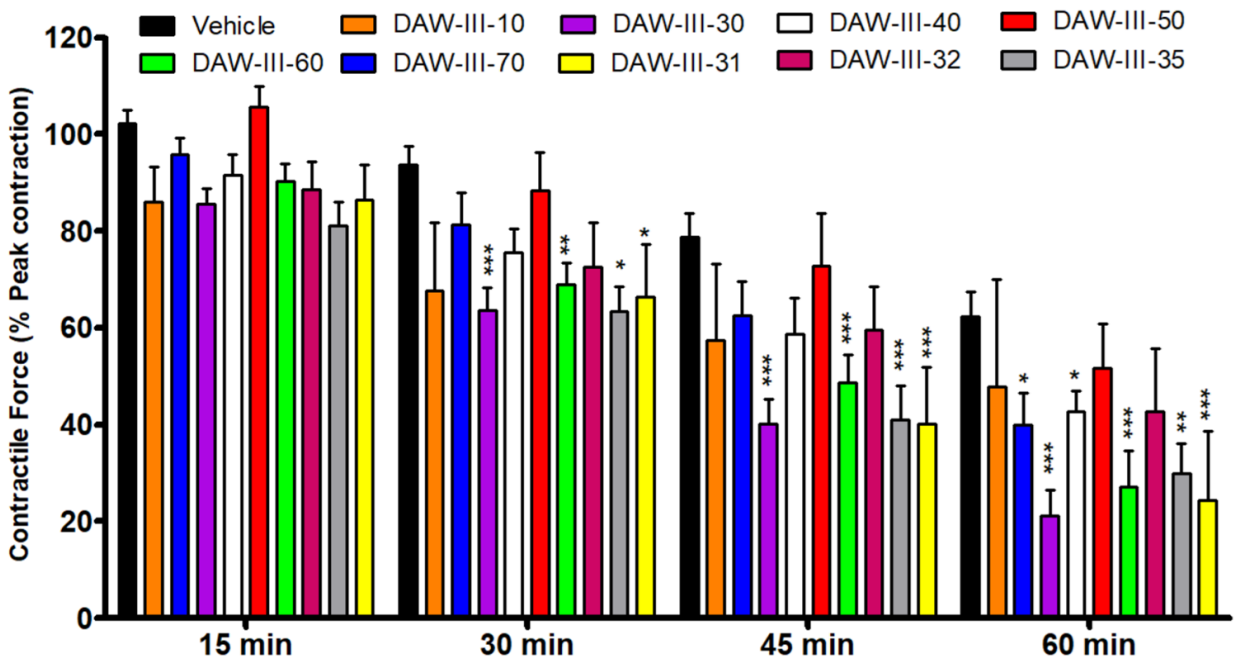

Figure 43: Ex vivo airway smooth muscle relaxation. Guinea pig trachea rings were contracted with substance P and treated with 25 μM of compound. Percent muscle force compared with the initial muscle contraction (0.1% DMSO) was determined at various time points and is depicted as mean and SEM (n = 10). A two-way analysis of variance (ANOVA) repeated measures was used to compare vehicle and test compound, with *p < 0.05, **p < 0.01, and ***p < 0.001.

compared to vehicle increased significantly thereafter for all four compounds. At 60 min, weak airway smooth muscle relaxation was also observed for DAW-III-70 and DAW-III-40. We noted the typical time-dependent reduction of muscle contractile force in the vehicle control due to the limited half-life of substance P. A good correlation was noticed between the relaxation of airway smooth muscle and the ability of compounds to bind $GABA_AR$s (Table 1). DAW-III-70, DAW-III-30, DAW-III-35, and DAW-III-31 interacted strongly with the $GABA_AR$s, especially compound DAW-III-30 with an IC_{50} of 9 nM. DAW-III-30 also showed the strongest effect on constricted airway smooth muscle with a p-value of <0.001 at 30 min. DAW-III-35 also strongly relaxes airway smooth muscle and is related to compound 68 (see Figure 39) with respect to the acetylene substitution. Compound 68 relaxed human airway smooth muscle, attenuated AHR, and decreased lung eosinophil numbers and, like MIDD0301, did not cross the blood−brain barrier.[180]

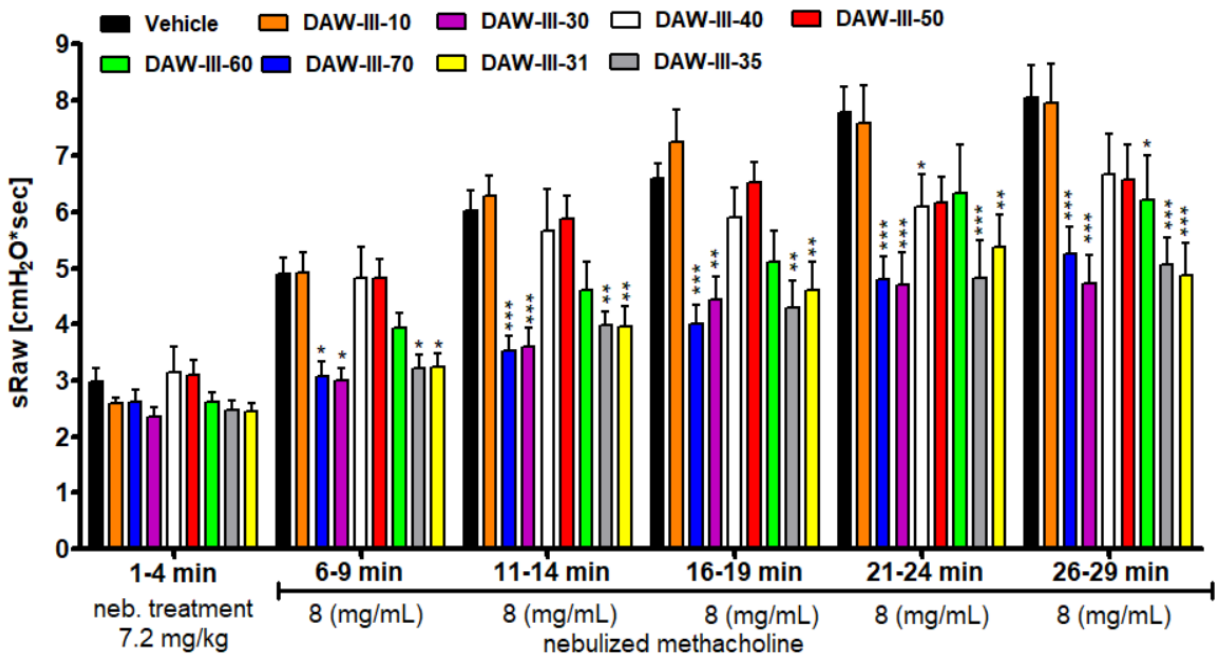

Figure 44: Compound effects on airway hyperresponsiveness. Female A/J mice received nebulized compound (7.2 mg/kg) followed by nebulized methacholine. Specific airway resistance (sRaw) was calculated at 3 min recording intervals and depicted as mean and SEM (n = 12). *p < 0.05, **p < 0.01, and ***p < 0.001 significance, respectively, between vehicle and compound treated groups as determined by two-way ANOVA repeated measures.

2.7.12 Bronchodilation

To demonstrate if DAW-III-10, 30, 40, 50, 60, 70, 31, 32, 33, and 35 could relax bronchoconstriction, we performed an AHR study using a double chamber plethysmograph that non-invasively quantifies airway mechanics in conscious mice (Figure 44).

A/J mice were used because they exhibit severe AHR to methacholine without the need for preexisting allergen sensitization and challenge.[184] DAW-III-10, 30, 40, 50, 60, 70, 31, 32, 33, and 35 were nebulized in phosphate buffered saline (7.2 mg/kg) followed by a sequence of five nebulized methacholine challenges, recording of airway mechanics, and calculation of specific airway resistance (sRaw). For the vehicle, increasing sRaw values were observed at successive methacholine challenges representing more labored breathing to overcome airway constriction. The weak $GABA_AR$ binders DAW-III-10 and DAW-III-40, 50, 60 showed little to no change of sRaw values in comparison with the vehicle. Interestingly, DAW-III-60 showed a much stronger *ex vivo* effect (Figure 43) than *in vivo* effect (Figure 44). DAW-III-70, DAW-III-30, DAW-III-35, and DAW-III-31 that bind strongly to the $GABA_ARs$ reduced sRaw values within the first methacholine challenge. The bronchodilatory effects of these compounds were observed throughout the experimental time course and aligned with the reversal of airway smooth muscle constriction using *ex vivo* tissue.

2.7.13 Conclusion

It can be concluded that the allosteric benzodiazepine binding site of $GABA_ARs$ located between the α and γ subunits can only accommodate spiro-imidazodiazepines with a three-

membered ring size. Larger ring sized spiro-imidazodiazepines showed diminished binding and reduced ability to relax constricted airway smooth muscle *ex vivo* and *in vivo*. Compound DAW-III-30 was the most promising compound in this study with the strongest $GABA_AR$ binding and excellent in vivo activity. The advantage of DAW-III-30 in comparison to MIDD0301, for which we have reported similar *ex vivo* and *in vivo* results, is the absence of a chiral center and the absence of a proton adjacent to the imine nitrogen, that when deprotonated will support the formation of a 6H isomer via a [1,3] hydrogen shift. Thus, very pure DAW-III-30 can be produced without the need of elaborate purification to remove the 6H isomer. In addition, DAW-III-30 has an improved microsomal stability in mice compared to MIDD0301 resulting in an anticipated longer *in vivo* half-life. It can be further concluded that an acetylene substituent in place of bromine retains $GABA_AR$ binding and resulted in DAW-III-35 with very good *in vivo* and *ex vivo* activity and excellent metabolic stability. DAW-III-31, without an aryl substituent, exhibited good *in vivo* activity and moderate $GABA_AR$ binding. Finally, DAW-III-70 bearing a racemic ethyl substituent retains very good $GABA_AR$ binding and good *in vivo* activity and is more metabolically stable than MIDD0301 with a methyl substituent. Thus, it can be concluded that our strategy to change diazepine ring substituents to suppress phase 2 metabolism resulted in metabolically more stable compounds, but it was limited by the restricted space of the allosteric $GABA_AR$ binding pocket to three-membered spiro imidazodiazepines.

2.7.14 Experimental Procedures

Aqueous Solubility: 5−50 mg of compound was added to 500 μL of PBS buffer at pH 7.4. The pH was adjusted if necessary, using a 1 M NaOH solution. The solutions were vortexed for

10 s, sonicated for 2 min, and agitated with a horizontal shaker in a closed vial for 24 h. The mixtures were transferred to an Eppendorf tube and centrifuged for 5 min at 16,000 × g followed by filtration through 0.22 μm cellulose acetate spin X centrifuge filter (Costar). 200 μL of filtrate was transferred to a new Eppendorf tube and 200 μL of methanol was added. Subsequent dilutions were made with 50:50 methanol/PBS buffer water to adjust concentrations suitable for UV detection. After mixing, 50 μL of this solution was transferred into a 384 well plate (Coring UV star, 781,801) for UV detection at 250− 600 nm (Tecan M1000). The assay was carried out with three independent samples of each compound. The concentration of each solution was determined with a calibration curve in 50:50 methanol/ PBS buffer water. Absorbance of corresponding methanol PBS blank was recorded and subtracted from the absorbance of calibration curve solutions and from the samples.

Permeability: The artificial membrane was prepared by carefully pipetting 15 μL of the 5% (v/v) hexadecane in hexane solution to each of the wells of the donor plate. The plate was placed into a fume hood for 1 h to ensure complete evaporation of the hexane. After the hexane had evaporated, 300 μL of PBS with 5% (v/ v) DMSO was added to each of the wells of the acceptor plate. The hexadecane treated donor plate was then placed on top of the acceptor plate taking care that the underside of the membrane is completely in contact with the solution in each of the acceptor wells. 300 μM of solution was prepared of each compound in 5% (v/v) DMSO in PBS, and 150 μM was transferred in triplicate to the donor wells. The lid was placed on the plates, and the entire plate sandwich was placed into a closed humid environment. The container was then placed on a reciprocal shaker for agitation at about 100 rpm. The time at the beginning of the incubation was recorded, as this is a thermodynamic-based assay. The incubation was then allowed

to continue for 18 h. The donor plate was removed, and 50 μL of the acceptor solution was transferred to the UV plate. Drug solutions at the theoretical equilibrium concentration (100 μM) were also prepared and transferred to the UV plate. The absorbance of the solutions in the UV plate was then scanned from 250 to 600 nm with 1 nm steps and a 5 nm bandwidth. log P_e was calculated as follows:

Equation 1:

$$P_{app} = C \times -\mathrm{Log}\left(1 - \frac{A_{acceptor}}{A_{equilibirum}}\right)$$

$$C = \frac{V_A \times V_D}{(V_A + V_D)\mathrm{Area} * t}$$

The relative permeability (cm/s) of the small molecules was calculated with equation 1, where VD is the volume of the donor well in cm^3 (150 μL), VA is the volume in the acceptor well in cm^3 (300 μL), A is the active surface area of the membrane in cm^2 (0.283 cm^2), T is the incubation time of the assay in seconds, $[drug]_A$ is the absorbance of the compound in the acceptor well after the incubation period, and $[drug]_E$ is the absorbance of the compound at the concentration of the theoretical equilibrium (as if the donor and acceptor solutions were simply combined).

Cell Viability: Human embryonic kidney HEK293T cells (ATCC) were cultured in 75 cm^2 flasks (CellStar). Cells were grown in DMEM/high glucose (Hyclone, #SH3024301) media to which non-essential amino acids (Hyclone, #SH30238.01), 10 mM HEPES (Hyclone, #SH302237.01), 5×10^6 units of penicillin and streptomycin (Hyclone, #SV30010), and 10% of heat inactivated fetal bovine serum (Gibco, #10082147) were added. HEK293T cells at 70−80% confluency were harvested with 0.05% trypsin (Hyclone, #SH3023601), added to 10 mL of the

assay buffer, DMEM/high-modified buffer without phenol red (Hyclone, #SH30284.01) containing all the above mentioned additives plus 10 mM sodium pyruvate and 10% percent heat inactivated FBS (Invitrogen, #12676- 011), and centrifuged for 3 min at 600 × g. The media was removed, and cells were resuspended in the same media. Cells were added to sterile white, optical bottom 384-well plates. To each well, 20 μL containing 15,000 cells was added. Plates were incubated for 4 h at 37°C with 5% CO_2 before two transfers of 100 nL of serially diluted (1:3 in DMSO) compounds (final maximum concentration at 300 μM) were transferred using a Tecan Freedom EVO liquid handling system with a 100 H stainless steel pin tool. The controls for the cytotoxicity assay were 3-dibutylamino-1-(4-hexyl-phenyl)-propan-1-one (150 μM in DMSO, positive) and DMSO (negative). After 18 h, assay plates were evaluated by adding 15 μL of Cell Titer-Glo Luminescence Assay Kit (Promega, Madison, WI) to each well and reading luminescence on a Tecan Infinite M1000 plate reader. Controls were measured in each plate to determine the z′ factor and enable data normalization. Three independent experiments were performed in quadruplicate, and data were analyzed using non-linear regression with variable slope (GraphPrism).

Rotarod: Ten-week-old female Swiss Webster adult mice were purchased from Charles River Laboratories and housed pathogen-free with a 12-h light and dark cycle. Animals had free access to food and water. All studies were conducted in accordance with institutional guidelines as defined by UWM Institutional Animal Care and Use Committee. Mice were trained to maintain balance at a constant speed of 15 rpm on the rotarod apparatus (Omnitech Electronics, Inc.) for 3 min. Compounds were dissolved in hot PEG400 (2.5% v/v) followed by the addition of 2% hydroxypropylmethylcellulose solution (97.5% v/v). Each mouse received a volume of 100 μL by

oral gavage. Mice were placed on the rotarod for 3 min at 10, 30, and 60 min after each administration. If a mouse fell before 3 min had elapsed, it was placed again on the rotating rod. If a mouse fell for the second time, the time of the fall was recorded. Data analysis was carried out with GraphPad Prism (GraphPad) using two-way analysis of variance (ANOVA) repeated measures and Bonferroni posttest (n = 12)

Microsomal Stability Assay (Phase 1): To 282 μL of water, 80 μL of phosphate buffer (0.5 M, pH 7.4), 20 μL of NADPH regenerating system solution A, and 4 μL of NADPH regenerating system solution B (BD Bioscience), was added 4 μL of a 1 mM DMSO solution of the test compound. The final assay concentration was 10 μM. The assay was preincubated at 37 °C for 5 min using a heating, shaking dry bath (Fischer Scientific), followed by a 50 μL aliquot being removed and quenched with 100 μL of cold methanol that contained 10 μM 4,5-diphenylimidazole as IS. 8.8 μL of 20 mg/mL human or mouse liver microsomes (Xenotech) was added to initiate the reaction. The assay protein concentration was 0.5 mg/mL. A final aliquot was taken after 120 min and quenched with 100 μL of cold methanol containing 10 μM IS. The samples were sonicated for 10 s, centrifuged at 11,000 × g for 5 min, and filtered using a spin-X HPLC filter tube (Corning Inc.), and centrifuged at 11,000 × g for 30 s. For the analysis by liquid chromatography with tandem mass spectrometry (LC−MS/MS; Shimadzu), the samples were diluted 20-fold. Peak area ratios between compound area and IS area were used to determine conversion between t = 0 and t = 120 min. The experiments were carried out in two independent assays in triplicate (n = 6). The activity of microsomes was tested with reference compound HZ166[199] for phase 1 and MIDD0301 for phase 2.[186]

Metabolic Stability Assay (Phase 2: Glucuronidation): To 0.230 mL water, 0.080 mL phosphate buffer (0.5 M, pH 7.4), 0.04 mL of a 50 mM of UDP-glucuronic acid in water (5 mM final concentration), 0.04 mL of a 50 mM solution of inhibitor sacharic-1,4-lactone in water (5 mM final concentration), 0.004 mL of a 100 mM MgCl2 solution in water (1 mM final concentration), 0.004 mL of a 1 mM DMSO solution of the test compound (10 μM assay concentration), and 1.8 μL of a 5 mg/mL alamethicin in DMSO (0.0225 mg/mL final concentration) were added. The assay was preincubated at 37 °C for 5 min using a heating shaking dry bath (Fischer Scientific), followed by a 50 μL aliquot being removed and quenched with 100 μL of cold methanol that contained 5 μM 4,5- diphenylimidazole as IS. 8.8 μL of either human or mouse liver S9 fraction or mouse kidney S9 fraction (each from Xenotech) was added to initiate the reaction. The protein assay concentration was 0.5 mg/mL. A final aliquot was taken after 120 min and quenched with 100 μL of cold methanol containing 5 μM IS. The samples were sonicated for 10 s, centrifuged at 11,000 × g for 5 min, filtered using a 0.22 μm nylon spin-X HPLC filter tube (Corning Inc.), and centrifuged at 11,000g for 30 s. For the analysis by LC−MS/MS (Shimadzu), the samples were diluted 10-fold. Peak area ratios between compound area and IS area were used to determine conversion between t = 0 and t = 120 min. The experiments were carried out in two independent assays in triplicate (n = 6). The activity of microsomes was tested with reference compound HZ166[199] for phase 1 and MIDD0301 for phase 2.[186]

Airway Smooth Muscle Relaxation: Adult male Hartley guinea pigs were purchased from Charles River Laboratory (435−450 g) and housed pathogen-free with a 12-h light and dark cycle. Animals had free access to food and water. Columbia University confirmed that all *in vivo* experiments were following their IACUC guidelines. Guinea pigs were euthanized with an

intraperitoneal injection of pentobarbital (100 mg/kg). Tracheas were removed and transected into rings containing two cartilaginous rings. The rings were washed five times with phosphate buffer (0.5 M, pH 7.4) to remove any pentobarbital. The epithelium was removed with a cotton swab, and two silk threads were used to suspend the rings in a 4 mL water jacked organ bath (Radnoti Glass Technology). A Grass FT03 force transducer was attached and connected to a computer that controlled and recorded the muscle tension using Acknowledge 7.3.3. software. The organ bath buffer consisted of 118 mM NaCl, 5.6 mM KCl, 0.5 mM $CaCl_2$, 0.2 mM $MgSO_4$, 25 mM $NaHCO_3$, 1.3 mM NaH_2PO_4, 5.6 mM, and 10 μM indomethacin. The solution was continuously bubbled with 5% carbon dioxide and 95% oxygen. Precontraction of the rings was carried out with 10 μM N-vanillylnonanamide (to deplete nonadrenergic, noncholinergic nerves). The bath buffer was replaced, and the resting tension reset to 1.0 g. The tracheal rings were then contracted with two cycles of increasing concentrations of acetylcholine (0.1−100 μM) with buffer exchanges and resetting of the resting tension to 1.0 g in between the cycles. The tracheal rings were then pretreated with 1 μM tetrodotoxin and 10 μM pyrilamine to remove the potential confounding effects on muscle force of endogenous airway nerves and histamine release. Tracheal rings were then contracted with substance P (1 μM) and at the plateau of their increased contractile force, compounds or vehicle (0.1% DMSO) was added to the organ bath. The amount of contractile force remaining at indicated times points was expressed as a percentage of the initial substance P induced contractile force and compared between compounds and vehicle. Experiments were repeated 6−10 times for each compound. Data were analyzed with GraphPad Prism (GraphPad) using two-way ANOVA repeated measures with Bonferroni posttest.

Airway Hyperresponsiveness Assay: Adult female A/J mice were purchased from Jackson Laboratory and housed pathogen-free with a 12-h light and dark cycle. Animals had free access to food and water. All studies were conducted in accordance with institutional guidelines as defined by UWM Institutional Animal Care and Use Committee. Mice were trained once a day for 5 days to become accustomed to the measuring chambers during nebulization and data acquisition. Instrument calibration was carried out before each experiment. sRaw was computed with FinePoint software using parameters recorded for the nasal and thoracic chambers. Compounds dissolved in phosphate buffered saline were nebulized as indicated for each experiment. Methacholine was dissolved in water and nebulized as indicated for each experiment. Nebulizers were calibrated for each measurement. Usually, nebulization occurred for <1 min followed by a 3 min data acquisition and 1 min pause before the next methacholine nebulization. Experiments were repeated 12 times for each compound. Data analysis was carried out with GraphPad Prism (GraphPad) using two-way ANOVA repeated measures with Bonferroni posttest.

2.7.15 Synthetic Methods

Chemicals and solvents were purchased from commercial sources and used without further purification. Reaction progress was monitored by silica gel TLC (Dynamic Adsorbents Inc.) with fluorescence indicator. ^{1}H, ^{13}C, and ^{19}F NMR spectra were obtained on Bruker 500 MHz instrument with the chemical shifts in δ (ppm) reported by reference to the deuterated solvents as an internal standard (IS) DMSO-D_6: δ = 2.50 ppm (^{1}H NMR) and δ = 39.52 ppm (^{13}C NMR) and $CDCl_3$: δ = 7.20 ppm (^{1}H NMR) and δ = 77.00 ppm (^{13}C NMR) (see below for NMR spectra). HRMS spectral data were recorded using a LCMS IT-TOF and LCMS QTOF spectrometers

(Shimadzu). High-performance liquid chromatography (Shimadzu Nexara series HPLC) coupled with a photo diode array detector (PDA, Shimidzu SPD-M30A) and a single quadrupole mass analyzer (LCMS 2020, Shimadzu, Kyoto, Japan) was used for purity analysis (absolute area %). Analytes were separated using a Restek Pinnacle-C18 (4.6 mm × 50 mm, 5 μm particle size) column with gradient elution of water and methanol (0.1% formic acid) at a flow rate of 0.8 mL/min. The purity of all tested compounds is >95%

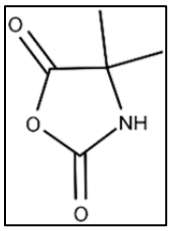

Synthesis of DAW-NCA-10: Boc-Aib-OH (5.51 g, 27.11 mmol) was added to anhydrous ethyl acetate (220 mL), followed by the addition of triphosgene (3.22 g, 10.84 mmol). The solution was stirred until a clear solution was obtained before triethyl amine (4.16 mL, 29.82 mmol) was added dropwise over a period of 15 min during which a white solid formed (TEA-HCl salt). The temperature was kept below 30 °C during the addition of triethyl amine. The solution was stirred at room temperature for 1 h followed by heating to reflux (80 °C) for 20 h. The reaction was cooled to room temperature and the solid was removed by filtration and washed with ethyl acetate. The filtrate was concentrated under reduced pressure to yield a brown residue. The residue was then dissolved in dichloromethane (10 mL) and hexanes was added dropwise (10 mL) over a period of 20 min while stirring. The mixture was allowed to sit at -20 °C for 24 h at which point the product precipitated out of solution. The product was collected by filtration to yield a crystalline white solid (2.31 g, 65.9%): ^{1}H NMR (500 MHz, $CDCl_3$) δ 6.94 (s, 1H), 1.60 (s, 6H); ^{13}C NMR (126 MHz, $CDCl_3$) δ 173.11, 151.73, 60.15, 25.25.

Figure 45: DAW-NCA-10 ^{1}H spectra:

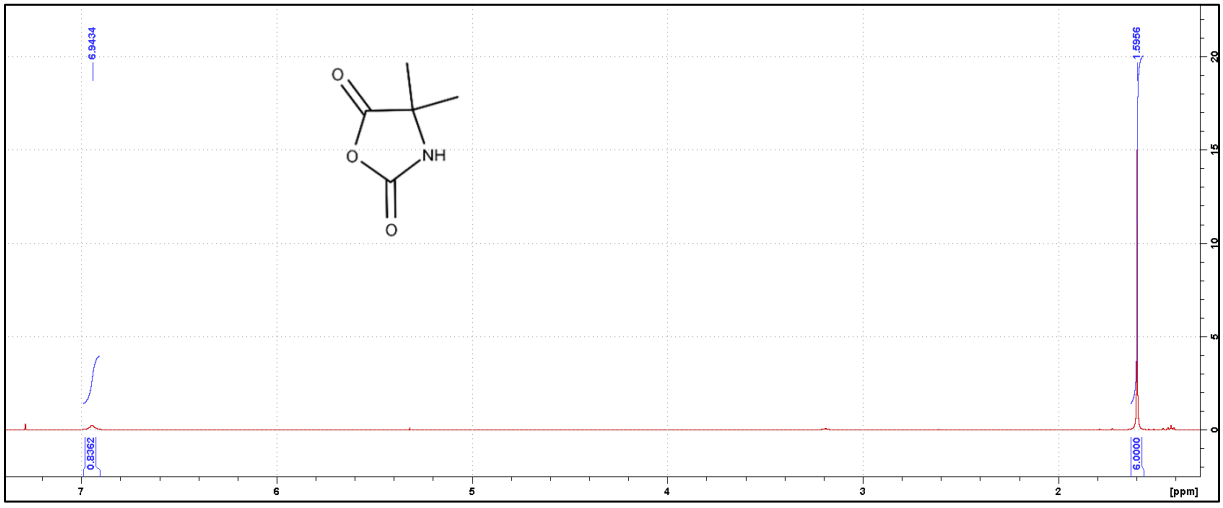

Figure 46: DAW-NCA-10 ^{13}C spectra:

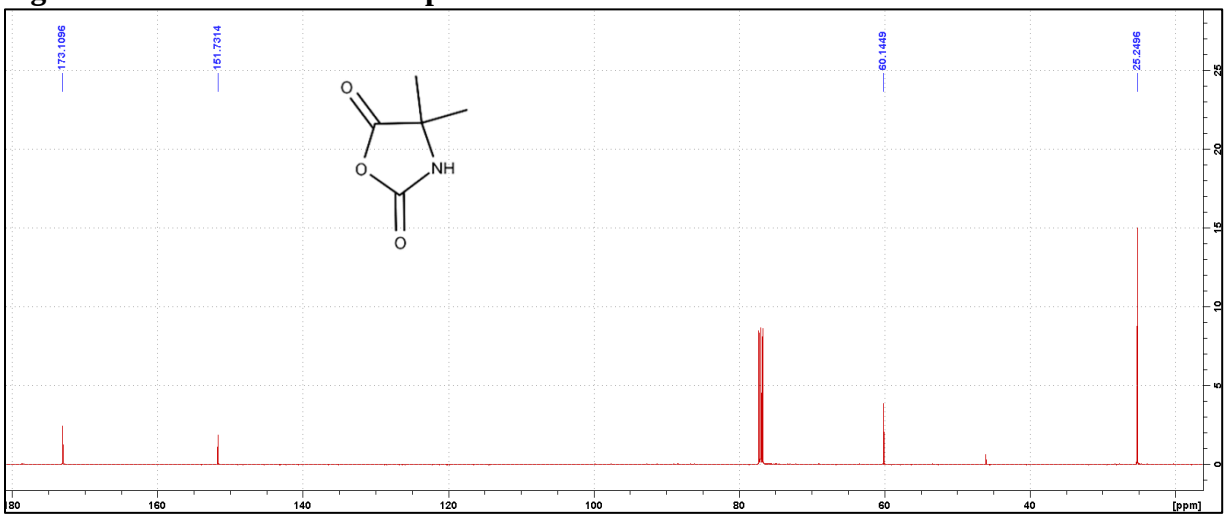

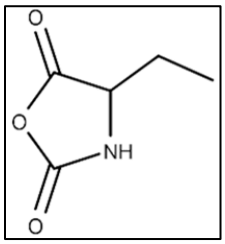

Synthesis of DAW-NCA-70: Boc-DL-Abu-OH (4.00 g, 19.68 mmol) was added to anhydrous ethyl acetate (90 mL), followed by the addition of triphosgene (2.34 g, 7.87 mmol). The solution was stirred until a clear solution was obtained before triethyl amine (3.02 mL, 21.65 mmol) was added dropwise

over a period of 15 min during which a white solid formed (TEA-HCl salt). The temperature was kept below 30 °C during the addition of triethyl amine. The solution was stirred at room temperature for 1 h followed by heating to reflux (80 °C) for 20 h. The reaction was cooled to room temperature and the solid was removed by filtration and washed with ethyl acetate. The filtrate was concentrated under reduced pressure to yield a brown residue. The residue was then dissolved in dichloromethane (10 mL). The mixture was allowed to sit at -20 °C for 24 h at which point the product precipitated out of solution. The product was collected by filtration to yield a crystalline white solid (1.11 g, 43.5%): ^{1}H NMR (500 MHz, $CDCl_3$) δ 6.71 (s, 1H), 4.36-4.34 (dt, *J* = 2.06, 0.75 Hz, 1H), 2.03-1.87 (m, 2H), 1.09-1.06 (t, *J* = 7.45 Hz, 3H); ^{13}C NMR (126 MHz, $CDCl_3$) δ 169.41, 152.81, 58.68, 25.06, 8.81.

Figure 47: DAW-NCA-70 ^{1}H spectra:

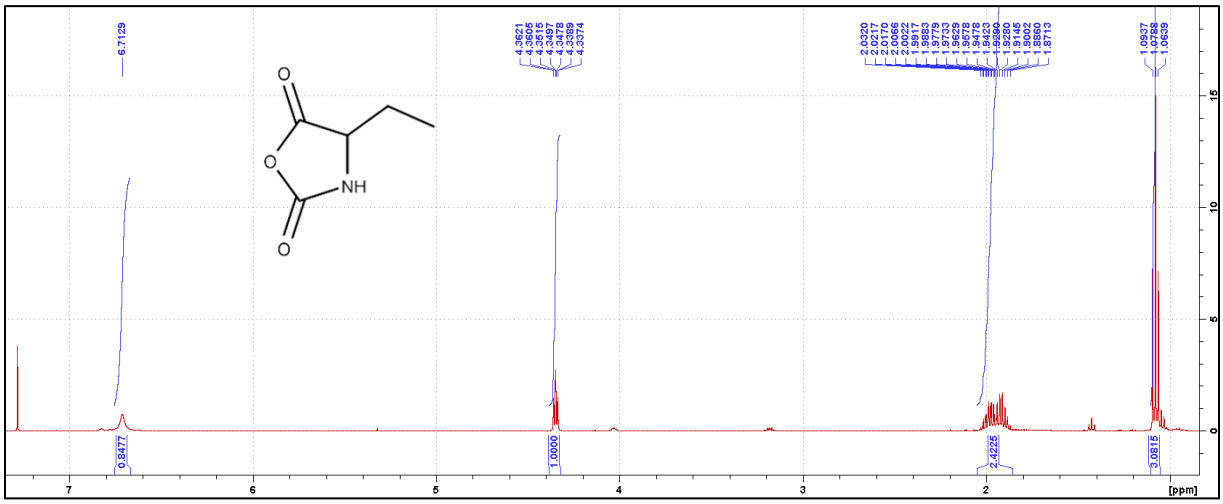

Figure 48: DAW-NCA-70 ^{13}C spectra:

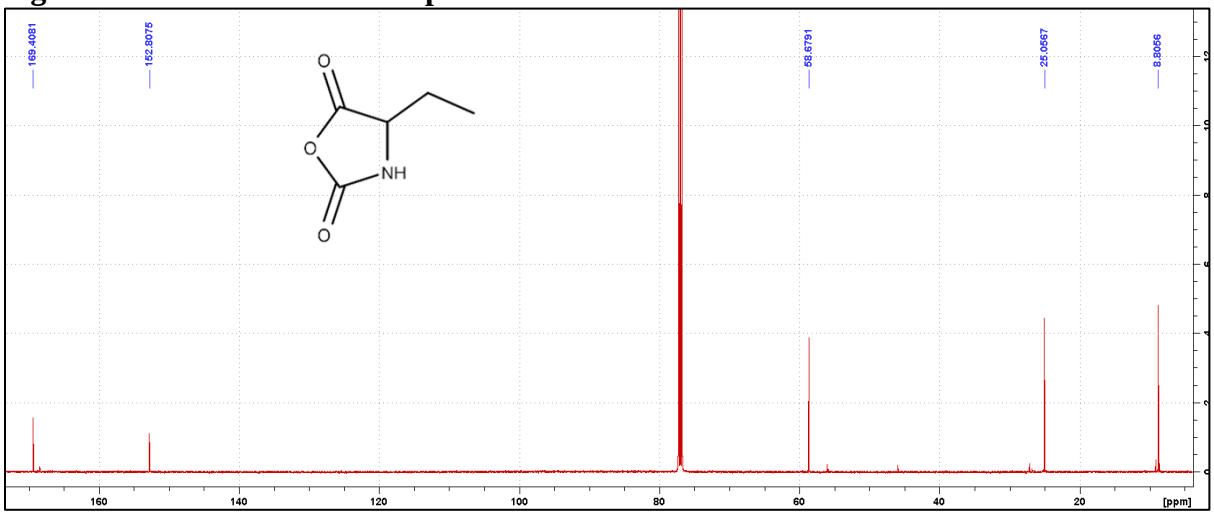

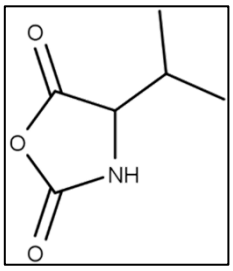

Synthesis of DAW-NCA-20: Boc-DL-Valine (10.03 g, 46.17 mmol) was added to anhydrous ethyl acetate (220 mL), followed by the addition of triphosgene (5.48 g, 18.47 mmol). The solution was stirred until a clear solution was obtained before triethyl amine (7.08 mL, 50.79 mmol) was added dropwise over a period of 15 min during which a white solid formed (TEA-HCl salt). The temperature was kept below 30 °C during the addition of triethyl amine. The solution was stirred at room temperature for 1 h followed by heating to reflux (80 °C) for 20 h. The reaction was cooled to room temperature and the solid was removed by filtration and washed with ethyl acetate. The filtrate was concentrated under reduced pressure to yield a brown residue. The residue was then dissolved in dichloromethane (20 mL) and hexanes was added dropwise (20 mL) over a period of 20 min while stirring. The mixture was allowed to sit at -20 °C for 24 h at which point the product precipitated out of solution. The product was collected by filtration to yield a crystalline white solid (4.54 g, 68.7%): ^{1}H NMR (500 MHz, $CDCl_3$) δ 6.96 (s, 1H), 4.25-4.24 (dd, *J* = 1.72, 0.90

Hz, 1H), 2.30-2.24 (m, 1H), 1.11-1.10 (d, *J* = 6.95 Hz, 3H), 1.06-1.04 (d, *J* = 6.85 Hz, 3H); ^{13}C NMR (126 MHz, $CDCl_3$) δ 168.79, 153.40, 63.11, 30.79, 18.24, 16.62.

Figure 49: DAW-NCA-20 ^{1}H spectra:

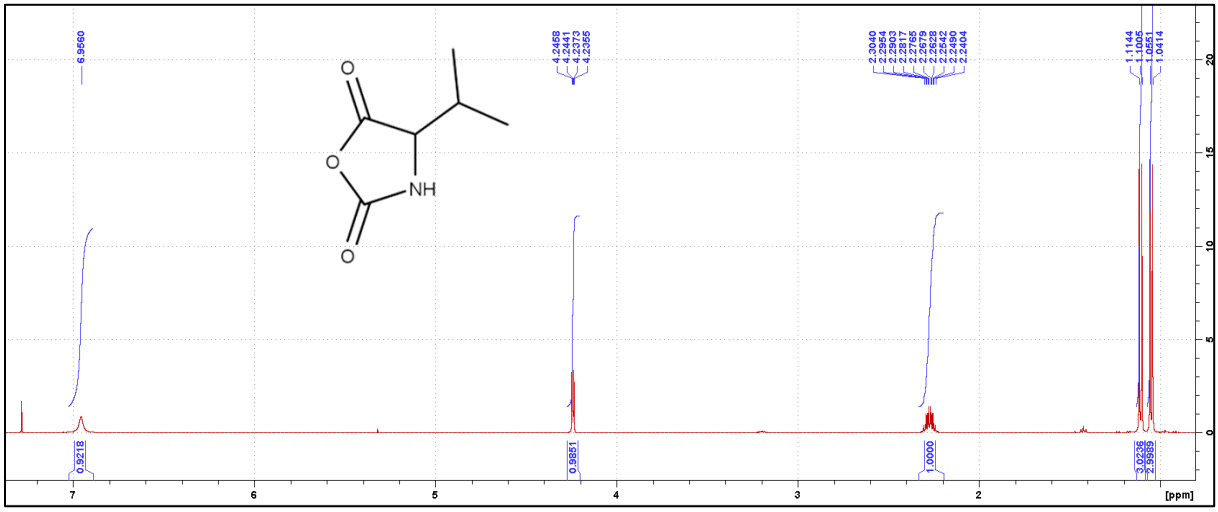

Figure 50: DAW-NCA-20 ^{13}C spectra:

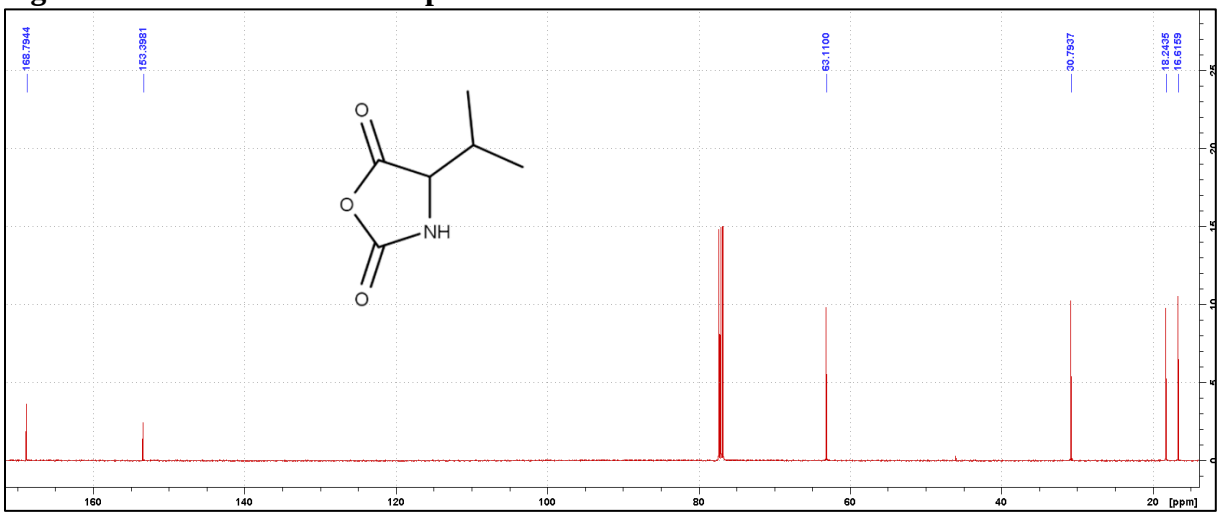

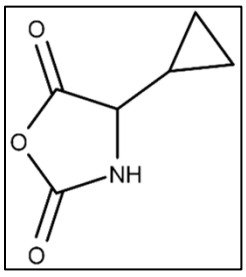

Synthesis of DAW-NCA-80: Boc-DL-cyclopropylglycine (4.01 g, 18.64 mmol) was added to anhydrous ethyl acetate (90 mL), followed by the addition of triphosgene (2.21 g, 7.46 mmol). The solution was stirred until a clear solution was obtained before triethyl amine (2.86 mL, 20.50 mmol) was

added dropwise over a period of 15 min during which a white solid formed (TEA-HCl salt). The temperature was kept below 30 °C during the addition of triethyl amine. The solution was stirred at room temperature for 1 h followed by heating to reflux (80 °C) for 20 h. The reaction was cooled to room temperature and the solid was removed by filtration and washed with ethyl acetate. The filtrate was concentrated under reduced pressure to yield a brown residue. The crude product was used for the subsequent reaction: ^{1}H NMR (500 MHz, $CDCl_3$) δ 6.08 (s, 1H), 3.91-3.89 (d, *J* = 7.54 Hz, 1H), 1.25-1.45 (m, 1H), 0.82 (m, 1H), 0.73 (m, 1H), 0.61-0.60 (m, 1H), 0.47-0.46 (m, 1H); ^{13}C NMR (126 MHz, $CDCl_3$) δ 168.45, 151.86, 60.82, 12.56, 2.31, 2.11.

Figure 51: DAW-NCA-80 ^{1}H spectra:

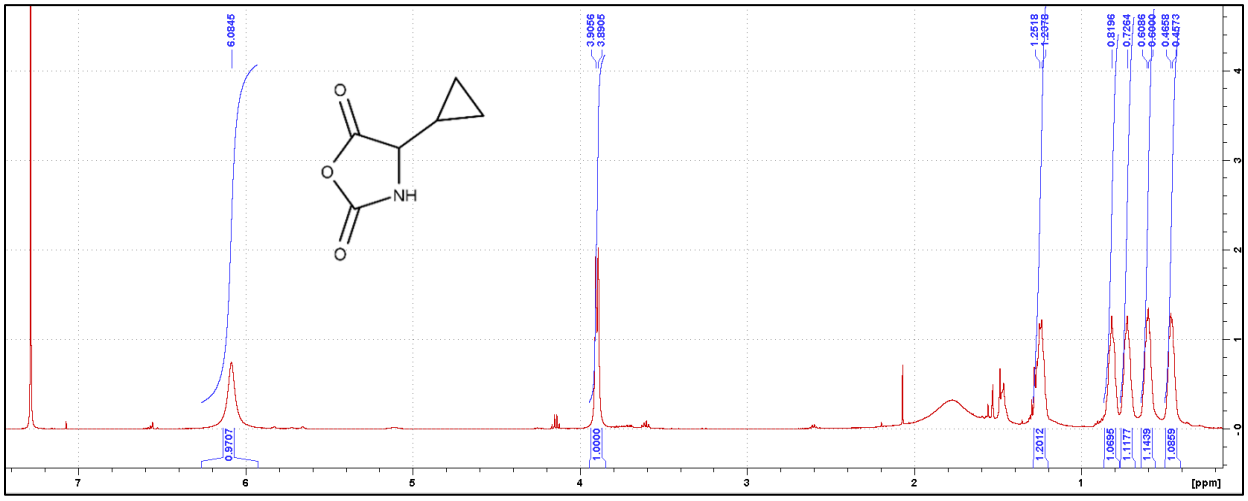

Figure 52: DAW-NCA-80 ^{13}C spectra:

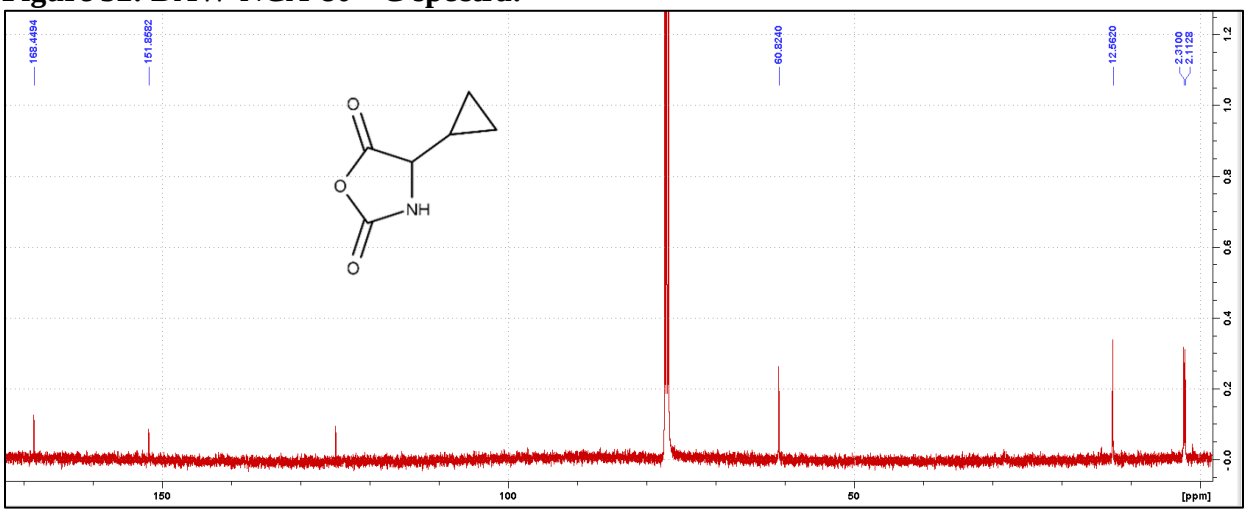

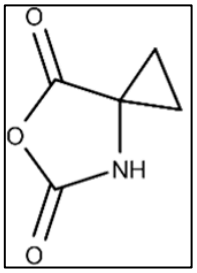

Synthesis of DAW-NCA-30: 1-(Boc-amino)cyclopropanecarboxylic acid (8.07 g, 40.11 mmol) was added to anhydrous ethyl acetate (600 mL), followed by the addition of triphosgene (4.75 g, 16.04 mmol). The solution was stirred until a clear solution was obtained before triethyl amine (6.15 mL, 44.12 mmol) was added dropwise over a period of 15 min during which a white solid formed (TEA-HCl salt). The temperature was kept below 30 °C during the addition of triethyl amine. The solution was stirred at room temperature for 1 h followed by heating to reflux (80 °C) for 20 h. The reaction was cooled to room temperature and the solid was removed by filtration and washed with ethyl acetate. The filtrate was concentrated under reduced pressure to yield a brown residue. The crude product was used for the subsequent reaction: ^{1}H NMR (500 MHz, d_6-DMSO) δ 9.19 (s, 1H), 1.43-1.37 (m, 4H); ^{13}C NMR (126 MHz, d_6-DMSO) δ 173.06, 151.96, 41.19, 14.52.

Figure 53: DAW-NCA-30 ^{1}H spectra:

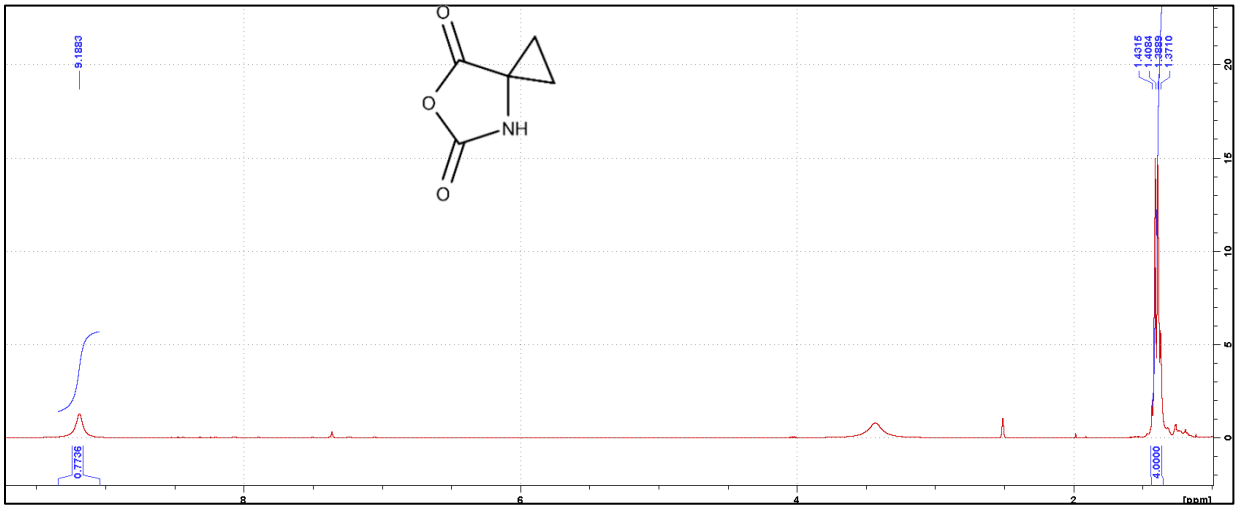

Figure 54: DAW-NCA-30 ^{13}C spectra:

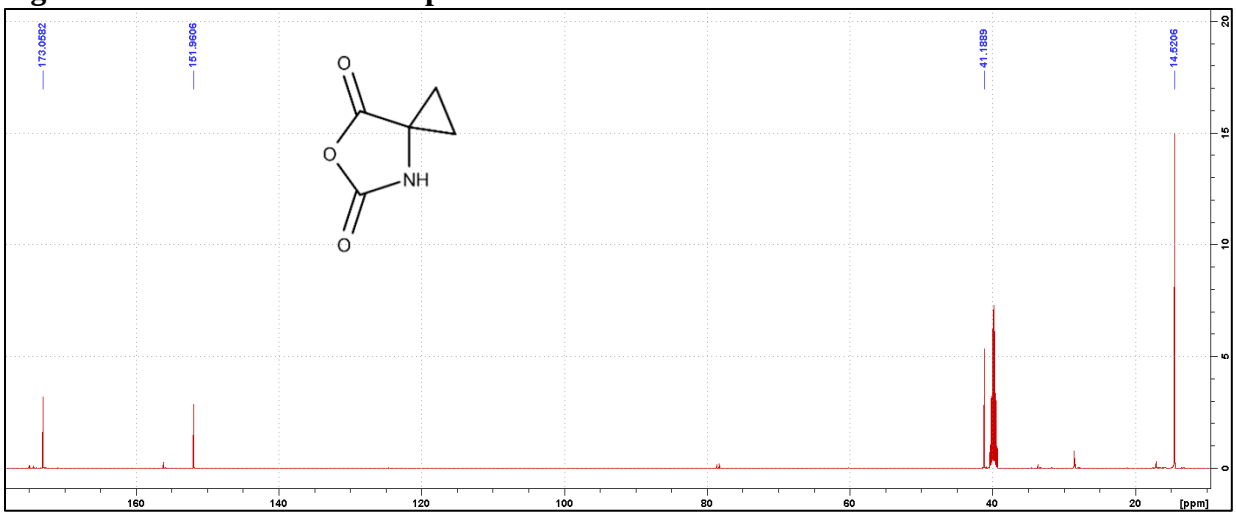

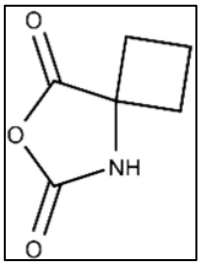

Synthesis of DAW-NCA-40: N-tert-Butoxycarbonyl-1-amino cyclobutane carboxylic acid (8.01 g, 37.22 mmol) was added to anhydrous ethyl acetate (250 mL), followed by the addition of triphosgene (4.42 g, 14.89 mmol). The solution was stirred until a clear solution was obtained before triethyl amine (5.71 mL, 40.94 mmol) was added dropwise over a period of 15 min during which a white solid formed (TEA-HCl salt). The temperature was kept below 30 °C during the addition of triethyl amine. The

solution was stirred at room temperature for 1 h followed by heating to reflux (80 °C) for 20 h. The reaction was cooled to room temperature and the solid was removed by filtration and washed with ethyl acetate. The filtrate was concentrated under reduced pressure to yield a brown residue. The residue was then dissolved in dichloromethane (20 mL). The mixture was allowed to sit at -20 °C for 24 h at which point the product precipitated out of solution. The product was collected by filtration to yield a crystalline white solid (2.53 g, 48.2%): ^{1}H NMR (500 MHz, $CDCl_3$) δ 7.24 (s, 1H), 2.72-2.67 (m, 2H), 2.55-2.48 (m, 2H), 2.25-2.15 (m, 1H), 1.96-1.88 (m, 1H); ^{13}C NMR (126 MHz, $CDCl_3$) δ 172.91, 151.89, 61.42, 33.36, 13.53.

Figure 55: DAW-NCA-40 ^{1}H spectra:

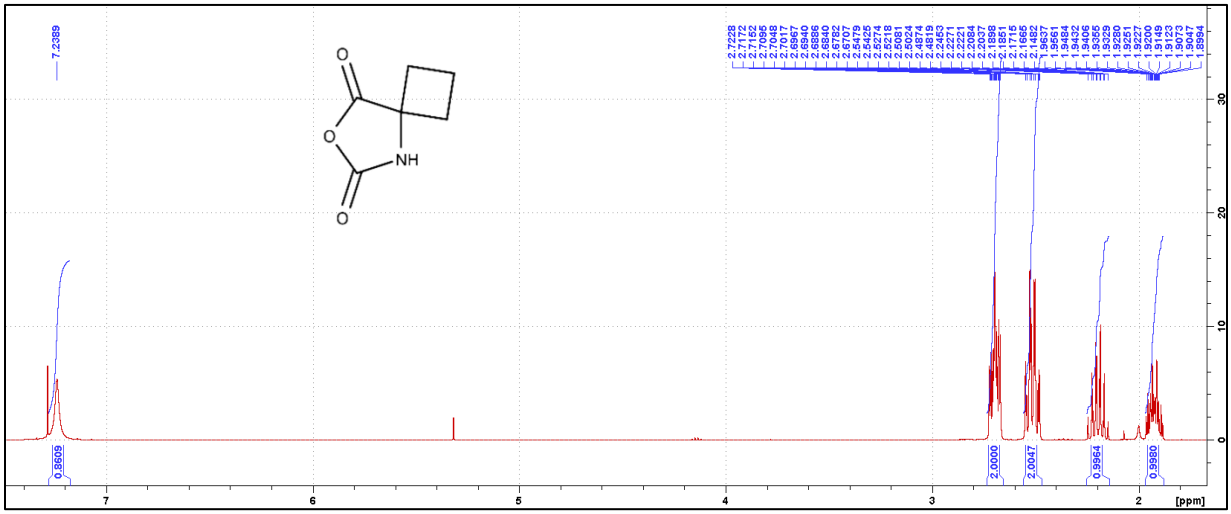

Figure 56: DAW-NCA-40 ^{13}C spectra:

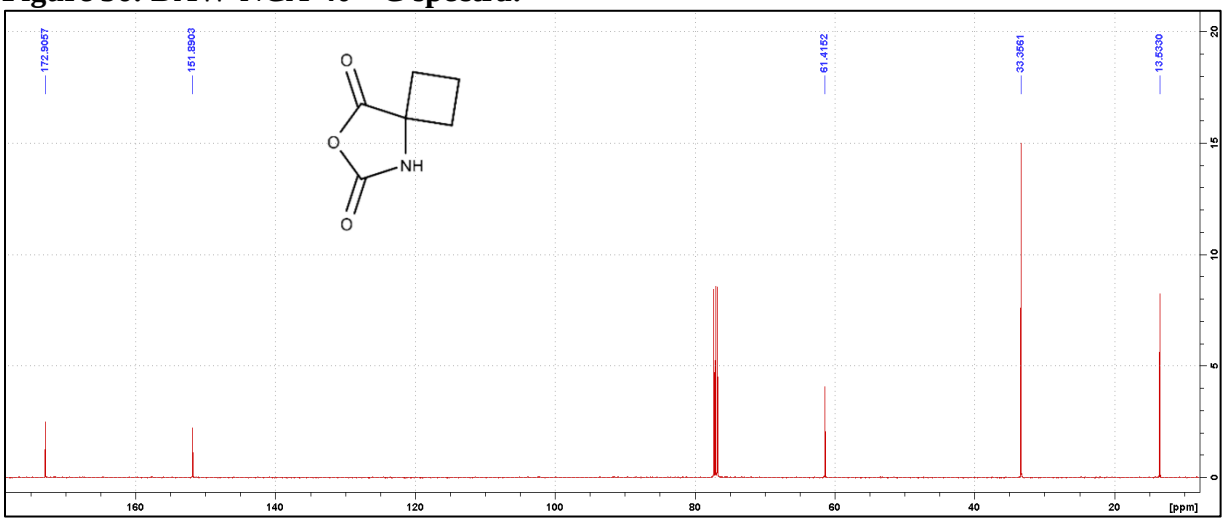

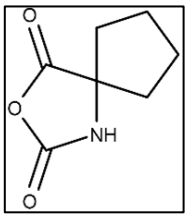

Synthesis of DAW-NCA-50: Boc-1-aminocyclopentane-1-carboxylic acid (12.17 g, 53.08 mmol) was added to anhydrous ethyl acetate (273 mL), followed by the addition of triphosgene (6.30 g, 21.23 mmol). The solution was stirred until a clear solution was obtained before triethyl amine (8.14 mL, 58.39 mmol) was added dropwise over a period of 15 min during which a white solid formed (TEA-HCl salt). The temperature was kept below 30 °C during the addition of triethyl amine. The solution was stirred at room temperature for 1 h followed by heating to reflux (80 °C) for 20 h. The reaction was cooled to room temperature and the solid was removed by filtration and washed with ethyl acetate. The filtrate was concentrated under reduced pressure to yield a brown residue. The residue was then dissolved in dichloromethane (30 mL). The mixture was allowed to sit at -20 °C for 24 h at which point the product precipitated out of solution. The product was collected by filtration to yield a crystalline white solid (5.46 g, 66.4%): ^{1}H NMR (500 MHz, $CDCl_3$) δ 7.10 (s, 1H), 2.22-2.17 (m, 2H), 1.92-1.82 (m, 4H), 1.79-1.76 (m, 2H); ^{13}C NMR (126 MHz, $CDCl_3$) δ 173.98, 152.45, 68.82, 38.42, 25.00.

Figure 57: DAW-NCA-50 ^{1}H spectra:

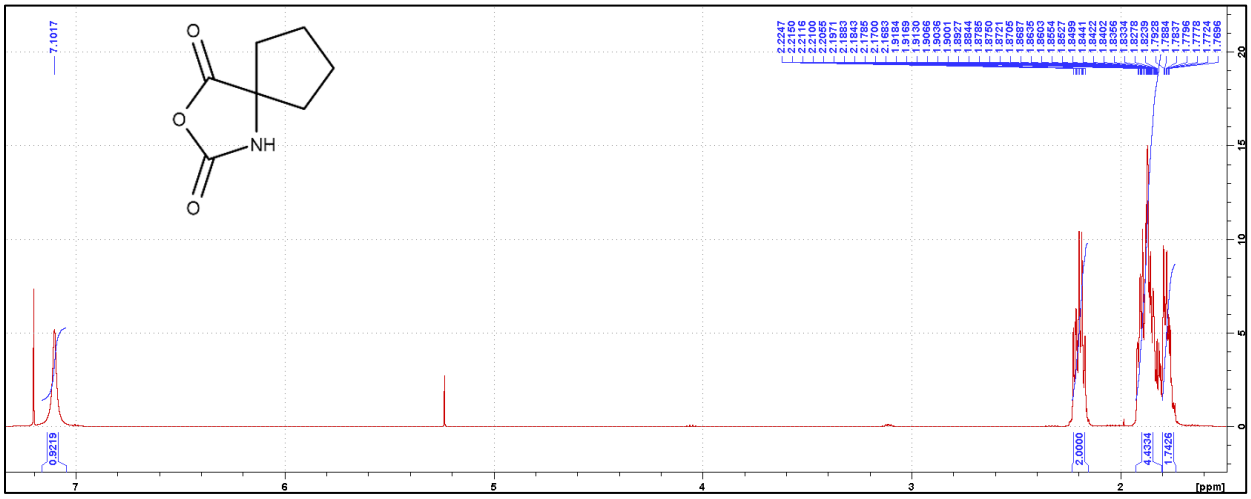

Figure 58: DAW-NCA-50 ^{13}C spectra:

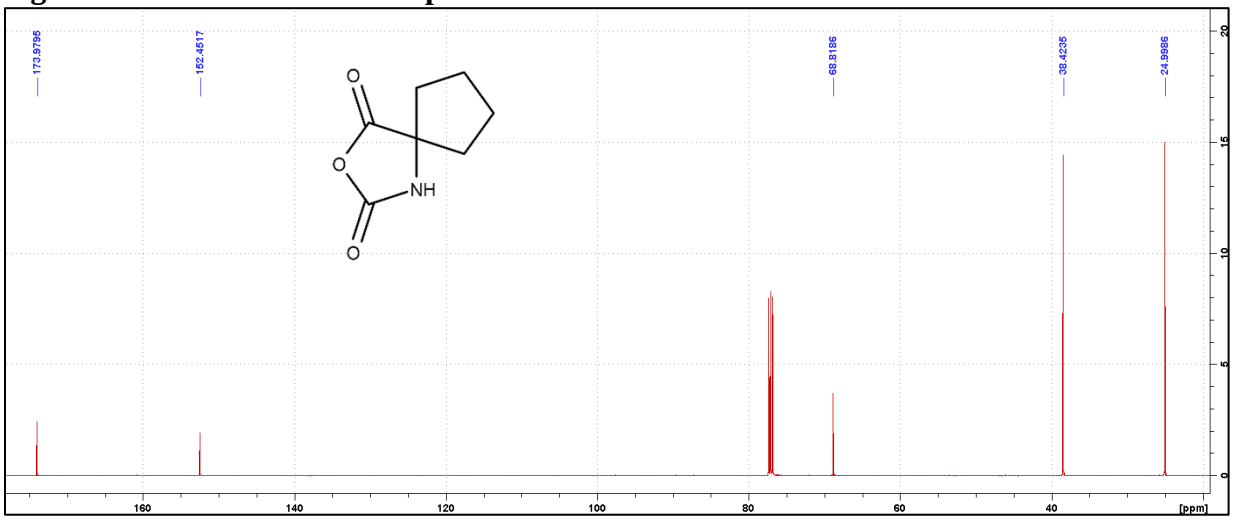

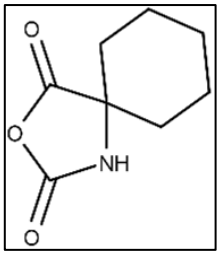

Synthesis of DAW-NCA-60: Boc-1-aminocyclohexane-1-carboxylic acid (5.01 g, 20.59 mmol) was added to anhydrous ethyl acetate (250 mL), followed by the addition of triphosgene (2.44 g, 8.24 mmol). The solution was stirred until a clear solution was obtained before triethyl amine (3.16 mL, 22.65 mol) was added dropwise over a period of 15 min during which a white solid formed (TEA-HCl salt). The temperature was kept below 30 °C during the addition of triethyl amine. The solution was

stirred at room temperature for 1 h followed by heating to reflux (80 °C) for 20 h. The reaction was cooled to room temperature and the solid was removed by filtration and washed with ethyl acetate. The filtrate was concentrated under reduced pressure to yield a brown residue. The residue was then dissolved in dichloromethane (20 mL) and the mixture was allowed to sit at -20°C for 24 h at which point the product precipitated out of solution. The product was collected by filtration and washed with 30% DCM:Hex to yield a crystalline white solid (1.73 g, 49.7%): ^{1}H NMR (500 MHz, $CDCl_3$) δ 7.57, (s, 1H), 1.90-1.79 (m, 4H), 1.74-1.71 (m, 2H), 1.63-1.63 (m, 1H), 1.45-1.33 (m, 3H); ^{13}C NMR (126 MHz, $CDCl_3$) δ 172.23, 152.72, 63.18, 33.87, 24.27, 21.42.

Figure 59: DAW-NCA-60 ^{1}H spectra:

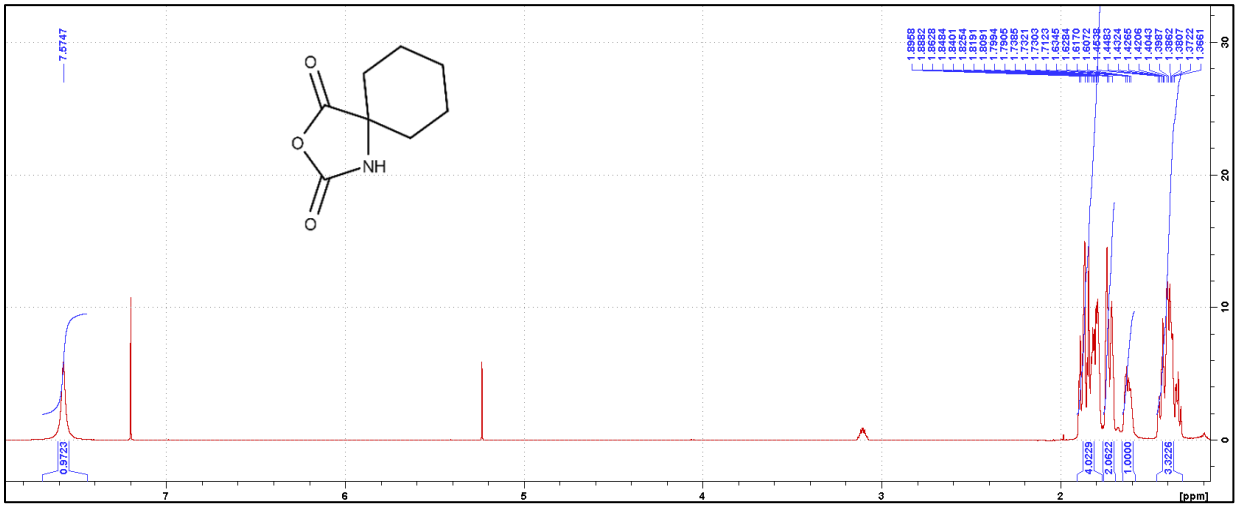

Figure 60: DAW-NCA-60 ^{13}C spectra:

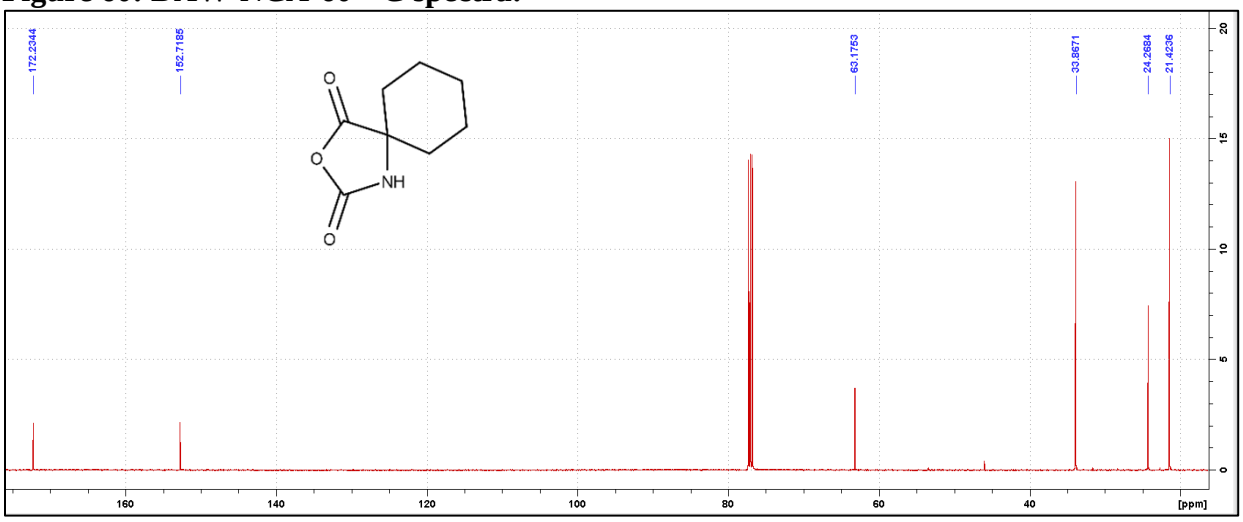

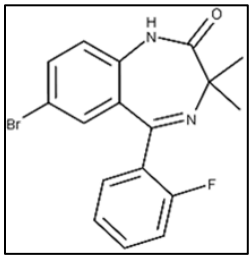

Synthesis of DAW-I-10: 2-Amino-5-bromo-2′-fluorobenzophenone (3.0 g, 10.20 mmol) was added to anhydrous toluene (100 mL), followed by the addition of trifluoroacetic acid (1.56 mL, 20.40 mmol) dropwise over a period of 10 min, and the mixture was allowed to stir at room temperature for 30 min. 4,4-Dimethyloxazolidine-2,5-dione (1.98 g, 15.30mmol) was added portion wise and the reaction was heated to 50 °C for 24 h. After the majority of the starting material had been consumed by TLC (50% EtOAc:Hex), triethylamine (2.99 mL, 21.42 mmol) was added dropwise over a period of 15 min at which point fuming was observed in the reaction. The reaction was then heated to 100 °C for 24 h at which point disappearance of the intermediate was observed via TLC (50% EtOAc:Hex). Upon cooling to room temperature, the solvent was removed under reduced pressure and the residue was dissolved in ethyl acetate (120 mL). The organic layer was washed with 5% aqueous sodium bicarbonate (120 mL), followed by 10% aqueous NaCl (120 mL). The organic layer was then dried with $MgSO_4$ and the solvent was removed under reduced pressure. The residue was stripped with 10% EtOAc:Heptane (50 mL, 2x) followed by a trituration in 10% EtOAc:Heptane (80 mL) at 60 °C for 4 h. The product was collected by filtration to yield a light

yellow solid (2.67 g, 72.3%): ^{1}H NMR (500 MHz, $CDCl_3$) δ 9.51 (s, 1H), 7.47-4.45 (dd, *J* = 3.62, 2.25 Hz, 1H), 7.44-7.41 (dt, *J* = 3.34, 1.75 Hz, 1H), 7.38-7.33 (m, 1H), 7.19-7.18 (m, 1H), 7.17-7.14 (dt, *J* = 3.23, 1.10 Hz, 1H), 7.01-6.97 (m, 1H), 6.96-6.94 (d, *J* = 8.6 Hz, 1H), 1.41 (s, 6H); ^{13}C NMR (126 MHz, $CDCl_3$) δ 174.61 (s), 162.68 (s), 160.28 (d, $^{1}J_{CF}$ = 250.70 Hz), 136.28 (s), 134.80 (s), 132.18 (d, $^{3}J_{CF}$ = 1.13 Hz), 131.70 (d, $^{2}J_{CF}$ = 8.24 Hz), 131.48 (d, $^{3}J_{CF}$ = 2.55 Hz), 129.87 (d, $^{4}J_{CF}$ = 0.89 Hz), 128.76 (d, $^{2}J_{CF}$ = 13.22 Hz), 124.46 (d, $^{3}J_{CF}$ = 3.55 Hz), 121.67 (s), 116.23 (d, $^{2}J_{CF}$ = 21.49 Hz), 115.74 (s), 63.73 (s), 25.13 (s); ^{19}F NMR (471 MHz, $CDCl_3$) δ -113.18; HRMS (ESI/IT-TOF): *m/z* $[M + H]^+$ calcd for $C_{17}H_{14}BrFN_2O$: 361.0346; found: 361.0312; HPLC Purity: 98.95%.

Figure 61: DAW-I-10 ^{1}H spectra:

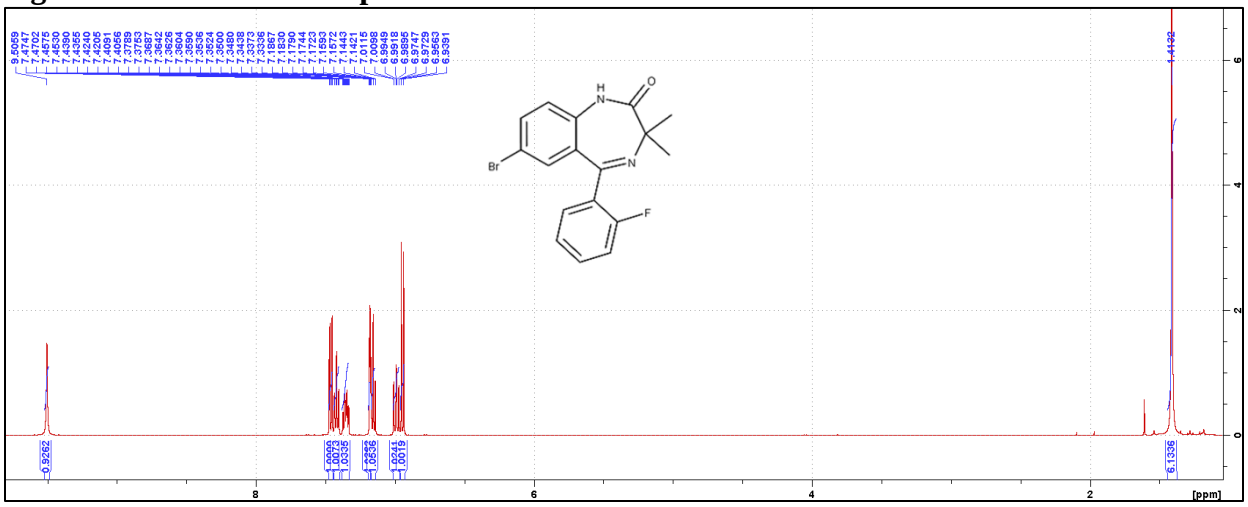

Figure 62: DAW-I-10 ^{13}C spectra:

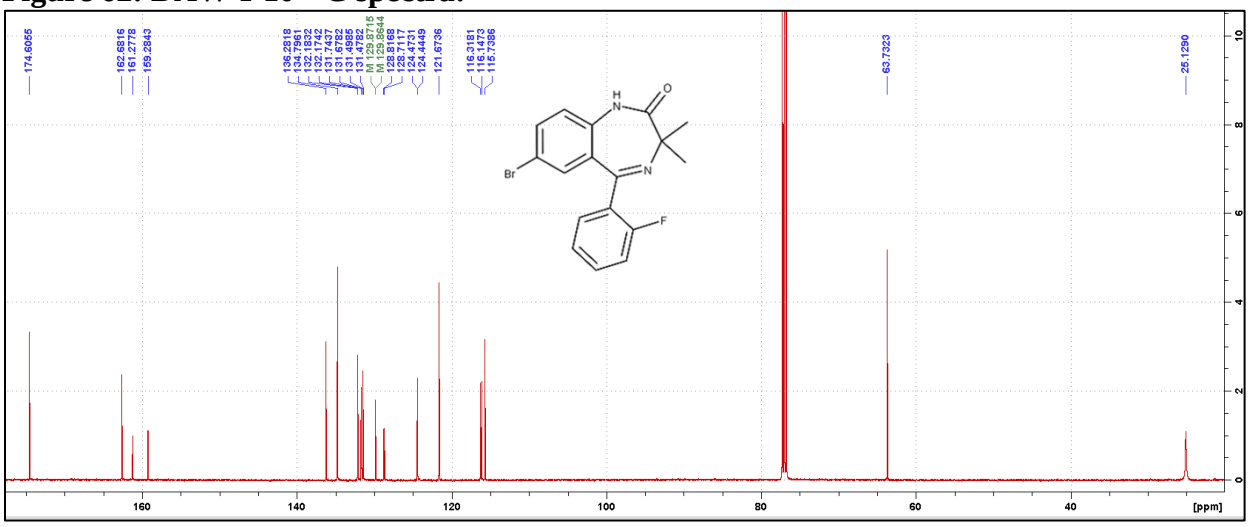

Figure 63: DAW-I-10 ^{19}F spectra:

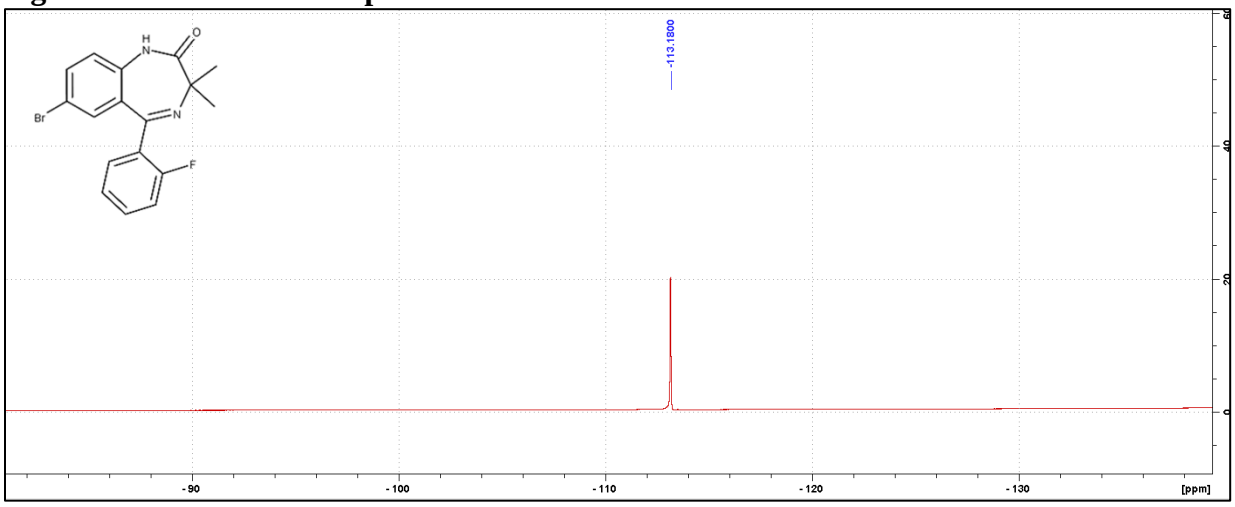

Figure 64: DAW-I-10 HPLC UV Chromatograph:

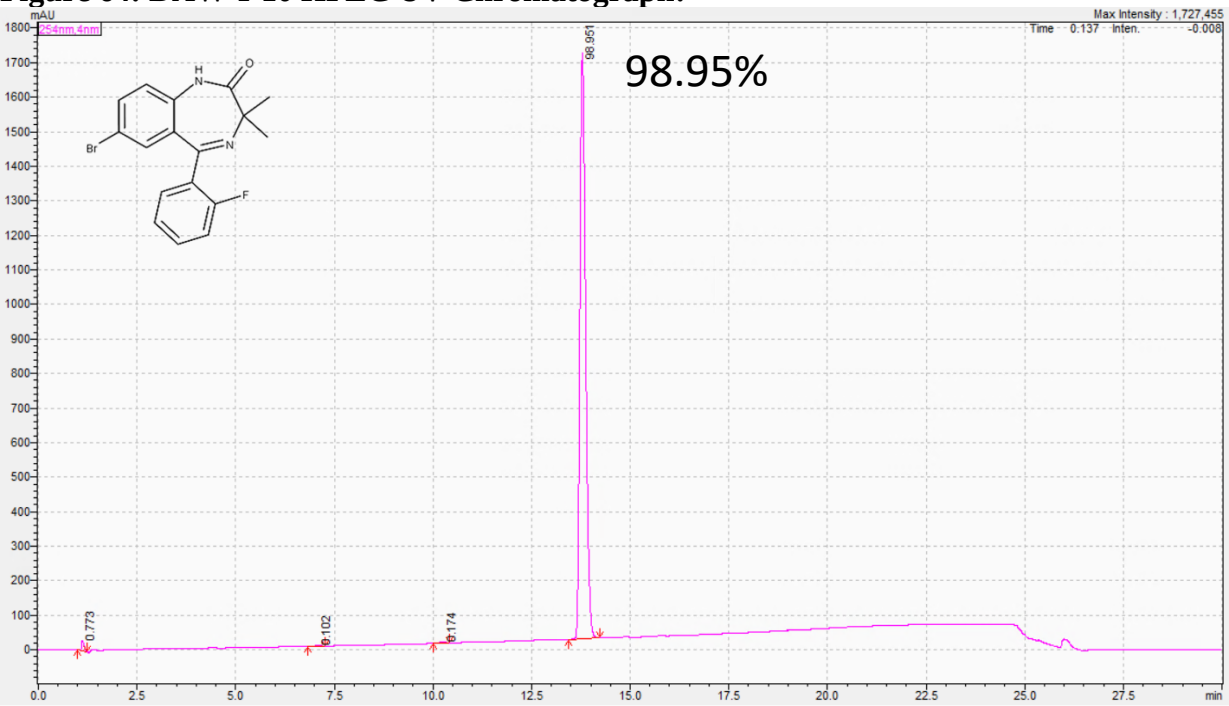

Figure 65: DAW-I-10 HRMS:

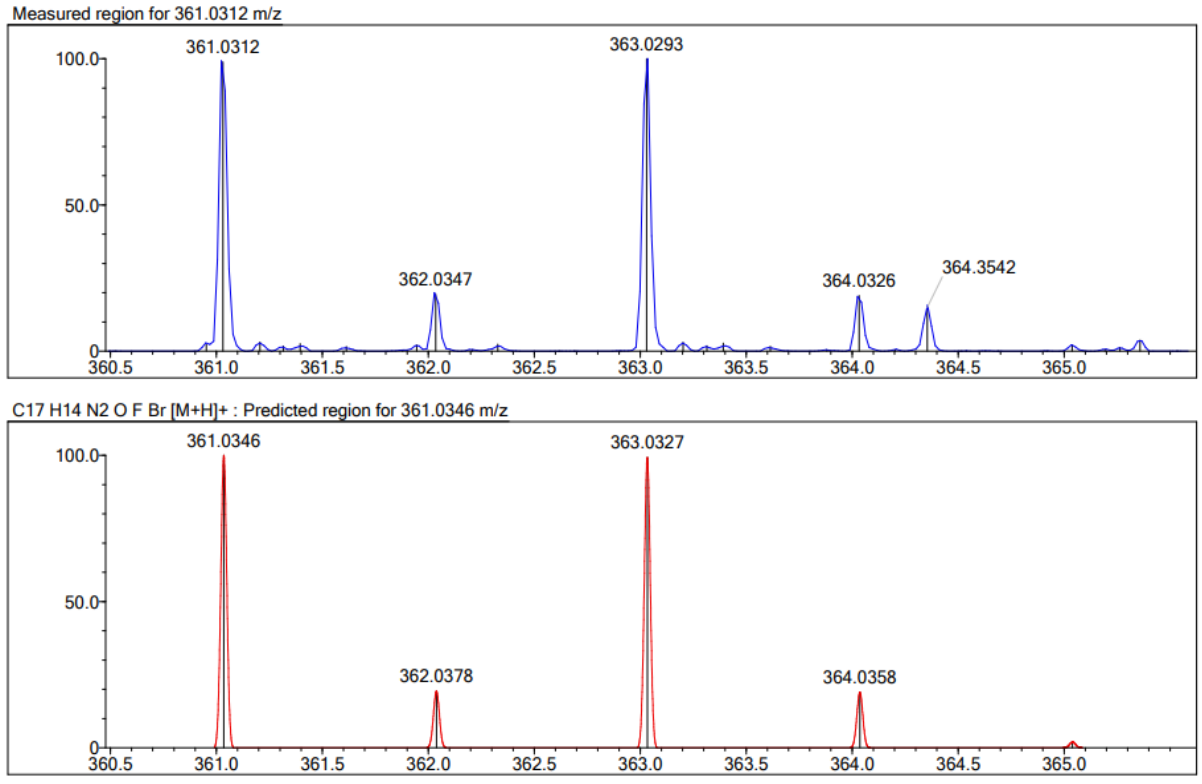

Rank	Score	Formula (M)	Ion	Meas. m/z	Pred. m/z	Df. (mDa)	Df. (ppm)	Iso	DBE
1	37.83	C17 H14 N2 O F Br	[M+H]+	361.0312	361.0346	-3.4	-9.42	82.59	11.0

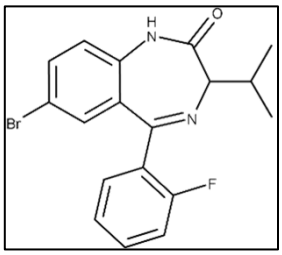

Synthesis of DAW-I-20: 2-Amino-5-bromo-2′-fluorobenzophenone (2.50 g, 8.50 mmol) was added to anhydrous toluene (100 mL), followed by the addition of trifluoroacetic acid (1.30 mL, 17.0 mmol) dropwise over a period of 10 min, and the mixture was allowed to stir at room temperature for 30 min. 4-Isopropyloxazolidine-2,5-dione (1.83 g, 12.75 mmol) was added portion wise and the reaction was heated to 50 °C for 24 h. After the majority of the starting material had been consumed by TLC (50% EtOAc:Hex), triethylamine (2.49 mL, 17.85 mmol) was added dropwise over a period of 15 min at which point fuming was observed in the reaction. The reaction was then heated to 100 °C for 24 h at which point disappearance of the intermediate was observed via TLC (50% EtOAc:Hex). Upon cooling to room temperature, the solvent was removed under reduced pressure and the residue was dissolved in ethyl acetate (100 mL). The organic layer was washed with 5% aqueous sodium bicarbonate (100 mL), followed by 10% aqueous NaCl (100 mL). The organic layer was then dried with $MgSO_4$ and the solvent was removed under reduced pressure. The residue was stripped with 10% EtOAc:Heptane (50 mL, 2x) followed by a trituration in 10% EtOAc:Heptane (80 mL) at 60 °C for 4 h. The product was collected by filtration to yield a light yellow solid (1.74 g, 54.0%): ^{1}H NMR (500 MHz, $CDCl_3$) δ 9.34 (s, 1H), 7.62-7.60 (dd, *J* = 3.60, 2.20 Hz, 1H), 7.59-7.56 (dt, *J* = 3.35, 1.70 Hz, 1H), 7.49-7.45 (m, 1H), 7.39-7.38 (d, *J* = 2.10 Hz, 1H), 7.27-7.24 (dt, *J* = 3.20, 0.95, 1H), 7.11-7.07 (m, 2H), 3.16 (d, *J* = 9.35 Hz, 1H), 2.80-2.73 (m, 1H), 1.23-1.21 (d, *J* = 6.70 Hz, 3H), 1.11-1.10 (d, *J* = 6.50 Hz, 3H); ^{13}C NMR (126 MHz, $CDCl_3$) δ 170.35 (s), 164.12 (s), 160.56 (d, $^{1}J_{CF}$ = 252.38 Hz), 136.52 (s), 134.65 (s), 132.21 (s), 132.14 (s), 131.70 (d, $^{4}J_{CF}$ = 1.33 Hz), 130.06 (s), 127.20 (d, $^{2}J_{CF}$ = 12.16 Hz), 124.37 (d, $^{3}J_{CF}$ = 3.57 Hz), 122.91 (s), 116.51 (s), 116.35 (d, $^{2}J_{CF}$ = 21.66 Hz), 69.50 (s), 28.97 (s), 20.28 (s), 18.99

(s); ^{19}F NMR (471 MHz, $CDCl_3$) δ -112.44, 112.45; HRMS (ESI/Q-TOF): *m/z* $[M + H]^+$ calcd for $C_{18}H_{16}BrFN_2O$: 375.05028; found: 375.05154; HPLC Purity: 99.99%.

Figure 66: DAW-I-20 ^1H spectra:

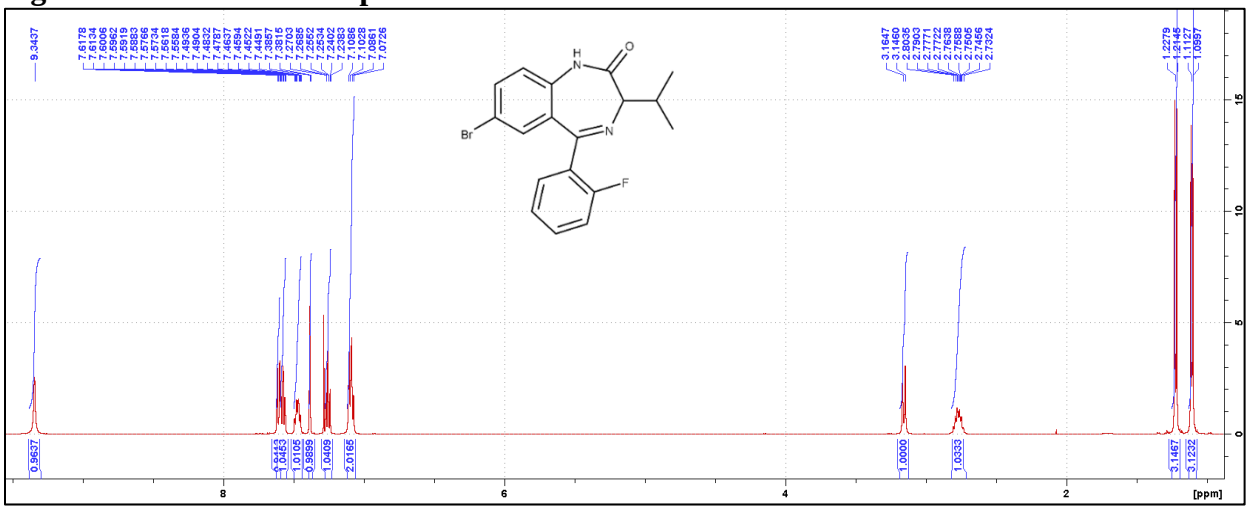

Figure 67: DAW-I-20 ^{13}C spectra:

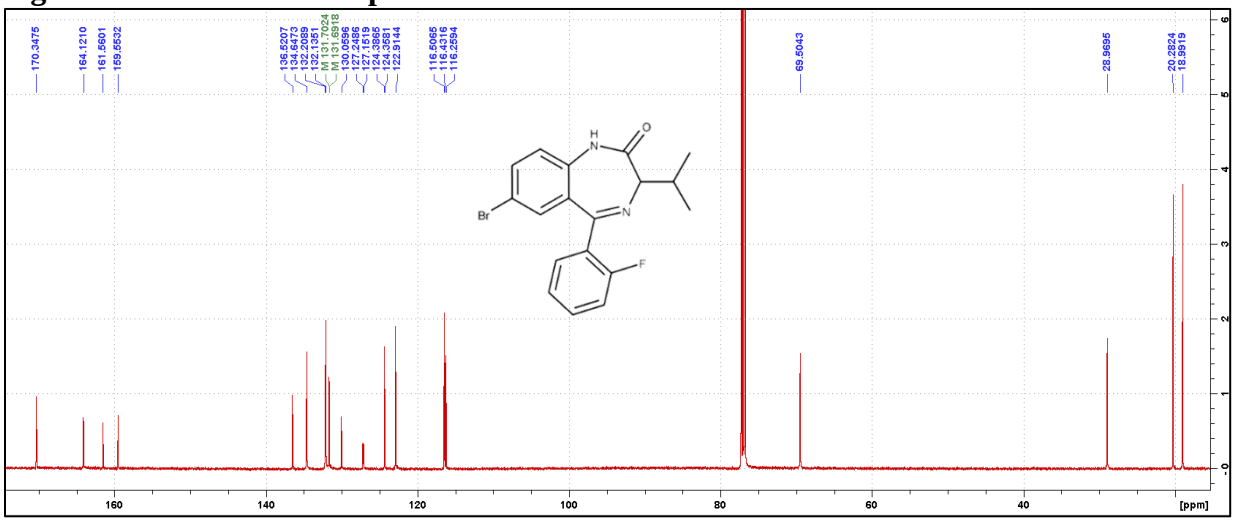

Figure 68: DAW-I-20 ^{19}F spectra:

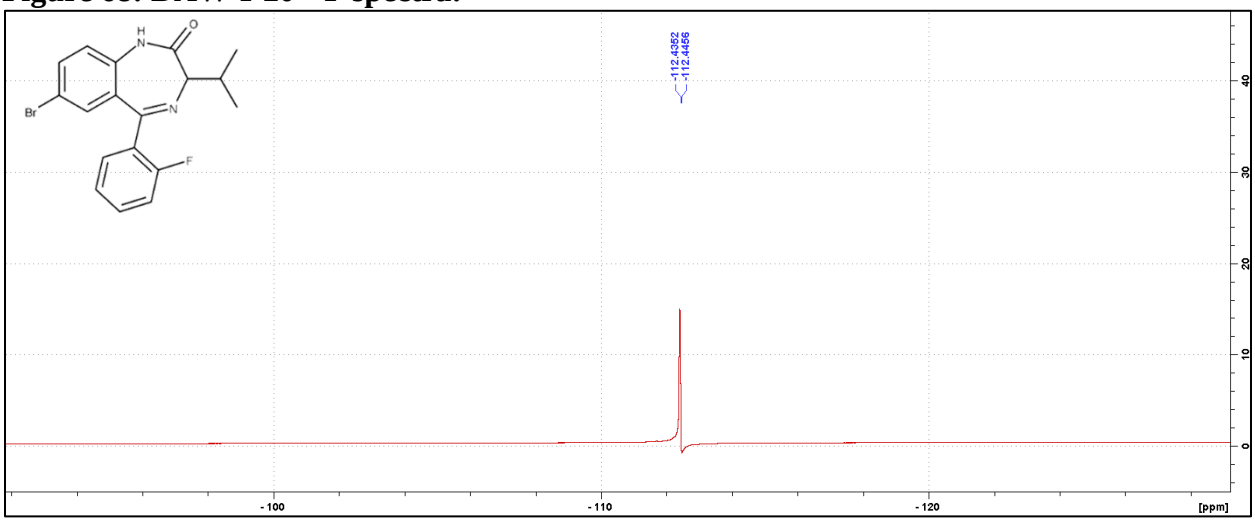

Figure 69: DAW-I-20 HPLC UV Chromatograph:

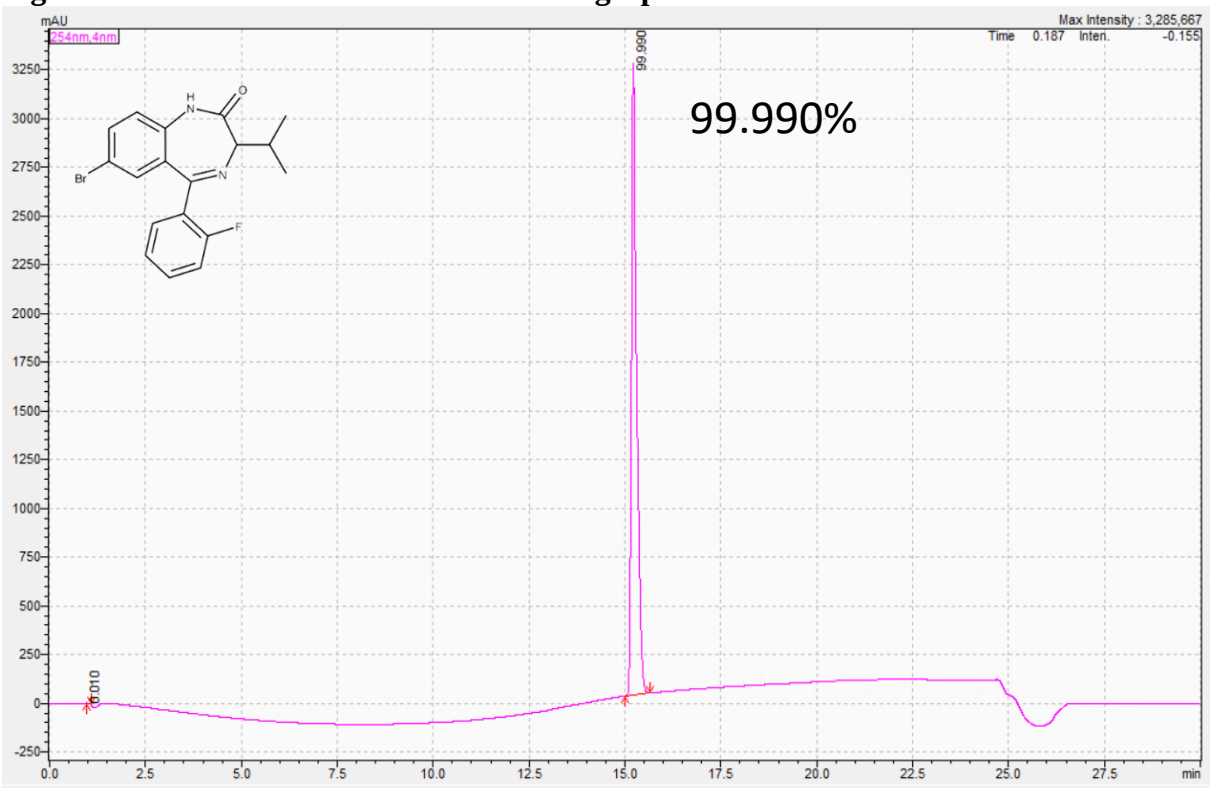

Figure 70: DAW-I-20 HRMS:

Score	Pred. (M)	Pred. m/z	Meas. m/z	Diff. (mDa)	Formulae (M)	Ion	Diff. (ppm)	Iso Score	DBE
32.00	374.04300	375.05028	375.05154	1.26	C18 H16 N2 O F Br	[M+H]+	3.360	27.06	11.0

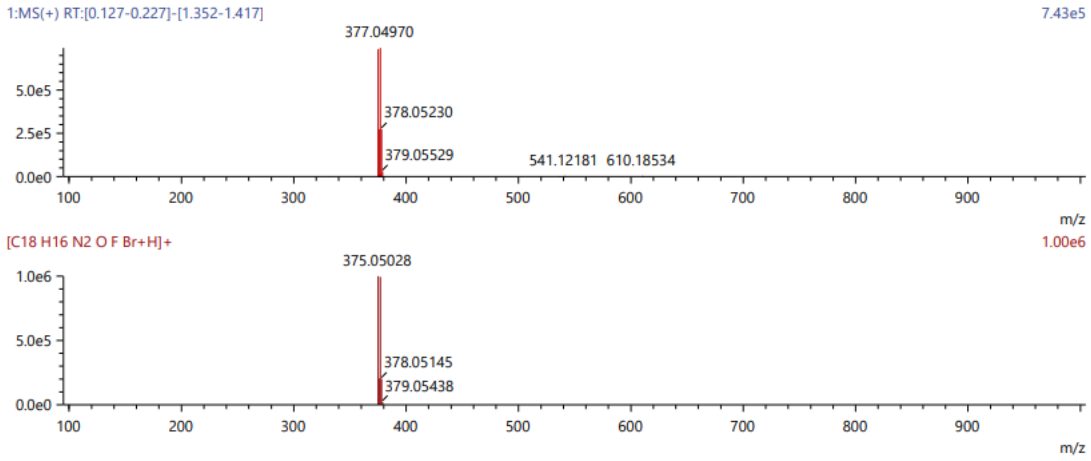

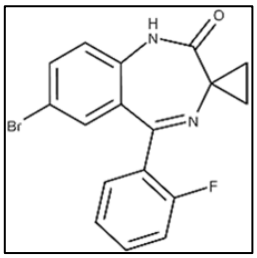

Synthesis of DAW-I-30: 2-Amino-5-bromo-2′-fluorobenzophenone (8.97 g, 30.50 mmol) was added to anhydrous toluene (242 mL), followed by the addition of trifluoroacetic acid (4.67 mL, 61.00mmol) dropwise over a period of 10 min, and the mixture was allowed to stir at room temperature for 30 min. Crude 6-oxa-4-azaspiro[2.4]heptane-5,7-dione (5.81g, 45.75 mmol) was added portion wise and the reaction was heated to 50 °C for 24 h. After the majority of the starting material had been consumed by TLC (50% EtOAc:Hex), triethylamine (8.93 mL, 64.05 mmol) was added dropwise over a period of 15 min at which point fuming was observed in the reaction. The reaction was then heated to 100 °C for 24 h at which point disappearance of the intermediate was observed via TLC (50% EtOAc:Hex). Upon cooling to room temperature, the solvent was removed under reduced pressure and the residue was dissolved in ethyl acetate (500 mL). The organic layer was washed with 5% aqueous sodium bicarbonate (500 mL), followed by 10% aqueous NaCl (500 mL). The organic layer was then dried with $MgSO_4$ and the solvent was removed under reduced pressure. The residue was stripped with 10% EtOAc:Heptane (100 mL, 2x) followed by a trituration in 10%

EtOAc:Heptane (200 mL) at 60 °C for 4 h. The product was collected by filtration to yield a light yellow solid (5.24 g, 47.8%): ^{1}H NMR (500 MHz, d_6-DMSO) δ 10.71 (s, 1H), 7.73-7.70 (dd, *J* = 3.67, 2.30 Hz, 1H), 7.60-7.55 (m, 1H), 7.54-7.51 (dt, *J* = 3.39, 1.75 Hz, 1H), 7.35-7.32 (dt, *J* = 3.21, 1.00 Hz, 1H), 7.29-7.25 (m, 1H), 7.20-7.18 (d, *J* = 8.70 Hz, 1H), 7.14-7.13 (d, *J* = 2.15 Hz, 1H), 1.20-1.18 (q, *J* = 4.03 Hz, 2H), 0.88-0.86 (q, *J* = 4.10 Hz, 2H); ^{13}C NMR (126 MHz, d_6-DMSO) δ 172.19 (s), 169.15 (s), 160.02 (d, $^{1}J_{CF}$ = 248.47 Hz), 138.01 (s), 134.98 (s), 132.94 (d, $^{3}J_{CF}$ = 8.35 Hz), 132.06 (d, $^{4}J_{CF}$ = 2.31 Hz), 131.42 (s), 130.67 (s), 127.66 (d, $^{2}J_{CF}$ = 12.64 Hz), 125.12 (d, $^{3}J_{CF}$ = 3.23 Hz), 123.55 (s), 116.45 (d, $^{2}J_{CF}$ = 21.35 Hz), 114.87 (s), 47.12 (s), 12.70 (s); ^{19}F NMR (471 MHz, d_6-DMSO) δ -113.85 - -113.90 (qu, *J* = 5.94 Hz); HRMS (ESI/Q-TOF): *m/z* $[M + H]^{+}$ calcd for $C_{17}H_{12}BrFN_2O$: 359.01898; found: 359.01997; HPLC Purity: 98.45%.

Figure 71: DAW-I-30 ^{1}H spectra:

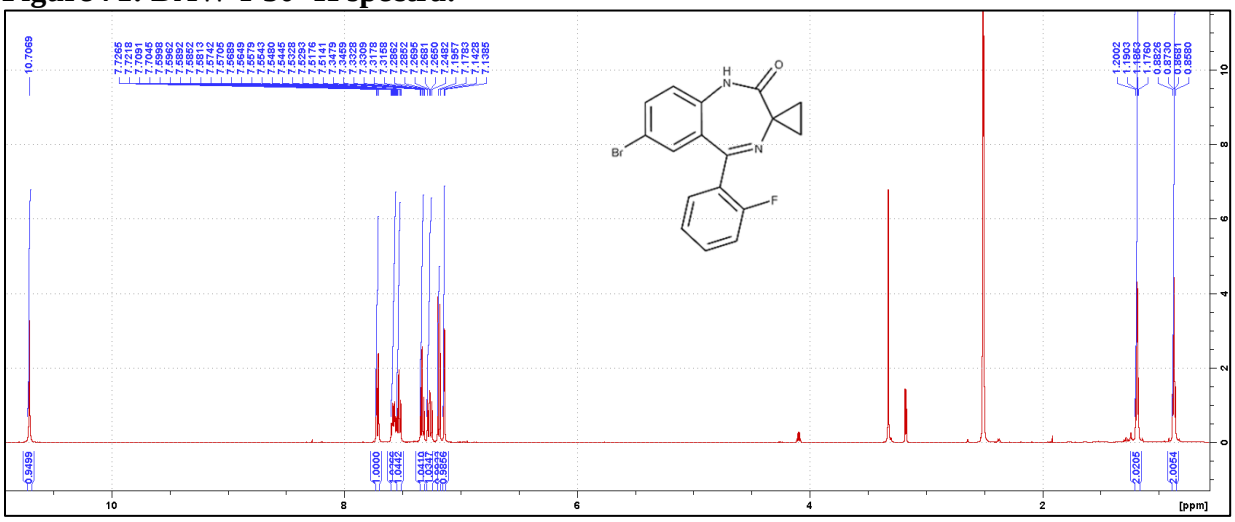

Figure 72: DAW-I-30 ^{13}C spectra:

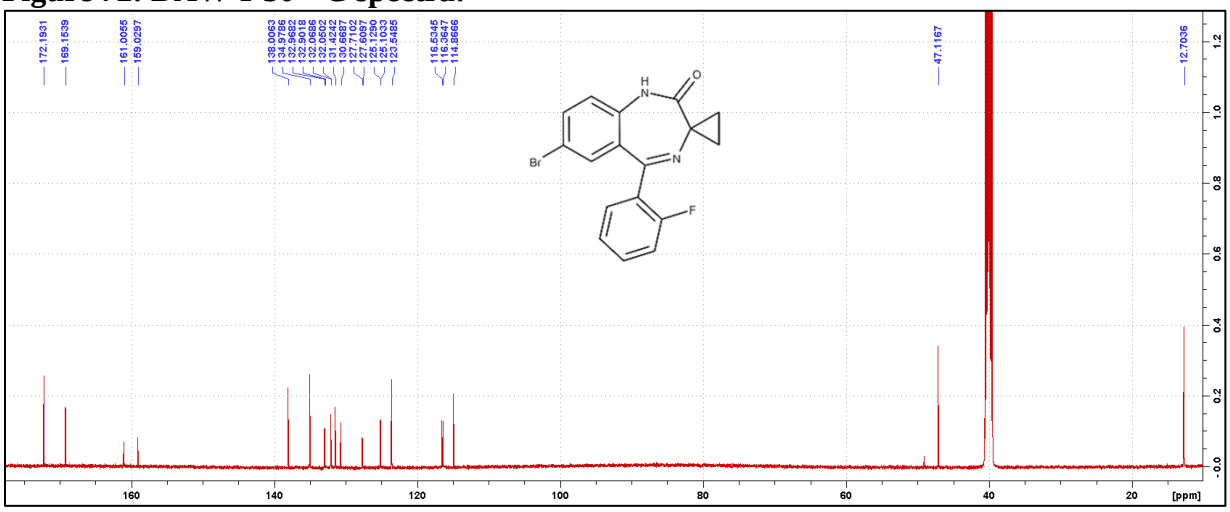

Figure 73: DAW-I-30 ^{19}F spectra:

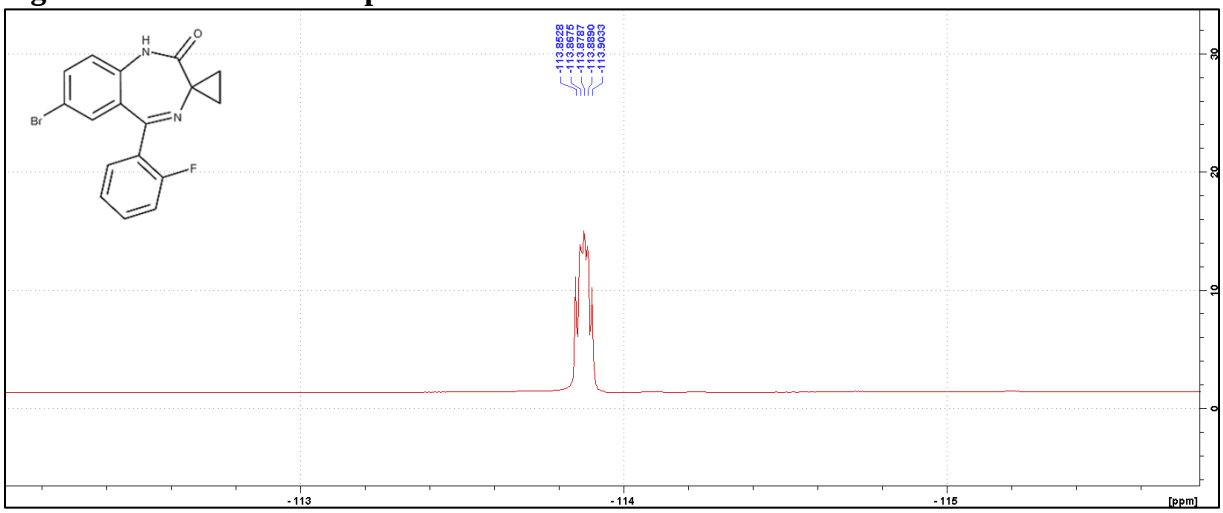

Figure 74: DAW-I-30 HPLC UV Chromatograph:

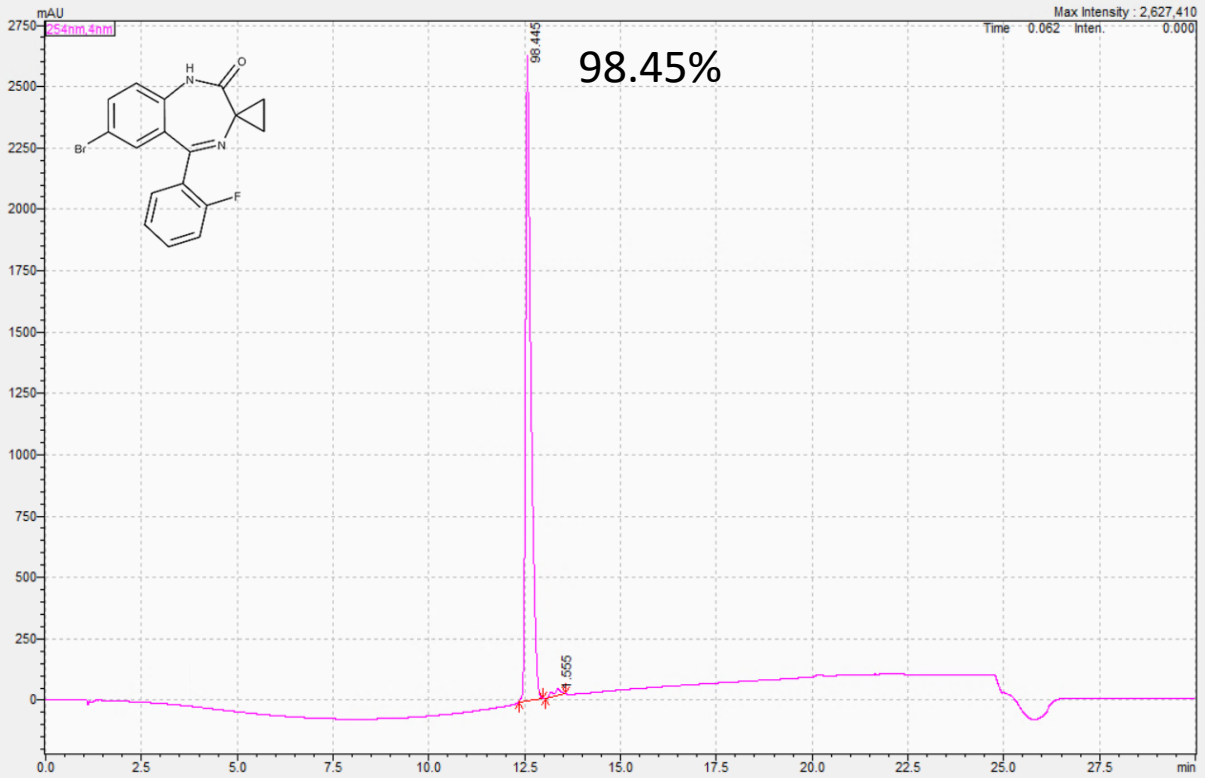

Figure 75: DAW-I-30 HRMS:

Score	Pred. (M)	Pred. m/z	Meas. m/z	Diff. (mDa)	Formulae (M)	Ion	Diff. (ppm)	Iso Score	DBE
52.25	358.01170	359.01898	359.01997	0.99	C17 H12 N2 O F Br	[M+H]+	2.758	48.82	12.0

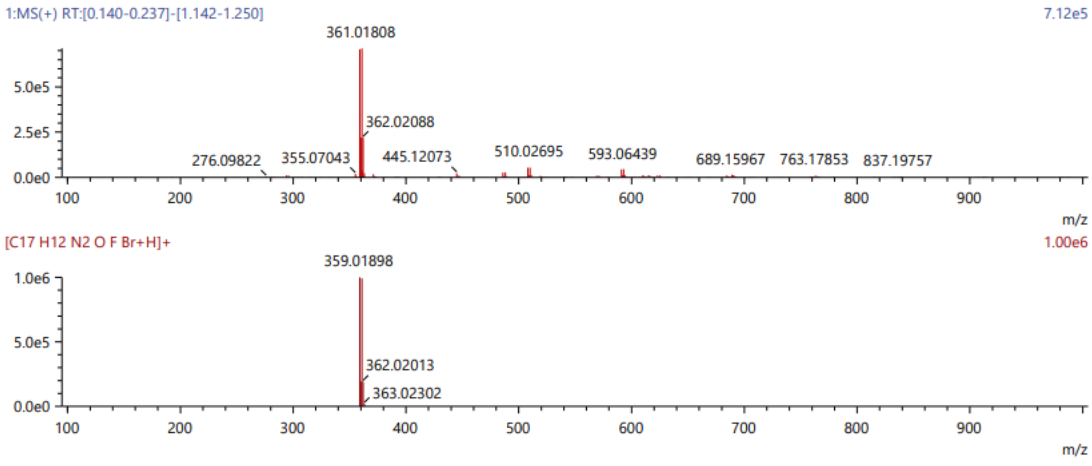

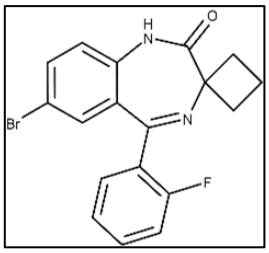

Synthesis of DAW-I-40: 2-Amino-5-bromo-2′-fluorobenzophenone (2.00 g, 6.80 mmol) was added to anhydrous toluene (70 mL), followed by the addition of trifluoroacetic acid (1.04 mL, 13.60 mmol) dropwise over a period of 10 min, and the mixture was allowed to stir at room temperature for 30 min. 7-oxa-5-azaspiro[3.4]octane-6,8-dione (1.44 g, 10.20 mmol) was added portion wise and the reaction was heated to 50 °C for 24 h. After the majority of the starting material had been consumed by TLC (50% EtOAc:Hex), triethylamine (1.99 mL, 14.28 mmol) was added dropwise over a period of 15 min at which point fuming was observed in the reaction. The reaction was then heated to 100 °C for 24 h at which point disappearance of the intermediate was observed via TLC (50% EtOAc:Hex). Upon cooling to room temperature, the solvent was removed under reduced pressure and the residue was dissolved in ethyl acetate (60 mL). The organic layer was washed with 5% aqueous sodium bicarbonate (60 mL), followed by 10% aqueous NaCl (60 mL). The organic layer was then dried with $MgSO_4$ and the solvent was removed under reduced pressure. The residue was stripped with 10% EtOAc:Heptane (20 mL, 2x) followed by a trituration in 10% EtOAc:Heptane (35 mL) at 60 °C for 4 h. The product was collected by filtration to yield a light yellow solid (2.16 g, 85.0%): ^{1}H NMR (500 MHz, $CDCl_3$) -25°C δ 10.18 (s, 1H), 7.56-7.53 (m, 1H), 7.51-7.49 (dd, *J* = 3.57, 2.10 Hz, 1H), 7.43-7.39 (m, 1H), 7.24-7.23 (d, *J* = 2.10 Hz, 1H), 7.22-7.19 (m, 1H), 7.05-7.00 (m, 1H), 3.27-3.24 (m, 1H), 2.64-2.63 (m, 1H), 2.00 (m, 1H), 1.73 (m, 3H); ^{13}C NMR (126 MHz, $CDCl_3$) -25°C δ 174.00 (s), 162.86 (s), 160.36 (d, $^{1}J_{CF}$ = 251.72 Hz), 136.60 (s), 134.98 (s), 132.37 (d, $^{3}J_{CF}$ = 8.25 Hz), 131.82 (s), 131.68 (s), 130.52 (s), 127.32 (d, $^{2}J_{CF}$ = 12.30 Hz), 124.66 (d, $^{3}J_{CF}$ = 3.03 Hz), 122.50 (s), 116.55 (s), 116.39 (d, $^{4}J_{CF}$ = 0.89 Hz), 116.18 (s), 67.36 (s), 33.99 (s), 32.01 (s), 14.72 (s); ^{19}F NMR (471 MHz, $CDCl_3$) -25°C δ -112.41;

HRMS (ESI/IT-TOF): *m/z* $[M + H]^+$ calcd for $C_{18}H_{14}BrFN_2O$: 373.0346; found: 373.0308; HPLC Purity: 98.27%.

Figure 76: DAW-I-40 ^{1}H spectra:

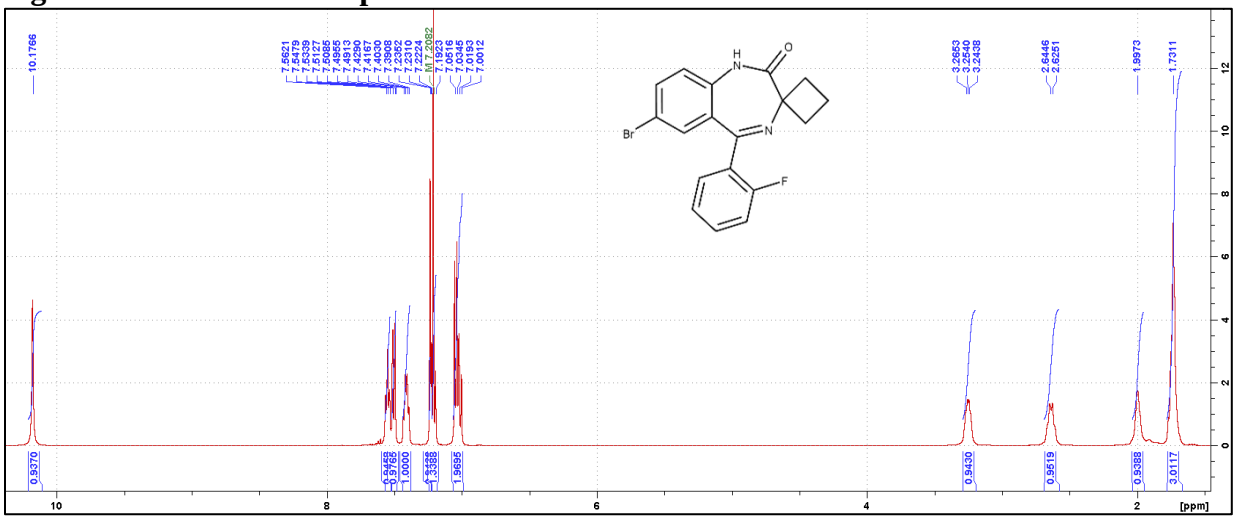

Figure 77: DAW-I-40 ^{13}C spectra:

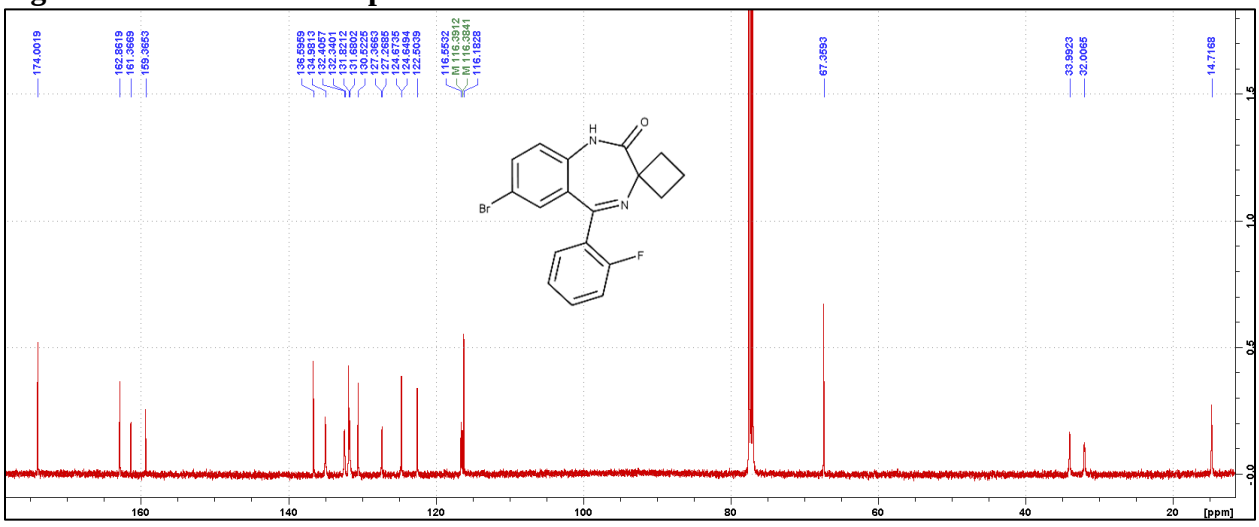

Figure 78: DAW-I-40 ^{19}F spectra:

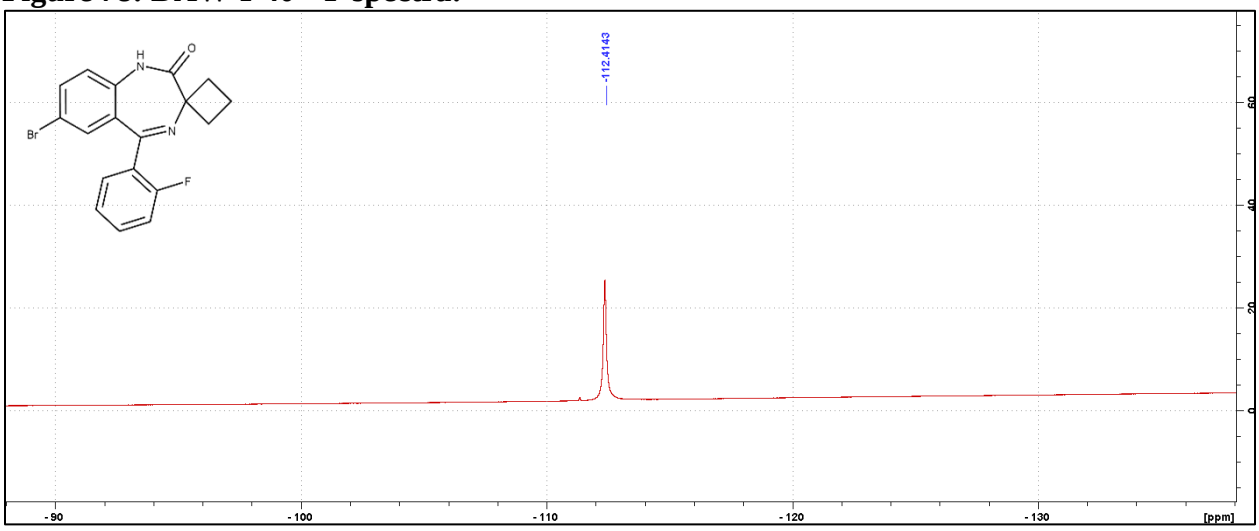

Figure 79: DAW-I-40 HPLC UV Chromatograph:

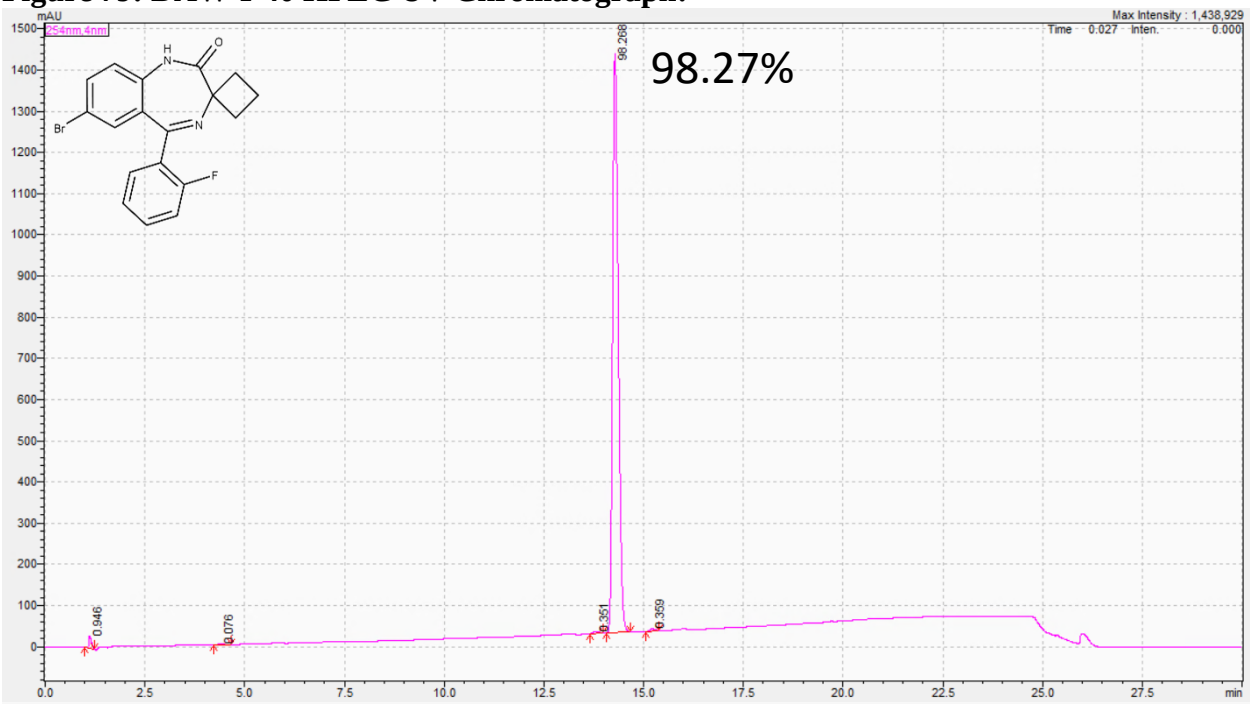

Figure 80: DAW-I-40 HRMS:

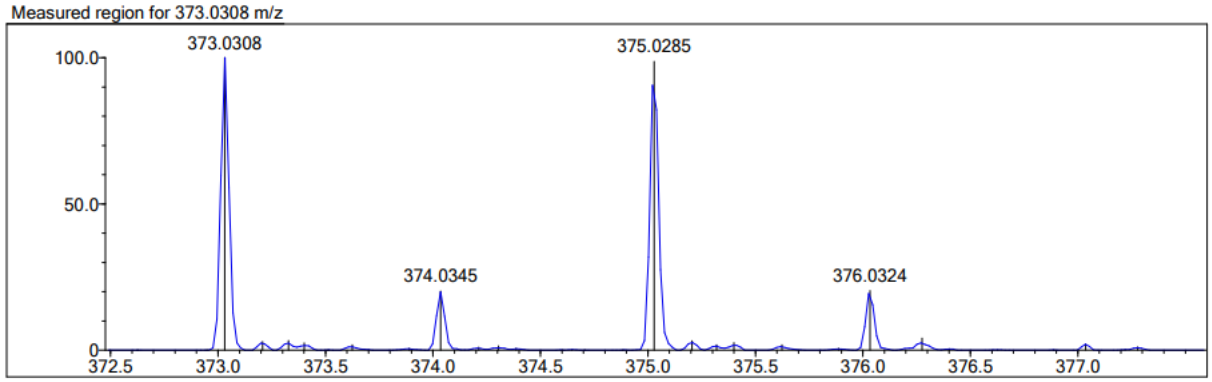

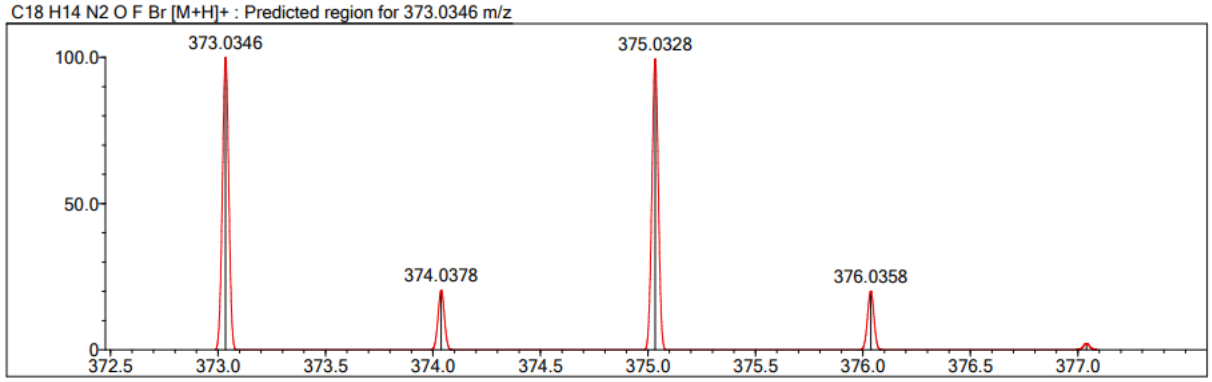

Rank	Score	Formula (M)	Ion	Meas. m/z	Pred. m/z	Df. (mDa)	Df. (ppm)	Iso	DBE
1	24.45	C18 H14 N2 O F Br	[M+H]+	373.0308	373.0346	-3.8	-10.19	61.92	12.0

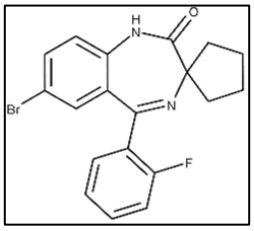

Synthesis of DAW-I-50: 2-Amino-5-bromo-2′-fluorobenzophenone (4.77 g, 16.22 mmol) was added to anhydrous toluene (130 mL), followed by the addition of trifluoroacetic acid (2.48 mL, 32.44 mmol) dropwise over a period of 10 min, and the mixture was allowed to stir at room temperature for 30 min. 3-Oxa-1-azaspiro[4.4]nonane-2,4-dione (377.4 mg, 24.32 mmol) was added portion wise and the reaction was heated to 50 °C for 24 h. After the majority of the starting material had been consumed by TLC (50% EtOAc:Hex), triethylamine (4.75 mL, 34.06 mmol) was added dropwise over a period of 15 min at which point fuming was observed in the reaction. The reaction was then heated to 100 °C for 24 h at which point disappearance of the intermediate was observed via TLC (50% EtOAc:Hex). Upon cooling to room temperature, the solvent was removed under reduced pressure and the residue was dissolved in ethyl acetate (150 mL). The organic layer was

washed with 5% aqueous sodium bicarbonate (150 mL), followed by 10% aqueous NaCl (150 mL). The organic layer was then dried with $MgSO_4$ and the solvent was removed under reduced pressure. The residue was stripped with 10% EtOAc:Heptane (50 mL, 2x) followed by a trituration in 10% EtOAc:Heptane (100 mL) at 60 °C for 4 h. The product was collected by filtration to yield a light yellow solid (5.23 g, 83.3%): ^{1}H NMR (500 MHz, $CDCl_3$) δ 10.27 (s, 1H), 7.58-7.56 (dd, *J* = 3.62, 2.25 Hz, 1H), 7.54-7.51 (m, 1H), 7.49-7.45 (m, 1H), 7.28-7.25 (m, 2H), 7.11-7.08 (m, 2H), 2.85 (m, 1H), 2.31 (m, 1H), 1.75 (m, 5H), 1.42 (m, 1H); ^{13}C NMR (126 MHz, $CDCl_3$) δ 174.72 (s), 163.73 (s), 160.28 (d, $^{1}J_{CF}$ = 251.26 Hz), 136.26 (s), 134.89 (d, $^{3}J_{CF}$ = 7.51 Hz), 132.18 (d, $^{3}J_{CF}$ = 7.09 Hz), 131.87 (s), 131.64 (s), 130.95 (s), 128.10 (d, $^{2}J_{CF}$ = 12.68 Hz), 124.69 (d, $^{3}J_{CF}$ = 3.08 Hz), 122.51 (d, $^{4}J_{CF}$ = 2.14 Hz), 116.45 (d, $^{2}J_{CF}$ = 20.86 Hz), 115.97 (s), 74.42 (s), 39.36 (s), 34.29 (s), 24.77 (s), 24.10 (s); ^{19}F NMR (471 MHz, $CDCl_3$) δ -112.64; HRMS (ESI/IT-TOF): *m/z* $[M + H]^+$ calcd for $C_{19}H_{16}BrFN_2O$: 387.0503; found: 387.0463; HPLC Purity: 98.48%.

Figure 81: DAW-I-50 ^{1}H spectra:

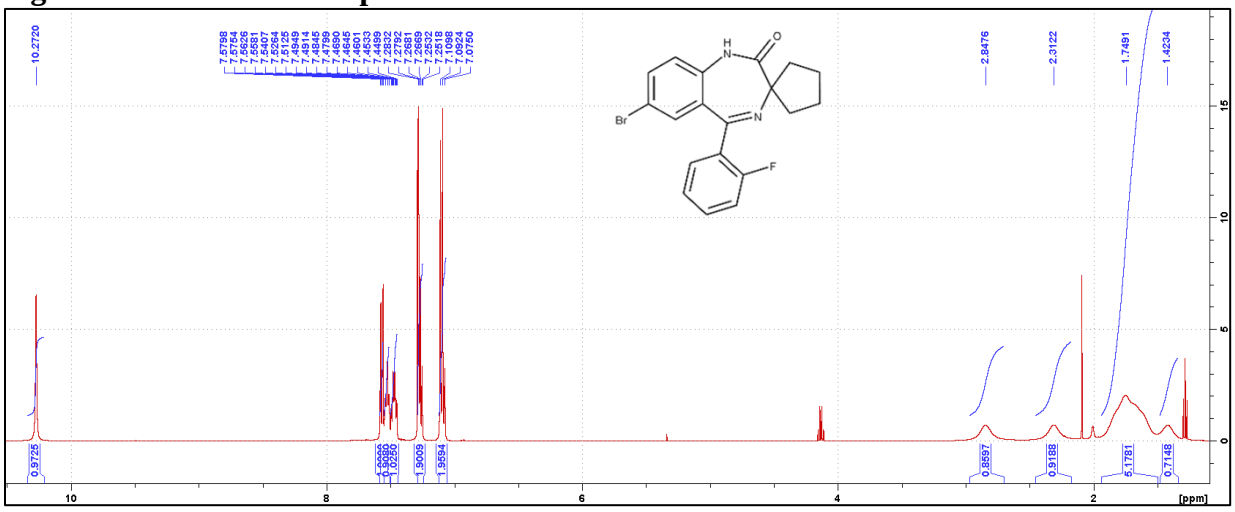

Figure 82: DAW-I-50 ^{13}C spectra:

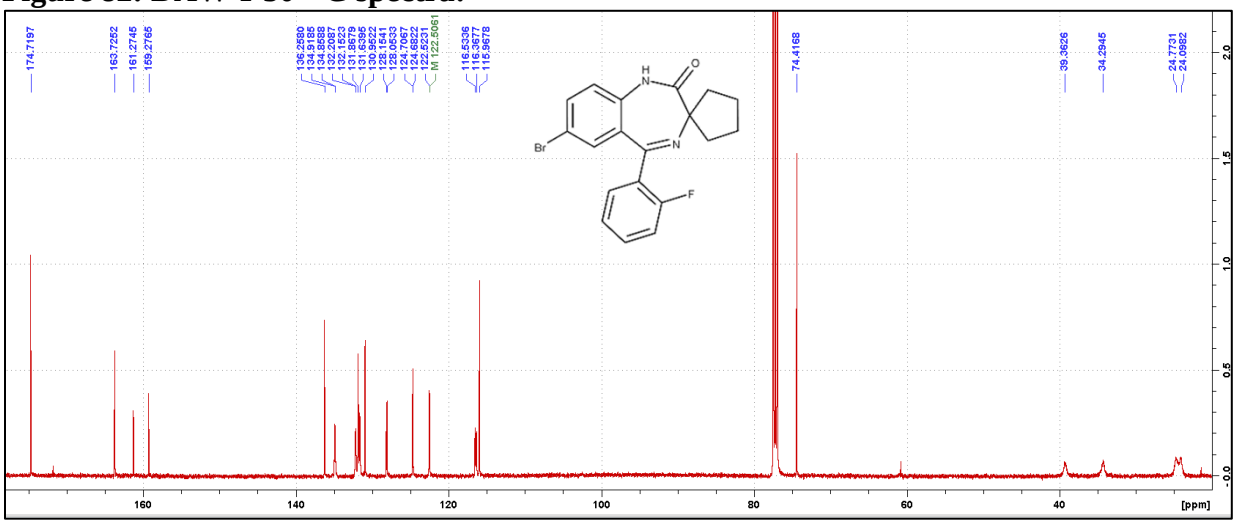

Figure 83: DAW-I-50 ^{19}F spectra:

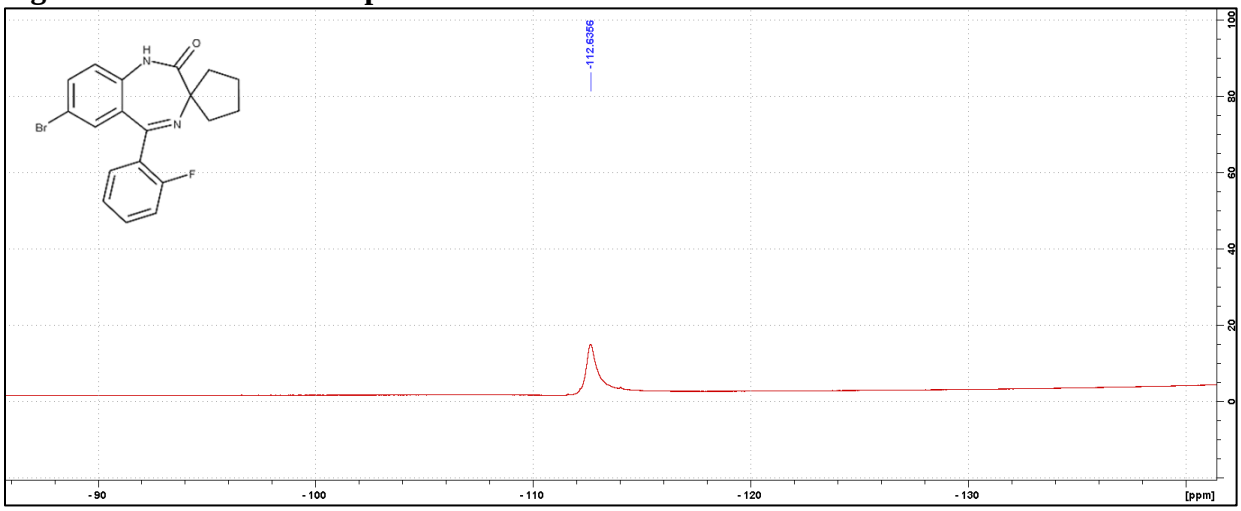

Figure 84: DAW-I-50 HPLC UV Chromatograph:

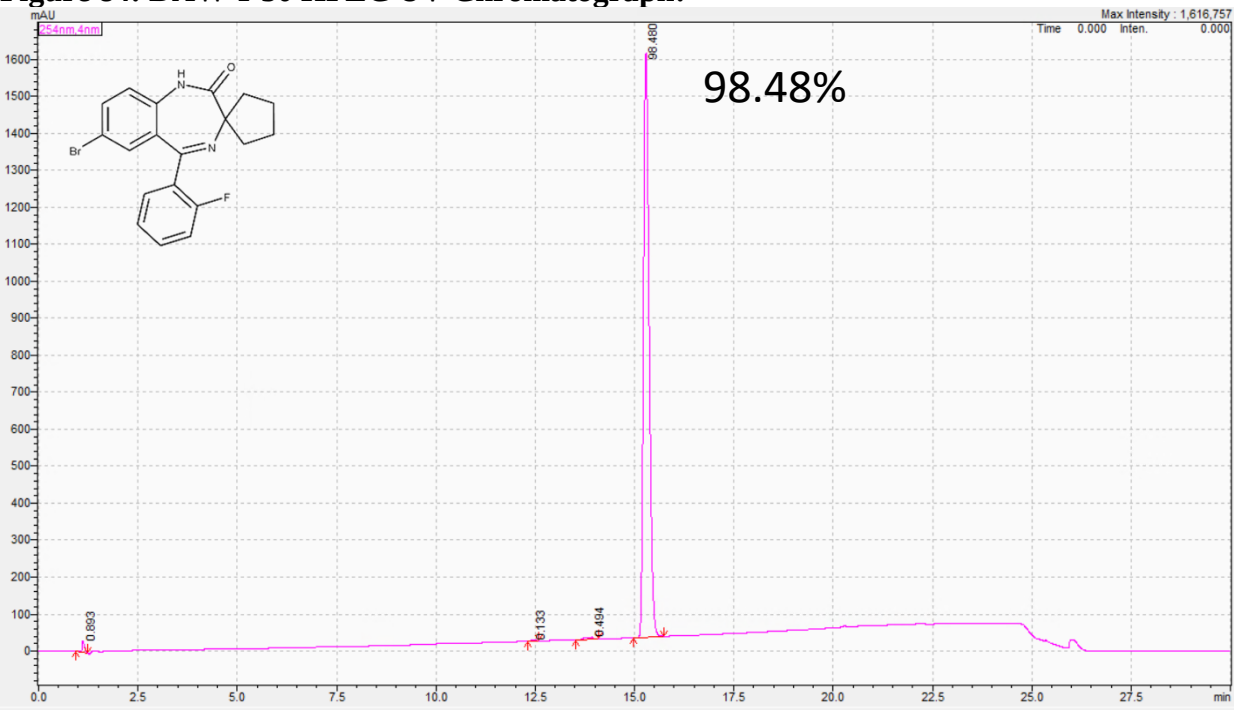

Figure 85: DAW-I-50 HRMS:

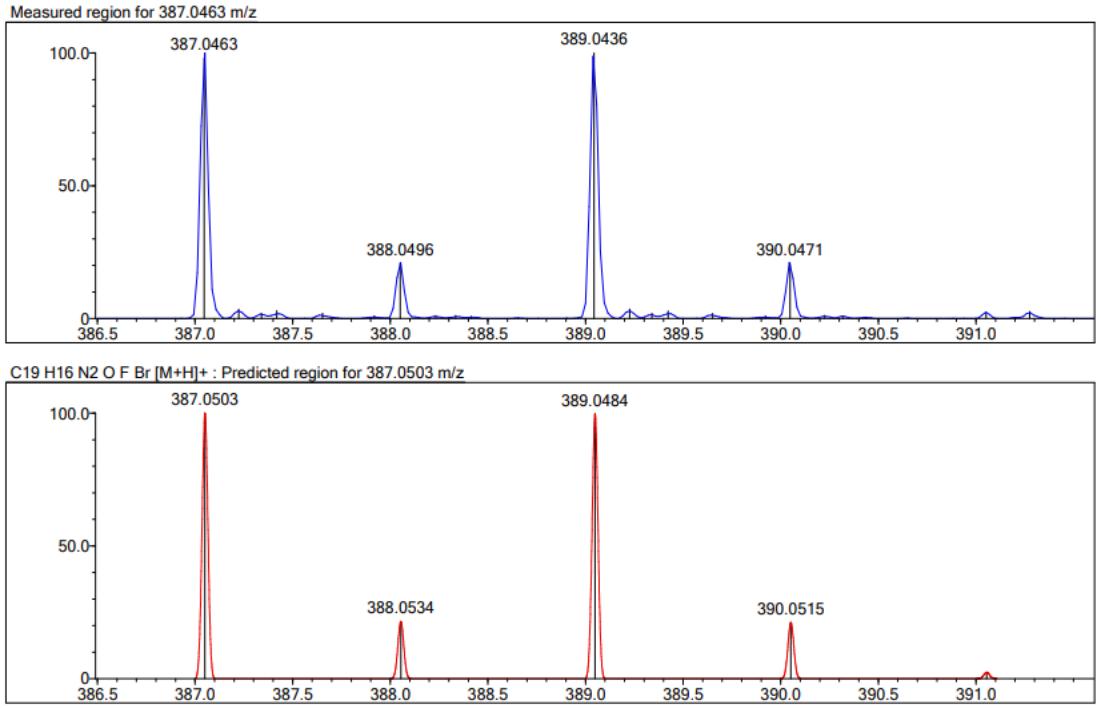

Rank	Score	Formula (M)	Ion	Meas. m/z	Pred. m/z	Df. (mDa)	Df. (ppm)	Iso	DBE
1	27.88	C19 H16 N2 O F Br	[M+H]+	387.0463	387.0503	-4.0	-10.33	71.26	12.0

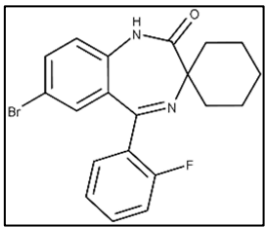

Synthesis of DAW-I-60: 2-Amino-5-bromo-2′-fluorobenzophenone (1.76 g, 5.98 mmol) was added to anhydrous toluene (60 mL), followed by the addition of trifluoroacetic acid (0.92 mL, 11.97 mmol) dropwise over a period of 10 min, and the mixture was allowed to stir at room temperature for 30 min. 3-oxa-1-azaspiro[4.5]decane-2,4-dione (2.02 g, 11.97 mmol) was added portion wise and the reaction was heated to 50 °C for 24 h. After the majority of the starting material had been consumed by TLC (50% EtOAc:Hex), triethylamine (1.75 mL, 12.57 mmol) was added dropwise over a period of 15 min at which point fuming was observed in the reaction. The reaction was then heated to 100 °C for 24 h at which point disappearance of the intermediate was observed via TLC (50% EtOAc:Hex). Upon cooling to room temperature, the solvent was removed under reduced pressure and the residue was dissolved in ethyl acetate (50 mL). The organic layer was washed with 5% aqueous sodium bicarbonate (50 mL), followed by 10% aqueous NaCl (50 mL). The organic layer was then dried with $MgSO_4$ and the solvent was removed under reduced pressure. The residue was stripped with 10% EtOAc:Heptane (20 mL, 2x) followed by a trituration in 10% EtOAc:Heptane (40 mL) at 60 °C for 4 h. The product was collected by filtration to yield a light yellow solid (1.52 g, 63.5%): ^{1}H NMR (500 MHz, $CDCl_3$) δ 9.74 (s, 1H), 7.49-7.47 (dd, *J* = 3.62, 2.24 Hz, 2H), 7.42-7.38 (m, 1H), 7.22-7.20 (d, *J* = 7.45 Hz, 1H), 7.19-7.18 (d, *J* = 2.20 Hz, 1H), 7.06-7.02 (t, *J* = 9.13 Hz, 1H), 6.97-6.95 (d, *J* = 8.65 Hz, 1H), 2.13 (m, 2H), 1.97 (m, 1H), 1.80 (m, 2H), 1.61 (m, 2H), 1.29 (m, 3H); ^{13}C NMR (126 MHz, $CDCl_3$) δ 173.82 (s), 162.22 (s), 160.39 (d, $^{1}J_{CF}$ = 251.03 Hz), 136.31, 134.67 (s), 132.10 (d, $^{3}J_{CF}$ = 1.08 Hz), 131.72 (d, $^{3}J_{CF}$ = 8.33 Hz), 131.60 (d, $^{3}J_{CF}$ = 2.50 Hz), 129.85 (s), 128.97 (d, $^{2}J_{CF}$ = 13.10 Hz), 124.43 (d, $^{4}J_{CF}$ = 3.55 Hz), 121.34 (s), 116.33 (d, $^{2}J_{CF}$ = 21.62 Hz), 115.62 (s), 66.40 (S), 25.76 (s), 22.00 (s); ^{19}F NMR (471

MHz, $CDCl_3$) δ -113.03; HRMS (ESI/Q-TOF): *m/z* $[M + H]^+$ calcd for $C_{20}H_{18}BrFN_2O$: 401.06593; found: 401.06740; HPLC Purity: 98.76%.

Figure 86: DAW-I-60 ^{1}H spectra:

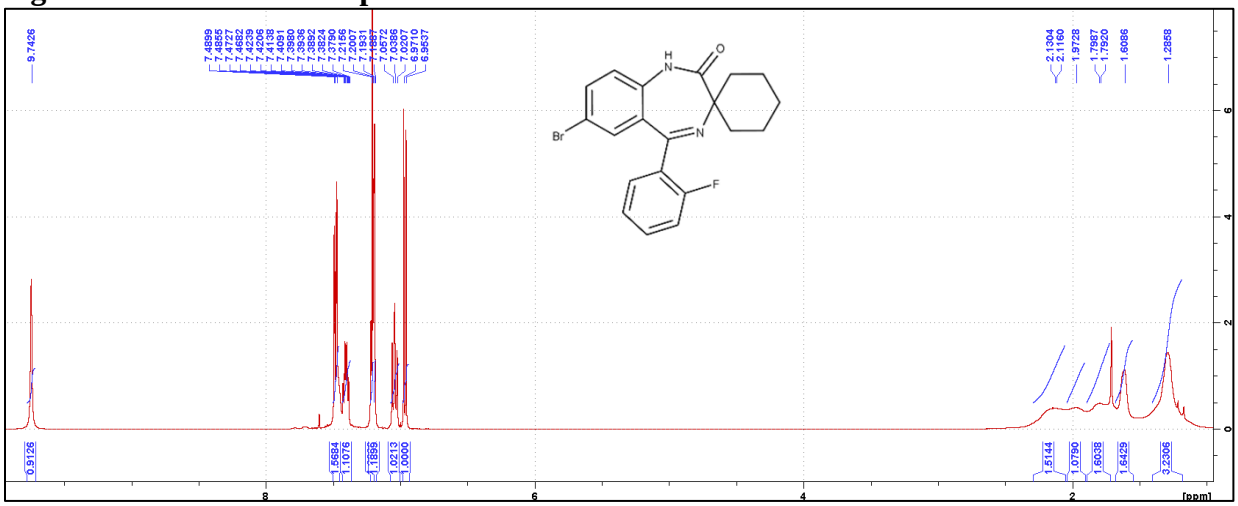

Figure 87: DAW-I-60 ^{13}C spectra:

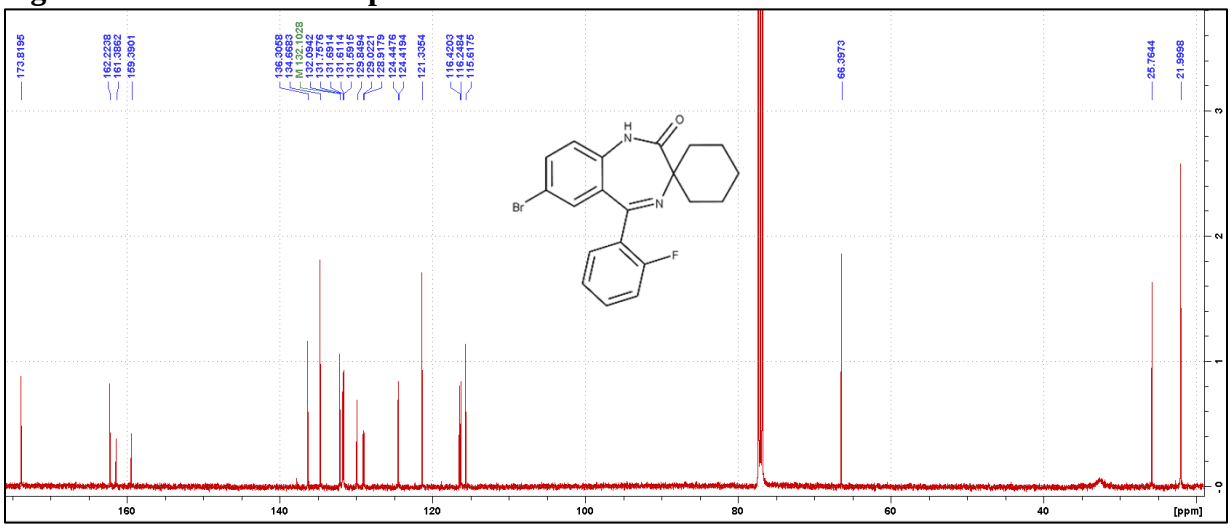

Figure 88: DAW-I-60 ^{19}F spectra:

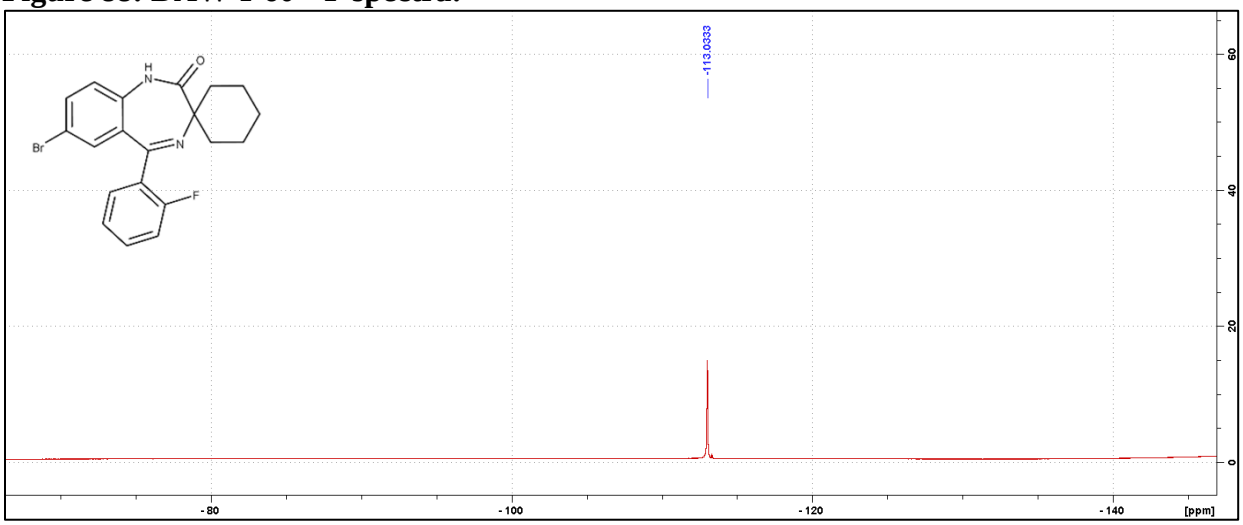

Figure 89: DAW-I-60 HPLC UV Chromatograph:

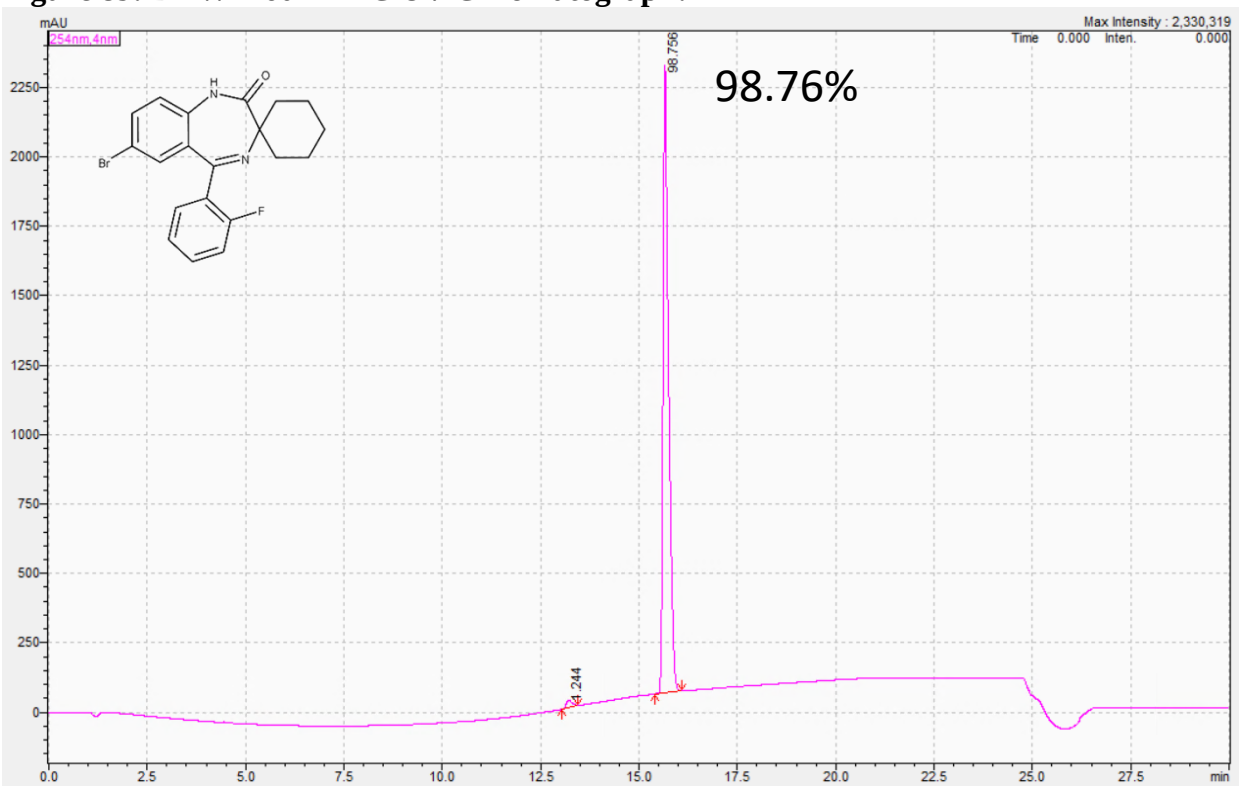

Figure 90: DAW-I-60 HRMS:

Score	Pred. (M)	Pred. m/z	Meas. m/z	Diff. (mDa)	Formulae (M)	Ion	Diff. (ppm)	Iso Score	DBE
30.50	400.05865	401.06593	401.06740	1.47	C20 H18 N2 O F Br	[M+H]+	3.665	25.88	12.0

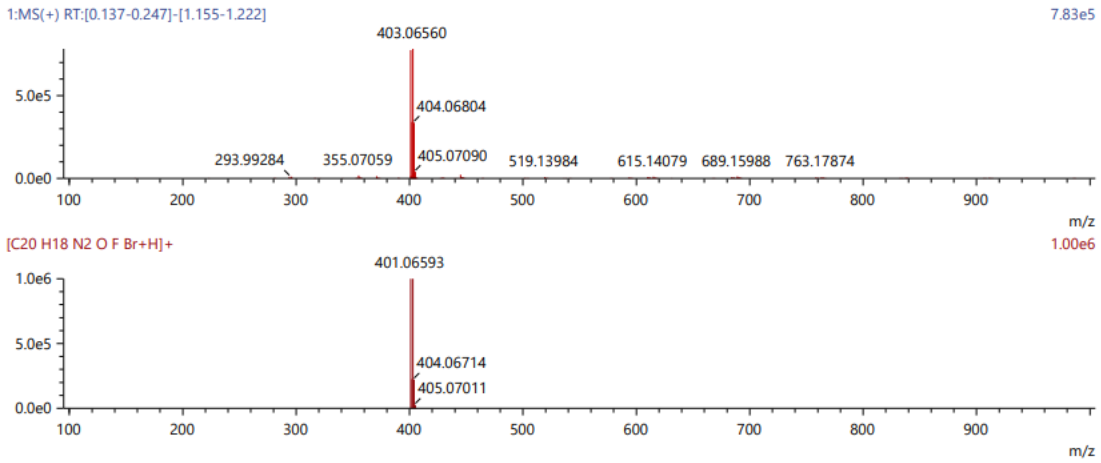

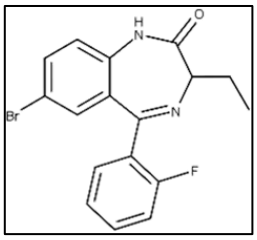

Synthesis of DAW-I-70: 2-Amino-5-bromo-2′-fluorobenzophenone (1.68g, 5.71 mmol) was added to anhydrous toluene (60 mL), followed by the addition of trifluoroacetic acid (0.87 mL, 11.42 mmol) dropwise over a period of 10 min, and the mixture was allowed to stir at room temperature for 30 min. 4-ethyloxazolidine-2,5-dione (1.11 g, 8.57 mmol) was added portion wise and the reaction was heated to 50 °C for 24 h. After the majority of the starting material had been consumed by TLC (50% EtOAc:Hex), triethylamine (1.67 mL, 12.00 mmol) was added dropwise over a period of 15 min at which point fuming was observed in the reaction. The reaction was then heated to 100 °C for 24 h at which point disappearance of the intermediate was observed via TLC (50% EtOAc:Hex). Upon cooling to room temperature, the solvent was removed under reduced pressure and the residue was dissolved in ethyl acetate (50 mL). The organic layer was washed with 5% aqueous sodium bicarbonate (50 mL), followed by 10% aqueous NaCl (50 mL). The organic layer was then dried with $MgSO_4$ and the solvent was removed under reduced pressure. The residue was stripped with 10% EtOAc:Heptane (20 mL, 2x) followed by a trituration in 10% EtOAc:Heptane (35 mL) at 60 °C for 4 h. The product was collected by filtration to yield a light yellow solid (1.64

g, 79.5%): ^{1}H NMR (500 MHz, $CDCl_3$) δ 8.96 (s, 1H), 7.52-7.49 (m, 2H), 7.41-7.36 (m, 1H), 7.29-7.28 (d, *J* = 2.05 Hz, 1H), 7.19-7.15 (m, 1H), 7.02-6.97 (m, 2H), 3.40-3.37 (t, *J* = 7.05 Hz, 1H), 2.22-2.16 (m, 2H), 1.04-1.01 (t, *J* = 7.43 Hz, 3H); ^{13}C NMR (126 MHz, $CDCl_3$) δ 171.39 (s), 164.66 (s), 160.49 (d, $^{1}J_{CF}$ = 252.08 Hz), 136.41 (s), 134.72 (d, $^{3}J_{CF}$ = 7.91 Hz), 132.19 (s), 131.60 (d, $^{3}J_{CF}$ = 10.68 Hz), 130.13 (s), 127.16 (d, $^{2}J_{CF}$ = 13.28 Hz), 124.45 (d, $^{4}J_{CF}$ = 3.53 Hz), 122.84 (d, $^{3}J_{CF}$ = 3.62 Hz), 116.57 (s), 116.33 (d, $^{2}J_{CF}$ = 22.06 Hz), 64.85 (s), 24.24 (s), 10.60 (q, *J* = 10.72 Hz); ^{19}F NMR (471 MHz, $CDCl_3$) δ -112.58; HRMS (ESI/Q-TOF): *m/z* $[M + H]^+$ calcd for $C_{17}H_{14}BrFN_2O$: 361.03463; found: 361.03605; HPLC Purity: 96.46%.

Figure 91: DAW-I-70 ^{1}H spectra:

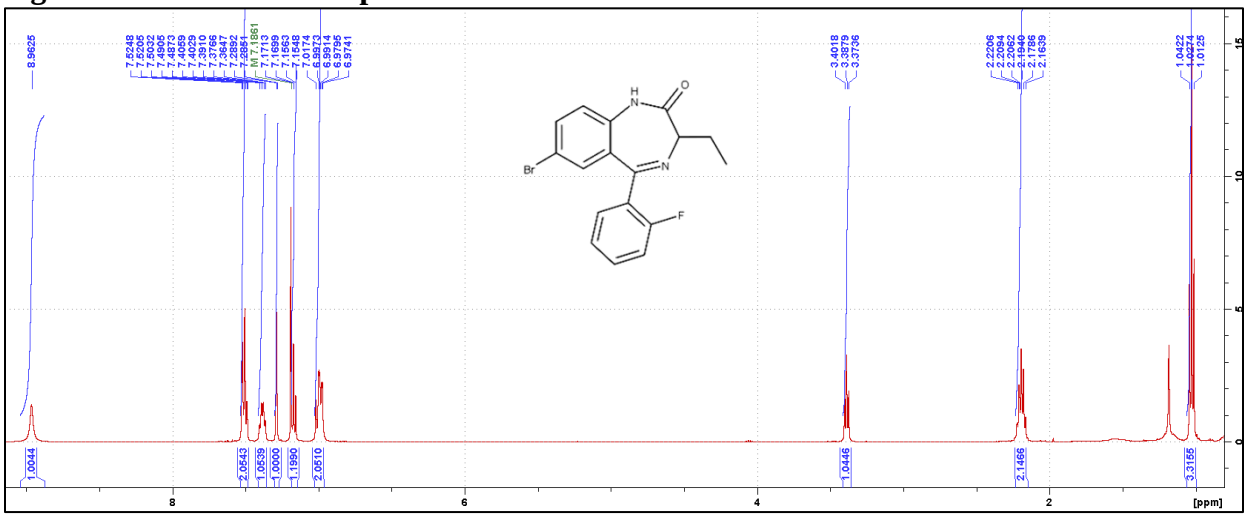

Figure 92: DAW-I-70 ^{13}C spectra:

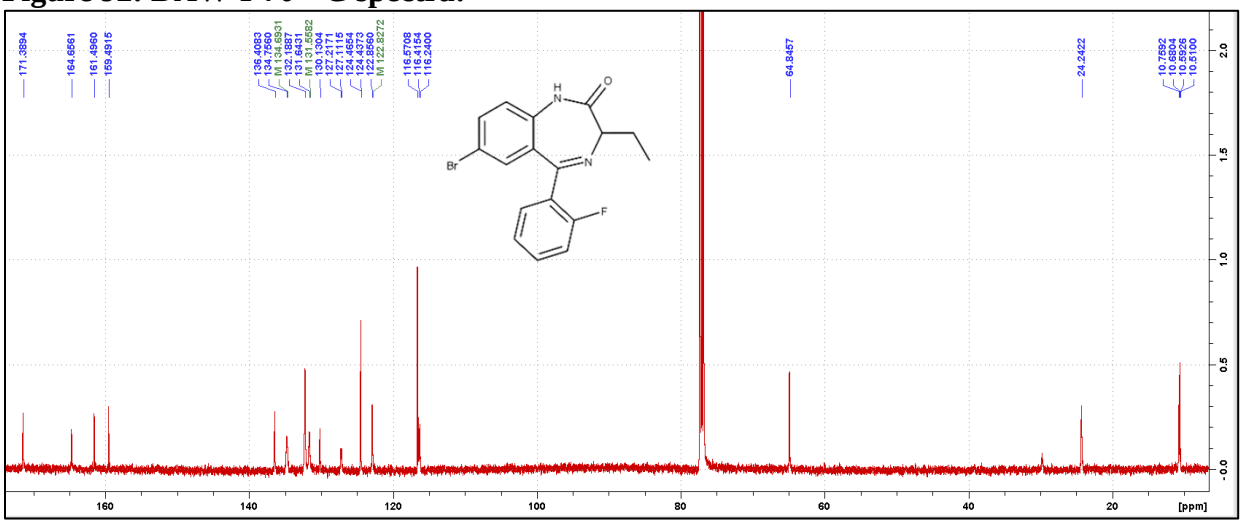

Figure 93: DAW-I-70 ^{19}F spectra:

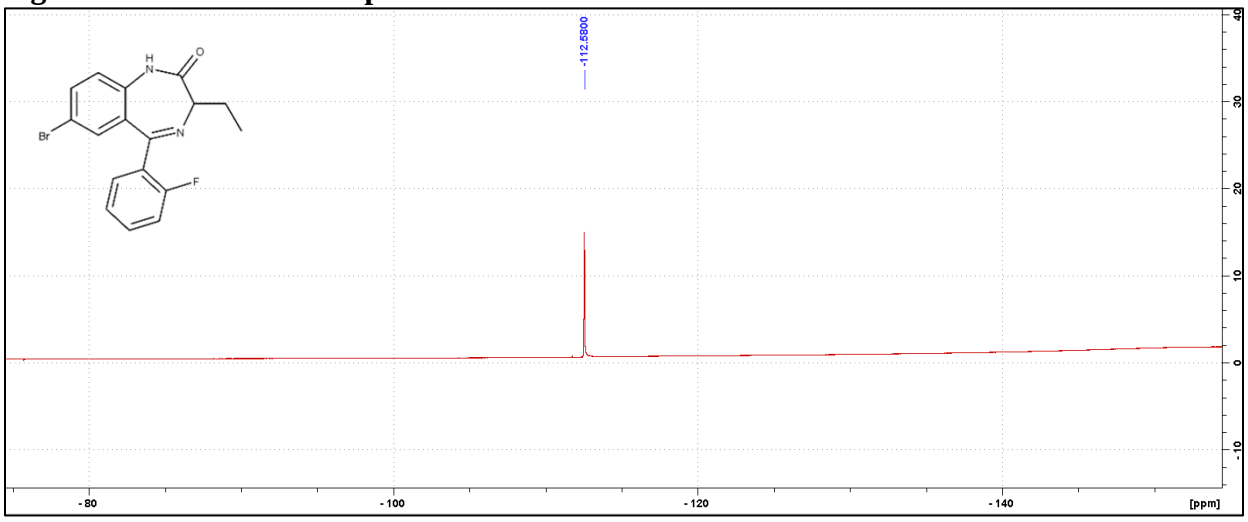

Figure 94: DAW-I-70 HPLC UV Chromatograph:

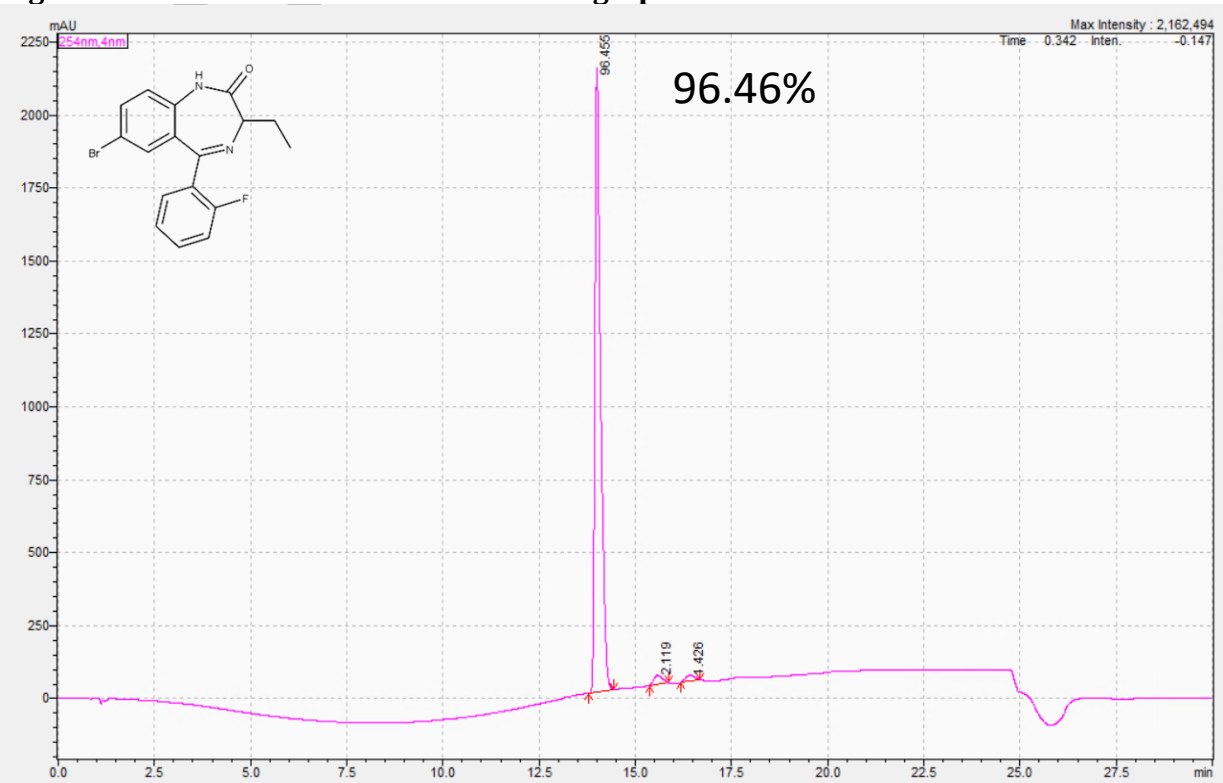

Figure 95: DAW-I-70 HRMS:

Score	Pred. (M)	Pred. m/z	Meas. m/z	Diff. (mDa)	Formulae (M)	Ion	Diff. (ppm)	Iso Score	DBE
29.88	360.02735	361.03463	361.03605	1.42	C17 H14 N2 O F Br	[M+H]+	3.933	25.71	11.0

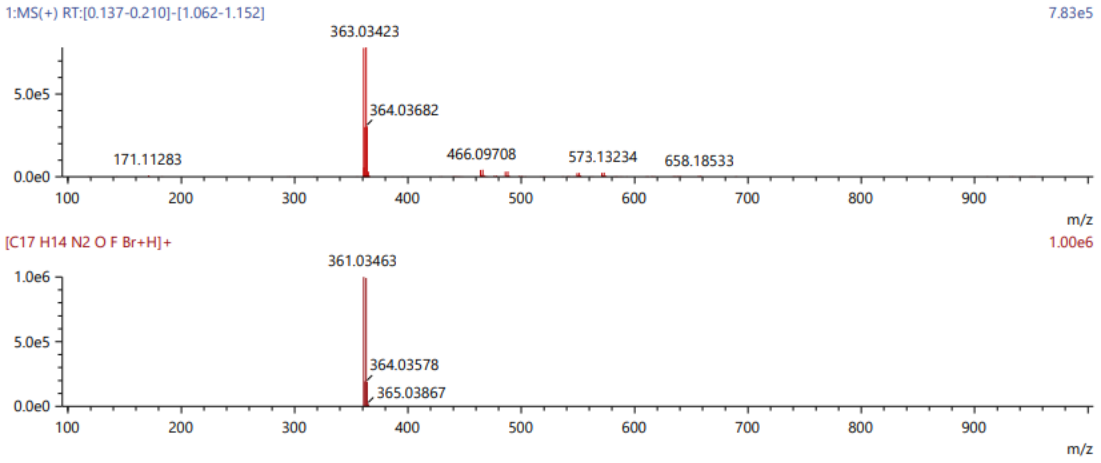

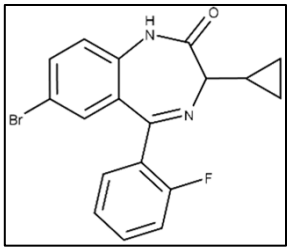

Synthesis of DAW-I-80: 2-Amino-5-bromo-2′-fluorobenzophenone (4.02 g, 13.68 mmol) was added to anhydrous toluene (50 mL), followed by the addition of trifluoroacetic acid (2.09 mL, 27.36 mmol) dropwise over a period of 10 min, and the mixture was allowed to stir at room temperature for 30 min. Crude 4-cyclopropyloxazolidine-2,5-dione (2.90 g, 20.52 mmol) was added portion wise and the reaction was heated to 50 °C for 24 h. After the majority of the starting material had been consumed by TLC (50% EtOAc:Hex), triethylamine (4.00 mL, 28.72 mmol) was added dropwise over a period of 15 min at which point fuming was observed in the reaction. The reaction was then heated to 100 °C for 24 h at which point disappearance of the intermediate was observed via TLC (50% EtOAc:Hex). Upon cooling to room temperature, the solvent was removed under reduced pressure and the residue was dissolved in ethyl acetate (80 mL). The organic layer was washed with 5% aqueous sodium bicarbonate (80 mL), followed by 10% aqueous NaCl (80 mL). The organic layer was then dried with $MgSO_4$ and the solvent was removed under reduced pressure. The residue was stripped with 10% EtOAc:Heptane (40 mL, 2x) followed by a trituration in 10% EtOAc:Heptane (60 mL) at 60 °C for 4 h. The product was collected by filtration to yield a light yellow solid (718.26 mg, 14.1%): ^{1}H NMR (500 MHz, $CDCl_3$) δ 8.81 (s, 1H), 7.63-7.59 (m, 2H), 7.50-7.45 (m, 1H), 7.36-35 (d, J = 2.05 Hz, 1H), 7.27-7.25 (dd, J = 2.85, 1.05 Hz, 1H), 7.11-7.05 (m, 2H), 3.09-3.08 (d, J = 8.05 Hz, 1H), 1.90-1.83 (m, 1H), 0.84-0.72 (m, 2H), 0.50-0.45 (m, 1H), 0.35-0.30 (m, 1H); ^{13}C NMR (126 MHz, $CDCl_3$) δ 168.90 (s), 161.75 (s), 158.03 (d, $^{1}J_{CF}$ = 251.84 Hz), 133.83 (s), 132.27 (s), 129.78 (s), 129.71 (s), 129.18 (d, $^{3}J_{CF}$ = 2.30 Hz), 127.57 (d, $^{4}J_{CF}$ = 1.48 Hz), 124.71 (d, $^{2}J_{CF}$ = 12.32 Hz), 122.00 (d, $^{3}J_{CF}$ = 3.58 Hz), 120.36 (s), 114.18 (s), 113.84 (d, $^{2}J_{CF}$ = 21.61 Hz), 65.23 (s), 9.43 (s), 0.00 (s), -0.14 (s); ^{19}F NMR (471

MHz, $CDCl_3$) δ -112.53-112.58 (qu, *J* = 5.6 Hz); HRMS (ESI/Q-TOF): *m/z* $[M + H]^+$ calcd for $C_{18}H_{14}BrFN_2O$: 373.03463; found: 373.03581; HPLC Purity: 98.57%.

Figure 96: DAW-I-80 ^{1}H spectra:

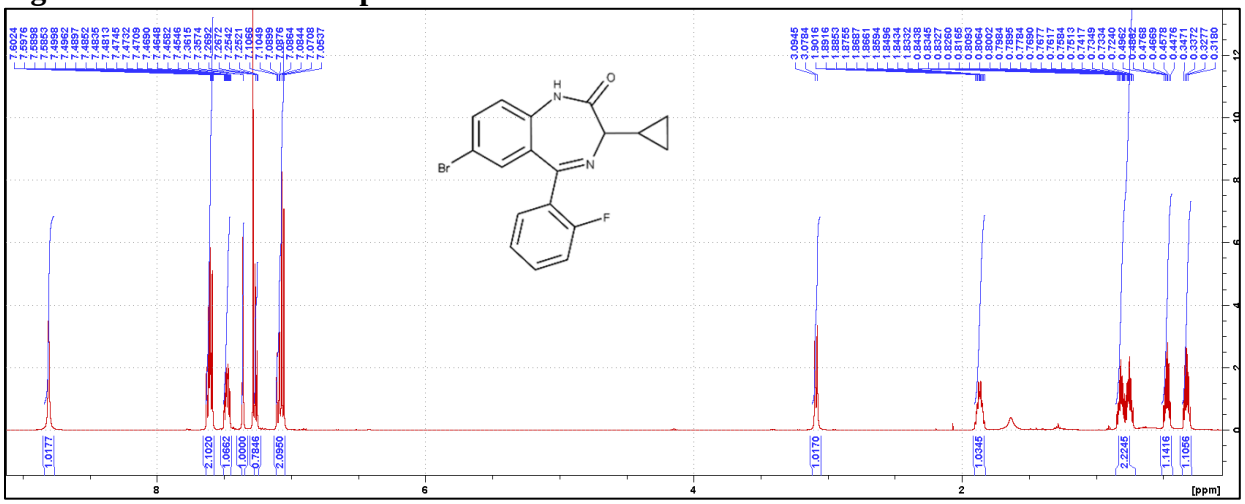

Figure 97: DAW-I-80 ^{13}C spectra:

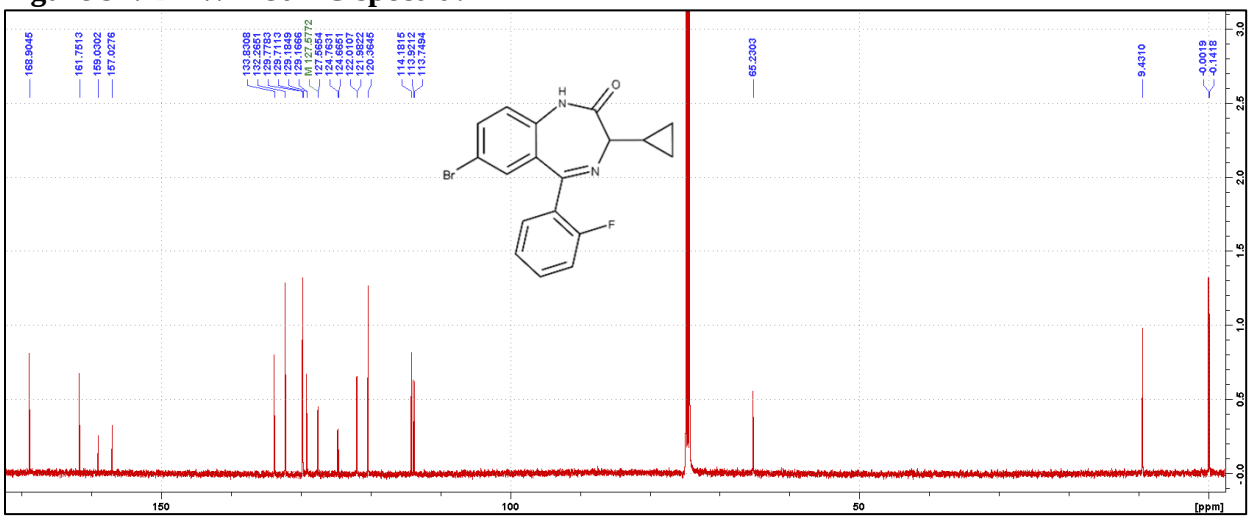

Figure 98: DAW-I-80 ^{19}F spectra:

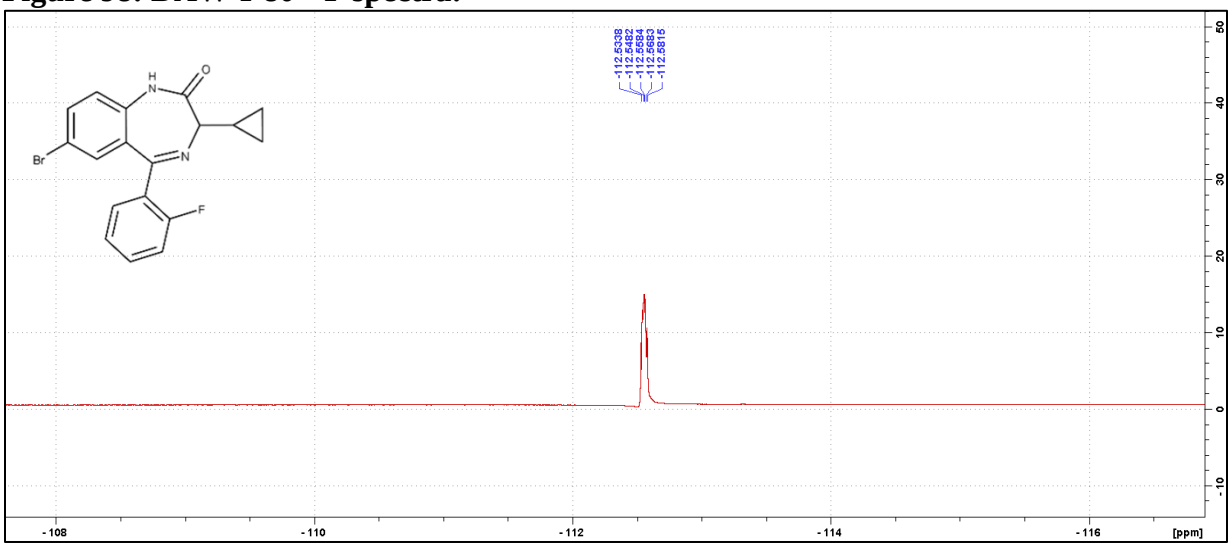

Figure 99: DAW-I-80 HPLC UV Chromatograph:

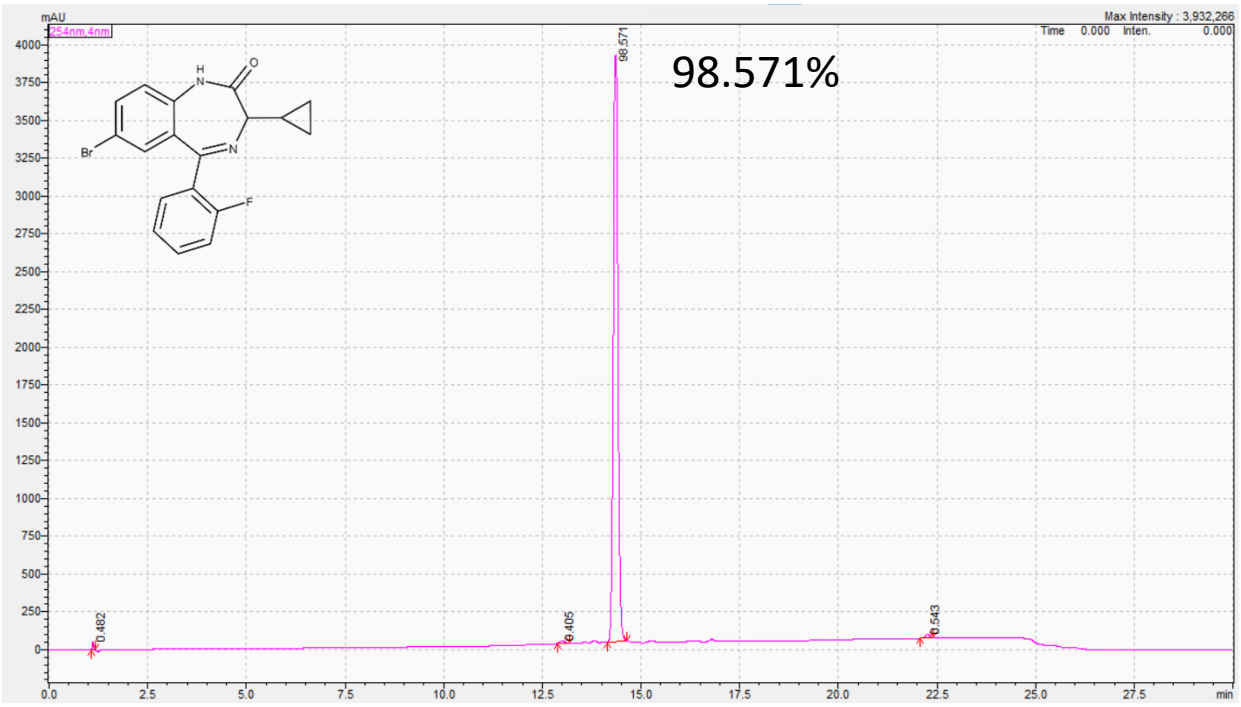

Figure 100: DAW-I-80 HRMS:

Score	Pred. (M)	Pred. m/z	Meas. m/z	Diff. (mDa)	Formulae (M)	Ion	Diff. (ppm)	Iso Score	DBE
40.46	372.02735	373.03463	373.03581	1.18	C18 H14 N2 O F Br	[M+H]+	3.163	36.19	12.0

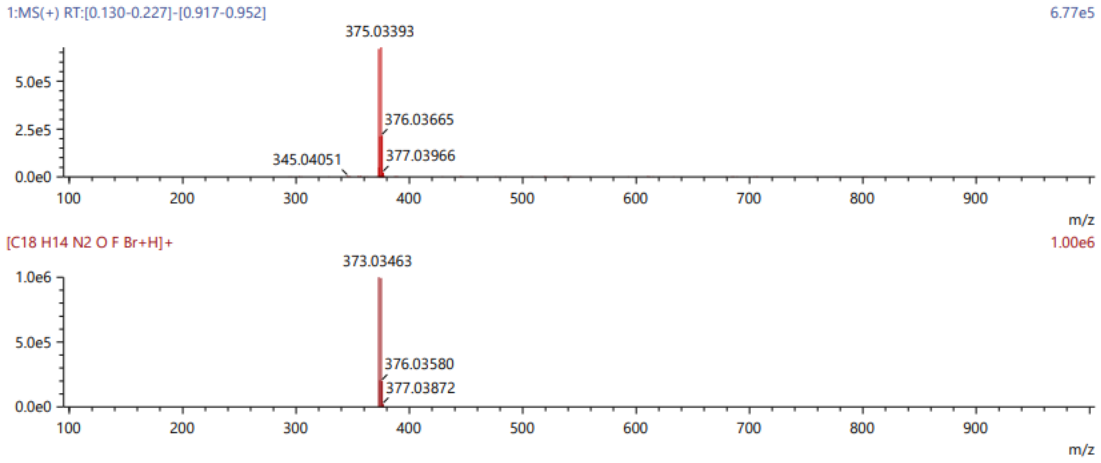

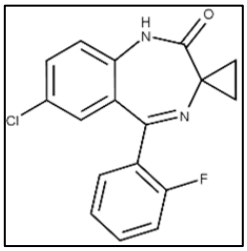

Synthesis of DAW-I-32: 2-Amino-5-chloro-2′-fluorobenzophenone (1.48 g, 5.92 mmol) was added to anhydrous toluene (40 mL), followed by the addition of trifluoroacetic acid (0.91 mL, 11.85 mmol) dropwise over a period of 10 min, and the mixture was allowed to stir at room temperature for 30 min. Crude 6-oxa-4-azaspiro[2.4]heptane-5,7-dione (1.13g, 8.89 mmol) was added portion wise and the reaction was heated to 50 °C for 24 h. After the majority of the starting material had been consumed by TLC (50% EtOAc:Hex), triethylamine (1.73mL, 12.44 mmol) was added dropwise over a period of 15 min at which point fuming was observed in the reaction. The reaction was then heated to 100 °C for 24 h at which point disappearance of the intermediate was observed via TLC (50% EtOAc:Hex). Upon cooling to room temperature, the solvent was removed under reduced pressure and the residue was dissolved in ethyl acetate (60 mL). The organic layer was washed with 5% aqueous sodium bicarbonate (60 mL), followed by 10% aqueous NaCl (60 mL). The organic layer was then dried with $MgSO_4$ and the solvent was removed under reduced pressure. The residue was stripped with 10% EtOAc:Heptane (20 mL, 2x) followed by a trituration in 10% EtOAc:Heptane (40 mL) at 60 °C for 4 h. The product was collected by filtration to yield a light

yellow solid (799 mg, 42.9%): ^{1}H NMR (500 MHz, d_6-DMSO) δ 10.71 (s, 1H), 7.61-7.59 (dd, *J* = 3.73, 2.45 Hz, 1H), 7.58-7.55 (m, 1H), 7.54-7.51 (m, 1H), 7.34-7.31 (dt, *J* = 3.19, 0.95 Hz, 1H), 7.28-7.24 (m, 2H), 7.02-7.01 (d, *J* = 2.25 Hz, 1H), 1.20-1.17 (m, 2H), 0.88-0.86 (m, 2H); ^{13}C NMR (126 MHz, d_6-DMSO) δ 172.20 (s), 169.23 (s), 160.02 (d, $^{1}J_{CF}$ = 248.55 Hz), 137.36 (s), 132.92 (d, $^{3}J_{CF}$ = 8.40 Hz), 132.16 (s), 132.04 (d, $^{4}J_{CF}$ = 2.19 Hz), 130.28 (s), 128.52 (s), 127.65 (d, $^{2}J_{CF}$ = 12.63 Hz), 126.99 (s), 125.11 (d, $^{3}J_{CF}$ = 3.19 Hz), 123.30 (s), 116.45 (d, $^{2}J_{CF}$ = 21.33 Hz), 47.12 (s), 12.69 (s); ^{19}F NMR (471 MHz, d_6-DMSO) δ -113.83 - -113.88 (qu, *J* = 5.80 Hz) HRMS (ESI/Q-TOF): *m/z* $[M + H]^+$ calcd for $C_{17}H_{12}ClFN_2O$: 315.06950; found: 315.06852; HPLC Purity 99.08%.

Figure 101: DAW-I-32 ^{1}H spectra:

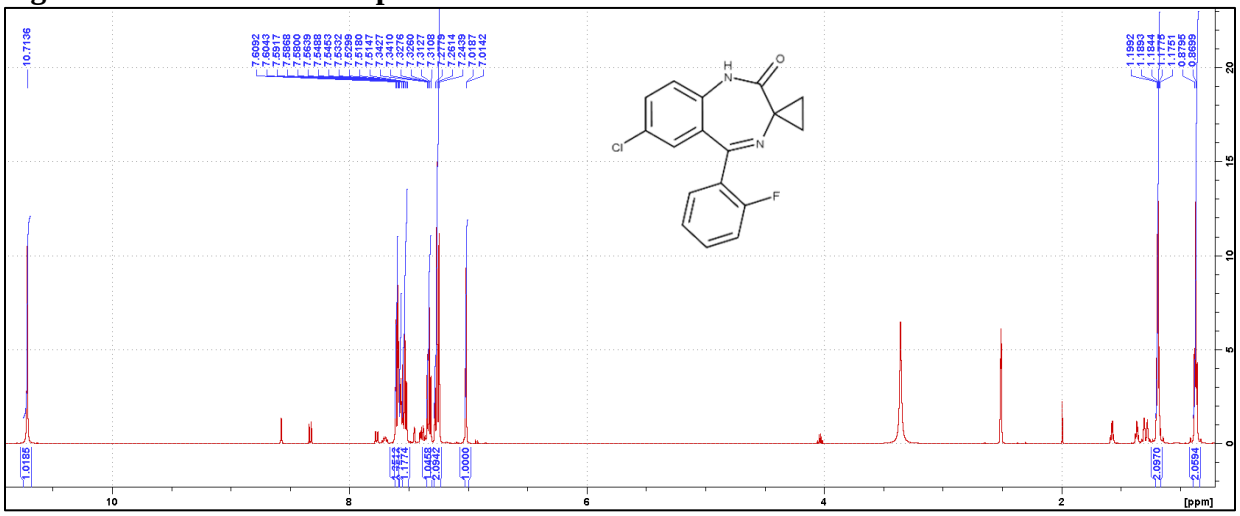

Figure 102: DAW-I-32 ^{13}C spectra:

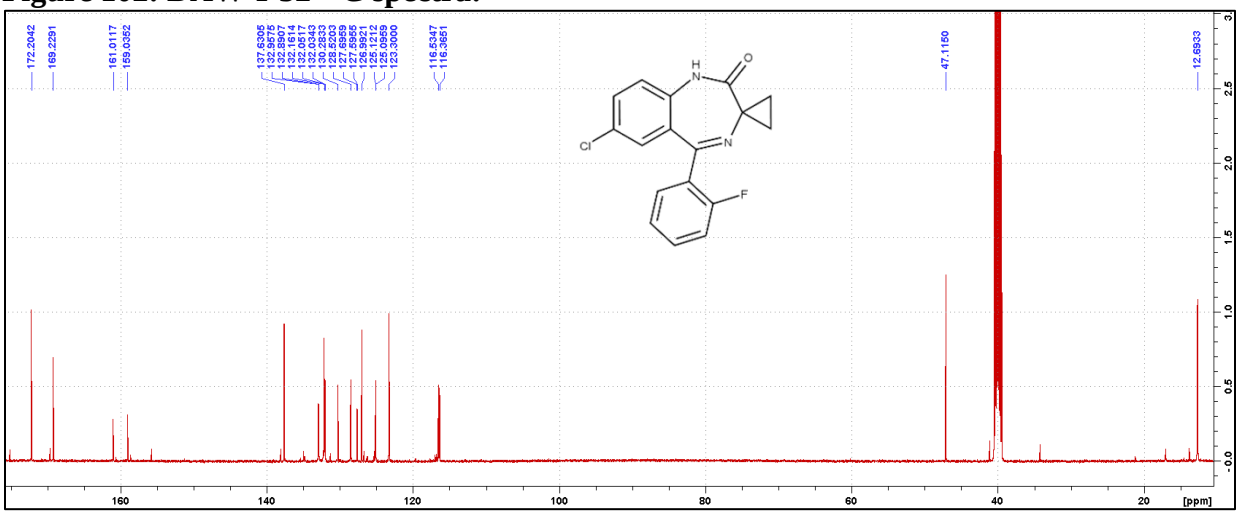

Figure 103: DAW-I-32 ^{19}F spectra:

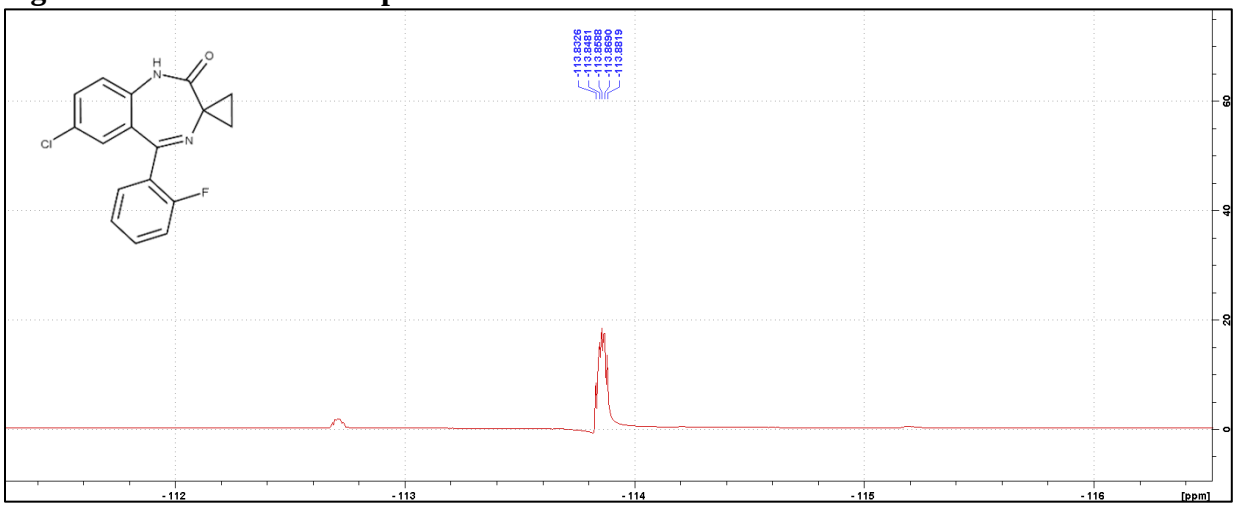

Figure 104: DAW-I-32 HPLC UV Chromatograph:

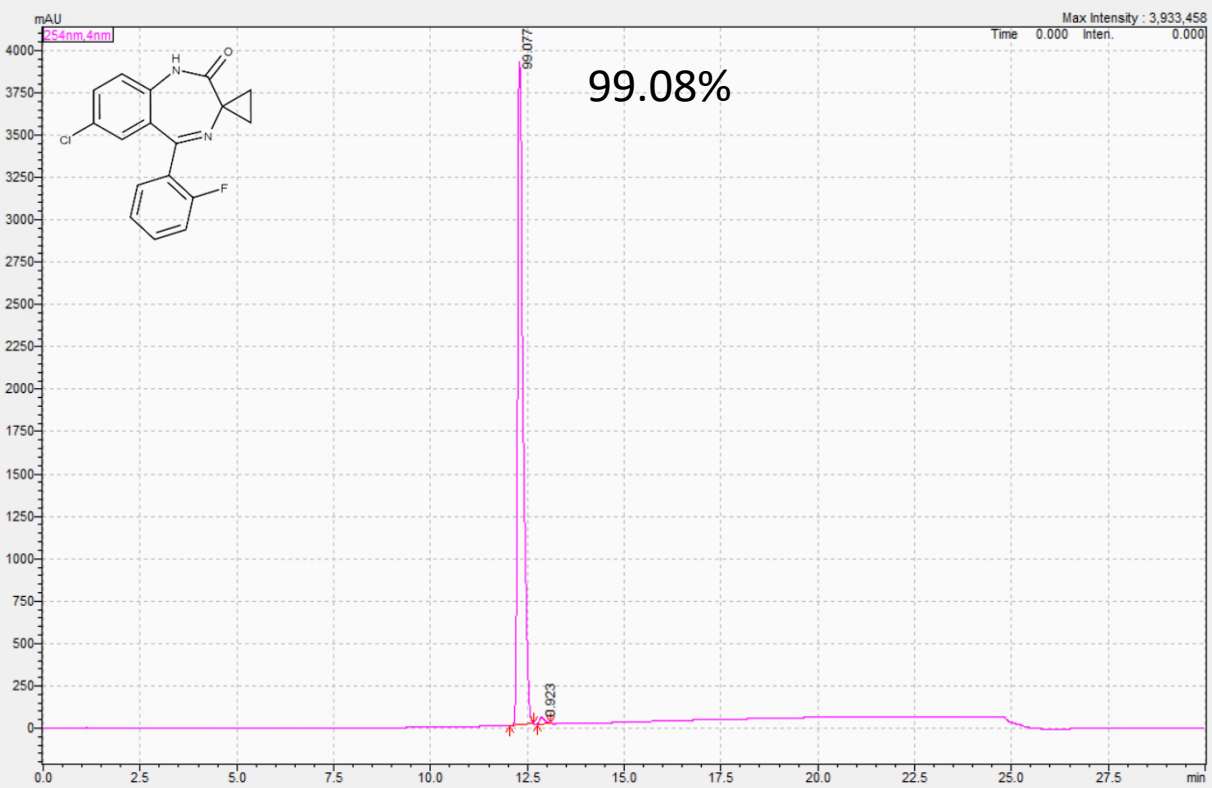

Figure 105: DAW-I-32 HRMS:

Score	Pred. (M)	Pred. m/z	Meas. m/z	Diff. (mDa)	Formulae (M)	Ion	Diff. (ppm)	Iso Score	DBE
53.02	314.06222	315.06950	315.06852	-0.98	C17 H12 N2 O F Cl	[M+H]+	-3.110	50.08	12.0

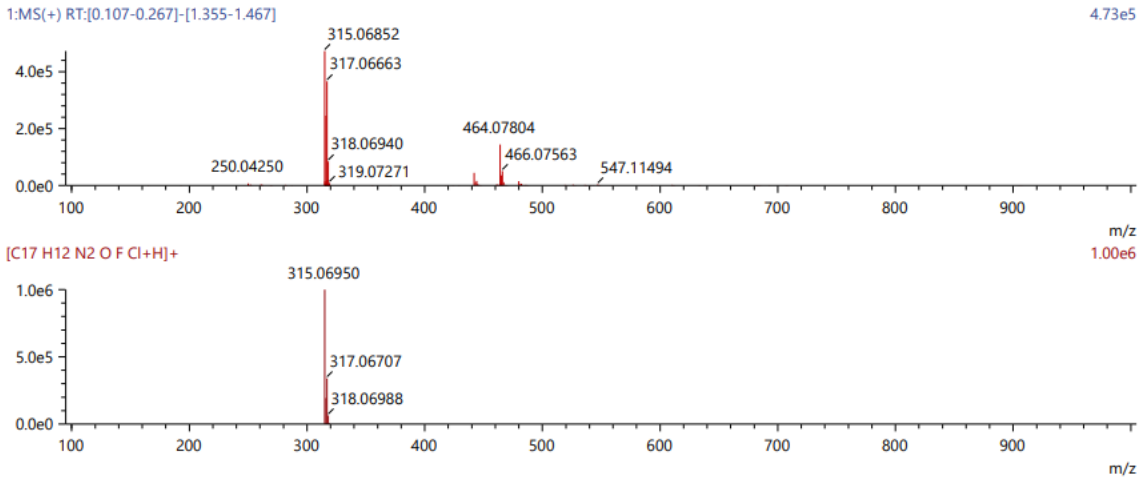

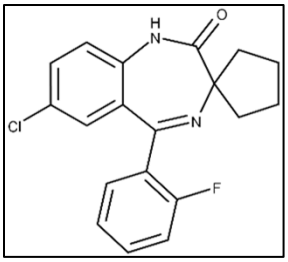

Synthesis of DAW-I-52: 2-Amino-5-chloro-2′-fluorobenzophenone (1.80 g, 7.21 mmol) was added to anhydrous toluene (52 mL), followed by the addition of trifluoroacetic acid (1.10 mL, 14.42 mmol) dropwise over a period of 10 min, and the mixture was allowed to stir at room temperature for 30 min. 3-Oxa-1-azaspiro[4.4]nonane-2,4-dione (1.68 g, 10.81 mmol) was added portion wise and the reaction was heated to 50 °C for 24 h. After the majority of the starting material had been consumed by TLC (50% EtOAc:Hex), triethylamine (2.11 mL, 15.14 mmol) was added dropwise over a period of 15 min at which point fuming was observed in the reaction. The reaction was then heated to 100 °C for 24 h at which point disappearance of the intermediate was observed via TLC (50% EtOAc:Hex). Upon cooling to room temperature, the solvent was removed under reduced pressure and the residue was dissolved in ethyl acetate (60 mL). The organic layer was washed with 5% aqueous sodium bicarbonate (60 mL), followed by 10% aqueous NaCl (60 mL). The organic layer was then dried with $MgSO_4$ and the solvent was removed under reduced pressure. The residue was stripped with 10% EtOAc:Heptane (25 mL, 2x) followed by a trituration in 10% EtOAc:Heptane (40 mL) at 60 °C for 4 h. The product was collected by filtration to yield a light yellow solid (2.40 g, 97.1%): ^{1}H NMR (500 MHz, $CDCl_3$) δ 9.30 (s, 1H), 7.53-7.50 (dt, *J* = 3.32, 1.70 Hz, 1H), 7.48-7.45 (m, 1H), 7.43-7.41 (m, 1H), 7.26-7.23 (dt, *J* = 3.17, 0.85 Hz, 1H), 7.15-7.14 (d, *J* = 2.25 Hz, 1H), 7.11-7.07 (m, 2H), 2.32 (m, 1H), 1.87 (m, 2H), 1.77-1.68 (m, 5H); ^{13}C NMR (126 MHz, $CDCl_3$) δ 174.15 (s), 163.36 (s), 160.41 (d, $^{1}J_{CF}$ = 251.28 Hz), 135.79 (s), 131.87 (s), 131.53 (s), 130.65 (s), 129.04 (s), 128.46 (s), 124.41 (d, $^{3}J_{CF}$ = 3.56 Hz), 121.81 (s), 116.26 (d, $^{2}J_{CF}$ = 21.50 Hz), 74.58 (s), 40.59 (s), 36.78 (s), 24.72 (s), 24.32 (s); ^{19}F NMR (471 MHz, $CDCl_3$) δ -112.99; HRMS (ESI/Q-TOF): *m/z* $[M + H]^+$ calcd for $C_{19}H_{16}ClFN_2O$: 343.10080; found: 343.10148; HPLC Purity 97.679%.

Figure 106: DAW-I-52 ^{1}H spectra:

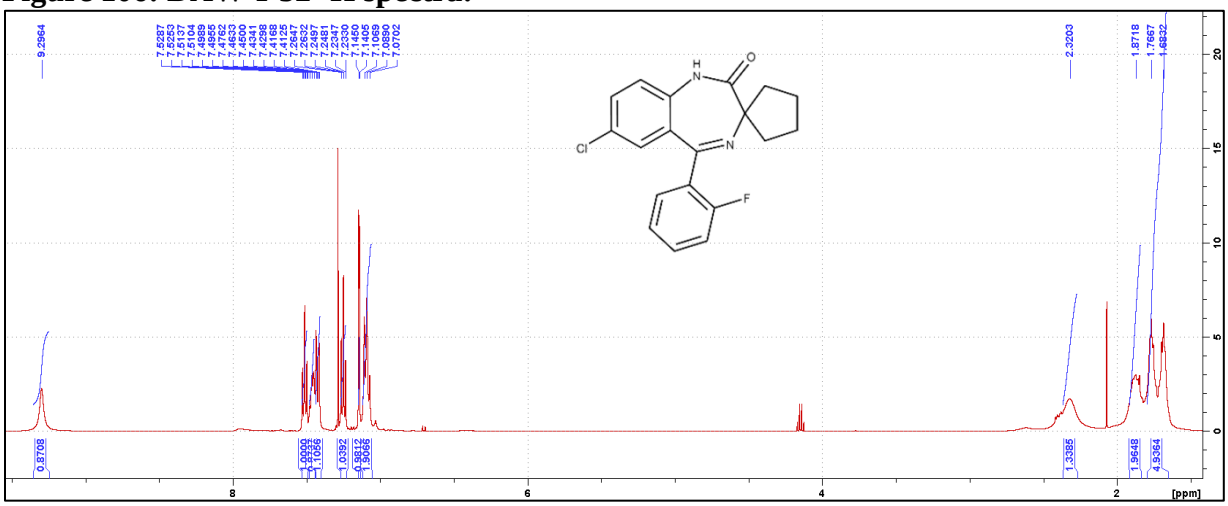

Figure 107: DAW-I-52 ^{13}C spectra:

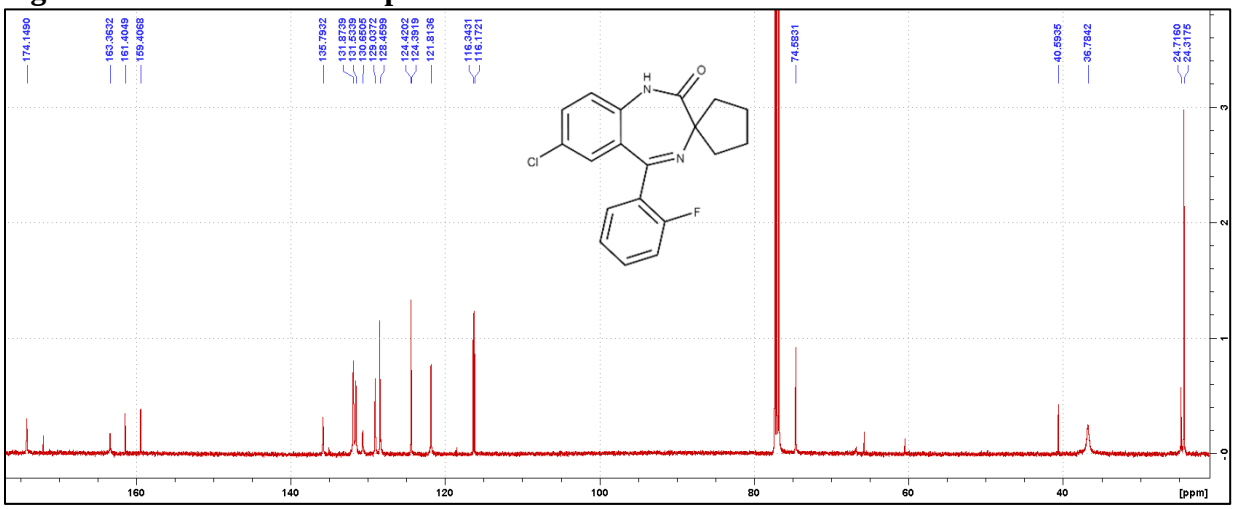

Figure 108: DAW-I-52 ^{19}F spectra:

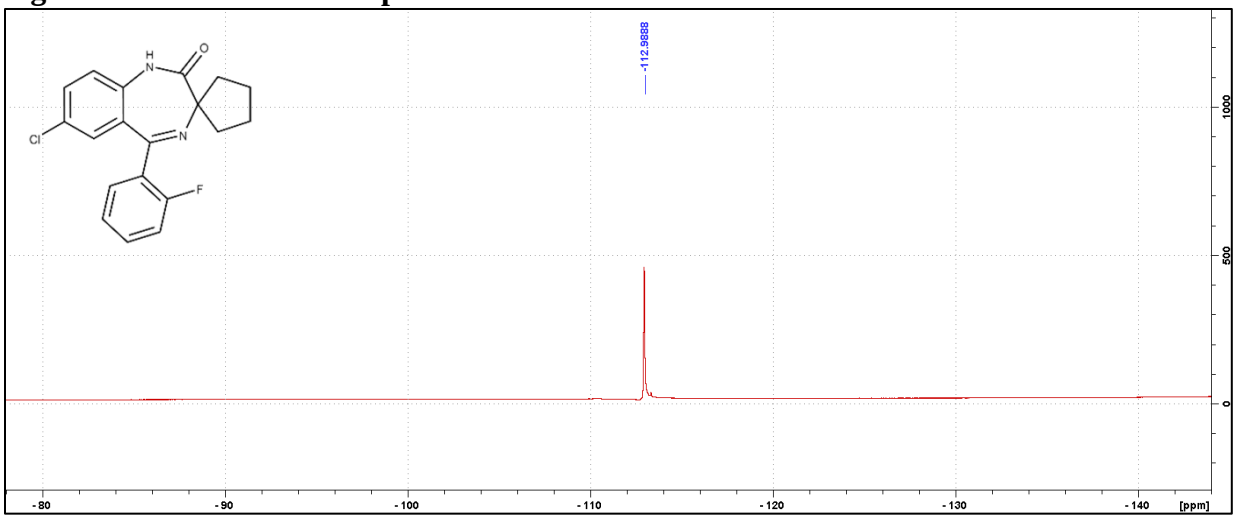

Figure 109: DAW-I-52 HPLC UV Chromatograph:

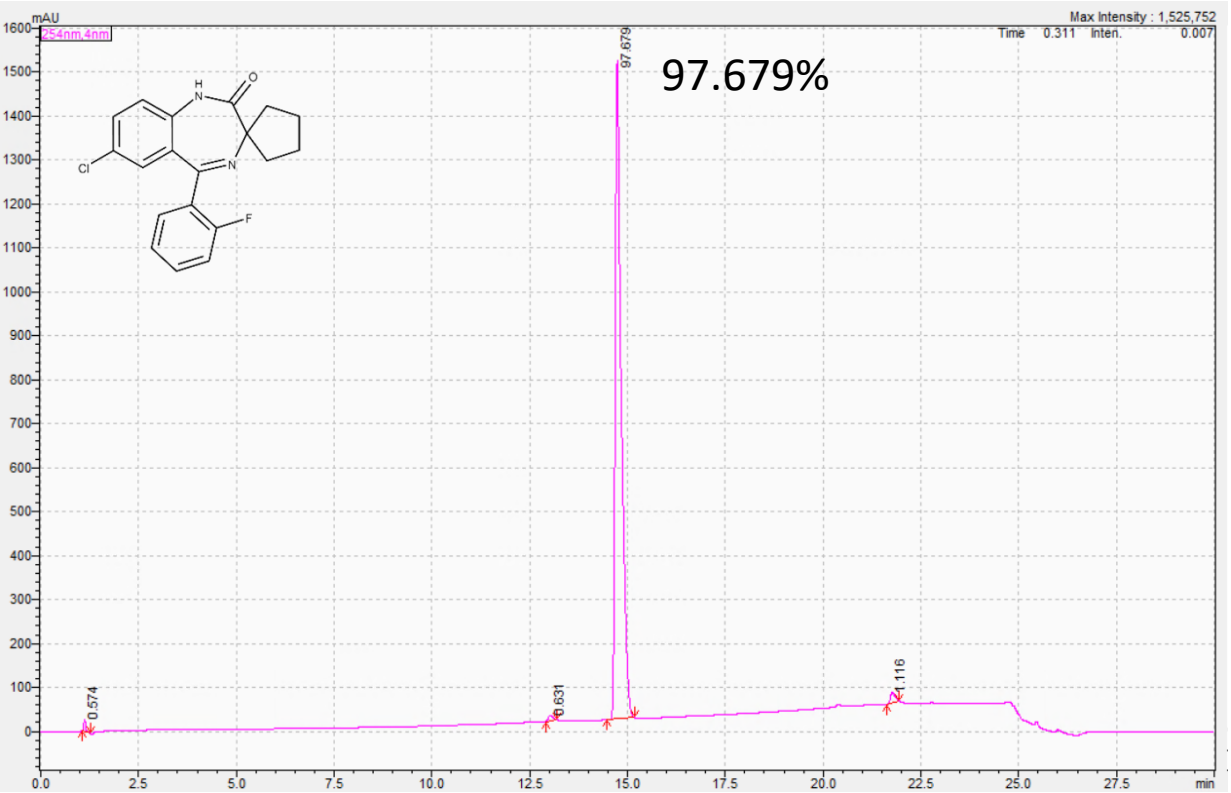

Figure 110: DAW-I-52 HRMS:

Score	Pred. (M)	Pred. m/z	Meas. m/z	Diff. (mDa)	Formulae (M)	Ion	Diff. (ppm)	Iso Score	DBE
57.61	342.09352	343.10080	343.10148	0.68	C19 H16 N2 O F Cl	[M+H]+	1.982	54.07	12.0

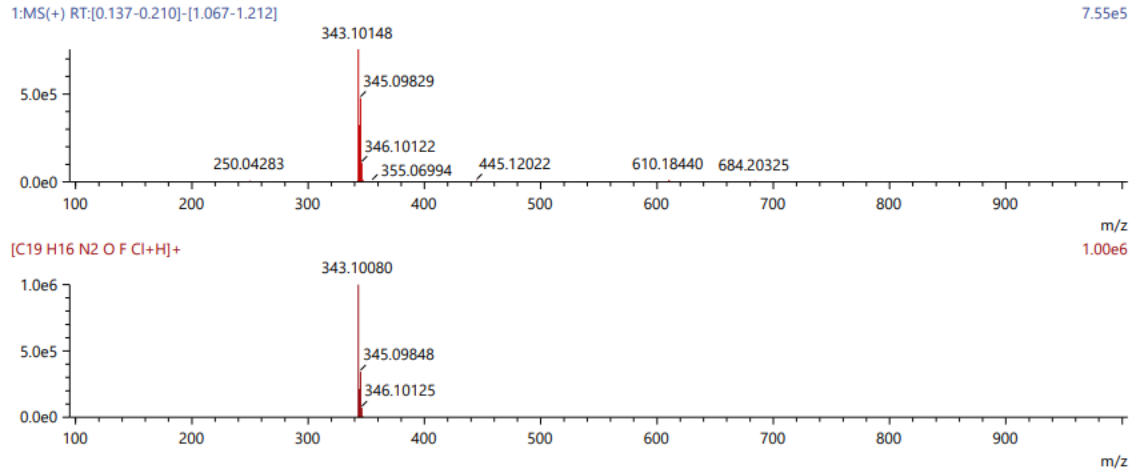

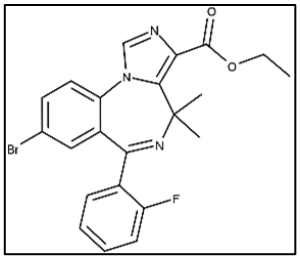

Synthesis of DAW-II-10: A three stopper RB flask was purged with nitrogen and vacuum 3 times. **DAW-I-10** (577.0 mg, 1.60 mmol) was dissolved in anhydrous tetrahydrofuran (6.8 mL) and added to the reaction flask. The mixture was cooled to -20 °C using a dry ice/IPA bath. A solution of 1M potassium *tert*-butoxide in anhydrous tetrahydrofuran (2.08 mL) was added dropwise over the course of 10 min, at which time the reaction color turned to a deep orange. Upon completion of the addition, the mixture was allowed to stir at -20 °C for 40 min. Diethyl chlorophosphate (0.32 mL, 2.24 mmol) was added dropwise over the course of 5 min while maintaining a temperature of -20 °C. After 3.5 h, no more conversion was observed via TLC (100% EtOAc) and ethyl isocyanoacetate (0.23 mL, 2.08 mmol) was added dropwise over the course of 5 min followed by the addition of a solution of 1M potassium *tert*-butoxide in anhydrous tetrahydrofuran (2.08 mL) at -20 °C. The reaction was then warmed to room temperature for 2 h at which point all intermediate had been consumed via TLC (100% EtOAc). The reaction was then quenched with 5% aqueous sodium bicarbonate (25 mL), and the product was extracted with ethyl acetate (25 mL). The organic layer was washed with 10% aqueous sodium bicarbonate (25 mL) followed by 20% aqueous NaCl (25 mL). The organic layer was then dried with $MgSO_4$ and then concentrated under reduced pressure. The resulting residue was triturated with a 50% mixture of tert-butyl methyl ether in hexanes (12 mL) at 55 °C for 20 h. The *tert*-butyl methyl ether/hexanes mixture was decanted, and the solid product was slurried in 100% hexanes (20 mL) at 55 °C for 4 h. The desired product was collected by filtration to yield an off-white solid (465.1 g, 63.8%): ^{1}H NMR (500 MHz, $CDCl_3$) -25°C δ 7.96 (s, 1H), 7.74-7.72 (dd, *J* = 3.60, 2.25 Hz, 1H), 7.59-7.56 (m, 1H), 7.47-7.43 (m, 2H), 7.38-7.37 (d, *J* = 2.15 Hz, 1H), 7.28-7.25 (dt, *J* = 3.20, 0.95 Hz, 1H), 7.06-7.02 (m, 1H), 4.44-4.30 (m, 2H), 2.14 (s, 3H), 1.40-1.36 (t, *J* = 7.15 Hz, 3H), 1.27 (s, 3H);

^{13}C NMR (126 MHz, $CDCl_3$) -25°C δ 164.62 (s), 160.91 (s), 160.07 (d, $^{1}J_{CF}$ = 250.72 Hz), 140.23 (s), 135.56 (s), 135.20 (s), 134.31 (s), 132.45 (s), 132.39 (s), 131.44 (d, $^{4}J_{CF}$ = 1.61 Hz), 131.02 (s), 130.81 (s), 127.97 (d, $^{2}J_{CF}$ = 12.48 Hz), 124.92 (d, $^{3}J_{CF}$ = 3.13 Hz), 124.33 (s), 121.20 (s), 116.42 (d, $^{2}J_{CF}$ = 21.13 Hz), 61.85 (s), 57.08 (s), 32.78 (s), 23.13 (s), 14.38 (d, *J* = 1.27 Hz); ^{19}F NMR (471 MHz, $CDCl_3$) -25°C δ -112.13; HRMS (ESI/IT-TOF): *m/z* $[M + H]^+$ calcd for $C_{22}H_{19}BrFN_3O_2$: 456.0717; found: 456.0711; HPLC Purity: 97.19%.

Figure 111: DAW-II-10 ^{1}H spectra:

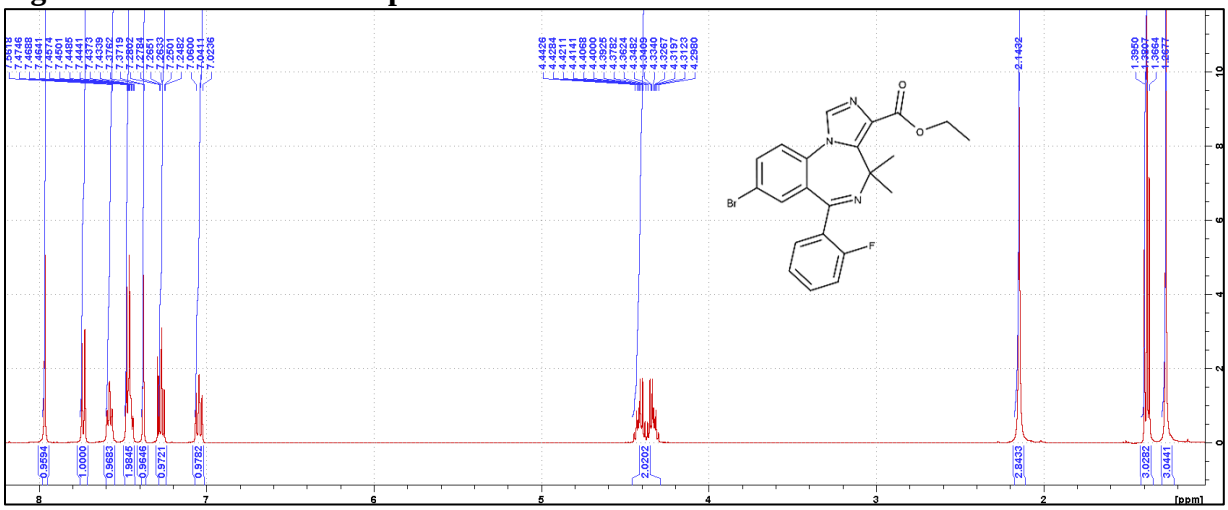

Figure 112: DAW-II-10 ^{13}C spectra:

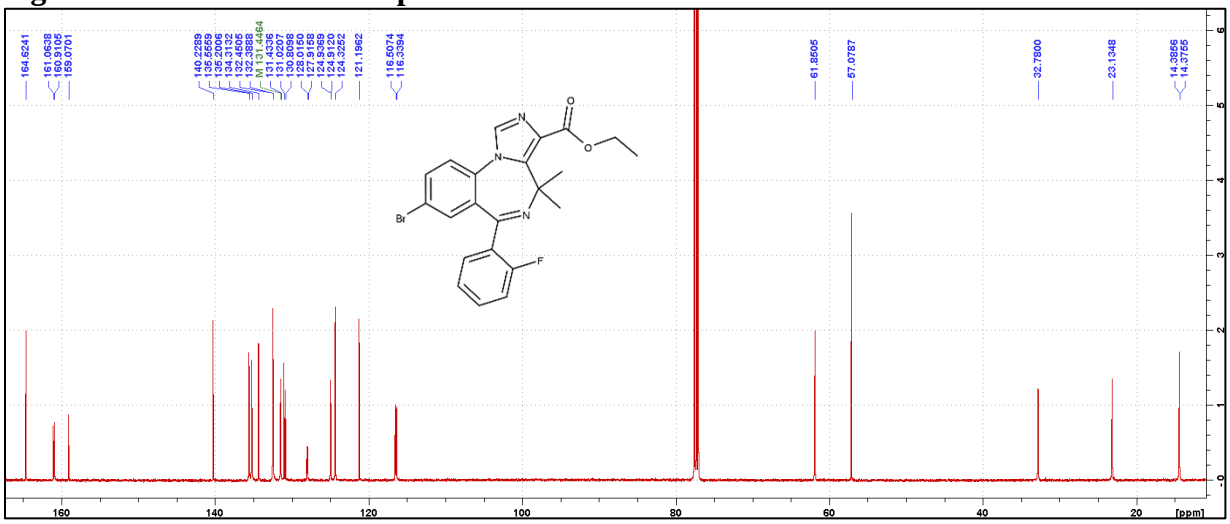

Figure 113: DAW-II-10 ^{19}F spectra:

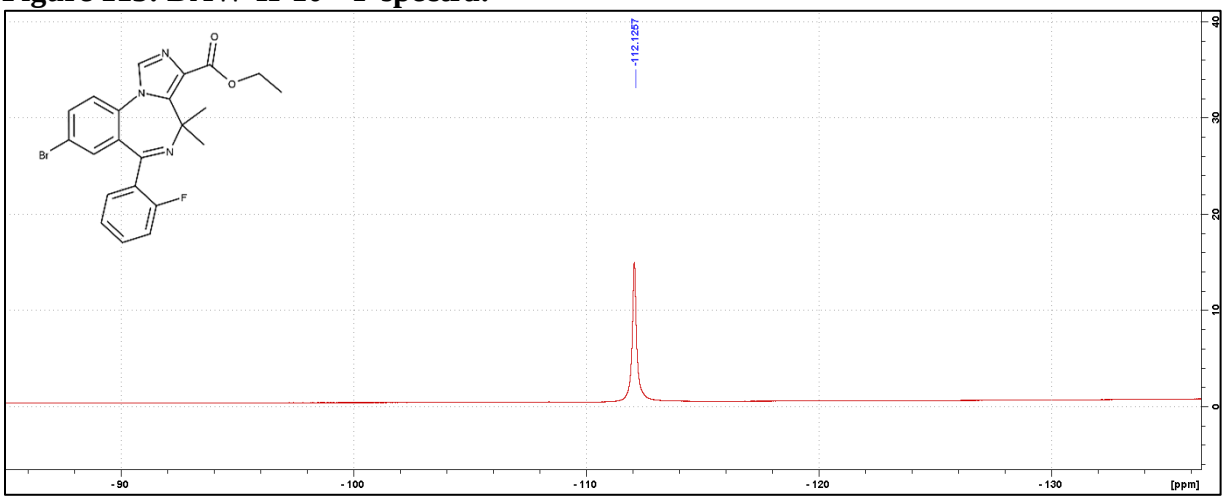

Figure 114: DAW-II-10 HPLC UV Chromatograph:

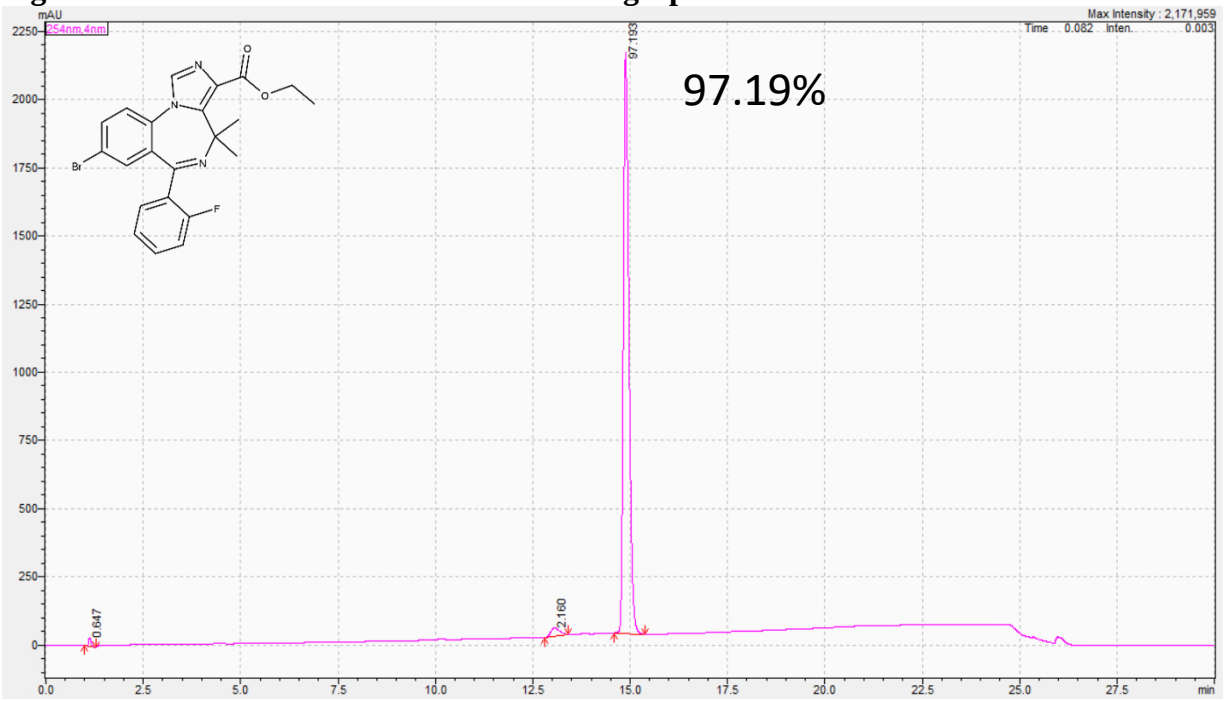

Figure 115: DAW-II-10 HRMS:

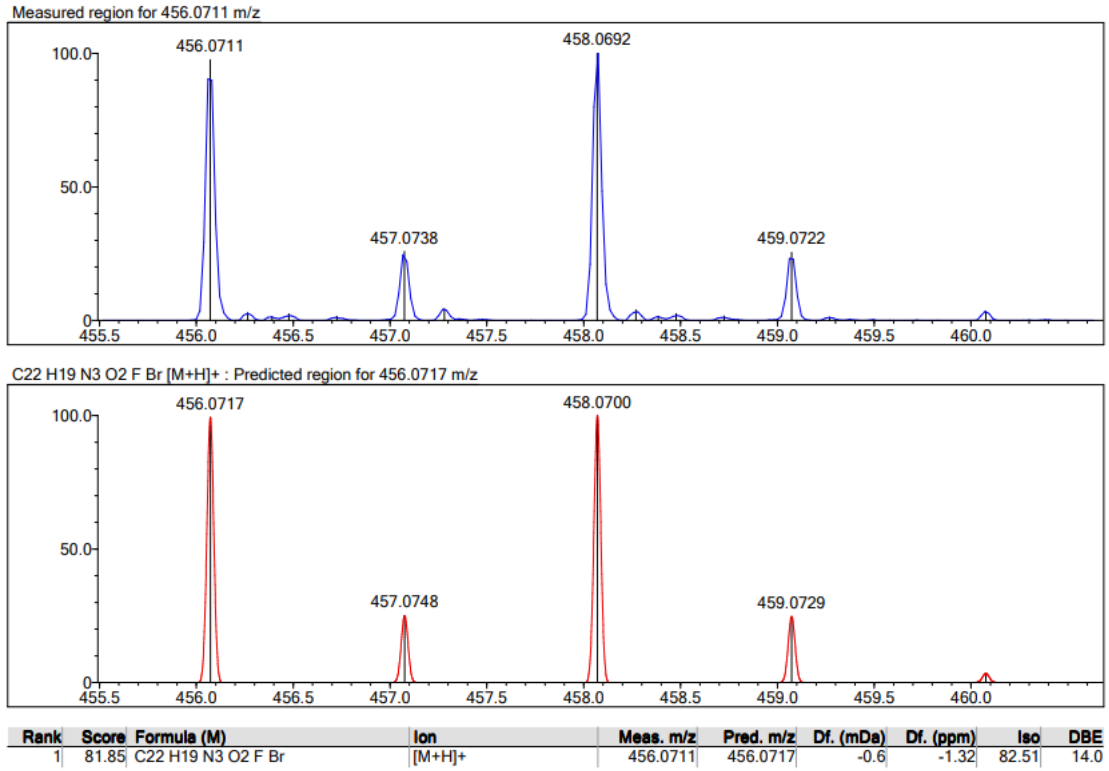

Rank	Score	Formula (M)	Ion	Meas. m/z	Pred. m/z	Df. (mDa)	Df. (ppm)	Iso	DBE
1	81.85	C22 H19 N3 O2 F Br	[M+H]+	456.0711	456.0717	-0.6	-1.32	82.51	14.0

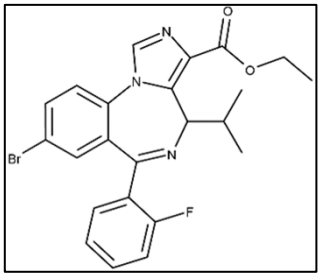

Synthesis of DAW-II-20: A three stopper RB flask was purged with nitrogen and vacuum 3 times. **DAW-I-20** (630.68 mg, 1.70 mmol) was dissolved in anhydrous tetrahydrofuran (8 mL) and added to the reaction flask. The mixture was cooled to -20 °C using a dry ice/IPA bath. A solution of 1M potassium *tert*-butoxide in anhydrous tetrahydrofuran (2.21 mL) was added dropwise over the course of 10 min, at which time the reaction color turned to a deep orange. Upon completion of the addition, the mixture was allowed to stir at -20 °C for 40 min. Diethyl chlorophosphate (0.34 mL, 2.38 mmol) was added dropwise over the course of 5 min while maintaining a temperature of -20 °C. After 3.5 h, no more conversion was observed via TLC (100% EtOAc) and ethyl isocyanoacetate (0.24 mL, 2.21 mmol) was added dropwise over the course of 5 min followed by the addition of a solution of 1M potassium *tert*-butoxide in anhydrous tetrahydrofuran (2.21 mL) at -20 °C. The reaction was then warmed to room temperature for 2 h

at which point all of the intermediate had been consumed via TLC (100% EtOAc). The reaction was then quenched with 5% aqueous sodium bicarbonate (30 mL), and the product was extracted with ethyl acetate (30 mL). The organic layer was washed with 10% aqueous sodium bicarbonate (30 mL) followed by 20% aqueous NaCl (30 mL). The organic layer was then dried with $MgSO_4$ and then concentrated under reduced pressure. The residue was loaded onto a precolumn with chloroform and separated by Biotage: 20-80% ethyl acetate in hexanes (30 CV). The desired product was obtained as an off-white solid (500.84 mg, 62.9%): ^{1}H NMR (500 MHz, $CDCl_3$) δ 7.92 (s, 1H), 7.73-7.71 (dd, *J* = 3.58, 2.20 Hz, 1H), 7.60-7.57 (dt, *J* = 3.33, 1.60 Hz, 1H), 7.49-7.45 (m, 2H), 7.43-7.42 (d, *J* = 1.95 Hz, 1H), 7.27-7.25 (m, 1H), 7.09-7.06 (m, 1H), 6.27-6.25 (d, *J* = 11.20, 1H), 4.51-4.33 (m, 2H), 1.91-1.84 (oct, *J* = 5.32 Hz, 1H), 1.45-1.42 (t, *J* = 7.13 Hz, 3H), 1.12-1.11 (d, *J* = 6.45 Hz, 3H), 0.82-0.80 (d, *J* = 6.55 Hz, 3H); ^{13}C NMR (126 MHz, $CDCl_3$) δ 162.92 (s), 162.32 (s), 160.13 (d, $^1J_{CF}$ = 251.07 Hz), 140.69 (s), 134.82 (s), 134.61 (s), 133.70 (s), 132.80 (s), 132.12 (d, $^3J_{CF}$ = 8.19 Hz), 131.52 (s), 131.25 (s), 131.21 (s), 128.40 (d, $^2J_{CF}$ = 12.94 Hz), 124.58 (d, $^4J_{CF}$ = 3.66 Hz), 123.53 (s), 120.99 (s), 116.31 (d, $^2J_{CF}$ = 21.54 Hz), 62.04 (s), 60.76 (s), 28.93 (s), 20.71 (s), 20.37 (s), 14.44 (s); ^{19}F NMR (471 MHz, $CDCl_3$) δ -112.23; HRMS (ESI/Q-TOF): *m/z* $[M + H]^+$ calcd for $C_{23}H_{21}BrFN_3O_2$: 470.08739; found: 470.08922; HPLC Purity: 96.55%.

Figure 116: DAW-II-20 ^{1}H spectra:

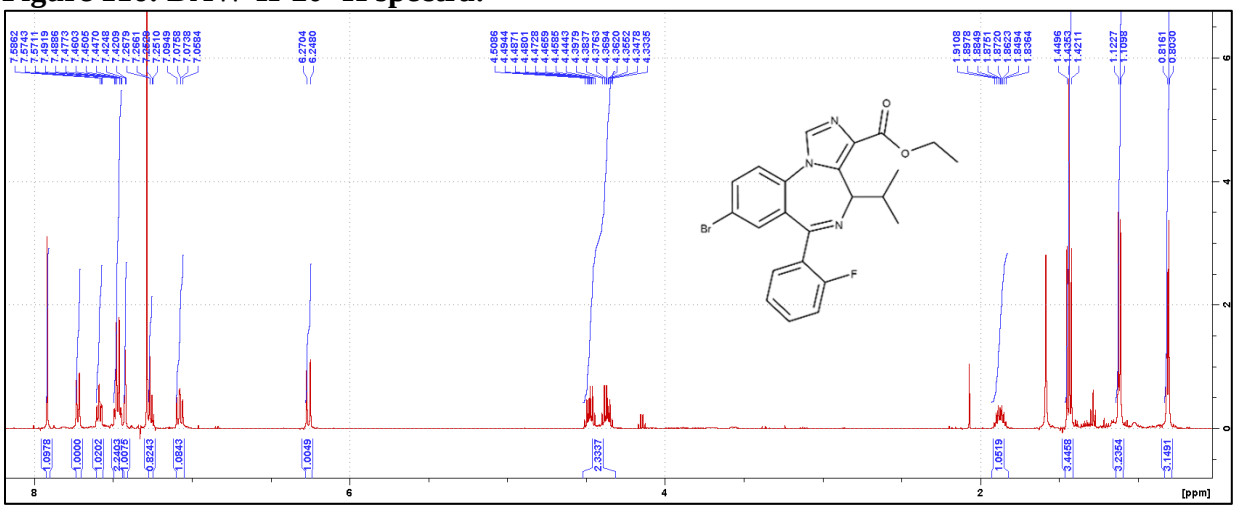

Figure 117: DAW-II-20 ^{13}C spectra:

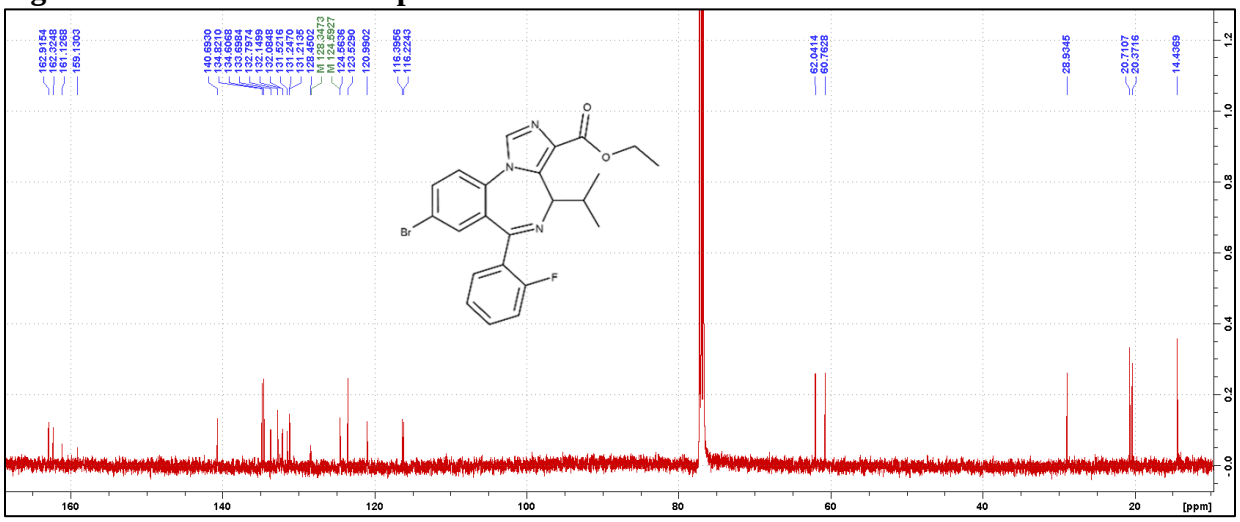

Figure 118: DAW-II-20 ^{19}F spectra:

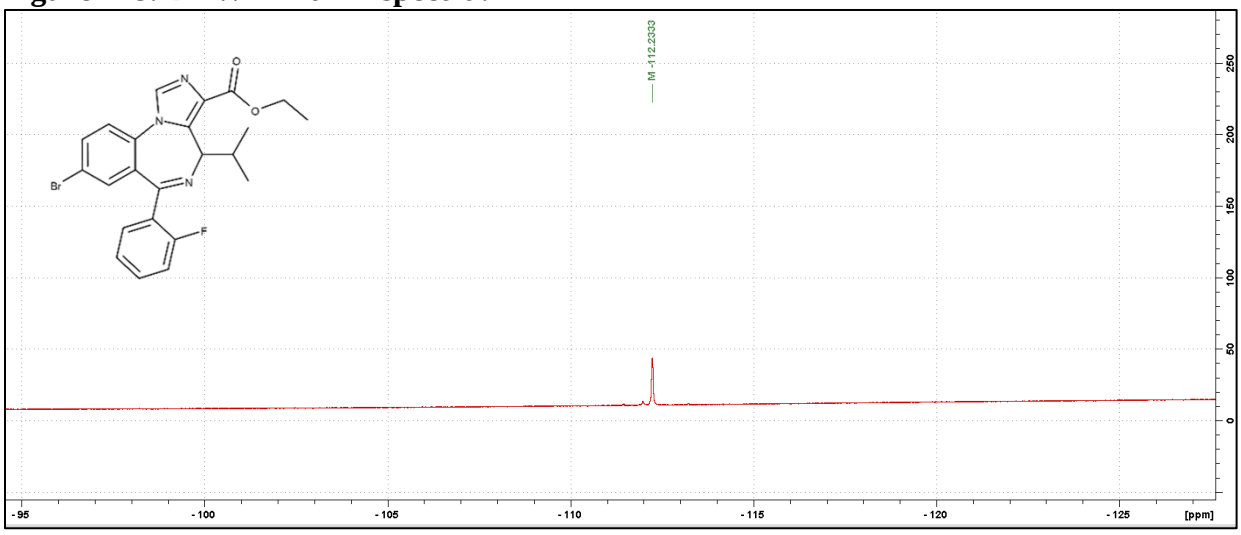

Figure 119: DAW-II-20 HPLC UV Chromatograph:

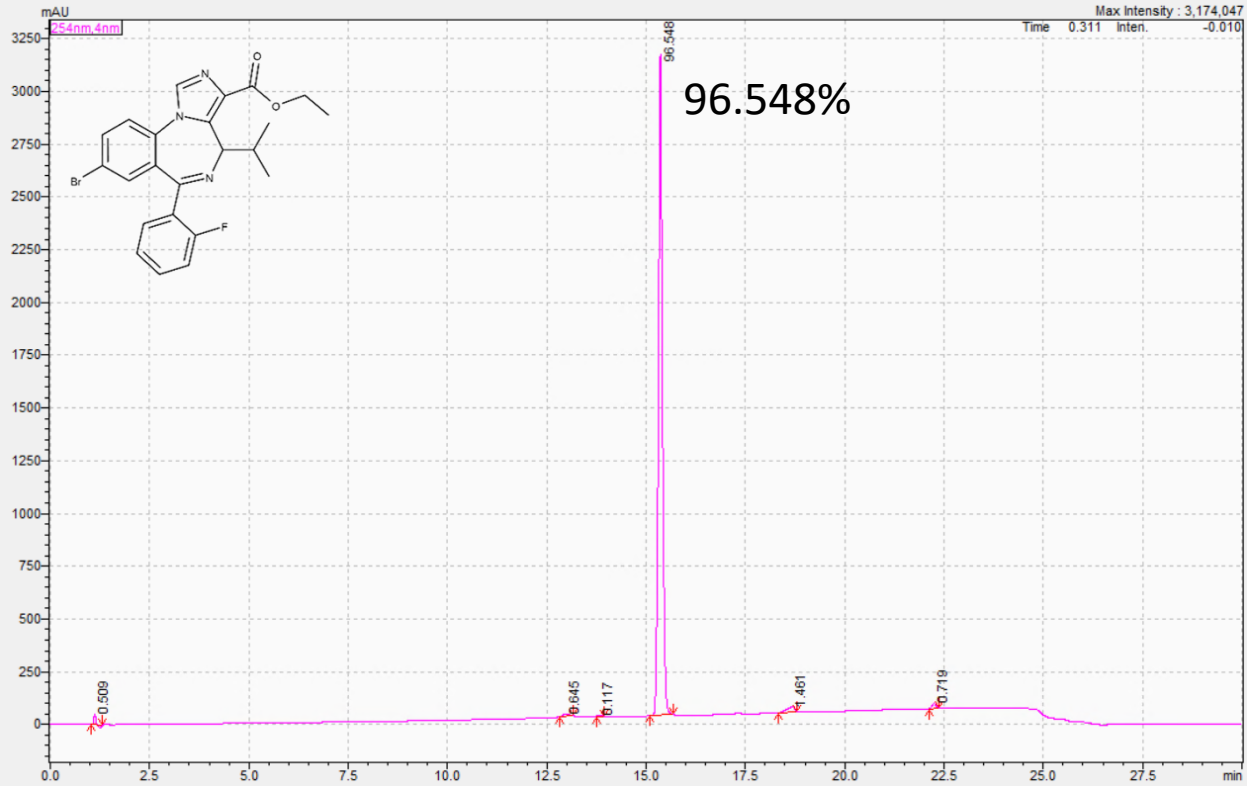

Figure 120: DAW-II-20 HRMS:

Score	Pred. (M)	Pred. m/z	Meas. m/z	Diff. (mDa)	Formulae (M)	Ion	Diff. (ppm)	Iso Score	DBE
29.29	469.08012	470.08739	470.08922	1.83	C23 H21 N3 O2 F Br	[M+H]+	3.893	24.97	14.0

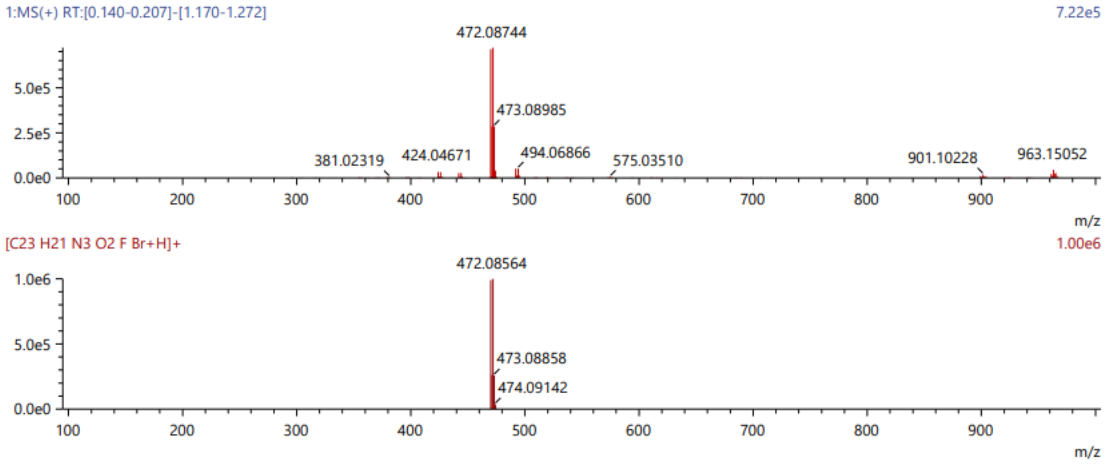

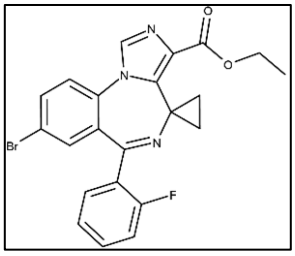

Synthesis of DAW-II-30: A three stopper RB flask was purged with nitrogen and vacuum 3 times. **DAW-I-30** (1.46 g, 4.06 mmol) was dissolved in anhydrous tetrahydrofuran (25 mL) and added to the reaction flask. The mixture was cooled to -20 °C using a dry ice/IPA bath. A solution of 1M potassium *tert*-butoxide in anhydrous tetrahydrofuran (5.28 mL) was added dropwise over the course of 10 min, at which time the reaction color turned to a deep orange. Upon completion of the addition, the mixture was allowed to stir at -20 °C for 40 min. Diethyl chlorophosphate (0.82 mL, 5.68 mmol) was added dropwise over the course of 5 min while maintaining a temperature of -20 °C. After 3.5 h, no more conversion was observed via TLC (100% EtOAc) and ethyl isocyanoacetate (0.58 mL, 5.28 mmol) was added dropwise over the course of 5 min followed by the addition of a solution of 1M potassium *tert*-butoxide in anhydrous tetrahydrofuran (5.28 mL) at -20 °C. The reaction was then warmed to room temperature for 2 h at which point all of the intermediate had been consumed via TLC (100% EtOAc). The reaction was then quenched with 5% aqueous sodium bicarbonate (60 mL), and the product was extracted with ethyl acetate (60 mL). The organic layer was washed with 10% aqueous sodium bicarbonate (60 mL) followed by 20% aqueous NaCl (60 mL). The organic layer was then dried with $MgSO_4$ and then concentrated under reduced pressure. The resulting residue was triturated with a 50% mixture of tert-butyl methyl ether in hexanes (25 mL) at 55 °C for 20 h. The *tert*-butyl methyl ether/hexanes mixture was decanted, and the solid product was slurried in 100% hexanes (30 mL) at 55 °C for 4 h. The desired product was collected by filtration to yield an off-white solid (1.07 g, 58.0%): ^{1}H NMR (500 MHz, $CDCl_3$) -18°C δ 7.90 (s, 1H), 7.73-7.70 (dd, *J* = 3.58, 2.20 Hz, 1H), 7.55-7.52 (dt, *J* = 3.33, 1.60 Hz, 1H), 7.46-7.45 (d, *J* = 8.60 Hz, 1H), 7.42-7.38 (m, 1H), 7.36-7.35 (d, *J* = 2.15 Hz, 1H), 7.19-7.16 (dt, *J* = 3.21, 0.90 Hz, 1H), 6.99-6.95 (m, 1H), 4.42-4.36 (m, 1H),

4.31-4.25 (m, 1H), 1.97-1.92 (m, 1H), 1.68-1.63 (m, 1H), 1.37-1.34 (t, J = 7.13 Hz, 3H), 0.72-0.63 (m, 2H); ^{13}C NMR (126 MHz, $CDCl_3$) -18°C δ 168.16 (s), 162.33 (s), 160.08 (d, $^{1}J_{CF}$ = 251.60 Hz), 140.21 (s), 135.07 (s), 134.31 (s), 133.80 (s), 132.81 (d, $^{3}J_{CF}$ = 8.43 Hz), 132.56 (d, $^{4}J_{CF}$ = 1.37 Hz), 132.29 (s), 131.34 (d, $^{3}J_{CF}$ = 1.75 Hz), 128.87 (s), 126.82 (d, $^{2}J_{CF}$ = 11.63 Hz), 124.72 (d, $^{3}J_{CF}$ = 3.26 Hz), 124.07 (s), 121.15 (s), 116.42 (d, $^{2}J_{CF}$ = 21.28 Hz), 61.11 (s), 37.20 (s), 15.28 (s), 14.59 (s), 14.52 (s); ^{19}F NMR (471 MHz, $CDCl_3$) -18°C δ -111.35; HRMS (ESI/Q-TOF): *m/z* $[M + H]^+$ calcd for $C_{22}H_{17}BrFN_3O_2$: 454.05609; found: 454.05755; HPLC Purity: 99.75%.

Figure 121: DAW-II-30 ^{1}H spectra:

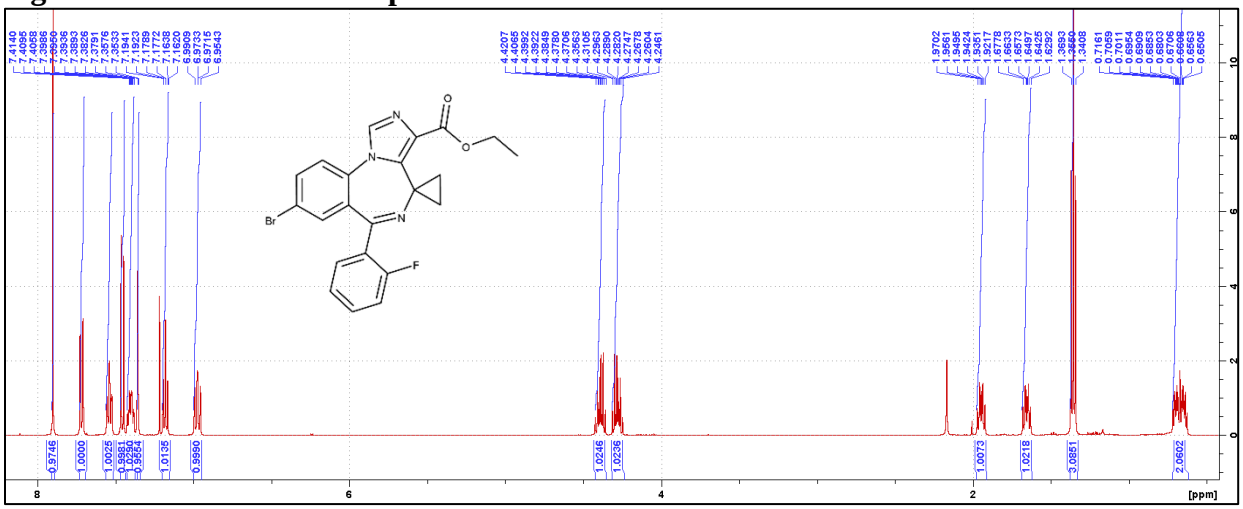

Figure 122: DAW-II-30 ^{13}C spectra:

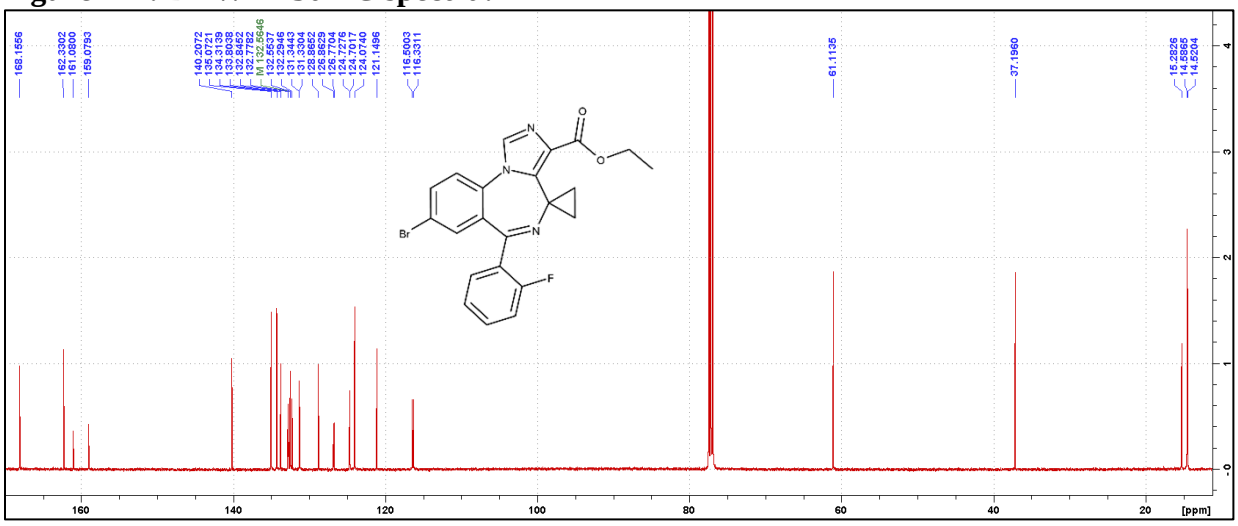

Figure 123: DAW-II-30 ^{19}F spectra:

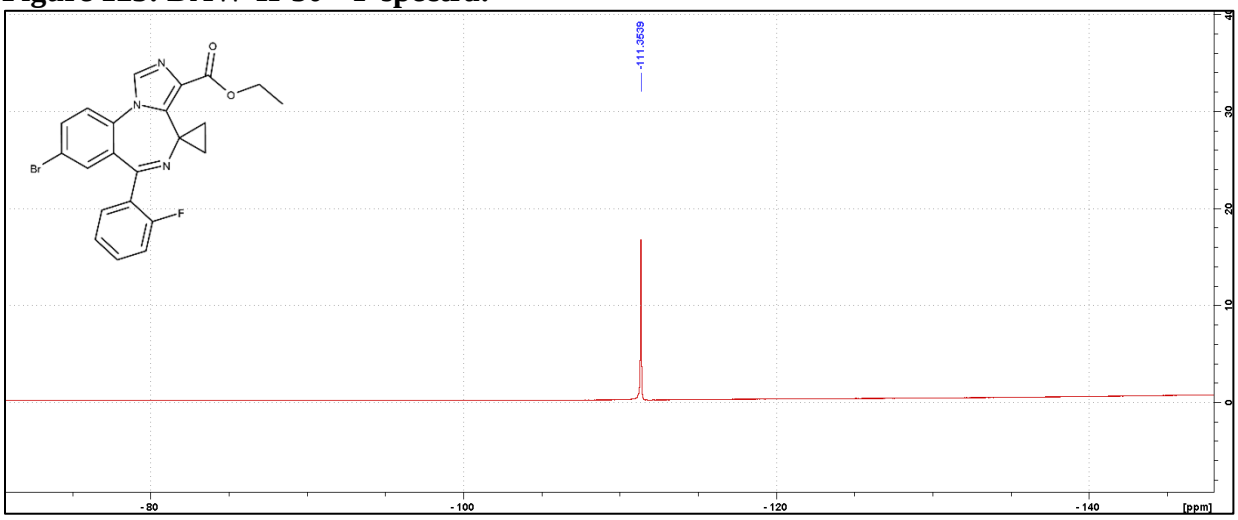

Figure 124: DAW-II-30 HPLC UV Chromatograph:

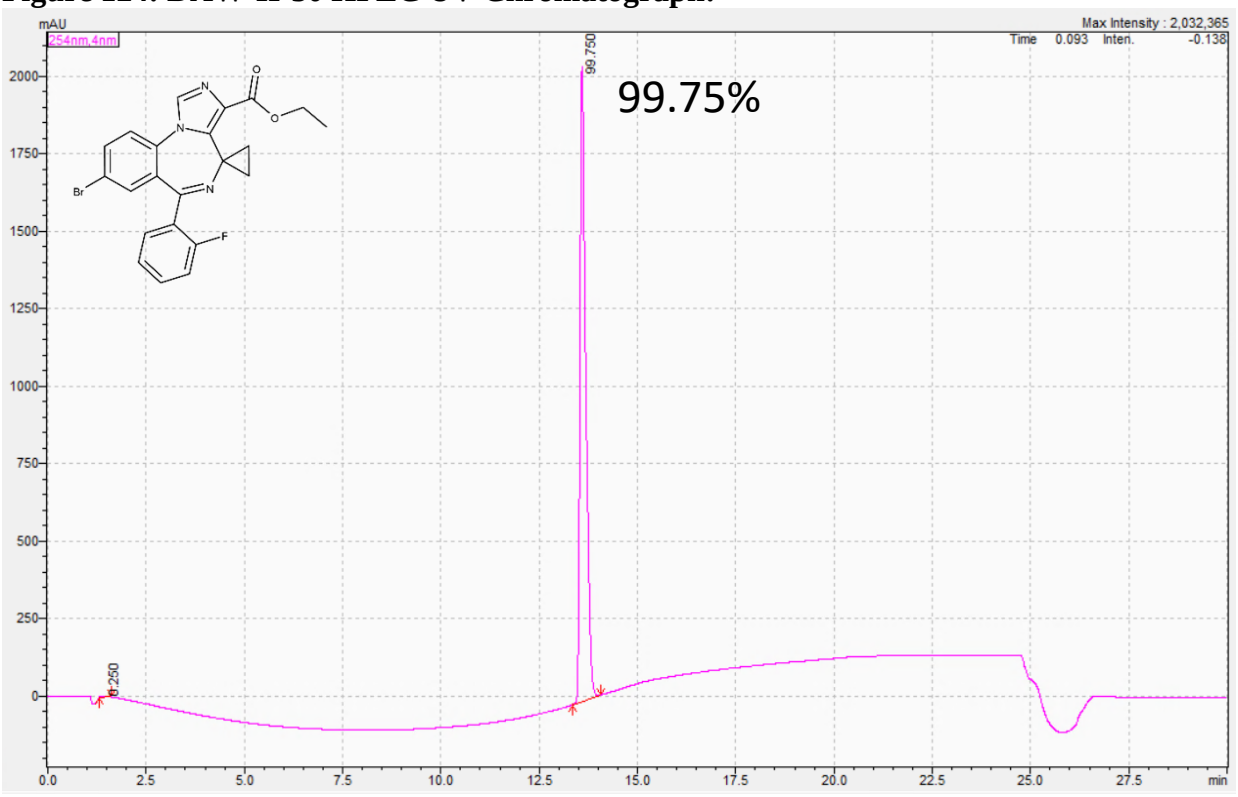

Figure 125: DAW-II-30 HRMS:

Score	Pred. (M)	Pred. m/z	Meas. m/z	Diff. (mDa)	Formulae (M)	Ion	Diff. (ppm)	Iso Score	DBE
45.77	453.04882	454.05609	454.05755	1.46	C22 H17 N3 O2 F Br	[M+H]+	3.215	42.16	15.0

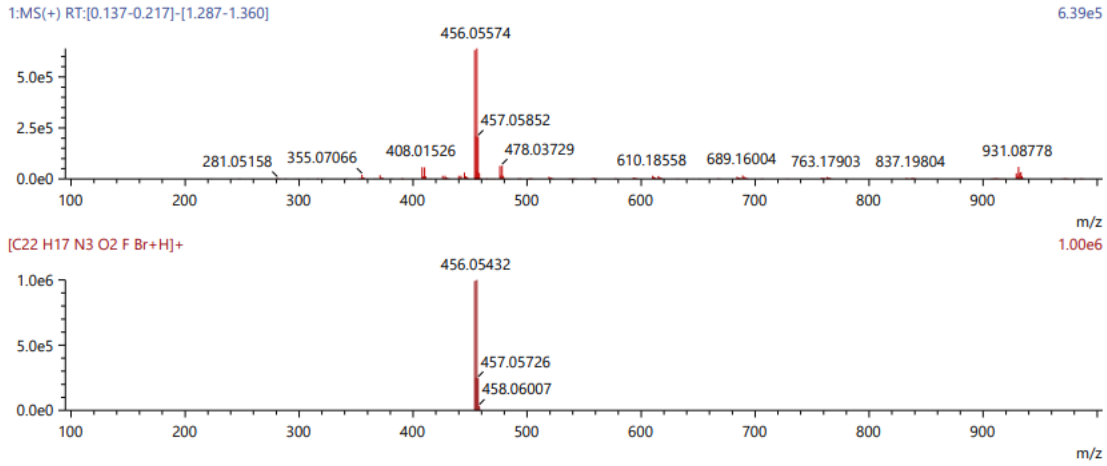

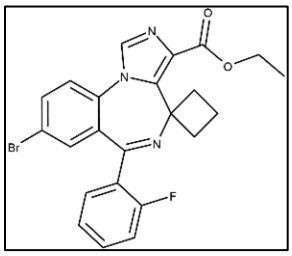

Synthesis of DAW-II-40: A three stopper RB flask was purged with nitrogen and vacuum 3 times. **DAW-I-40** (749.43 mg, 2.01 mmol) was dissolved in anhydrous tetrahydrofuran (8mL) and added to the reaction flask. The mixture was cooled to -20 °C using a dry ice/IPA bath. A solution of 1M potassium *tert*-butoxide in anhydrous tetrahydrofuran (2.61 mL) was added dropwise over the course of 10 min, at which time the reaction color turned to a deep orange. Upon completion of the addition, the mixture was allowed to stir at -20 °C for 40 min. Diethyl chlorophosphate (0.41 mL, 2.81 mmol) was added dropwise over the course of 5 min while maintaining a temperature of -20 °C. After 3.5 h, no more conversion was observed via TLC (100% EtOAc) and ethyl isocyanoacetate (0.29 mL, 2.61 mmol) was added dropwise over the course of 5 min followed by the addition of a solution of 1M potassium *tert*-butoxide in anhydrous tetrahydrofuran (2.61 mL) at -20 °C. The reaction was then warmed to room temperature for 2 h at which point all of the intermediate had been consumed via TLC (100% EtOAc). The reaction was then quenched with 5% aqueous sodium bicarbonate (35 mL), and the product was extracted with ethyl acetate (35 mL). The organic layer was washed with 10% aqueous sodium bicarbonate

(35 mL) followed by 20% aqueous NaCl (35 mL). The organic layer was then dried with $MgSO_4$ and then concentrated under reduced pressure. The resulting residue was triturated with a 50% mixture of *tert*-butyl methyl ether in hexanes (15 mL) at 55 °C for 20 h. The tert-butyl methyl ether/hexanes mixture was decanted, and the solid product was slurried in 100% hexanes (20 mL) at 55 °C for 4 h. The desired product was collected by filtration to yield an off-white solid (562.7 mg, 59.8%): ^{1}H NMR (500 MHz, $CDCl_3$) -20°C δ 7.79 (s, 1H), 7.65-7.63 (dd, *J* = 3.58, 2.20 Hz, 1H), 7.62-7.59 (dt, *J* = 3.39, 1.80 Hz, 1H), 7.39-7.35 (m, 3H), 7.20-7.17 (dt, *J* = 4.03, 1.00 Hz, 1H), 6.98-6.94 (m, 1H), 4.35-4.28 (m, 2H), 3.61-3.55 (m, 1H), 2.97-2.91 (m, 1H), 2.06-2.00 (m, 1H), 1.93-1.85 (m, 1H), 1.81-1.75 (m, 1H), 1.73-1.68 (m, 1H), 1.35-1.32 (t, *J* = 7.13 Hz, 3H); ^{13}C NMR (126 MHz, $CDCl_3$) -20°C δ 162.86 (s), 161.03 (s), 160.33 (d, $^{1}J_{CF}$ = 251.31 Hz), 141.84 (s), 134.85 (d, $^{3}J_{CF}$ = 5.89 Hz), 134.56 (d, $^{3}J_{CF}$ = 9.12 Hz), 133.80 (s), 132.41 (s), 132.29 (s), 132.23 (s), 131.57 (d, $^{4}J_{CF}$ = 2.50 Hz), 129.18 (s), 127.41 (d, $^{2}J_{CF}$ = 12.11 Hz), 124.54 (d, $^{3}J_{CF}$ = 3.47 Hz), 123.92 (s), 121.12 (s), 116.24 (d, $^{2}J_{CF}$ = 21.43 Hz), 62.26 (s), 61.03 (t, *J* = 7.72 Hz), 36.26 (s), 35.06 (s), 16.30 (s), 14.41 (q, *J* = 8.07 Hz); ^{19}F NMR (471 MHz, $CDCl_3$) -20 °C δ -112.00 - -112.05 (qu, *J* = 5.59 Hz); HRMS (ESI/IT-TOF): *m/z* $[M + H]^+$ calcd for $C_{23}H_{19}BrFN_3O_2$: 468.0717; found: 468.0702; HPLC Purity: 98.85%.

Figure 126: DAW-II-40 ^{1}H spectra:

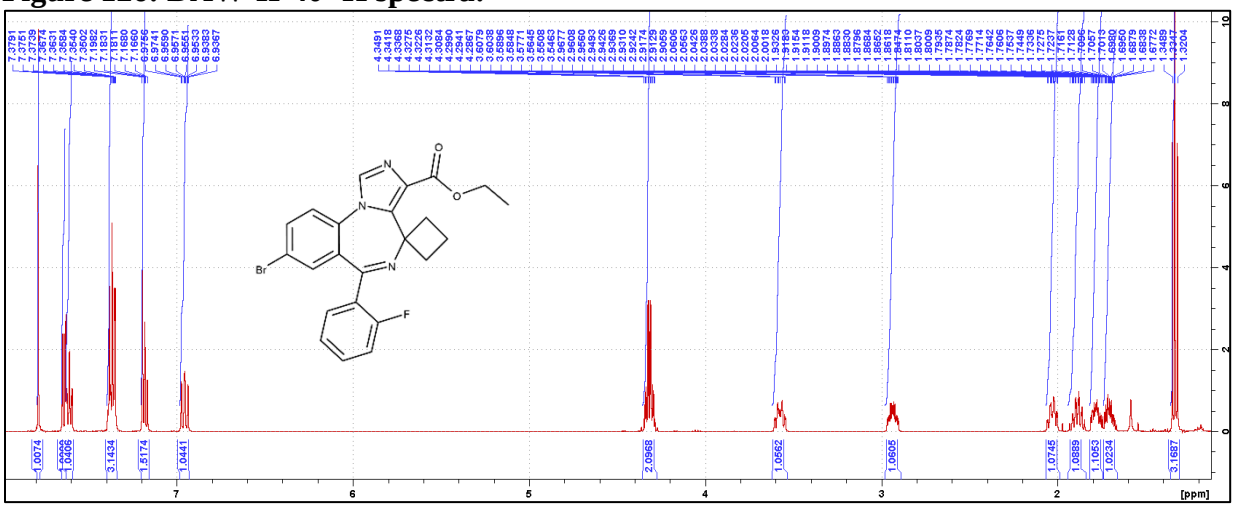

Figure 127: DAW-II-40 ^{13}C spectra:

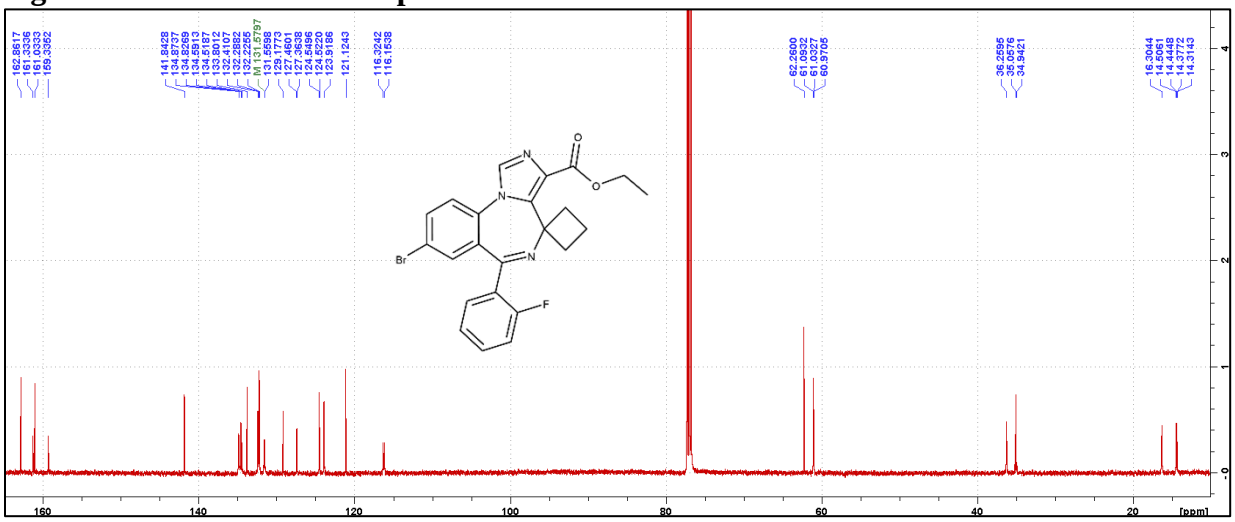

Figure 128: DAW-II-40 ^{19}F spectra:

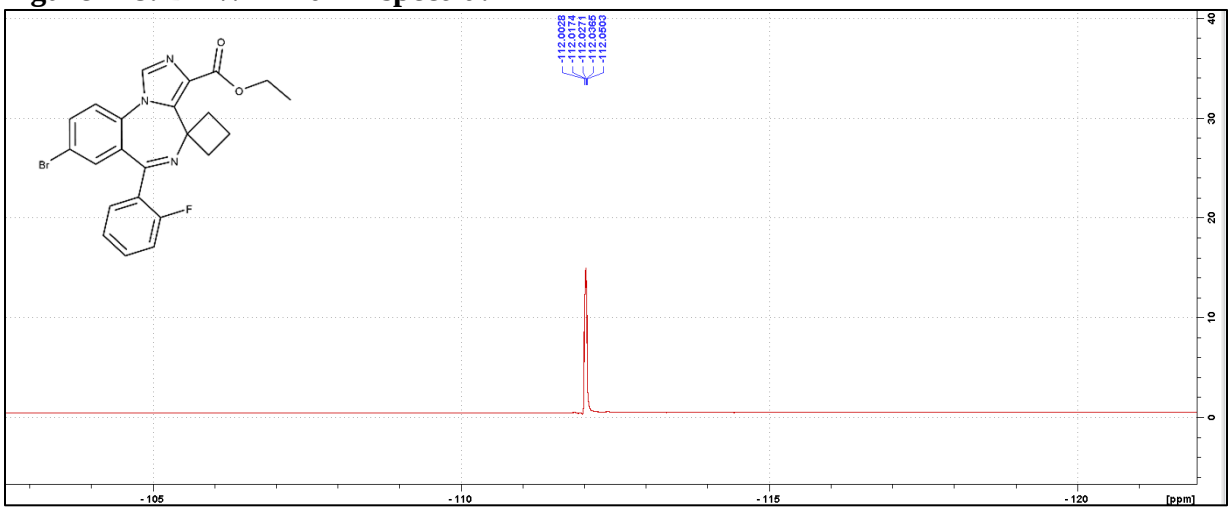

Figure 129: DAW-II-40 HPLC UV Chromatograph:

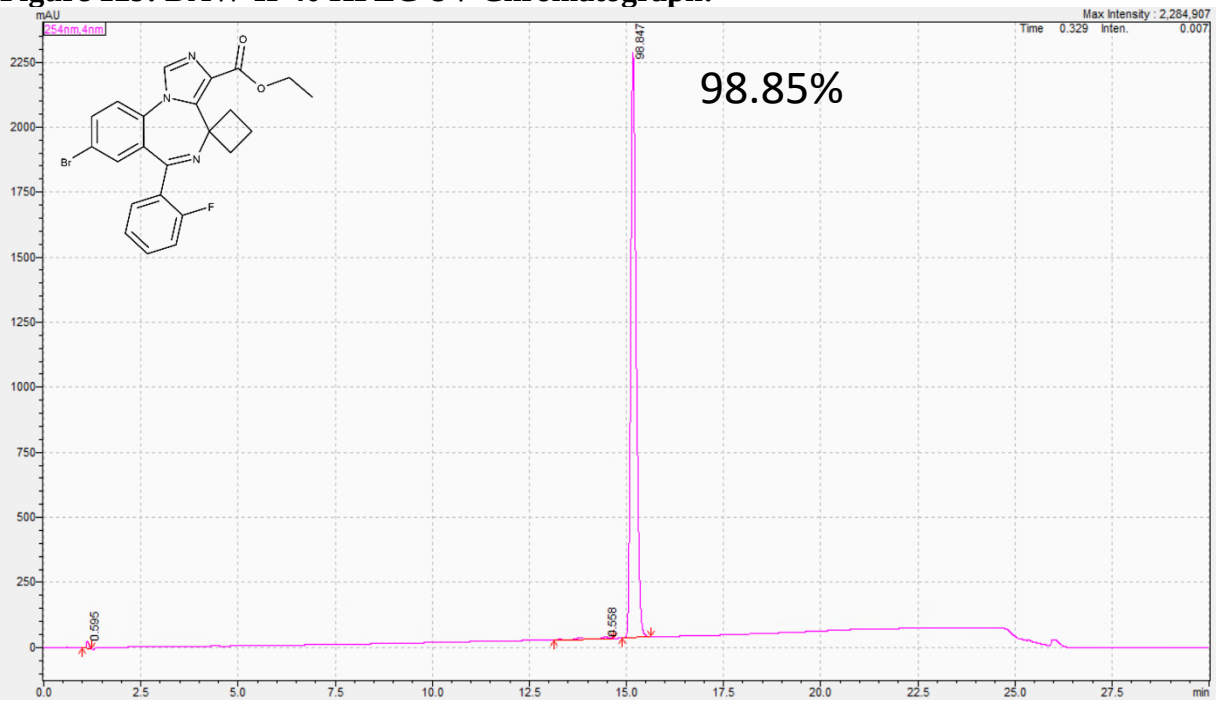

Figure 130: DAW-II-40 HRMS:

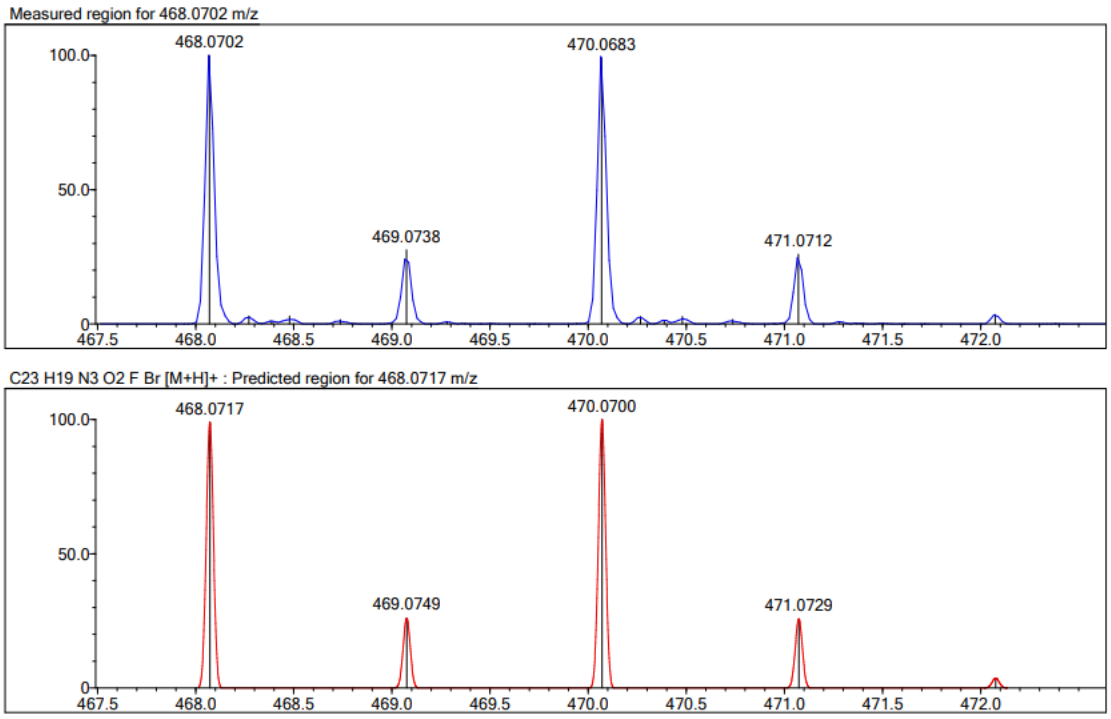

Rank	Score	Formula (M)	Ion	Meas. m/z	Pred. m/z	Df. (mDa)	Df. (ppm)	Iso	DBE
1	75.43	C23 H19 N3 O2 F Br	[M+H]+	468.0702	468.0717	-1.5	-3.20	79.82	15.0

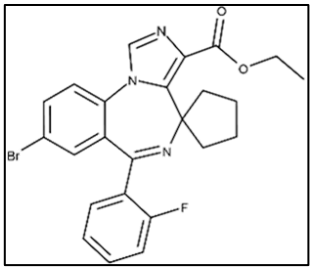

Synthesis of DAW-II-50: A three stopper RB flask was purged with nitrogen and vacuum 3 times. **DAW-I-50** (1.25 g, 3.22 mmol) was dissolved in anhydrous tetrahydrofuran (13.6 mL) and added to the reaction flask. The mixture was cooled to -20 °C using a dry ice/IPA bath. A solution of 1M potassium *tert*-butoxide in anhydrous tetrahydrofuran (4.19 mL) was added dropwise over the course of 10 min, at which time the reaction color turned to a deep orange. Upon completion of the addition, the mixture was allowed to stir at -20 °C for 40 min. Diethyl chlorophosphate (0.65 mL, 4.51 mmol) was added dropwise over the course of 5 min while maintaining a temperature of -20 °C. After 3.5 h, no more conversion was observed via TLC (100% EtOAc) and ethyl isocyanoacetate (0.46 mL, 4.19 mmol) was added dropwise over the course of 5 min followed by the addition of a solution of 1M potassium *tert*-butoxide in anhydrous tetrahydrofuran (4.19 mL) at -20 °C. The reaction was then warmed to room temperature for 2 h at which point all the intermediate had been consumed via TLC (100% EtOAc). The reaction was then quenched with 5% aqueous sodium bicarbonate (50 mL), and the product was extracted with ethyl acetate (50 mL). The organic layer was washed with 10% aqueous sodium bicarbonate (50 mL) followed by 20% aqueous NaCl (50 mL). The organic layer was then dried with $MgSO_4$ and then concentrated under reduced pressure. The resulting residue was triturated with a 50% mixture of *tert*-butyl methyl ether in hexanes (25 mL) at 55 °C for 20 h. The tert-butyl methyl ether/hexanes mixture was decanted, and the solid product was slurried in 100% hexanes (35 mL) at 55 °C for 4 h. The desired product was collected by filtration to yield an off-white solid (1.15 g, 74.1%): ^{1}H NMR (500 MHz, $CDCl_3$) -20°C δ 7.84 (s, 1H), 7.68-7.66 (dd, *J* = 3.58, 2.20 Hz, 1H), 7.49-7.46 (m, 1H), 7.42-7.37 (m, 2H), 7.32-7.31 (d, *J* = 2.15 Hz, 1H), 7.21-7.17 (dt, *J* = 3.19, 0.90 Hz, 1H), 7.00-6.97 (m, 1H), 4.32-4.28 (q, *J* = 7.14 Hz, 2H), 2.80-2.77 (m, 1H), 2.54-2.48 (m, 1H), 1.86-

1.82 (m, 2H), 1.66-1.56 (m, 2H), 1.52-1.48 (m, 2H), 1.35-1.32 (t, J = 7.13 Hz, 3H); ^{13}C NMR (126 MHz, $CDCl_3$) -20°C δ 162.53 (s), 160.10 (s), 158.97 (d, $^{1}J_{CF}$ = 251.06 Hz), 139.88 (s), 134.14 (s), 133.83 (s), 133.26 (s), 131.23 (s), 131.15 (s), 130.67 (s), 130.26 (d, $^{3}J_{CF}$ = 1.94 Hz), 128.54 (s), 126.55 (d, $^{2}J_{CF}$ = 12.27 Hz), 123.62 (d, $^{3}J_{CF}$ = 3.23 Hz), 123.23, 119.99, 115.25 (d, $^{2}J_{CF}$ = 21.24 Hz), 66.08 (s), 60.33 (s), 39.98 (s), 34.77 (s), 22.59 (s), 22.03 (s), 13.25 (s); ^{19}F NMR (471 MHz, $CDCl_3$) -20 °C δ -112.00; HRMS (ESI/IT-TOF): *m/z* $[M + H]^+$ calcd for $C_{24}H_{21}BrFN_3O_2$: 482.0874; found: 482.0869; HPLC Purity: 99.05%.

Figure 131: DAW-II-50 ^{1}H spectra:

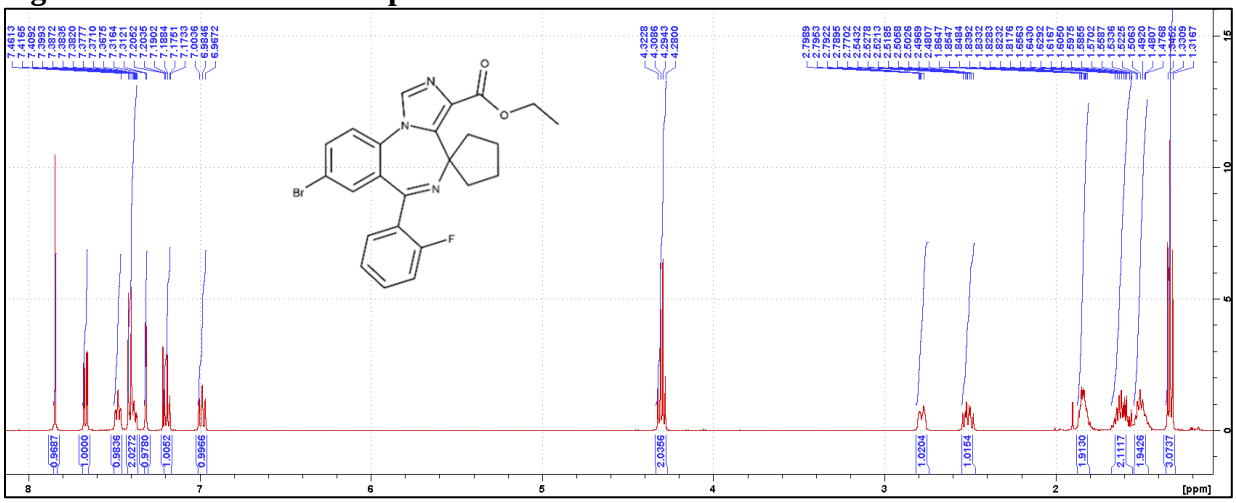

Figure 132: DAW-II-50 ^{13}C spectra:

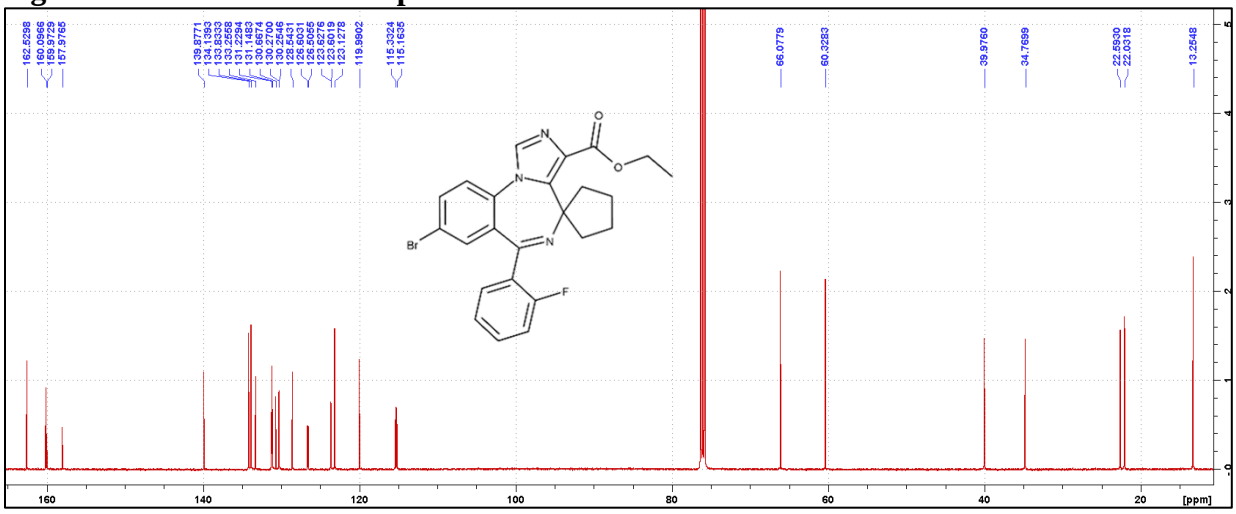

Figure 133: DAW-II-50 ^{19}F spectra:

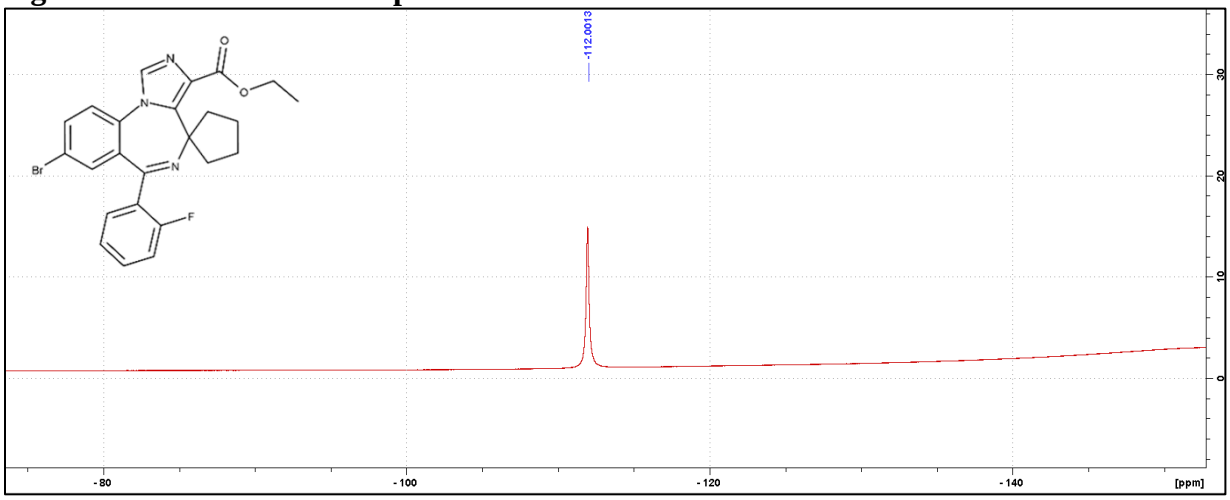

Figure 134: DAW-II-50 HPLC UV Chromatograph:

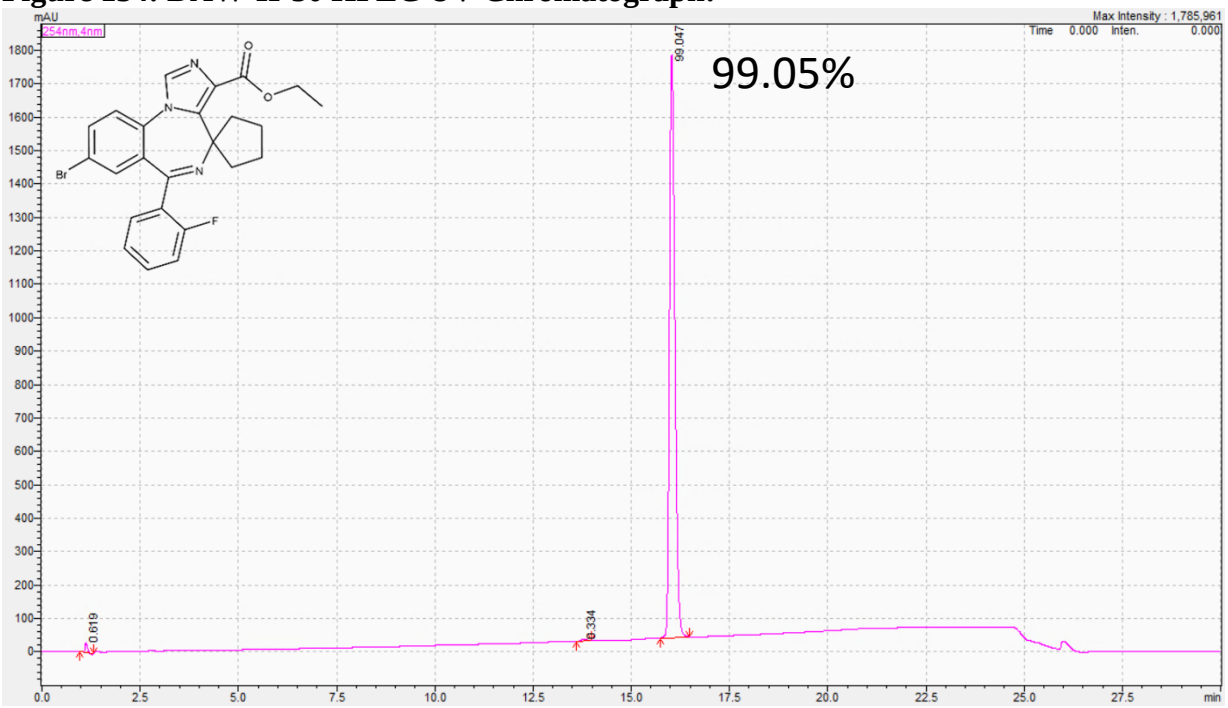

Figure 135: DAW-II-50 HRMS:

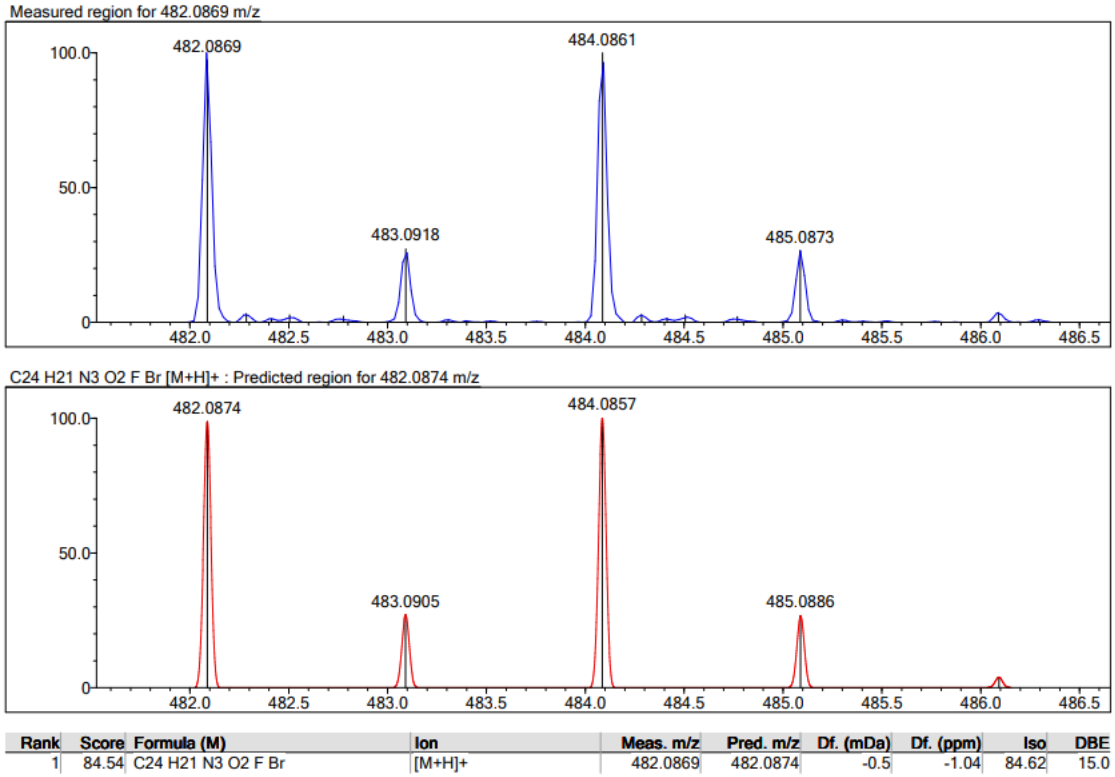

Rank	Score	Formula (M)	Ion	Meas. m/z	Pred. m/z	Df. (mDa)	Df. (ppm)	Iso	DBE
1	84.54	C24 H21 N3 O2 F Br	[M+H]+	482.0869	482.0874	-0.5	-1.04	84.62	15.0

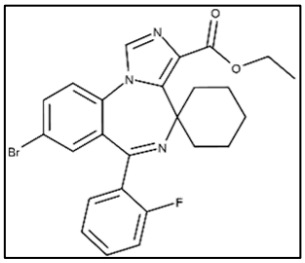

Synthesis of DAW-II-60: A three stopper RB flask was purged with nitrogen and vacuum 3 times. **DAW-I-60** (1.06 g, 2.63 mmol) was dissolved in anhydrous tetrahydrofuran (11.5 mL) and added to the reaction flask. The mixture was cooled to -20 °C using a dry ice/IPA bath. A solution of 1M potassium *tert*-butoxide in anhydrous tetrahydrofuran (2.63 mL) was added dropwise over the course of 10 min, at which time the reaction color turned to a deep orange. Upon completion of the addition, the mixture was allowed to stir at -20 °C for 40 min. Diethyl chlorophosphate (0.53 mL, 3.68 mmol) was added dropwise over the course of 5 min while maintaining a temperature of -20 °C. After 3.5 h, no more conversion was observed via TLC (100% EtOAc) and ethyl isocyanoacetate (0.37 mL, 3.42 mmol) was added dropwise over the course of 5 min followed by the addition of a solution of 1M potassium *tert*-butoxide in anhydrous tetrahydrofuran (2.63 mL) at -20 °C. The reaction was then warmed to room temperature for 2 h

at which point all the intermediate had been consumed via TLC (100% EtOAc). The reaction was then quenched with 5% aqueous sodium bicarbonate (40 mL), and the product was extracted with ethyl acetate (40 mL). The organic layer was washed with 10% aqueous sodium bicarbonate (40 mL) followed by 20% aqueous NaCl (40 mL). The organic layer was then dried with $MgSO_4$ and then concentrated under reduced pressure. The resulting residue was triturated with a 50% mixture of *tert*-butyl methyl ether in hexanes (15 mL) at 55 °C for 20 h. The tert-butyl methyl ether/hexanes mixture was decanted, and the solid product was slurried in 100% hexanes (20 mL) at 55 °C for 4 h. The desired product was collected by filtration to yield an off-white solid (591.4 mg, 45.3%): ^{1}H NMR (500 MHz, $CDCl_3$) -20 °C δ 7.84 (s, 1H), 7.65-7.63 (dd, *J* = 3.58, 2.20 Hz, 1H), 7.54-7.51 (m, 1H), 7.41-7.35 (m, 2H), 7.30-7.29 (d, *J* = 2.15 Hz, 1H), 7.21-7.18 (dt, *J* = 3.16, 0.80 Hz, 1H), 7.01-6.97 (m, 1H), 4.36-4.23 (m, 2H), 2.50-2.48 (m, 1H), 2.43-2.38 (m, 1H), 2.09-2.01 (m, 1H), 1.89-1.86 (m, 1H), 1.79-1.77 (m, 1H), 1.66-1.64 (m, 1H), 1.37-1.25 (m, 6H), 1.16-1.11 (m, 1H); ^{13}C NMR (126 MHz, $CDCl_3$) -20 °C δ 165.00 (s), 160.56 (s), 160.15 (d, $^1J_{CF}$ = 251.09 Hz), 140.14 (s), 135.50 (s), 135.08 (s), 134.61 (s), 132.36 (d, $^3J_{CF}$ = 8.28 Hz), 132.21 (s), 131.46 (d, $^4J_{CF}$ = 1.70 Hz), 130.93 (d, $^3J_{CF}$ = 9.16 Hz), 128.28 (d, $^2J_{CF}$ = 12.52 Hz), 124.84 (d, $^3J_{CF}$ = 3.11 Hz), 123.98 (s), 121.05 (s), 116.51 (d, $^2J_{CF}$ = 21.24 Hz), 61.80 (s), 59.64 (s), 38.30 (s), 31.16 (s), 25.53 (s), 22.17 (s), 22.05 (s), 14.35 (s); ^{19}F NMR (471 MHz, $CDCl_3$) -20°C δ -112.22; HRMS (ESI/Q-TOF): *m/z* $[M + H]^+$ calcd for $C_{25}H_{23}BrFN_3O_2$: 496.10304; found: 496.10492; HPLC Purity: 99.29%.

Figure 136: DAW-II-60 ^{1}H spectra:

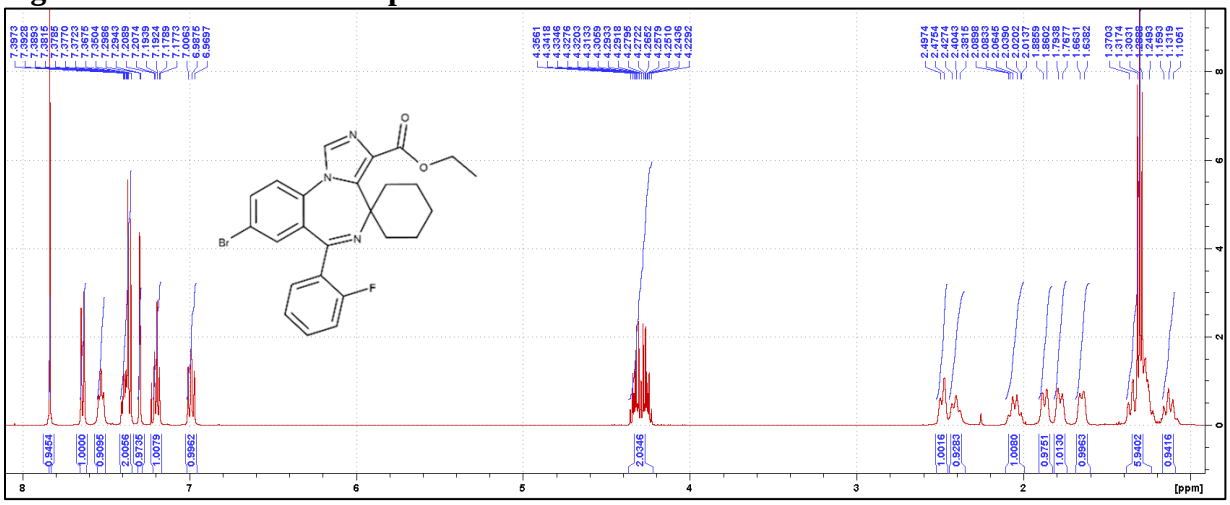

Figure 137: DAW-II-60 ^{13}C spectra:

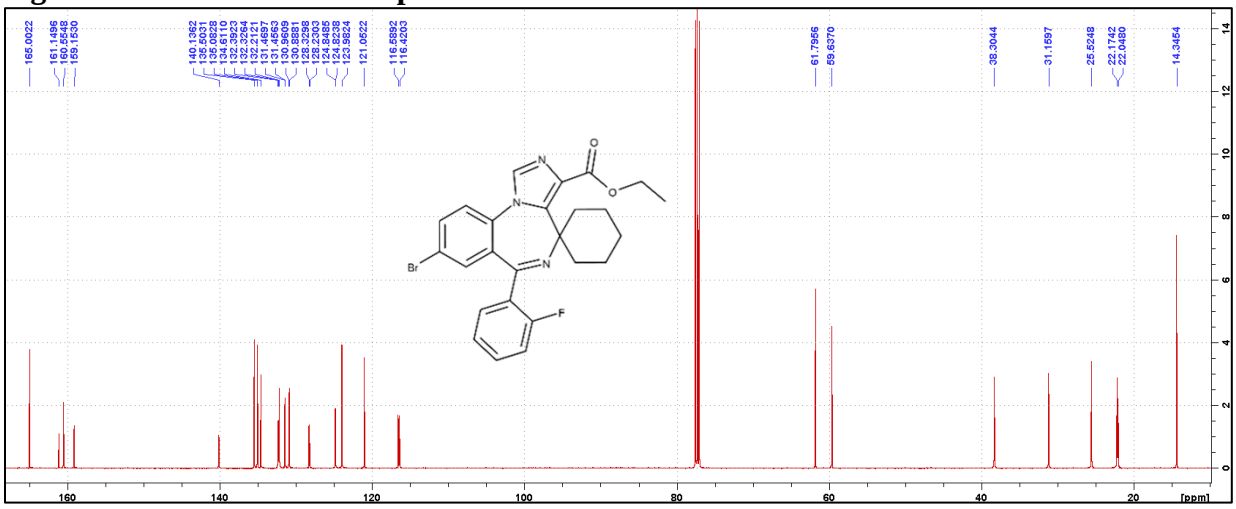

Figure 138: DAW-II-60 ^{19}F spectra:

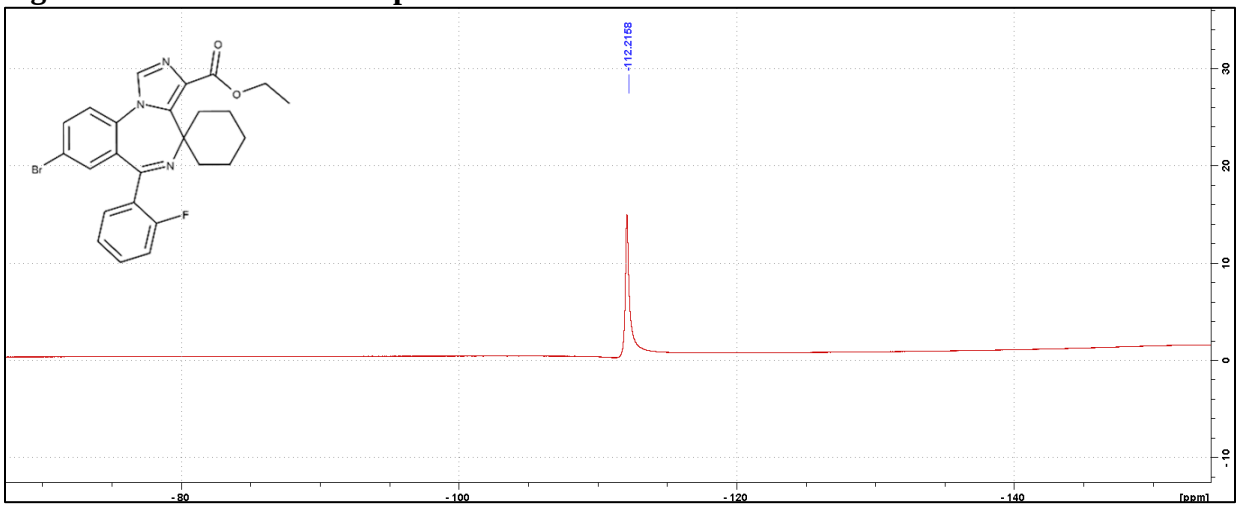

Figure 139: DAW-II-60 HPLC UV Chromatograph:

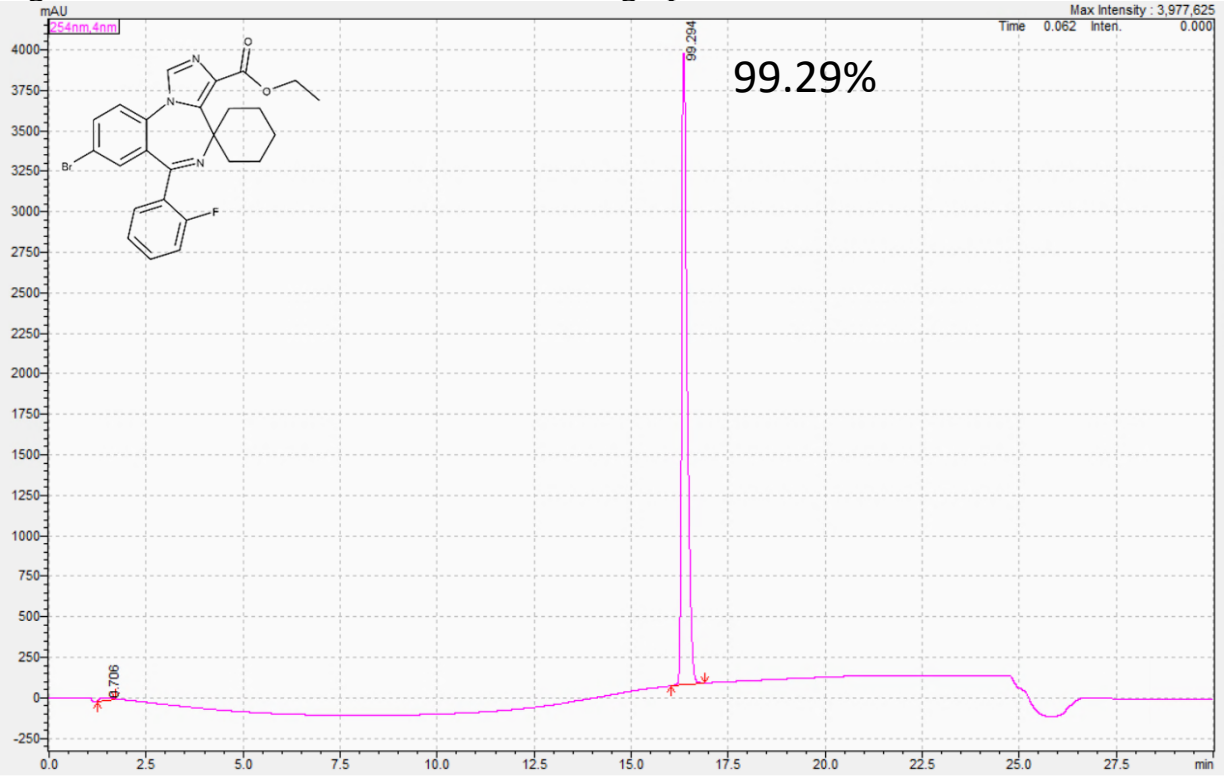

Figure 140: DAW-II-60 HRMS:

Score	Pred. (M)	Pred. m/z	Meas. m/z	Diff. (mDa)	Formulae (M)	Ion	Diff. (ppm)	Iso Score	DBE
36.78	495.09577	496.10304	496.10492	1.88	C25 H23 N3 O2 F Br	[M+H]+	3.790	33.07	15.0

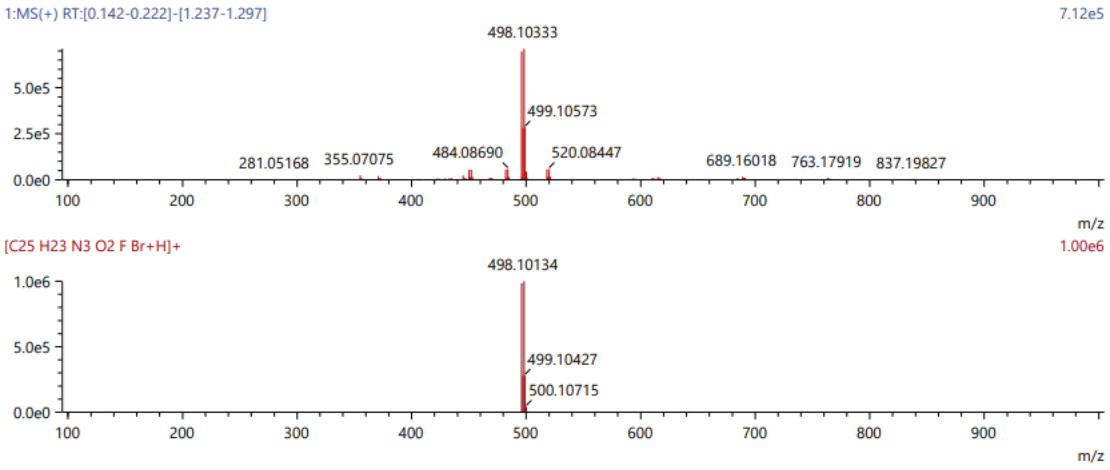

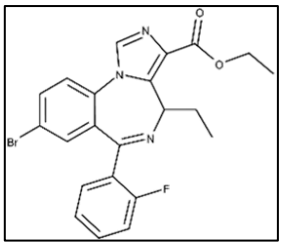

Synthesis of DAW-II-70: A three stopper RB flask was purged with nitrogen and vacuum 3 times. **DAW-I-70** (1.02 g, 2.83 mmol) was dissolved in anhydrous tetrahydrofuran (10.7 mL) and added to the reaction flask. The mixture was cooled to -20 °C using a dry ice/IPA bath. A solution of 1M potassium *tert*-butoxide in anhydrous tetrahydrofuran (3.68 mL) was added dropwise over the course of 10 min, at which time the reaction color turned to a deep orange. Upon completion of the addition, the mixture was allowed to stir at -20 °C for 40 min. Diethyl chlorophosphate (0.57 mL, 3.96 mmol) was added dropwise over the course of 5 min while maintaining a temperature of -20 °C. After 3.5 h, no more conversion was observed via TLC (100% EtOAc) and ethyl isocyanoacetate (0.40 mL, 3.68 mmol) was added dropwise over the course of 5 min followed by the addition of a solution of 1M potassium *tert*-butoxide in anhydrous tetrahydrofuran (3.68 mL) at -20 °C. The reaction was then warmed to room temperature for 2 h at which point all the intermediate had been consumed via TLC (100% EtOAc). The reaction was then quenched with 5% aqueous sodium bicarbonate (40 mL), and the product was extracted with ethyl acetate (40 mL). The organic layer was washed with 10% aqueous sodium bicarbonate (40 mL) followed by 20% aqueous NaCl (mL). The organic layer was then dried with $MgSO_4$ and then concentrated under reduced pressure. The resulting residue was triturated with a 50% mixture of tert-butyl methyl ether in hexanes (15 mL) at 55 °C for 20 h. The tert-butyl methyl ether/hexanes mixture was decanted, and the solid product was slurried in 100% hexanes (20 mL) at 55 °C for 4 h. The desired product was collected by filtration to yield an off-white solid (755.27 mg, 58.5%): ^{1}H NMR (500 MHz, $CDCl_3$) -20°C δ 7.90 (s, 1H), 7.67-7.65 (dd, *J* = 3.60, 2.25 Hz, 1H), 7.54-7.51 (m, 1H), 7.44-7.38 (m, 2H), 7.34-7.33 (d, *J* = 2.10 Hz, 1H), 7.22-7.19 (dt, *J* = 3.19, 0.85 Hz, 1H), 7.01-6.98 (m, 1H), 6.44-6.40 (q, *J* = 5.43 Hz, 1H), 4.41-4.24 (m, 2H), 1.70-1.61 (m, 1H),

1.53-1.44 (m, 1H), 1.36-1.33 (t, J = 7.15, 3H), 0.86-0.83 (t, J = 7.37 Hz, 3H); ^{13}C NMR (126 MHz, $CDCl_3$) -20°C δ 161.83 (s), 161.72 (s), 158.78 (d, $^{1}J_{CF}$ = 250.77 Hz), 139.27 (s), 133.80 (d, $^{3}J_{CF}$ = 3.77 Hz), 132.28 (s), 131.80 (s), 131.20 (d, $^{3}J_{CF}$ = 8.28 Hz), 130.06 (d, $^{4}J_{CF}$ = 2.01 Hz), 129.82 (s), 129.42 (s), 127.06 (d, $^{2}J_{CF}$ = 12.35 Hz), 123.58 (d, $^{3}J_{CF}$ = 3.36 Hz), 122.6 (s), 119.91 (s), 115.23 (d, $^{2}J_{CF}$ = 21.23 Hz), 59.86 (s), 55.43 (s), 21.40 (s), 13.36 (s), 10.45 (s); ^{19}F NMR (471 MHz, $CDCl_3$) -20°C δ -111.73, -111.96; HRMS (ESI/Q-TOF): *m/z* $[M + H]^+$ calcd for $C_{22}H_{19}BrFN_3O_2$: 456.07174; found: 456.07166; HPLC Purity: 99.85%.

Figure 141: DAW-II-70 ^{1}H spectra:

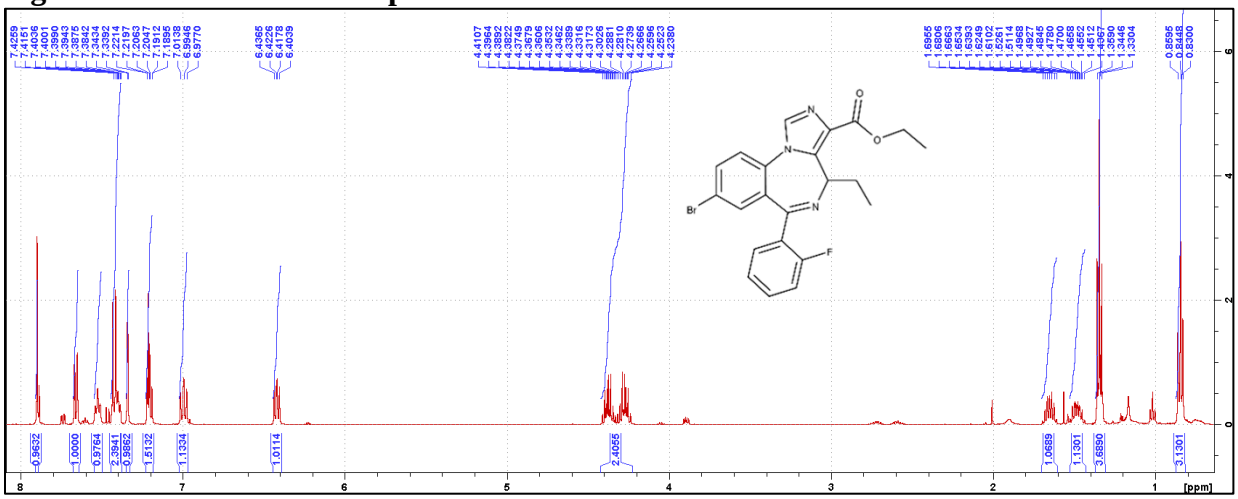

Figure 142: DAW-II-70 ^{13}C spectra:

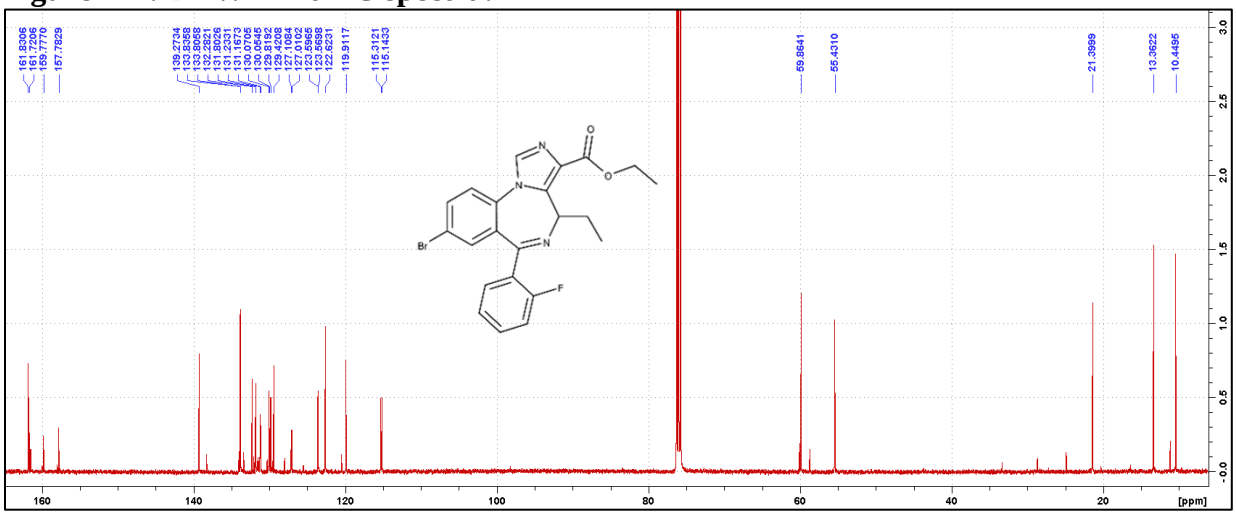

Figure 143: DAW-II-70 ^{19}F spectra:

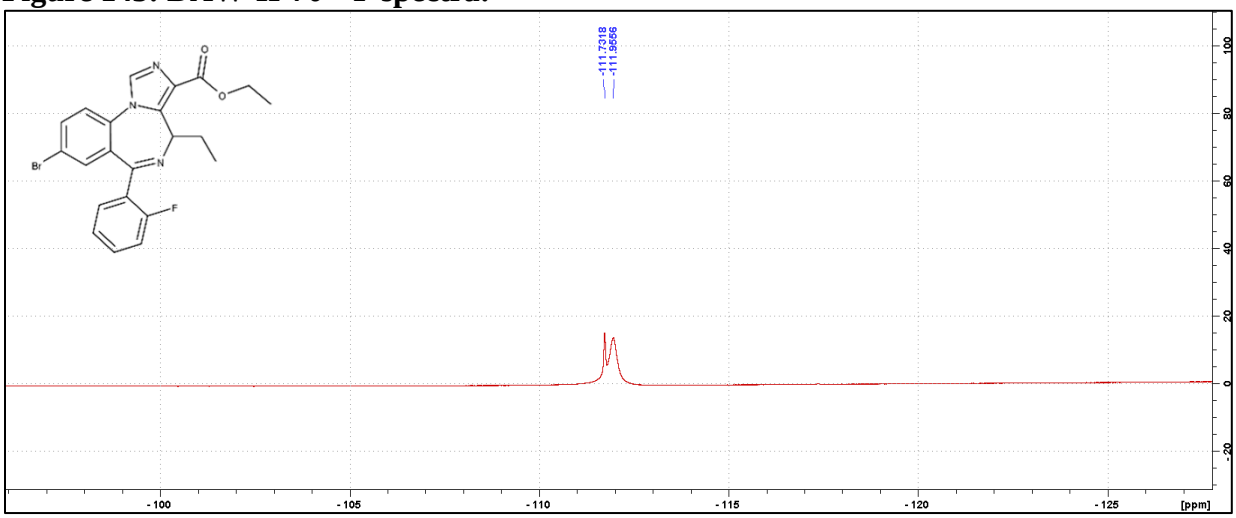

Figure 144: DAW-II-70 HPLC UV Chromatograph:

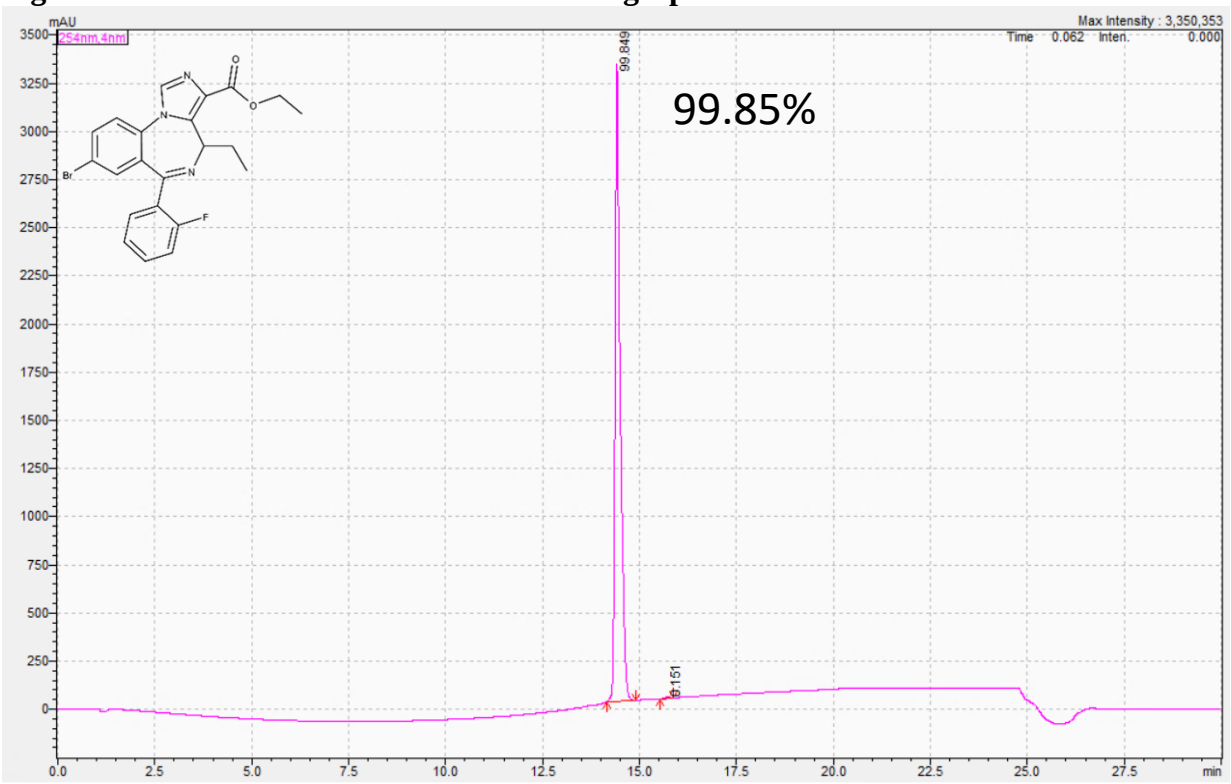

Figure 145: DAW-II-70 HRMS:

Score	Pred. (M)	Pred. m/z	Meas. m/z	Diff. (mDa)	Formulae (M)	Ion	Diff. (ppm)	Iso Score	DBE
58.32	455.06447	456.07174	456.07166	-0.08	C22 H19 N3 O2 F Br	[M+H]+	-0.175	53.75	14.0

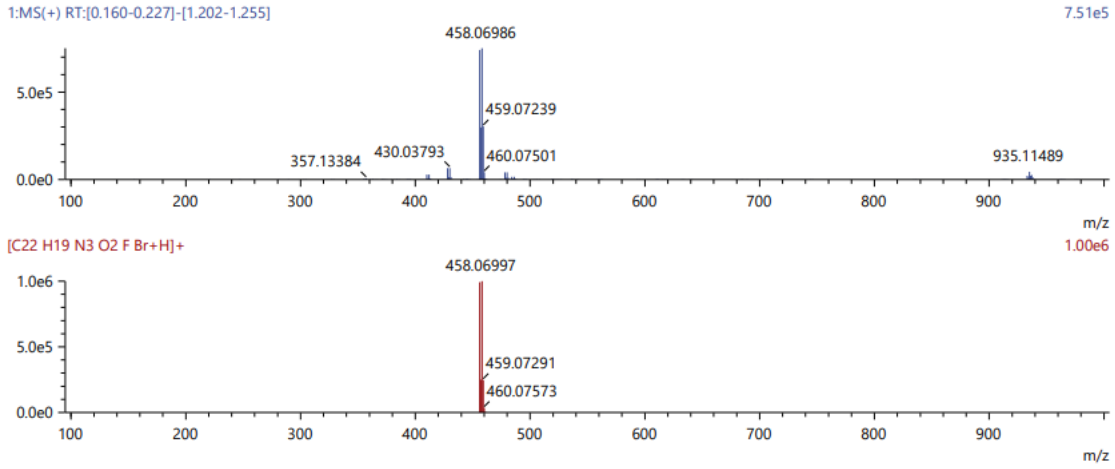

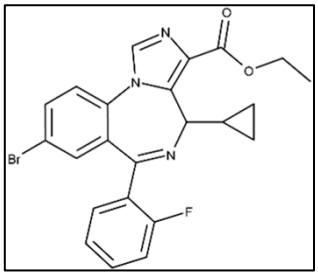

Synthesis of DAW-II-80: A three stopper RB flask was purged with nitrogen and vacuum 3 times. **DAW-I-80** (251.64 mg, 0.67 mmol) was dissolved in anhydrous tetrahydrofuran (2.7 mL) and added to the reaction flask. The mixture was cooled to -20 °C using a dry ice/IPA bath. A solution of 1M potassium *tert*-butoxide in anhydrous tetrahydrofuran (0.87 mL) was added dropwise over the course of 10 min, at which time the reaction color turned to a deep orange. Upon completion of the addition, the mixture was allowed to stir at -20 °C for 40 min. Diethyl chlorophosphate (0.14 mL, 0.94 mmol) was added dropwise over the course of 5 min while maintaining a temperature of -20 °C. After 3.5 h, no more conversion was observed via TLC (100% EtOAc) and ethyl isocyanoacetate (95.8 uL, 0.88 mmol) was added dropwise over the course of 5 min followed by the addition of a solution of 1M potassium *tert*-butoxide in anhydrous tetrahydrofuran (0.87 mL) at -20 °C. The reaction was then warmed to room temperature for 2 h at which point all the intermediate had been consumed via TLC (100% EtOAc). The reaction was then quenched with 5% aqueous sodium bicarbonate (10 mL), and the product was extracted with ethyl acetate (10 mL). The organic layer was washed with 10% aqueous sodium bicarbonate (10

mL) followed by 20% aqueous NaCl (10 mL). The organic layer was then dried with $MgSO_4$ and then concentrated under reduced pressure. The resulting residue was triturated with a 50% mixture of tert-butyl methyl ether in hexanes (5 mL) at 55 °C for 20 h. The tert-butyl methyl ether/hexanes mixture was decanted, and the solid product was slurried in 100% hexanes (10 mL) at 55 °C for 4 h. The desired product was collected by filtration to yield an off-white solid (176.24 mg, 55.8%): ^{1}H NMR (500 MHz, $CDCl_3$) δ 7.73 (s, 1H), 7.52-7.50 (dd, J = 3.60, 2.20 Hz, 1H), 7.47-7.43 (dt, J = 3.37, 1.75 Hz, 1H), 7.29-7.28 (d, J = 8.55 Hz, 1H), 7.27-7.22 (m, 2H), 7.07-7.04 (m, 1H), 6.86-6.82 (m, 1H), 5.46-5.44 (d, J = 3.60 Hz, 1H), 4.25-4.18 (m, 1H), 4.15-4.08 (m, 1H), 1.20-1.17 (t, J = 7.13 Hz, 3H), 0.66-0.59 (m, 1H), 0.49-0.45 (m, 1H), 0.34-0.29 (m, 1H), 0.26-0.22 (m, 1H), 0.13-0.07 (m, 1H); ^{13}C NMR (126 MHz, $CDCl_3$) δ 162.90 (s), 162.74 (s), 160.13 (d, $^{1}J_{CF}$ = 250.93 Hz), 141.37 (s), 134.81 (s), 134.65 (s), 133.84 (s), 133.10 (d, $^{4}J_{CF}$ = 2.01 Hz), 132.16 (d, $^{3}J_{CF}$ = 8.28 Hz), 131.62 (s), 131.42 (d, $^{3}J_{CF}$ = 2.45 Hz), 129.72 (s), 128.45 (d, $^{2}J_{CF}$ = 12.34 Hz), 124.57 (d, $^{3}J_{CF}$ = 3.40 Hz), 123.83 (s), 120.94 (s), 116.23 (d, $^{2}J_{CF}$ = 21.45 Hz), 60.76 (s), 60.02 (s), 14.40 (s), 10.51 (s), 5.03 (s), 3.21 (s); ^{19}F NMR (471 MHz, $CDCl_3$) δ -112.06; HRMS (ESI/Q-TOF): m/z $[M + H]^+$ calcd for $C_{23}H_{19}BrFN_3O_2$: 468.07174; found: 468.07171; HPLC Purity: 99.20%.

Figure 146: DAW-II-80 ^{1}H spectra:

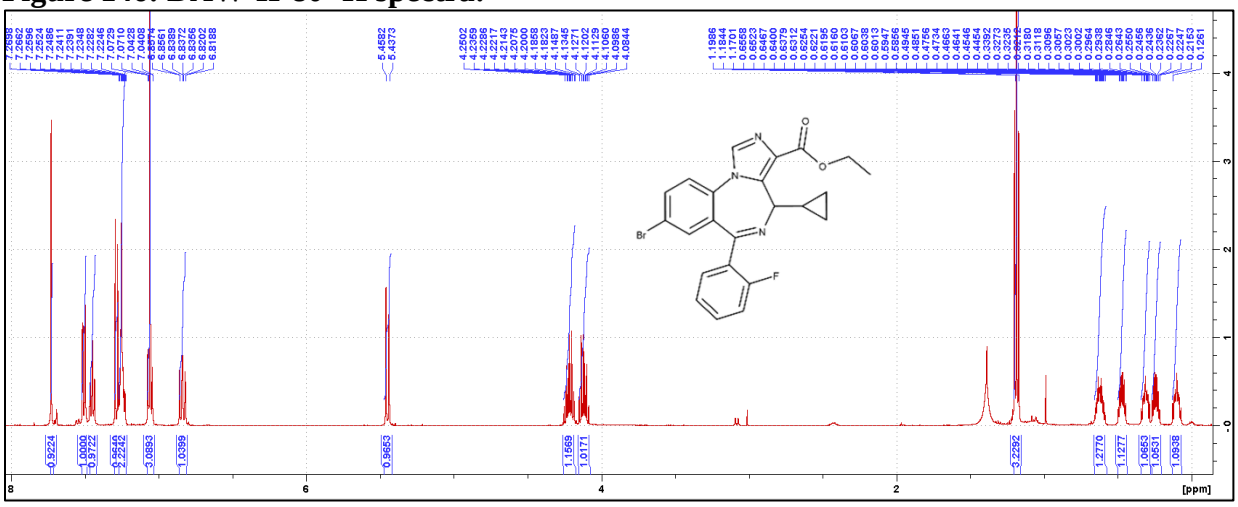

Figure 147: DAW-II-80 ^{13}C spectra:

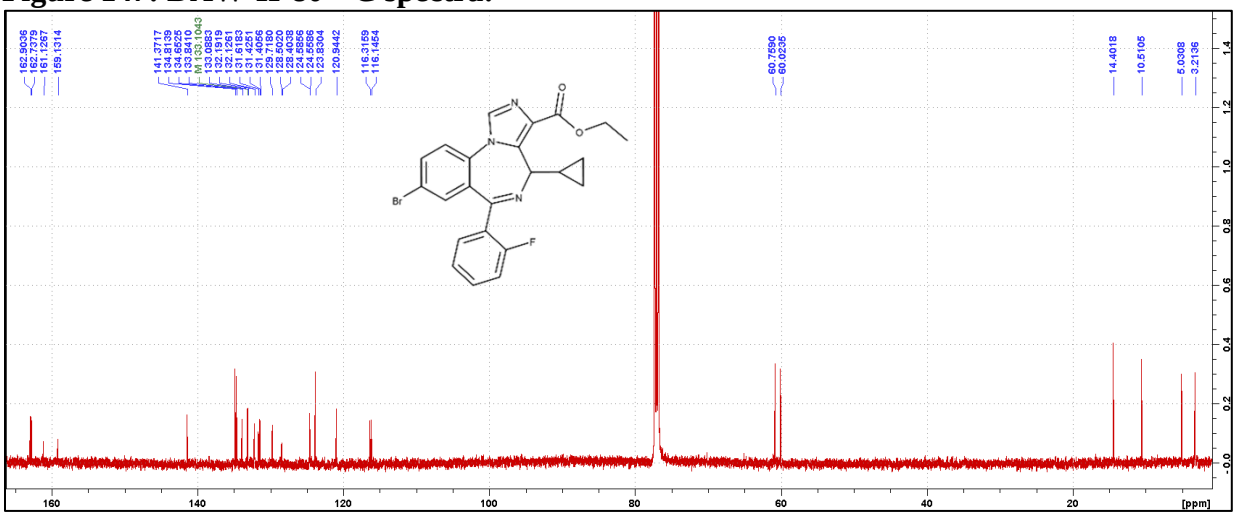

Figure 148: DAW-II-80 ^{19}F spectra:

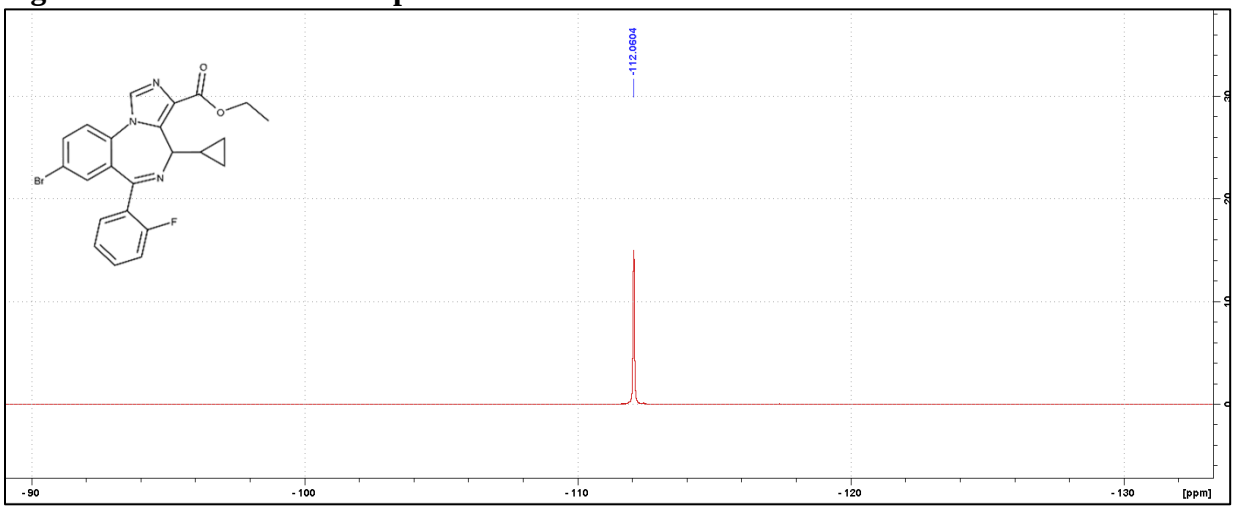

Figure 149: DAW-II-80 HPLC UV Chromatograph:

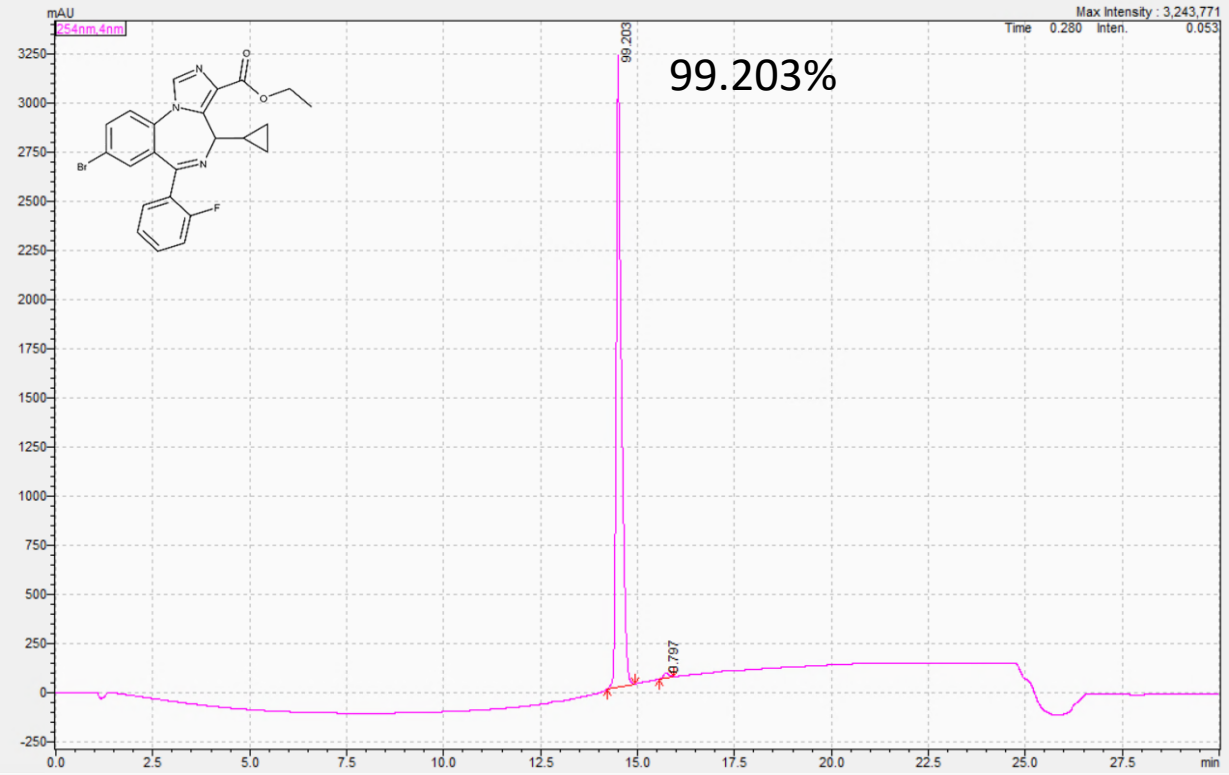

Figure 150: DAW-II-80 HRMS:

Score	Pred. (M)	Pred. m/z	Meas. m/z	Diff. (mDa)	Formulae (M)	Ion	Diff. (ppm)	Iso Score	DBE
59.05	467.06447	468.07174	468.07171	-0.03	C23 H19 N3 O2 F Br	[M+H]+	-0.064	54.51	15.0

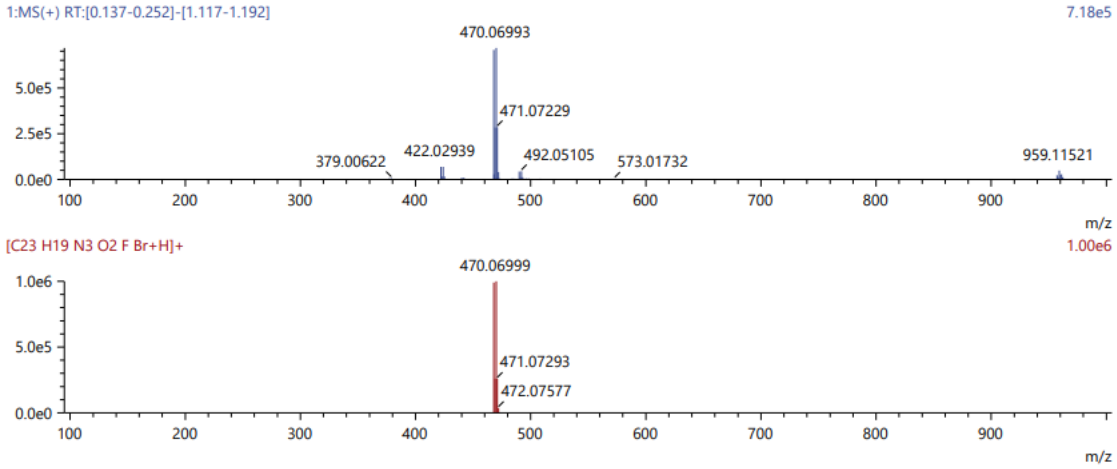

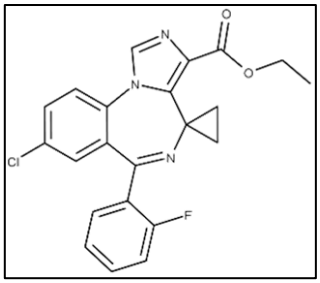

Synthesis of DAW-II-32: A three stopper RB flask was purged with nitrogen and vacuum 3 times. **DAW-I-32** (574.6 mg, 1.83 mmol) was dissolved in anhydrous tetrahydrofuran (18 mL) and added to the reaction flask. The mixture was cooled to -20 °C using a dry ice/IPA bath. A solution of 1M potassium *tert*-butoxide in anhydrous tetrahydrofuran (2.37 mL) was added dropwise over the course of 10 min, at which time the reaction color turned to a deep orange. Upon completion of the addition, the mixture was allowed to stir at -20 °C for 40 min. Diethyl chlorophosphate (0.37 mL, 2.56 mmol) was added dropwise over the course of 5 min while maintaining a temperature of -20 °C. After 3.5 h, no more conversion was observed via TLC (100% EtOAc) and ethyl isocyanoacetate (0.26 mL, 2.37 mmol) was added dropwise over the course of 5 min followed by the addition of a solution of 1M potassium *tert*-butoxide in anhydrous tetrahydrofuran (2.37 mL) at -20 °C. The reaction was then warmed to room temperature for 2 h at which point all the intermediate had been consumed via TLC (100% EtOAc). The reaction was then quenched with 5% aqueous sodium bicarbonate (30 mL), and the product was extracted with ethyl acetate (30 mL). The organic layer was washed with 10% aqueous sodium bicarbonate (30 mL) followed by 20% aqueous NaCl (30 mL). The organic layer was then dried with $MgSO_4$ and then concentrated under reduced pressure. The resulting residue was triturated with a 50% mixture of tert-butyl methyl ether in hexanes (12 mL) at 55 °C for 20 h. The *tert*-butyl methyl ether/hexanes mixture was decanted, and the solid product was slurried in 100% hexanes (20 mL) at 55 °C for 4 h. The desired product was collected by filtration to yield an off-white solid (447.94 mg, 59.8%): ^{1}H NMR (500 MHz, $CDCl_3$) δ 7.93 (s, 1H), 7.63-7.61 (dd, *J* = 3.63, 2.30 Hz, 1H), 7.60-7.58 (m, 1H), 7.57-7.56 (m, 1H), 7.48-7.43 (m, 1H), 7.28-7.27 (d, *J* = 2.25 Hz, 1H), 7.25-7.22 (dt, *J* = 3.22, 0.95 Hz, 1H), 7.06-7.02 (m, 1H), 4.50-4.34 (m, 2H), 2.08-2.03 (m, 1H), 1.74-1.69 (m, 1H), 1.45-

1.42 (t, J = 7.13 Hz, 3H), 0.78-0.69 (m, 2H); ^{13}C NMR (126 MHz, $CDCl_3$) δ 167.89 (s), 162.24 (s), 160.19 (d, $^{1}J_{CF}$ = 251.59 Hz), 140.16 (s), 134.16 (d, $^{2}J_{CF}$ = 17.31 Hz), 133.53 (s), 133.29 (s), 132.49 (d, $^{3}J_{CF}$ = 7.59 Hz), 132.25 (d, $^{4}J_{CF}$ = 1.42 Hz), 131.93 (d, $^{3}J_{CF}$ = 10.33 Hz), 131.23 (d, $^{3}J_{CF}$ = 8.20 Hz), 129.66 (d, $^{4}J_{CF}$ = 1.65 Hz), 129.14 (s), 127.03 (d, $^{2}J_{CF}$ = 11.89 Hz), 124.50 (d, $^{3}J_{CF}$ = 3.39 Hz), 123.70 (d, $^{3}J_{CF}$ = 4.71 Hz), 116.25 (d, $^{2}J_{CF}$ = 24.30 Hz), 60.83 (t, J = 9.64 Hz), 37.29 (s), 15.11 (s), 14.45 (d, J = 14.58 Hz); ^{19}F NMR (471 MHz, $CDCl_3$) δ -111.75 - -111.80 (qu, J = 5.63 Hz); HRMS (ESI/Q-TOF): m/z $[M + H]^+$ calcd for $C_{22}H_{17}ClFN_3O_2$: 410.10661; found: 410.10166; HPLC Purity: 99.18%.

Figure 151: DAW-II-32 ^{1}H spectra:

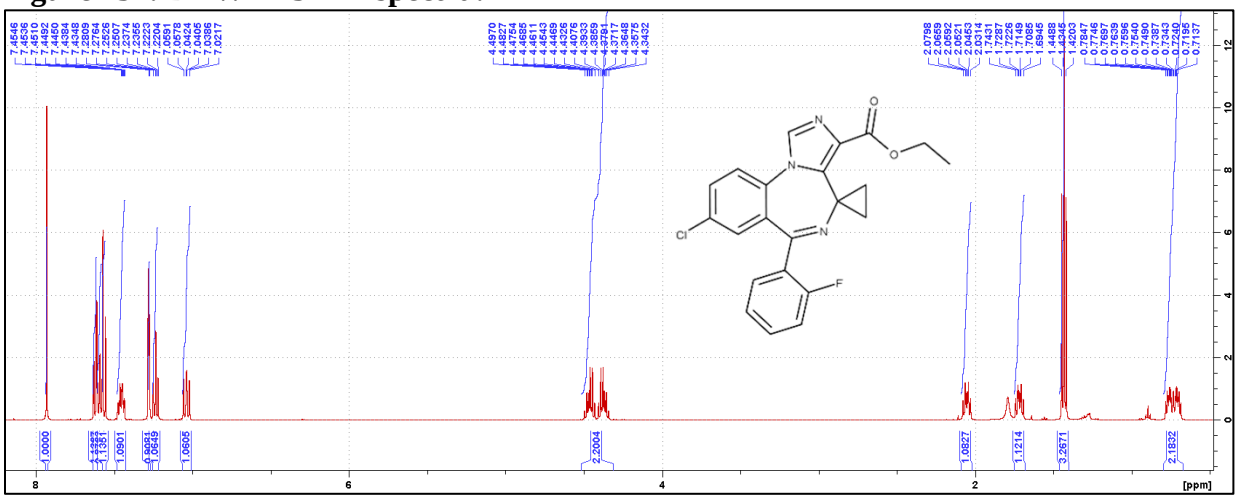

Figure 152: DAW-II-32 ^{13}C spectra:

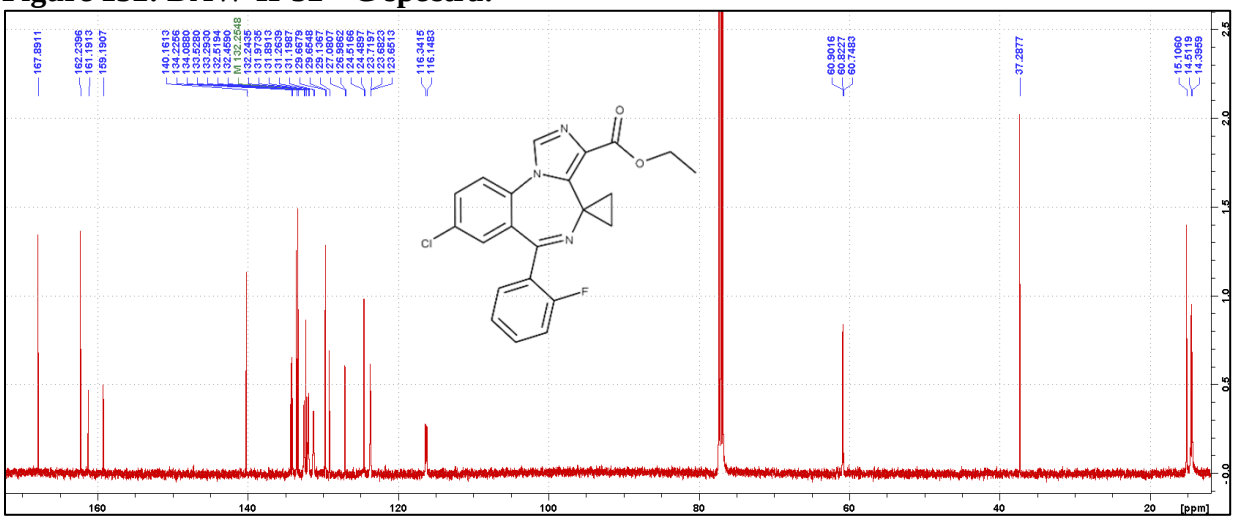

Figure 153: DAW-II-32 ^{19}F spectra:

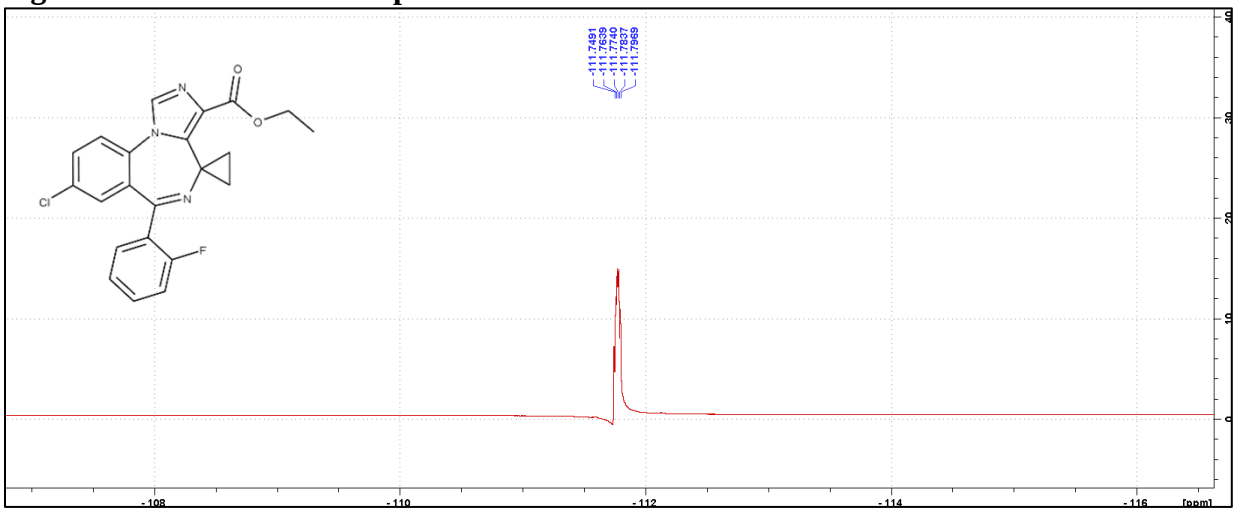

Figure 154: DAW-II-32 HPLC UV Chromatograph:

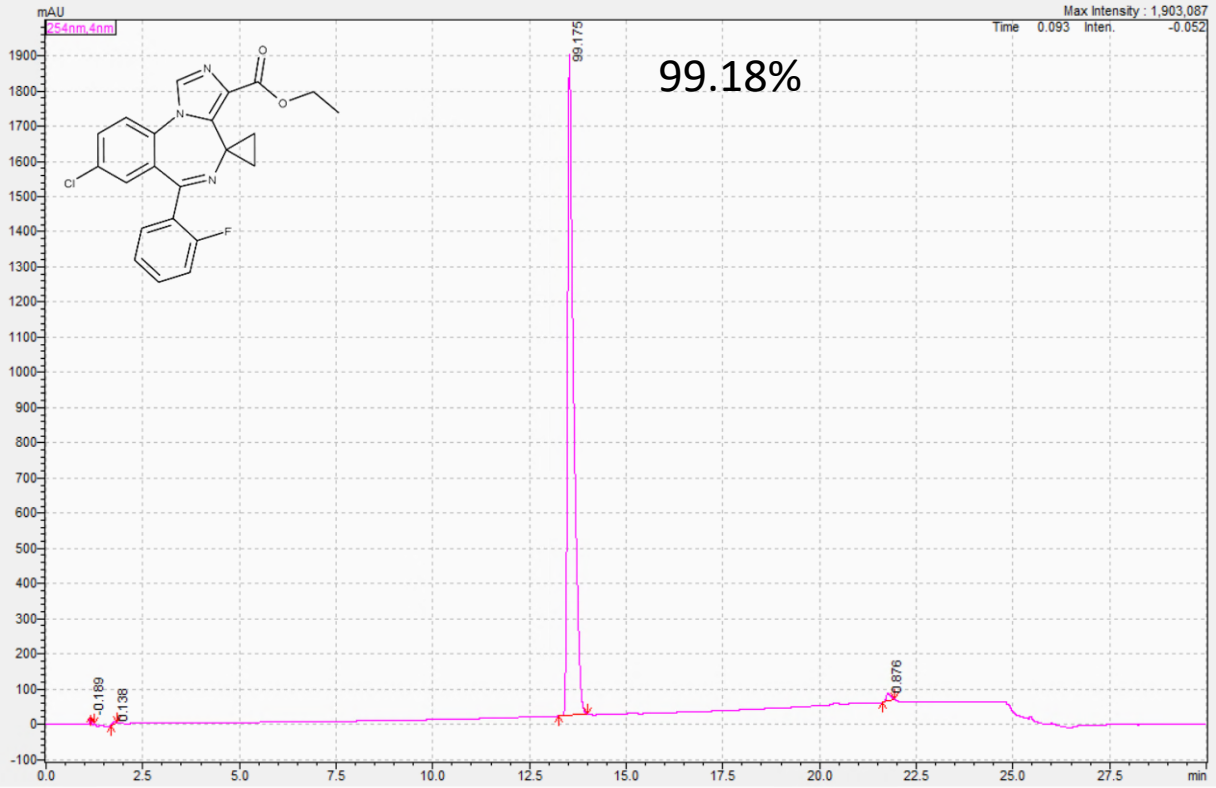

Figure 155: DAW-II-32 HRMS:

Score	Pred. (M)	Pred. m/z	Meas. m/z	Diff. (mDa)	Formulae (M)	Ion	Diff. (ppm)	Iso Score	DBE
10.56	409.09933	410.10661	410.10166	-4.95	C22 H17 N3 O2 F Cl	[M+H]+	-12.070	11.73	15.0

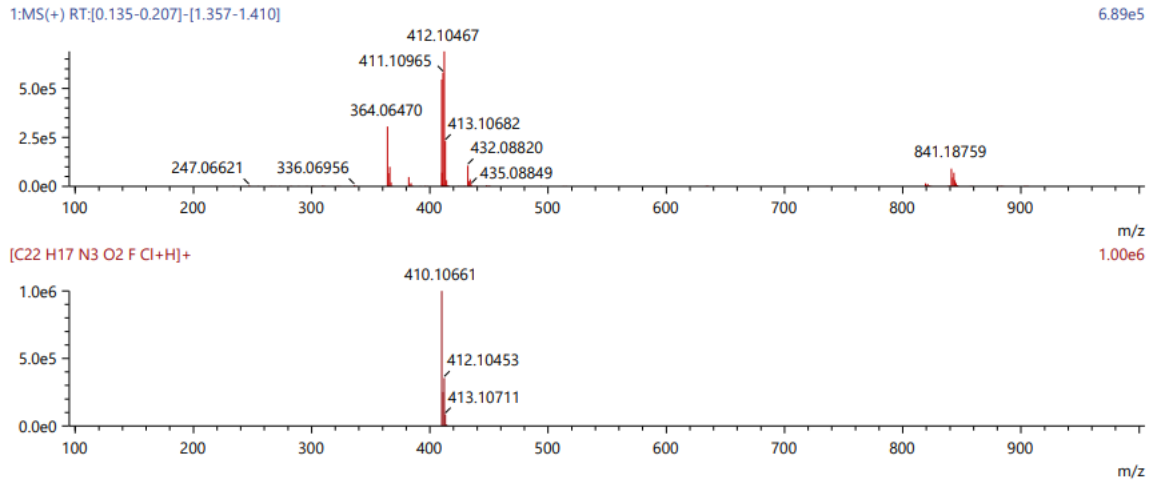

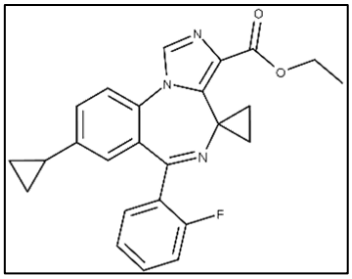

Synthesis of DAW-II-33: A mixture of toluene (19.9 mL) and water (2.88 mL) was degassed with nitrogen before **DAW-II-30** (1.00 g, 2.20 mmol) was added. Cyclopropyl boronic acid (94.6 mg, 11.02 mmol) was then added, followed by potassium phosphate (2.01 g, 9.48 mmol), palladium acetate (49.5 mg, 0.22 mmol), and tri(*o*-tolyl)phosphine (134.1g, 0.44 mmol). The reaction was then heated to 100 °C for 18 h before being cooled back to room temperature and H_2O (50 mL) was added. The aqueous layer was extracted with ethyl acetate (50 mL, 3x) and the organic layers were combined before being washed with brine (150 mL) and dried with $MgSO_4$. The solvent was removed under reduced pressure and the residue was loaded onto a precolumn with chloroform and separated by Biotage: 25-95% ethyl acetate in hexanes (20 CV). The desired product was obtained as an off-white solid (534.19 mg, 58.3%): ^{1}H NMR (500 MHz, $CDCl_3$) δ 7.91 (s, 1H), 7.59-7.55 (dt, *J* = 3.36, 1.75 Hz, 1H), 7.49-7.48 (d, *J* = 8.30 Hz, 1H), 7.45-7.41 (m, 1H), 7.28-7.26 (dd, *J* = 3.47, 2.05 Hz, 1H), 7.24-7.20 (dt, *J* = 3.23, 1.00 Hz, 1H), 7.04-7.01 (m, 1H), 6.99-6.98 (m, 1H), 4.50-4.34 (m, 2H), 2.06-2.01 (m, 1H), 1.92-1.87 (m, 1H), 1.71-1.66 (m, 1H), 1.45-1.42 (t, *J* = 7.15 Hz, 3H), 1.04-1.01 (m, 2H), 0.76-0.62 (m, 4H); ^{13}C NMR (126 MHz, $CDCl_3$) δ 169.22 (s), 162.45 (s), 160.26 (d, $^1J_{CF}$ = 251.55 Hz), 143.80 (s), 140.18 (s), 134.19 (s), 132.53 (s), 131.99 (d, $^3J_{CF}$ = 8.40 Hz), 131.33 (d, $^3J_{CF}$ = 2.39 Hz), 130.55 (d, $^4J_{CF}$ = 1.01 Hz), 128.67 (s), 128.51 (s), 127.83 (d, $^2J_{CF}$ = 12.09 Hz), 127.43 (d, $^3J_{CF}$ = 1.48 Hz), 124.47 (d, $^3J_{CF}$ = 3.54 Hz), 122.11 (s), 116.06 (d, $^2J_{CF}$ = 21.60 Hz), 60.68 (s), 37.19 (s), 15.09 (d, *J* = 6.47 Hz), 14.47 (d, *J* = 3.62 Hz), 9.91 (s); ^{19}F NMR (471 MHz, $CDCl_3$) δ -112.04 - -112.09 (qu, *J* = 5.46 Hz); HRMS (ESI/Q-TOF): *m/z* $[M + H]^+$ calcd for $C_{25}H_{22}FN_3O_2$: 416.17688; found: 416.17756; HPLC Purity: 98.90%.

Figure 156: DAW-II-33 ^{1}H spectra:

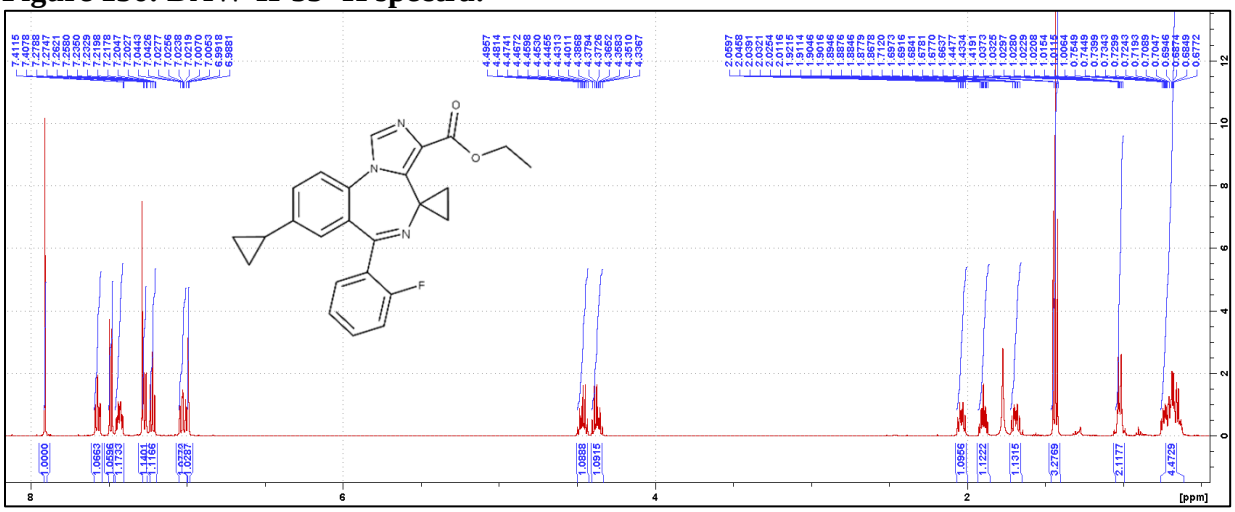

Figure 157: DAW-II-33 ^{13}C spectra:

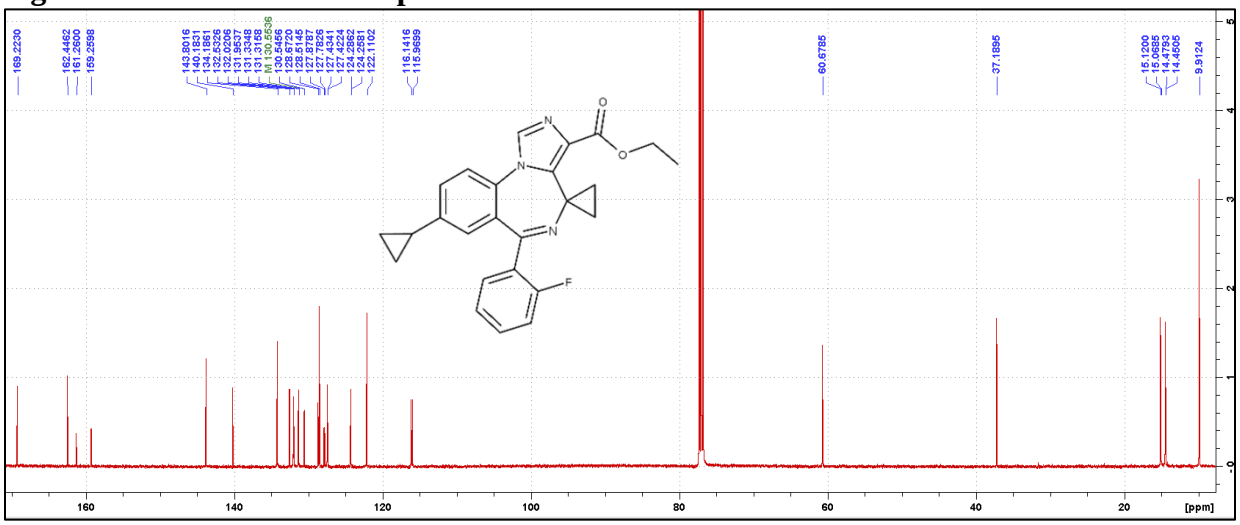

Figure 158: DAW-II-33 ^{19}F spectra:

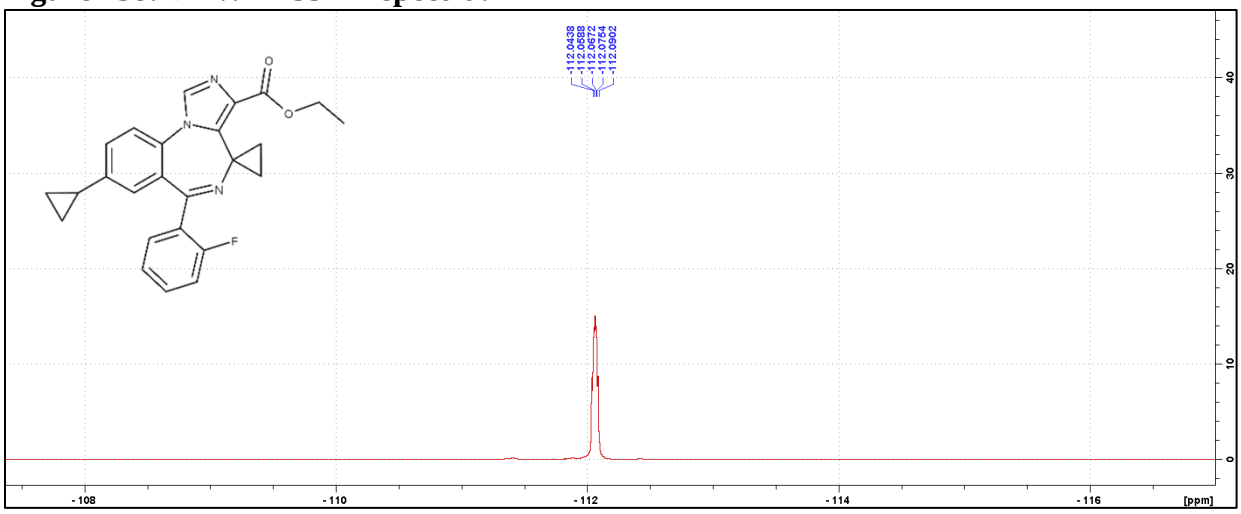

Figure 159: DAW-II-33 HPLC UV Chromatograph:

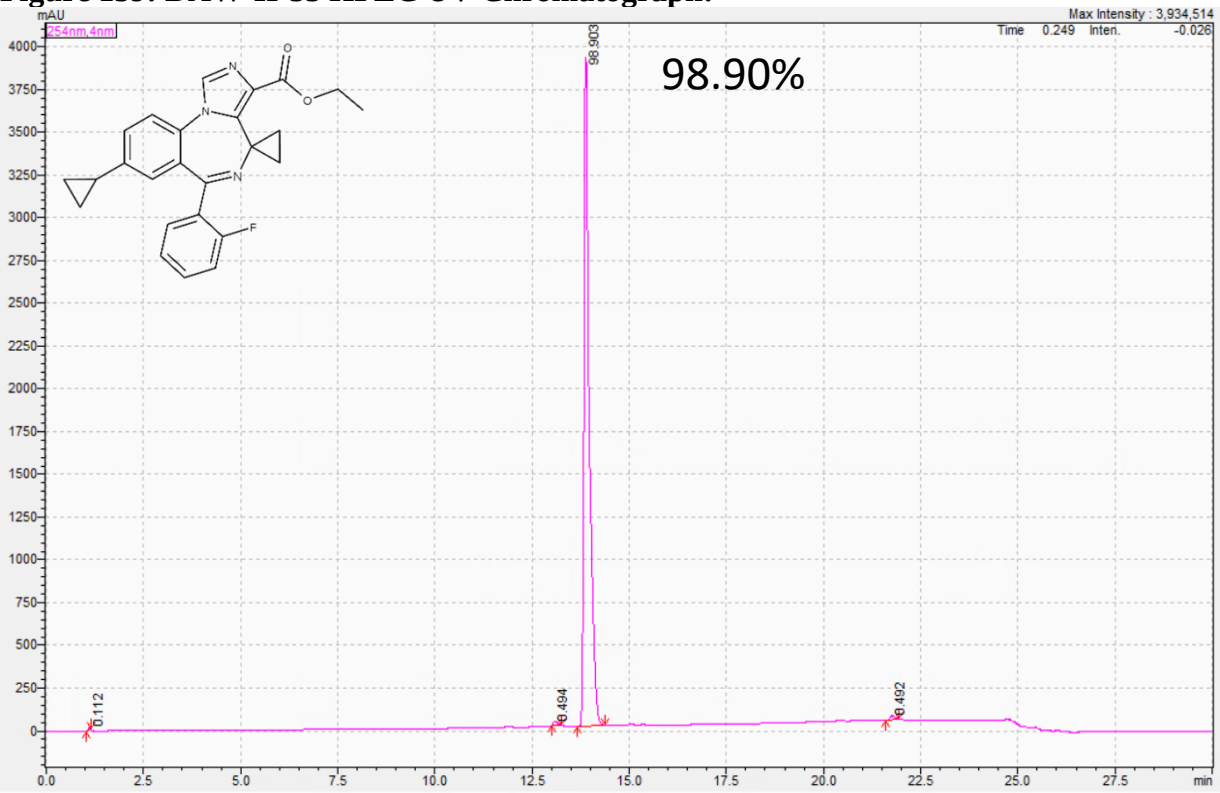

Figure 160: DAW-II-33 HRMS:

Score	Pred. (M)	Pred. m/z	Meas. m/z	Diff. (mDa)	Formulae (M)	Ion	Diff. (ppm)	Iso Score	DBE
57.47	415.16961	416.17688	416.17756	0.68	C25 H22 N3 O2 F	[M+H]+	1.634	53.66	16.0

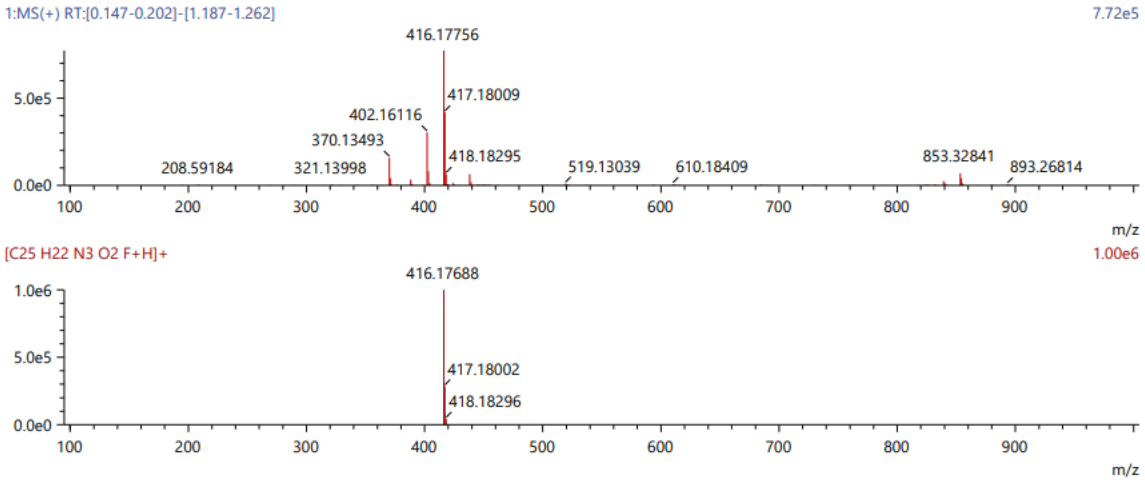

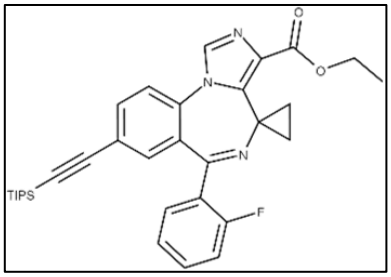

Synthesis of DAW-II-35T: A three stopper RB flask was purged with vacuum and nitrogen 3 times. Anhydrous acetonitrile (6.5 mL) was added to the flask and the solvent was degassed with nitrogen. Palladium acetate (25 mg, 0.11 mmol) was added followed by the addition of tri(*o*-tolyl)phosphine (67 mg, 0.22 mmol) and the mixture was stirred at room temperature for 30 min. **DAW-II-30** (1.07 g, 2.35 mmol) was added followed by the addition of triethyl amine (0.66 mL, 4.77 mmol), TIPS acetylene (0.63 mL, 2.83 mmol), and additional nitrogen degassed acetonitrile (8.7 mL). The reaction was heated to 75 °C for 4 h. Upon completion by TLC (100% EtOAc), silica gel (550 mg) was added to the reaction and the reaction was cooled to room temperature while stirring for 30 min. The mixture was filtered over celite and washed with acetonitrile. The solvent was removed under reduced pressure and the residue was dissolved in dichloromethane (50 mL) before the organic layer was washed with 5% aqueous sodium bicarbonate (50 mL), followed by 10% aqueous NaCl (50 mL). The organic layer was dried with $MgSO_4$, and the solvent was removed under reduced pressure. The residue was loaded onto a precolumn with chloroform and separated by Biotage: 5-55% ethyl acetate in hexanes (20 CV), 55-90% ethyl acetate in hexanes (5 CV). The desired product was obtained as a yellow solid (996.59 mg, 76.2%): ^{1}H NMR (500 MHz, $CDCl_3$) δ 7.94 (s, 1), 7.72-7.70 (dd, *J* = 3.38, 1.85 Hz, 1H), 7.60-7.57 (dt, *J* = 3.35, 1.70 Hz, 1H), 7.55-7.53 (d, *J* = 8.30 Hz, 1H), 7.46-7.42 (m, 1H), 7.33-7.32 (m, 1H), 7.24-7.21 (dt, *J* = 3.21, 0.95 Hz, 1H), 7.05-7.02 (m, 1H), 4.49-4.43 (m, 1H), 4.40-4.34 (m, 1H), 2.07-2.02 (m, 1H), 1.72-1.67 (m, 1H), 1.44-1.41 (t, *J* = 7.13 Hz, 3H), 1.12-1.10 (m, 21H), 0.76-0.69 (m, 2H); ^{13}C NMR (126 MHz, $CDCl_3$) δ 168.46 (s), 162.28 (s), 160.25 (d, $^1J_{CF}$ = 251.64 Hz), 140.27 (s), 135.39 (s), 134.39 (s), 134.18 (s), 132.85 (d, $^4J_{CF}$ = 1.28 Hz), 132.26 (d, $^3J_{CF}$ = 8.36 Hz), 131.26 (d, $^3J_{CF}$ = 2.06 Hz), 130.93 (s), 129.04 (s), 127.34 (d, $^2J_{CF}$ = 11.87 Hz),

124.36 (d, $^{3}J_{CF}$ = 3.42 Hz), 123.03 (s), 122.29 (s), 116.18 (d, $^{2}J_{CF}$ = 21.49 Hz), 104.66 (s), 94.06 (s), 77.27 (s), 60.78 (s), 37.26 (s), 18.61 (s), 15.11 (s), 14.46 (s), 14.42 (s), 11.23 (s); ^{19}F NMR (471 MHz, $CDCl_3$) δ -111.87 - -111.91 (qu, *J* = 5.56 Hz); HRMS (ESI/Q-TOF): *m/z* $[M + H]^+$ calcd for $C_{33}H_{38}FN_3O_2Si$: 556.27901; found: 556.27742; HPLC Purity: 98.02%.

Figure 161: DAW-II-35T ^{1}H spectra:

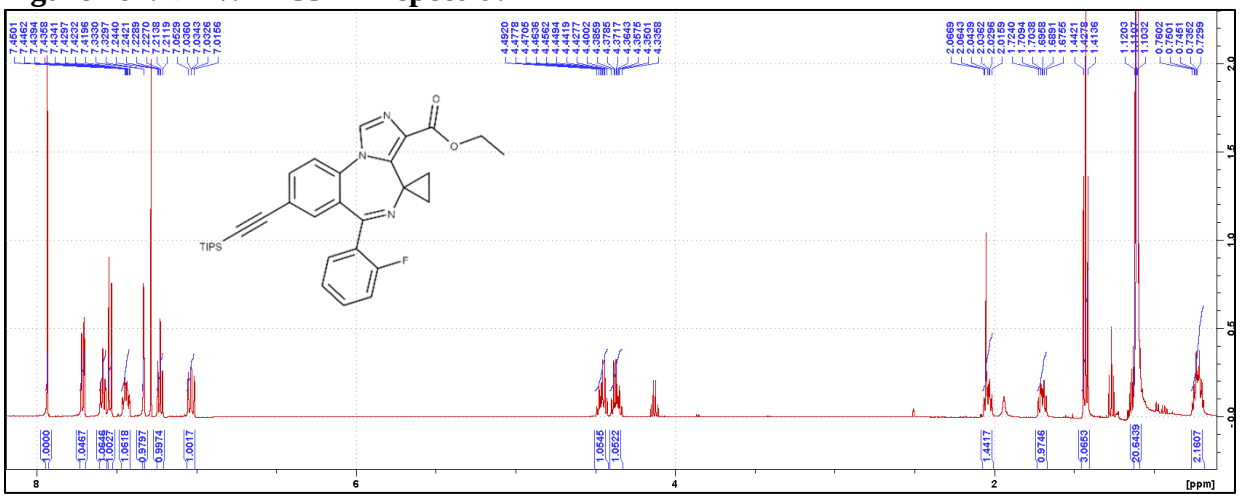

Figure 162: DAW-II-35T ^{13}C spectra:

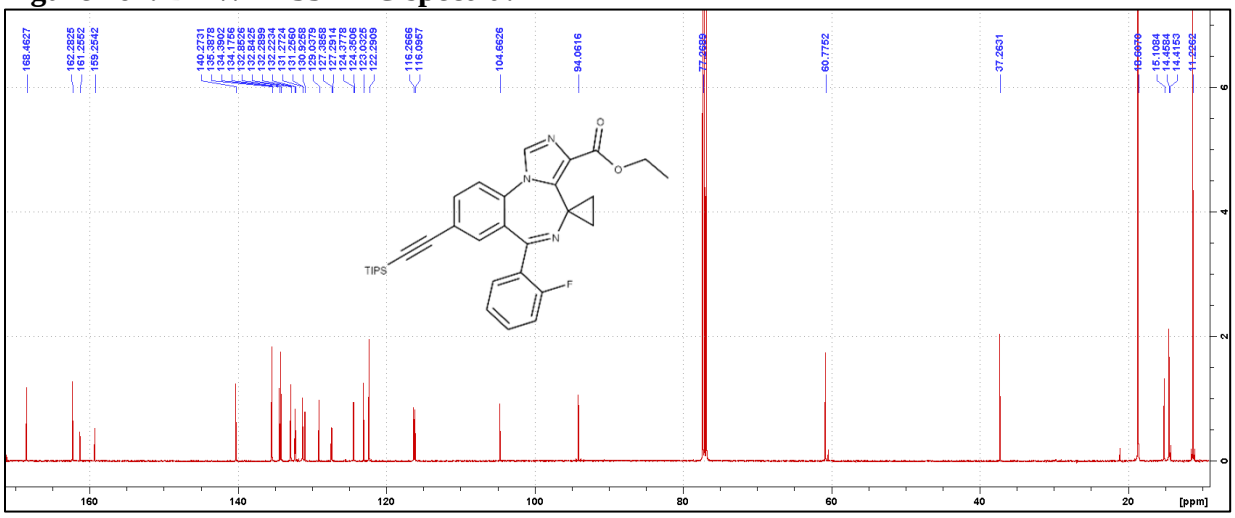

Figure 163: DAW-II-35T ^{19}F spectra:

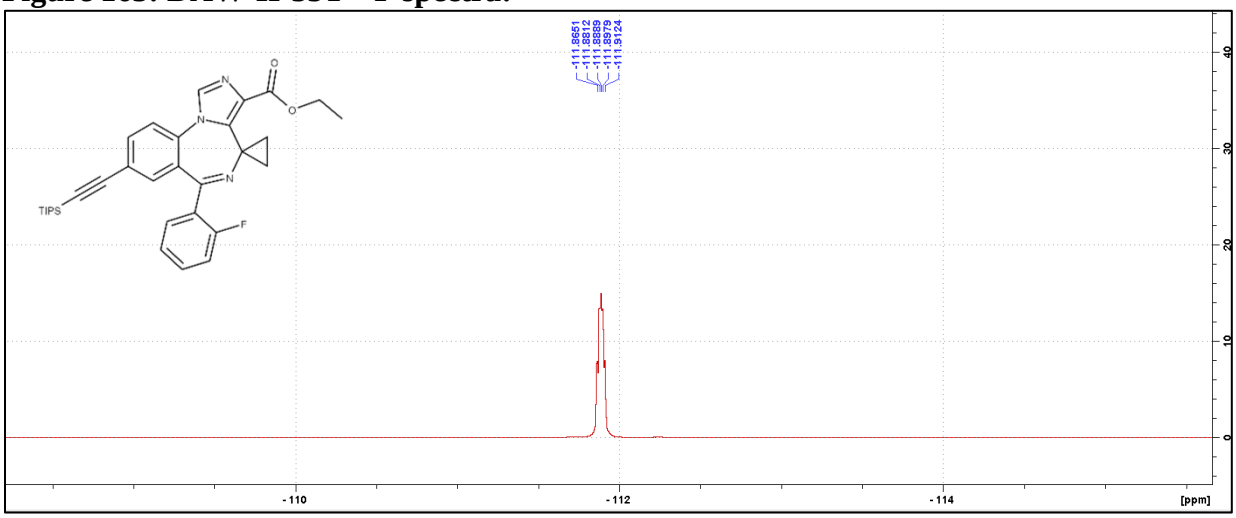

Figure 164: DAW-II-35T HPLC UV Chromatograph:

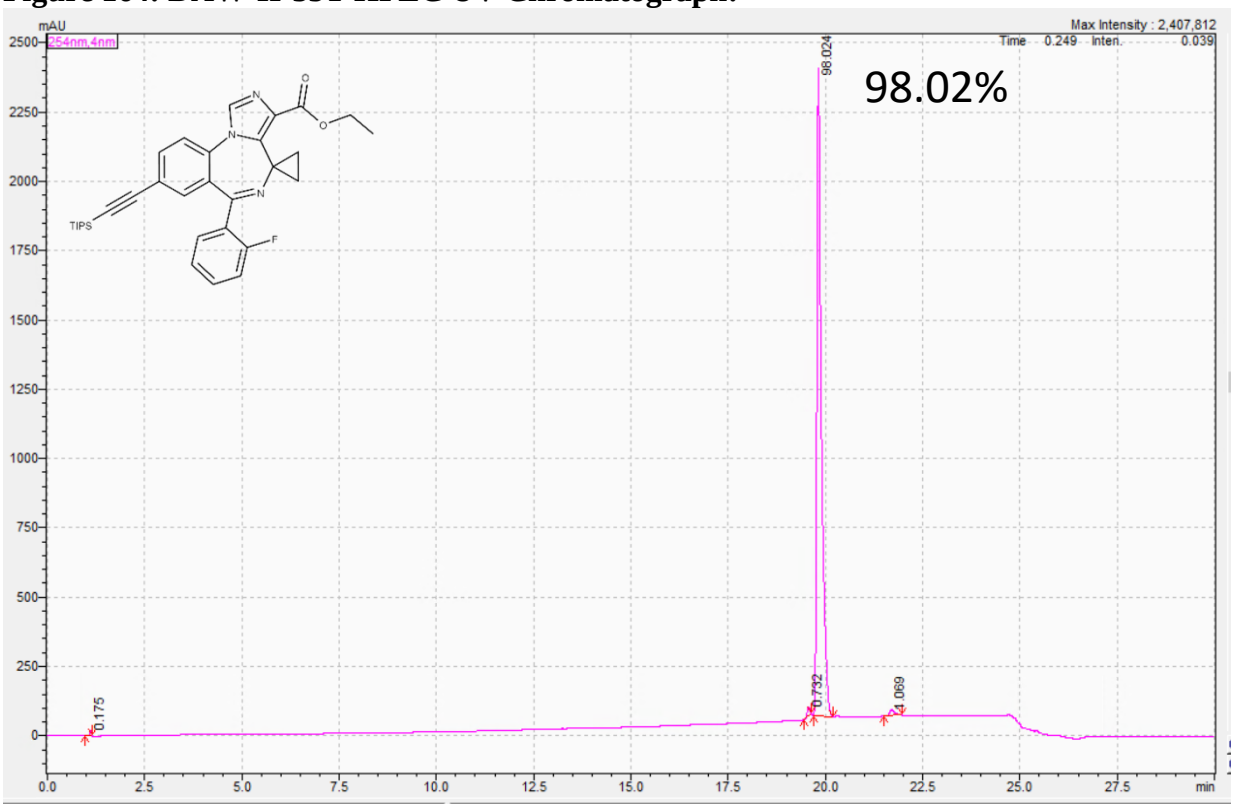

Figure 165: DAW-II-35T HRMS:

Score	Pred. (M)	Pred. m/z	Meas. m/z	Diff. (mDa)	Formulae (M)	Ion	Diff. (ppm)	Iso Score	DBE
34.51	555.27173	556.27901	556.27742	-1.59	C33 H38 N3 O2 F Si	[M+H]+	-2.858	29.23	16.0

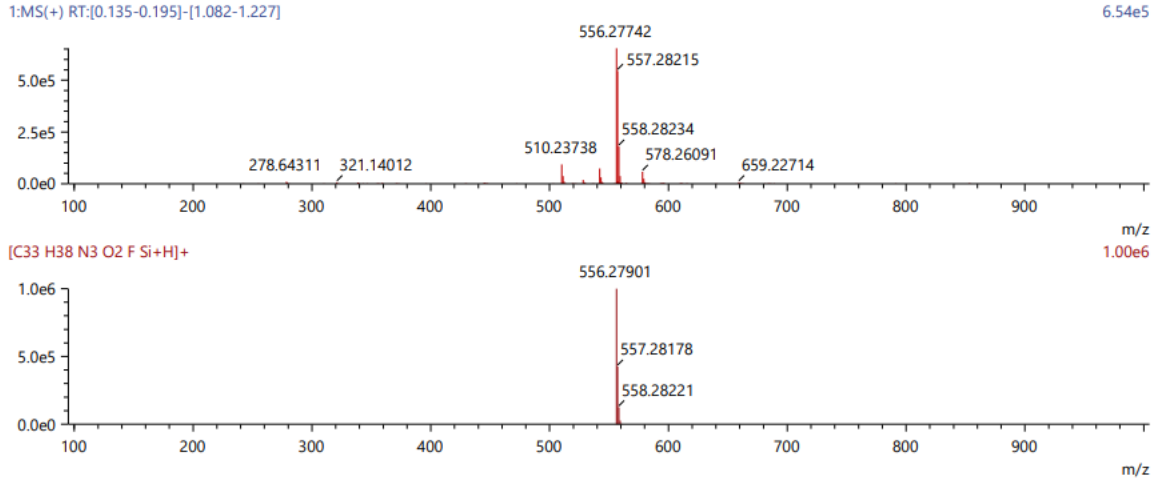

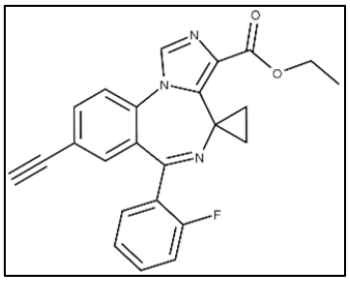

Synthesis of DAW-II-35: DAW-II-35T (939.69 mg, 1.69 mmol) was dissolved in a solution of THF (9.32 mL) and H_2O (93.2 uL). The mixture was cooled to -20 °C in a dry ice/IPA bath before 1M TBAF in THF (1.94 mL) was added dropwise over 5 min. The reaction was then warmed to room temperature and stirred for 1.5 h upon which all the starting material had been consumed by TLC (100% EtOAc:Hex). The reaction was then diluted with ethyl acetate (60 mL), and the organic layer was washed with 10% aqueous NaCl (60 mL, 2x). The organic layer was dried with $MgSO_4$, and the solvent was removed under reduced pressure. The residue was loaded onto a precolumn with chloroform and separated by Biotage: 35-90% ethyl acetate in hexanes (25 CV). The desired product was obtained as an off-white solid (666.2 mg, 98.6%): ^{1}H NMR (500 MHz, $CDCl_3$) δ 7.95 (s, 1H), 7.76-7.74 (dd, J = 3.37, 1.80 Hz, 1H), 7.60-7.58 (m, 2H), 7.48-7.43 (m, 1H), 7.42-7.41 (d, J = 1.60 Hz, 1H), 7.25-7.22 (dt, J = 3.23, 1.00 Hz, 1H), 7.06-7.02 (m, 1H), 4.50-4.35 (m, 2H), 3.17 (s, 1H), 2.07-2.03 (m, 1H), 1.74-1.71 (m, 1H), 1.46-1.43 (t, J = 7.13 Hz, 3H), 0.78-0.68 (m, 2H); ^{13}C NMR (126 MHz, $CDCl_3$) δ 168.35 (s), 162.25 (s), 160.22 (d, $^1J_{CF}$ = 251.55 Hz), 140.26 (s), 135.20 (d, $^3J_{CF}$ = 6.10 Hz), 134.88 (s), 134.18 (d, $^3J_{CF}$ = 8.90 Hz),

133.47 (s), 132.35 (d, $^{3}J_{CF}$ = 8.38 Hz), 131.24 (s), 131.01 (d, $^{4}J_{CF}$ = 1.39 Hz), 129.13 (s), 127.27 (d, $^{2}J_{CF}$ = 11.94 Hz), 124.44 (d, $^{3}J_{CF}$ = 3.47 Hz), 122.43 (s), 121.66 (s), 116.24 (d, $^{2}J_{CF}$ = 21.59 Hz), 81.54 (d, *J* = 2.25 Hz), 79.63 (d, *J* = 10.29 Hz), 60.83 (t, *J* = 7.01 Hz), 37.26 (s), 15.11 (s), 14.46 (d, *J* = 8.23 Hz); ^{19}F NMR (471 MHz, $CDCl_3$) δ -111.82 - -111.87 (qu, *J* = 5.59 Hz); HRMS (ESI/Q-TOF): *m/z* $[M + H]^+$ calcd for $C_{24}H_{18}FN_3O_2$: 400.14558; found: 400.14606; HPLC Purity: 97.27%.

Figure 166: DAW-II-35 ^{1}H spectra:

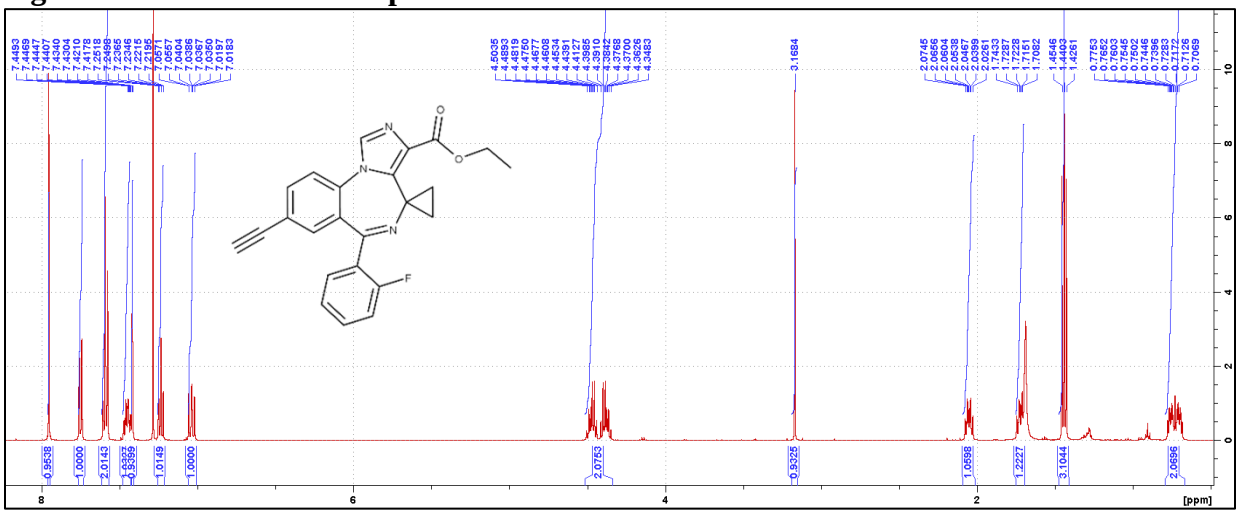

Figure 167: DAW-II-35 ^{13}C spectra:

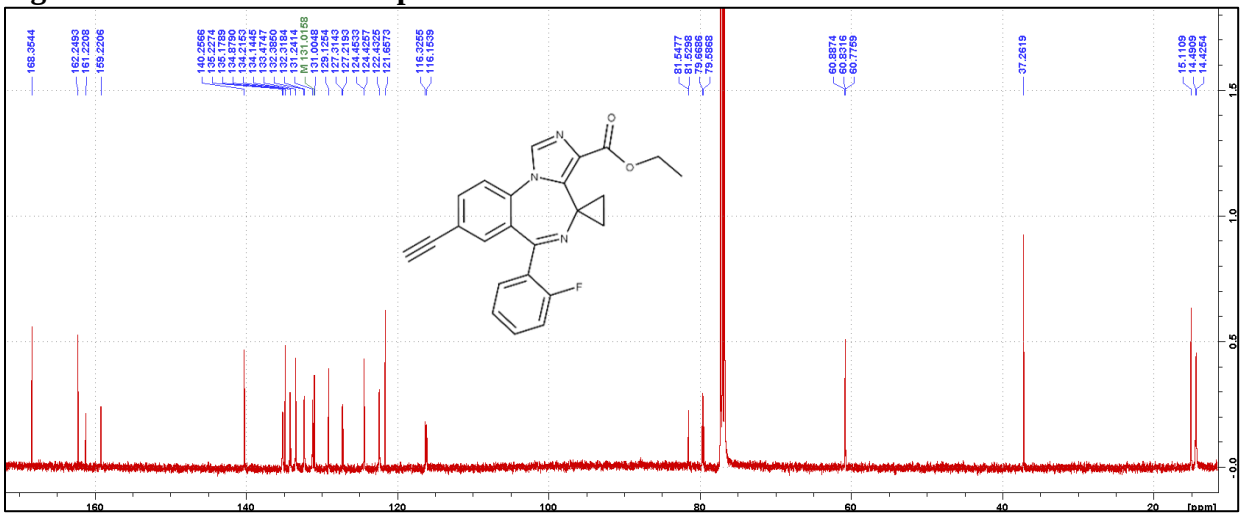

Figure 168: DAW-II-35 ^{19}F spectra:

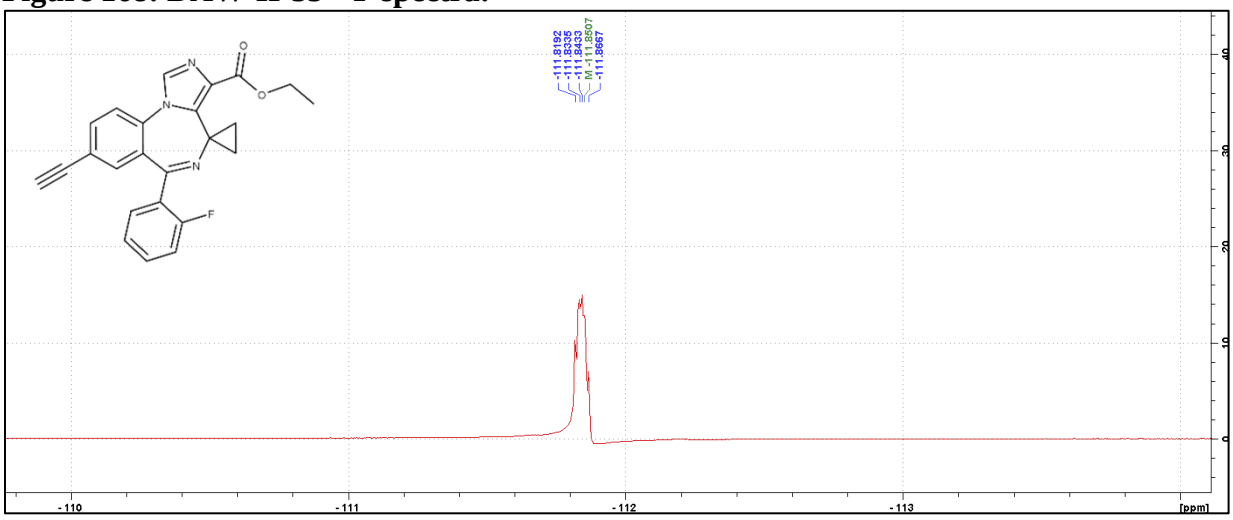

Figure 169: DAW-II-35 HPLC UV Chromatograph:

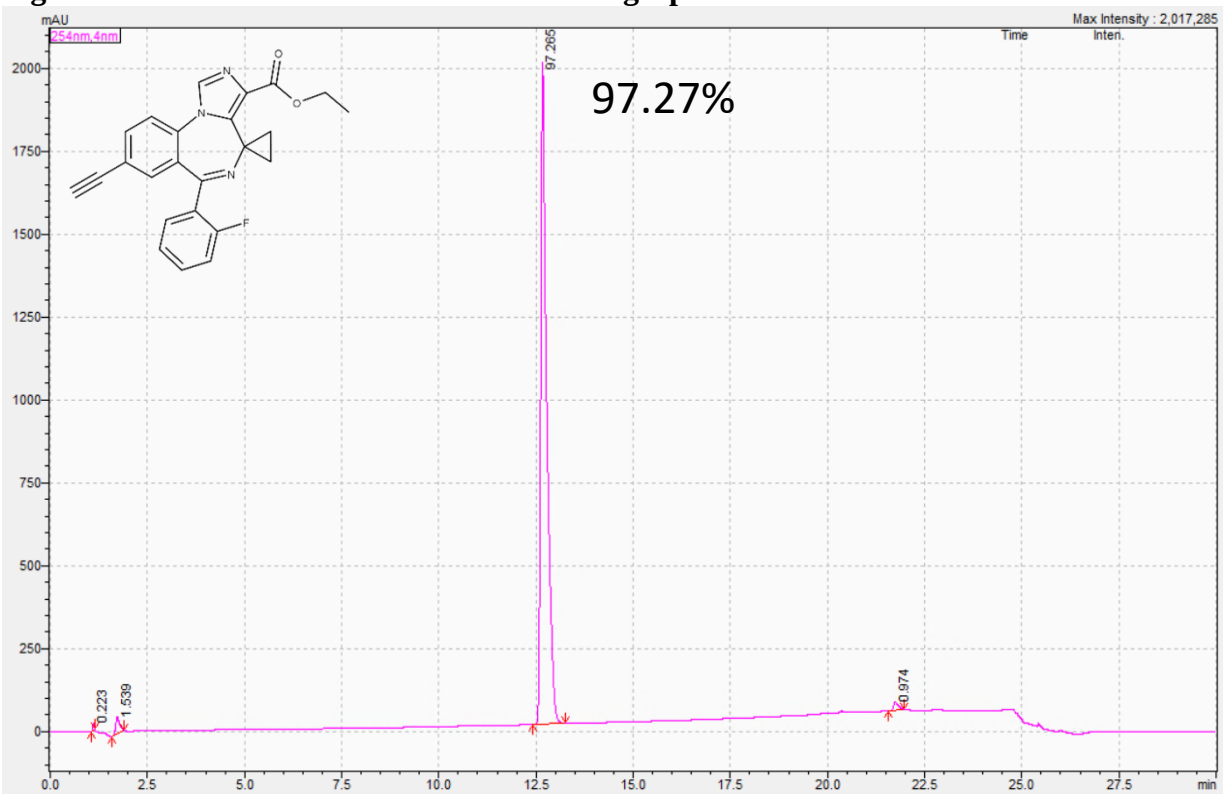

Figure 170: DAW-II-35 HRMS:

Score	Pred. (M)	Pred. m/z	Meas. m/z	Diff. (mDa)	Formulae (M)	Ion	Diff. (ppm)	Iso Score	DBE
58.61	399.13830	400.14558	400.14606	0.48	C24 H18 N3 O2 F	[M+H]+	1.200	54.64	17.0

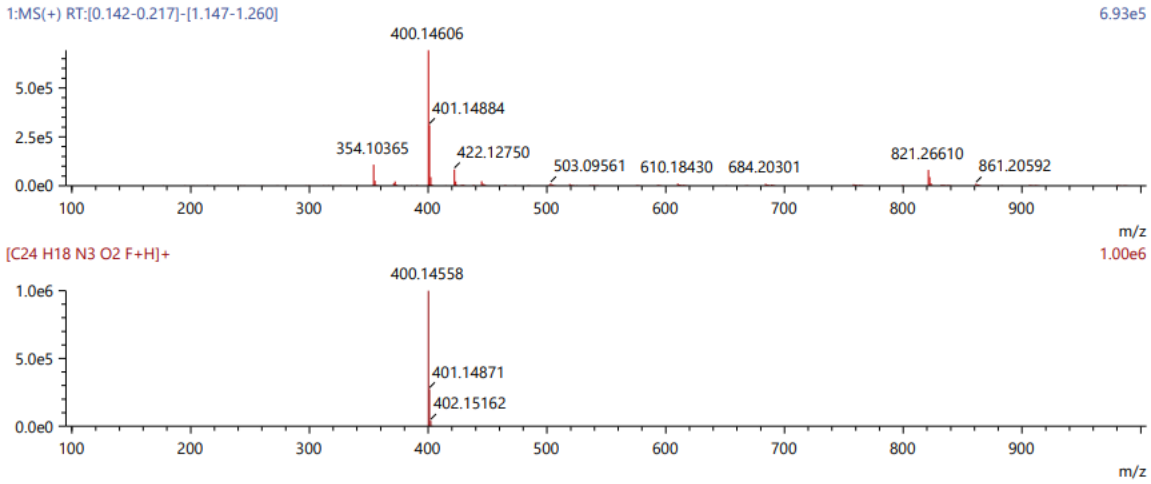

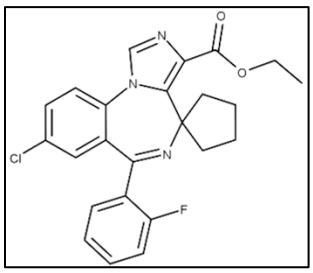

Synthesis of DAW-II-52: A three stopper RB flask was purged with nitrogen and vacuum 3 times. **DAW-I-52** (1.20 g, 3.50 mmol) was dissolved in anhydrous tetrahydrofuran (13.6 mL) and added to the reaction flask. The mixture was cooled to -20 °C using a dry ice/IPA bath. A solution of 1M potassium *tert*-butoxide in anhydrous tetrahydrofuran (4.55 mL) was added dropwise over the course of 10 min, at which time the reaction color turned to a deep orange. Upon completion of the addition, the mixture was allowed to stir at -20 °C for 40 min. Diethyl chlorophosphate (0.71 mL, 4.90 mmol) was added dropwise over the course of 5 min while maintaining a temperature of -20 °C. After 3.5 h, no more conversion was observed via TLC (100% EtOAc) and ethyl isocyanoacetate (0.50 mL, 4.55 mmol) was added dropwise over the course of 5 min followed by the addition of a solution of 1M potassium *tert*-butoxide in anhydrous tetrahydrofuran (4.55 mL) at -20 °C. The reaction was then warmed to room temperature for 2 h at which point all of the intermediate had been consumed via TLC (100% EtOAc). The reaction was then quenched with 5% aqueous sodium bicarbonate (50 mL), and the product was extracted with ethyl acetate (50 mL). The organic layer was washed with 10% aqueous sodium bicarbonate

(50 mL) followed by 20% aqueous NaCl (50 mL). The organic layer was then dried with $MgSO_4$ and then concentrated under reduced pressure. The resulting residue was triturated with a 50% mixture of *tert*-butyl methyl ether in hexanes (20 mL) at 55 °C for 20 h. The *tert*-butyl methyl ether/hexanes mixture was decanted, and the solid product was slurried in 100% hexanes (30 mL) at 55 °C for 4 h. The desired product was collected by filtration to yield an off-white solid (935.4 mg, 61.0%): ^{1}H NMR (500 MHz, $CDCl_3$) δ 7.86 (s, 1H), 7.51-7.48 (dd, *J* = 3.60, 2.25 Hz, 1H), 7.47-7.43 (m, 2H), 7.38-7.34 (m, 1H), 7.17-7.14 (dt, *J* = 3.23, 1.05 Hz, 2H), 6.99-6.95 (m, 1H), 4.32-4.28 (q, *J* = 7.15 Hz, 2H), 2.76-2.74 (m, 1H), 2.57-2.55 (m, 1H), 1.83 (m, 2H), 1.62-1.60 (m, 2H), 1.51-1.50 (m, 2H), 1.34-1.31 (t, *J* = 7.13 Hz, 3H); ^{13}C NMR (126 MHz, $CDCl_3$) δ 163.65 (s), 161.03 (s), 160.30 (d, $^1J_{CF}$ = 251.15 Hz), 140.74 (s), 135.20 (s), 134.10 (s), 133.41 (s), 132.10 (d, $^3J_{CF}$ = 8.38 Hz), 131.91 (s), 131.79 (s), 131.37 (d, $^3J_{CF}$ = 2.34 Hz), 129.87 (s), 129.47 (d, $^4J_{CF}$ = 1.51 Hz), 127.92 (d, $^2J_{CF}$ = 12.36 Hz), 124.55 (d, $^3J_{CF}$ = 3.52 Hz), 124.00 (s), 116.29 (d, $^2J_{CF}$ = 21.44 Hz), 67.44 (s), 61.33 (s), 40.99 (s), 36.00 (s), 23.62 (s), 23.29 (s), 14.31 (s); ^{19}F NMR (471 MHz, $CDCl_3$) δ -112.27; HRMS (ESI/Q-TOF): *m/z* $[M + H]^+$ calcd for $C_{24}H_{21}ClFN_3O_2$: 438.13791; found: 438.13868; HPLC Purity: 98.06%.

Figure 171: DAW-II-52 ^{1}H spectra:

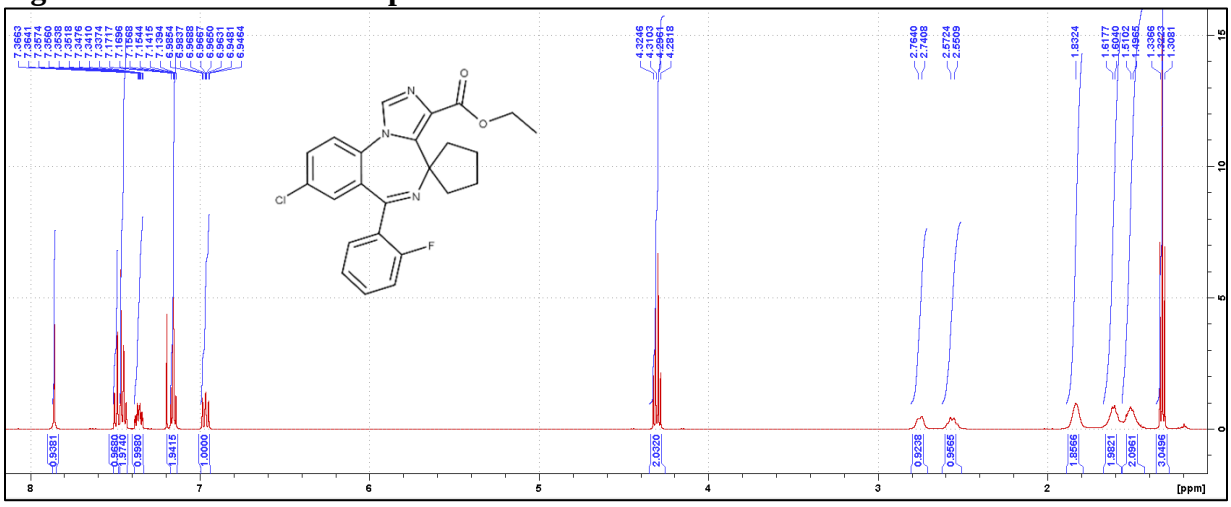

Figure 172: DAW-II-52 ^{13}C spectra:

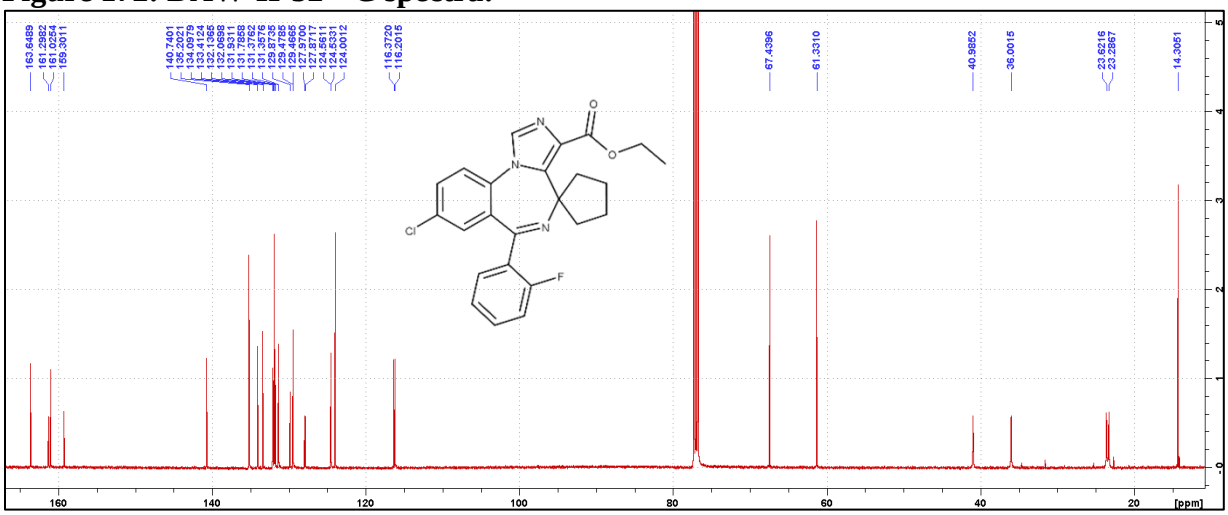

Figure 173: DAW-II-52 ^{19}F spectra:

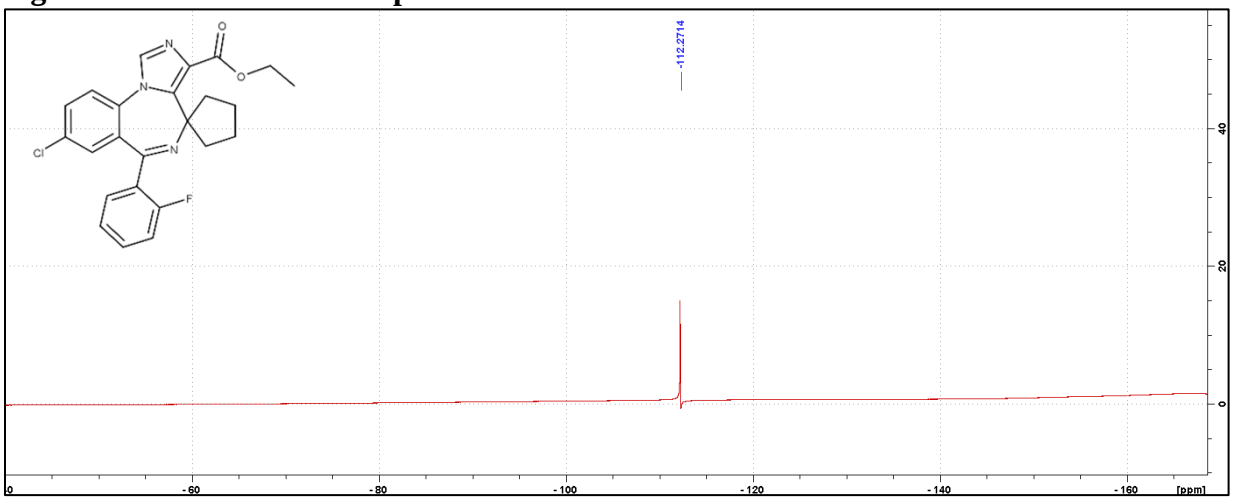

Figure 174: DAW-II-52 HPLC UV Chromatograph:

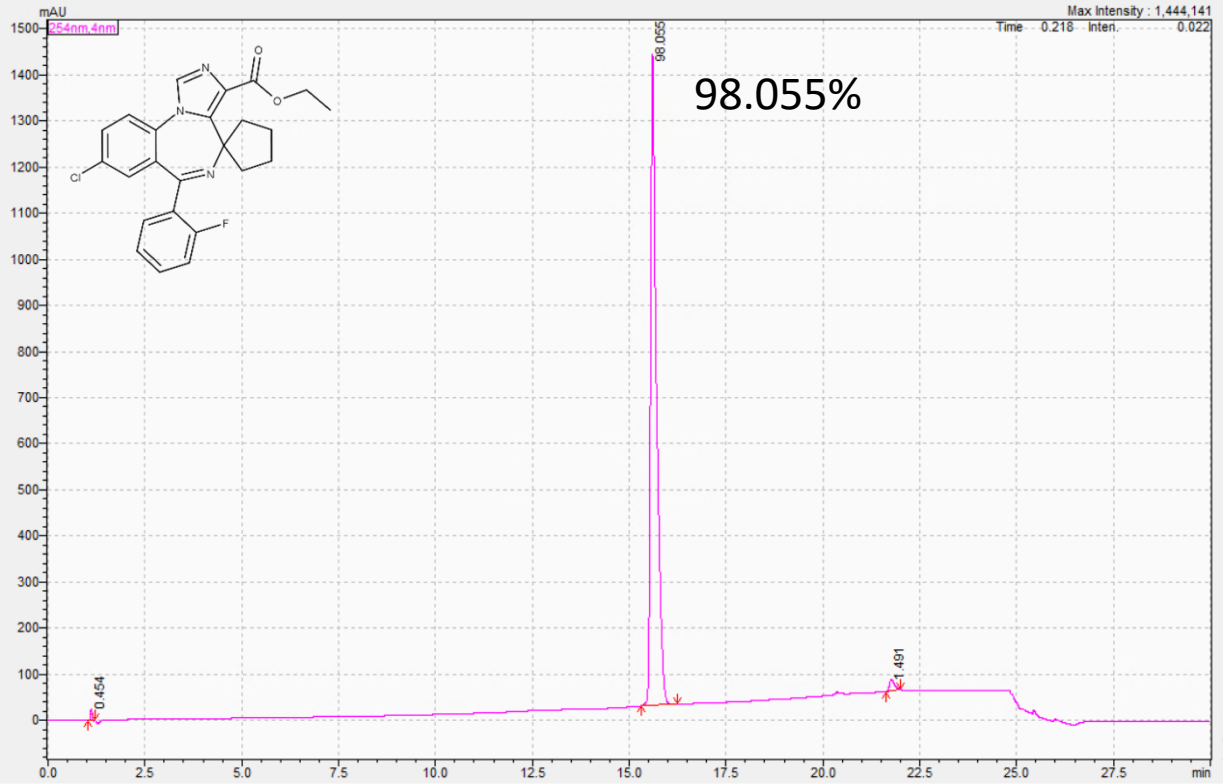

Figure 175: DAW-II-52 HRMS:

Score	Pred. (M)	Pred. m/z	Meas. m/z	Diff. (mDa)	Formulae (M)	Ion	Diff. (ppm)	Iso Score	DBE
56.83	437.13063	438.13791	438.13868	0.77	C24 H21 N3 O2 F Cl	[M+H]+	1.757	53.04	15.0

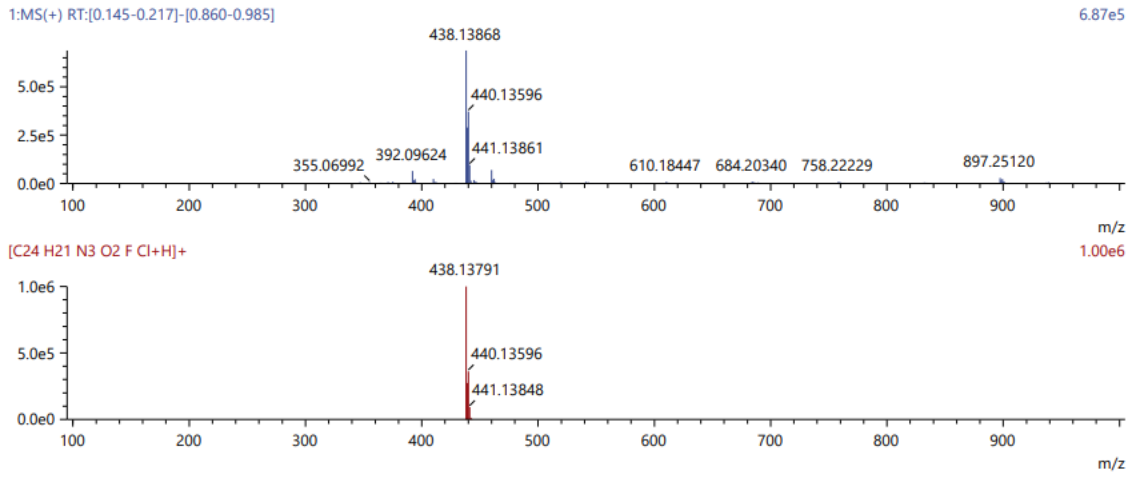

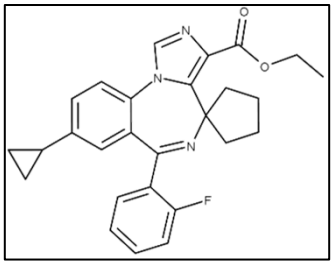

Synthesis of DAW-II-53: A mixture of toluene (11.2 mL) and water (1.62 mL) was degassed with nitrogen before **DAW-II-50** (560.2 mg, 1.16 mmol) was added. Cyclopropyl boronic acid (498.8 mg, 5.81 mmol) was then added, followed by potassium phosphate (1.06 g, 4.99 mmol), palladium acetate (26.1 mg, 0.12 mmol), and tri(*o*-tolyl)phosphine (70.7 mg, 0.23 mmol). The reaction was then heated to 100 °C for 18 h before being cooled back to room temperature and H_2O (50 mL) was added. The aqueous layer was extracted with ethyl acetate (50 mL, 3x) and the organic layers were combined before being washed with brine (150 mL) and dried with $MgSO_4$. The solvent was removed under reduced pressure and the residue was loaded onto a precolumn with chloroform and separated by Biotage: 25-95% ethyl acetate in hexanes (20 CV). The desired product was obtained as an off-white solid (331.6 mg, 64.4%): ^{1}H NMR (500 MHz, $CDCl_3$) -20°C δ 7.93 (s, 1H), 7.55-7.53 (m, 1H), 7.48-7.46 (m, 1H), 7.45-7.42 (m, 1H), 7.26-7.23 (dt, *J* = 3.14, 0.70 Hz, 1H), 7.19-7.17 (dd, *J* = 3.35, 1.75 Hz, 1H), 7.06-7.03 (m, 1H), 6.97-6.96 (m, 1H), 4.39-4.34 (q, *J* = 7.12 Hz, 2H), 2.87-2.85 (m, 1H), 2.63-2.56 (m, 1H), 1.92-1.90 (m, 2H), 1.88-1.83 (m, 1H), 1.75-1.70 (m, 1H), 1.66-1.52 (m, 3H), 1.41-1.38 (t, *J* = 7.15 Hz, 3H), 1.05-1.02 (m, 2H), 0.72-0.62 (m, 2H); ^{13}C NMR (126 MHz, $CDCl_3$) -20°C δ 163.78 (s), 162.85 (s), 160.26 (d, $^1J_{CF}$ = 251.03 Hz), 144.26 (s), 141.20 (s), 135.45 (s), 132.87 (s), 132.00 (d, $^3J_{CF}$ = 6.81 Hz), 131.58 (s), 129.28 (s), 129.07 (s), 128.47 (d, $^2J_{CF}$ = 15.49 Hz), 127.99 (s), 127.30 (s), 124.64 (d, $^3J_{CF}$ = 3.15 Hz), 122.69 (s), 116.28 (d, $^2J_{CF}$ = 21.32 Hz), 67.16 (s), 61.42 (s), 41.19 (s), 35.57 (s), 23.78 (s), 23.15 (s), 15.20 (s), 14.49 (s), 10.70 (s); ^{19}F NMR (471 MHz, $CDCl_3$) -20°C δ -112.29; HRMS (ESI/Q-TOF): *m/z* $[M + H]^+$ calcd for $C_{27}H_{26}FN_3O_2$: 444.20818; found: 444.20450; HPLC Purity: 98.93%.

Figure 176: DAW-II-53 ^{1}H spectra:

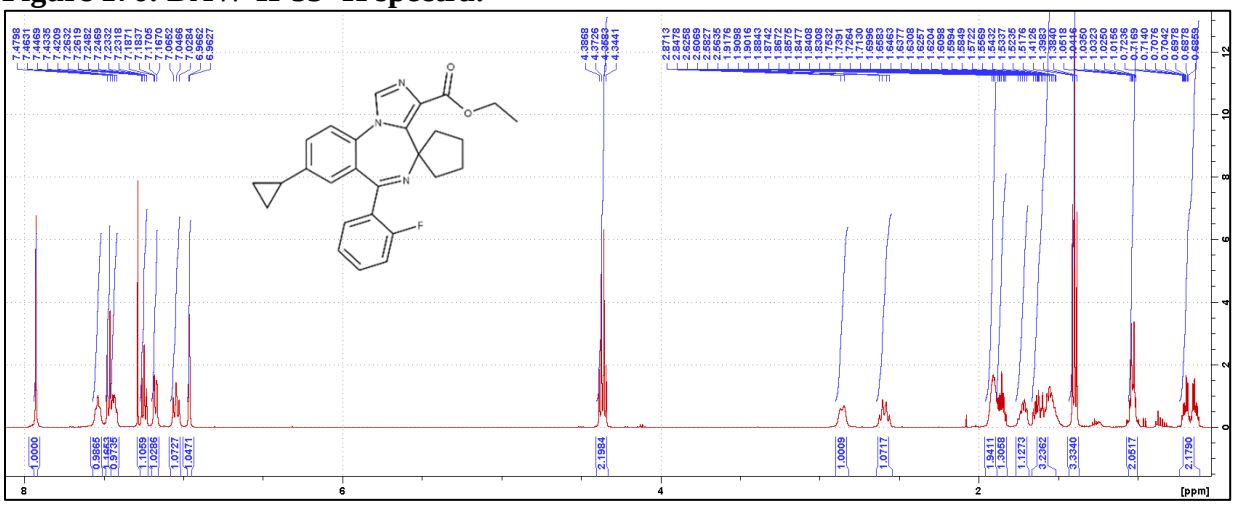

Figure 177: DAW-II-53 ^{13}C spectra:

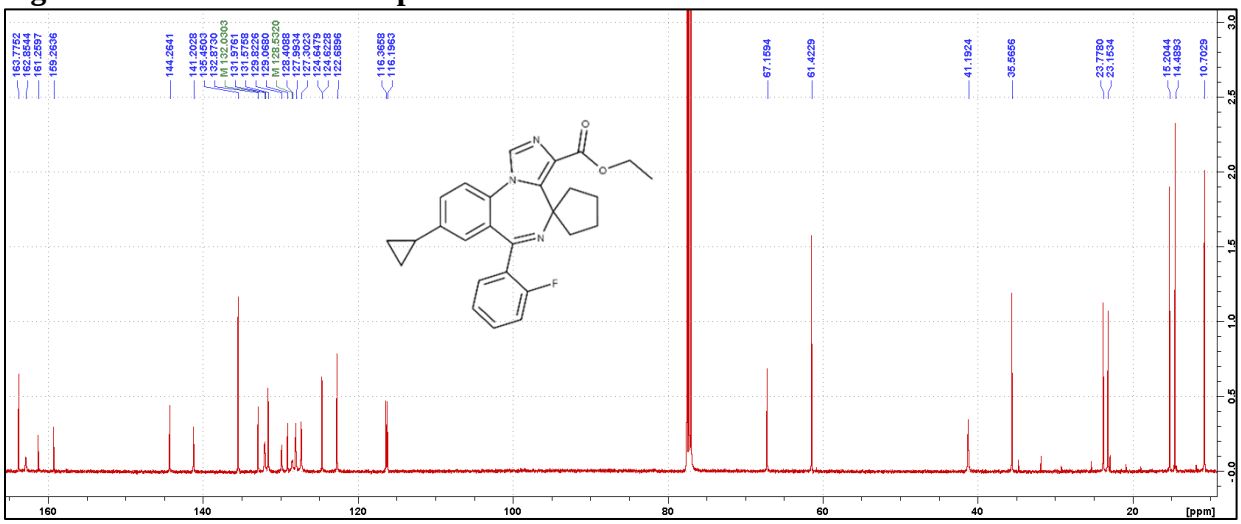

Figure 178: DAW-II-53 ^{19}F spectra:

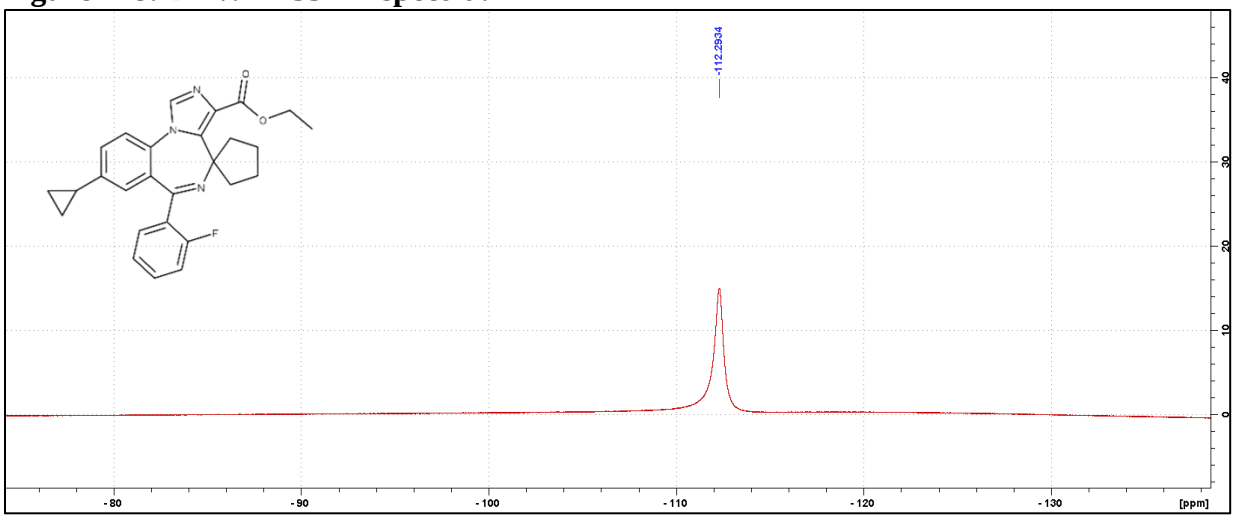

Figure 179: DAW-II-53 HPLC UV Chromatograph:

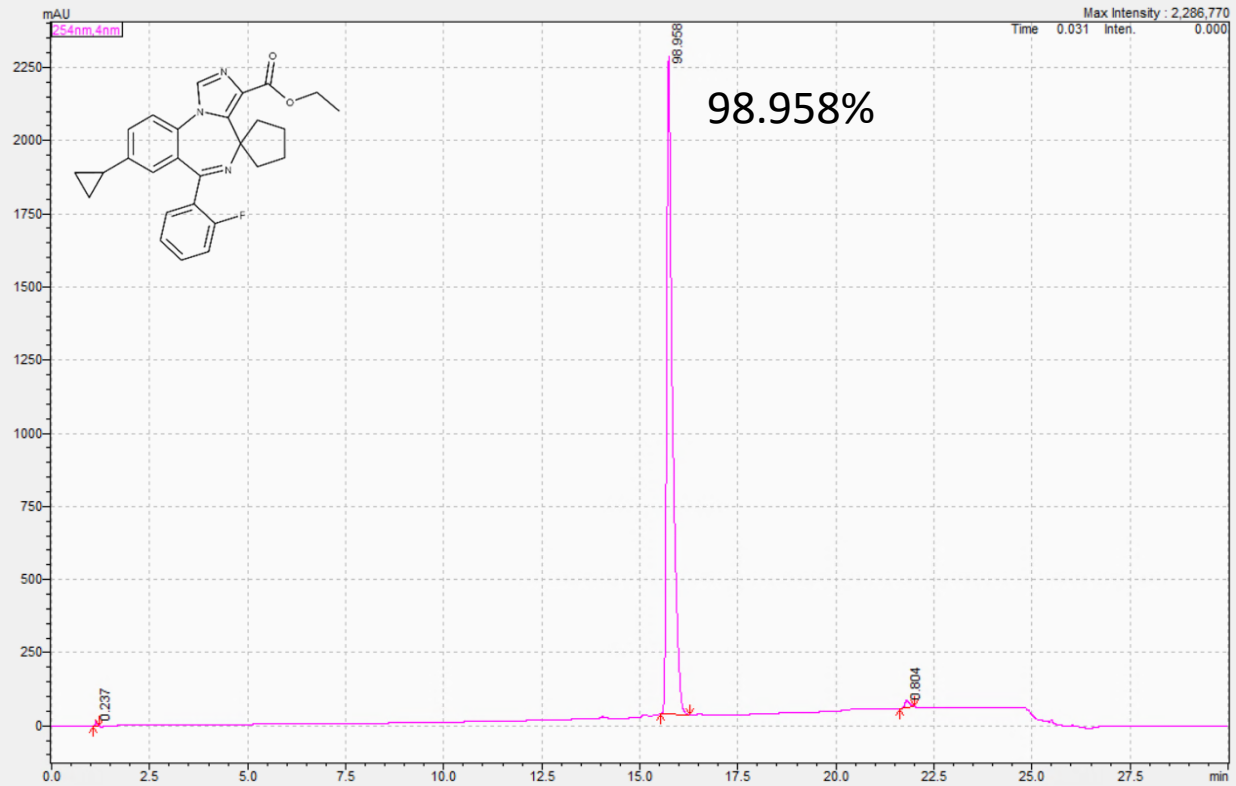

Figure 180: DAW-II-53 HRMS:

Score	Pred. (M)	Pred. m/z	Meas. m/z	Diff. (mDa)	Formulae (M)	Ion	Diff. (ppm)	Iso Score	DBE
14.63	443.20091	444.20818	444.20450	-3.68	C27 H26 N3 O2 F	[M+H]+	-8.284	16.25	16.0

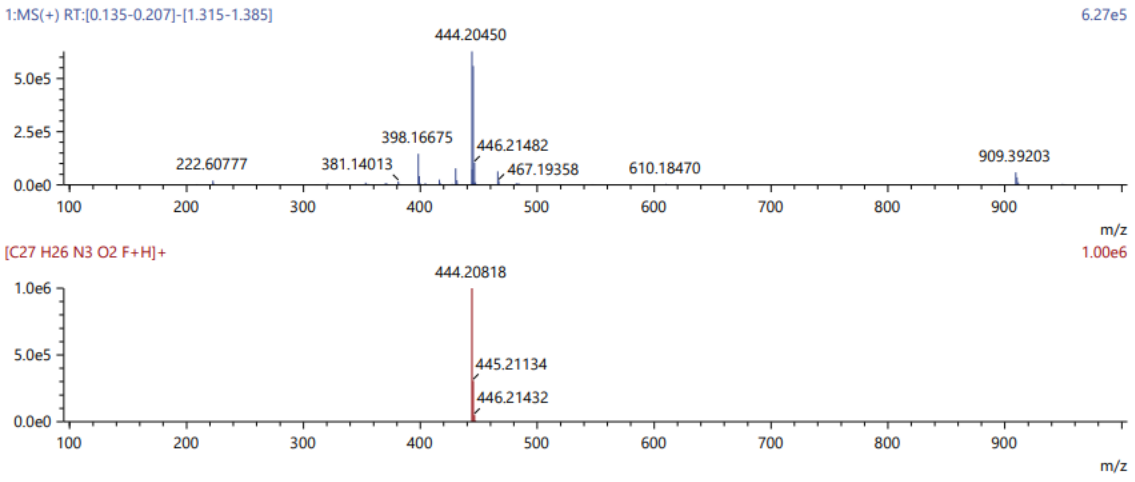

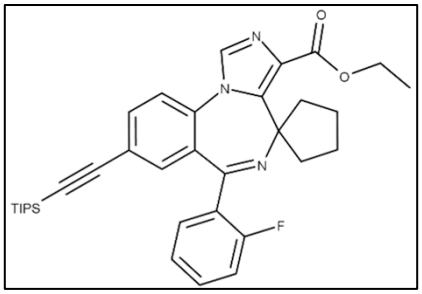

Synthesis of DAW-II-55T: A three stopper RB flask was purged with vacuum and nitrogen 3 times. Anhydrous acetonitrile (7.3 mL) was added to the flask and the solvent was degassed with nitrogen. Palladium acetate (28.1 mg, 0.125 mmol) was added followed by the addition of tri(*o*-tolyl)phosphine (75.7 mg, 0.25 mmol) and the mixture was stirred at room temperature for 30 min. **DAW-II-50** (1.20 g, 2.49 mmol) was added followed by the addition of triethyl amine (0.69 mL, 4.98 mmol), TIPS acetylene (0.67 mL, 2.99 mmol), and additional nitrogen degassed acetonitrile (9.75 mL). The reaction was heated to 75 °C for 4 h. Upon completion by TLC (100% EtOAc), silica gel (600 mg) was added to the reaction and the reaction was cooled to room temperature while stirring for 30 min. The mixture was filtered over celite and washed with acetonitrile. The solvent was removed under reduced pressure and the residue was dissolved in dichloromethane (50 mL) before the organic layer was washed with 5% aqueous sodium bicarbonate (50 mL), followed by 10% aqueous NaCl (50 mL). The organic layer was dried with $MgSO_4$, and the solvent was removed under reduced pressure. The residue was loaded onto a precolumn with chloroform and separated by Biotage: 5-55% ethyl acetate in hexanes (20 CV), 55-90% ethyl acetate in hexanes (5 CV). The desired product was obtained as a yellow solid (1.32 g, 91.2%): ^{1}H NMR (500 MHz, $CDCl_3$) δ 7.89 (s, 1H), 7.67-7.65 (dd, *J* = 3.38, 1.85 Hz, 1H), 7.54-7.49 (m, 2H), 7.44-7.40 (m, 1H), 7.29-7.28 (m, 1H), 7.24-7.21 (dt, *J* = 3.22, 1.05 Hz, 1H), 7.06-7.02 (m, 1H), 4.40-4.35 (q, *J* = 7.14 Hz, 2H), 2.83-2.81 (m, 1H), 2.67-2.61 (m, 1H), 1.90 (m, 2H), 1.72-1.57 (m, 4H), 1.41-1.38 (t, *J* = 7.13 Hz, 3H), 1.11-1.09 (m, 21H); ^{13}C NMR (126 MHz, $CDCl_3$) δ 163.78 (s), 161.50 (s), 160.32 (d, $^{1}J_{CF}$ = 251.19 Hz), 140.82 (s), 135.42 (d, *J* = 5.51 Hz), 135.26 (d, *J* = 8.58 Hz), 135.01 (d, *J* = 12.35 Hz), 132.56 (s), 131.79 (d, $^{3}J_{CF}$ = 7.41 Hz), 131.35 (d, $^{3}J_{CF}$ = 9.54 Hz), 130.41 (s), 129.91 (s), 128.22 (d, $^{2}J_{CF}$ = 12.32 Hz), 124.35

(d, $^{3}J_{CF}$ = 3.29 Hz), 123.02 (s), 122.51 (m), 116.13 (m), 104.62 (s), 94.00 (s), 67.34 (s), 61.18 (t, *J* = 12.41 Hz), 40.97 (t, *J* = 17.85 Hz), 35.86 (t, *J* = 15.68 Hz), 23.42 (m), 18.56 (m), 14.26 (m), 11.18 (m); ^{19}F NMR (471 MHz, $CDCl_3$) δ -112.39; HRMS (ESI/Q-TOF): *m/z* $[M + H]^+$ calcd for $C_{35}H_{42}FN_3O_2Si$: 584.31031; found: 584.30819; HPLC Purity: 98.46%.

Figure 181: DAW-II-55T ^{1}H spectra:

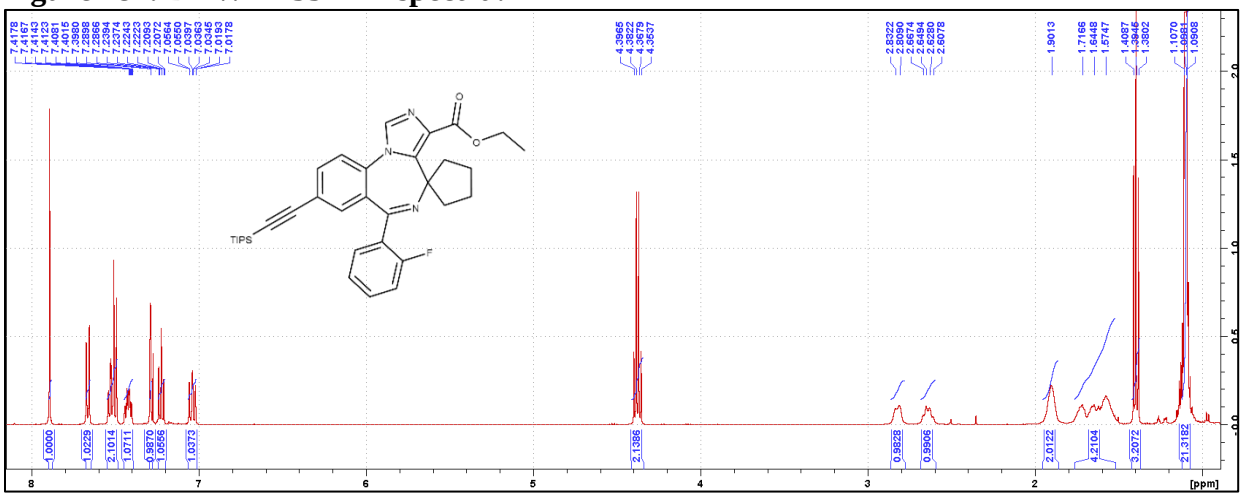

Figure 182: DAW-II-55T ^{13}C spectra:

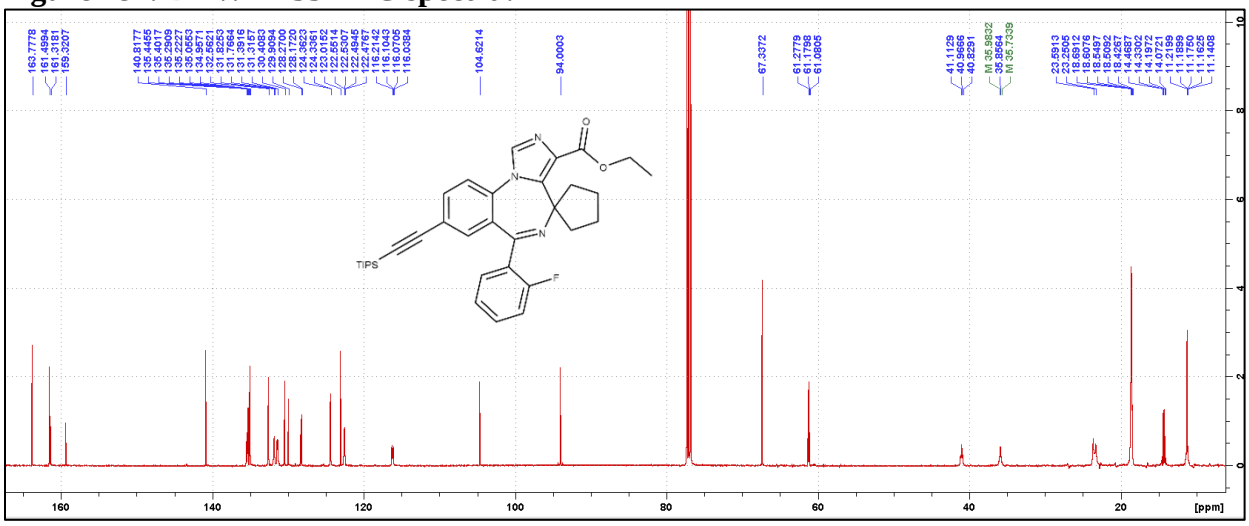

Figure 183: DAW-II-55T ^{19}F spectra:

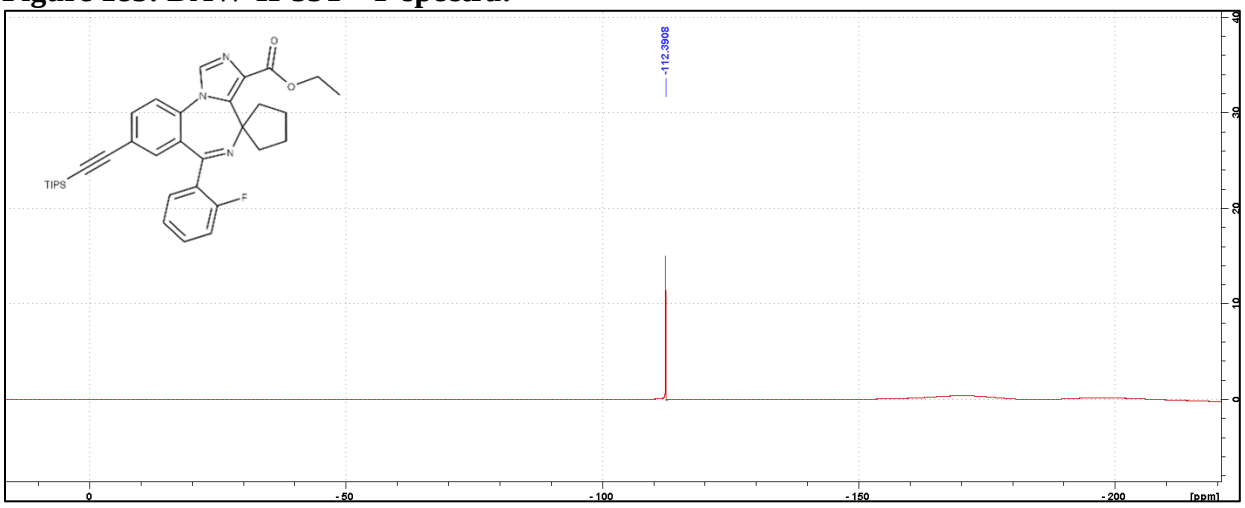

Figure 184: DAW-II-55T HPLC UV Chromatograph:

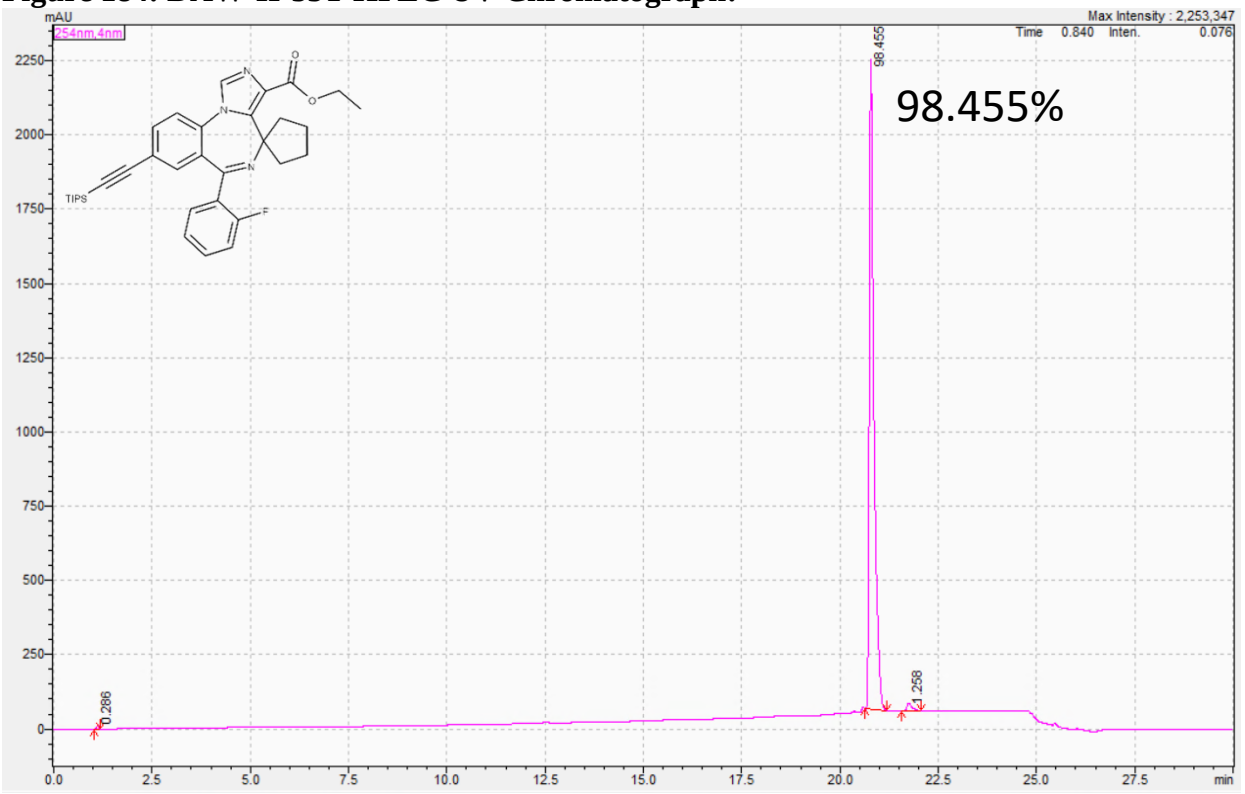

Figure 185: DAW-II-55T HRMS:

Score	Pred. (M)	Pred. m/z	Meas. m/z	Diff. (mDa)	Formulae (M)	Ion	Diff. (ppm)	Iso Score	DBE
28.00	583.30303	584.31031	584.30819	-2.12	C35 H42 N3 O2 F Si	[M+H]+	-3.628	23.04	16.0

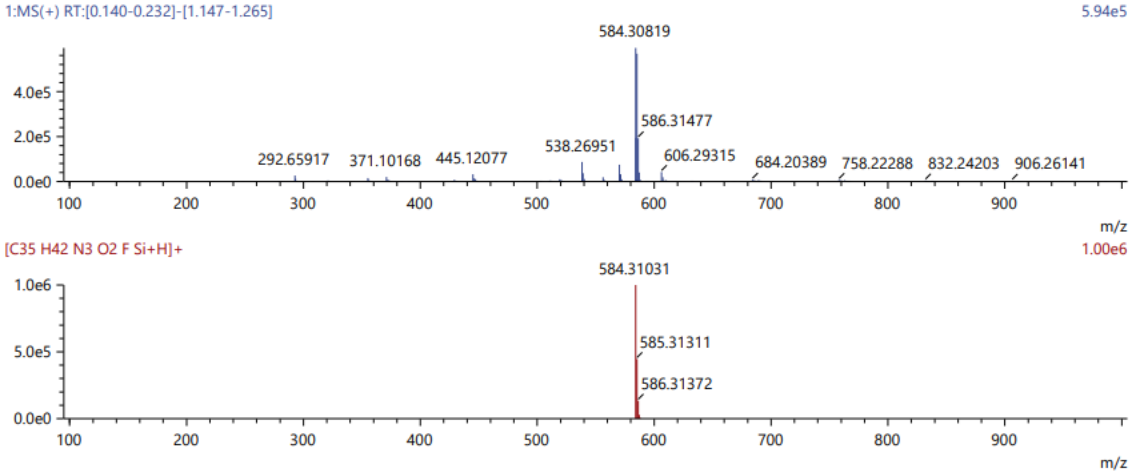

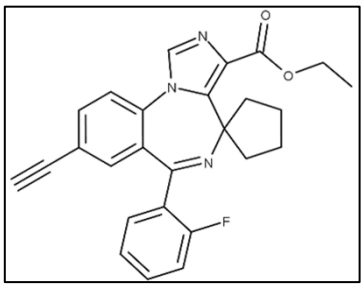

Synthesis of DAW-II-55: DAW-II-55T (1.24 g, 2.12 mmol) was dissolved in a solution of THF (12.4 mL) and H_2O (123.7 uL). The mixture was cooled to -20 °C in a dry ice/IPA bath before 1M TBAF in THF (2.6 mL) was added dropwise over 5 min. The reaction was then warmed to room temperature and stirred for 1.5 h upon which all the starting material had been consumed by TLC (100% EtOAc:Hex). The reaction was then diluted with ethyl acetate (80 mL), and the organic layer was washed with 10% aqueous NaCl (80 mL, 2x). The organic layer was dried with $MgSO_4$, and the solvent was removed under reduced pressure. The residue was loaded onto a precolumn with chloroform and separated by Biotage: 35-90% ethyl acetate in hexanes (25 CV). The desired product was obtained as an off-white solid (868.9 mg, 95.1%): ^{1}H NMR (500 MHz, $CDCl_3$) δ 7.88 (s, 1H), 7.69-7.67 (dd, *J* = 3.38, 1.85 Hz, 1H), 7.53-7.50 (m, 2H), 7.44-7.40 (m, 1H), 7.37-7.36 (m, 1H), 7.24-7.20 (dt, *J* = 3.22, 1.00 Hz, 1H), 7.05-7.01 (m, 1H), 4.40-4.35 (q, *J* = 3.38 Hz, 2H), 3.14 (s, 1H), 2.81 (m, 1H), 2.64-2.62 (m, 1H), 1.90 (m, 2H), 1.69-1.57 (m, 4H), 1.41-1.38 (t, *J* = 7.13 Hz, 3H); ^{13}C NMR (126 MHz, $CDCl_3$) δ 163.85 (s), 161.39 (s), 160.31 (d, $^1J_{CF}$ = 251.09 Hz), 140.79 (s), 135.50 (s), 135.19 (s), 135.15

(s), 133.24 (d, $^{4}J_{CF}$ = 1.31 Hz), 131.89 (d, $^{3}J_{CF}$ = 8.31 Hz), 131.36 (d, $^{3}J_{CF}$ = 2.20 Hz), 130.51 (s), 130.12 (s), 128.23 (d, $^{2}J_{CF}$ = 12.45 Hz), 124.46 (d, $^{3}J_{CF}$ = 3.48 Hz), 122.65 (s), 121.63 (s), 116.24 (d, $^{2}J_{CF}$ = 21.49 Hz), 81.52 (s), 79.59 (d, *J* = 5.24 Hz), 67.38 (s), 61.25 (t, *J* = 4.68 Hz), 40.98 (s), 35.93 (s), 23.59 (s), 23.25 (s), 14.30 (d, *J* = 4.01 Hz); ^{19}F NMR (471 MHz, $CDCl_3$) δ -112.37; HRMS (ESI/Q-TOF): *m/z* $[M + H]^+$ calcd for $C_{26}H_{22}FN_3O_2$: 428.17688; found: 428.17330; HPLC Purity: 99.21%.

Figure 186: DAW-II-55 ^{1}H spectra:

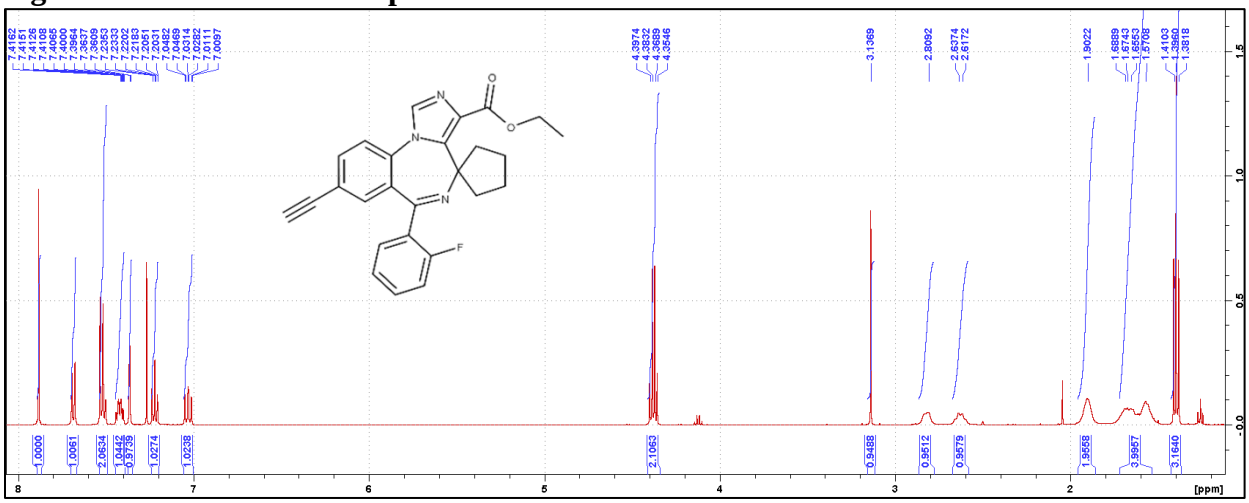

Figure 187: DAW-II-55 ^{13}C spectra:

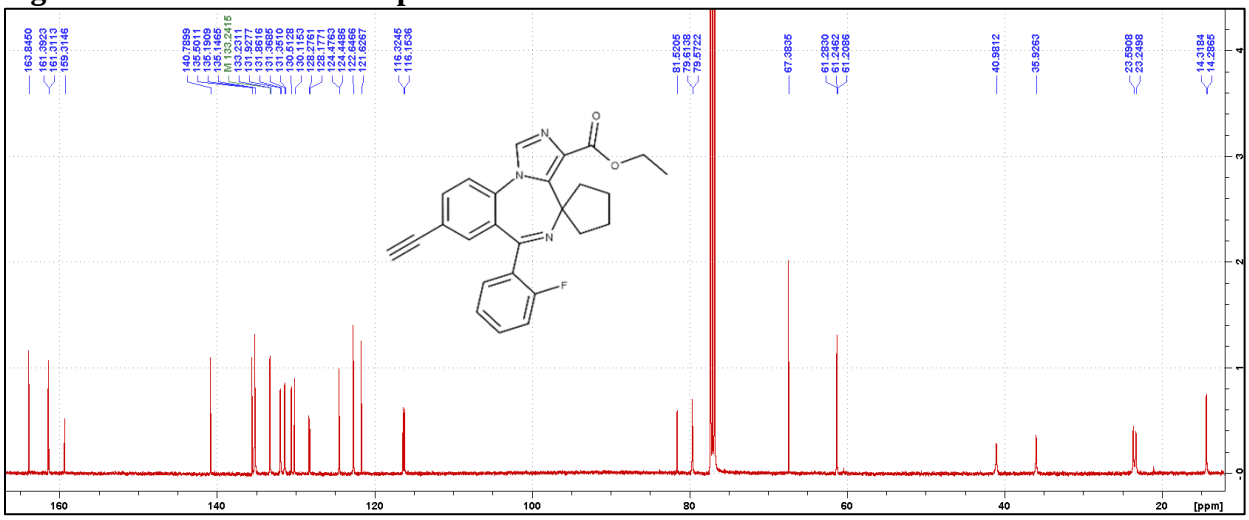

Figure 188: DAW-II-55 ^{19}F spectra:

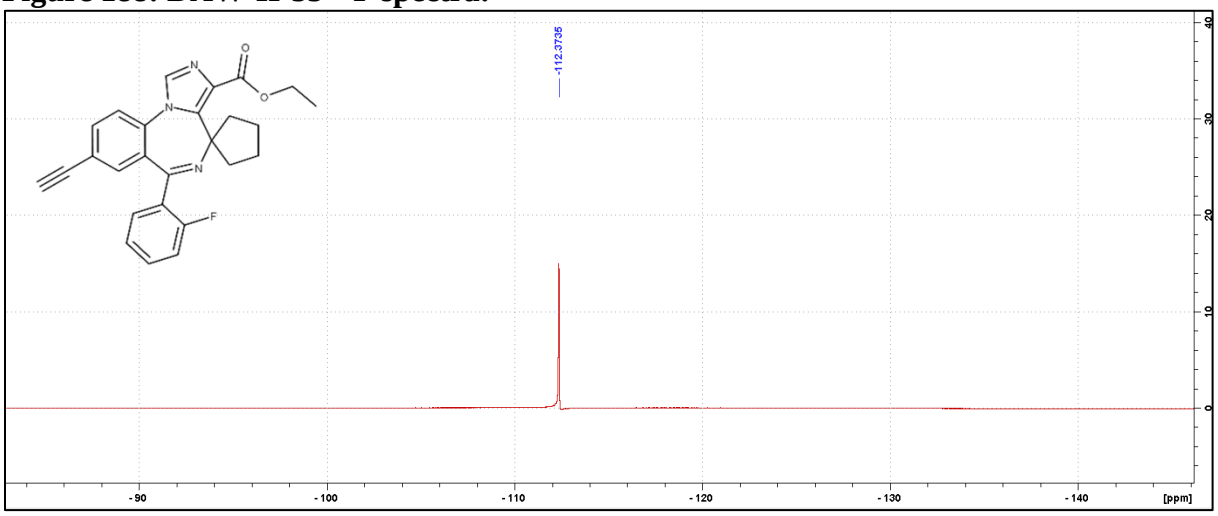

Figure 189: DAW-II-55 HPLC UV Chromatograph:

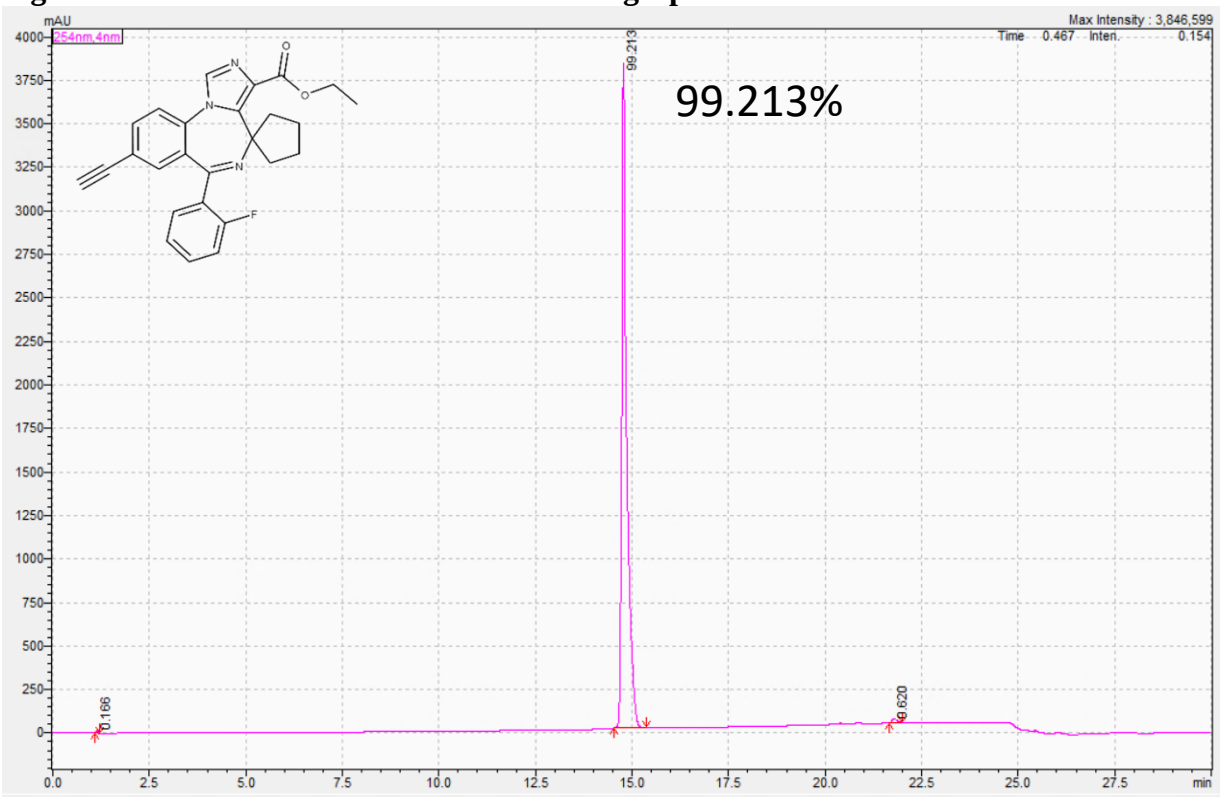

Figure 190: DAW-II-55 HRMS:

Score	Pred. (M)	Pred. m/z	Meas. m/z	Diff. (mDa)	Formulae (M)	Ion	Diff. (ppm)	Iso Score	DBE
14.90	427.16961	428.17688	428.17330	-3.58	C26 H22 N3 O2 F	[M+H]+	-8.361	16.55	17.0

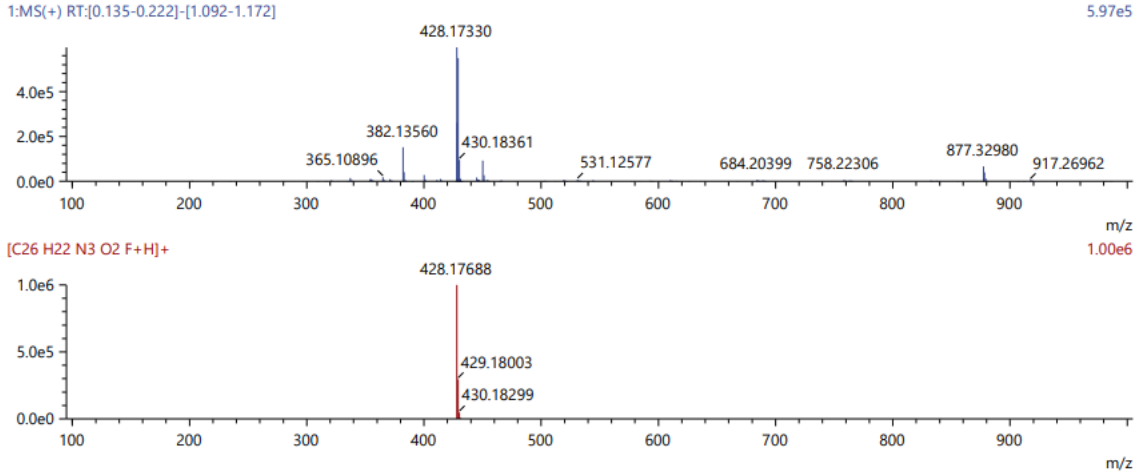

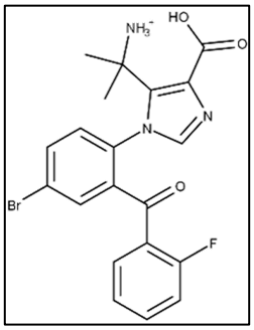

Synthesis of DAW-III-10: DAW-II-10 (202.1 mg, 0.44 mmol) was dissolved in tetrahydrofuran (14.3 mL) and cooled to 0 °C. Solid sodium hydroxide was added (531.5 mg, 13.29 mmol), followed by the addition of H_2O (340 uL). The reaction was then removed from the ice bath and gently heated to 80 °C for 18 h. When all the starting material had dropped to the baseline via TLC (100% EtOAc), the reaction was cooled to room temperature. Acetic acid was added until the pH was observed to be ~5, and the reaction was then warmed to 50 °C and allowed to stir for 20 h. The reaction was then concentrated to dryness under reduced pressure. The residue was dissolved in H_2O (3.5 mL) and portioned into 0.5 mL fractions. To each fraction was added an additional 1 mL of H_2O causing the desired product to precipitate out of solution. The fractions were centrifuged and the solution was decanted. The solid fractions were combined and washed with an additional 6 mL of H_2O to remove any residual acetic acid. The product was then collected by filtration to yield a white powder. The solid was slurried in 5 mL of 5 M HCl at 95 °C for 18 h upon which the diazepine ring had been completely broken by TLC (1.8 mL MeOH + 0.1 mL

AcOH + 4.3 mL chloroform). The mixture was then cooled to room temperature and the product was collected by filtration. The solid material was then washed with hot IPA (1 mL, 2x) and the product was again filtered to yield pure material. (59.3 mg, 31.2%): ^{1}H NMR (500 MHz, MeOD) δ 8.05-8.03 (dd, *J* = 3.56-2.25 Hz, 1H), 7.87-7.86 (m, 2H), 7.81-7.79 (m, 1H), 7.77-7.70 (m, 2H), 7.41-7.38 (m, 1H), 7.32-7.28 (m, 1H), 1.77 (s, 3H), 1.53 (s, 3H); ^{13}C NMR (126 MHz, MeOD) δ 190.18 (s), 166.65 (s), 161.10 (d, $^{1}J_{CF}$ = 254.49 Hz), 139.80 (s), 139.43 (s), 138.47 (s), 136.11 (d, $^{3}J_{CF}$ = 9.12 Hz), 135.63 (s), 133.04 (s), 132.07 (s), 131.39 (s), 124.88 (d, $^{3}J_{CF}$ = 3.43 Hz), 124.76 (d, $^{2}J_{CF}$ = 11.14 Hz), 124.65 (s), 116.51 (d, $^{2}J_{CF}$ = 21.86 Hz), 52.86 (s), 25.77 (s), 25.63 (s); ^{19}F NMR (471 MHz, MeOD) δ -110.50, -114.21; HRMS (ESI/Q-TOF): *m/z* [M + H]$^{+}$ calcd for $C_{20}H_{17}BrFN_3O_3$: 446.05101; found: 446.05095; HPLC Purity: 96.12%.

Figure 191: DAW-III-10 ^{1}H spectra:

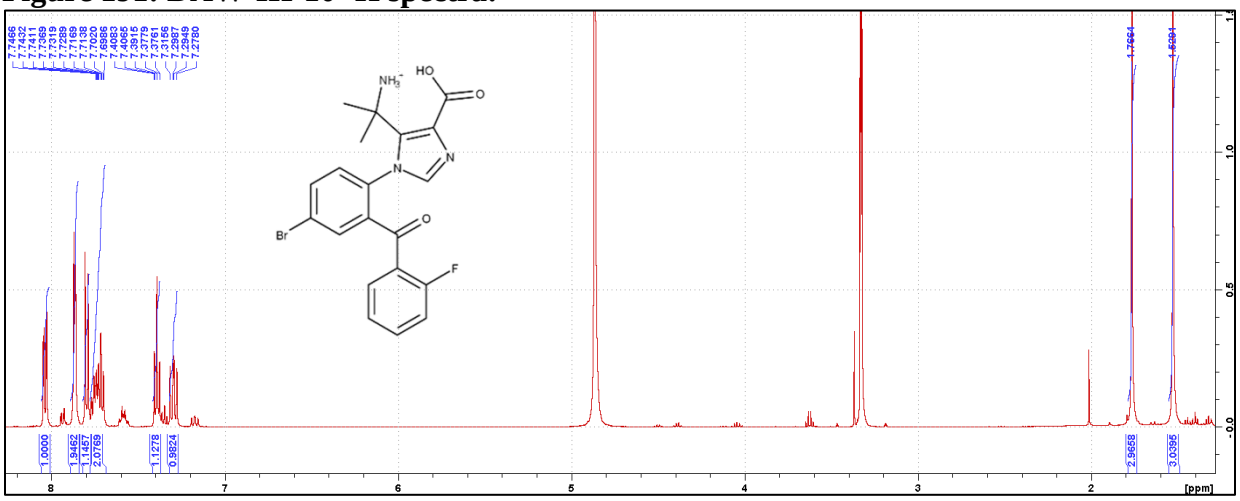

Figure 192: DAW-III-10 ^{13}C spectra:

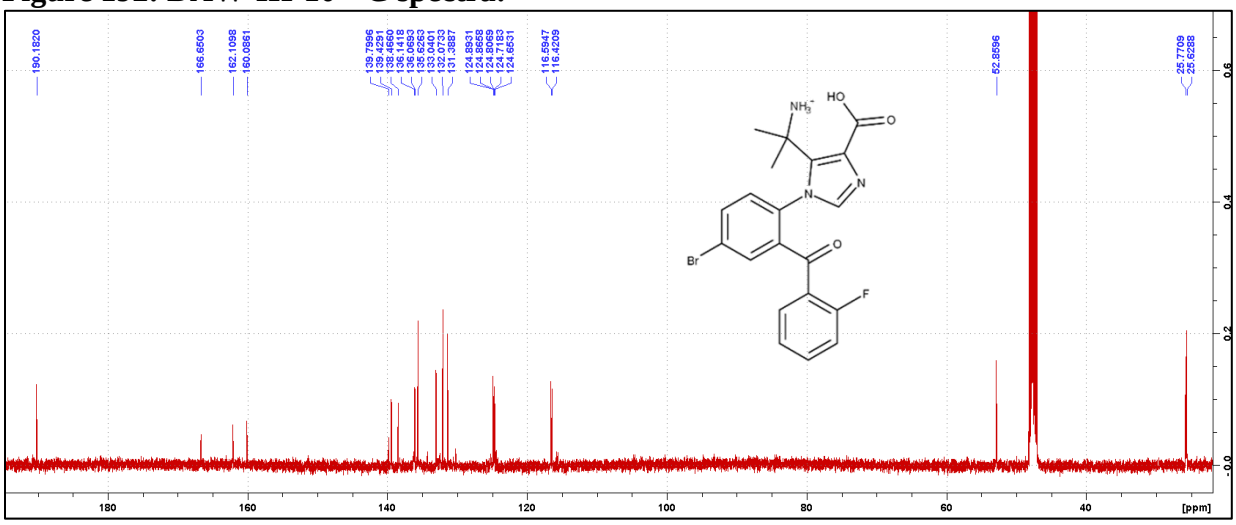

Figure 193: DAW-III-10 ^{19}F spectra:

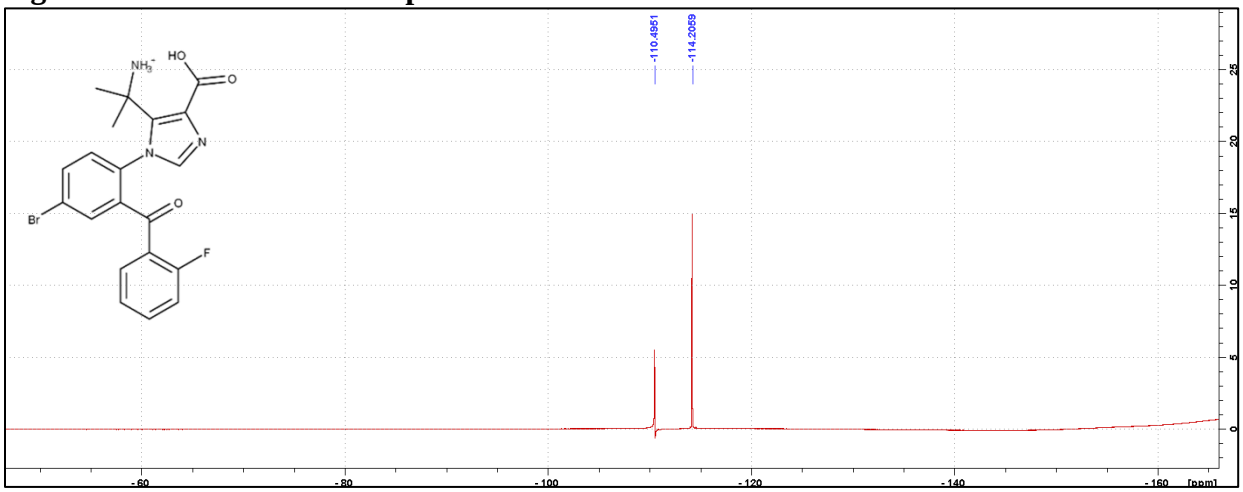

Figure 194: DAW-III-10 HPLC UV Chromatograph:

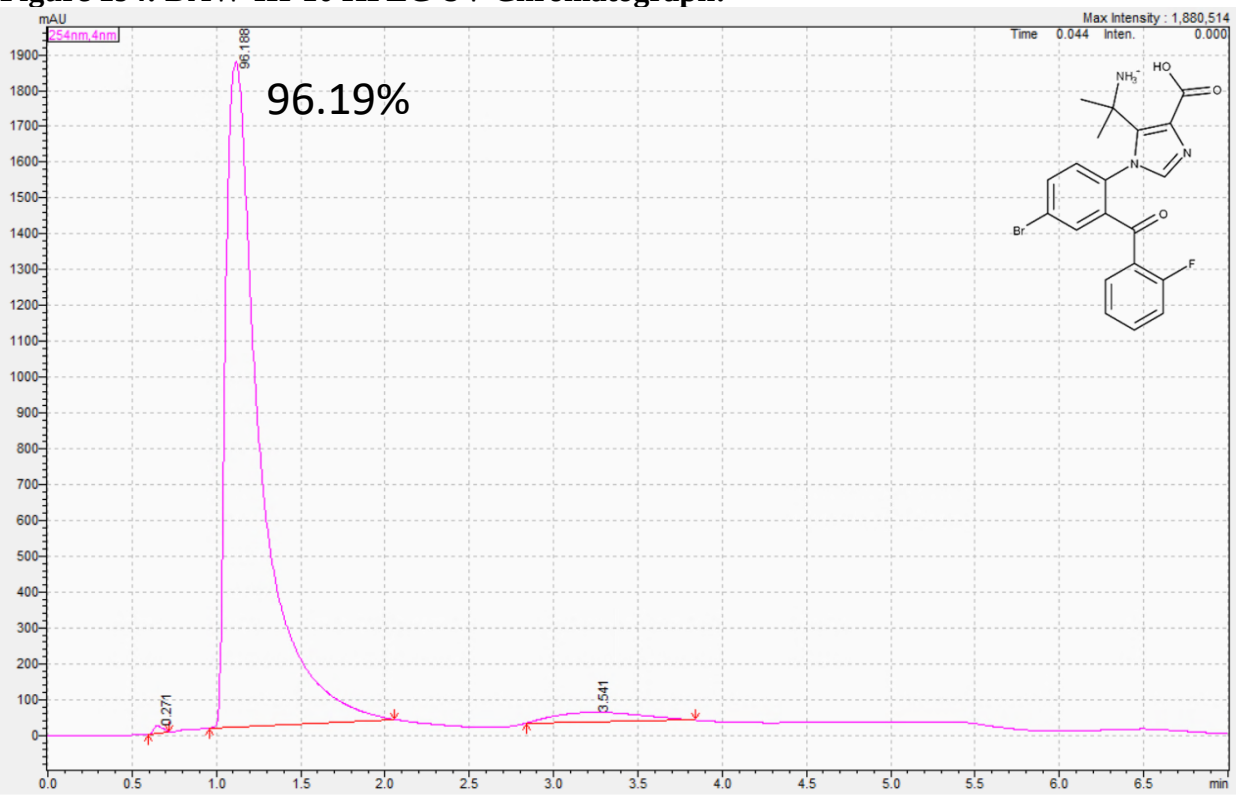

Figure 195: DAW-III-10 HRMS:

Score	Pred. (M)	Pred. m/z	Meas. m/z	Diff. (mDa)	Formulae (M)	Ion	Diff. (ppm)	Iso Score	DBE
98.02	445.04373	446.05101	446.05095	-0.06	C20 H17 N3 O3 F Br	[M+H]+	-0.135	97.84	13.0

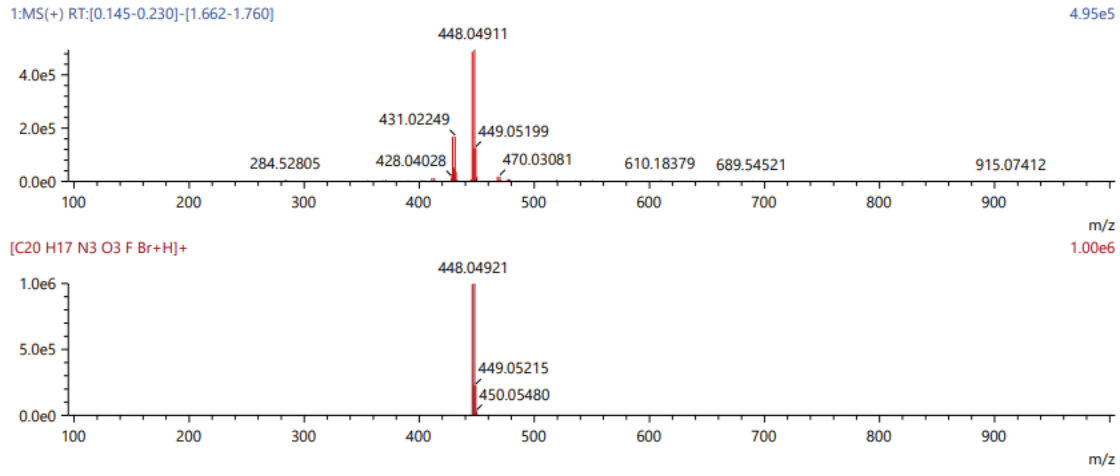

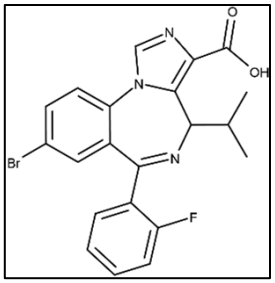

Synthesis of DAW-III-20: DAW-II-20 (172.25 mg, 0.36 mmol) was dissolved in tetrahydrofuran (15 mL) and cooled to 0 °C. Solid sodium hydroxide was added (436.9 mg, 10.92 mmol), followed by the addition of H_2O (281 uL). The reaction was then removed from the ice bath and gently heated to 80 °C for 18 h. When all the starting material had dropped to the baseline via TLC (100% EtOAc), the reaction was cooled to room temperature. Acetic acid was added until the pH was observed to be ~5, and the reaction was then warmed to 50 °C and allowed to stir for 20 h. The reaction was then concentrated to dryness under reduced pressure. The residue was dissolved in H_2O (3 mL) and portioned into 0.5 mL fractions. To each fraction was added an additional 1 mL of H_2O causing the desired product to precipitate out of solution. The fractions were centrifuged and the solution was decanted. The solid fractions were combined and washed with an additional 5 mL of H_2O to remove any residual acetic acid. The product was then collected by filtration to yield a white powder. No further purification was conducted. (91.33 g, 56.7%): ^{1}H NMR (500 MHz, d_6-DMSO) δ 8.17 (s, 1H), 7.76 (m, 2H), 7.41-7.37 (m, 2H), 7.18-7.15 (m, 2H), 7.10-7.07 (m, 1H), 6.03-6.01 (d, J = 11.15 Hz, 1H), 1.65-1.57 (sep, J = 6.16 Hz, 1H), 0.84-0.83 (d, J = 6.40 Hz, 3H), 0.51-0.50 (d, J = 6.55 Hz, 3H); ^{13}C NMR (126 MHz, d_6-DMSO) δ 165.25 (s), 161.94 (s), 159.88 (d, $^{1}J_{CF}$ = 247.92 Hz), 138.67 (s), 135.84 (s), 135.39 (s), 134.24 (s), 132.65 (d, $^{3}J_{CF}$ = 8.26 Hz), 132.14 (s), 131.87 (d, $^{4}J_{CF}$ = 1.69 Hz), 131.21 (s), 128.83 (d, $^{2}J_{CF}$ = 12.80 Hz), 125.45 (s), 125.21 (d, $^{3}J_{CF}$ = 3.07 Hz), 120.02 (s), 116.47 (d, $^{2}J_{CF}$ = 21.47 Hz), 61.72 (s), 28.63 (s), 20.98 (s), 20.56 (s); ^{19}F NMR (471 MHz, d_6-DMSO) δ -114.25; HRMS (ESI/Q-TOF): *m/z* $[M + H]^+$ calcd for $C_{21}H_{17}BrFN_3O_2$: 442.05609; found: 442.05743; HPLC Purity: 99.71%.

Figure 196: DAW-III-20 ^{1}H spectra:

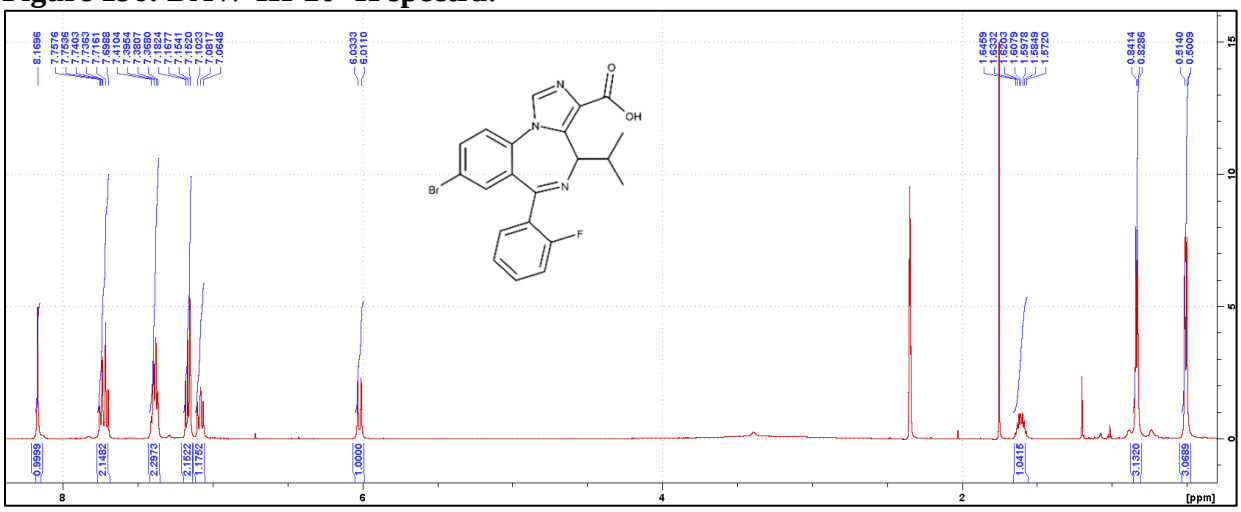

Figure 197: DAW-III-20 ^{13}C spectra:

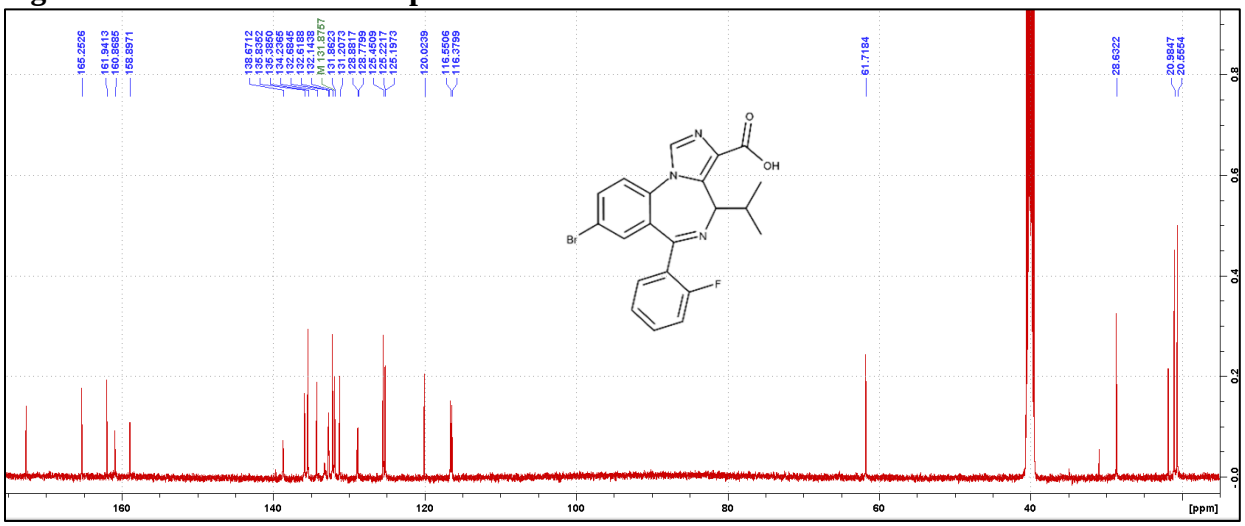

Figure 198: DAW-III-20 ^{19}F spectra:

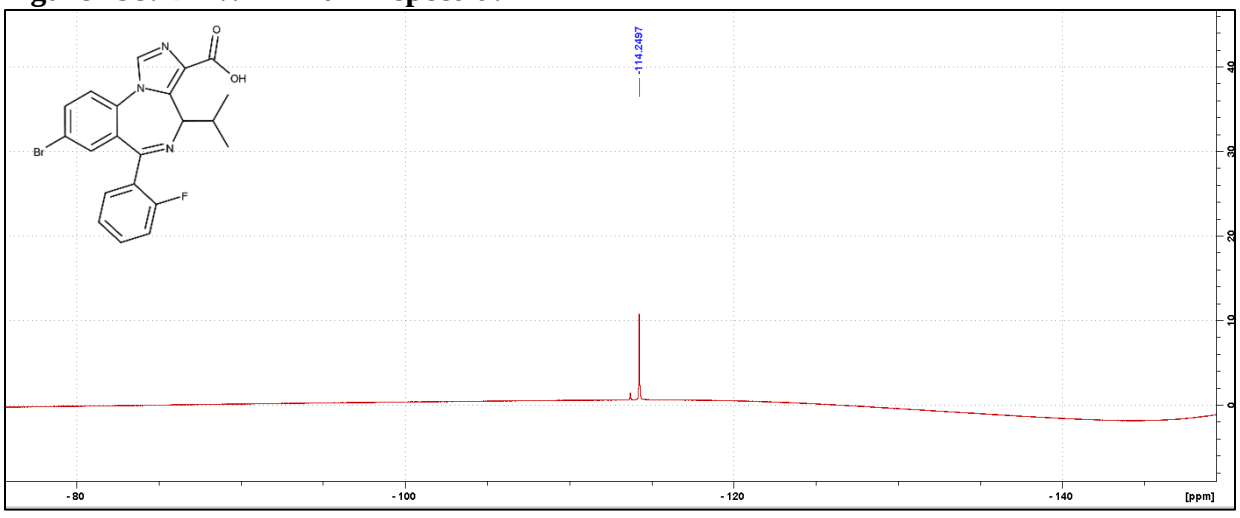

Figure 199: DAW-III-20 HPLC UV Chromatograph:

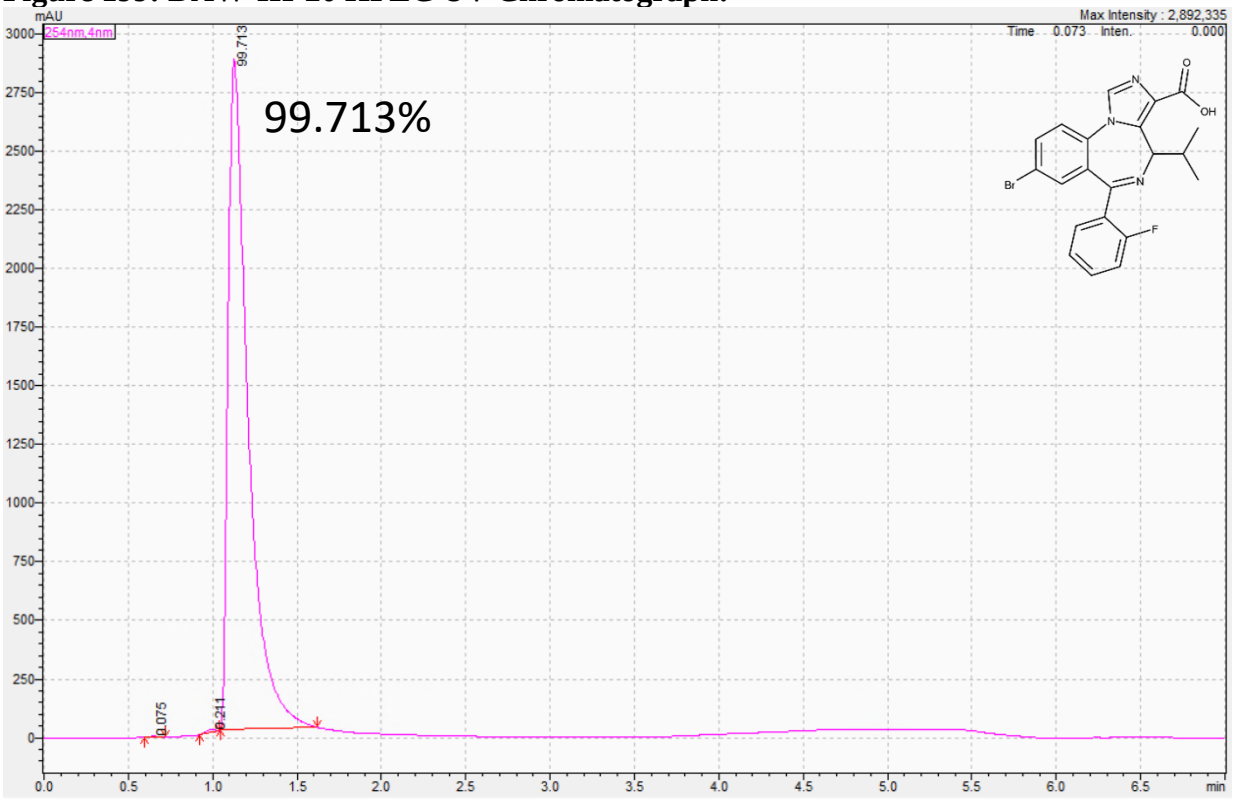

Figure 200: DAW-III-20 HRMS:

Score	Pred. (M)	Pred. m/z	Meas. m/z	Diff. (mDa)	Formulae (M)	Ion	Diff. (ppm)	Iso Score	DBE
63.79	441.04882	442.05609	442.05743	1.34	C21 H17 N3 O2 F Br	[M+H]+	3.031	61.95	14.0

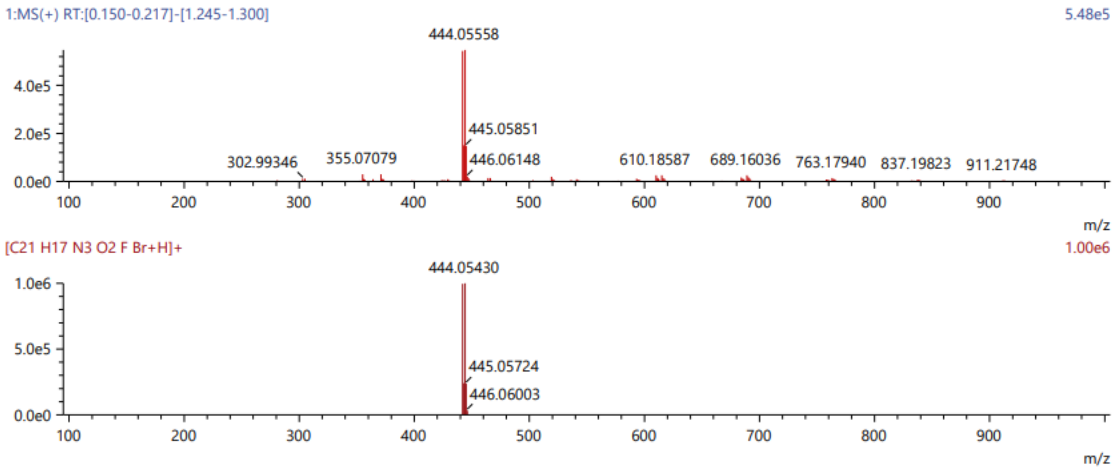

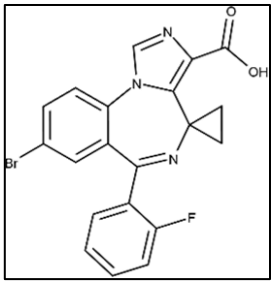

Synthesis of DAW-III-30: DAW-II-30 (186.89 mg, 0.41 mmol) was dissolved in tetrahydrofuran (13 mL) and cooled to 0 °C. Solid sodium hydroxide was added (493.6 mg, 12.34 mmol), followed by the addition of H_2O (307 uL). The reaction was then removed from the ice bath and gently heated to 80 °C for 18 h. When all the starting material had dropped to the baseline via TLC (100% EtOAc), the reaction was cooled to room temperature. Acetic acid was added until the pH was observed to be ~5, and the reaction was then warmed to 50 °C and allowed to stir for 20 h. The reaction was then concentrated to dryness under reduced pressure. The residue was dissolved in H_2O (3.5 mL) and portioned into 0.5 mL fractions. To each fraction was added an additional 1 mL of H_2O causing the desired product to precipitate out of solution. The fractions were centrifuged and the solution was decanted. The solid fractions were combined and washed with an additional 6 mL of H_2O to remove any residual acetic acid. The product was then collected by filtration to yield a white powder. No further purification was conducted. (140.57 mg, 80.2%): ^{1}H NMR (500 MHz, d_6-DMSO) δ 8.26 (s, 1H), 7.89-7.86 (dd, *J* = 3.62, 2.25 Hz, 1H), 7.77-7.75 (d, *J* = 8.65 Hz, 1H), 7.49-7.45 (m, 2H), 7.25-7.22 (m, 2H), 7.16-7.12 (m, 1H), 1.78 (m, 1H), 1.34 (m, 1H), 0.61 (m, 2H); ^{13}C NMR (126 MHz, d_6-DMSO) δ 167.26 (s), 164.18 (s), 159.91 (d, $^{1}J_{CF}$ = 248.64 Hz), 135.49 (s), 135.35 (s), 134.50 (s), 133.13 (d, $^{3}J_{CF}$ = 8.46 Hz), 132.07 (d, $^{3}J_{CF}$ = 4.73 Hz), 131.94 (d, $^{4}J_{CF}$ = 1.62 Hz), 127.43 (d, $^{2}J_{CF}$ = 12.05 Hz), 125.84 (s), 125.16 (d, $^{3}J_{CF}$ = 3.13 Hz), 120.03 (s), 116.48 (d, $^{2}J_{CF}$ = 21.29 Hz), 37.64 (s), 31.78 (S), 14.80 (s), 14.40 (s); ^{19}F NMR (471 MHz, d_6-DMSO) δ -113.54 - -113.59 (qu, *J* = 5.84 Hz); HRMS (ESI/Q-TOF): *m/z* $[M + H]^+$ calcd for $C_{20}H_{13}BrFN_3O_2$: 426.02479; found: 426.02602; HPLC Purity: 99.96%.

Figure 201: DAW-III-30 ^{1}H spectra:

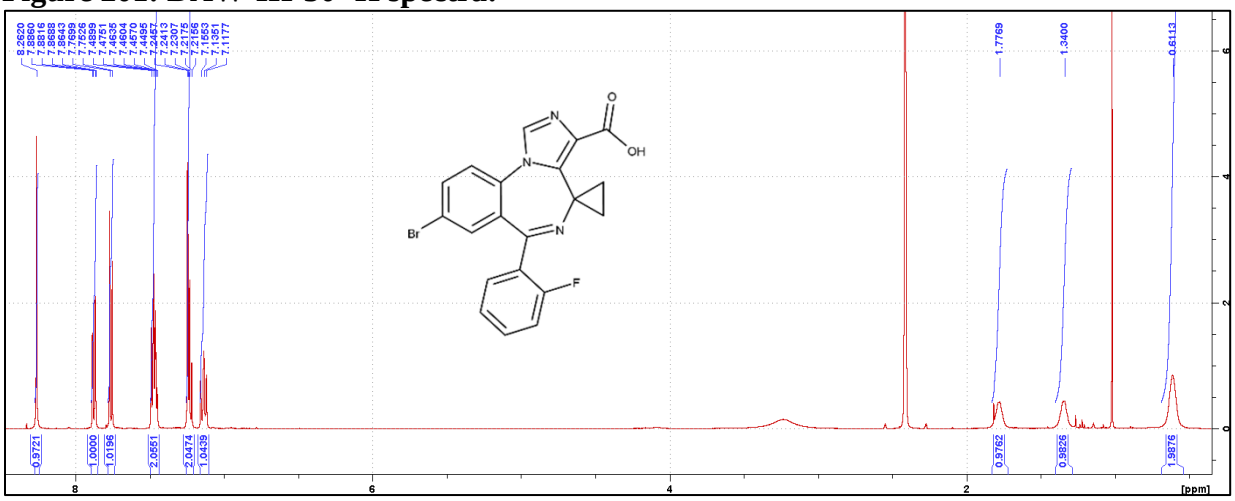

Figure 202: DAW-III-30 ^{13}C spectra:

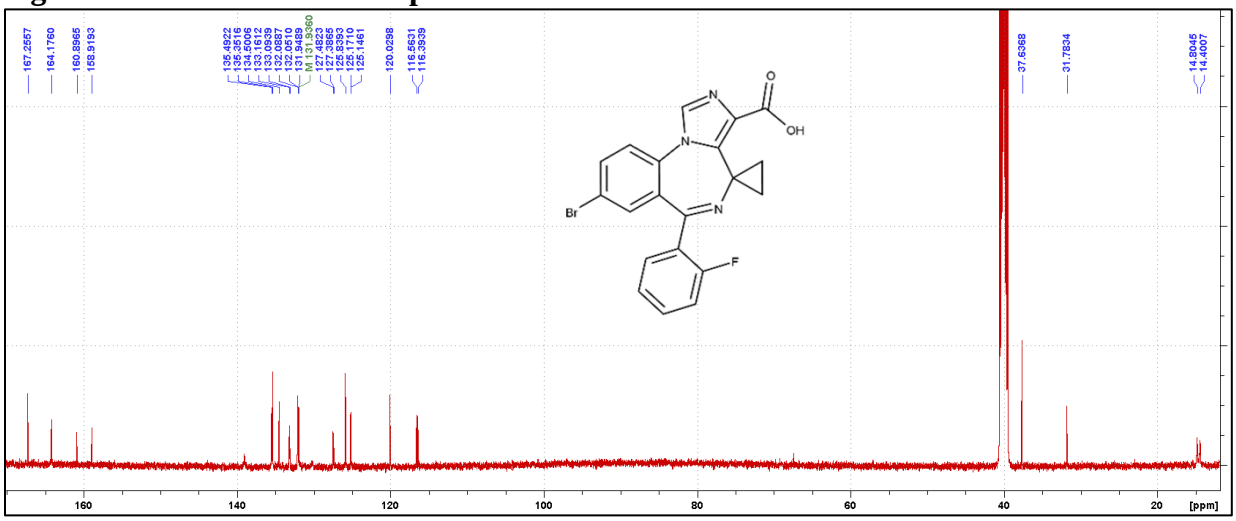

Figure 203: DAW-III-30 ^{19}F spectra:

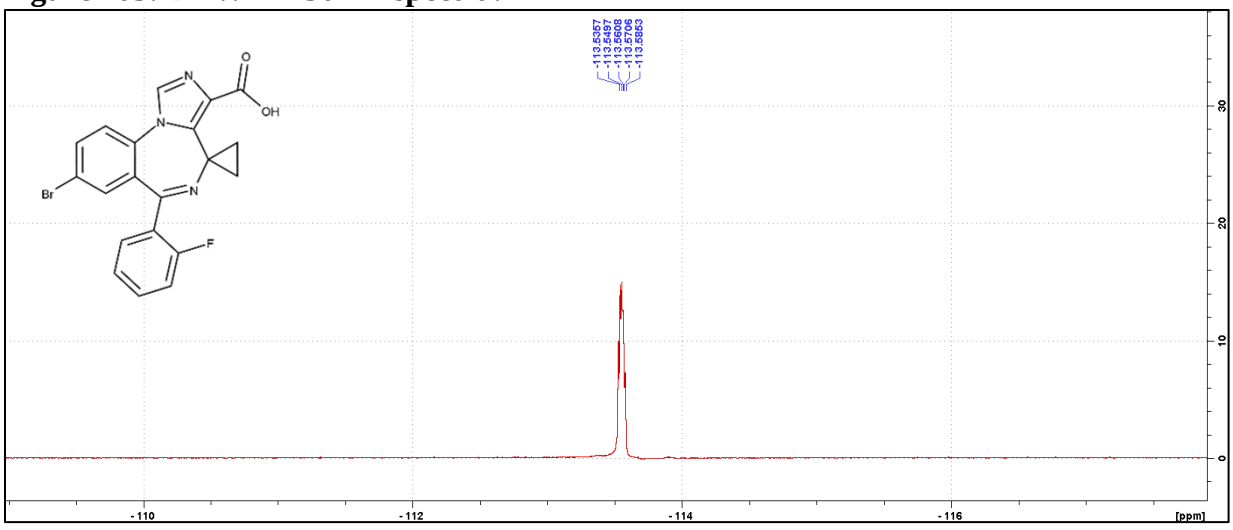

Figure 204: DAW-III-30 HPLC UV Chromatograph:

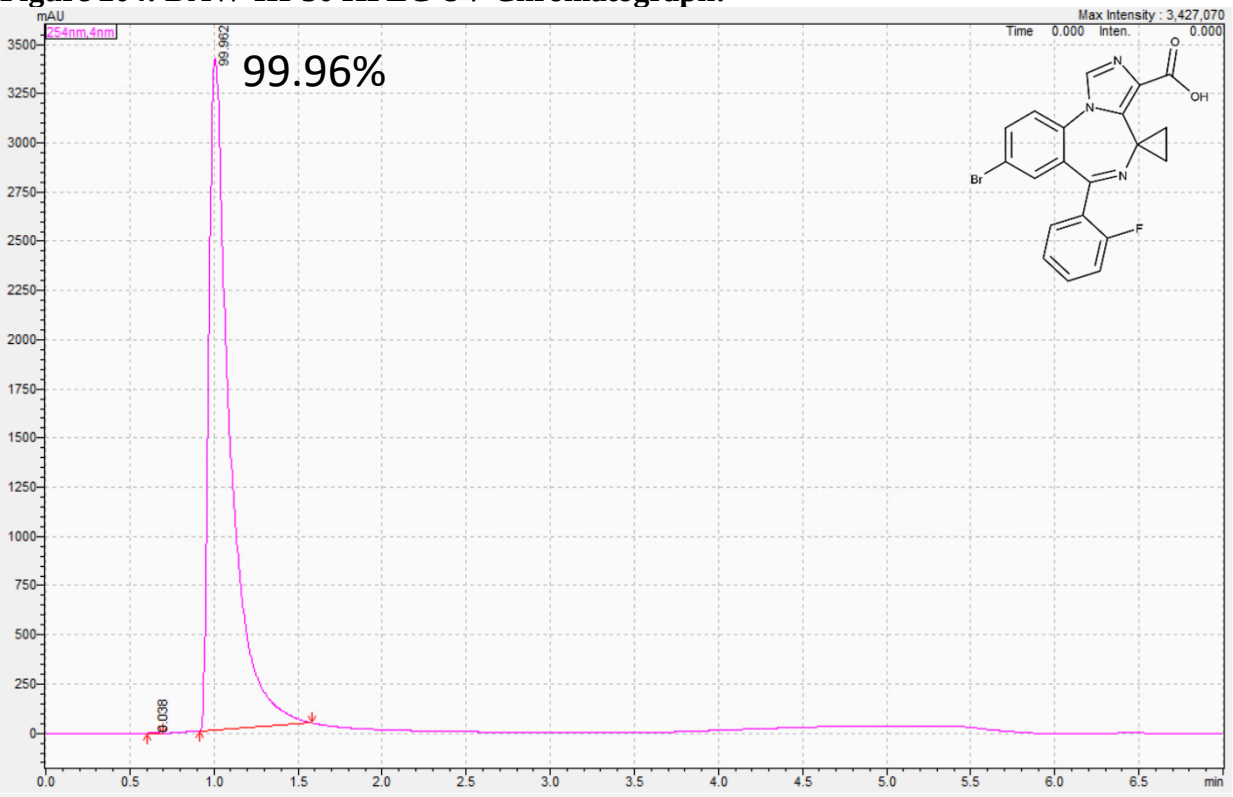

Figure 205: DAW-III-30 HRMS:

Score	Pred. (M)	Pred. m/z	Meas. m/z	Diff. (mDa)	Formulae (M)	Ion	Diff. (ppm)	Iso Score	DBE
71.47	425.01752	426.02479	426.02602	1.23	C20 H13 N3 O2 F Br	[M+H]+	2.887	70.32	15.0

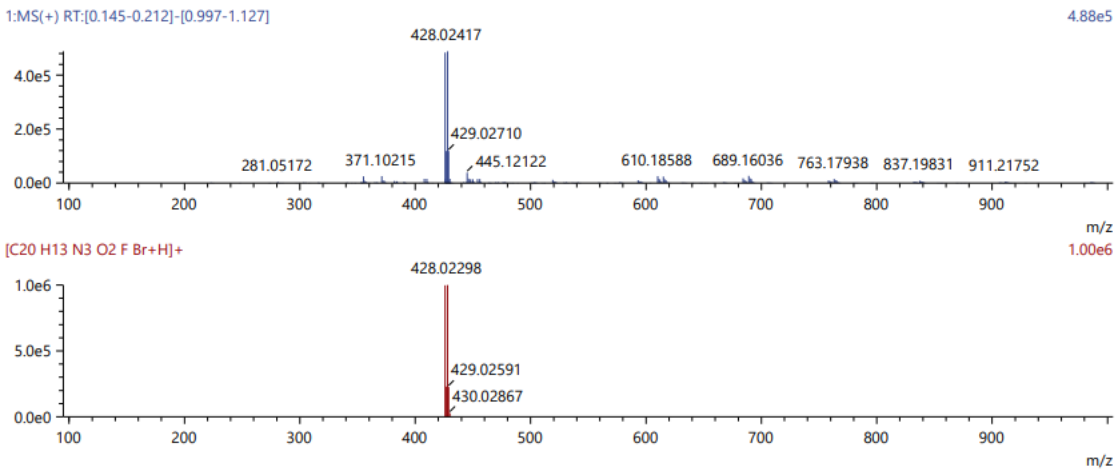

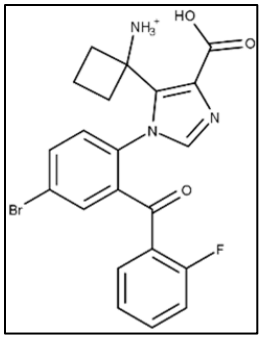

Synthesis of DAW-III-40: DAW-II-40 (158.89 mg, 0.34 mmol) was dissolved in tetrahydrofuran (11.3 mL) and cooled to 0 °C. Solid sodium hydroxide was added (407.1 mg, 10.18 mmol), followed by the addition of H_2O (260 uL). The reaction was then removed from the ice bath and gently heated to 80 °C for 18 h. When all the starting material had dropped to the baseline via TLC (100% EtOAc), the reaction was cooled to room temperature. Acetic acid was added until the pH was observed to be ~5, and the reaction was then warmed to 50 °C and allowed to stir for 20 h. The reaction was then concentrated to dryness under reduced pressure. The residue was dissolved in H_2O (3.5 mL) and portioned into 0.5 mL fractions. To each fraction was added an additional 1 mL of H_2O causing the desired product to precipitate out of solution. The fractions were centrifuged and the solution was decanted. The solid fractions were combined and washed with an additional 6 mL of H_2O to remove any residual acetic acid. The product was then collected by filtration to yield a white powder. The solid was slurried in 5 mL of 5 M HCl at 95 °C for 18 h upon which the diazepine ring had been completely broken by TLC (1.8 mL MeOH + 0.1 mL AcOH + 4.3 mL chloroform). The mixture was then cooled to room temperature and the product was collected by filtration. The solid material was then washed with hot IPA (1 mL, 2x) and the product was again filtered to yield pure material. (92.78 mg, 62.1%): ^{1}H NMR (500 MHz, d_6-DMSO) δ 8.54 (s, 1H), 7.99-7.96 (dd, *J* = 3.63, 2.25 Hz, 1H), 7.88-7.86 (d, *J* = 2.25 Hz, 1H), 7.68-7.65 (dt, *J* = 3.40, 1.70 Hz, 1H), 7.60-7.55 (m, 1H), 7.40-7.39 (m, 1H), 7.37-7.34 (dt, *J* = 3.21, 1.00 Hz, 1H), 7.26-7.22 (m, 1H), 3.51-3.46 (m, 1H), 2.82-2.76 (m, 1H), 2.07-2.02 (m, 1H), 1.88-1.79 (m, 2H), 1.69-1.62 (m, 1H); ^{13}C NMR (126 MHz, d_6-DMSO) δ 165.08 (s), 160.39 (s), 157.71 (d, $^1J_{CF}$ = 336.58 Hz), 139.95 (s), 135.99 (s), 135.48 (s), 134.24 (s), 132.95 (d, $^3J_{CF}$ = 8.24 Hz), 132.17 (d, $^4J_{CF}$ = 1.57 Hz), 131.94 (s), 131.75 (s), 127.69 (d, $^2J_{CF}$ = 12.05 Hz), 125.87 (s), 125.19

(d, $^{3}J_{CF}$ = 3.51 Hz), 120.32 (s), 118.91 (s), 117.86 (s), 116.47 (d, $^{2}J_{CF}$ = 21.27 Hz), 61.99 (s), 35.91 (s), 34.56 (s), 15.87 (s); ^{19}F NMR (471 MHz, d_6-DMSO) δ -113.78 - -113.83 (qu, *J* = 5.69 Hz); HRMS (ESI/Q-TOF): *m/z* $[M + H]^+$ calcd for $C_{21}H_{17}BrFN_3O_3$: 458.05101; found: 458.05074; HPLC Purity: 99.67%

Figure 206: DAW-III-40 ^{1}H spectra:

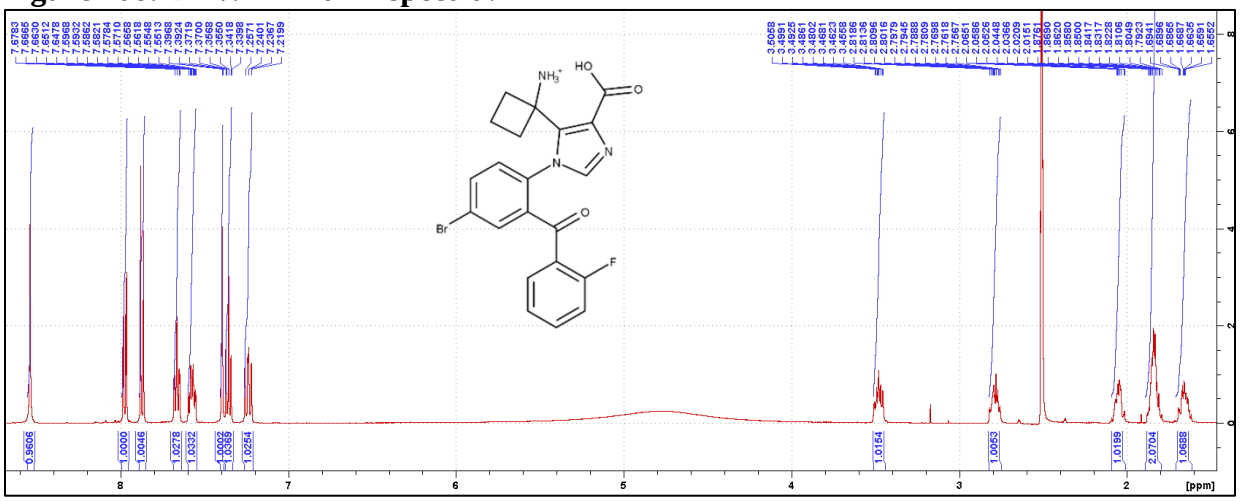

Figure 207: DAW-III-40 ^{13}C spectra:

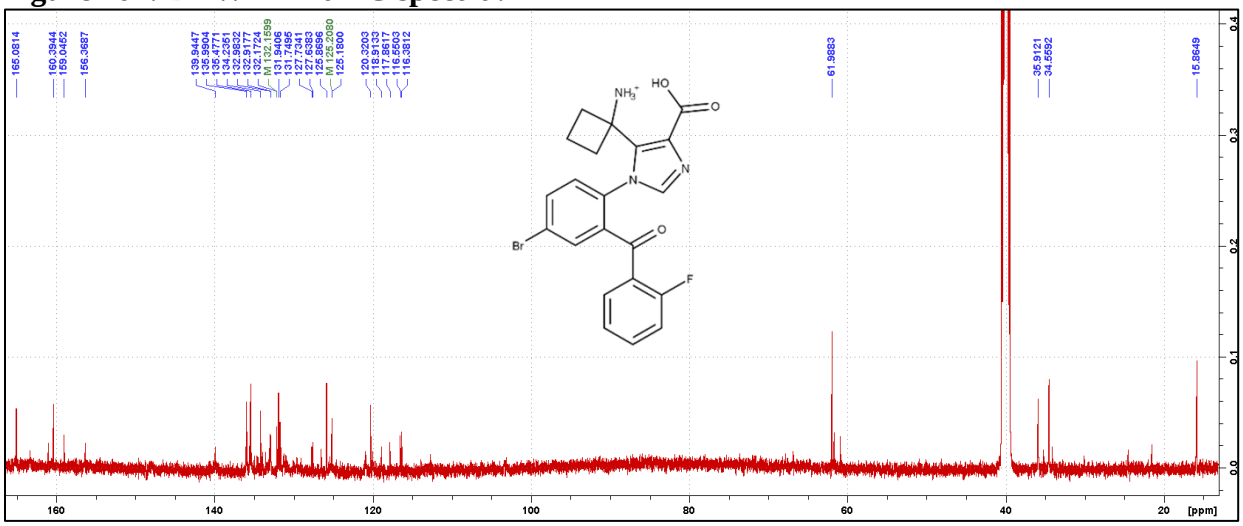

Figure 208: DAW-III-40 ^{19}F spectra:

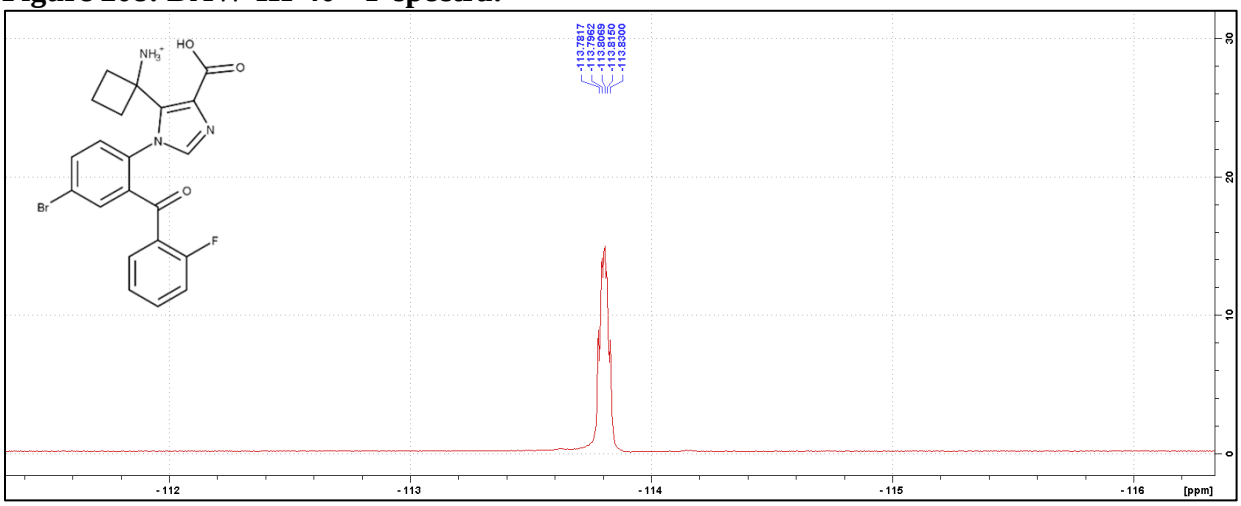

Figure 209: DAW-III-40 HPLC UV Chromatograph:

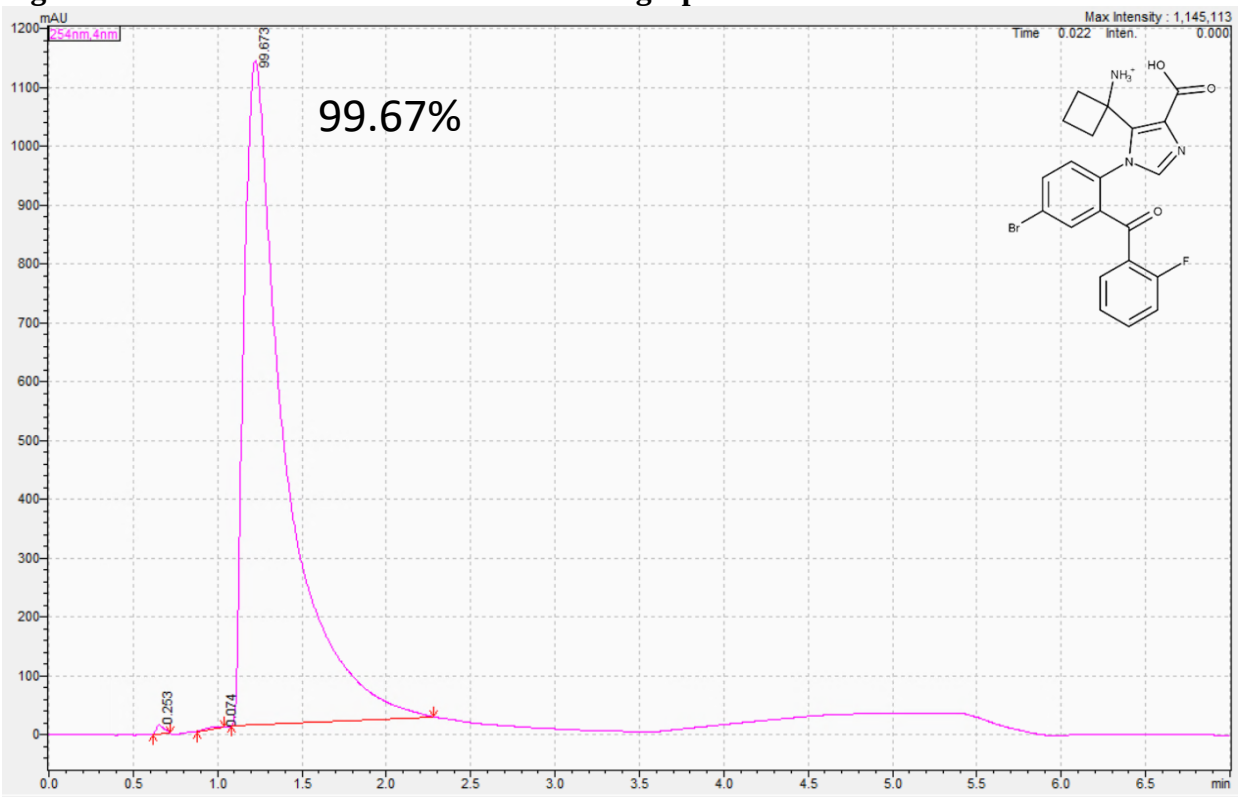

Figure 210: DAW-III-40 HRMS:

Score	Pred. (M)	Pred. m/z	Meas. m/z	Diff. (mDa)	Formulae (M)	Ion	Diff. (ppm)	Iso Score	DBE
98.89	457.04373	458.05101	458.05074	-0.27	C21 H17 N3 O3 F Br	[M+H]+	-0.589	99.05	14.0

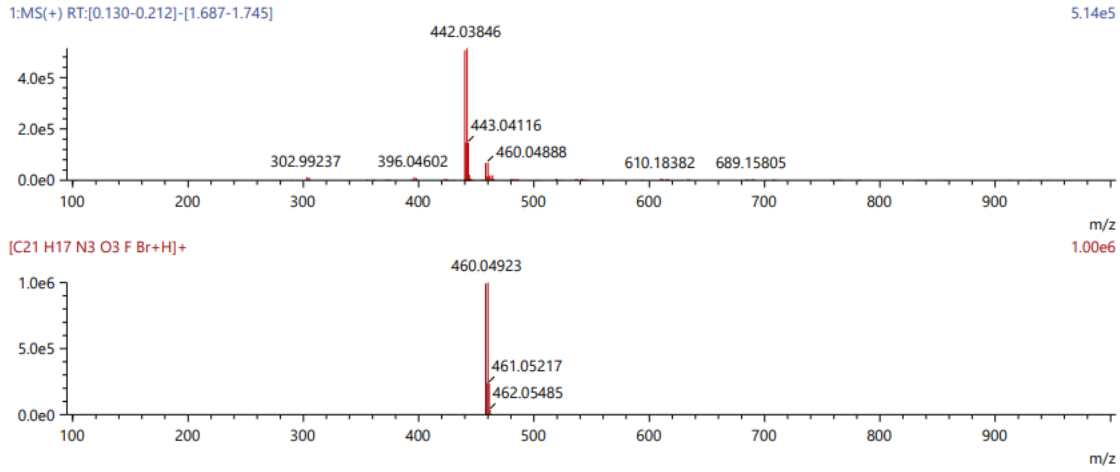

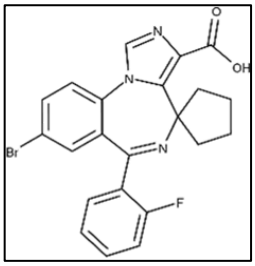

Synthesis of DAW-III-50: DAW-II-50 (286.1 mg, 0.59 mmol) was dissolved in tetrahydrofuran (20.3 mL) and cooled to 0 °C. Solid sodium hydroxide was added (712 mg, 17.79 mmol), followed by the addition of H_2O (481 uL). The reaction was then removed from the ice bath and gently heated to 80 °C for 18 h. When all the starting material had dropped to the baseline via TLC (100% EtOAc), the reaction was cooled to room temperature. Acetic acid was added until the pH was observed to be ~5, and the reaction was then warmed to 50 °C and allowed to stir for 20 h. The reaction was then concentrated to dryness under reduced pressure. The residue was dissolved in H_2O (6 mL) and portioned into 0.5 mL fractions. To each fraction was added an additional 1 mL of H_2O causing the desired product to precipitate out of solution. The fractions were centrifuged and the solution was decanted. The solid fractions were combined and washed with an additional 15 mL of H_2O to remove any residual acetic acid. The product was then collected by filtration to yield a white powder. No further purification was conducted. (125.4 mg, 46.5%): ^{1}H NMR (500 MHz, d_6-DMSO) δ 8.25 (s, 1H), 7.92-7.90 (dd, *J* = 3.57, 2.11 Hz, 1H), 7.83-7.81 (d, *J* = 8.65 Hz, 1H), 7.56-7.51 (m, 2H), 7.33-7.32 (d, *J* = 7.40 Hz, 1H), 7.30-7.29 (m, 1H), 7.24-7.21 (dt, *J* = 6.29,

1.41 Hz, 1H), 2.55 (m, 2H), 1.77 (m, 2H), 1.61 (m, 3H), 1.48 (m, 1H); ^{13}C NMR (126 MHz, d_6-DMSO) δ 167.27 (S), 160.47 (S), 159.99 (d, $^{1}J_{CF}$ = 248.16 Hz), 136.33 (S), 135.93 (S), 135.36 (S), 135.03 (S), 133.47 (S), 132.65 (d, $^{3}J_{CF}$ = 8.15 Hz), 132.01 (d, $^{4}J_{CF}$ = 1.38 Hz), 131.84 (S), 131.63 (S), 128.42 (d, $^{2}J_{CF}$ = 12.50 Hz), 125.94 (S), 125.15 (d, $^{4}J_{CF}$ = 2.64 Hz), 119.93 (S), 116.43 (d, $^{2}J_{CF}$ = 21.39 Hz), 67.17 (S), 36.16 (S), 23.61 (S); ^{19}F NMR (471 MHz, d_6-DMSO) δ -114.11; HRMS (ESI/Q-TOF): *m/z* $[M + H]^+$ calcd for $C_{22}H_{17}BrFN_3O_2$: 454.05609; found: 454.05775; HPLC Purity: : 99.48%.

Figure 211: DAW-III-50 ^{1}H spectra:

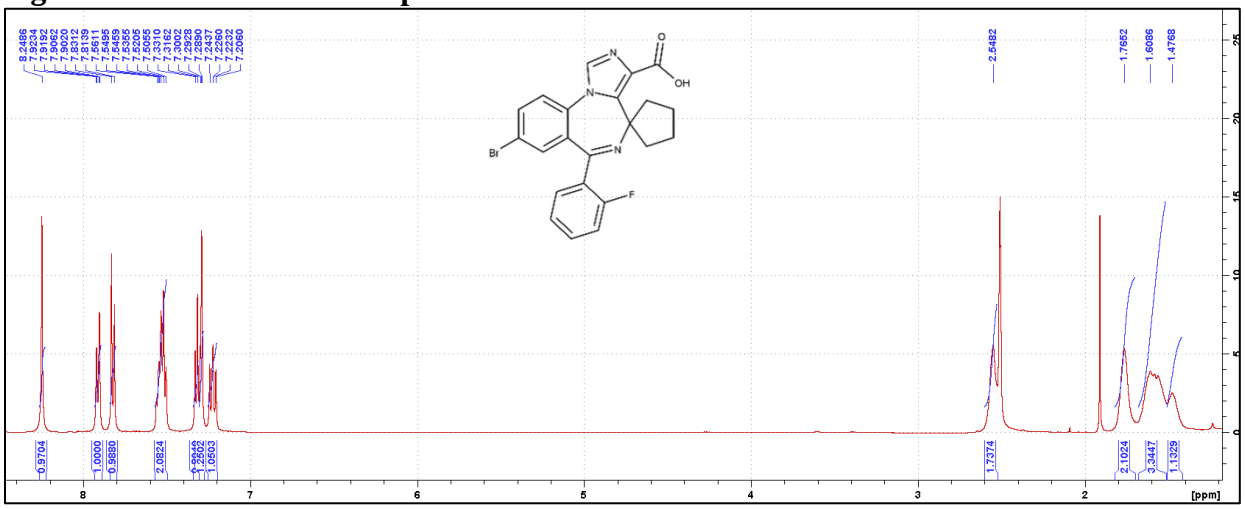

Figure 212: DAW-III-50 ^{13}C spectra:

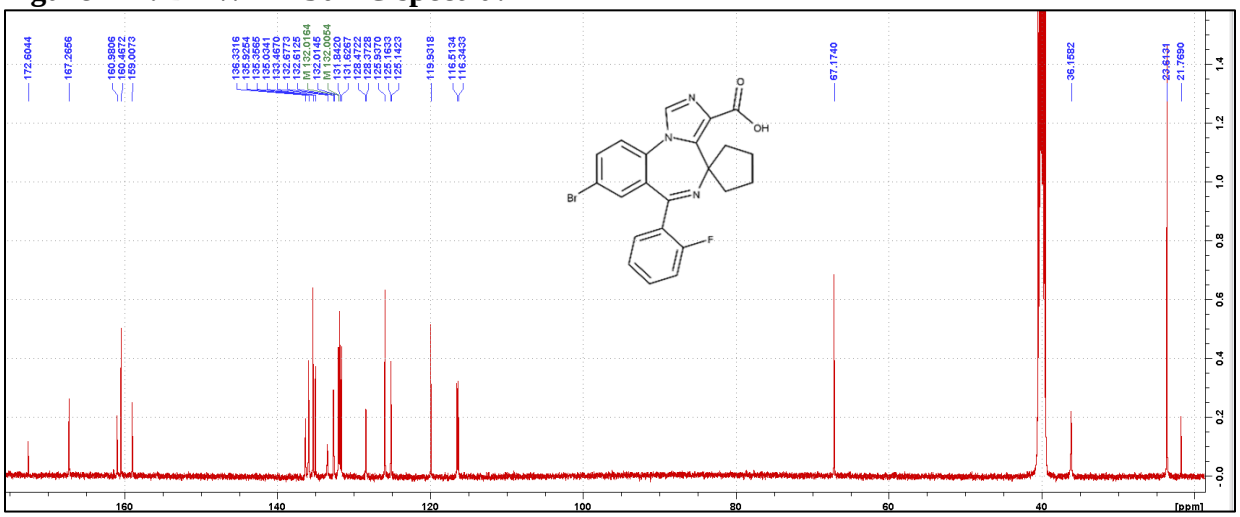

Figure 213: DAW-III-50 ^{19}F spectra:

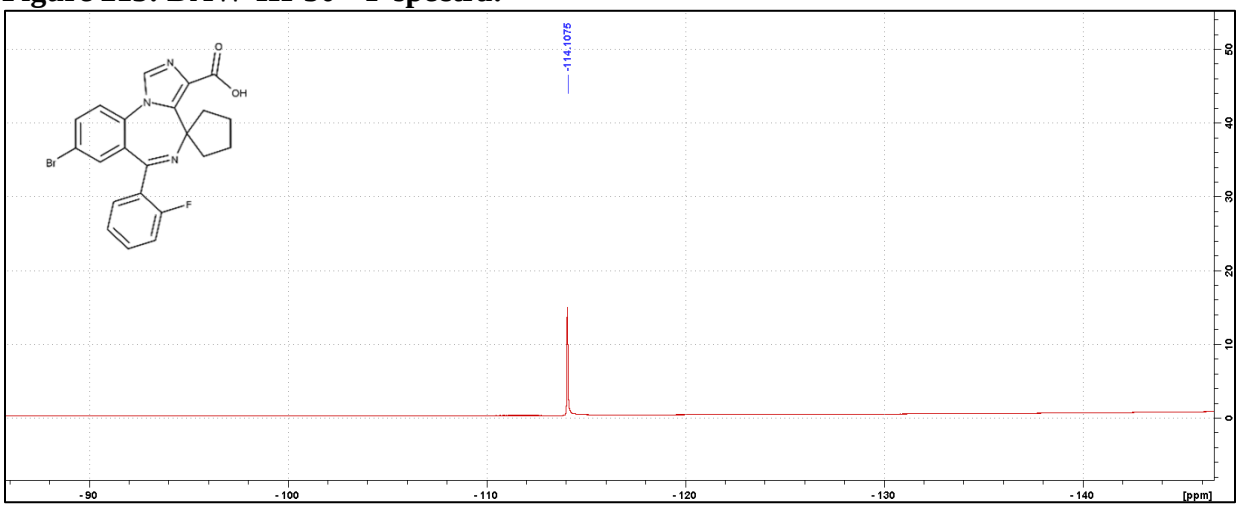

Figure 214: DAW-III-50 HPLC UV Chromatograph:

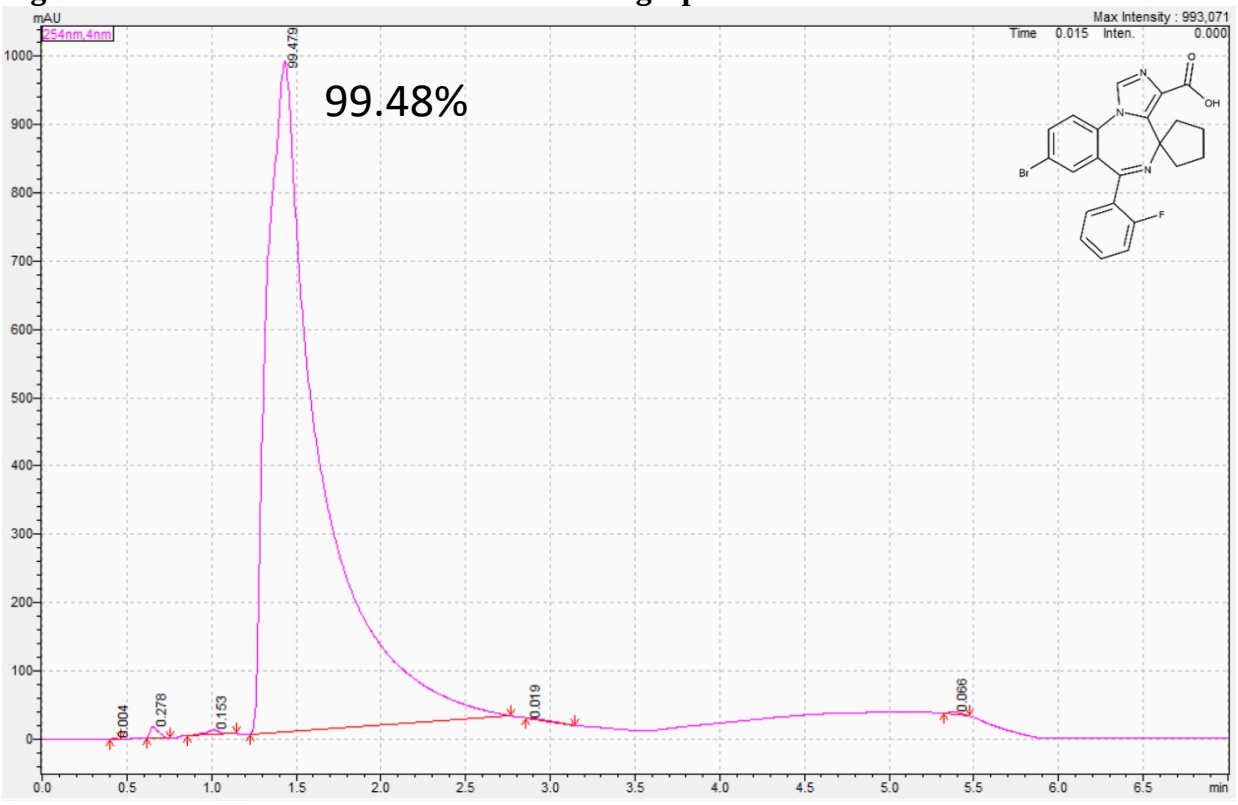

Figure 215: DAW-III-50 HRMS:

Score	Pred. (M)	Pred. m/z	Meas. m/z	Diff. (mDa)	Formulae (M)	Ion	Diff. (ppm)	Iso Score	DBE
67.65	453.04882	454.05609	454.05775	1.66	C22 H17 N3 O2 F Br	[M+H]+	3.656	67.14	15.0

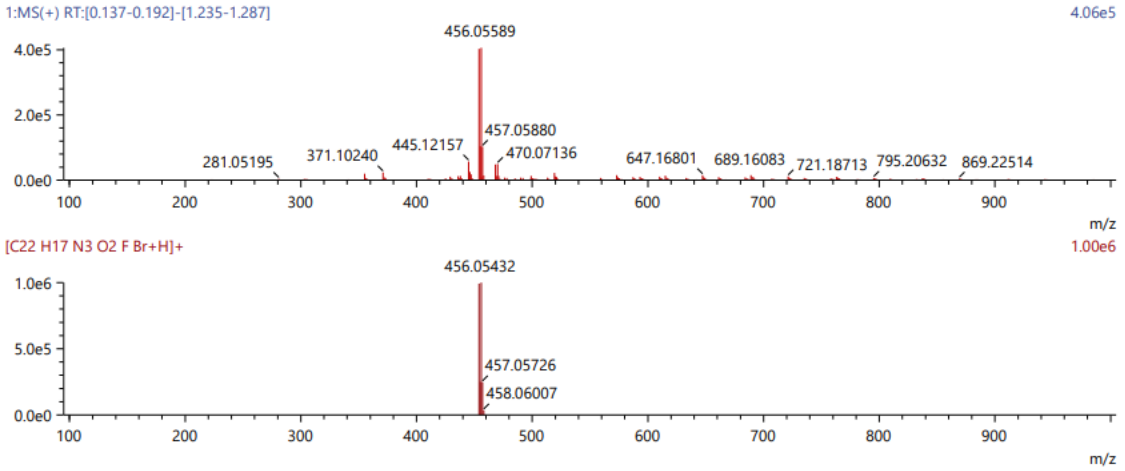

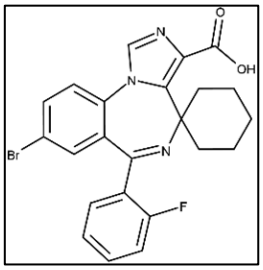

Synthesis of DAW-III-60: DAW-II-60 (168.93 mg, 0.34 mmol) was dissolved in tetrahydrofuran (12 mL) and cooled to 0 °C. Solid sodium hydroxide was added (432.8 mg, 10.82 mmol), followed by the addition of H_2O (284 uL). The reaction was then removed from the ice bath and gently heated to 80 °C for 18 h. When all the starting material had dropped to the baseline via TLC (100% EtOAc), the reaction was cooled to room temperature. Acetic acid was added until the pH was observed to be ~5, and the reaction was then warmed to 50 °C and allowed to stir for 20 h. The reaction was then concentrated to dryness under reduced pressure. The residue was dissolved in H_2O (4 mL) and portioned into 0.5 mL fractions. To each fraction was added an additional 1 mL of H_2O causing the desired product to precipitate out of solution. The fractions were centrifuged, and the solution was decanted. The solid fractions were combined and washed with an additional 6 mL of H_2O to remove any residual acetic acid. The product was then collected by filtration to yield a white powder. No further purification was conducted. (143.2 mg, 89.8%): ^{1}H NMR (500 MHz, d_6-DMSO) δ 8.07 (s, 1H), 7.76-7.74 (dd, *J* = 3.63, 2.25 Hz, 1H), 7.65-7.64 (d, *J* =8.65 Hz, 1H), 7.43-7.39 (m, 2H), 7.21-7.18 (dt, *J* = 3.20, 0.95 Hz, 1H), 7.15-7.14 (d, *J* = 2.15 Hz, 1H), 7.13-

7.09 (m, 1H), 2.24 (m, 2H), 1.89 (m, 1H), 1.73 (m, 1H), 1.52-1.49 (m, 2H), 1.14-1.10 (m, 4H); ^{13}C NMR (126 MHz, d_6-DMSO) δ 168.45 (s), 160.01 (d, $^{1}J_{CF}$ = 248.17 Hz), 159.67 (s), 135.91 (s), 135.41 (s), 135.29 (s), 132.55 (d, $^{3}J_{CF}$ = 8.31 Hz), 131.95 (d, $^{4}J_{CF}$ = 2.57 Hz), 131.71 (s), 130.69 (s), 129.00 (d, $^{2}J_{CF}$ = 12.70 Hz), 125.47 (s), 125.21 (d, $^{3}J_{CF}$ = 3.05 Hz), 119.70 (s), 116.51 (d, $^{2}J_{CF}$ = 21.37 Hz), 59.21 (s), 37.24 (s), 31.72 (s), 25.68 (s), 21.96 (s); ^{19}F NMR (471 MHz, d_6-DMSO) δ -114.14; HRMS (ESI/Q-TOF): *m/z* $[M + H]^+$ calcd for $C_{23}H_{19}BrFN_3O_2$: 468.07174; found: 467.07357; HPLC Purity: 99.78%.

Figure 216: DAW-III-60 ^{1}H spectra:

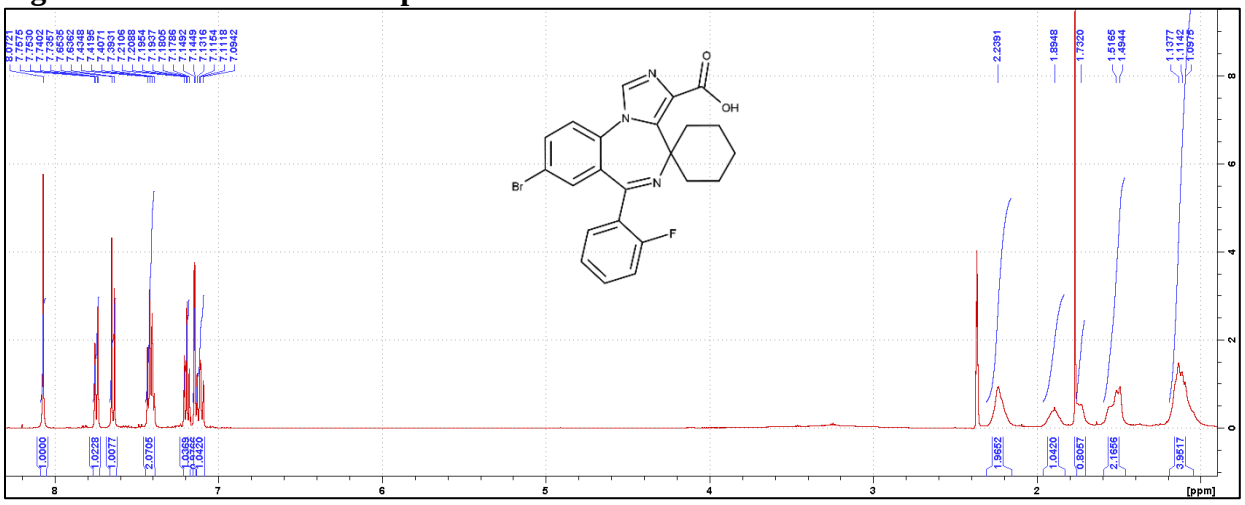

Figure 217: DAW-III-60 ^{13}C spectra:

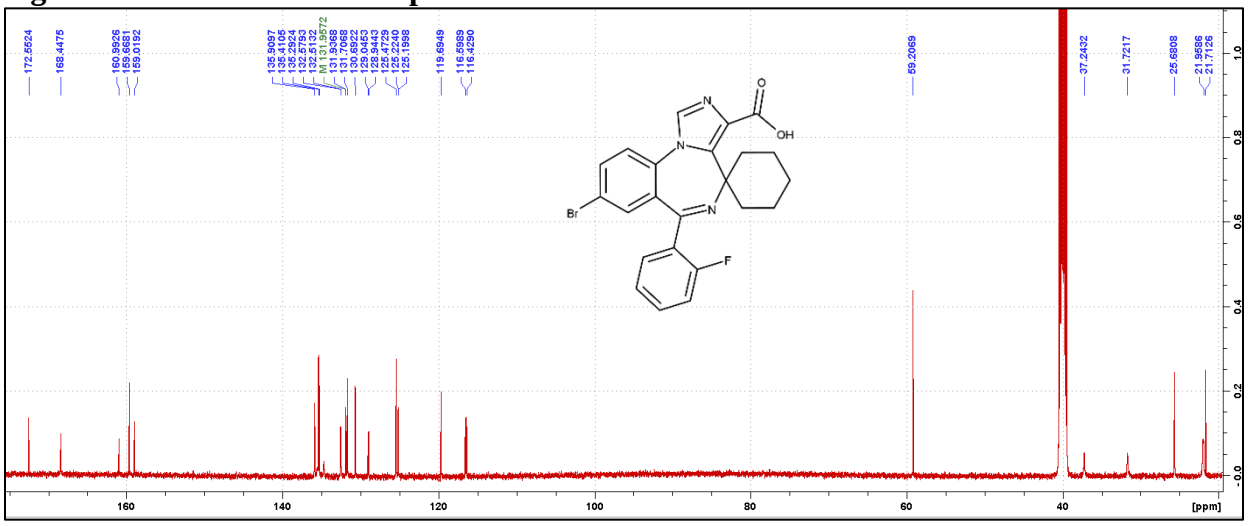

Figure 218: DAW-III-60 ^{19}F spectra:

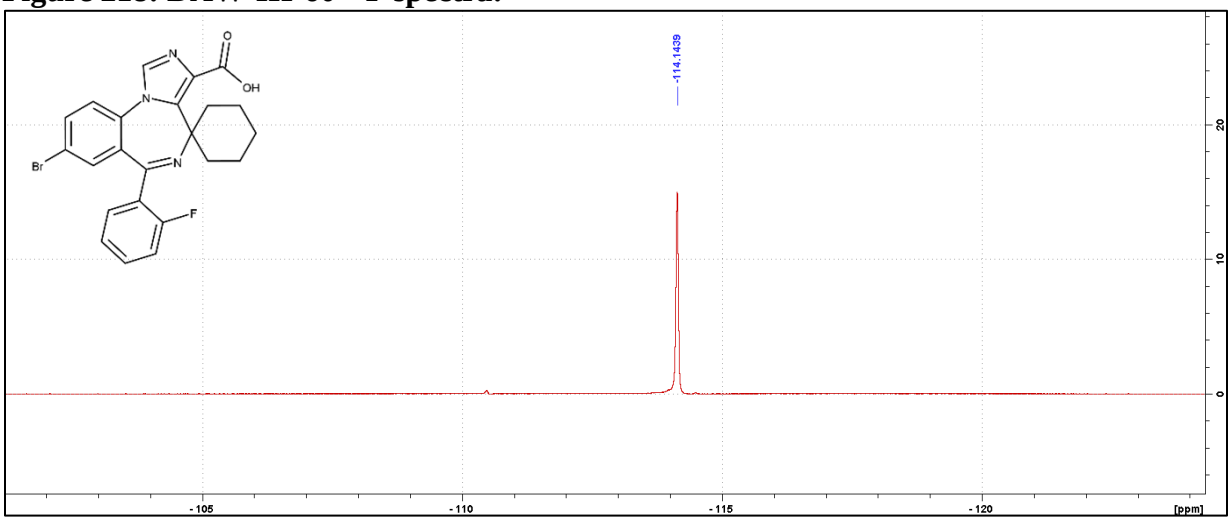

Figure 219: DAW-III-60 HPLC UV Chromatograph:

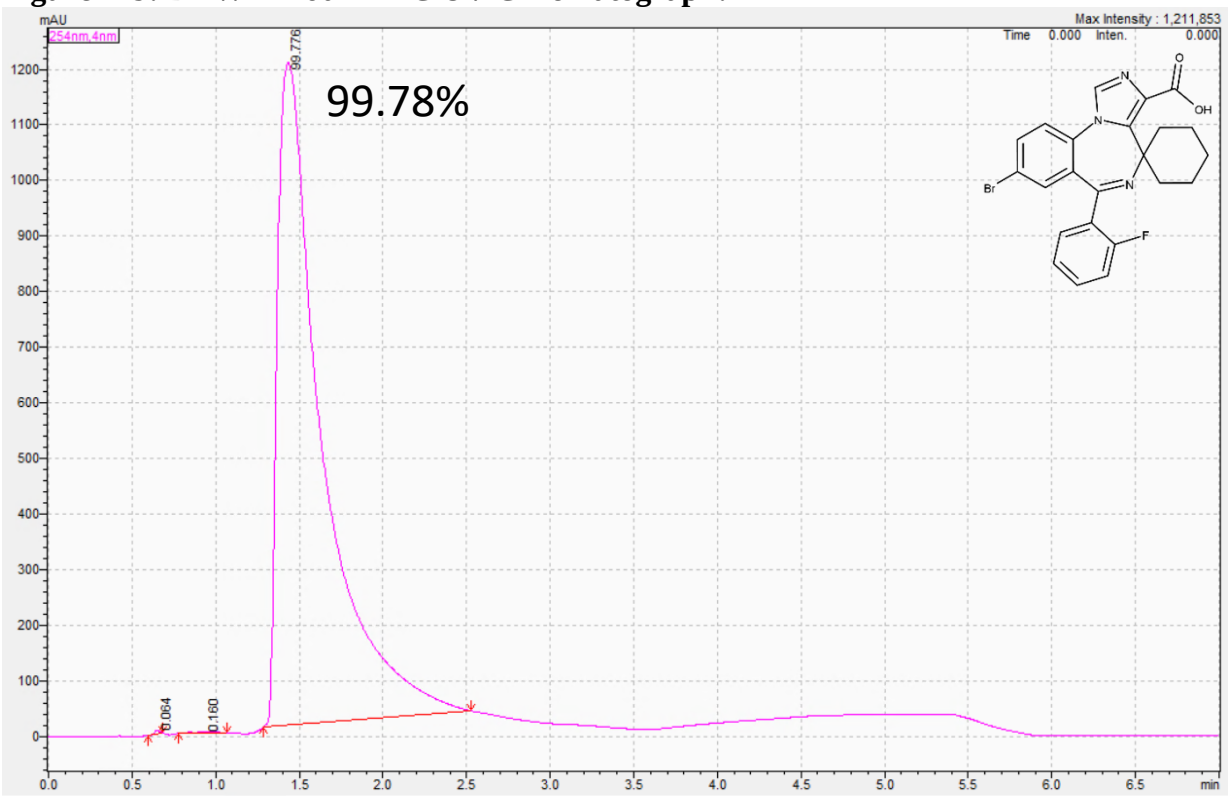

Figure 220: DAW-III-60 HRMS:

Score	Pred. (M)	Pred. m/z	Meas. m/z	Diff. (mDa)	Formulae (M)	Ion	Diff. (ppm)	Iso Score	DBE
58.37	467.06447	468.07174	468.07357	1.83	C23 H19 N3 O2 F Br	[M+H]+	3.910	57.31	15.0

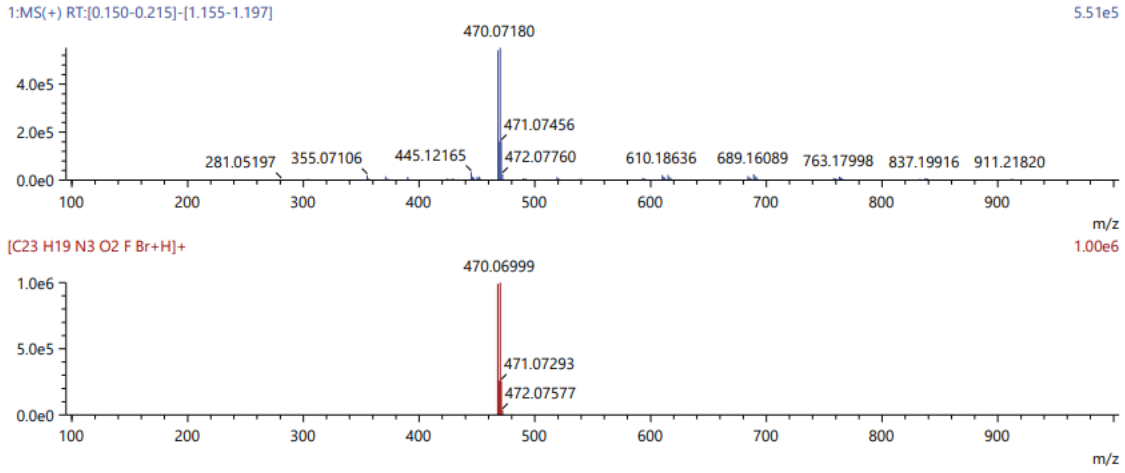

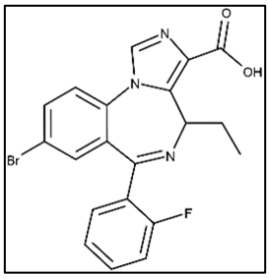

Synthesis of DAW-III-70: DAW-II-70 (248.31 mg, 0.54 mmol) was dissolved in tetrahydrofuran (17.5 mL) and cooled to 0 °C. Solid sodium hydroxide was added (652.9 mg, 16.32 mmol), followed by the addition of H_2O (410 uL). The reaction was then removed from the ice bath and gently heated to 80 °C for 18 h. When all the starting material had dropped to the baseline via TLC (100% EtOAc), the reaction was cooled to room temperature. Acetic acid was added until the pH was observed to be ~5, and the reaction was then warmed to 50 °C and allowed to stir for 20 h. The reaction was then concentrated to dryness under reduced pressure. The residue was dissolved in H_2O (4.5 mL) and portioned into 0.5 mL fractions. To each fraction was added an additional 1 mL of H_2O causing the desired product to precipitate out of solution. The fractions were centrifuged and the solution was decanted. The solid fractions were combined and washed with an additional 7 mL of H_2O to remove any residual acetic acid. The product was then collected by filtration to yield a white powder. The solid was slurried in 5 mL of 5 M HCl at 95 °C for 18 h upon which the diazepine ring had been completely broken by TLC (1.8 mL MeOH + 0.1 mL AcOH + 4.3 mL chloroform). The mixture was then cooled to room temperature and the product

was collected by filtration. The solid material was then washed with hot IPA (1 mL, 2x) and the product was again filtered to yield pure material. (189.23 g, 81.2%): ^{1}H NMR (500 MHz, MeOD) δ 8.32 (s, 1H), 7.89-7.87 (m, 1H), 7.81-7.79 (d, *J* = 8.65 Hz, 1H), 7.59-7.55 (m, 2H), 7.38 (m, 1H), 7.35-7.32 (dd, *J* = 3.20, 0.90 Hz, 1H), 7.19-7.15 (m, 1H), 6.49-6.45 (d, *J* = 8.13 Hz, 1H), 1.80-1.72 (m, 1H), 1.64-1.55 (m, 1H), 0.95-0.92 (t, *J* = 7.35 Hz, 3H); ^{13}C NMR (126 MHz, MeOD) δ 164.74 (s), 164.06 (s), 160.02 (d, $^{1}J_{CF}$ = 249.14 Hz), 139.33 (s), 135.76 (d, $^{2}J_{CF}$ = 28.40 Hz), 135.42 (d, $^{4}J_{CF}$ = 2.21 Hz), 135.16 (s), 133.78 (s), 132.72 (d, $^{3}J_{CF}$ = 17.25 Hz), 131.07 (s), 130.82 (s), 128.10 (d, $^{3}J_{CF}$ = 12.87 Hz), 124.55 (s), 124.42 (s), 124.30 (s), 121.77 (s), 120.57 (s), 115.74 (d, $^{2}J_{CF}$ = 21.04 Hz), 56.43 (d, *J* = 39.09 Hz), 22.18 (t, *J* = 33.97 Hz), 10.24 (d, *J* = 7.56 Hz); ^{19}F NMR (471 MHz, MeOD) δ -115.63; HRMS (ESI/Q-TOF): *m/z* $[M + H]^{+}$ calcd for $C_{20}H_{15}BrFN_3O_2$: 428.04044; found: 428.04032; HPLC Purity: 95.76%.

Figure 221: DAW-III-70 ^{1}H spectra:

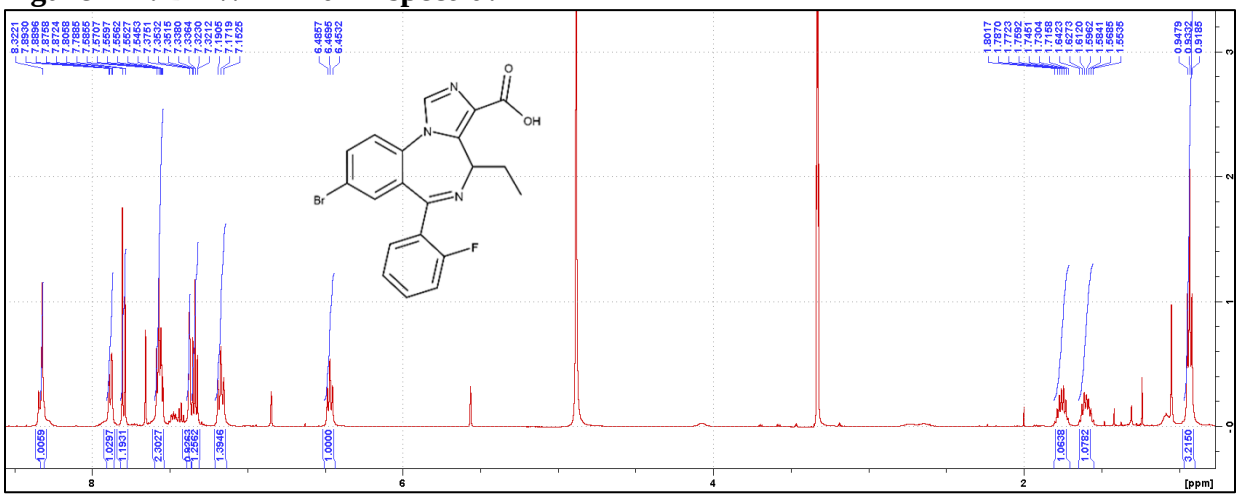

Figure 222: DAW-III-70 ^{13}C spectra:

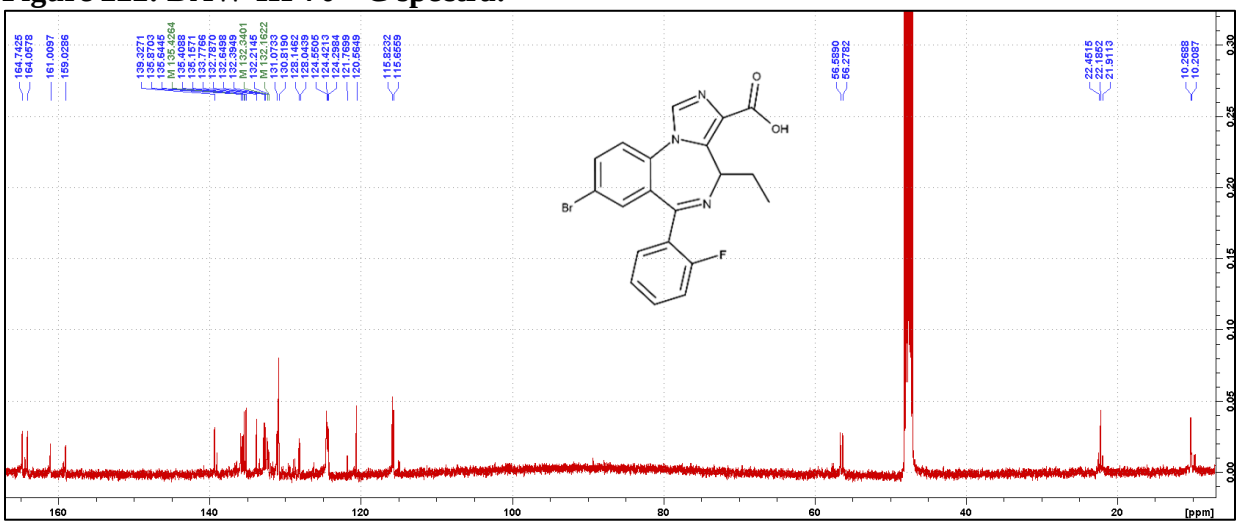

Figure 223: DAW-III-70 ^{19}F spectra:

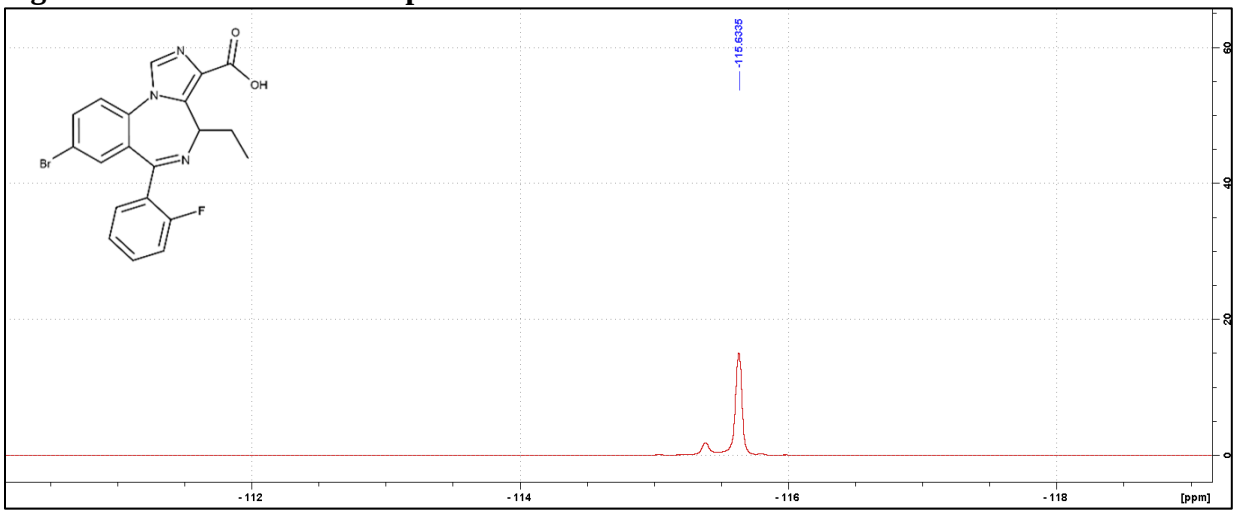

Figure 224: DAW-III-70 HPLC UV Chromatograph:

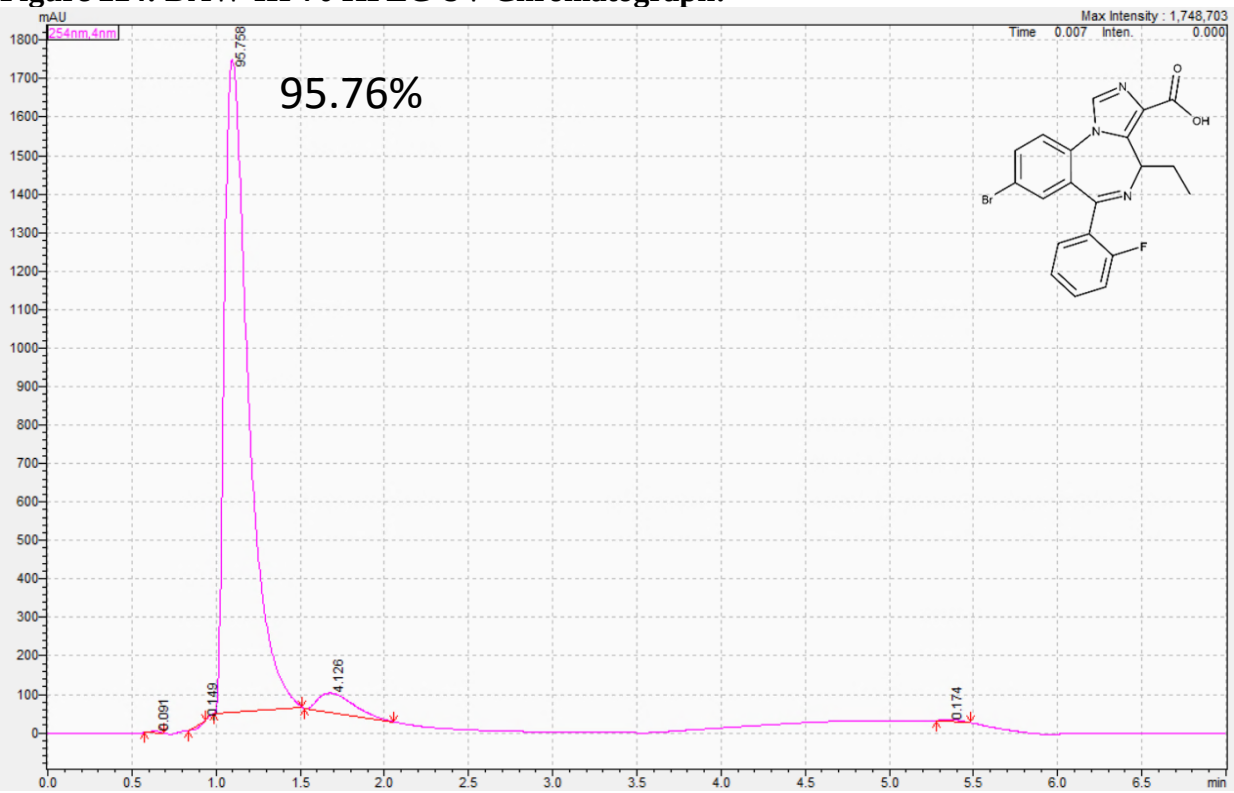

Figure 225: DAW-III-70 HRMS:

Score	Pred. (M)	Pred. m/z	Meas. m/z	Diff. (mDa)	Formulae (M)	Ion	Diff. (ppm)	Iso Score	DBE
99.74	427.03317	428.04044	428.04032	-0.12	C20 H15 N3 O2 F Br	[M+H]+	-0.280	99.83	14.0

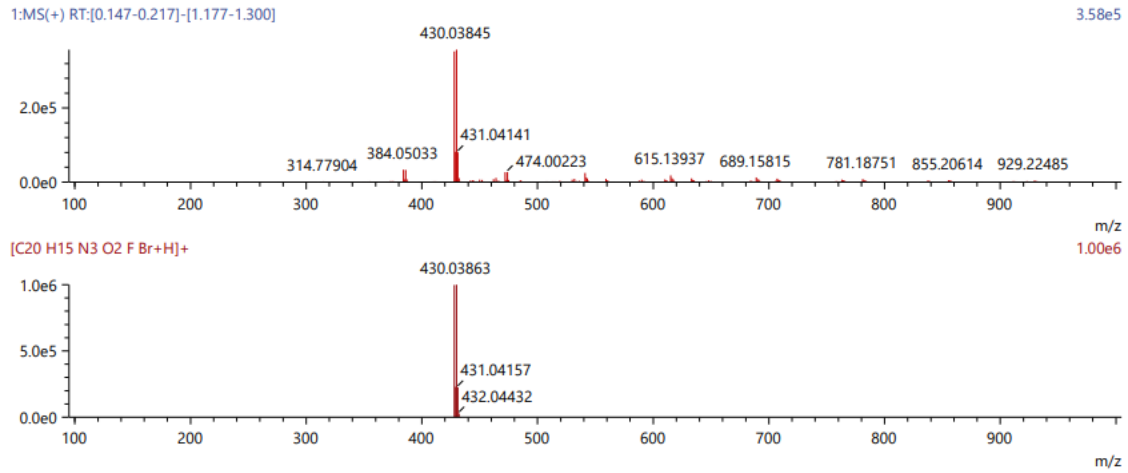

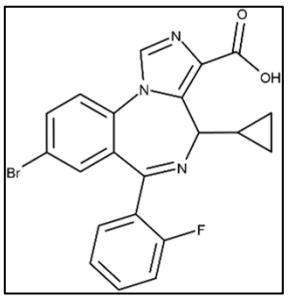

Synthesis of DAW-III-80: DAW-II-80 (143.99 mg, 0.31 mmol) was dissolved in tetrahydrofuran (10 mL) and cooled to 0 °C. Solid sodium hydroxide was added (369 mg, 9.22 mmol), followed by the addition of H_2O (242 uL). The reaction was then removed from the ice bath and gently heated to 80 °C for 18 h. When all the starting material had dropped to the baseline via TLC (100% EtOAc), the reaction was cooled to room temperature. Acetic acid was added until the pH was observed to be ~5, and the reaction was then warmed to 50 °C and allowed to stir for 20 h. The reaction was then concentrated to dryness under reduced pressure. The residue was dissolved in H_2O (3.5 mL) and portioned into 0.5 mL fractions. To each fraction was added an additional 1 mL of H_2O causing the desired product to precipitate out of solution. The fractions were centrifuged and the solution was decanted. The solid fractions were combined and washed with an additional 6 mL of H_2O to remove any residual acetic acid. The product was then collected by filtration to yield a white powder. No further purification was conducted. (101.46 mg, 75.0%): ^{1}H NMR (500 MHz, d_6-DMSO) δ 7.96 (s, 1H), 7.66 (m, 2H), 7.41-7.37 (dt, *J* = 3.38, 1.65 Hz, 1H), 7.36-7.33 (m, 1H), 7.16-7.13 (dt, *J* = 3.20, 0.95 Hz, 1H), 7.11 (m, 1H), 7.05-7.01 (m, 1H), 5.81-5.79 (d, *J* = 10.40 Hz, 1H), 0.61-0.54 (m, 1H), 0.27-0.23 (m, 2H), 0.20-0.15 (m, 1H), 0.02 - -0.03 (m, 1H); ^{13}C NMR (126 MHz, d_6-DMSO) δ 166.53 (s), 161.71 (s), 159.86 (d, $^{1}J_{CF}$ = 247.64 Hz), 138.06 (s), 136.15 (s), 135.09 (s), 134.98 (s), 133.77 (s), 132.49 (d, $^{3}J_{CF}$ = 8.34 Hz), 132.28 (s), 131.93 (d, $^{4}J_{CF}$ = 1.78 Hz), 131.27 (s), 129.22 (d, $^{2}J_{CF}$ = 12.74 Hz), 125.48 (s), 125.21 (d, $^{3}J_{CF}$ = 2.39 Hz), 119.31 (s), 116.40 (d, $^{2}J_{CF}$ = 21.44 Hz), 59.51 (s), 11.37 (s), 5.45 (s), 3.17 (s); ^{19}F NMR (471 MHz, d_6-DMSO) δ -113.97; HRMS (ESI/Q-TOF): *m/z* $[M + H]^+$ calcd for $C_{21}H_{15}BrFN_3O_2$: 440.04044; found: 440.04219; HPLC Purity: 97.68%.

Figure 226: DAW-III-80 ^{1}H spectra:

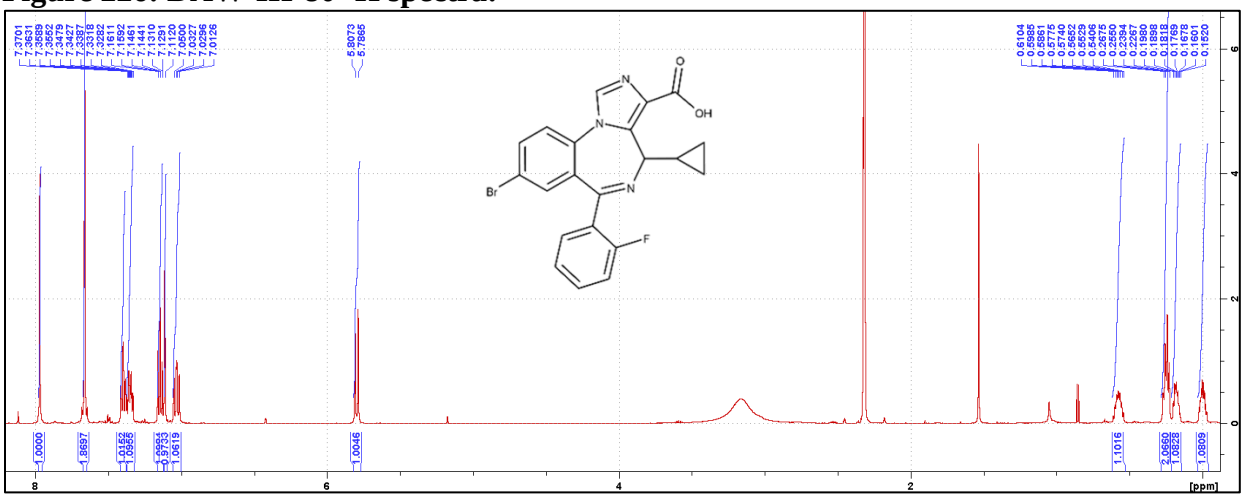

Figure 227: DAW-III-80 ^{13}C spectra:

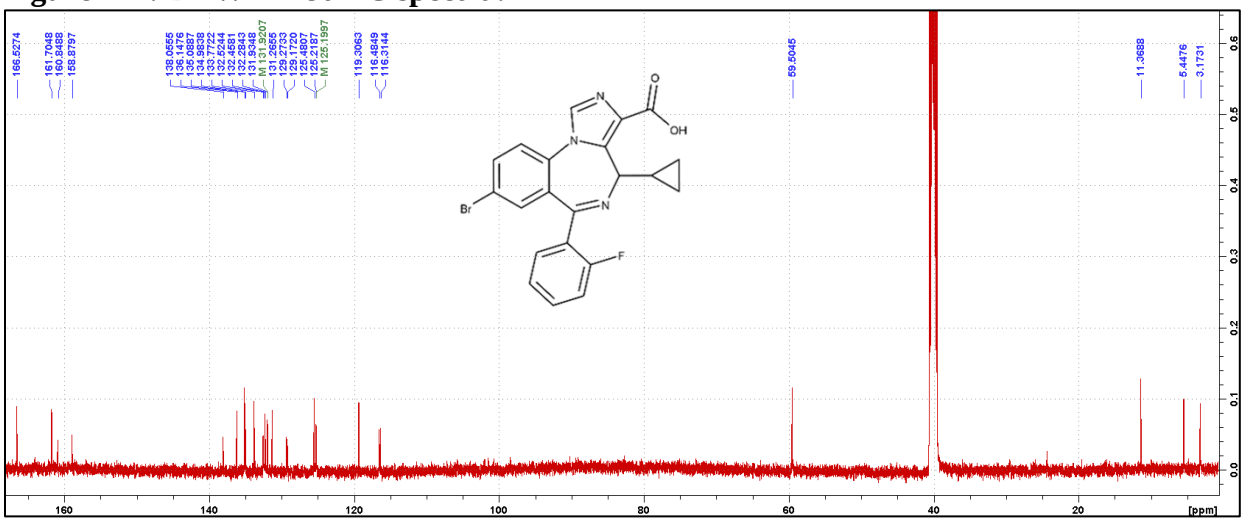

Figure 228: DAW-III-80 ^{19}F spectra:

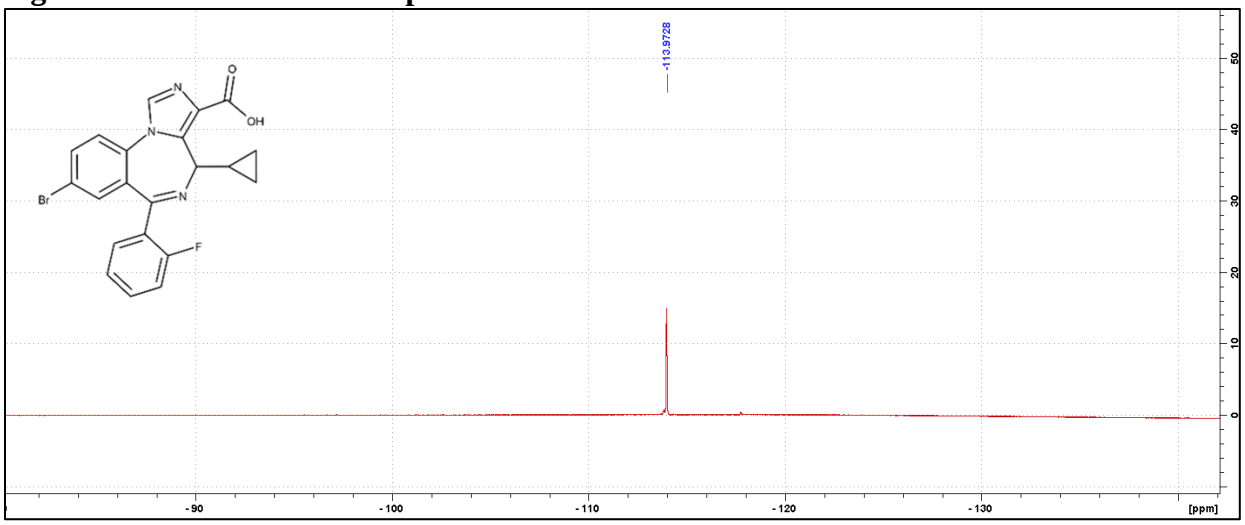

Figure 229: DAW-III-80 HPLC UV Chromatograph:

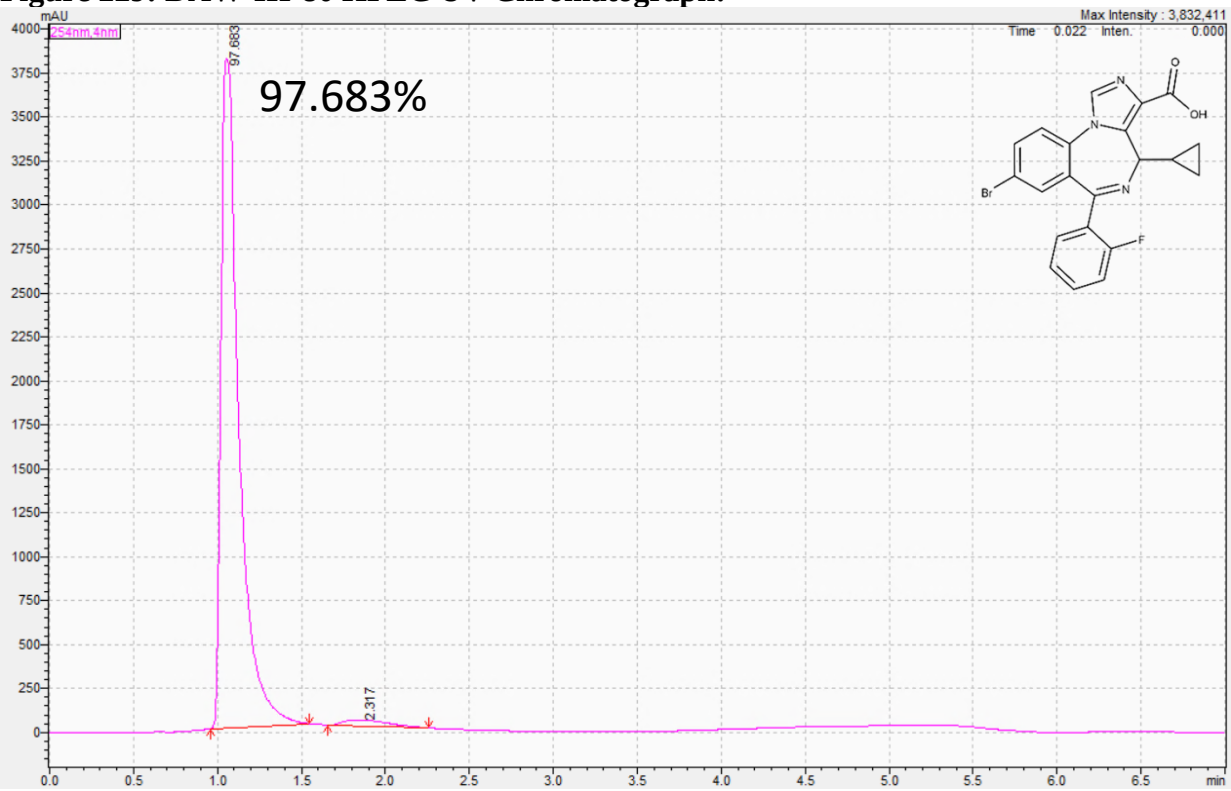

Figure 230: DAW-III-80 HRMS:

Score	Pred. (M)	Pred. m/z	Meas. m/z	Diff. (mDa)	Formulae (M)	Ion	Diff. (ppm)	Iso Score	DBE
65.13	439.03317	440.04044	440.04219	1.75	C21 H15 N3 O2 F Br	[M+H]+	3.977	64.97	15.0

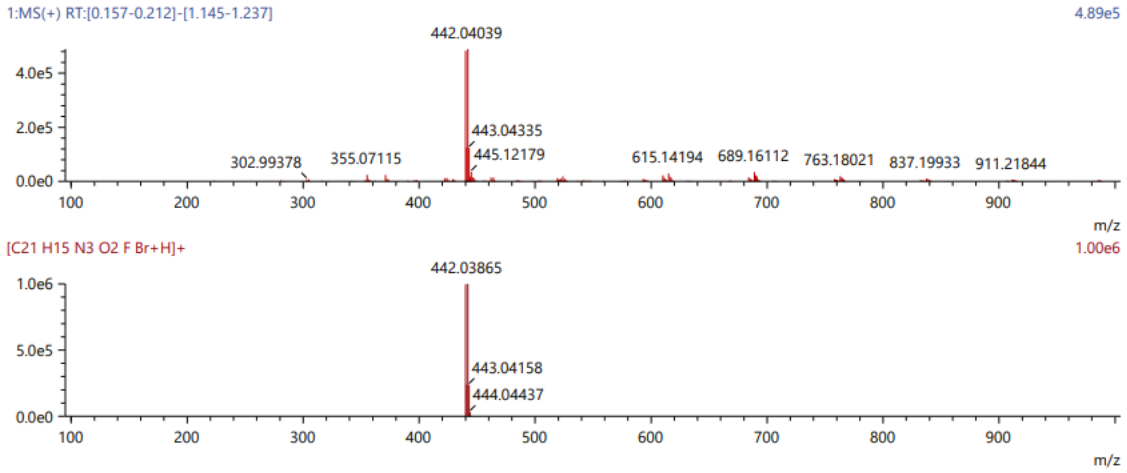

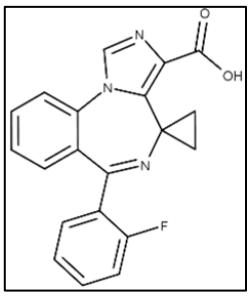

Synthesis of DAW-III-31: A three stopper RB flask was purged with vacuum and nitrogen 3 times. Anhydrous methanol (47 mL) was added, and the solvent was degassed with nitrogen. Sodium bicarbonate (281 mg, 3.35 mmol) was added followed by the addition of **DAW-III-30** (470.62 mg, 1.10 mmol) and 10% palladium on activated carbon (114 mg). A hydrogen balloon was attached to the flask and the flask was gently purged with vacuum and hydrogen 3 times. The hydrogen was then allowed to freely flow into the reaction with vigorous stirring for 5 min. The reaction mixture was then filtered over celite and washed with methanol. The solvent was removed under reduced pressure and the residue was sonicated in H_2O (2 mL) for 2 min. The product was then collected by filtration to yield a white powder (313.98 mg, 81.9%): ^{1}H NMR (500 MHz, d_6-DMSO) δ 8.37 (s, 1H), 7.90-7.88 (d, *J* = 7.90 Hz, 1H), 7.77-7.74 (m, 1H), 7.56-7.52 (m, 2H), 7.50-7.47 (m, 1H), 7.33-7.29 (m, 1H), 7.25-7.18 (m, 2H), 1.86-1.82 (m, 1H), 1.48-1.43 (m, 1H), 0.71-0.67 (m, 1H), 0.63-0.58 (m, 1H); ^{13}C NMR (126 MHz, d_6-DMSO) δ 168.80 (s), 164.09 (s), 159.94 (d, $^{1}J_{CF}$ = 248.48 Hz), 139.76 (s), 135.65 (d, $^{3}J_{CF}$ = 19.73 Hz), 135.09 (s), 132.68 (d, $^{2}J_{CF}$ = 20.59 Hz), 131.80 (d, $^{3}J_{CF}$ = 16.10 Hz), 130.26 (s), 130.04 (s), 129.12 (s), 128.07 (d, $^{3}J_{CF}$ = 12.27 Hz), 127.81 (d, $^{3}J_{CF}$ = 12.27 Hz), 125.04 (s), 123.49 (d, $^{2}J_{CF}$ = 22.88 Hz), 116.40 (d, $^{2}J_{CF}$ = 21.17 Hz), 37.48 (s), 14.89 (s), 14.48 (s); ^{19}F NMR (471 MHz, d_6-DMSO) δ -113.54 - -113.59 (qu, *J* = 5.42 Hz); HRMS (ESI/Q-TOF): *m/z* $[M + H]^+$ calcd for $C_{20}H_{14}FN_3O_2$: 348.11428; found: 348.11441; HPLC Purity: 99.51%.

Figure 231: DAW-III-31 ^{1}H spectra:

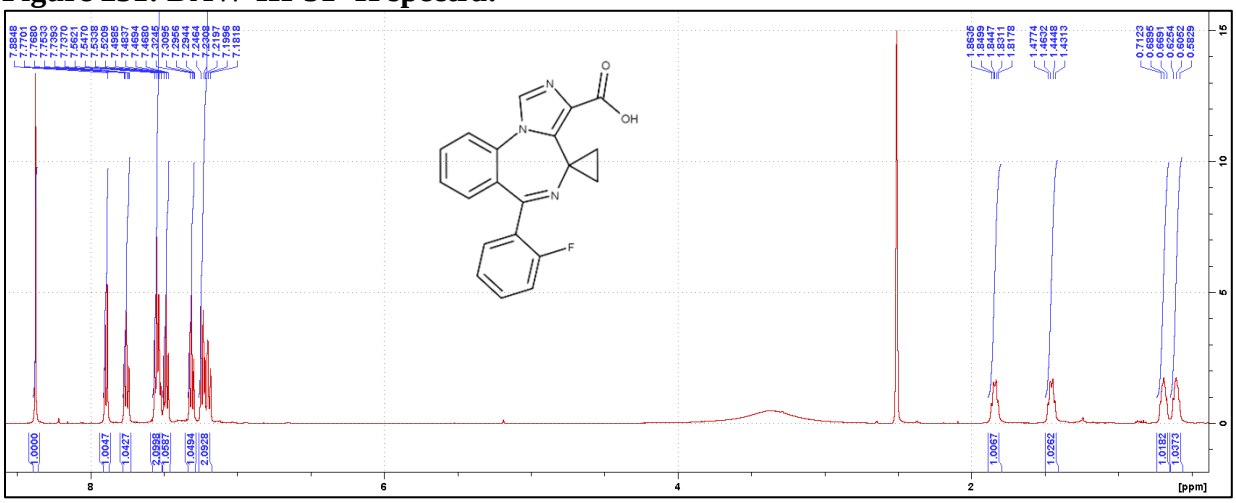

Figure 232: DAW-III-31 ^{13}C spectra:

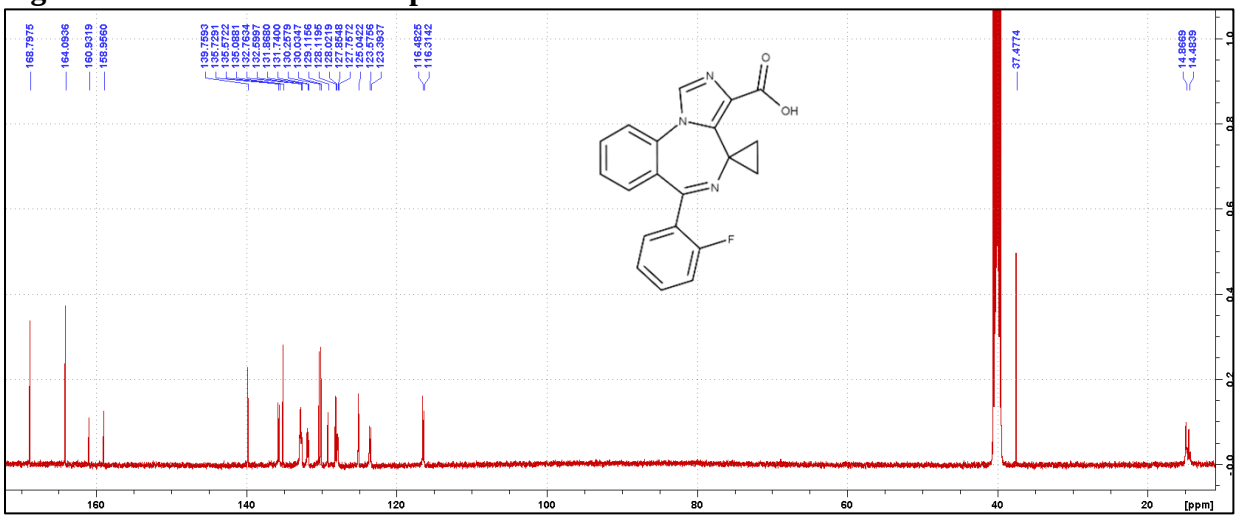

Figure 233: DAW-III-31 ^{19}F spectra:

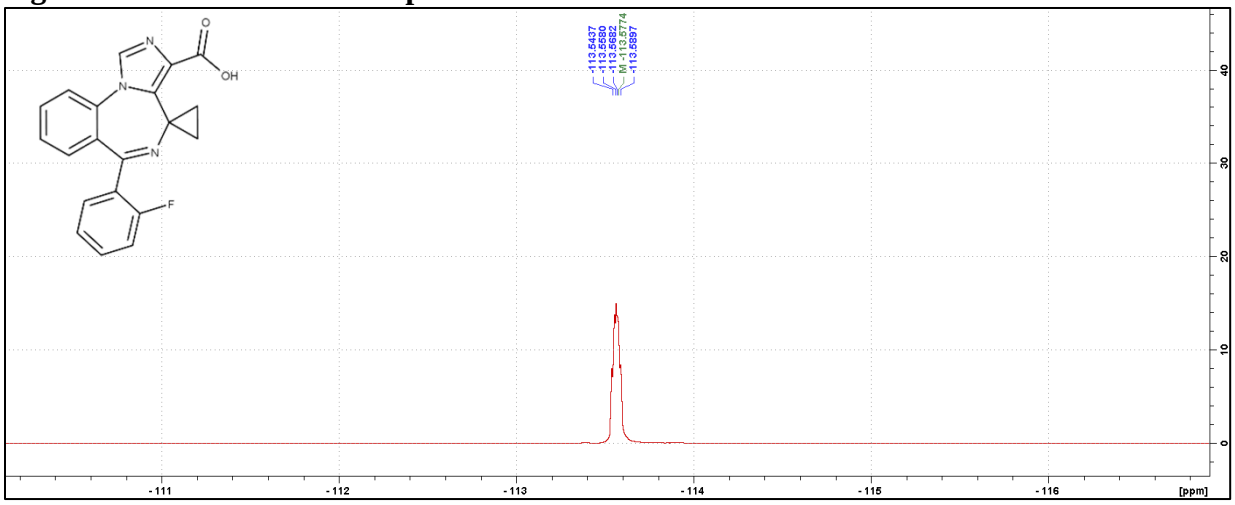

Figure 234: DAW-III-31 HPLC UV Chromatograph:

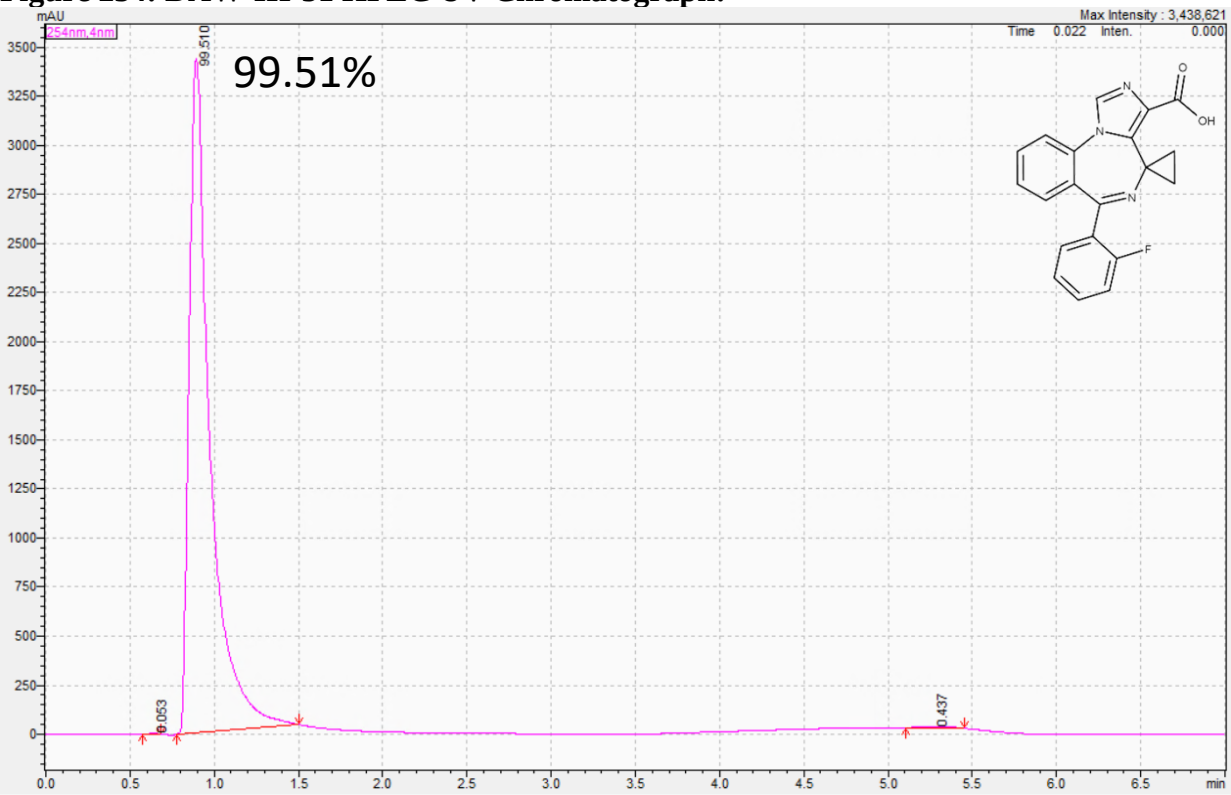

Figure 235: DAW-III-31 HRMS:

Score	Pred. (M)	Pred. m/z	Meas. m/z	Diff. (mDa)	Formulae (M)	Ion	Diff. (ppm)	Iso Score	DBE
62.32	347.10700	348.11428	348.11441	0.13	C20 H14 N3 O2 F	[M+H]+	0.373	58.30	15.0

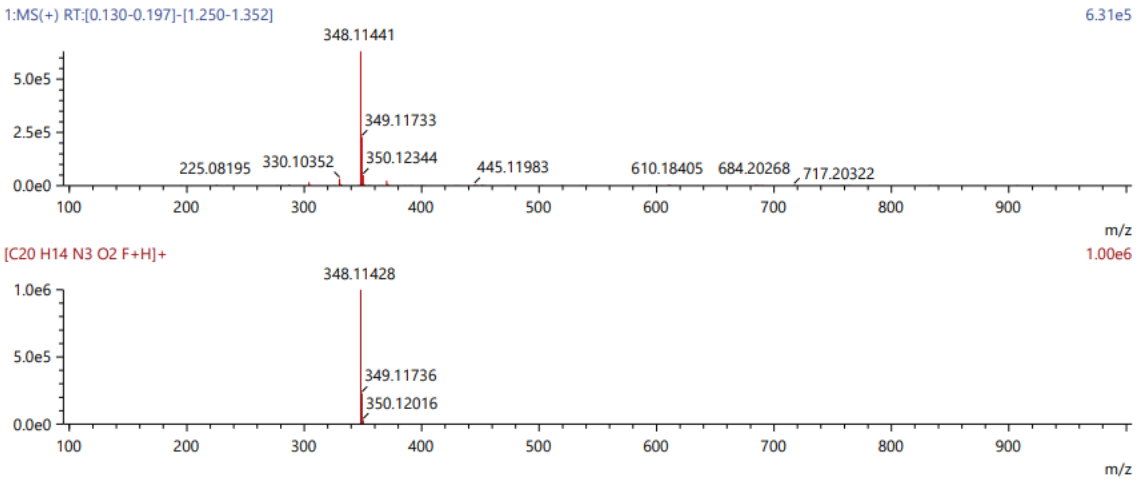

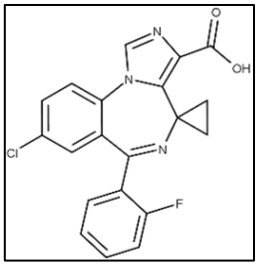

Synthesis of DAW-III-32: DAW-II-32 (210.1 mg, 0.51 mmol) was dissolved in tetrahydrofuran (14.9 mL) and cooled to 0 °C. Solid sodium hydroxide was added (615.2 mg, 15.38 mmol), followed by the addition of H_2O (353.5 μL). The reaction was then removed from the ice bath and gently heated to 80 °C for 18 h. When all of the starting material had dropped to the baseline via TLC (100% EtOAc), the reaction was cooled to room temperature. Acetic acid was added until the pH was observed to be ~5, and the reaction was then warmed to 50 °C and allowed to stir for 20 h. The reaction was then concentrated to dryness under reduced pressure. The residue was dissolved in H_2O (4 mL) and portioned into 0.5 mL fractions. To each fraction was added an additional 1 mL of H_2O causing the desired product to precipitate out of solution. The fractions were centrifuged and the solution was decanted. The solid fractions were combined and washed with an additional 6 mL of H_2O to remove any residual acetic acid. The product was then collected by filtration to yield a white powder. No further purification was conducted. (172.6 mg, 88.2%): ^{1}H NMR (500 MHz, d_6-DMSO) δ 8.40 (s, 1H), 7.95-7.94 (d, *J* = 8.65 Hz, 1H), 7.87-785 (dd, *J* = 3.68, 2.40 Hz, 1H), 7.59-7.55 (m, 2H), 7.35-7.31 (m, 1H), 7.25-7.21 (m, 2H), 1.85-1.80 (m, 1H), 1.49-1.45 (m, 1H), 0.75-0.69 (m, 2H); ^{13}C NMR (126 MHz, d_6-DMSO) δ 167.47 (s), 163.88 (s), 159.91 (d, $^{1}J_{CF}$ = 248.68 Hz), 139.72 (s), 135.84 (d, $^{3}J_{CF}$ = 10.35 Hz), 133.99 (s), 133.20 (s), 132.51 (d, $^{3}J_{CF}$ = 11.56 Hz), 131.96 (s), 131.87 (s), 129.26 (s), 128.96 (s), 127.35 (d, $^{2}J_{CF}$ = 11.96 Hz), 125.71 (d, $^{2}J_{CF}$ = 12.00 Hz), 125.17 (d, $^{4}J_{CF}$ = 2.50 Hz), 116.49 (d, $^{2}J_{CF}$ = 21.02 Hz), 37.60 (s), 14.82 (s), 14.41(s); ^{19}F NMR (471 MHz, d_6-DMSO) δ -113.53 - -113.58 (qu, *J* = 5.69 Hz) HRMS (ESI/Q-TOF): *m/z* $[M + H]^+$ calcd for $C_{20}H_{13}ClFN_3O_2$: 382.07531; found: 382.07606; HPLC Purity: 99.82%.

Figure 236: DAW-III-32 ^{1}H spectra:

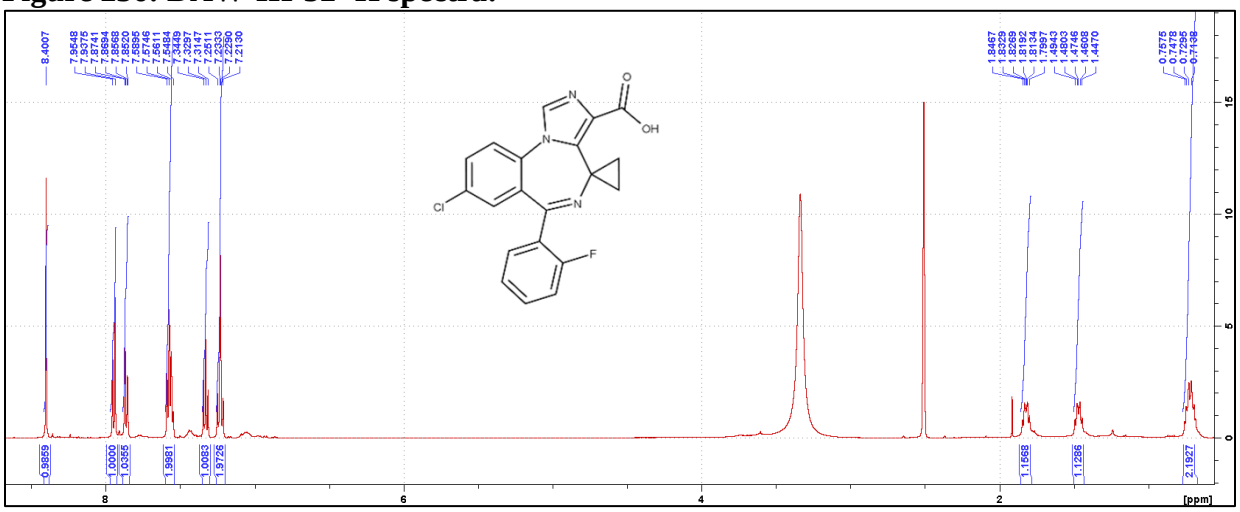

Figure 237: DAW-III-32 ^{13}C spectra:

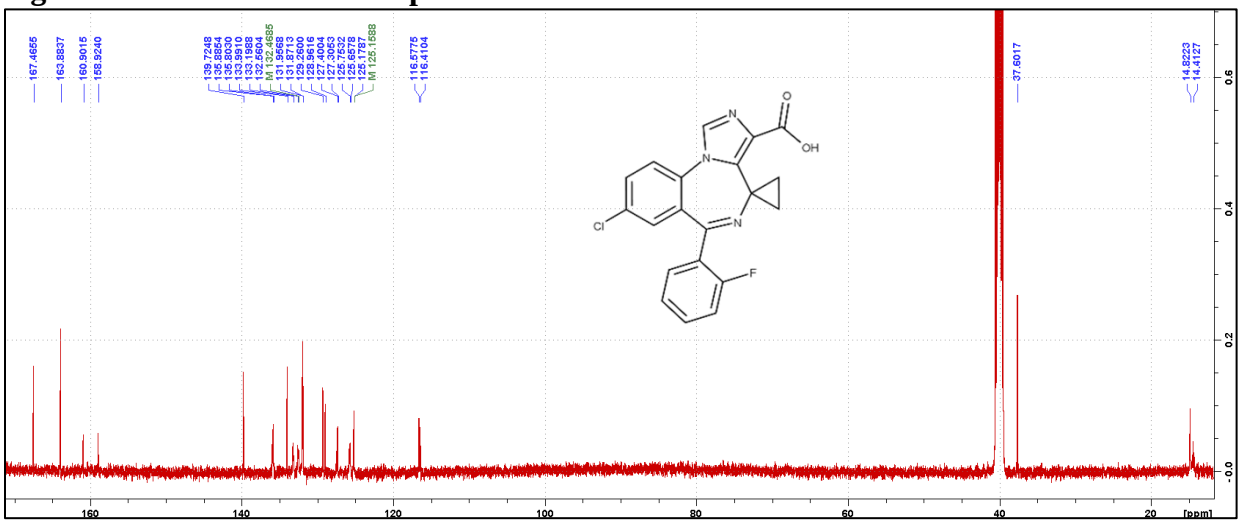

Figure 238: DAW-III-32 ^{19}F spectra:

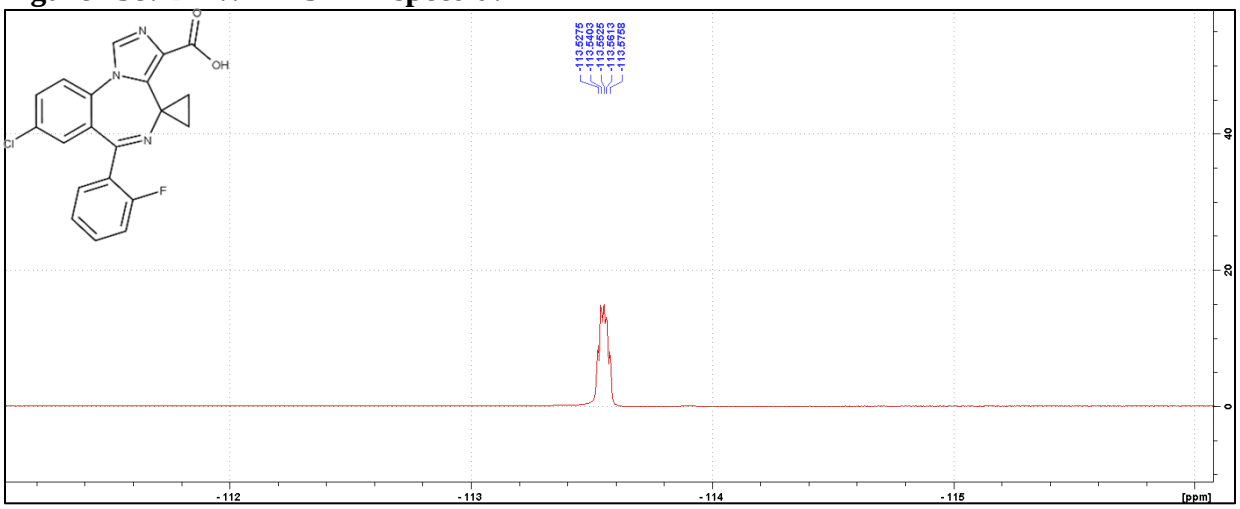

Figure 239: DAW-III-32 HPLC UV Chromatograph:

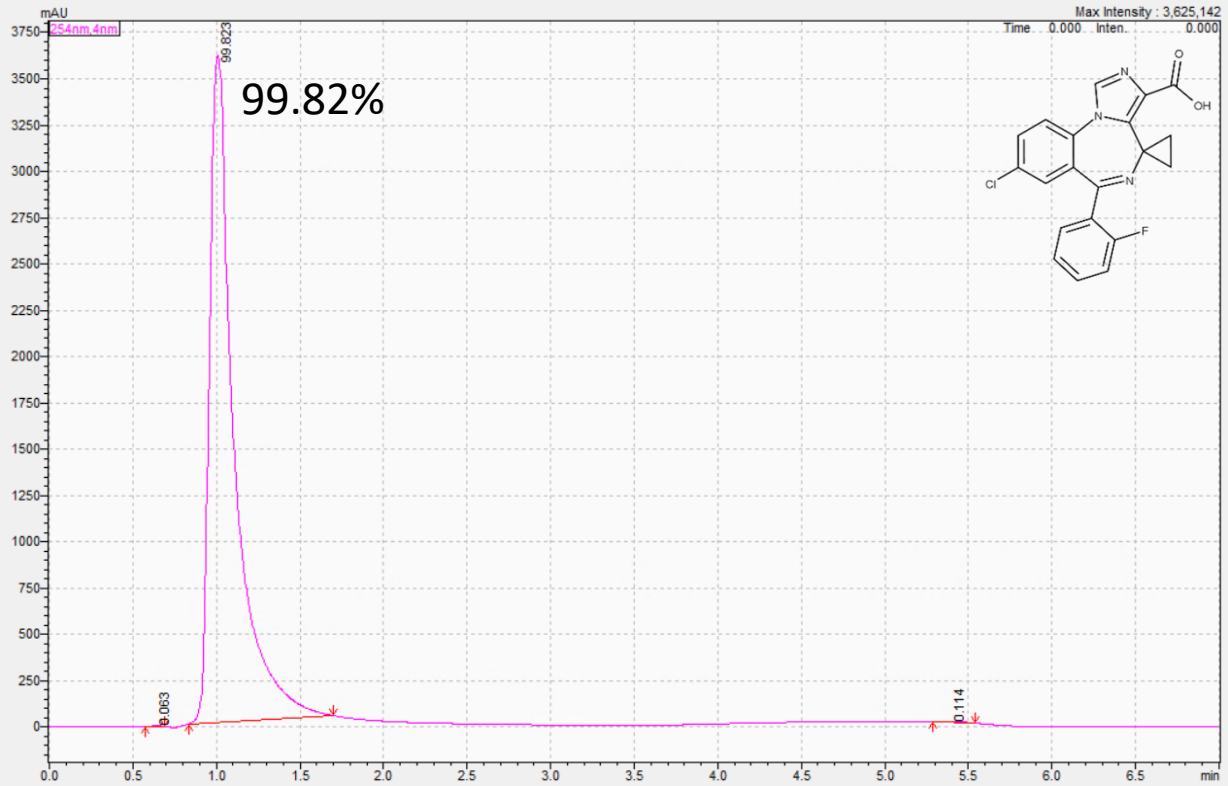

Figure 240: DAW-III-32 HRMS:

Score	Pred. (M)	Pred. m/z	Meas. m/z	Diff. (mDa)	Formulae (M)	Ion	Diff. (ppm)	Iso Score	DBE
56.65	381.06803	382.07531	382.07606	0.75	C20 H13 N3 O2 F Cl	[M+H]+	1.963	53.00	15.0

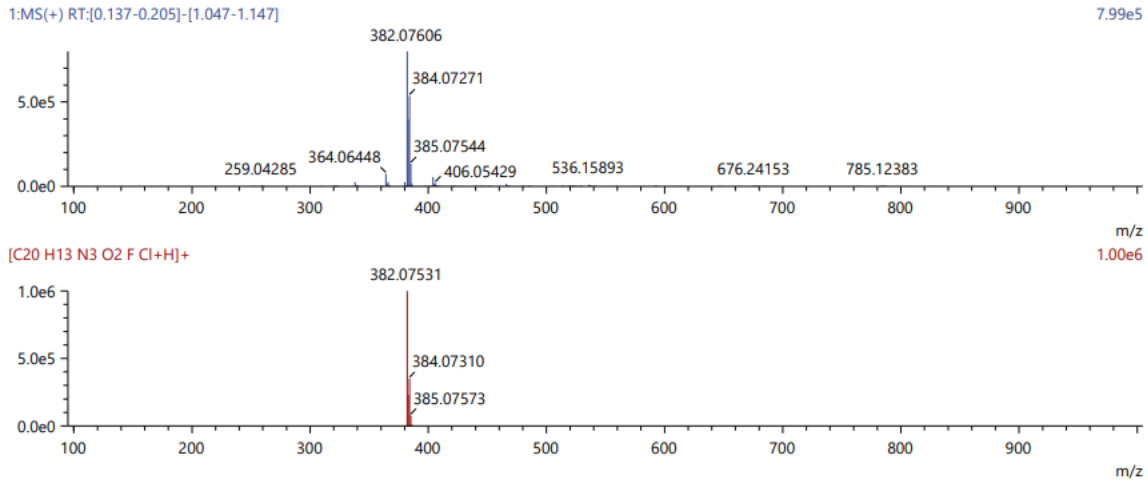

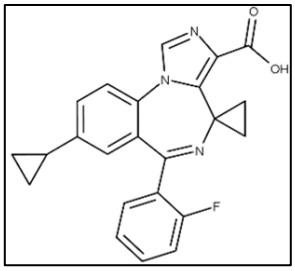

Synthesis of DAW-III-33: DAW-II-33 (236.18 g, 0.57 mmol) was dissolved in tetrahydrofuran (16.7 mL) and cooled to 0 °C. Solid sodium hydroxide was added (682.2 mg, 17.05 mmol), followed by the addition of H_2O (397.4 μL). The reaction was then removed from the ice bath and gently heated to 80 °C for 18 h. When all the starting material had dropped to the baseline via TLC (100% EtOAc), the reaction was cooled to room temperature. Acetic acid was added until the pH was observed to be ~5, and the reaction was then warmed to 50 °C and allowed to stir for 20 h. The reaction was then concentrated to dryness under reduced pressure. The residue was dissolved in H_2O (3.5 mL) and portioned into 0.5 mL fractions. To each fraction was added an additional 1 mL of H_2O causing the desired product to precipitate out of solution. The fractions were centrifuged and the solution was decanted. The solid fractions were combined and washed with an additional 6 mL of H_2O to remove any residual acetic acid. The product was then collected by filtration to yield a white powder. No further purification was conducted. (151.45 g, 68.7%): ^{1}H NMR (500 MHz, d_6-DMSO) δ 8.30 (s, 1H), 7.76-7.74 (d, *J* = 8.35 Hz, 1H), 7.57-7.52 (m, 2H), 7.36-7.34 (dd, *J* = 3.50, 2.05 Hz, 1H), 7.33-7.30 (dt, *J* = 3.21, 0.95 Hz, 1H), 7.23-7.19 (m, 1H), 6.96-6.95 (m, 1H), 1.97-1.92 (m, 1H), 1.84 (m, 1H), 1.43-1.42 (m, 1H), 0.97-0.96 (m, 2H), 0.67-0.62 (m, 4H); ^{13}C NMR (126 MHz, d_6-DMSO) δ 168.73 (s), 164.11 (s), 159.95 (d, $^{1}J_{CF}$ = 248.61 Hz), 143.59 (s), 139.49 (s), 135.45 (s), 132.77 (d, $^{3}J_{CF}$ = 8.33 Hz), 132.64 (s), 132.58 (s), 131.84 (d, $^{4}J_{CF}$ = 2.26 Hz), 130.01 (s), 128.47 (s), 128.07 (d, $^{3}J_{CF}$ = 12.26 Hz), 127.21 (s), 126.32 (d, $^{2}J_{CF}$ = 12.40 Hz), 125.02 (d, $^{3}J_{CF}$ = 2.98 Hz), 123.51 (s), 116.38 (d, $^{2}J_{CF}$ = 21.42 Hz), 37.48 (s), 15.06 (s), 14.69 (d, *J* = 53.58 Hz), 10.51 (d, *J* = 32.82 Hz); ^{19}F NMR (471 MHz, d_6-DMSO) δ -113.51; HRMS (ESI/Q-TOF): *m/z* $[M + H]^+$ calcd for $C_{23}H_{18}FN_3O_2$: 388.14558; found: 388.14551; HPLC Purity: 99.49%.

Figure 241: DAW-III-33 ^{1}H spectra:

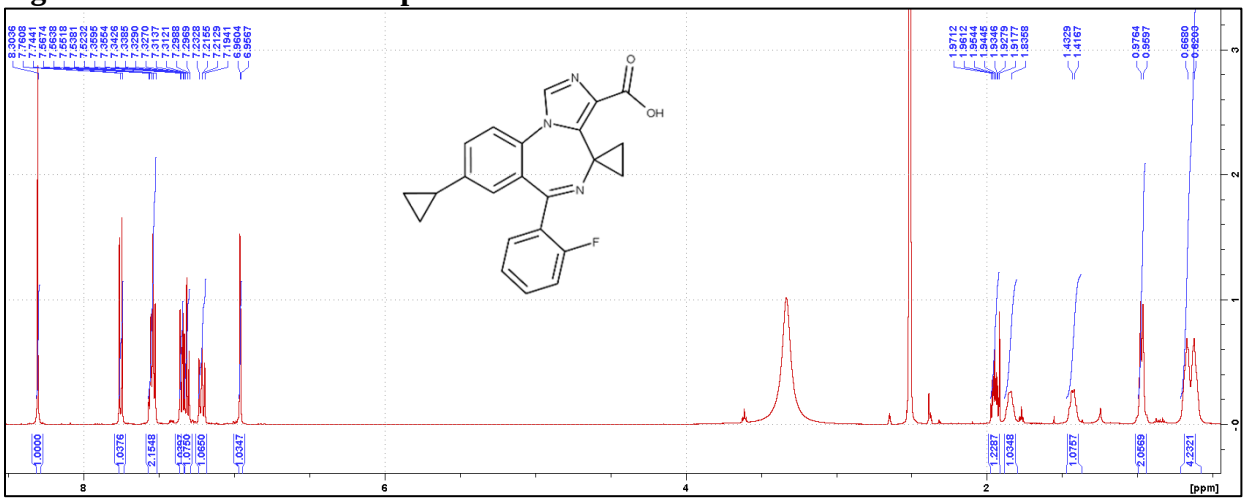

Figure 242: DAW-III-33 ^{13}C spectra:

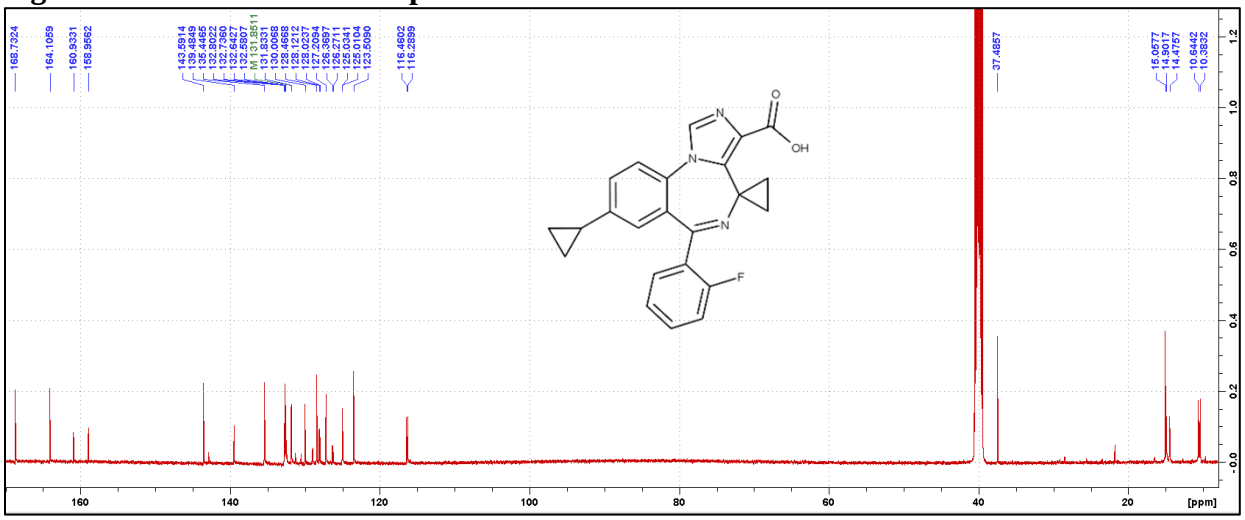

Figure 243: DAW-III-33 ^{19}F spectra:

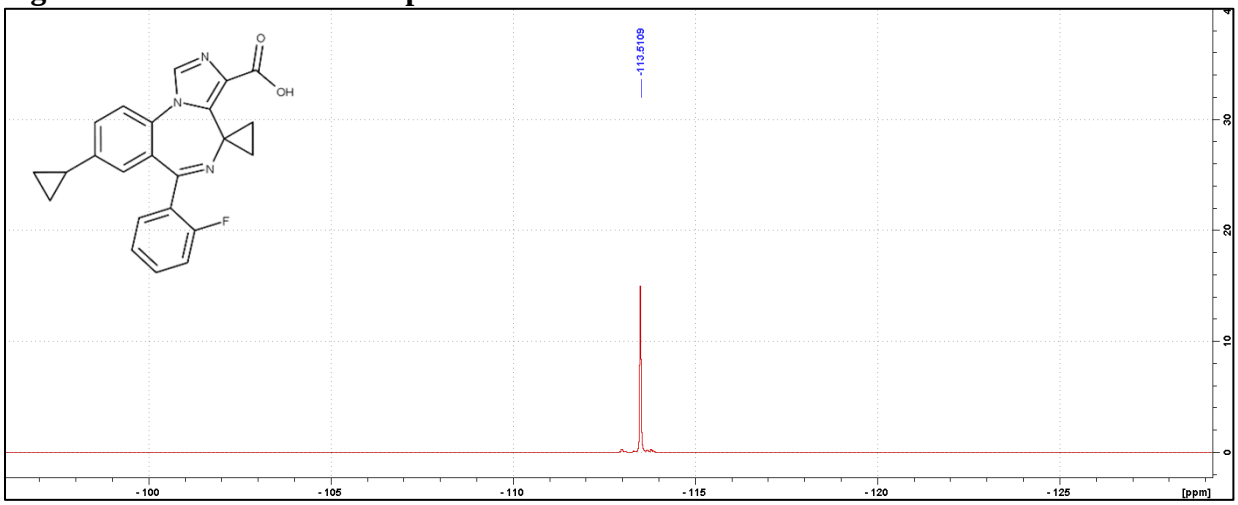

Figure 244: DAW-III-33 HPLC UV Chromatograph:

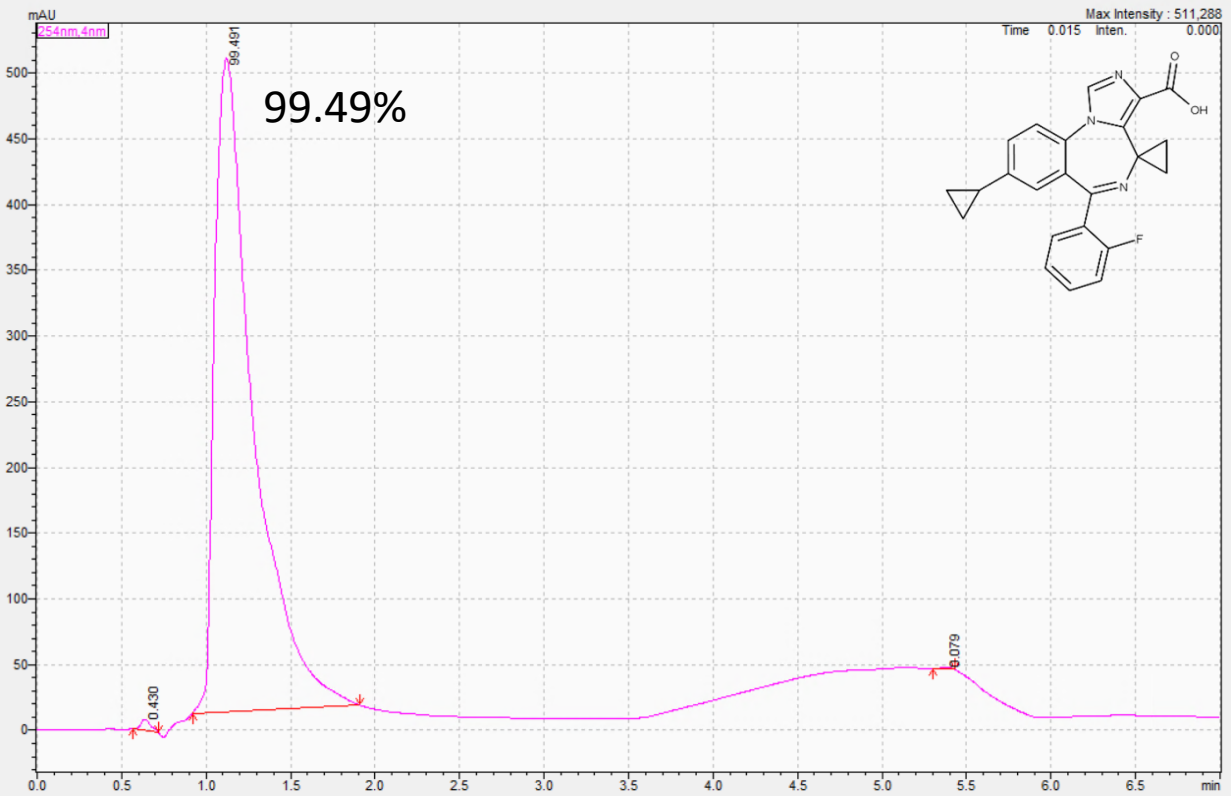

Figure 245: DAW-III-33 HRMS:

Score	Pred. (M)	Pred. m/z	Meas. m/z	Diff. (mDa)	Formulae (M)	Ion	Diff. (ppm)	Iso Score	DBE
99.91	387.13830	388.14558	388.14551	-0.07	C23 H18 N3 O2 F	[M+H]+	-0.180	99.97	16.0

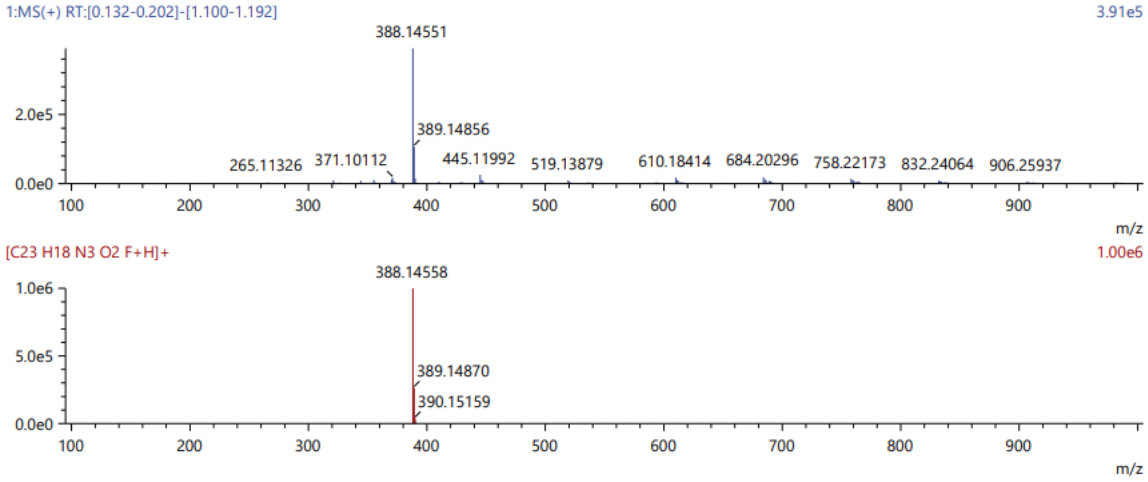

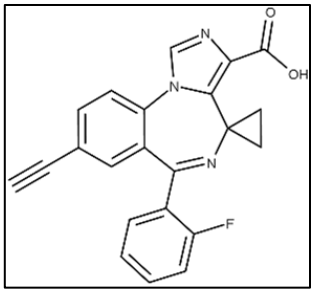

Synthesis of DAW-III-35: DAW-II-35 (116.05 mg, 0.29 mmol) was dissolved in tetrahydrofuran (8.2 mL) and cooled to 0 °C. Solid sodium hydroxide was added (348.6 mg, 8.72 mmol), followed by the addition of H_2O (195.3 μL). The reaction was then removed from the ice bath and gently heated to 80 °C for 18 h. When all of the starting material had dropped to the baseline via TLC (100% EtOAc), the reaction was cooled to room temperature. Acetic acid was added until the pH was observed to be ~5, and the reaction was then warmed to 50 °C and allowed to stir for 20 h. The reaction was then concentrated to dryness under reduced pressure. The residue was dissolved in H_2O (3 mL) and portioned into 0.5 mL fractions. To each fraction was added an additional 1 mL of H_2O causing the desired product to precipitate out of solution. The fractions were centrifuged and the solution was decanted. The solid fractions were combined and washed with an additional 5 mL of H_2O to remove any residual acetic acid. The product was then collected by filtration to yield a white powder. No further purification was conducted. (61.01 mg, 59.3%): ^{1}H NMR (500 MHz, d_6-DMSO) δ 8.41 (s, 1H), 7.93-7.92 (d, *J* = 8.40 Hz, 1H), 7.87-7.85 (dd, *J* = 3.35, 1.75 Hz, 1H), 7.59-7.56 (m, 2H), 7.34-7.32 (m, 1H), 7.26 (m, 1H), 7.25-7.21 (m, 1H), 4.37 (s, 1H), 1.84-1.84 (m, 1H), 1.49-1.44 (m, 1H), 0.73-0.67 (m, 2H); ^{13}C NMR (126 MHz, d_6-DMSO) δ 167.88 (s), 163.90 (s), 159.89 (d, $^1J_{CF}$ = 248.62 Hz), 139.73 (s), 135.83 (s), 135.48 (s), 135.11 (s), 133.06 (d, $^3J_{CF}$ = 8.73 Hz), 132.95 (s), 131.93 (d, $^4J_{CF}$ = 1.82 Hz), 130.58 (s), 129.05 (s), 127.59 (d, $^2J_{CF}$ = 12.03 Hz), 125.14 (d, $^3J_{CF}$ = 3.38 Hz), 124.23 (s), 121.01 (s), 116.46 (d, $^2J_{CF}$ = 21.22 Hz), 83.36 (d, *J* = 11.62 Hz), 82.13 (d, *J* = 2.02 Hz), 35.57 (s), 14.84 (s), 14.45 (s); ^{19}F NMR (471 MHz, d_6-DMSO) δ -113.65 - -113.70 (qu, *J* = 5.59 Hz); HRMS (ESI/Q-TOF): *m/z* $[M + H]^+$ calcd for $C_{22}H_{14}FN_3O_2$: 372.11428; found: 372.11403; HPLC Purity: 99.88%.

Figure 246: DAW-III-35 ^{1}H spectra:

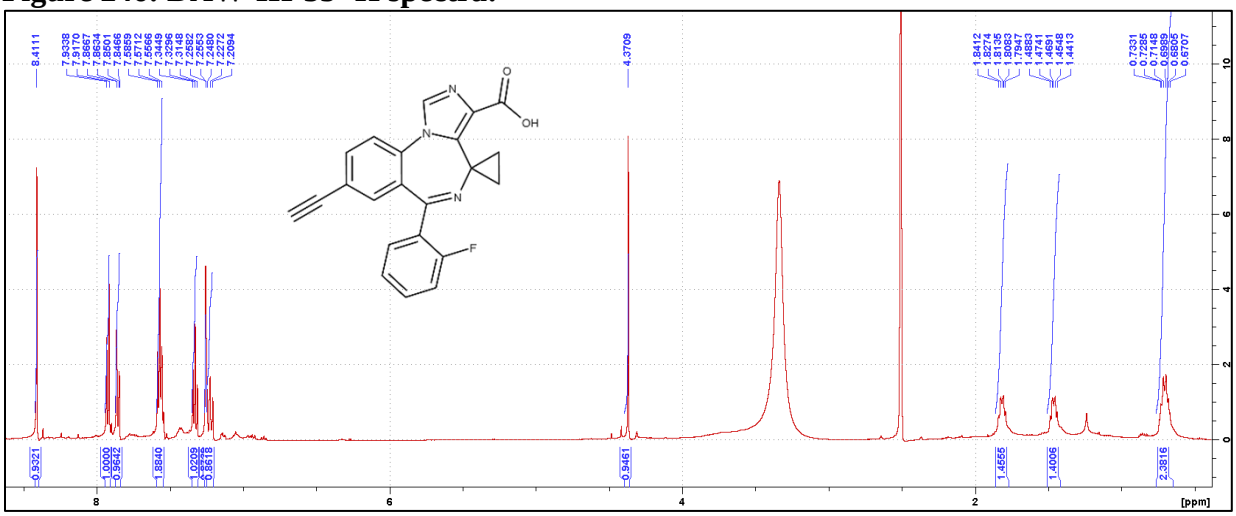

Figure 247: DAW-III-35 ^{13}C spectra:

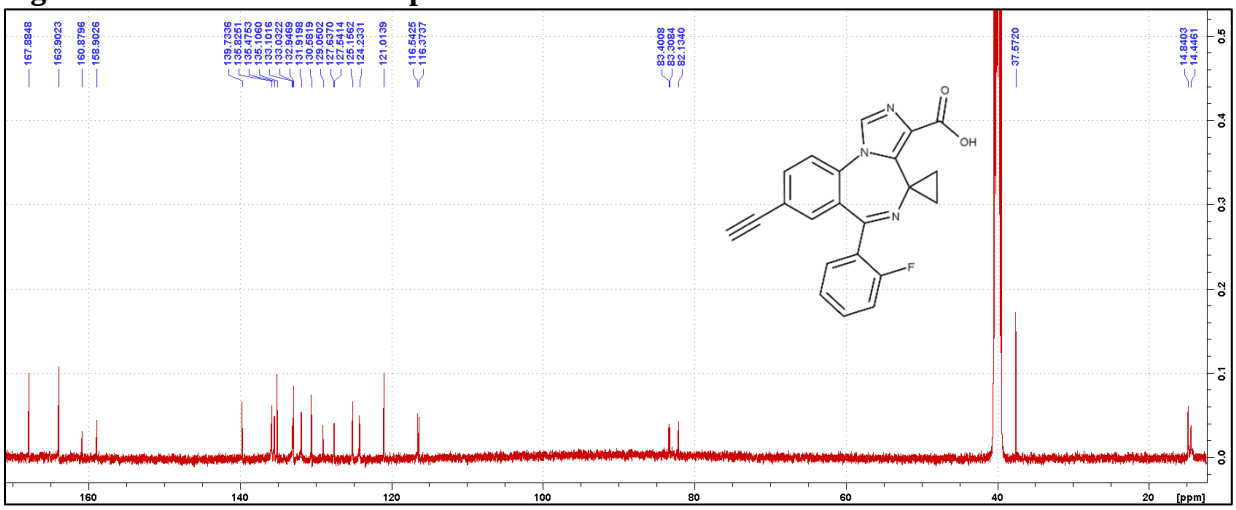

Figure 248: DAW-III-35 ^{19}F spectra:

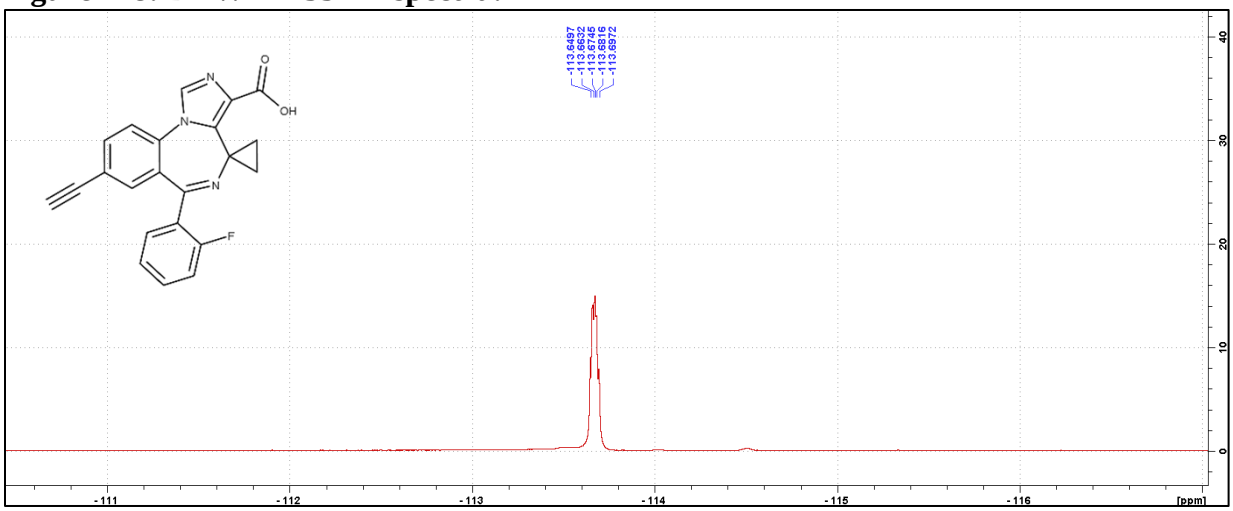

Figure 249: DAW-III-35 HPLC UV Chromatograph:

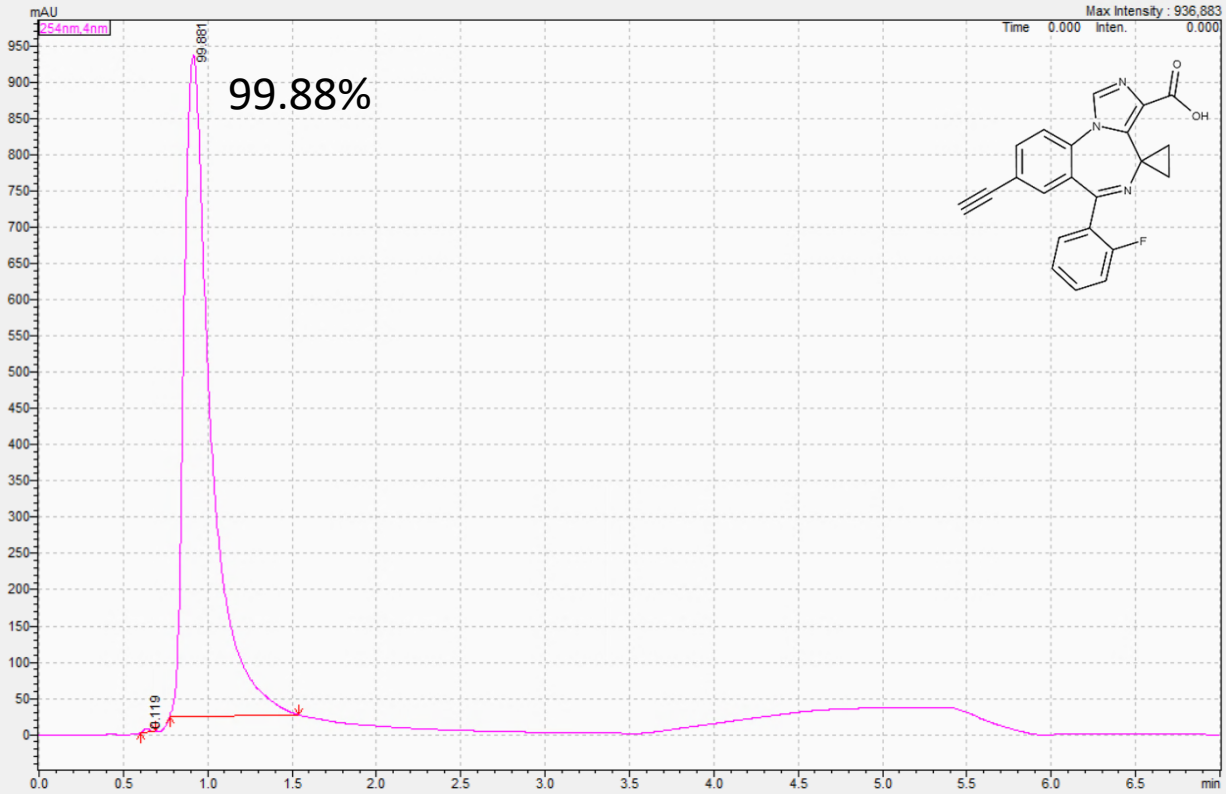

Figure 250: DAW-III-35 HRMS:

Score	Pred. (M)	Pred. m/z	Meas. m/z	Diff. (mDa)	Formulae (M)	Ion	Diff. (ppm)	Iso Score	DBE
98.85	371.10700	372.11428	372.11403	-0.25	C22 H14 N3 O2 F	[M+H]+	-0.672	99.05	17.0

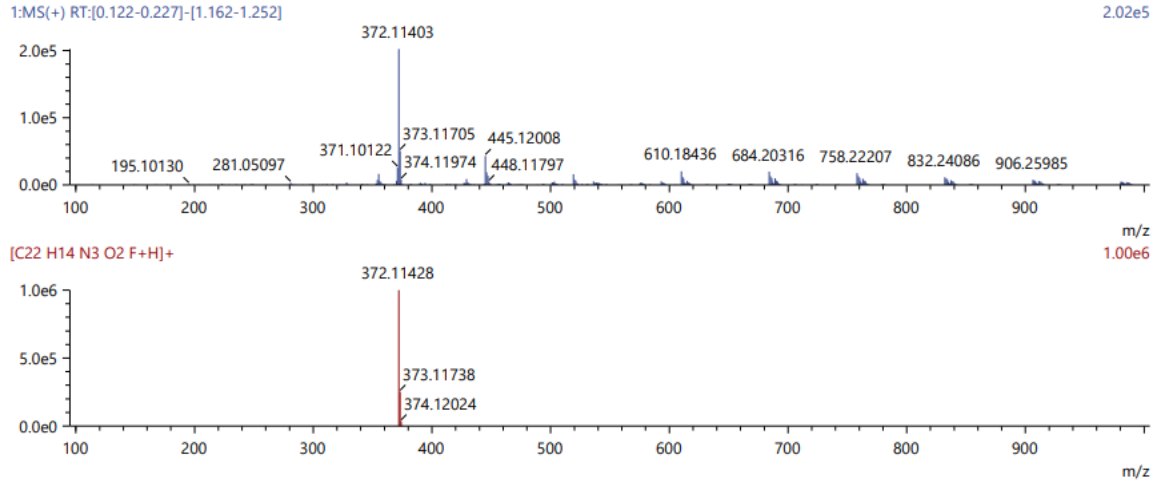

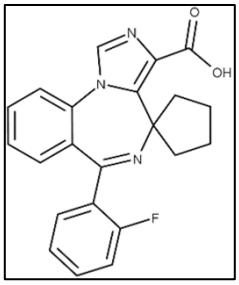

Synthesis of DAW-III-51: A three stopper RB flask was purged with vacuum and nitrogen 3 times. Anhydrous methanol (17 mL) was added, and the solvent was degassed with nitrogen. Sodium bicarbonate (102 mg, 1.21 mmol) was added followed by the addition of **DAW-III-50** (170.4 mg, 0.38 mmol) and 10% palladium on activated carbon (42 mg). A hydrogen balloon was attached to the flask and the flask was gently purged with vacuum and hydrogen 3 times. The hydrogen was then allowed to freely flow into the reaction with vigorous stirring for 5 min. The reaction mixture was then filtered over celite and washed with methanol. The solvent was removed under reduced pressure and the residue was sonicated in H_2O (2 mL) for 2 min. The product was then collected by filtration to yield a white powder (69.6 mg, 49.4%): ^{1}H NMR (500 MHz, d_6-DMSO) δ 8.27 (s, 1H), 7.86-7.85 (m, 1H), 7.72-7.70 (m, 1H), 7.55-7.49 (m, 2H), 7.46-7.43 (m, 1H), 7.32-7.29 (m, 1H), 7.22-7.19 (m, 2H), 2.57 (m, 1H), 2.47 (m, 1H), 1.78 (m, 2H), 1.53 (m, 4H); ^{13}C NMR (126 MHz, d_6-DMSO) δ 166.69 (s), 162.10 (s), 160.05 (d, $^{1}J_{CF}$ = 248.05 Hz), 136.16 (s), 135.61 (s), 132.70 (s), 132.33 (d, $^{3}J_{CF}$ = 8.51 Hz), 131.89 (d, $^{4}J_{CF}$ = 2.46 Hz), 129.81 (s), 129.01 (d, $^{2}J_{CF}$ = 12.72 Hz), 127.79 (s), 125.05 (d, $^{3}J_{CF}$ = 3.15 Hz), 123.64 (s), 116.36 (d, $^{2}J_{CF}$ = 21.47 Hz), 67.00 (s), 35.76 (s), 23.46 (s); ^{19}F NMR (471 MHz, d_6-DMSO) δ -114.13; HRMS (ESI/Q-TOF): *m/z* $[M + H]^+$ calcd for $C_{22}H_{18}FN_3O_2$: 376.14558; found: 376.14589; HPLC Purity: 99.27%.

Figure 251: DAW-III-51 ^{1}H spectra:

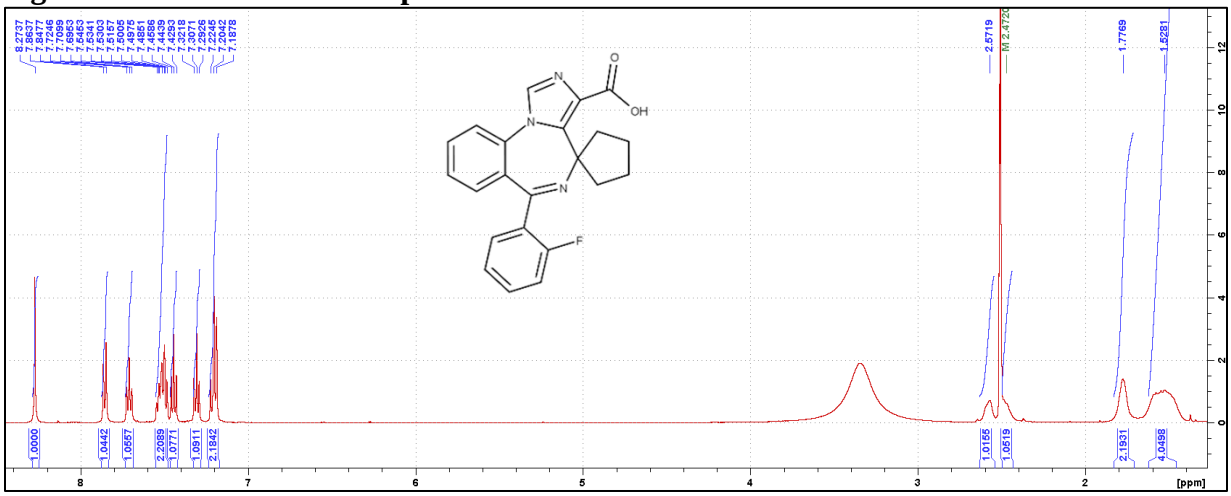

Figure 252: DAW-III-51 ^{13}C spectra:

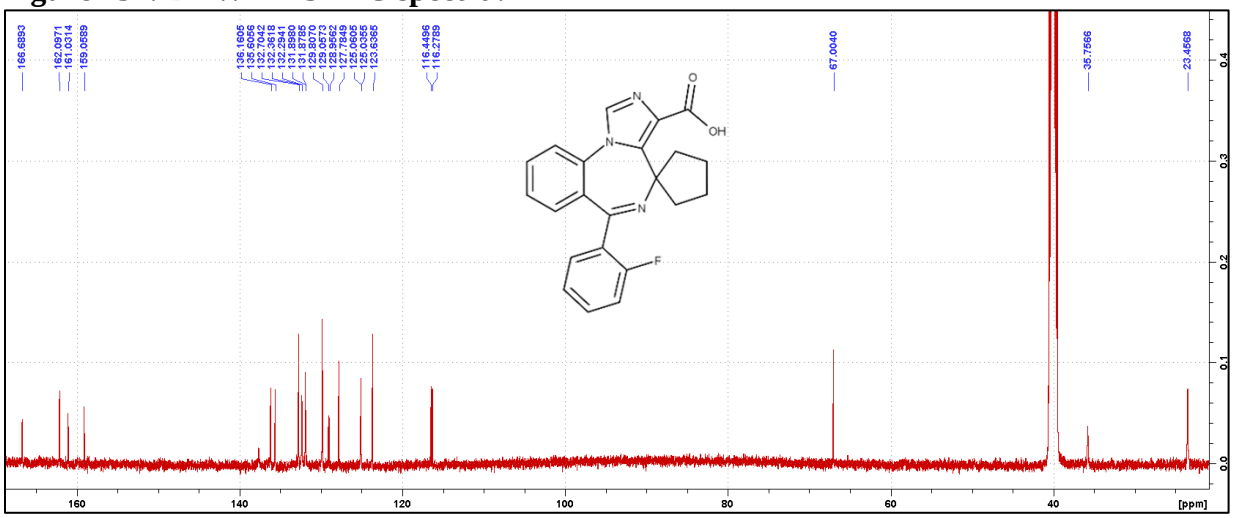

Figure 253: DAW-III-51 ^{19}F spectra:

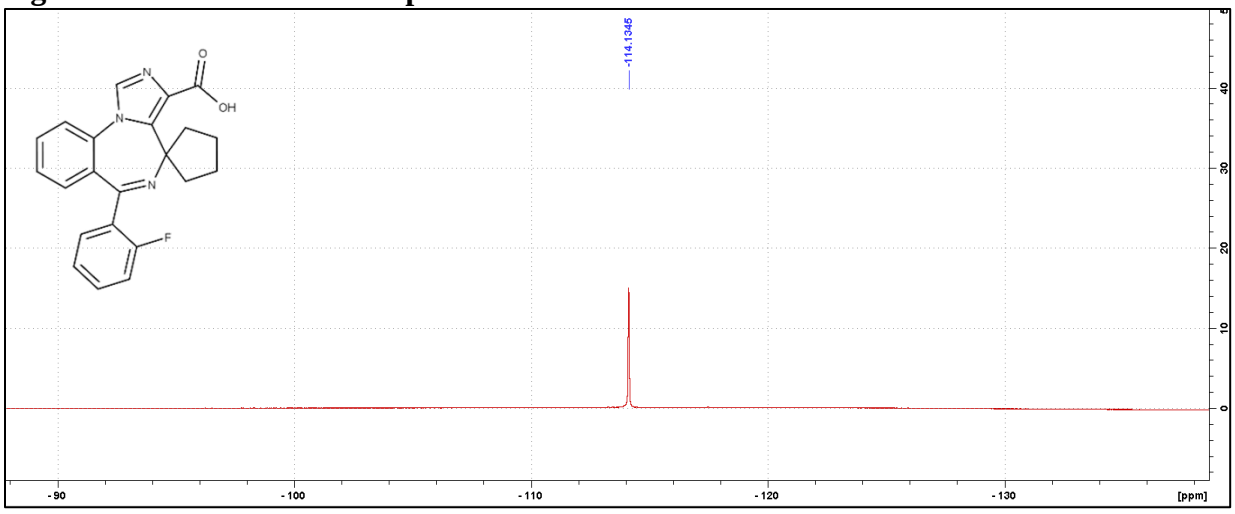

Figure 254: DAW-III-51 HPLC UV Chromatograph:

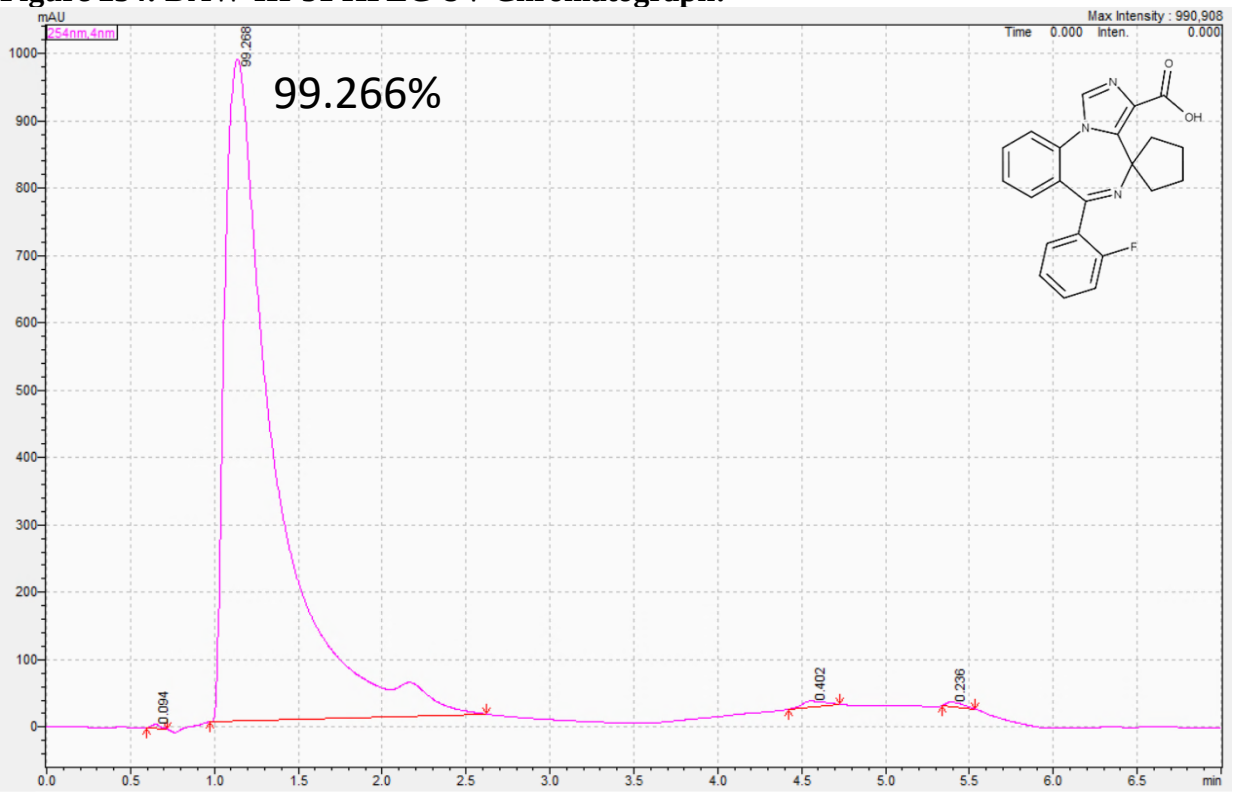

Figure 255: DAW-III-51 HRMS:

Score	Pred. (M)	Pred. m/z	Meas. m/z	Diff. (mDa)	Formulae (M)	Ion	Diff. (ppm)	Iso Score	DBE
62.49	375.13830	376.14558	376.14589	0.31	C22 H18 N3 O2 F	[M+H]+	0.824	58.73	15.0

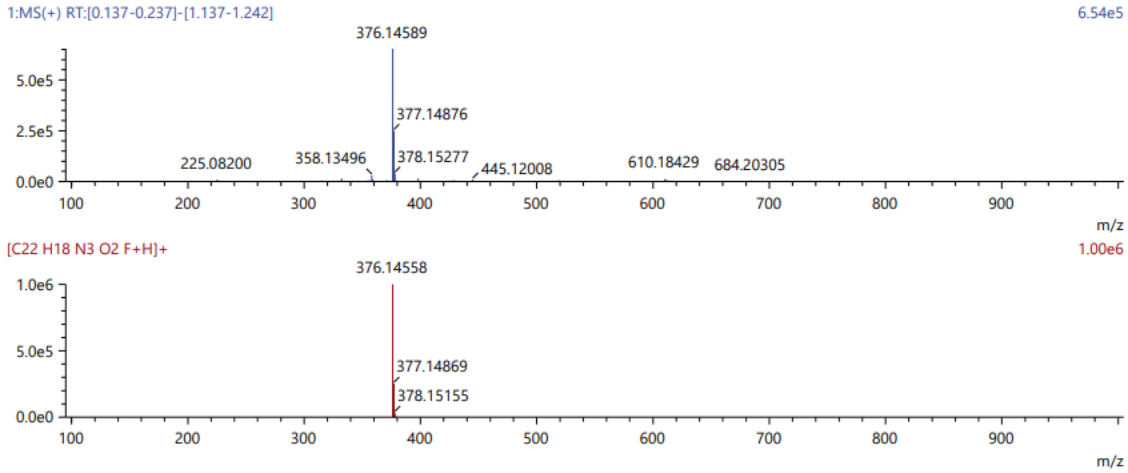

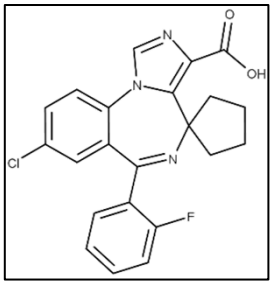

Synthesis of DAW-III-52: DAW-II-52 (314.2 mg, 0.72 mmol) was dissolved in tetrahydrofuran (22.3 mL) and cooled to 0 °C. Solid sodium hydroxide was added (861.0 mg, 21.53 mmol), followed by the addition of H_2O (529.5 μL). The reaction was then removed from the ice bath and gently heated to 80 °C for 18 h. When all the starting material had dropped to the baseline via TLC (100% EtOAc), the reaction was cooled to room temperature. Acetic acid was added until the pH was observed to be ~5, and the reaction was then warmed to 50 °C and allowed to stir for 20 h. The reaction was then concentrated to dryness under reduced pressure. The residue was dissolved in H_2O (5 mL) and portioned into 0.5 mL fractions. To each fraction was added an additional 1 mL of H_2O causing the desired product to precipitate out of solution. The fractions were centrifuged and the solution was decanted. The solid fractions were combined and washed with an additional 9 mL of H_2O to remove any residual acetic acid. The product was then collected by filtration to yield a white powder. No further purification was conducted. (314.9 mg, 84.0%): ^{1}H NMR (500 MHz, d_6-DMSO) δ 8.32 (s, 1H), 7.93-7.92 (d, *J* = 8.70 Hz, 1H), 7.83-7.81 (dd, *J* = 3.70, 2.45 Hz, 1H), 7.58-7.51 (m, 2H), 7.34-7.31 (dt, *J* = 3.21, 1.00 Hz, 1H), 7.25-7.21 (m, 1H), 7.20-7.19 (d, *J* = 2.40 Hz, 1H), 2.58 (m, 1H), 2.46 (m, 1H), 1.78 (m, 2H), 1.63-1.49 (m, 4H); ^{13}C NMR (126 MHz, d_6-DMSO) δ 166.31 (s), 160.77 (s), 160.00 (d, $^{1}J_{CF}$ = 248.25 Hz), 137.96 (s), 136.59 (s), 136.43 (s), 134.43 (s), 132.55 (d, $^{2}J_{CF}$ = 21.13 Hz), 132.05 (s), 131.42 (s), 131.03 (s), 129.04 (s), 128.27 (d, $^{3}J_{CF}$ = 12.36 Hz), 125.97 (d, $^{3}J_{CF}$ = 3.75 Hz), 125.78 (s), 125.17 (s), 116.46 (d, $^{2}J_{CF}$ = 21.27 Hz), 67.12 (s), 36.00 (s), 23.57 (s); ^{19}F NMR (471 MHz, d_6-DMSO) δ -114.11; HRMS (ESI/Q-TOF): *m/z* $[M + H]^+$ calcd for $C_{22}H_{17}ClFN_3O_2$: 410.10661; found: 410.10755; HPLC Purity: 99.82%.

Figure 256: DAW-III-52 ^{1}H spectra:

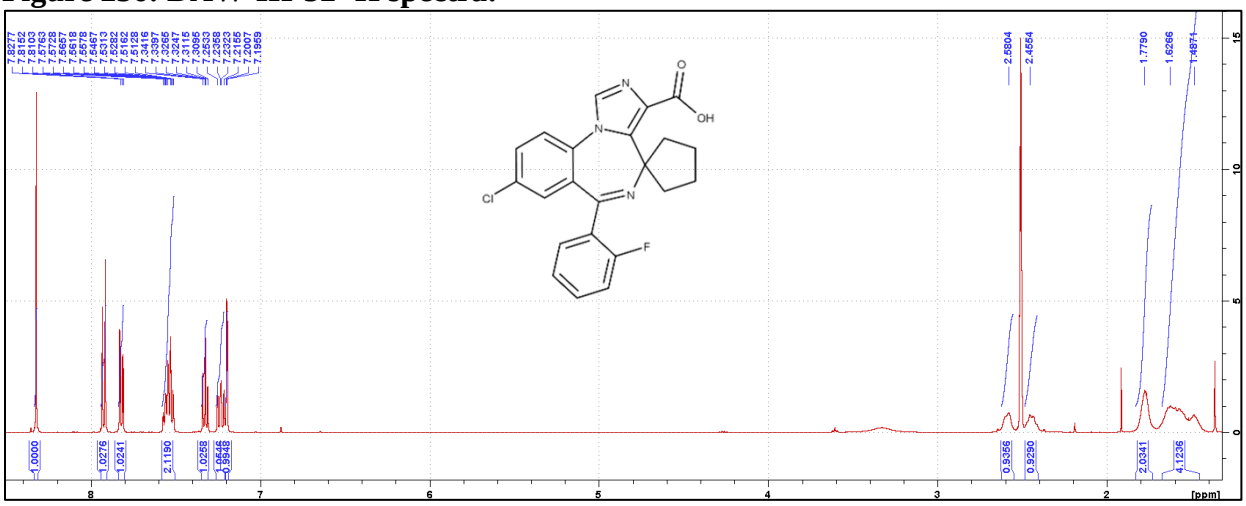

Figure 257: DAW-III-52 ^{13}C spectra:

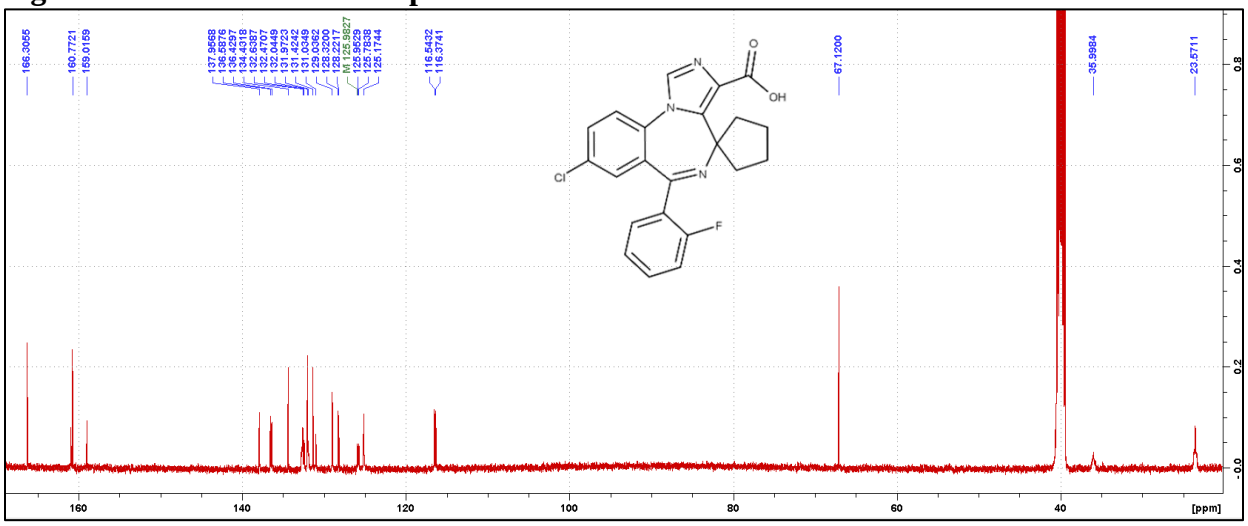

Figure 258: DAW-III-52 ^{19}F spectra:

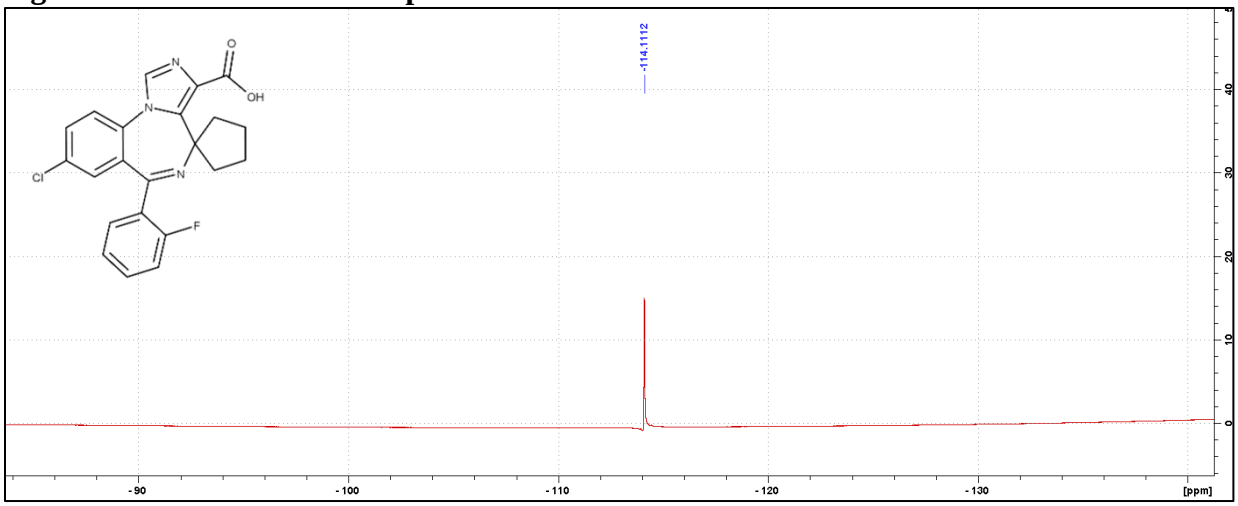

Figure 259: DAW-III-52 HPLC UV Chromatograph:

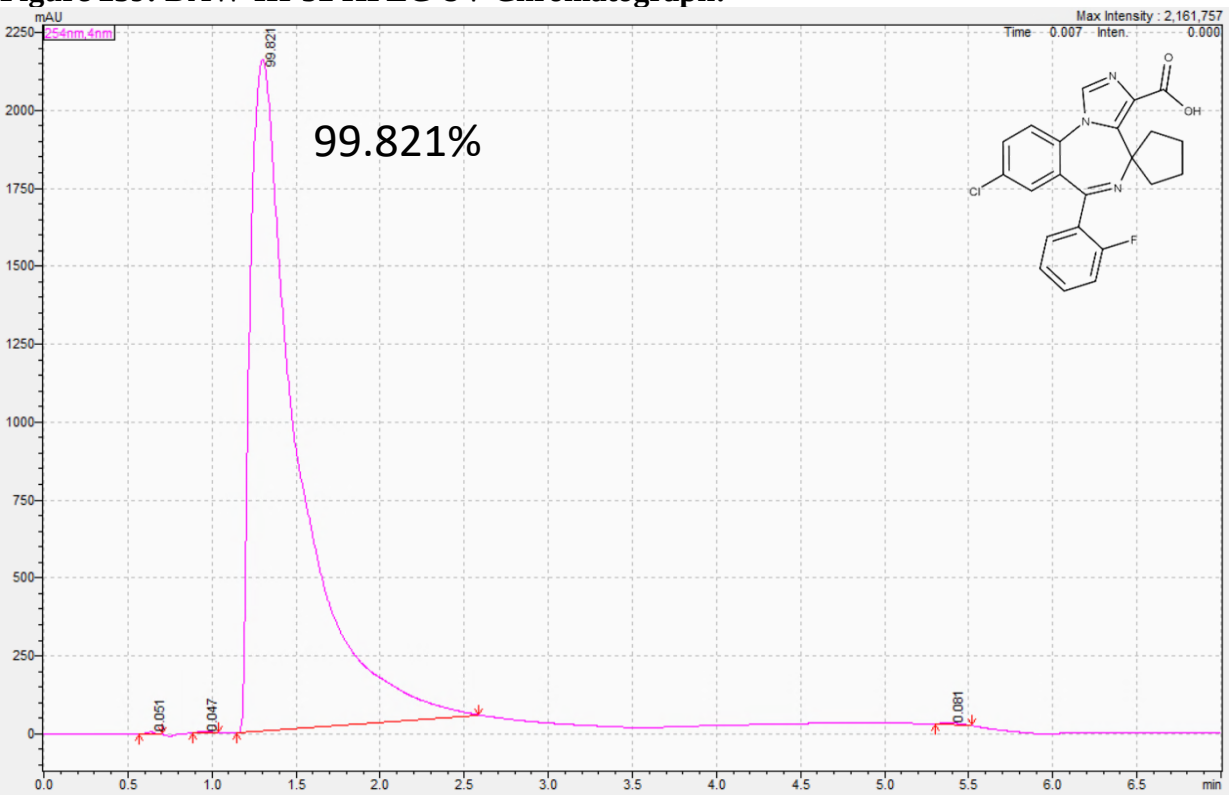

Figure 260: DAW-III-52 HRMS:

Score	Pred. (M)	Pred. m/z	Meas. m/z	Diff. (mDa)	Formulae (M)	Ion	Diff. (ppm)	Iso Score	DBE
55.54	409.09933	410.10661	410.10755	0.94	C22 H17 N3 O2 F Cl	[M+H]+	2.292	52.04	15.0

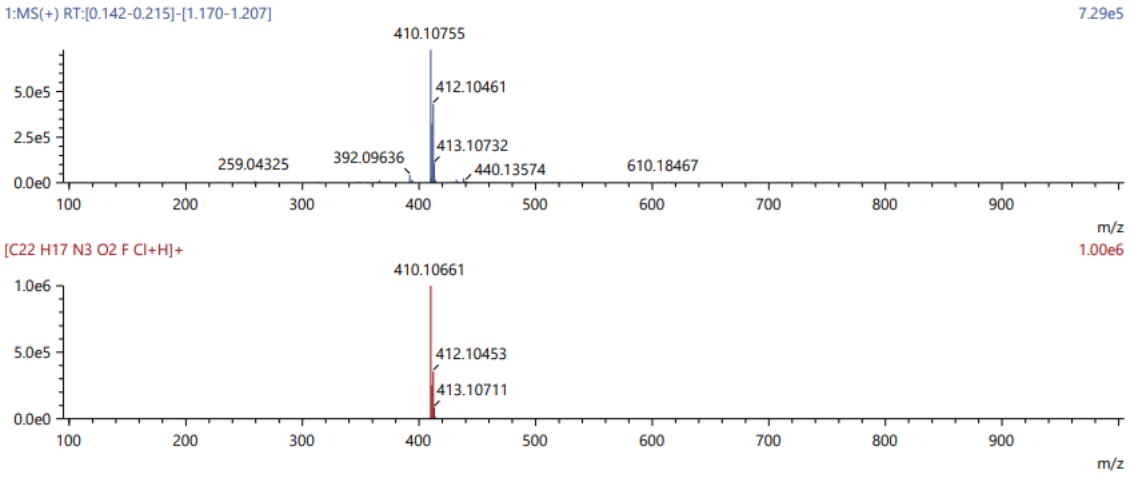

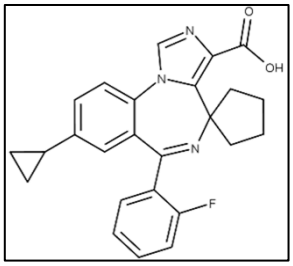

Synthesis of DAW-III-53: DAW-II-53 (196.2 g, 0.44 mmol) was dissolved in tetrahydrofuran (13.9 mL) and cooled to 0 °C. Solid sodium hydroxide was added (0.53 mg, 13.27 mmol), followed by the addition of H_2O (330 μL). The reaction was then removed from the ice bath and gently heated to 80 °C for 18 h. When all the starting material had dropped to the baseline via TLC (100% EtOAc), the reaction was cooled to room temperature. Acetic acid was added until the pH was observed to be ~5, and the reaction was then warmed to 50 °C and allowed to stir for 20 h. The reaction was then concentrated to dryness under reduced pressure. The residue was dissolved in H_2O (3.5 mL) and portioned into 0.5 mL fractions. To each fraction was added an additional 1 mL of H_2O causing the desired product to precipitate out of solution. The fractions were centrifuged and the solution was decanted. The solid fractions were combined and washed with an additional 6 mL of H_2O to remove any residual acetic acid. The product was then collected by filtration to yield a white powder. No further purification was conducted. (121.0 mg, 65.8%): ^{1}H NMR (500 MHz, d_6-DMSO) δ 8.22 (s, 1H), 7.73-7.71 (d, *J* = 8.35, 1H), 7.55-7.49 (m, 2H), 7.32-7.29 (m, 2H), 7.23-7.20 (m, 1H), 6.93-6.92 (m, 1H), 2.56 (m, 1H), 2.48 (m, 1H), 1.96-1.91 (m, 1H), 1.77 (m, 2H), 1.61-1.47 (m, 4H), 0.96-0.95 (m, 2H), 0.65-0.63 (m, 2H); ^{13}C NMR (126 MHz, d_6-DMSO) δ 166.62 (s), 162.04 (s), 160.05 (d, $^{1}J_{CF}$ = 248.18 Hz), 143.65 (s), 137.59 (s), 136.05 (s), 135.89 (s), 133.13 (s), 132.35 (s), 131.91 (s), 129.61 (s), 128.97 (d, $^{3}J_{CF}$ = 12.54 Hz), 128.42 (s), 127.03 (d, $^{3}J_{CF}$ = 13.99 Hz), 125.03 (d, $^{3}J_{CF}$ = 3.92 Hz), 123.72 (d, $^{2}J_{CF}$ = 15.89 Hz), 116.35 (d, $^{2}J_{CF}$ = 21.26 Hz), 67.00 (s), 35.74 (s), 23.54 (s), 15.07 (s), 14.95 (s), 10.63 (s), 10.30 (s); ^{19}F NMR (471 MHz, d_6-DMSO) δ -114.06; HRMS (ESI/Q-TOF): *m/z* $[M + H]^+$ calcd for $C_{25}H_{22}FN_3O_2$: 416.17688; found: 416.17786; HPLC Purity: 99.67%.

Figure 261: DAW-III-53 ^{1}H spectra:

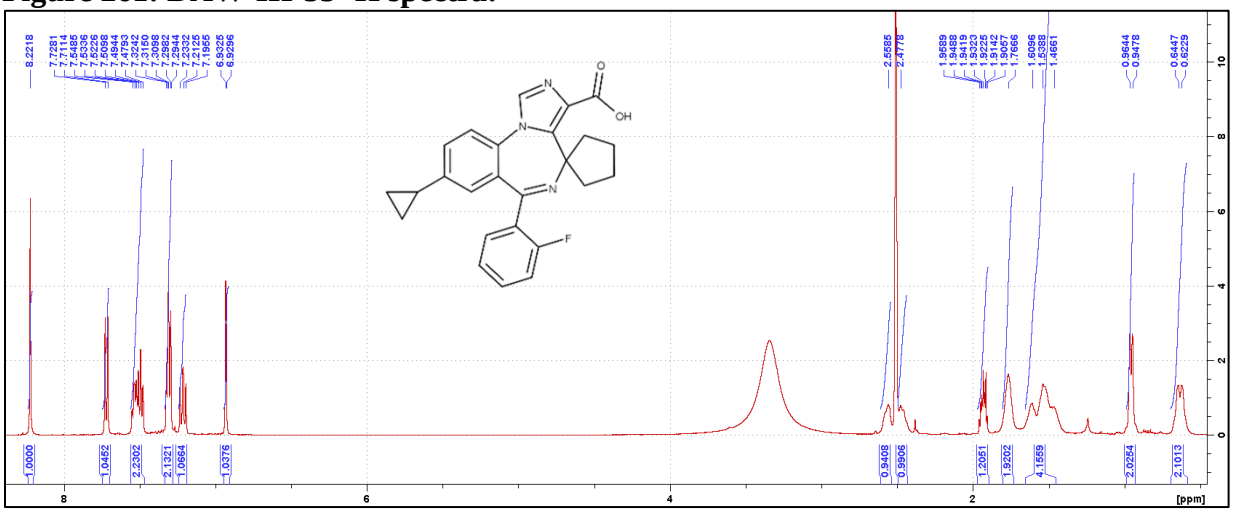

Figure 262: DAW-III-53 ^{13}C spectra:

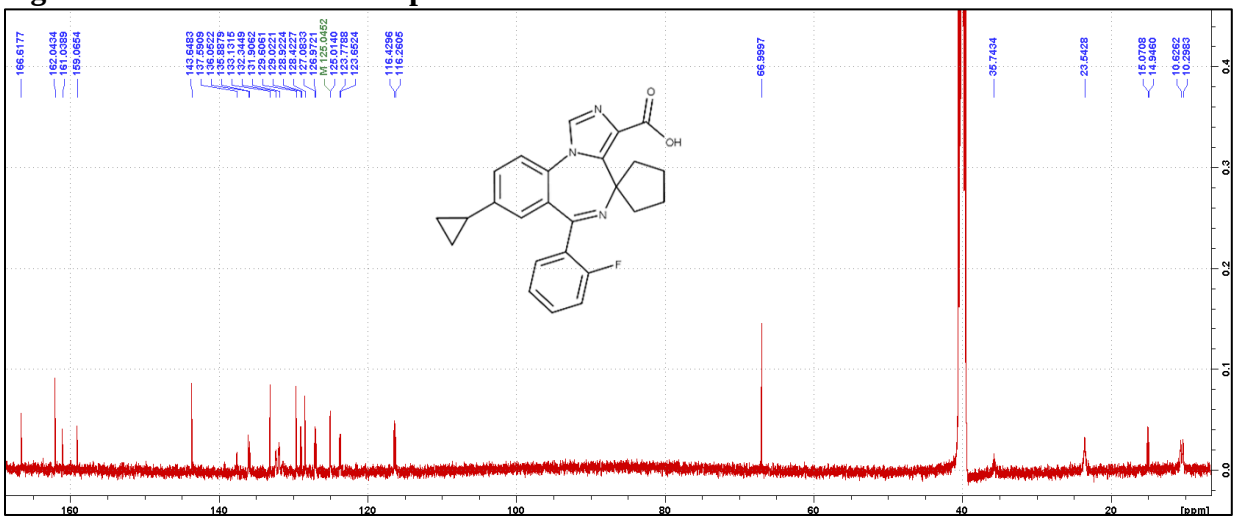

Figure 263: DAW-III-53 ^{19}F spectra:

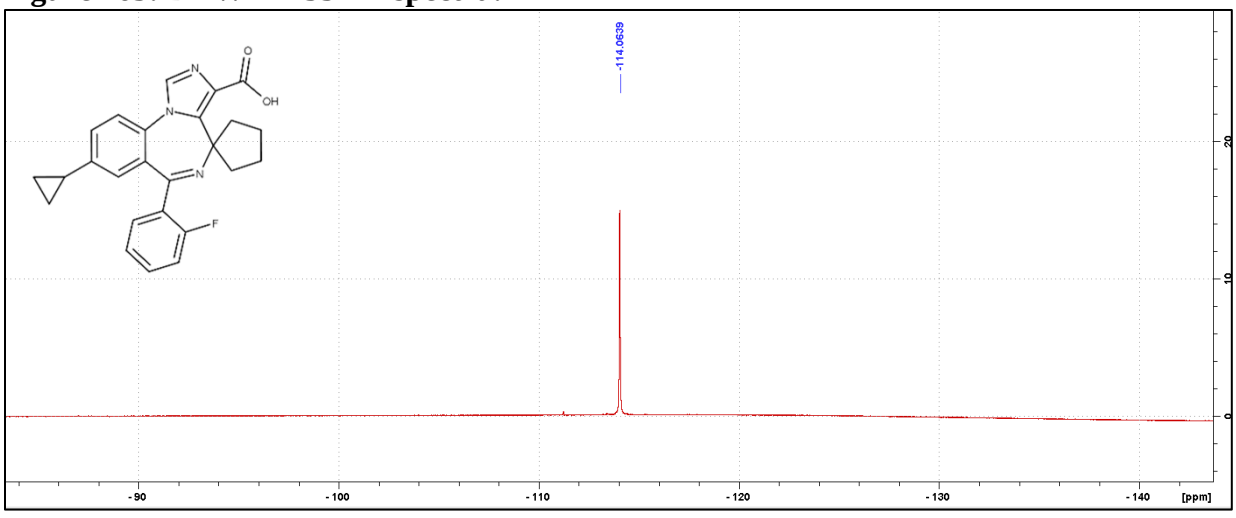

Figure 264: DAW-III-53 HPLC UV Chromatograph:

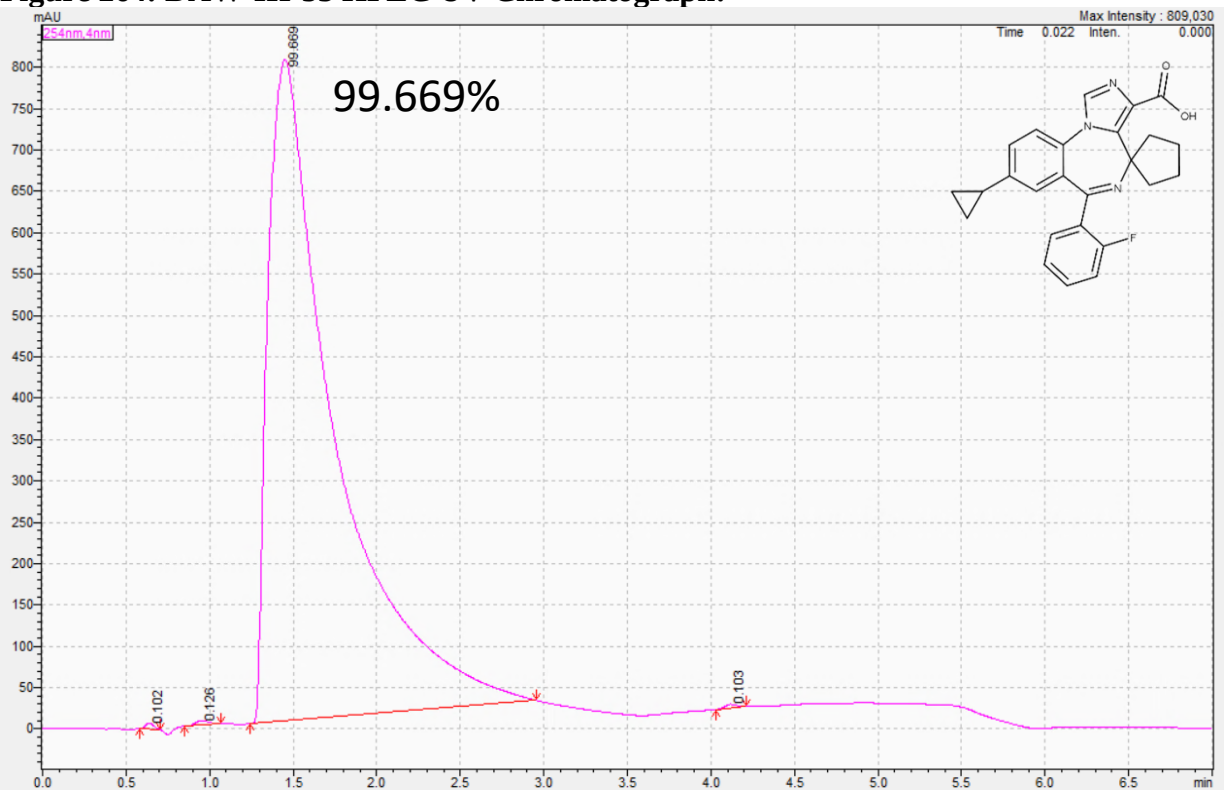

Figure 265: DAW-III-53 HRMS:

Score	Pred. (M)	Pred. m/z	Meas. m/z	Diff. (mDa)	Formulae (M)	Ion	Diff. (ppm)	Iso Score	DBE
52.60	415.16961	416.17688	416.17786	0.98	C25 H22 N3 O2 F	[M+H]+	2.355	48.82	16.0

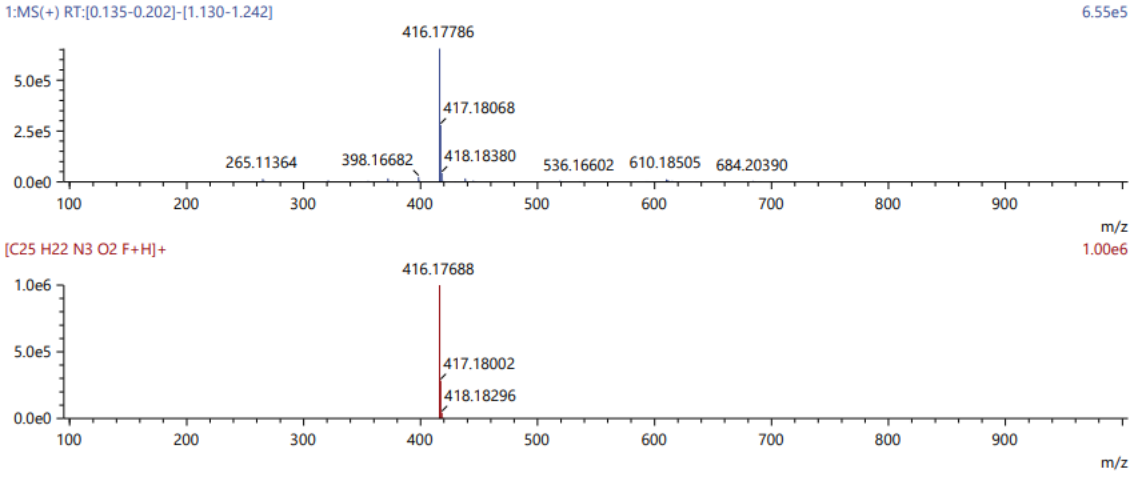

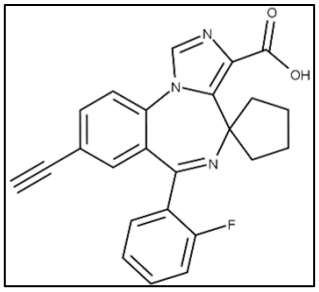

Synthesis of DAW-III-55: DAW-II-55 (529.1 mg, 1.24 mmol) was dissolved in tetrahydrofuran (37.5 mL) and cooled to 0 °C. Solid sodium hydroxide was added (1.49 g, 37.12 mmol), followed by the addition of H_2O (889.7 μL). The reaction was then removed from the ice bath and gently heated to 80 °C for 18 h. When all the starting material had dropped to the baseline via TLC (100% EtOAc), the reaction was cooled to room temperature. Acetic acid was added until the pH was observed to be ~5, and the reaction was then warmed to 50 °C and allowed to stir for 20 h. The reaction was then concentrated to dryness under reduced pressure. The residue was dissolved in H_2O (6 mL) and portioned into 0.5 mL fractions. To each fraction was added an additional 1 mL of H_2O causing the desired product to precipitate out of solution. The fractions were centrifuged and the solution was decanted. The solid fractions were combined and washed with an additional 15 mL of H_2O to remove any residual acetic acid. The product was then collected by filtration to yield a white powder. No further purification was conducted. (276.8 mg, 56.0%): ^{1}H NMR (500 MHz, d_6-DMSO) δ 8.27 (s, 1H), 7.89-7.87 (d, *J* = 8.4 Hz, 1H), 7.81 (dd, *J* = 3.40, 1.85 Hz, 1H), 7.56-7.50 (m, 2H), 7.34-7.30 (dt, *J* = 3.17, 0.85 Hz, 1H), 7.24-7.23 (m, 1H), 7.20-7.19 (m, 1H), 4.35 (s, 1H), 2.55 (m, 1H), 1.77 (m, 2H), 1.62-1.48 (m, 5H); ^{13}C NMR (126 MHz, d_6-DMSO) δ 167.09 (s), 161.01 (s), 159.98 (d, $^{1}J_{CF}$ = 248.03 Hz), 136.02 (s), 135.75 (s), 135.48 (s), 132.68 (s), 132.55 (d, $^{3}J_{CF}$ = 8.40 Hz), 131.98 (d, $^{4}J_{CF}$ = 2.19 Hz), 130.05 (s), 128.64 (d, $^{2}J_{CF}$ = 12.63 Hz), 125.14 (d, $^{3}J_{CF}$ = 3.09 Hz), 124.26 (s), 120.80 (s), 116.40 (d, $^{2}J_{CF}$ = 21.29 Hz), 83.25 (s), 82.14 (s), 67.12 (s), 36.09 (s), 23.56 (s); ^{19}F NMR (471 MHz, d_6-DMSO) δ -114.22; HRMS (ESI/Q-TOF): *m/z* $[M + H]^+$ calcd for $C_{24}H_{18}FN_3O_2$: 400.14558; found: 400.14649; HPLC Purity: 99.71%.

Figure 266: DAW-III-55 ^{1}H spectra:

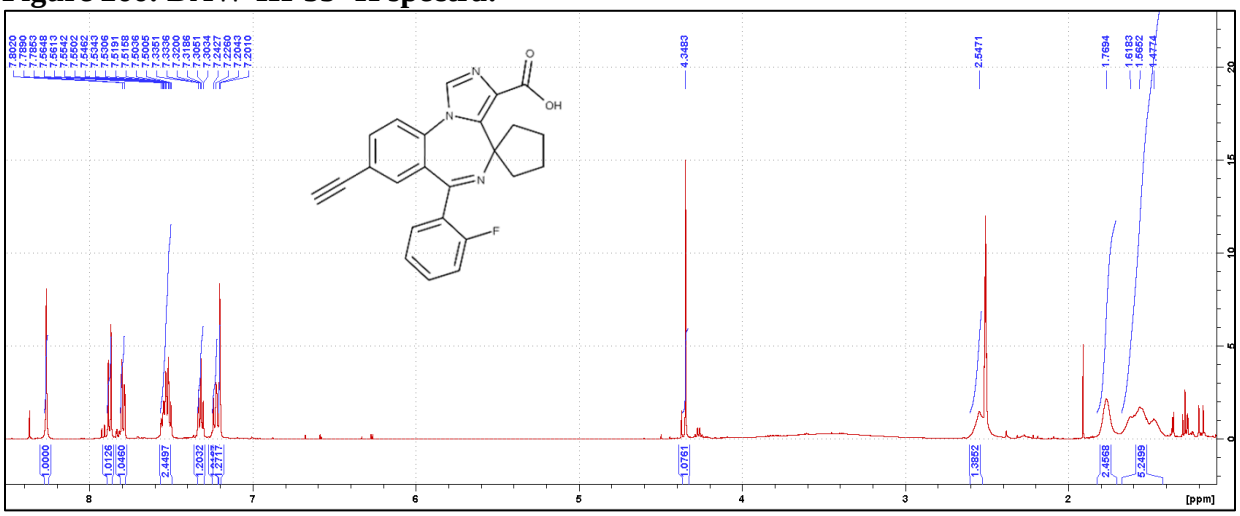

Figure 267: DAW-III-55 ^{13}C spectra:

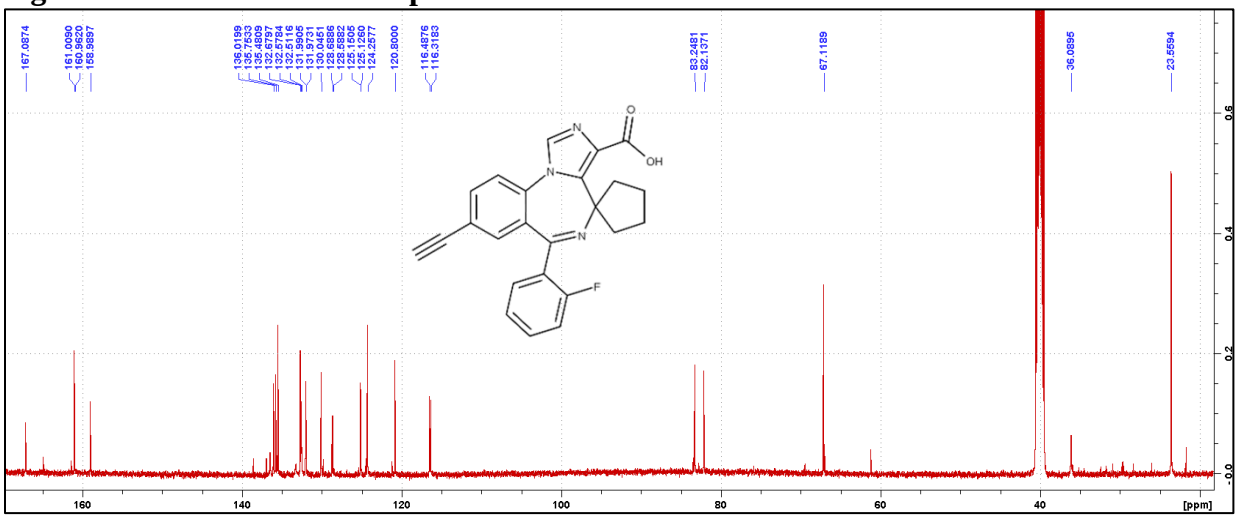

Figure 268: DAW-III-55 ^{19}F spectra:

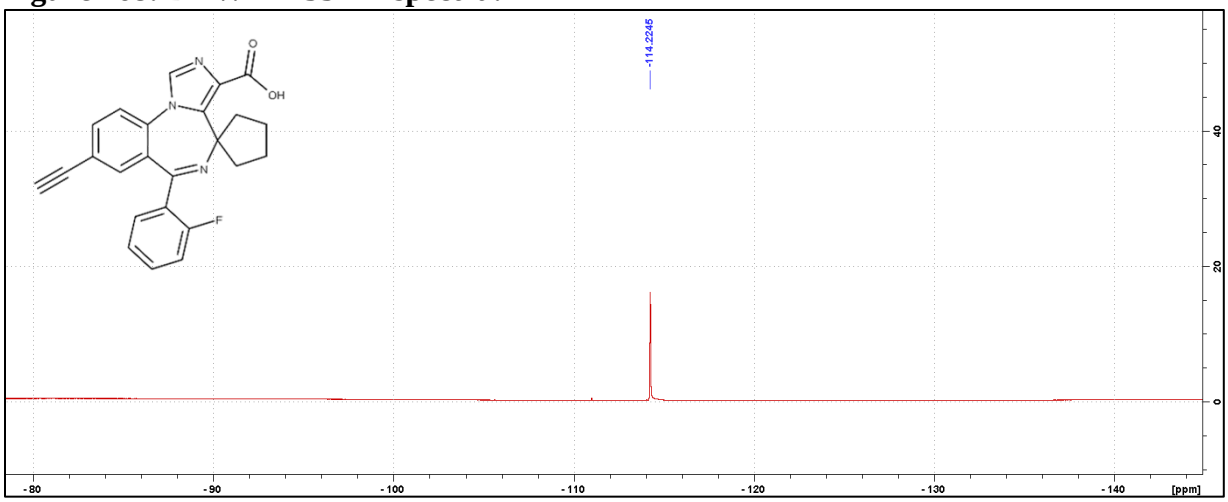

Figure 269: DAW-III-55 HPLC UV Chromatograph:

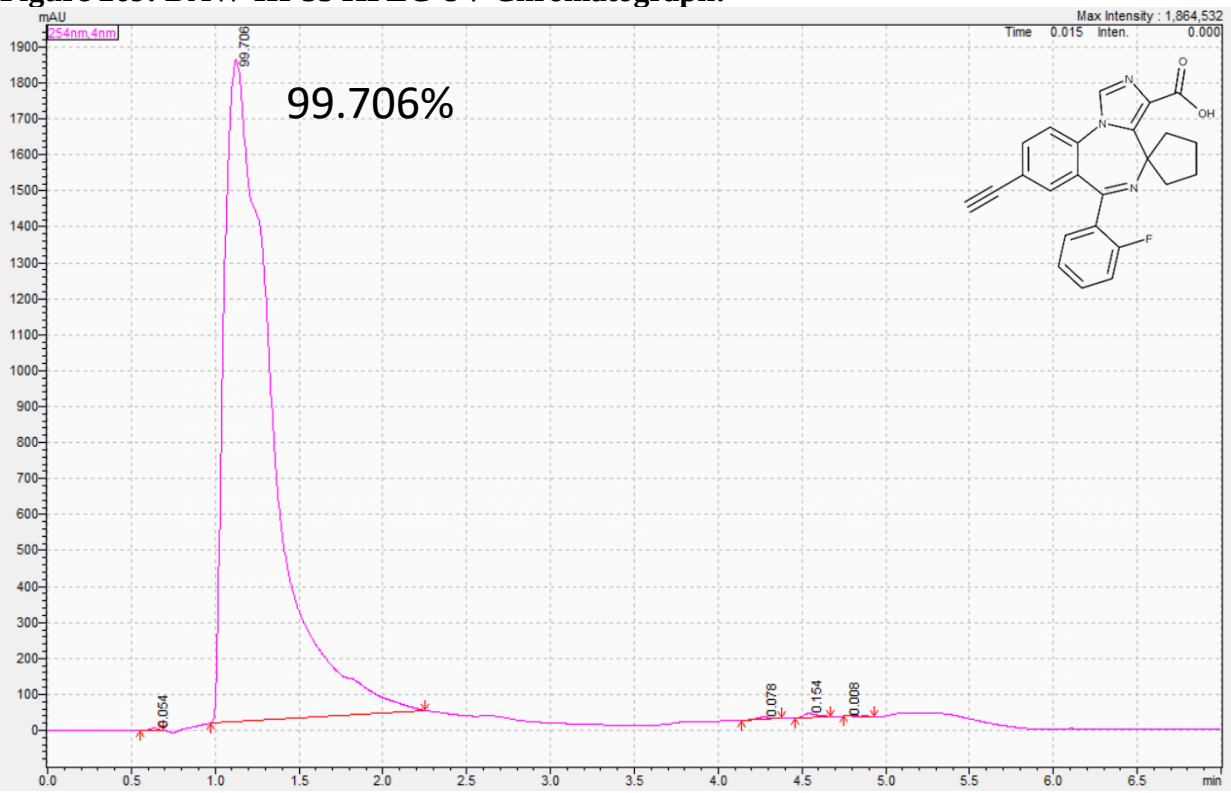

Figure 270: DAW-III-55 HRMS:

Score	Pred. (M)	Pred. m/z	Meas. m/z	Diff. (mDa)	Formulae (M)	Ion	Diff. (ppm)	Iso Score	DBE
59.99	399.13830	400.14558	400.14649	0.91	C24 H18 N3 O2 F	[M+H]+	2.274	56.96	17.0

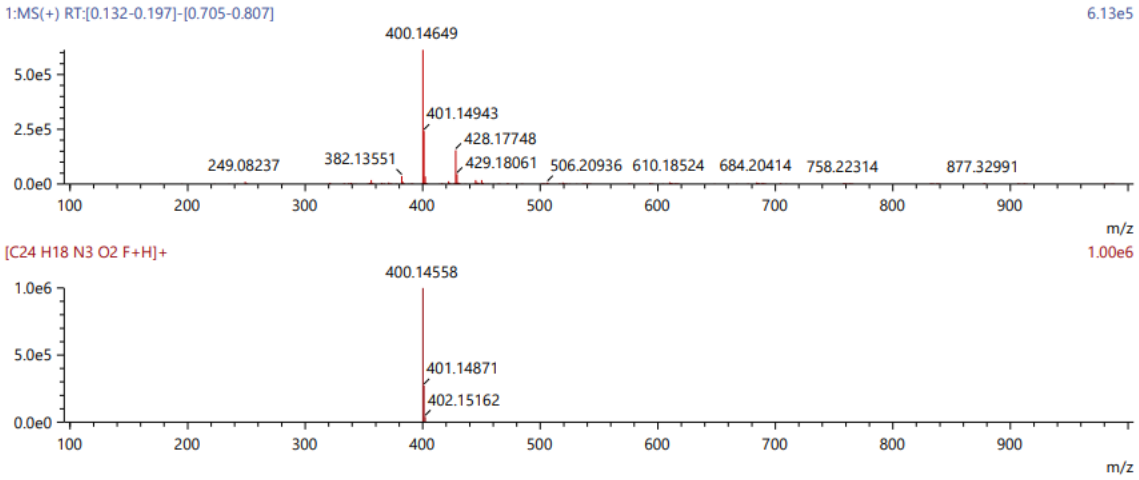

Figure 271: DAW-I-10 BZP rat brain site dose response:

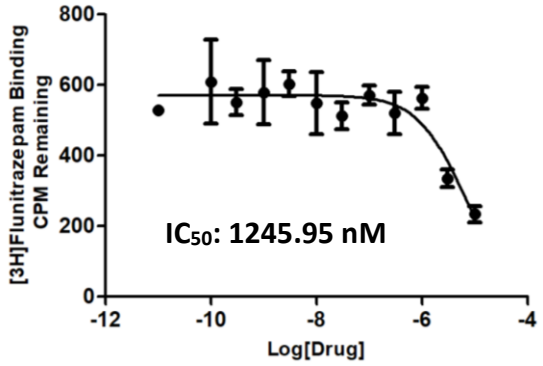

Figure 272: DAW-I-20 BZP rat brain site dose response:

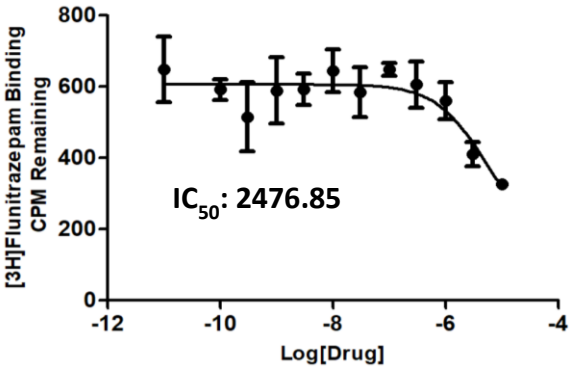

Figure 273: DAW-I-70 BZP rat brain site dose response:

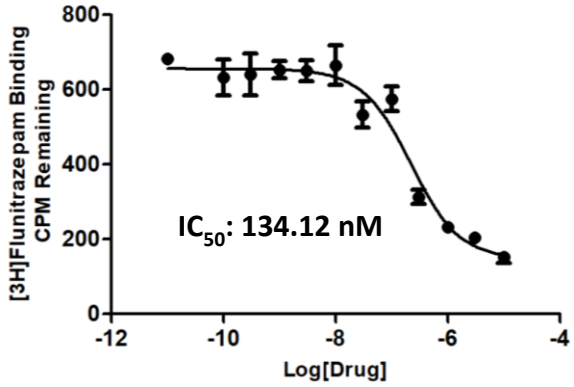

Figure 274: DAW-I-30 BZP rat brain site dose response:

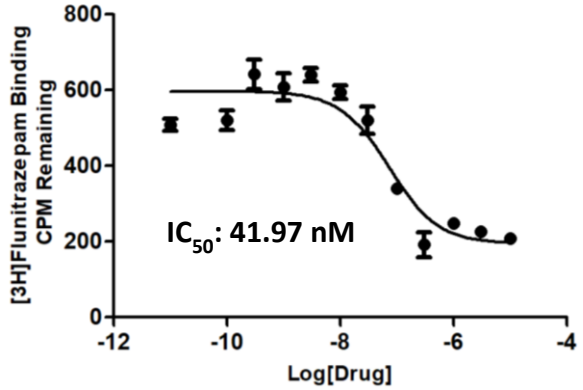

Figure 275: DAW-I-40 BZP rat brain site dose response:

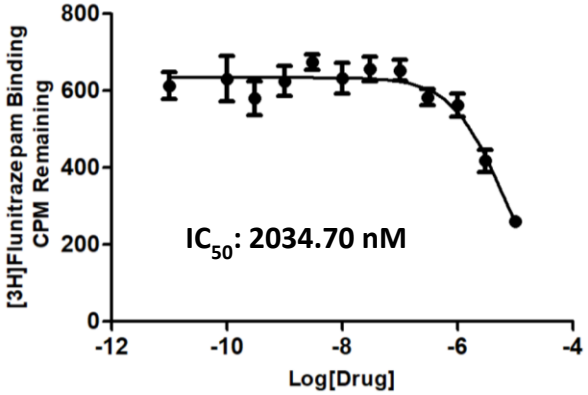

Figure 276: DAW-I-32 BZP rat brain site dose response:

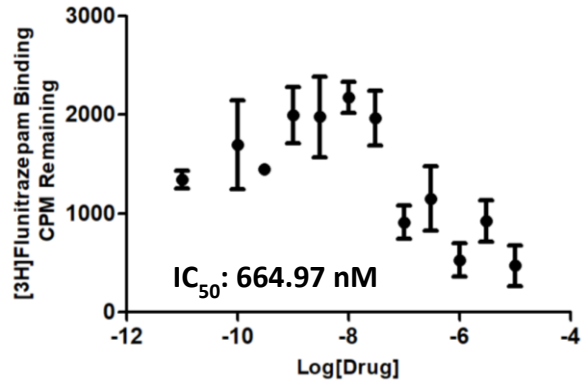

Figure 277: DAW-I-80 BZP rat brain site dose response:

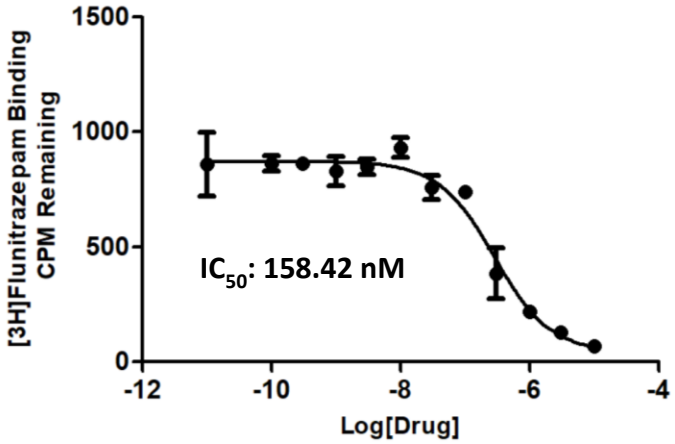

Figure 278: DAW-II-10 BZP rat brain site dose response:

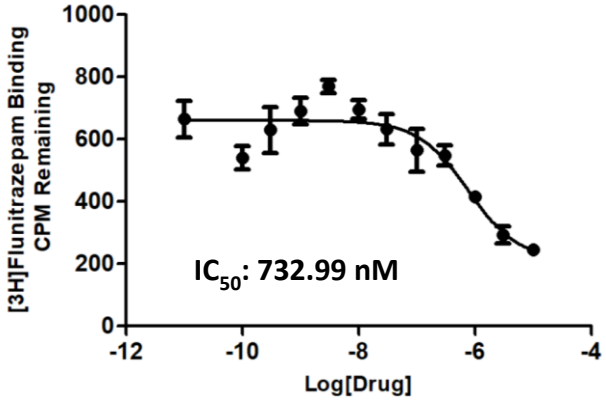

Figure 279: DAW-II-70 BZP rat brain site dose response:

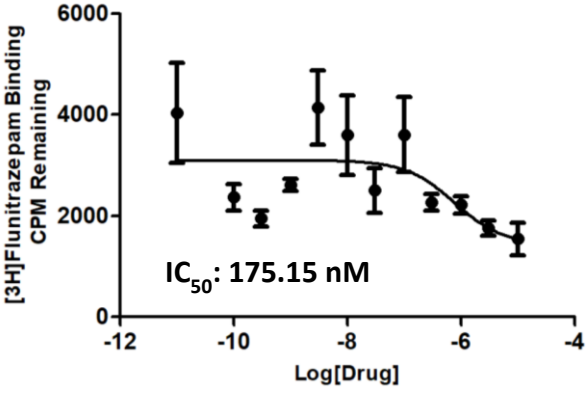

Figure 280: DAW-II-30 BZP rat brain site dose response:

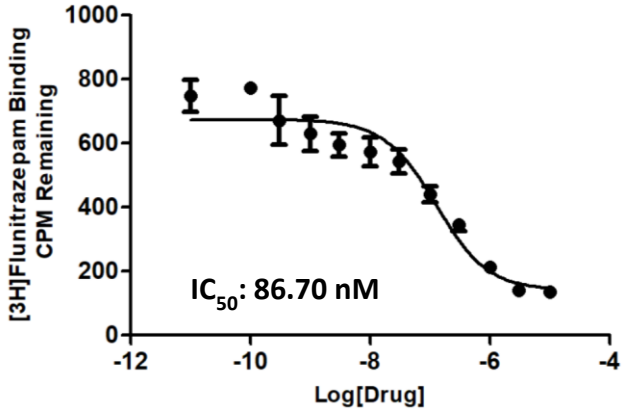

Figure 281: DAW-II-40 BZP rat brain site dose response:

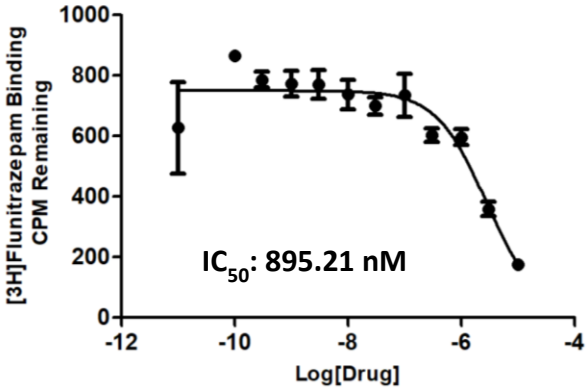

Figure 282: DAW-II-60 BZP rat brain site dose response:

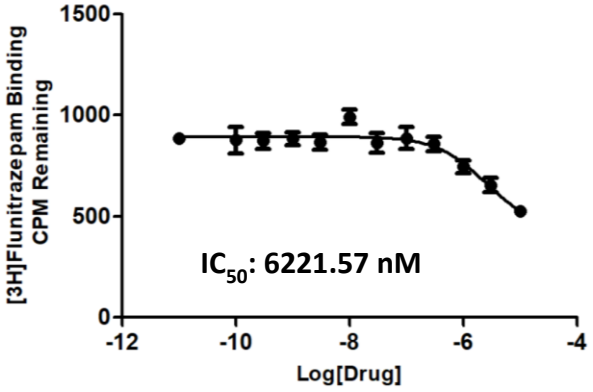

Figure 283: DAW-II-80 BZP rat brain site dose response:

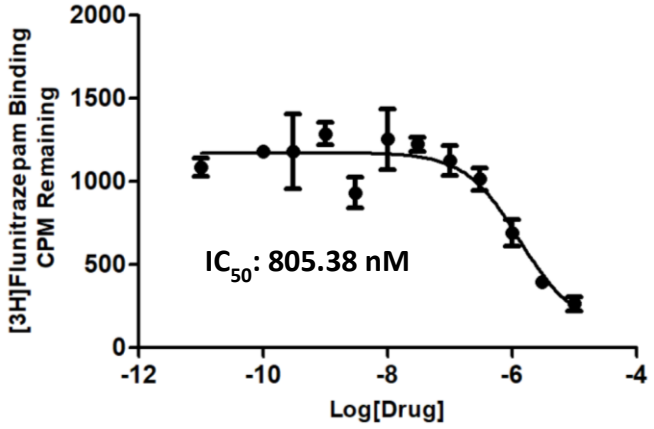

Figure 284: DAW-II-35 BZP rat brain site dose response:

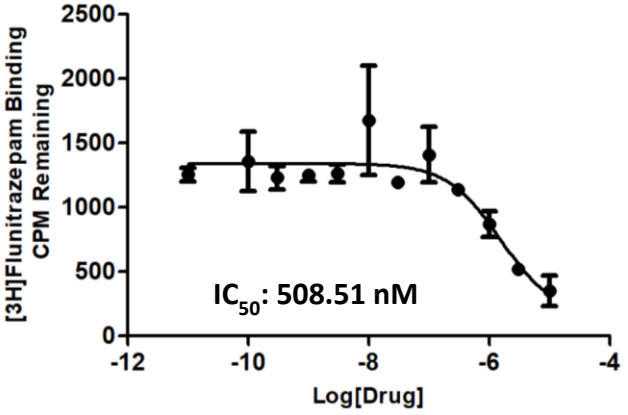

Figure 285: DAW-III-10 BZP rat brain site dose response:

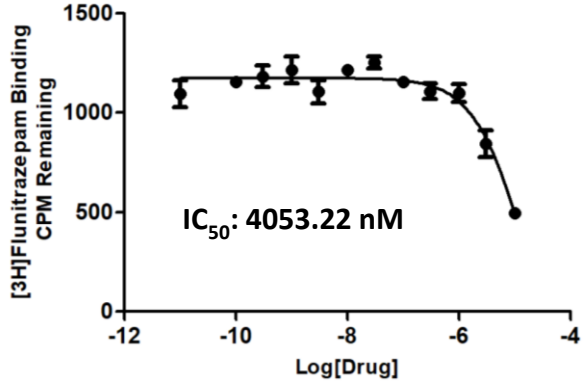

Figure 286: DAW-III-70 BZP rat brain site dose response:

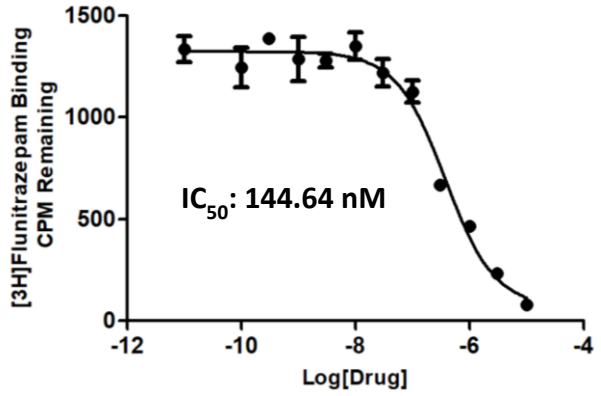

Figure 287: DAW-III-30 BZP rat brain site dose response:

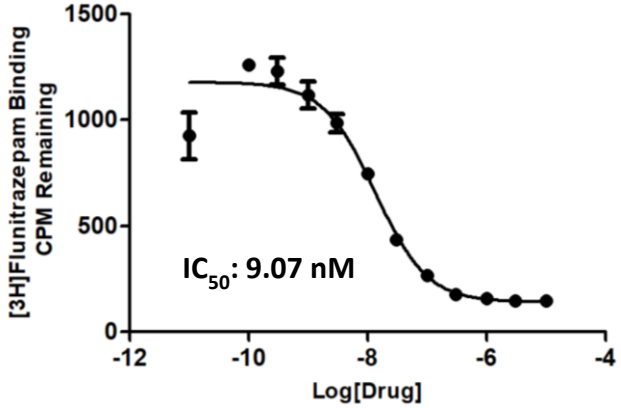

Figure 288: DAW-III-40 BZP rat brain site dose response:

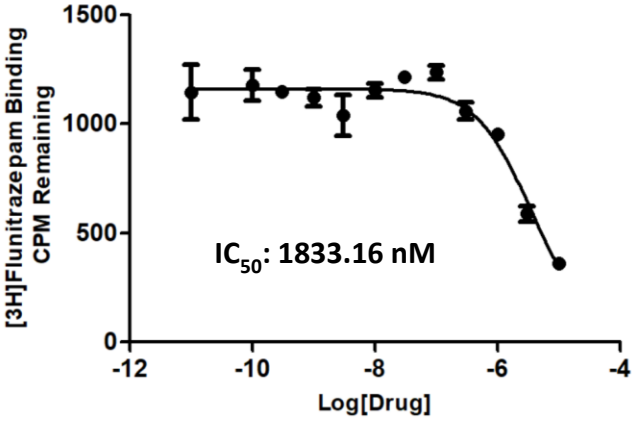

Figure 289: DAW-III-35 BZP rat brain site dose response:

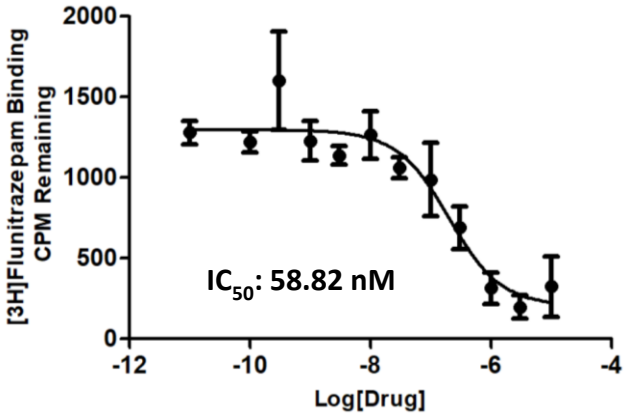

Figure 290: DAW-III-33 BZP rat brain site dose response:

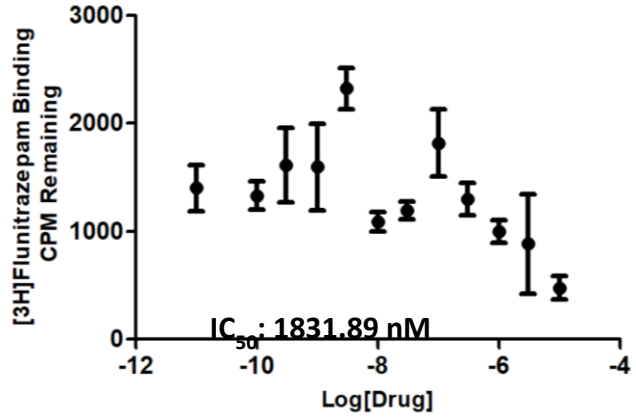

Figure 291: DAW-III-31 BZP rat brain site dose response:

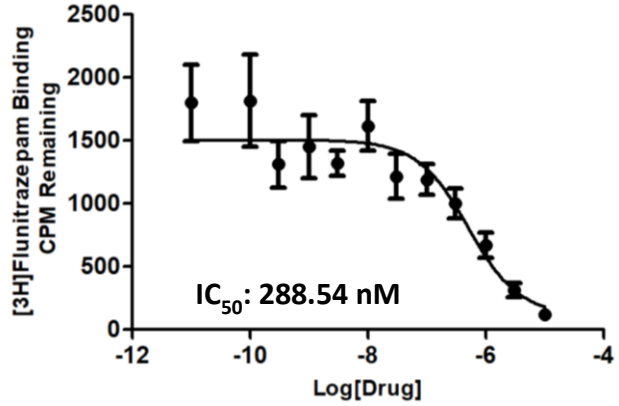

Figure 292: DAW-III-80 BZP rat brain site dose response:

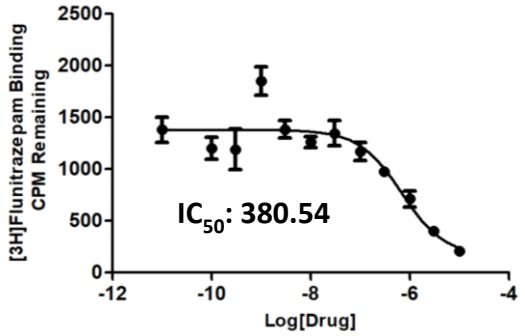

Figure 293: DAW-I-10, 70, 30, 40 cell viability concentration vs luminescence:

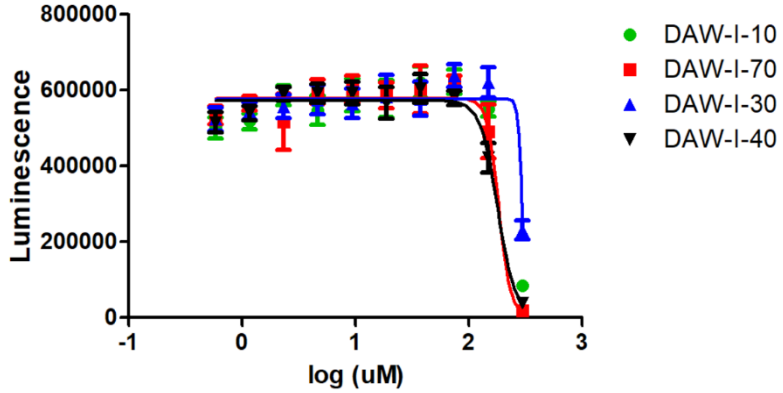

Figure 294: DAW-I-50, 60, 32 cell viability concentration vs luminescence:

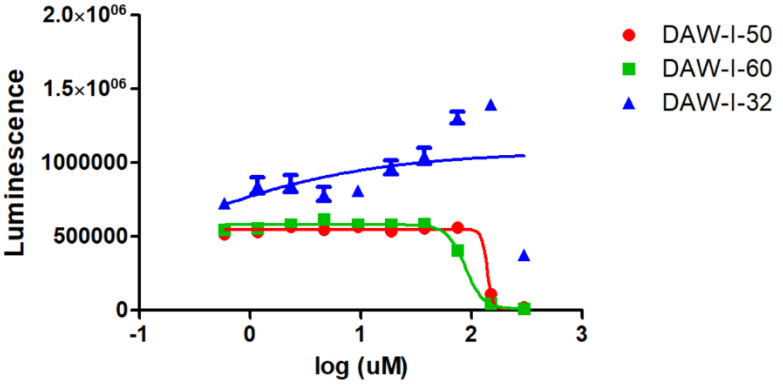

Figure 295: DAW-II-10, 70, 30, 40, 50 cell viability concentration vs luminescence:

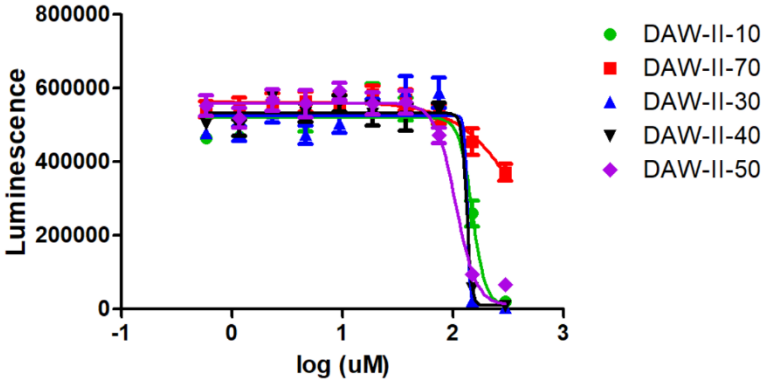

Figure 296: DAW-II-60, 32, 35, 33 cell viability concentration vs luminescence:

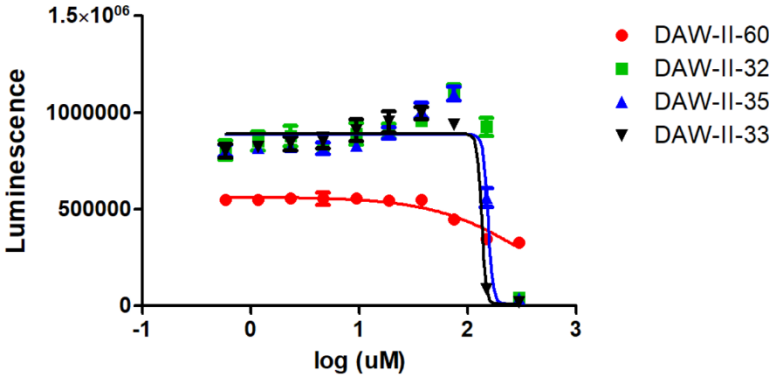

Figure 297: DAW-III-10, 70, 30, 40, 50 cell viability concentration vs luminescence:

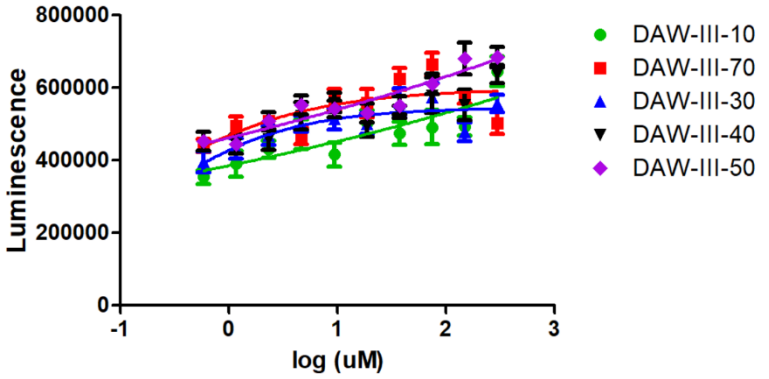

Figure 298: DAW-III-60, 32, 35, 33, 31 cell viability concentration vs luminescence:

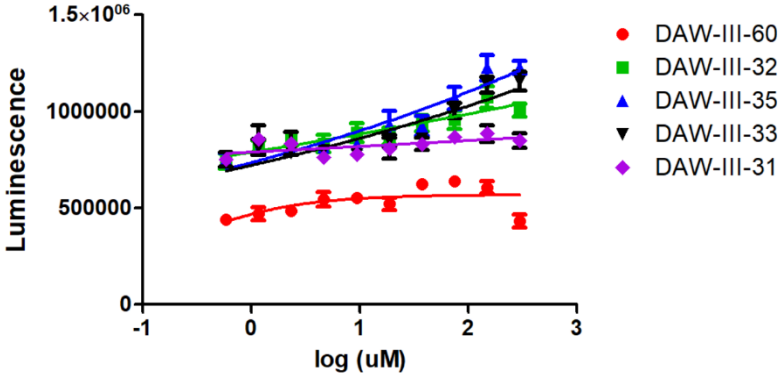

Figure 299: DAW-I-20, 80, DAW-II-20, 80, DAW-III-20, 80 cell viability concentration vs luminescence:

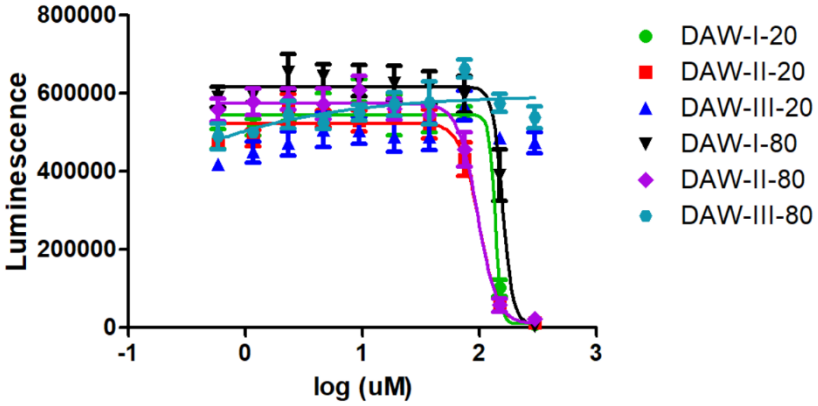

Figure 300: DAW-I-52, DAW-II-52, 53, 55 cell viability concentration vs luminescence:

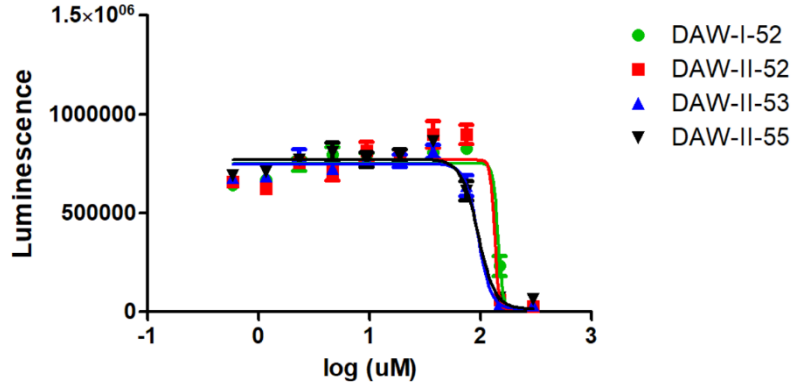

Figure 301: DAW-III-51, 52, 53, 55 cell viability concentration vs luminescence:

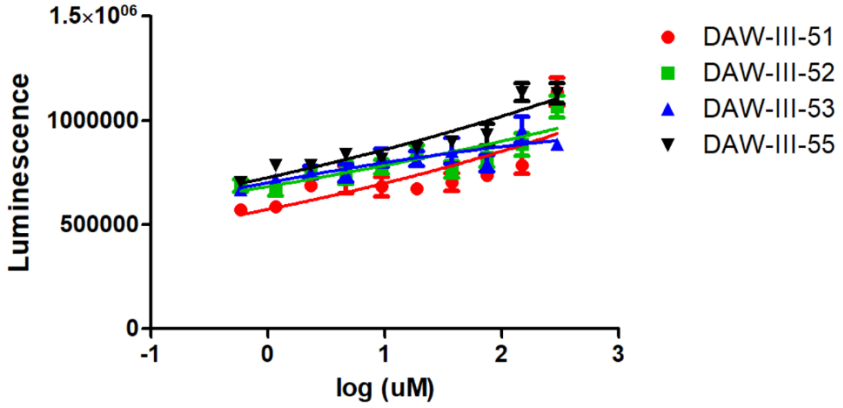

2.8 Large Scale Synthesis of MIDD0301 and PI560: Discussion and Synthetic Methods

2.8.1 Discussion

Due to the need of an effective non-steroidal oral treatment for asthma, MIDD0301 was developed as a novel asthma medication that specifically targets α_5-GABA$_A$Rs in airway smooth muscle (ASM) and inflammatory cells.[200] Building upon the foundational synthetic work by the

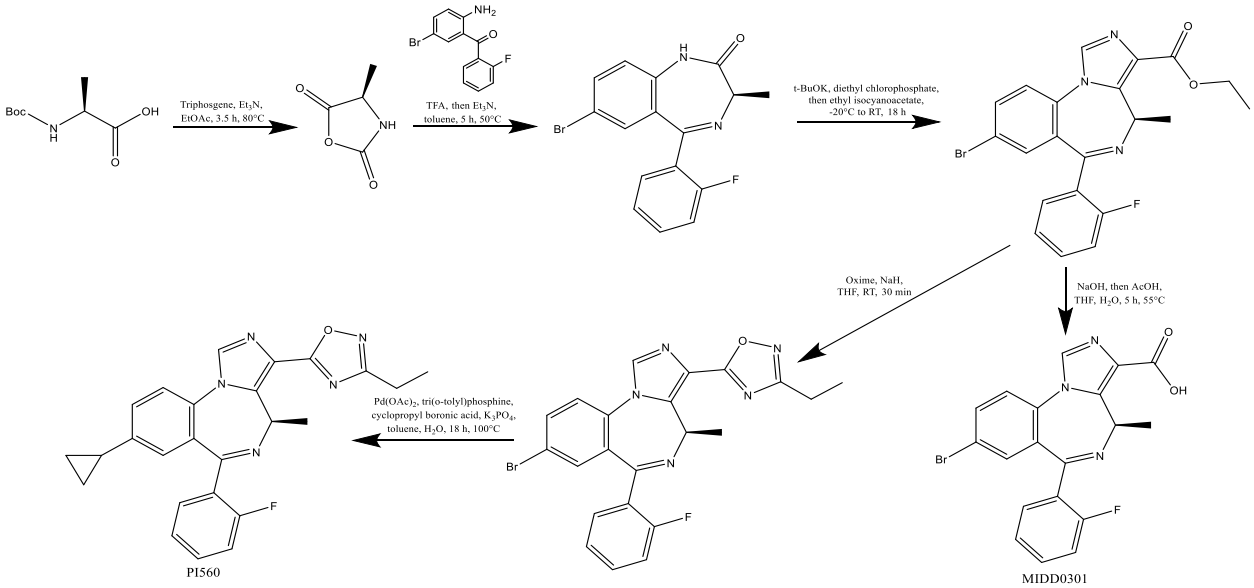

Scheme 8: Scalable synthetic route of MIDD0301 and PI560

Cook group, MIDD0301 underwent three critical structural modifications to enhance its potential as a leading candidate for asthma treatment.[201] MIDD0301 functions as an allosteric $GABA_AR$ agonist and has demonstrated its ability to alleviate asthmatic symptoms in animal models through oral administration. Importantly, the introduction of a chiral R-CH_3 group improved metabolic stability, while the incorporation of a 2'F substituent increased its potency. Additionally, the presence of a carboxylic acid function significantly reduced its ability to cross the blood-brain barrier (BBB) while retaining its ability to reach cells of the lungs as an oral medication.

The process of developing a scalable synthesis is necessary for any clinical drug candidate as a successful drug would need to be produced on the kilogram scale. Extensive work in the scale up synthesis of clinical asthma drug candidate MIDD0301 has been conducted by Knutson, et. al.[202]. To obtain enough material to conduct *in vivo* atopic dermatitis studies as well as other relevant pre-clinical studies, the procedures outlined by Knutson, et. al. were followed with small modifications in order to obtain roughly 200 g of MIDD0301. Furthermore, PI560 (aka GL-IV-03) is an imidazobenzodiazepine containing an oxadiazole ring that has previously been evaluated for its ability to reduce nitric oxide production,[203] as well as being screened for receptor binding.[204] Currently PI560 is also being evaluated for the oral treatment of asthma as well as atopic dermatitis. Both MIDD0301 and PI560 are structurally related and therefore much of the synthesis could be conducted with the same methods.[204] However, the final two steps in the synthesis of PI560 follow different synthetic methods and have previously not been scaled past approximately 15 g reactions. Following optimization of the reaction methods, the synthesis of PI560 was successfully scaled to greater than 100 g reaction sizes to obtain roughly 200 g of PI560.

The synthetic scheme for MIDD0301 and PI560 is outlined in Scheme 8. The synthesis started with a BOC protected D-alanine which was converted to the corresponding amino acid N-

carboxyanhydride (NCA). This process was done with triphosgene and triethylamine in ethyl acetate. This synthesis could also be conducted with phosgene and the non-protected amino acid, however, due to triphosgene being a crystalline solid and phosgene being a highly hazardous gas, we found that triphosgene is much easier to work with. Furthermore, we have found that using the BOC protected amino acid rather than the free amino acid results in higher yields. This reaction could be conducted successfully on a 300 g scale using a 5 L RB flask. The reaction was successfully run at a 500 g scale, however, slight overheating during the addition of the triethylamine and a large amount of off gassing made this reaction difficult and resulted in lower yields. Therefore, it would only be recommended to scale up this reaction past 300 g if the appropriate equipment is used. The first step of this reaction involved dissolving the protected alanine in ethyl acetate. Often the starting material would not fully dissolve until the triphosgene was added. This was followed by the dropwise addition of triethylamine. It was necessary to conduct the triethylamine addition very carefully as this step produced a small amount of phosgene gas which is very hazardous. If necessary, this gas can be trapped using a methanolic scrubber system. This step produced a white precipitate in the reaction which is known to be a triethylamine-HCl salt. During the triethylamine addition, the reaction would ideally be kept under 30 °C. However, due to the hazardous phosgene gas being produced, it would have been difficult and hazardous to begin with the reaction in an ice bath and then switch to a heating mantle once heating was required. Therefore, the triethylamine was added slow enough such that the reaction was prevented from overheating. The reaction temperature was monitored internally with a thermometer, and the reaction could often be kept under 40 °C, and at this temperature, no detrimental effects to the yield or product purity were observed. For future work, a jacketed flask could be employed for easier and safer control over the temperature. Once all the reagents were

added, the reaction was brought to reflux. It was determined that refluxing for approximately 3 h was the ideal time to produce as much product as possible without the production of too many impurities. Once complete, the reaction was cooled and the precipitate was filtered. The reaction was then concentrated, however, upon reaching near dryness, a white powder began to precipitate. Upon NMR analysis this precipitate appeared to be alanine. This alanine could have come from a small amount of BOC-alanine becoming deprotected during the reaction, or it could be an impurity in the purchased BOC-alanine as the material is listed as 99% pure and approximately 3 g of this alanine was usually collected from a 300 g reaction. This impurity could be removed by filtration to allow for easier purification of the desired product. Once concentrated to dryness, a small amount of DCM could be added which was often enough to recrystallize the desired product at -20 °C, however, hexanes could be added if no crystal formed. One would have to be cautious not to add too much hexanes, which could result in the formation of an oil. The desired product could be isolated in multiple crops of crystals which as many as 5 crops being collected per reaction, however, the purity of the product diminishes greatly after the third crop.

The second step of this synthesis involves the coupling of the synthesized NCA to a commercially available aniline. The reactivity of the NCA allows for easy coupling under acidic conditions, followed by cyclization to yield the 7-membered benzodiazepine ring under basic conditions. As outlined by Knutson, et. al., it is possible to synthesize this benzodiazepine via coupling the aniline directly to BOC-D-alanine using various coupling agents such as N,N'-dicyclohexylcarbodiimide (DCC) and 1-ethyl-3-(3-dimethylaminopropyl)carbodiimide (EDC). While this process does not involve the use of the NCAs, the coupling and subsequent cyclization is done as two separate reactions with a work-up in between. Therefore, due to both synthetic routes involving multiple steps, and comparable yields for each pathway, these routes would likely

be comparable in both time and cost of materials. The first step of the coupling reaction was done with the NCA was completed with TFA as the acid, and no further conversion to the intermediate was observed after 4 h. The reaction was then neutralized with a slight excess of triethylamine and the reaction intermediate was often fully converted to the cyclized product within 2 h. Due to similar TLC retention factors, full consumption of the intermediate to the final product was often confirmed via mass spectrometry. Full cyclization often occurred at 50 °C, however, to encourage complete and faster cyclization, the reaction could be gently heated to 70 °C. This increase in temperature proved to not affect the optical purity of the final product, however, one would likely have to be cautious about high temperatures due to the risk racemization. Upon completion of this reaction, the mixture was worked-up with washes of water, sodium bicarbonate, and brine. Interestingly, if this reaction was conducted on a 150 g scale, horrible emulsions occurred during the work-up that often-needed filtration, large amounts of extra solvent, or extra extractions to fully clear. However, if this reaction was run on a 300 g scale, no such emulsions were observed, and a clear biphasic mixture was observed in the separatory funnel after sitting for 15 min. This reaction was not scaled up past 300 g, however it would be expected that the work-up would remain or become easier the larger the scale. Purification of the desired product was accomplished via trituration with 10% ethyl acetate:heptane. Often two trituration's were required to obtain acceptable purity. These trituration's were conducted at room temperature as it was observed that under elevated temperatures, the product would sometimes clump into approximately 1 cm^2 sized balls which would have to be ground up and re-purified.

The next step of this synthesis involved the formation of the imidazole ring fused to the benzodiazepine. This reaction had to be conducted with oven dried glassware, performed under nitrogen, and anhydrous THF had to be used. Due to the first step of the reaction being a

deprotonation step with potassium *tert*-butoxide, and water present would cause this reaction to fail. This reaction was conducted on a scale of up to 215 g with the only limitation to scaling up larger being the flask size and cooling bath size, however, with the appropriate equipment, this reaction could easily be scaled much larger. Upon dissolving the starting material in THF, the mixture was cooled to -20 °C. This was found to be the optimum temperature as too warm would risk racemization and too cold would slow the rate of the reaction. However, successful deprotonation was indicated by the reaction turning a deep red upon addition of the base. This color usually began to persist once approximately ¾ of the base was added, and if this color change was not observed or the red color did not persist, the reaction was likely quenched by water stemming from the solvent or staring material. When using different benzodiazepine starting materials, the color change of the reaction upon deprotonation could range from a deep orange to a deep red, all of which signaled a successful deprotonation. Once significant time had passed for the deprotonation to occur, diethyl chlorophosphate was added to act as a leaving group. This was eventually followed by the addition of ethyl isocyanoacetate and potassium *t*-butoxide. Significant conversion was observed after 4 h once all reagents had been added, however, greater conversion was observed if the reaction was allowed to stir overnight for approximately 12 h after all reagents had been added. Once the reaction was complete, the work-up often did yield a significant emulsion, however it could always be cleared by sitting for a reasonable amount of time. Once the work-up was complete, the solvent was removed and the product was purified via a single trituration in 50% MTBE:Hex. This single trituration often yielded acceptable purity to carry forward with the synthesis, however, multiple trituration's could be conducted if needed.

From the synthesized ethyl ester, multiple routes could be taken to synthesize a variety of products. A simple hydrolysis yielded MIDD0301. The addition of an oxadiazole ring followed

by a Suzuki coupling yielded PI560. The hydrolysis was conducted with NaOH in a water:THF mixture and was often conducted on a 150 g scale. It was determined that the use of 4 eq of NaOH was sufficient to hydrolyze the ethyl ester while not racemizing the desired product. Full conversion of this reaction was often observed after approximately 5 h at 55 °C. Often the greater the scale for this reaction, the faster and more easily the reaction was completed. Small scale reactions would sometimes stall, and if this happened, one would have to be cautious in using more NaOH or more heat with the risk of racemizing the product. Once complete, the reaction was acidified to a pH of ~5 with AcOH and the THF was removed under reduced pressure. During the THF removal, there was a point at which the solution became cloudy followed by the precipitation of a sticky oil. It was at this point that the mixture was about to bump on the rotovap, and once the solution began to climb into the rotovap trap, the pressure should be released immediately as all or nearly all of the THF had been removed. A small amount of methanol was then added to the flask and the mixture was then stirred at 50 °C, followed by colling to RT to stir overnight. The desired product could then be filtered to yield a light tan solid. Purification could be conducted via a recrystallization in 200 proof ethanol which would yield the product as a white powder. Multiple crops could be collected to obtain the best yield possible.

For the synthesis of PI560, the ethyl ester was reacted with an ethyl oxime ((E)-N'-hydroxypropionimidamide) under basic conditions to afford the desired oxadiazole ring. This reaction had previously not been scaled past 15 g, therefore some R&D was needed to obtain acceptable yields. The first step of this reaction involves the deprotonation of the oxime with sodium hydride (NaH). This step as well as the entirety of the reaction needs to be kept very dry. Anhydrous THF is necessary as well as the addition of oven dried 3Å molecular sieves to the oxime flask to remove any residual water. The NaH could be added portion wise to the oxime,

followed by an hour of stirring at RT to ensure complete deprotonation. 1.1 eq of NaH was determined to be the ideal amount of NaH to ensure complete deprotonation but not allow significant formation of an unwanted 6H isomer of the methyl substituted imidazodiazepine. Minimization of the formation of the 6H isomer in this step proved to be difficult. Using the standard reaction conditions, approximately 13% of isolated products were the 6H isomer. Many trials were conducted in an effort to limit the formation of this byproduct including: using 0.7 eq of NaH, running the reaction at -20 °C, running the reaction at reflux, using potassium tert-butoxide as base, adding the ethyl ester solution to the oxime solution rather than the other way around per standard, using 1.5 eq of oxime rather than 4 eq, adding 1 eq of magnesium chloride to act as a weak Lewis acid, using carbonyldiimidazole (CDI) as a coupling agent. While all trials were successful in yielding product, they were all unsuccessful in limiting the formation of the 6H isomer. Next, numerous trials were conducted to remove the byproduct via trituration or purification. Numerous solvent systems were tested with some crystals being obtained in solutions of MeOH and EtOH, however, the crystals contained a mixture of the 6H isomer and the desired product. Therefore, it was determined that column chromatography would have to be used to successfully purify the desired product. It was determined to be the most efficient to run columns after the final step of the synthesis to avoid having to run multiple columns. Following the addition of all the reagents to this reaction, full conversion was often achieved between 30 min to 1.5 h. It is recommended that the reaction should be quenched as soon as full conversion is achieved to limit the formation of the 6H isomer. It is not recommended that this reaction be run overnight. After work-up, the crude product can be triturated in a 50% MTBE:Hex mixture in order to remove all impurities except for the 6H isomer. Upon optimization, this reaction could successfully be run on a 115 g scale with further scale-up likely very possible.

The final step in the PI560 synthesis involves a Suzuki coupling to add the cyclopropane ring in place of the bromine. This reaction utilized palladium acetate as a catalyst and tri(o-tolyl)phosphine as a ligand. Cyclopropyl boronic acid was used as boronic acid to install the cyclopropane group. The solvent mixture of toluene and water had to be degassed by bubbling nitrogen through the solution for 40 min. Once degassed, all the reagents could be added, and the reaction could be heated to 100 °C for 18 h. The starting material and product have identical retention factors via TLC; therefore the reaction progress was monitored via mass spectrometry. It was important to ensure full conversion of the starting material because separation of the starting material and product would be extremely difficult due to the identical retention factors. Following completion of the reaction, the work-up was conducted and the final product was purified via column chromatography. The desired product was eluted by an isocratic gradient of 45:45:10 EtOAc:Hex:$CHCl_3$. Post column, the product had a slight undesirable smell and was a darker brown color than expected. This could be solved by a brief trituration in MTBE which would also transform the product into a fine powder suitable for filtration. Product purity post column and trituration was >95%. It would be expected that post column, any residual palladium would be removed, however, to ensure the complete removal of palladium, it may be beneficial to run the Suzuki reaction before the addition of the oxadiazole ring as this product would then go through multiple purifications before the final product is obtained.

2.8.2 Synthetic Methods

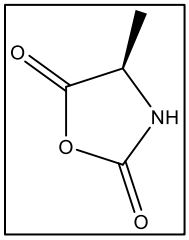

Synthesis of (R)-4-methyloxazolidine-2,5-dione: Boc-D-alanine (300 g, 1.59 mol) was dissolved in EtOAc (3.5 L). Triphosgene was added (190.7 g, 0.634 mol) followed by the dropwise addition of Et_3N (246 mL, 1.74 mol) over the course of

40 min. The reaction was then stirred at RT for 1 h before being heated to reflux for 3 h. Once complete, the reaction was cooled to RT and the precipitate (TEA-HCl salt) was removed via filtration. The filtered solid was washed with EtOAc (2 x 250 mL). The EtOAc was then removed under reduced pressure until approximately ¾ of the organic solution remained. At this point the formed precipitate (D-alanine) was removed via filtration and the rest of the solvent was removed under reduced pressure. The residue was dissolved in DCM (150 mL) and the solution was placed at -20 °C for 20 h to allow for crystal formation. If no crystals formed, hexanes could be added dropwise until the solution first becomes cloudy, and the mixture could be placed back at -20 °C for further crystal formation. The collected crystals were collected by filtration and the filtrate was collected to collect further crops of crystals. The product was obtained as a clear to yellow crystalline solid (82.1 g, 45.0%): ^{1}H NMR (500 MHz, $CDCl_3$) δ 9.00 (s, 1H), 4.50-4.45 (q, *J* = 3.12 Hz, 1H), 1.35-1.34 (d, *J* = 7.03 Hz, 3H); ^{13}C NMR (126 MHz, $CDCl_3$) δ 172.86, 152.15, 53.28, 17.21.

Figure 302: ^{1}H spectra of D-alanine NCA:

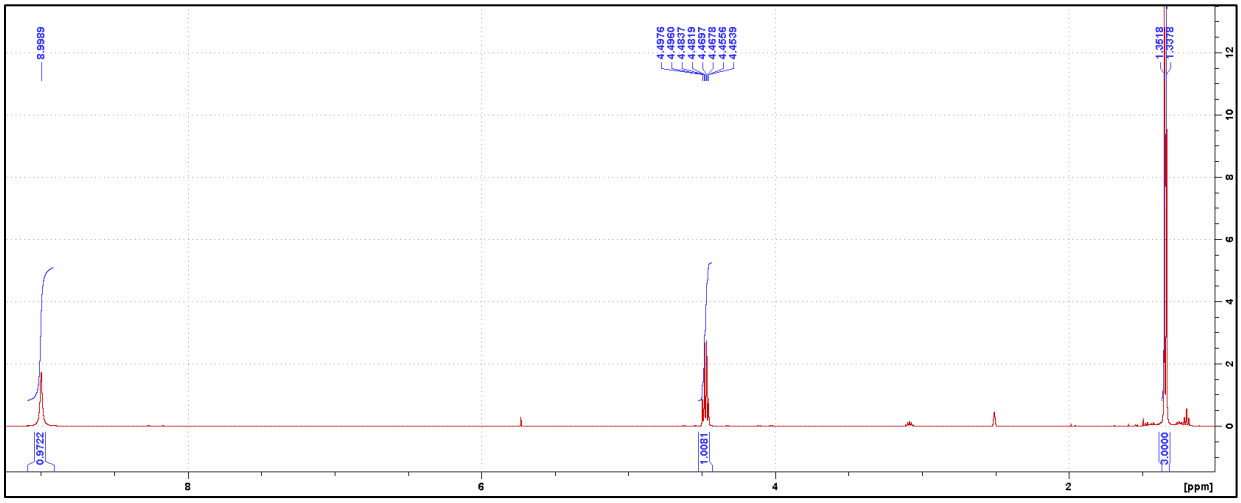

Figure 303: ^{13}C spectra of D-alanine NCA:

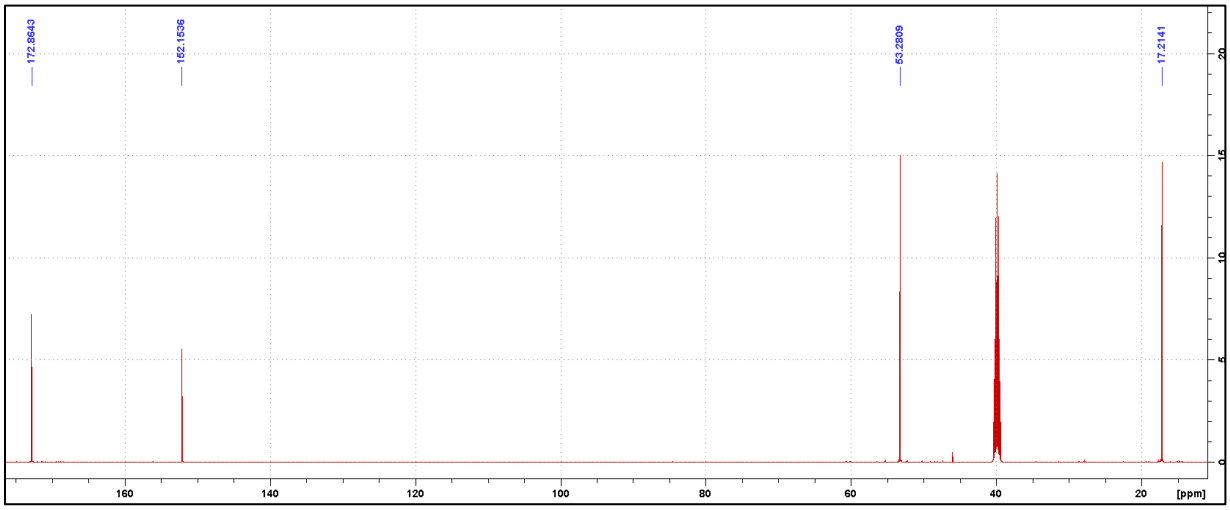

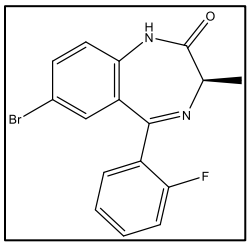

Synthesis of (R)-7-bromo-5-(2-fluorophenyl)-3-methyl-1,3-dihydro-2H-benzo[e][1,4]diazepin-2-one: 2-Amino-5-bromophenyl-2-fluorophenyl methanone (300 g, 1.02 mol) was dissolved in toluene (3.5 L) before the dropwise addition of TFA (156 mL, 2.04 mol) over the course of 15 min. The mixture was then stirred at RT for 30 min before the (R)-4-methyloxazolidine-2,5-dione (140.9 g, 1.22 mol) was added portion wise. The mixture was then heated to 50 °C for 3 h until no further conversion was observed via TLC (50% EtOAc:Hex). Triethylamine (298.6 mL, 2.14) was then added dropwise over the course of 30 min and the reaction was stirred for an additional 1.5 h at 50 °C until the intermediate was fully converted into the desired product. The reaction was then concentrated to dryness and the residue was dissolved in EtOAc (1 L). The organic layer was washed with H_2O (1 L), 5% aqueous $NaHCO_3$ (1 L), and brine (1 L). The organic layer was then dried with anhydrous $MgSO_4$ before being concentrated to dryness. The crude material was then triturated with 10% EtOAc:Heptane (2 x 500 mL). The first trituration was 12 h at RT, and the second trituration was 2 h at RT. The Pure product was collected as a yellow solid (304.9 g, 83.4%): ^1H NMR (500 MHz, $CDCl_3$) δ 9.26 (s, 1H), 7.62-7.59 (m, 2H), 7.49-7.44 (m, 1H), 7.37-

7.36 (d, *J* = 2.08 Hz, 1H), 7.27-7.24 (dt, *J* = 3.23, 1.00 Hz, 1H), 7.11-7.09 (d, *J* = 8.60 Hz, 1H), 7.08-7.06 (m, 1H), 3.82-3.78 (q, *J* = 6.49 Hz, 1H), 1.80-1.78 (d, *J* = 6.52 Hz, 3H) ; ^{13}C NMR (126 MHz, $CDCl_3$) δ 172.11 (s), 164.47 (s), 160.44 (d, $^{1}J_{CF}$ = 251.91 Hz), 136.36 (s), 134.72 (s), 132.18 (d, $^{3}J_{CF}$ = 8.37 Hz), 132.09 (d, $^{4}J_{CF}$ = 1.49 Hz), 131.53 (d, $^{3}J_{CF}$ = 2.22 Hz), 130.15 (s), 127.11 (d, $^{2}J_{CF}$ = 12.31 Hz), 124.45 (d, $^{3}J_{CF}$ = 3.58 Hz), 122.82 (s), 116.56 (s), 166.29 (d, $^{2}J_{CF}$ = 21.53 Hz), 58.83 (s), 16.94 (s).

Figure 304: ^{1}H spectra of (R)-7-bromo-5-(2-fluorophenyl)-3-methyl-1,3-dihydro-2H benzo[e][1,4]diazepin-2-one:

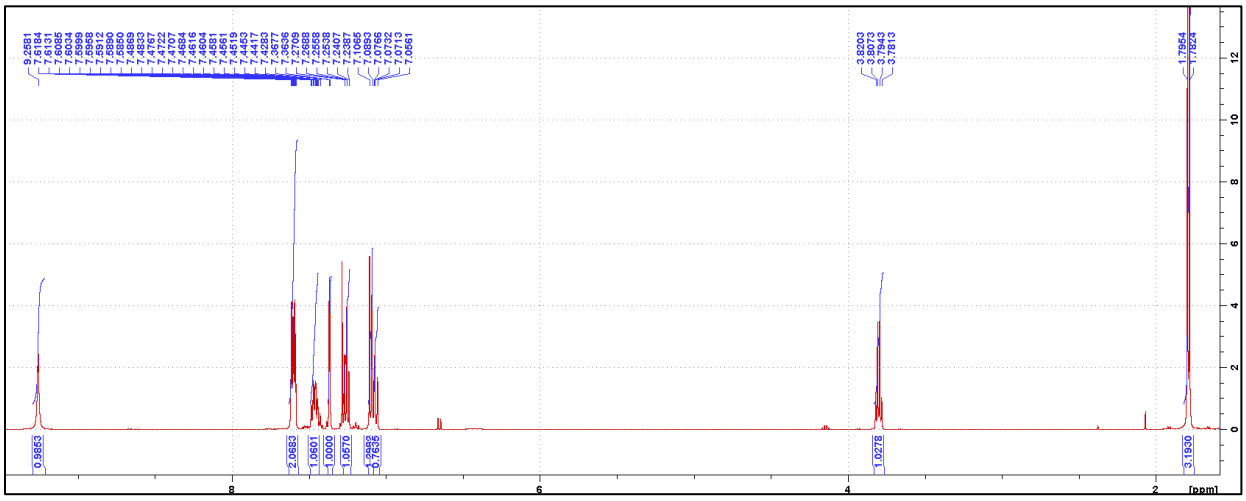

Figure 305: ^{13}C spectra of (R)-7-bromo-5-(2-fluorophenyl)-3-methyl-1,3-dihydro-2H benzo[e][1,4]diazepin-2-one:

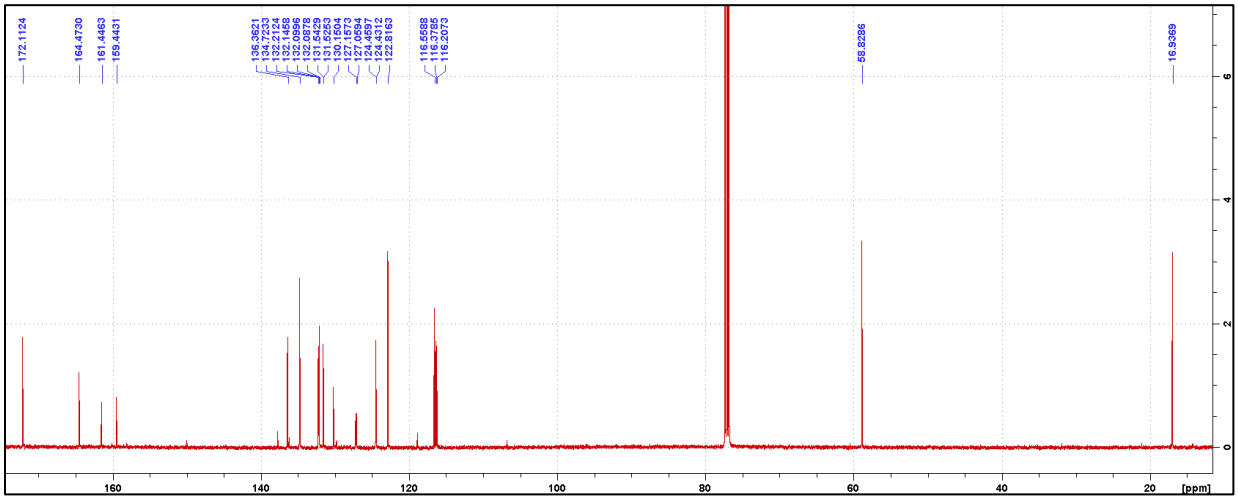

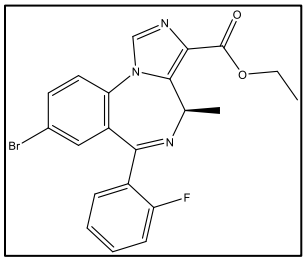

Synthesis of ethyl (R)-8-bromo-6-(2-fluorophenyl)-4-methyl-4H-benzo[f]imidazo[1,5-a][1,4]diazepine-3-carboxylate: (R)-7-Bromo-5-(2-fluorophenyl)-3-methyl-1,3- dihydro-2H-benzo [e][1,4] diazepin-2-one (217.0 g, 0.625 mol) was dissolved in anhydrous THF (2 L). The mixture was then cooled to -20 °C before the dropwise addition of a 1 M in THF *t*-BuOK solution (805 mL, 0.815 mol) over the course of 20 min. The reaction was then stirred at -20 °C for 40 min before diethyl chlorophosphate (125 mL, 0.875 mol) was added dropwise over the course of 5 min. The reaction was stirred at -20 °C for 3.5 h at which point no further conversion was observed via TLC (50% EtOAc:Hex) and ethyl isocyanoacetate (88 mL, 0.815 mol) was added dropwise over the course of 5 min, followed by the dropwise addition of *t*-BuOK (1 M in THF, 805 mL, 0.815 mol) over the course of 20 min. The reaction was then allowed to warm to RT and stir for an additional 12 h at which point the intermediate was converted to product via TLC. The reaction was then quenched with 5% $NaHCO_3$ (1 L) and diluted with EtOAc (1 L). The organic layer was

then washed with 10% $NaHCO_3$ (1 L), and brine (1 L). The organic layer was then dried with anhydrous $MgSO_4$ before being concentrated to dryness. The crude material was triturated with 50% MTBE:Hex (500 mL). The desired product was collected as a tan solid (175.8 g, 63.6%): ^{1}H NMR (500 MHz, $CDCl_3$) δ 7.92 (s, 1H), 7.73-7.72 (m, 1H), 7.61-7.59 (m, 1H), 7.49-7.42 (m, 3H), 7.28-7.25 (dt, *J* = 3.22, 0.97 Hz, 1H), 7.07-7.03 (t, *J* = 9.26 Hz, 1H), 6.73-6.69 (q, *J* = 7.27 Hz, 1H), 4.43-4.38 (m, 2H), 1.43-1.41 (t, *J* = 7.13 Hz, 3H), 1.30-1.28 (d, *J* = 7.32 Hz, 3H); ^{13}C NMR (126 MHz, $CDCl_3$) δ 162.92 (s), 162.66 (s), 161.00 (d, $^1J_{CF}$ = 250.77 Hz), 141.59 (s), 134.85 (s), 134.75 (s), 133.68 (s), 133.04 (s), 132.11 (d, $^3J_{CF}$ = 8.28 Hz), 131.18 (s), 129.59 (s), 128.42 (d, $^2J_{CF}$ = 12.47 Hz), 124.57 (d, $^4J_{CF}$ = 3.18 Hz), 123.65 (s), 120.95 (s), 116.24 (d, $^2J_{CF}$ = 21.47 Hz), 60.81 (s), 50.12 (s), 14.88 (s), 14.44 (s).

Figure 306: ^{1}H spectra of ethyl (R)-8-bromo-6-(2-fluorophenyl)-4-methyl-4H-benzo[f]imidazo[1,5-a][1,4]diazepine-3-carboxylate:

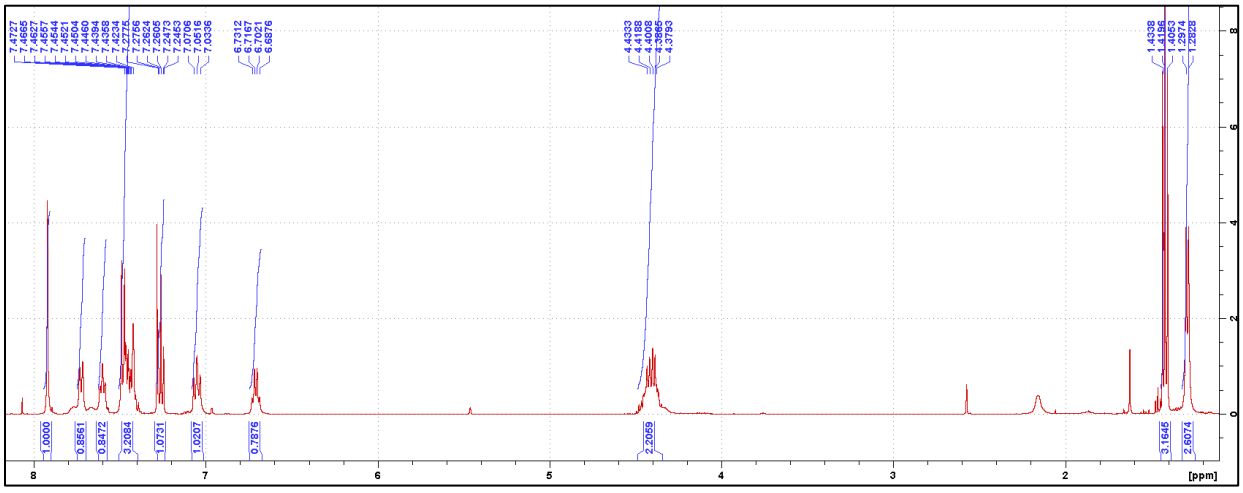

Figure 307: ^{13}C spectra of ethyl (R)-8-bromo-6-(2-fluorophenyl)-4-methyl-4H-benzo[f]imidazo[1,5-a][1,4]diazepine-3-carboxylate:

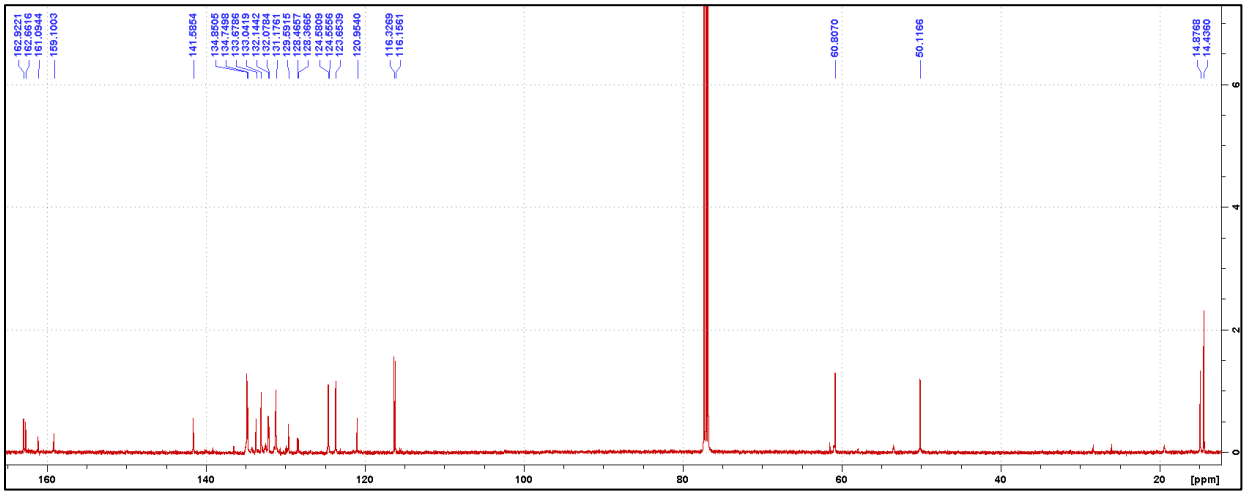

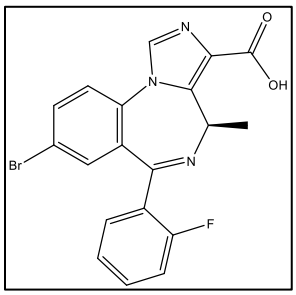

Synthesis of MIDD0301: Ethyl (R)-8-bromo-6-(2-fluorophenyl)-4-methyl-4H-benzo[f]imidazo[1,5-a][1,4]diazepine-3-carboxylate (134.2 g, 0.303 mol) was dissolved in THF (2 L) before being cooled to 0 °C. A 1.74 M solution of NaOH is H_2O (680 mL) was prepared and added to the reaction flask dropwise over the course of 30 min. The reaction was then heated to 55 °C for 5 h at which point all of the starting material dropped to the baseline via TLC (100% EtOAc). The reaction was cooled to RT before the addition of H_2O (1350 mL) and acetic acid (101 mL, 1.77 mol). The THF was removed under reduced pressure and MeOH (1 L) was added. The mixture was heated to 60 °C for 30 min before being cooled to RT and allowed to continue stirring for 12 h. The crude product was then collected by filtration and washed with H_2O (100 mL). The product was recrystallized in hot EtOH (4 L). The desired product was collected as a white powder (108.1 g, 86.0%): ^{1}H NMR (500 MHz, $CDCl_3$) δ 12.70 (s, 1H), 8.42 (s, 1H), 7.96-7.95 (m, 1H), 7.90-7.88 (m, 1H), 7.60-7.54 (m, 2H), 7.35-7.32 (m, 2H), 7.26-7.22 (t, *J* = 9.44 Hz, 1H), 6.53-6.49 (q, *J* = 7.03 Hz, 1H), 1.94 (m, 0.5H), 1.18-1.17 (d, *J* = 7.28 Hz, 2.5H); ^{13}C NMR (126 MHz, $CDCl_3$) δ

164.60 (s), 162.39 (s), 159.85 (d, $^{1}J_{CF}$ = 247.84 Hz), 141.00 (s), 136.72 (s), 135.50 (s), 134.00 (s), 132.76 (d, $^{3}J_{CF}$ = 8.30 Hz), 132.39 (s), 131.94 (s), 130.89 (s), 129.32 (s), 128.69 (d, $^{2}J_{CF}$ = 12.88 Hz), 125.65 (s), 125.20 (s), 120.29 (s), 116.44 (d, $^{2}J_{CF}$ = 21.23 Hz), 49.83 (s), 15.04 (s).

Figure 308: ^{1}H spectra of MIDD0301:

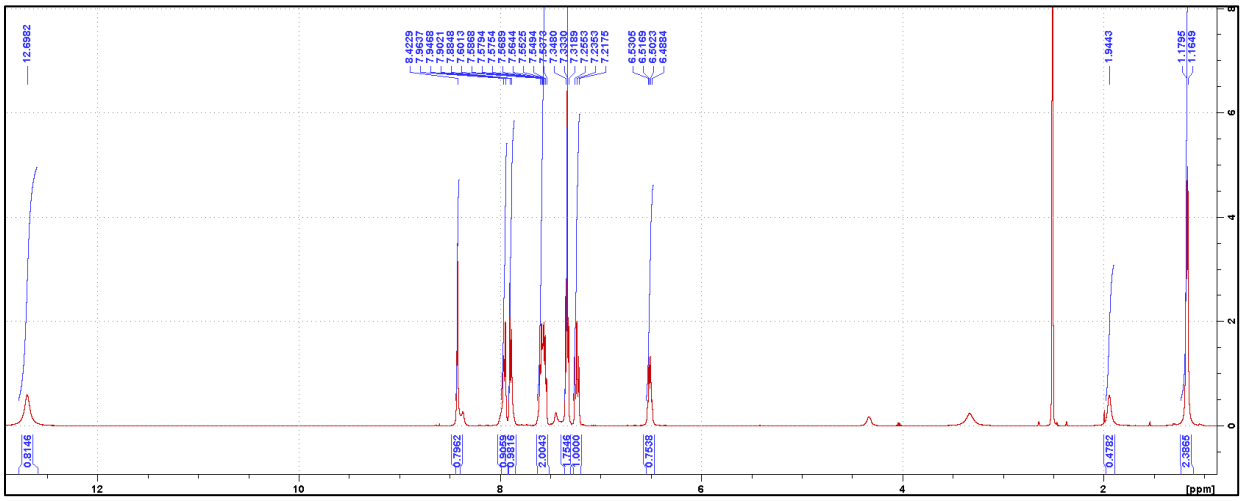

Figure 309: ^{13}C spectra of MIDD0301:

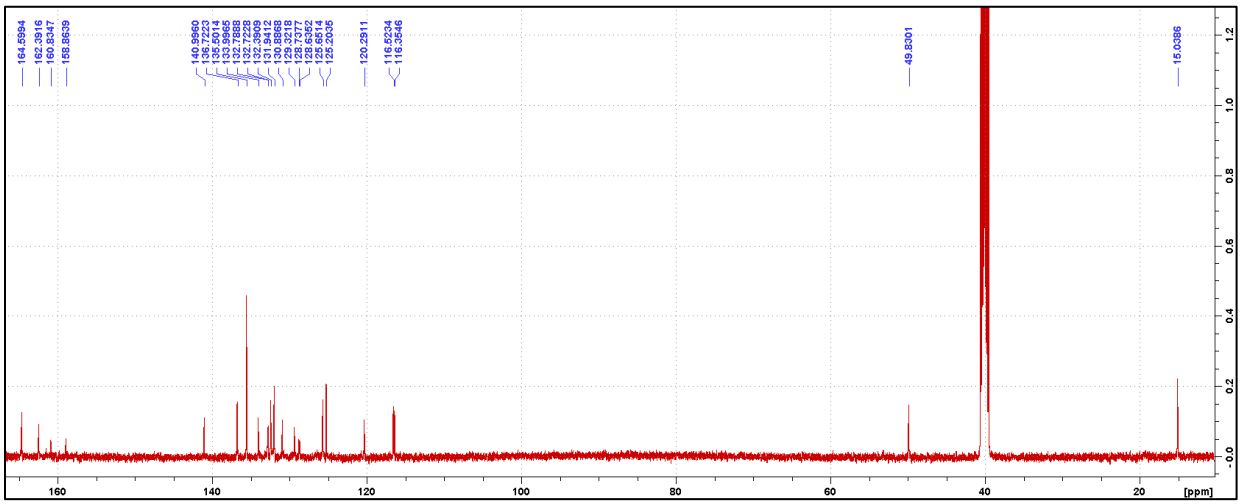

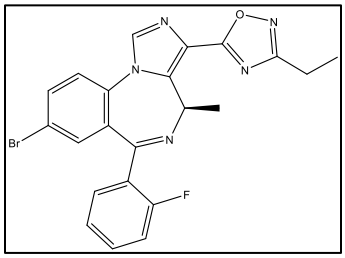

Synthesis of (R)-5-(8-bromo-6- (2-fluorophenyl)-4-methyl-4H-benzo [f] imidazo [1,5-a] [1,4] diazepin-3-yl)-3-ethyl-1,2,4-oxadiazole: (E)-N'-Hydroxypropionimidamide (91 g, 1.03 mol) was

dissolved in anhydrous THF (102 mL). Enough oven dried 3Å molecular sieves were added to fill approximately ¼ of the flask. NaH (60% dispersion in mineral oil, 11.4 g, 0.285 mol) was added portion wise, and the mixture was allowed to stir at RT for 1 h. In a separate flask, ethyl (R)-8-bromo-6-(2-fluorophenyl)-4-methyl-4H-benzo [f]imidazo[1,5-a][1,4] diazepine-3-carboxylate (114.4 g, 0.259 mol) was mixed in anhydrous THF (1.7 L). The oxime solution was then added dropwise over the course of 15 min. The reaction was then allowed to stir at RT until full consumption of the starting material was observed via TLC (100% EtOAc). Full consumption was observed between 0.5-1.5 h. Once complete, the reaction was quenched with aqueous 10% $NaHCO_3$ (1 L) and the mixture was extracted with EtOAc (3 x 500 mL). The organic fractions were pooled and washed with brine (1 L) before being dried with anhydrous $MgSO_4$. The organic layer was concentrated to dryness and the crude material was triturated with 50% MTBE:Hex to yield the desired product as a tan solid (97.2 g, 80.6%): ^{1}H NMR (500 MHz, $CDCl_3$) δ 7.98 (s, 1H), 7.72-7.70 (m, 0.25H), 7.67-7.65 (dd, *J* = 3.30, 1.42 Hz, 0.75H), 7.59-7.56 (m, 0.25H), 7.52-7.49 (m, 0.75H), 7.47-7.45 (d, *J* = 8.57 Hz, 1H), 7.38-7.34 (m, 2H), 7.18-7.15 (dt, *J* = 3.21, 0.88 Hz, 1H), 6.97-6.94 (t, *J* = 9.23 Hz, 1H), 6.67-6.63 (q, *J* = 7.25 Hz, 0.75H), 4.33-4.31 (m, 0.25H), 2.75-2.71 (q, *J* = 7.55 Hz, 2H), 2.08-2.07 (m, 1H), 1.30-1.25 (m, 5H); ^{13}C NMR (126 MHz, $CDCl_3$) δ 171.88 (s), 170.67 (s), 162.86 (s), 160.07 (d, $^1J_{CF}$ = 250.91 Hz), 139.13 (s), 136.23 (s), 135.05 (s), 133.39 (s), 133.18 (s), 132.22 (d, $^3J_{CF}$ = 8.24 Hz), 131.16 (s), 131.09 (s), 128.32 (d, $^2J_{CF}$ = 12.18 Hz), 125.00 (s), 124.58 (d, $^4J_{CF}$ = 2.92 Hz), 123.68 (s), 121.18 (s), 116.26 (d, $^2J_{CF}$ = 21.41 Hz), 50.24 (s), 19.76 (s), 14.98 (s), 11.54 (s).

Figure 310: ^{1}H spectra of (R)-5-(8-bromo-6-(2-fluorophenyl)-4-methyl-4H-benzo [f]imidazo[1,5-a][1,4] diazepin-3-yl)-3-ethyl-1,2,4-oxadiazole:

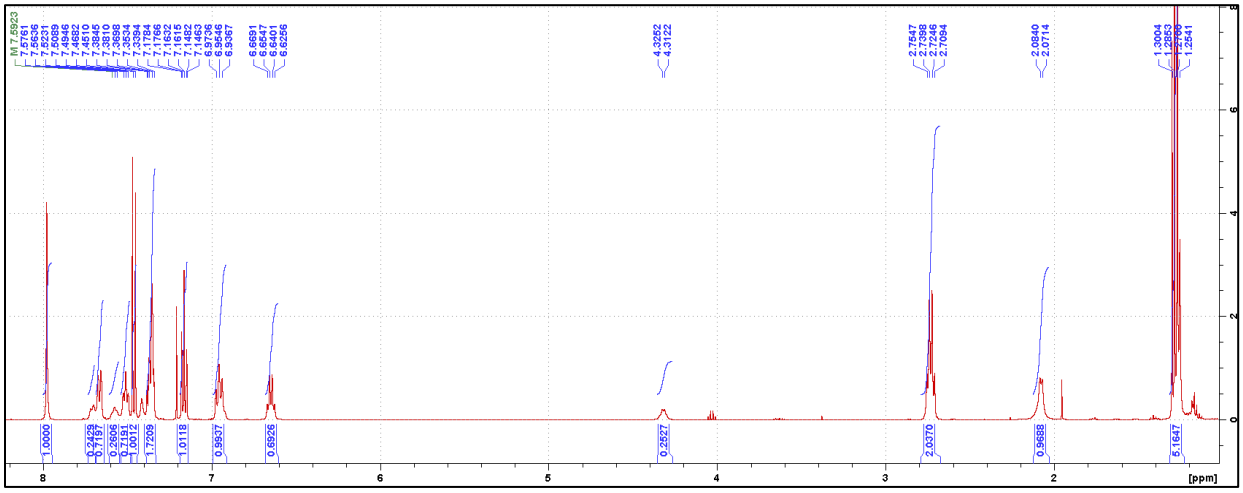

Figure 311: ^{13}C spectra of (R)-5-(8-bromo-6-(2-fluorophenyl)-4-methyl-4H-benzo [f]imidazo[1,5-a][1,4] diazepin-3-yl)-3-ethyl-1,2,4-oxadiazole:

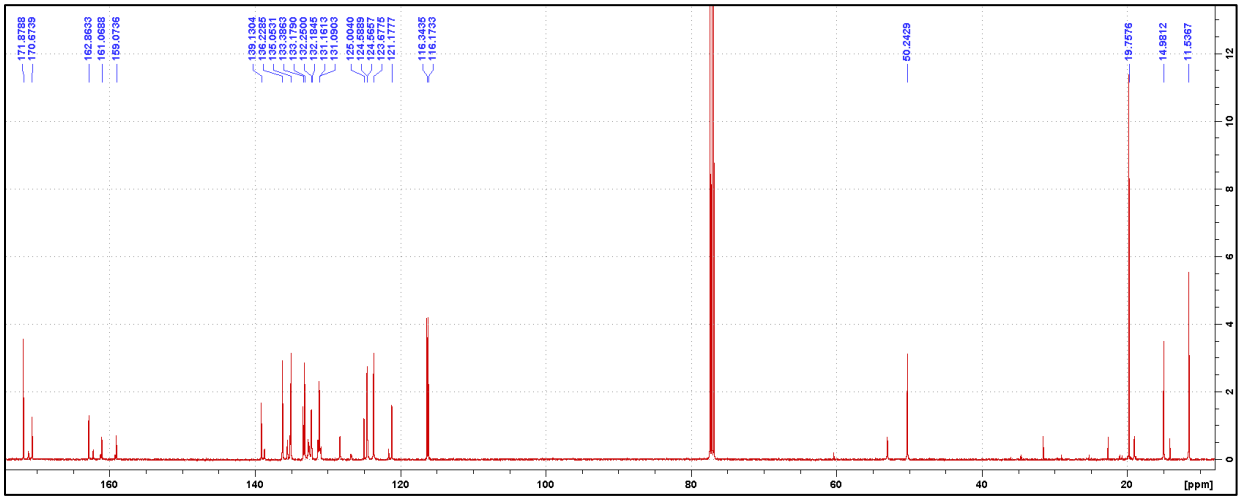

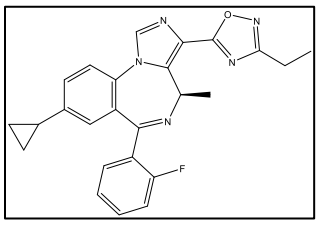

Synthesis of PI560: Toluene (1900 mL) and H_2O (280 mL) were degassed with nitrogen before the addition of (R)-5-(8-bromo-6-(2-fluorophenyl)-4-methyl-4H-benzo [f]imidazo[1,5-a][1,4] diazepin-3-yl)-3-ethyl-1,2,4-oxadiazole (97.2 g, 0.208 mol). Cyclopropane boronic acid was added (89.5 g, 1.04 mol), followed by the addition of potassium phosphate tribasic (190.2 g, 0.986 mol),

$Pd(OAc)_2$ (4.7 g, 20.8 mmol), and tri(o-tolyl)phosphine (12.7 g, 41.7 mmol). The reaction was then heated to 100 °C for 18 h at which point full consumption of the starting material was confirmed via mass spectrometry. The reaction was then cooled to RT before the addition of H_2O (1 L) and the mixture was extracted with EtOAc (3 x 500 mL). The organic fractions were pooled and washed with brine (1 L) before being dried over anhydrous $MgSO_4$. The organic layer was then concentrated to dryness before the crude material was purified via column chromatography (isocratic: 45:45:10 EtOAc:Hex:$CHCl_3$). The material that was collected from the column could be triturated with MTBE (200 mL) before the desired product was collected as a tan solid (51.7 g, 58%): ^{1}H NMR (500 MHz, $CDCl_3$) δ 7.94 (s, 1H), 7.52-7.49 (m, 1H), 7.44-7.42 (d, *J* = 8.35 Hz, 1H), 7.37-7.33 (m, 1H), 7.17-7.14 (dt, *J* = 3.16, 0.79 Hz, 2H), 6.97-6.92 (m, 2H), 6.63-6.59 (q, *J* = 7.39 Hz, 1H), 2.76-2.72 (q, *J* = 7.50 Hz, 2H), 2.09-2.07 (m, 0.8H), 1.82-1.77 (m, 1H), 1.31-1.28 (t, *J* = 7.58 Hz, 1H), 1.26-1.24 (d, *J* = 7.29 Hz, 2.2H), 0.94-0.92 (m, 2H), 0.61-0.52 (m, 2H); ^{13}C NMR (126 MHz, $CDCl_3$) δ 170.81 (s), 169.94 (s), 163.29 (s), 159.13 (d, $^1J_{CF}$ = 250.82 Hz), 143.11 (s), 138.19 (s), 135.19 (s), 130.83 (s), 130.72 (s), 130.66 (s), 130.19 (s), 128.19 (s), 127.57 (s), 127.04 (s), 123.54 (s), 123.34 (d, $^3J_{CF}$ = 5.66 Hz), 120.86 (s), 115.03 (d, $^2J_{CF}$ = 21.56 Hz), 49.19 (s), 18.74 (s), 14.06 (s), 13.75 (s), 10.53 (s), 8.91 (s).

Figure 312: ^{1}H spectra of PI560:

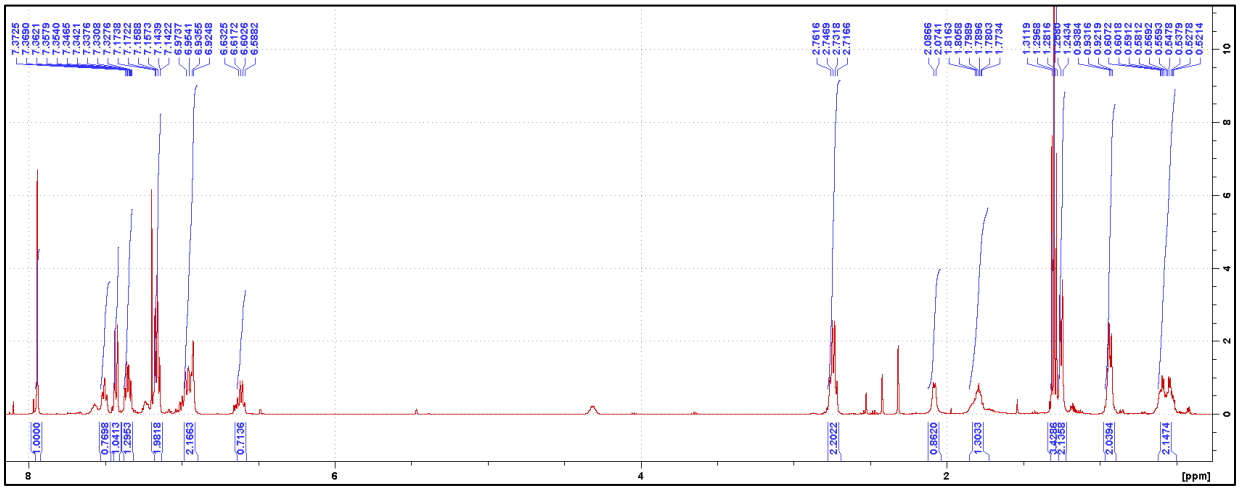

Figure 313: ^{13}C spectra of PI560:

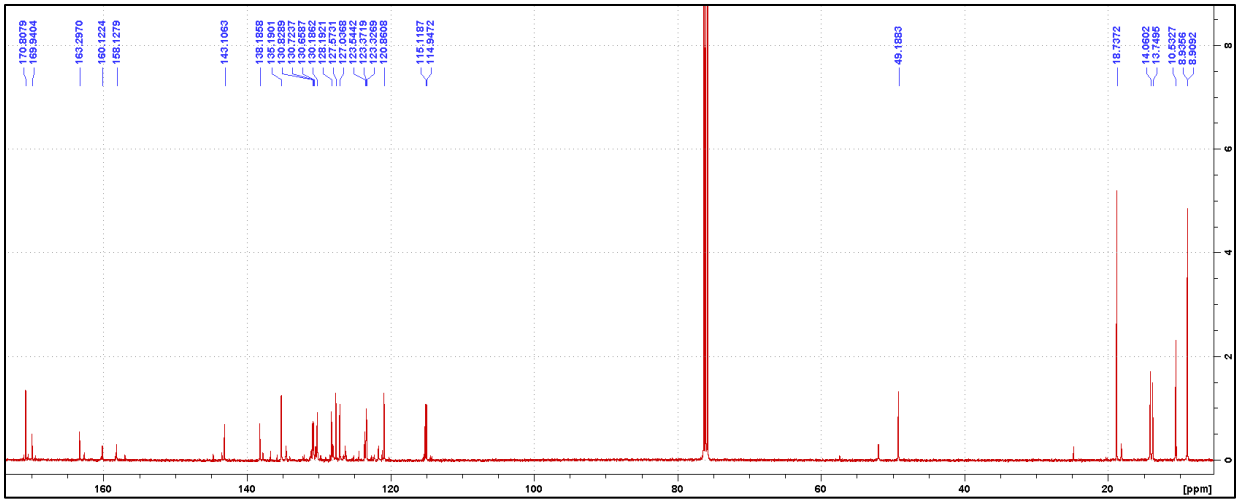

2.9 TSPO Ligand Design and Synthesis

2.9.1 Background

The Translocator Protein (TSPO), holds great promise in the development of novel anxiolytic drugs. Setting itself apart from benzodiazepine tranquilizers which known for their side effects.[205] TSPO is a carrier protein situated on the outer mitochondrial membrane, responsible for transporting cholesterol from the outer to the inner mitochondrial membrane. This process is vital

in the synthesis of neurosteroids, which positively influence the $GABA_A$ receptor's function by binding to their unique sites,[206] separate from benzodiazepines.[207]

Over the past 25 years, researchers have devised around 20 different classes of TSPO ligands,[208] with some demonstrating neuropsychotropic effects in *in vivo* models.[209] Despite their efficacy in various animal models for anxiety,[210] depression,[211] and other behavioral tests,[208] no TSPO ligands have successfully made it through clinical trials or been approved for clinical use.[205] This limitation is likely due to their adverse effects, linked to the xenobiotic nature of these compounds.

The Zakusov Research Institute of Pharmacology[212] has introduced an innovative approach for creating potent, safe, and physiologically compatible drugs using dipeptides.[213] This approach centers around crafting dipeptides structurally resembling non-peptide bioactive compounds, appropriately named Drug-Based Peptide Design (DBPD). Dipeptides, owing to their small molecular size and the presence of an active transport system, can readily traverse biological barriers. Additionally, their enzymatic stability is maintained due to a limited number of protease-targeted bonds, making them suitable for oral administration. Furthermore, dipeptides are cost-effective and simple to synthesize. An example of this strategy is the dipeptide nootropic drug Noopept (N-phenylacetyl-L-prolylglycine ethyl ester), developed based on the classic nootropic drug piracetam (N-carbamidomethylpyrrolidone-2).[214] Noopept has been available on the pharmaceutical market since 2006.[215]

With progress in the generation of novel TSPO ligands, we gained interest when some of our synthesized benzodiazepines proved to have low μM binding affinity to this receptor. Here we present initial binding data as well as the synthetic methods for novel compounds having a high affinity towards TSPO.

2.9.2 Benzodiazepine TSPO Ligand Design

As previously stated, synthesized benzodiazepines were sent to PDSP program (University of NC Chapel Hill)[194] to screen for receptor binding. Of all synthesized ligands only two compounds (DAW-II-20 and DAW-II-80) displayed significant TSPO receptor binding (Table 3). DAW-II-20 contains a racemic isopropyl substituent attached to the 7-membered ring, and DAW-II-80 contains a racemic cyclopropane substituent. Due to the geometric similarity of these two groups, it is unsurprising these compounds exhibited similar binding. Compounds were initially screened at 10 μM, and any compound to achieve greater than 50% inhibition was then subjected to a dose response analysis. DAW-II-20 and DAW-II-80 achieved 109.7% and 112.68% respectively in the primary binding screening. These two compounds were then subjected to a dose response study in which DAW-II-20 and DAW-II-80 have an IC_{50} value of 755.9 nM and 366.4 nM, respectively (see dose response curves below). Both compounds were docked into TSPO crystal structure 1EQ1[216] using MOE where only moderate docking scores were calculated. Future optimization of the docking approach would be needed as obtained docking scores did not correlate with binding data obtained from PDSP. However, MOE was able to strongly predict a significant difference in binding between the R and S enantiomers of the synthesized compounds. DAW-II-20 and DAW-II-80 were synthesized as racemic compounds, which could explain the significant difference in IC_{50} values whereas the primary data was nearly identical. Because of the data obtained from MOE, we decided to synthesize the enantiomerically pure R and S forms of DAW-II-20. Due to the cost of the enantiomerically pure amino acid required to synthesize DAW-II-80, this compound was not studied further.

Table 3: TSPO binding data obtained from the Psychoactive Drug Screening Program

Compound	TSPO binding % inhibition at 10 µM
DAW-I-10	-1.41
DAW-I-20	26.37
DAW-I-30	-12.11
DAW-I-40	-1.33
DAW-I-50	8.00
DAW-I-60	31.14
DAW-I-70	32.89
DAW-I-80	66.55
DAW-II-10	49.78
DAW-II-20	109.70
DAW-II-30	44.45
DAW-II-40	47.30
DAW-II-50	12.15
DAW-II-60	67.70
DAW-II-70	7.45
DAW-II-80	112.68
DAW-III-10	8.83
DAW-III-20	-13.11
DAW-III-30	27.33
DAW-III-40	15.26
DAW-III-50	44.27
DAW-III-60	21.35
DAW-III-70	26.92
DAW-III-80	17.04

(R)-DAW-II-20 was successfully synthesized by the same synthesis route outlined in Scheme 5. The enantiomerically pure amino acid was converted into the corresponding N-carboxy anhydride (NCA) before being coupled to the desired aniline. The conversion to the imidazobenzodiazepine yielded the final product. Surprisingly, the synthesis of (S)-DAW-II-20 proved much more challenging. The NCA was successfully synthesized, however, subsequent coupling to the aniline proved completely unsuccessful. Due to the first step of this reaction being a protonation of the NCA with TFA, we hypothesized that a stronger acid may be needed to successfully protonate the NCA. Therefore, we performed reactions with sulfuric acid as well as

triflic acid but without success. Attempts were then made to use Lewis acids such as boron trifluoride and titanium tetrachloride, however, no reactions were successful. Previously, it had

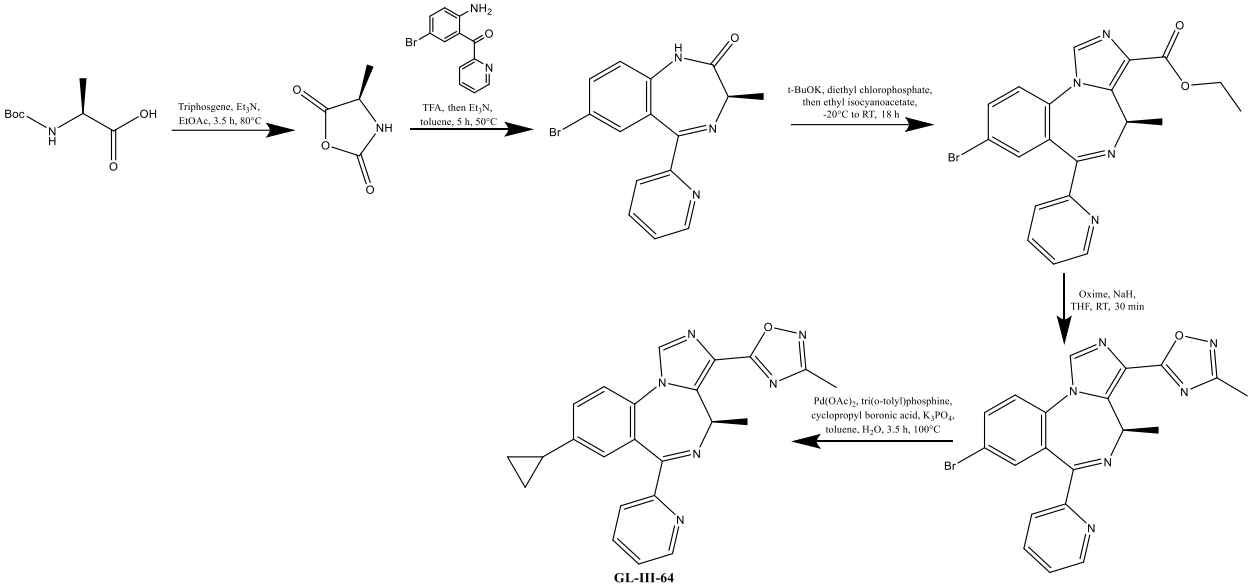

Scheme 9: Synthesis of GL-III-64

been determined that synthesizing the NCA was a superior synthetic route to a DCC peptide coupling reaction due to the higher yields obtained when using sterically hindered amino acids. However, due to the unsuccessful nature of this particular NCA, a DCC coupling reaction was attempted with a small amount of product being obtained. (S)-DAW-II-20 could be successfully synthesized by coupling the BOC protected amino acid directly to the aniline using DCC, followed by deprotection and cyclization to yield the corresponding benzodiazepine. The formation of the fused imidazole ring yielded the final product. (S)-DAW-II-20 was obtained in extremely low yield due to the lack of product being formed in the DCC coupling step, and more work is needed to find a better synthetic route, however, enough product was obtained to successfully complete the binding studies. Upon screening the R and S forms of DAW-II-20 for TSPO binding, the S form yielded an IC_{50} value of 316.2 nM and the R form yielded an IC_{50} value of 728.1 nM. Therefore, it can be concluded that the S form of the synthesized benzodiazepines has greater TSPO binding than the R form.

In the process to search for how benzodiazepines could be further modified for greater TSPO binding, GL-III-64 which was first synthesized by Guanguan Li (see Scheme 9), was noted as a TSPO binder due to its IC_{50} value of 29 nM. GL-III-64 contains a pyridine nitrogen in the 2' position rather than the 2' fluorine functionality as shown in many of the synthesized benzodiazepines in this chapter. Upon looking into other TSPO hit compounds, nearly all benzodiazepines showing strong binding have a nitrogen in the 2' position, therefore it can be concluded that this functionality increases the binding affinity. Due to the strong binding of GL-III-64, this compound was synthesized for future in vivo studies in respect to atopic dermatitis studies (see synthetic methods below). Much of the synthesis of GL-III-64 follows what was outlined in Scheme 5 with the NCA, benzodiazepine, and ethyl ester all being synthesized via the same methods outlined in Scheme 5, albeit with the use of a different aniline. Subsequently, the oxadiazole ring was added using the same method used in the PI560 synthesis, however, a methyl oxime was used rather than an ethyl oxime. Finally, the cyclopropane ring was added using the same Suzuki coupling reaction outlined in the PI560 synthesis with small modifications. The formation of the product was monitored by mass spectrometry and deemed complete after approximately 3.5 h. The reaction should be stopped at this point to prevent the formation of unwanted impurities. Due to the unique dinitrogen configuration of GL-III-64 (the imine nitrogen and the 2' pyridine nitrogen), it seemed that the compound was acting as a palladium ligand preventing the Suzuki reaction from taking place. This resulted in the lack of full conversion despite stirring for 18 h. To overcome this, 0.2 eq of $Pd(OAc)_2$ was used rather than the standard 0.1 eq. The equivalents of the phosphine were also doubled to account for the increased catalyst loading. The results of this increased amount of catalyst proved to yield full conversion to the desired product in a shorter amount of time.

2.9.3 Synthetic Methods

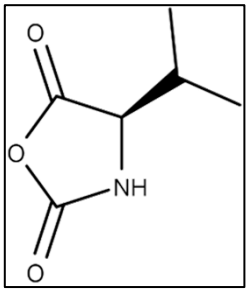

Synthesis of (R)-Valine NCA: Boc-D-Valine (10.0 g, 46.17 mmol) was added to anhydrous ethyl acetate (200 mL), followed by the addition of triphosgene (5.48 g, 18.47 mmol). The solution was stirred until a clear solution was obtained before triethyl amine (7.08 mL, 50.79 mmol) was added dropwise over a period of 15 min during which a white solid formed (TEA-HCl salt). The temperature was kept below 30°C during the addition of triethyl amine. The solution was stirred at room temperature for 1 h followed by heating to reflux (80°C) for 20 hr. The reaction was cooled to room temperature and the solid was removed by filtration and washed with ethyl acetate. The filtrate was concentrated under reduced pressure to yield a brown residue. The residue was then dissolved in dichloromethane (40 mL) and hexanes was added dropwise (110 mL) over a period of 20 min while stirring. The mixture was allowed to sit at -20 °C for 24 h at which point the product precipitated out of solution. The product was collected by filtration to yield a crystalline white solid (3.7 g, 56.2%): ^{1}H NMR (500 MHz, $CDCl_3$) δ 6.23 (s, 1H), 4.23-4.22 (d, J = 4.24 Hz, 1H), 2.31-2.24 (m, 1H), 1.12-1.10 (d, J = 6.95 Hz, 3H), 1.07-1.05 (d, J = 6.82 Hz, 3H); ^{13}C NMR (126 MHz, $CDCl_3$) δ 168.65, 152.52, 62.99, 30.81, 18.27, 16.62.

Figure 314: ^{1}H spectra of (R)-Valine NCA:

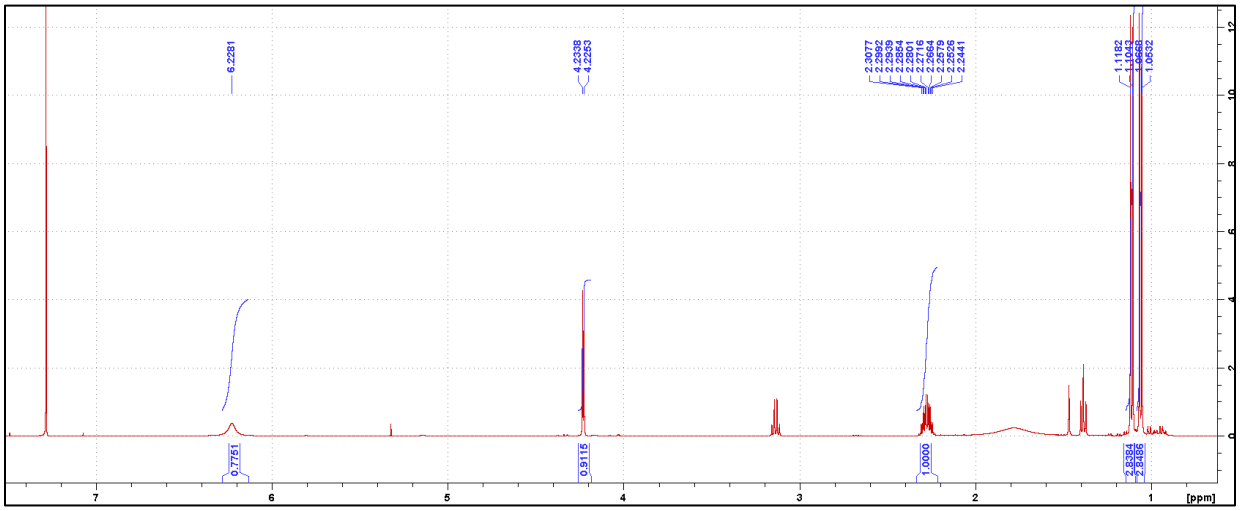

Figure 315: ^{13}C spectra of (R)-Valine NCA:

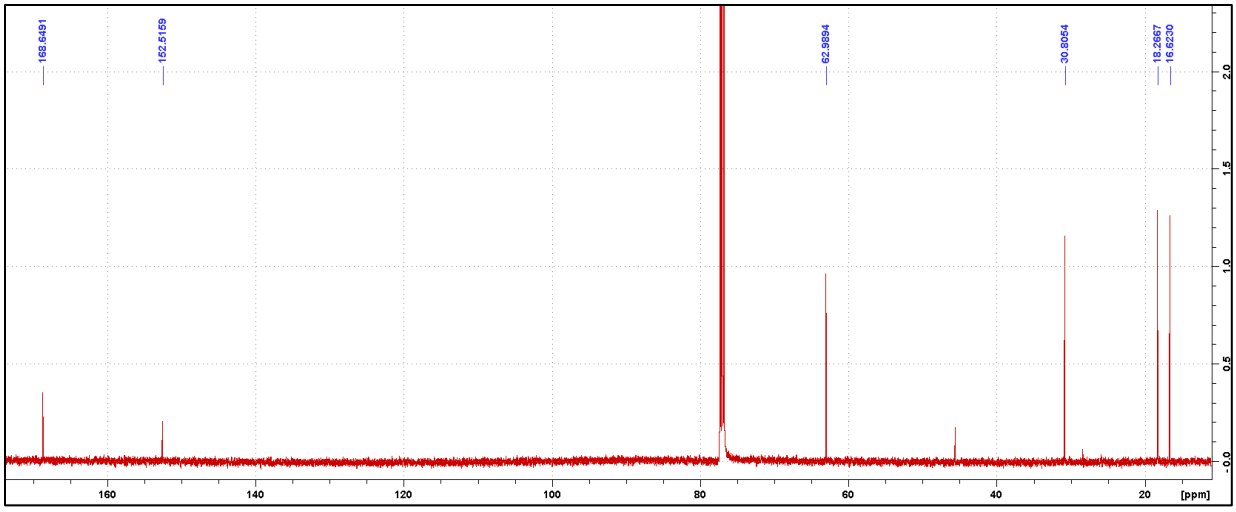

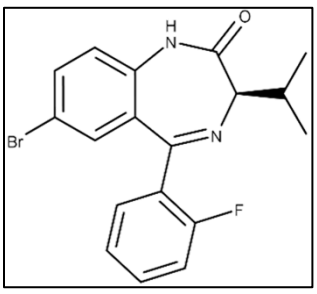

Synthesis of (R)-DAW-I-20: 2-Amino-5-bromo-2′-fluorobenzophenone (4.4 g, 14.96 mmol) was added to anhydrous toluene (100 mL), followed by the addition of trifluoroacetic acid (2.3 mL, 29.92 mmol) dropwise over a period of 10 min, and the mixture was allowed to stir at room temperature for 30 min. (R)-4-isopropyloxazolidine-2,5-dione (3.21 g, 22.42 mmol) was added portion wise and the reaction was heated to 50 °C for 24 h. After the

majority of the starting material had been consumed by TLC (50% EtOAc:Hex), triethylamine (4.4 mL, 31.42 mmol) was added dropwise over a period of 15 min at which point fuming was observed in the reaction. The reaction was then heated to 100 °C for 24 h at which point disappearance of the intermediate was observed via TLC (50% EtOAc:Hex). Upon cooling to room temperature, the solvent was removed under reduced pressure and the residue was dissolved in ethyl acetate (100 mL). The organic layer was washed with 5% aqueous sodium bicarbonate (100 mL), followed by 10% aqueous NaCl (100 mL). The organic layer was then dried with $MgSO_4$ and the solvent was removed under reduced pressure. The residue was stripped with 10% EtOAc:Heptane (50 mL, 2x) followed by a trituration in 10% EtOAc:Heptane (80 mL) at 60 °C for 4 h. The product was collected by filtration to yield a light yellow solid (3.59 g, 64.0%): ^{1}H NMR (500 MHz, $CDCl_3$) δ 8.23 (s, 1H), 7.63-7.61 (dd, *J* = 3.62, 2.26 Hz, 1H), 7.60-7.57 (dt, *J* = 3.36, 1.78 Hz, 1H), 7.50-7.45 (m, 1H), 7.39-7.38 (d, *J* = 2.12 Hz, 1H), 7.27-7.24 (dt, *J* = 3.23, 1.07 Hz, 1H), 7.11-7.07 (m, 1H), 7.04-7.03 (d, *J* = 8.62 Hz, 1H), 3.17-3.15 (d, *J* = 9.35 Hz, 1H), 2.79-2.73 (m, 1H), 1.22-1.21 (d, *J* = 6.69 Hz, 3H), 1.12-1.11 (d, *J* = 6.53 Hz, 3H); ^{13}C NMR (126 MHz, $CDCl_3$) δ 169.66 (s), 164.04 (s), 160.54 (d, $^{1}J_{CF}$ = 252.23 Hz), 136.21 (s), 134.64 (s), 132.21 (q, *J* = 4.17 Hz), 131.63 (d, $^{4}J_{CF}$ = 2.38 Hz), 130.16 (s), 127.17 (d, $^{2}J_{CF}$ = 12.14 Hz), 124.40 (d, $^{3}J_{CF}$ = 3.58 Hz), 122.64 (s), 116.64 (s), 116.33 (d, $^{2}J_{CF}$ = 21.58 Hz), 69.44 (s), 28.99 (s), 22.70 (s), 20.25 (s).

Figure 316: ^{1}H spectra of (R)-DAW-I-20:

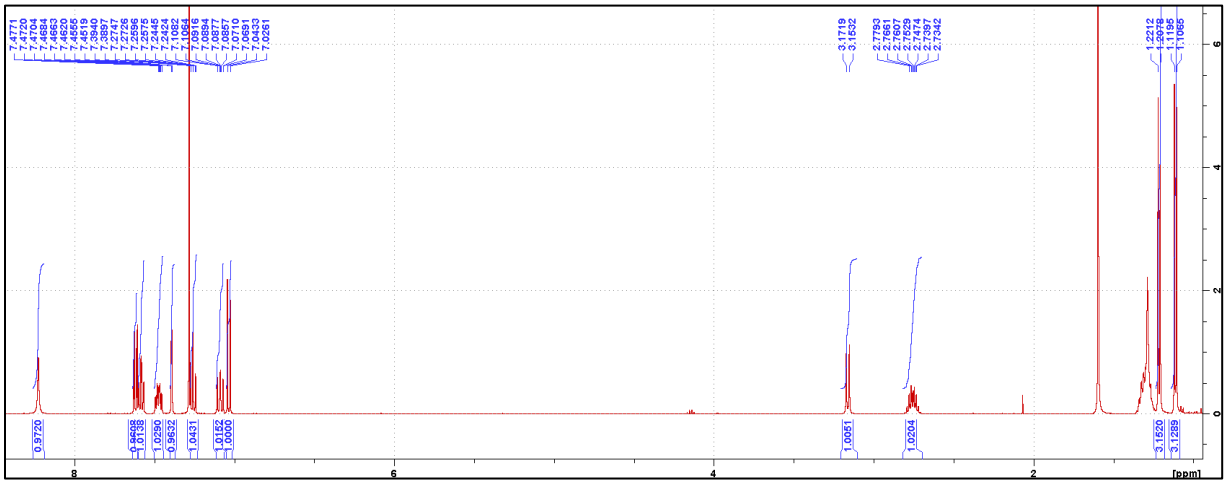

Figure 317: ^{13}C spectra of (R)-DAW-I-20:

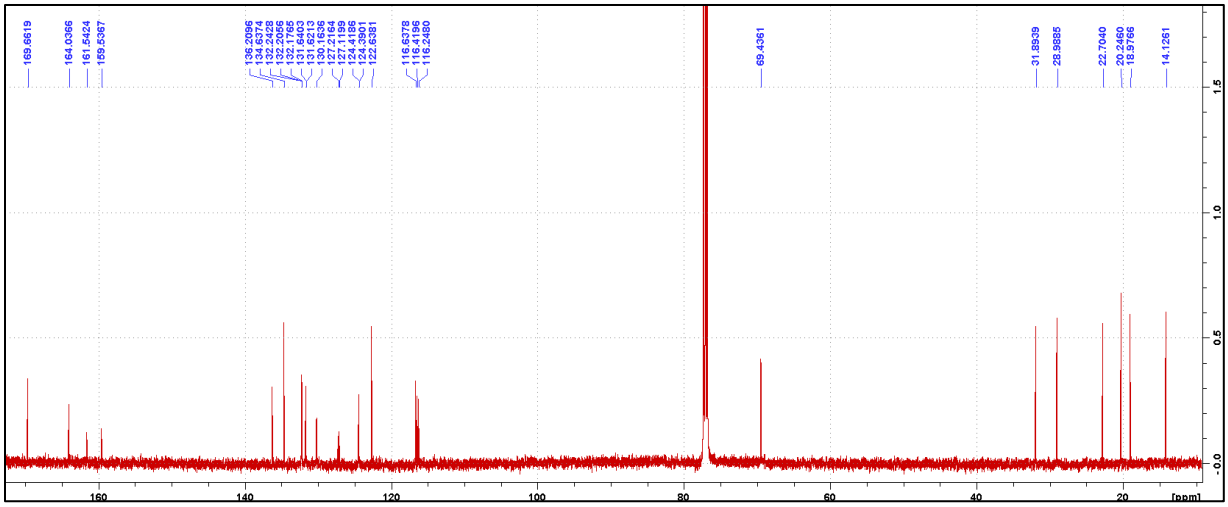

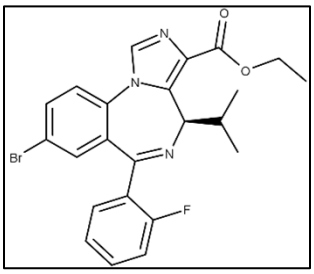

Synthesis of (R)-DAW-II-20: A three stopper RB flask was purged with nitrogen and vacuum 3 times. **(R)-DAW-I-20** (502.5 mg, 1.34 mmol) was dissolved in anhydrous tetrahydrofuran (6 mL) and added to the reaction flask. The mixture was cooled to -20 °C using a dry ice/IPA bath. A solution of 1M potassium tert-butoxide in anhydrous tetrahydrofuran (1.74 mL) was added dropwise over the course of 10 min, at which time the reaction color turned to a deep orange. Upon

completion of the addition, the mixture was allowed to stir at -20 °C for 40 min. Diethyl chlorophosphate (0.27 mL, 1.87 mmol) was added dropwise over the course of 5 min while maintaining a temperature of -20 °C. After 3.5 h, no more conversion was observed via TLC (100% EtOAc) and ethyl isocyanoacetate (0.19 mL, 1.74 mmol) was added dropwise over the course of 5 min followed by the addition of a solution of 1M potassium tert-butoxide in anhydrous tetrahydrofuran (1.74 mL) at -20 °C. The reaction was then warmed to room temperature for 2 h at which point all of the intermediate had been consumed via TLC (100% EtOAc). The reaction was then quenched with 5% aqueous sodium bicarbonate (30 mL), and the product was extracted with ethyl acetate (30 mL). The organic layer was washed with 10% aqueous sodium bicarbonate (30 mL) followed by 20% aqueous NaCl (30 mL). The organic layer was then dried with $MgSO_4$ and then concentrated under reduced pressure. The residue was loaded onto a precolumn with chloroform and separated by Biotage: 20-80% ethyl acetate in hexanes (30 CV). The desired product was obtained as an off-white solid (366.6 mg, 58.2%): ^{1}H NMR (500 MHz, $CDCl_3$) δ 7.92 (s, 1H), 7.73-7.71 (dd, *J* = 3.58, 2.19 Hz, 1H), 7.60-7.57 (dt, *J* = 3.32, 1.60 Hz, 1H), 7.49-7.45 (m, 2H), 7.42-7.41 (d, *J* = 1.99 Hz, 1H), 7.28-7.25 (dt, *J* = 3.22, 0.86 Hz, 1H), 7.09-7.05 (m, 1H), 6.27-6.25 (d, *J* = 11.22 Hz, 1H), 4.49-4.44 (m, 1H), 4.40-4.35 (m, 1H), 1.90-1.85 (m, 1H), 1.47-1.42 (t, *J* = 7.13 Hz, 3H), 1.12-1.11 (d, *J* = 6.44 Hz, 3H), 0.81-0.80 (d, *J* = 6.57 Hz, 3H); ^{13}C NMR (126 MHz, $CDCl_3$) δ 162.91 (s), 162.34 (s), 160.13 (d, $^{1}J_{CF}$ = 250.94 Hz), 140.68 (s), 134.72 (d, $^{2}J_{CF}$ = 27.83 Hz), 133.70 (s), 132.80 (s), 132.13 (d, $^{3}J_{CF}$ = 8.29 Hz), 131.51 (s), 131.24 (s), 131.21 (d, $^{4}J_{CF}$ = 2.31 Hz), 128.38 (d, $^{3}J_{CF}$ = 12.43 Hz), 124.57 (d, $^{4}J_{CF}$ = 3.48 Hz), 123.54 (s), 120.99 (s), 116.31 (d, $^{2}J_{CF}$ = 21.48 Hz), 60.76 (s), 28.93 (s), 20.71 (s), 20.37 (s).

Figure 318: ^{1}H spectra of (R)-DAW-II-20:

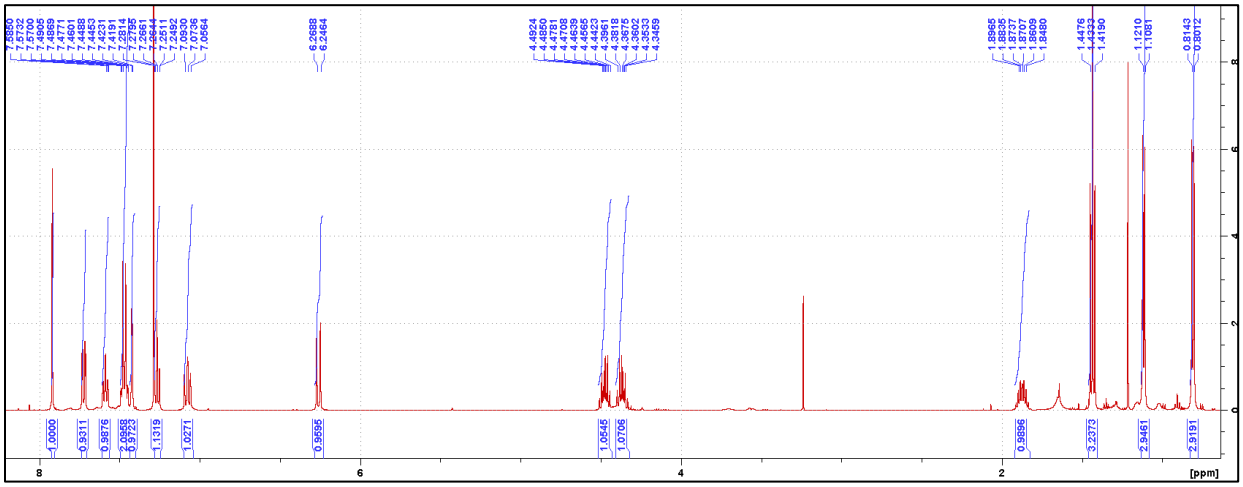

Figure 319: ^{13}C spectra of (R)-DAW-II-20:

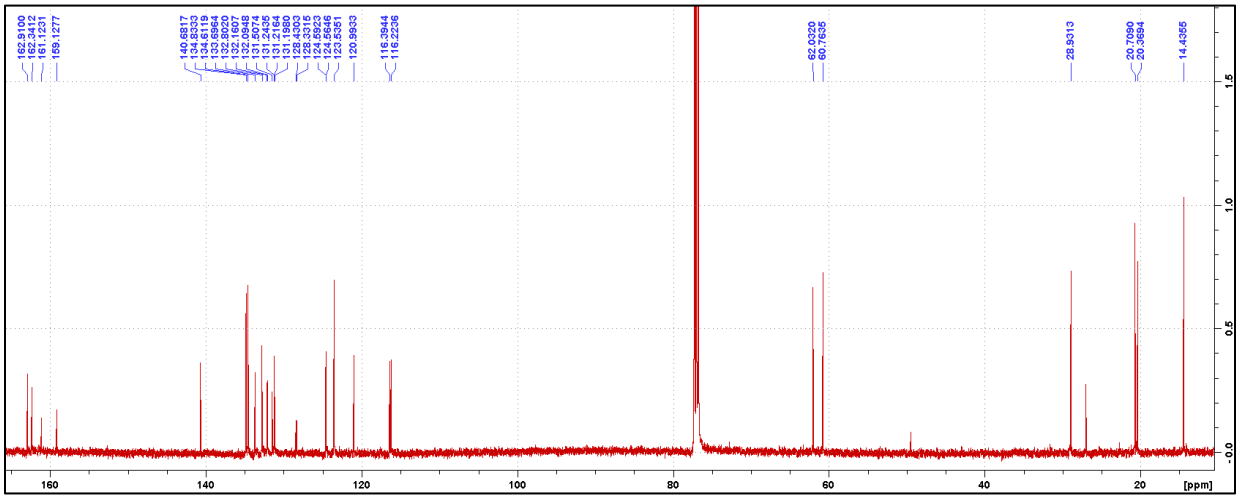

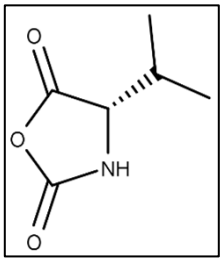

Synthesis of (S)-valine NCA: Boc-D-valine (10.0 g, 46.17 mmol) was added to anhydrous ethyl acetate (200 mL), followed by the addition of triphosgene (5.48 g, 18.47 mmol). The solution was stirred until a clear solution was obtained before triethyl amine (7.08 mL, 50.79 mmol) was added dropwise over a period of 15 min during which a white solid formed (TEA-HCl salt). The temperature was kept

below 30 °C during the addition of triethyl amine. The solution was stirred at room temperature for 1 h followed by heating to reflux (80°C) for 20 h. The reaction was cooled to room temperature and the solid was removed by filtration and washed with ethyl acetate. The filtrate was concentrated under reduced pressure to yield a brown residue. The residue was then dissolved in dichloromethane (25 mL) and hexanes was added dropwise (25 mL) over a period of 20 min while stirring. The mixture was allowed to sit at -20 °C for 24 h at which point the product precipitated out of solution. The product was collected by filtration to yield a crystalline white solid (2.85 g, 43.2%): ^{1}H NMR (500 MHz, $CDCl_3$) δ 6.16 (s, 1H), 4.23-4.22 (d, *J* = 4.25 Hz, 1H), 2.31-2.25 (m, 1H), 1.12-1.11 (d, *J* = 6.95 Hz, 3H), 1.07-1.05 (d, *J* = 6.82 Hz, 3H); ^{13}C NMR (126 MHz, $CDCl_3$) δ 168.58, 152.55, 62.99, 30.80, 18.27, 16.62.

Figure 320: ^{1}H spectra of (S)-valine NCA:

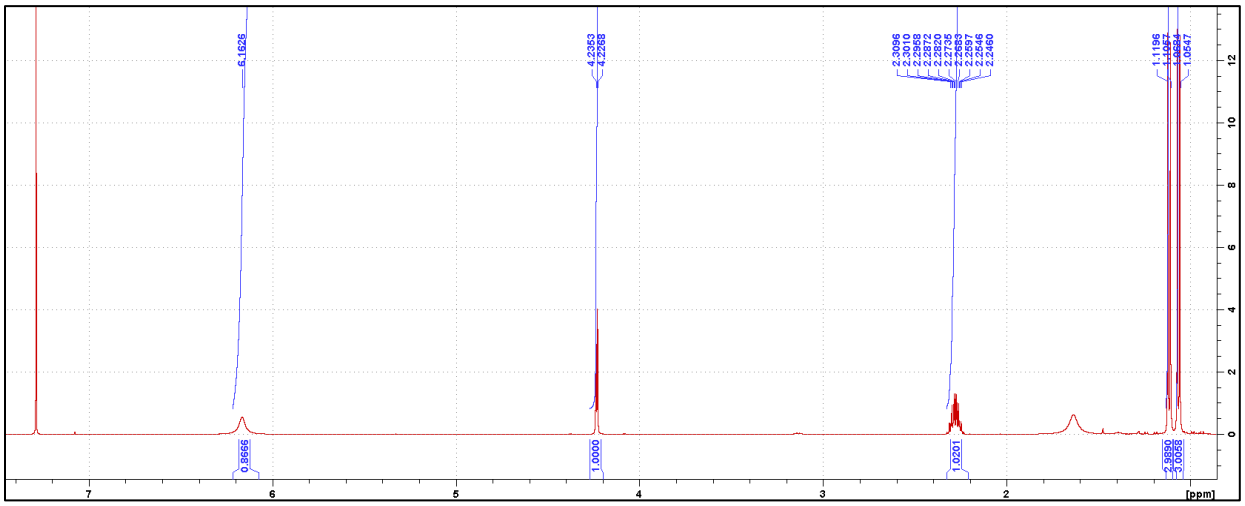

Figure 321: ^{13}C spectra of (S)-valine NCA:

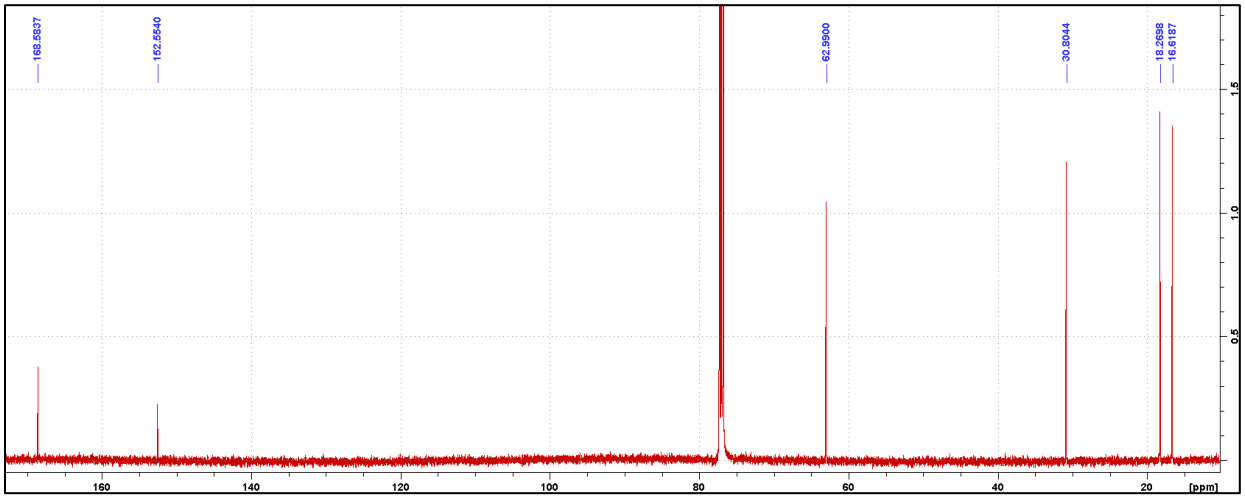

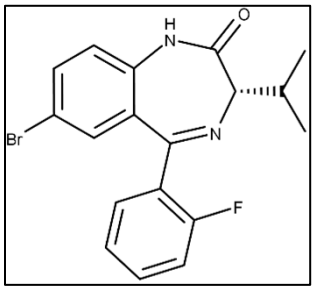

Synthesis of (S)-DAW-I-20: 2-Amino-5-bromo-2′-fluorobenzophenone (15.08 g, 51.27 mmol) was dissolved in DCM (75 mL) before being cooled to 0 °C. DCC (12.91 g, 62.55 mmol) was dissolved in DCM (50 mL) and added dropwise to the mixture while stirring at 0 °C. upon completion of the addition, the reaction was warmed to RT for 36 h. The reaction was then filtered and washed with DCM to remove the urea byproduct. The filtrate was then concentrated to dryness before the crude material was dissolved in DCM (100 mL) and TFA (28.6 mL, 307.62 mmol) was added dropwise. The mixture was then stirred overnight at RT. Boc deprotection was confirmed with the material dropping to the baseline via TLC (50% EtOAc:Hex) while the 2-amino-5-bromo-2′-fluorobenzophenone remained unchanged via TLC. The reaction was then neutralized with Et_3N (52.9 mL, 312.75 mmol) and the reaction was then heated to 80 °C for 3.5 h. Cyclization was confirmed with the material moving off the baseline via TLC (50% EtOAc:Hex). The reaction was then concentrated to dryness before the crude material was

dissolved in EtOAc (250 mL). The organic layer was washed with H_2O (250 mL), followed by a wash with 5% aqueous $NaHCO_3$ (250 mL), and brine (250 mL). The organic layer was then dried with anhydrous $MgSO_4$ before being concentrated to dryness. The crude material was loaded onto a precolumn with chloroform and separated by Biotage: 5-5% ethyl acetate in hexanes (3 CV), followed by 5-50% ethyl acetate in hexanes (15 CV). The desired product was collected as a yellow solid. (3.05 g, 15.8%): ^{1}H NMR (500 MHz, $CDCl_3$) δ 9.52 (s, 1H), 7.62-7.60 (dd, *J* = 3.61, 2.22 Hz, 1H), 7.59-7.54 (dt, *J* = 3.32, 1.54 Hz, 1H), 7.48-7.44 (m, 1H), 7.38-7.37 (d, *J* = 2.09 Hz, 1H), 7.25-7.22 (m, 1H), 7.12-7.06 (m, 1H), 3.17-3.15 (d, *J* = 9.36 Hz, 1H), 2.81-2.74 (m, 1H), 1.23-1.21 (d, *J* = 6.68 Hz, 3H), 1.14-1.13 (d, *J* = 6.52 Hz, 3H); ^{13}C NMR (126 MHz, $CDCl_3$) δ 170.38 (s), 164.10 (s), 160.55 (d, $^1J_{CF}$ = 252.53 Hz), 136.58 (s), 134.62 (s), 132.14 (t, *J* = 3.94 Hz), 131.70 (d, $^4J_{CF}$ = 1.79 Hz), 130.03 (s), 127.18 (d, $^2J_{CF}$ = 12.13 Hz), 124.33 (d, $^3J_{CF}$ = 3.57 Hz), 122.91 (s), 116.46 (s), 116.34 (d, $^2J_{CF}$ = 21.68 Hz), 69.54 (s), 28.98 (s), 20.31 (s), 19.01 (s).

Figure 322: ^{1}H spectra of (S)-DAW-I-20:

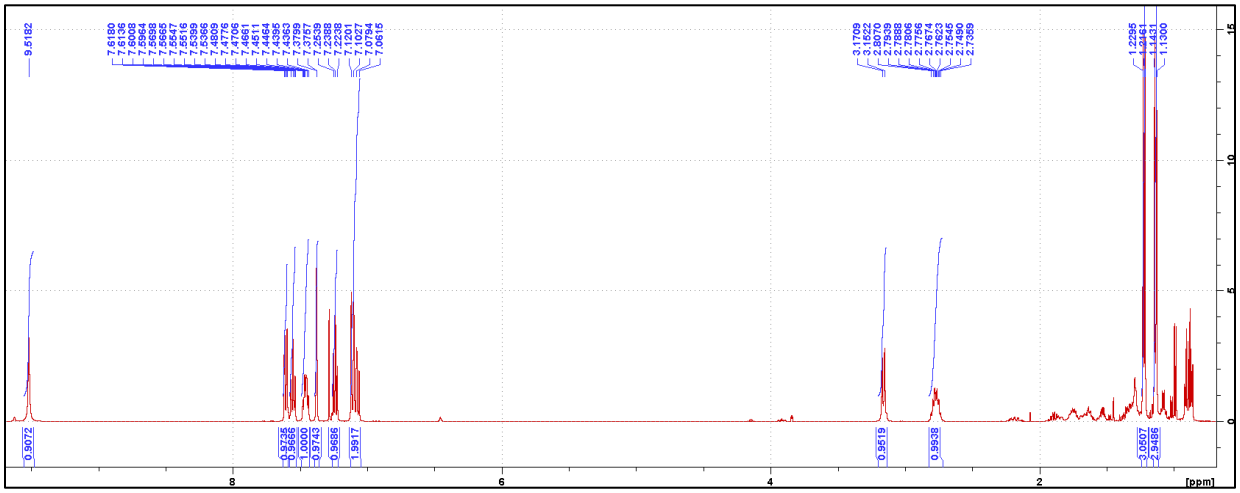

Figure 323: ^{13}C spectra of (S)-DAW-I-20:

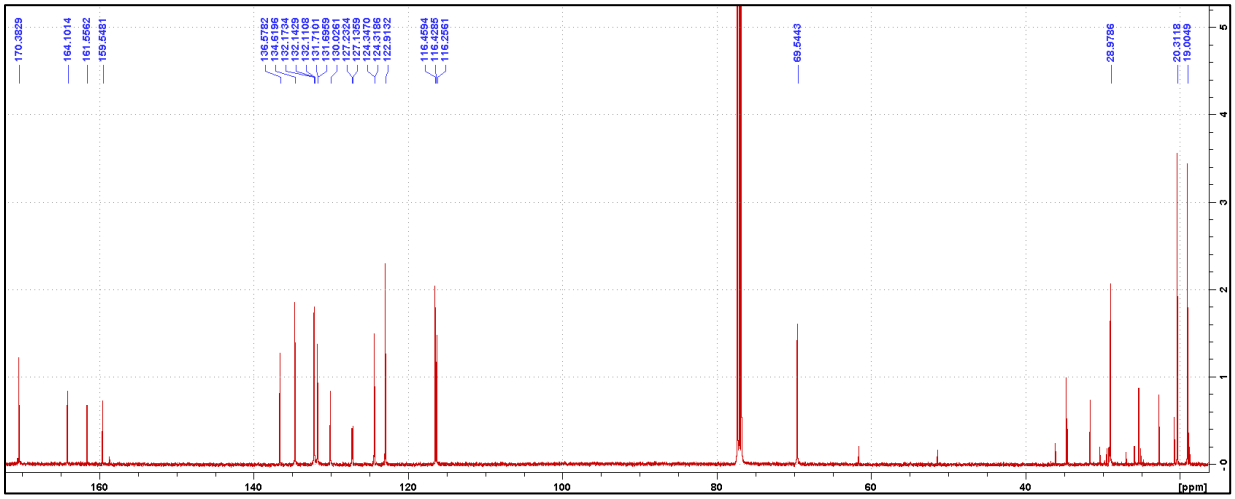

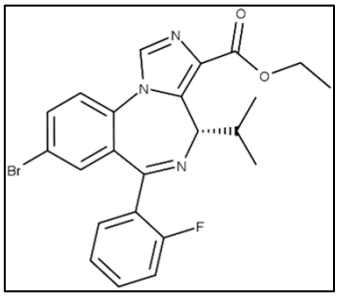

Synthesis of (S)-DAW-II-20: A three stopper RB flask was purged with nitrogen and vacuum 3 times. **(S)-DAW-I-20** (250.84 mg, 0.67 mmol) was dissolved in anhydrous tetrahydrofuran (2.7 mL) and added to the reaction flask. The mixture was cooled to -20 °C using a dry ice/IPA bath. A solution of 1M potassium tert-butoxide in anhydrous tetrahydrofuran (0.87 mL) was added dropwise over the course of 10 min, at which time the reaction color turned to a deep orange. Upon completion of the addition, the mixture was allowed to stir at -20 °C for 40 min. Diethyl chlorophosphate (0.135 mL, 0.94 mmol) was added dropwise over the course of 5 min while maintaining a temperature of -20 °C. After 3.5 h, no more conversion was observed via TLC (100% EtOAc) and ethyl isocyanoacetate (0.095 mL, 0.87 mmol) was added dropwise over the course of 5 min followed by the addition of a solution of 1M potassium tert-butoxide in anhydrous tetrahydrofuran (0.87 mL) at -20 °C. The reaction was then warmed to room temperature and stirred overnight at which point all of the intermediate had been consumed via

TLC (100% EtOAc). The reaction was then quenched with 5% aqueous sodium bicarbonate (30 mL), and the product was extracted with ethyl acetate (30 mL). The organic layer was washed with 10% aqueous sodium bicarbonate (30 mL) followed by 20% aqueous NaCl (30 mL). The organic layer was then dried with $MgSO_4$ and then concentrated under reduced pressure. The residue was loaded onto a precolumn with chloroform and separated by Biotage: 30-90% ethyl acetate in hexanes (45 CV). The desired product was obtained as an off-white solid (159.25 mg, 50.7%): ^{1}H NMR (500 MHz, $CDCl_3$) δ 7.92 (s, 1H), 7.73-7.71 (dd, *J* = 3.57, 2.16 Hz, 1H), 7.60-7.57 (dt, *J* = 3.29, 1.42 Hz, 1H), 7.49-7.45 (m, 2H), 7.42-7.41 (d, *J* = 1.93 Hz, 1H), 7.28-7.25 (dt, *J* = 3.92, 0.46 Hz, 1H), 7.09-7.06 (m, 1H), 6.27-6.25 (d, *J* = 11.22 Hz, 1H), 4.51-4.44 (m, 1H), 4.40-4.33 (m, 1H), 1.90-1.83 (m, 1H), 1.44-1.42 (t, *J* = 7.13 Hz, 3H), 1.12-1.11 (d, *J* = 6.43 Hz, 3H), 0.81-0.80 (d, *J* = 6.57 Hz, 3H); ^{13}C NMR (126 MHz, $CDCl_3$) δ 162.90 (s), 162.36 (s), 160.13 (d, $^1J_{CF}$ = 250.94 Hz), 140.67 (s), 134.89 (d, $^2J_{CF}$ = 27.83 Hz), 133.70 (s), 132.81 (s), 132.18 (d, $^3J_{CF}$ = 8.28 Hz), 131.49 (s), 131.23 (s), 128.36 (d, $^3J_{CF}$ = 12.43 Hz), 124.58 (d, $^4J_{CF}$ = 3.38 Hz), 123.54 (d, $^3J_{CF}$ = 6.12 Hz), 120.99 (s), 116.30 (d, $^2J_{CF}$ = 23.87 Hz), 60.77 (t, *J* = 9.91 Hz), 28.93 (d, *J* = 11.26 Hz), 20.75 (s), 20.37 (s).

Figure 324: ^{1}H spectra of (S)-DAW-II-20:

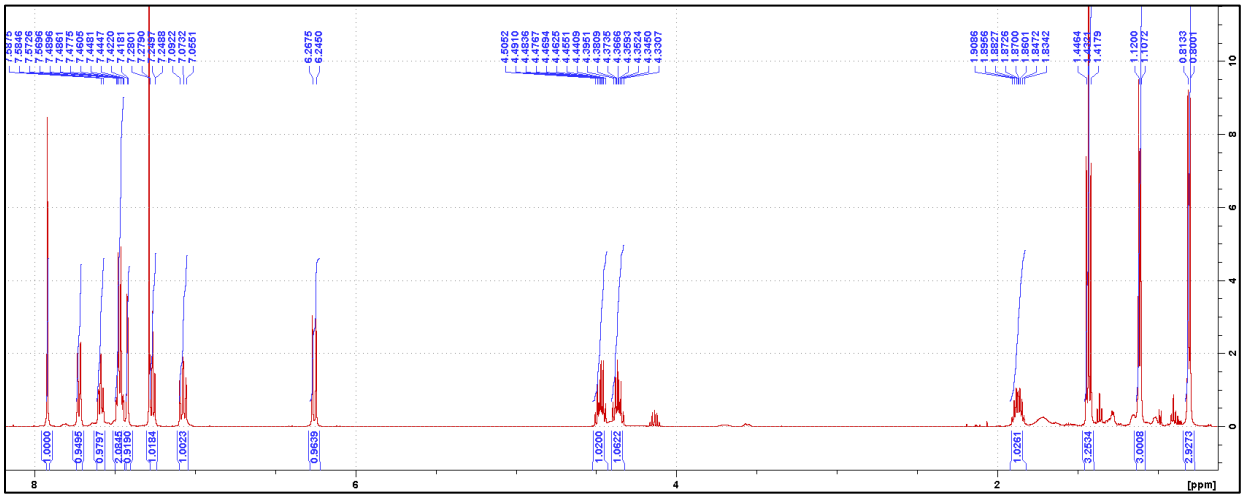

Figure 325: ^{13}C spectra of (S)-DAW-II-20:

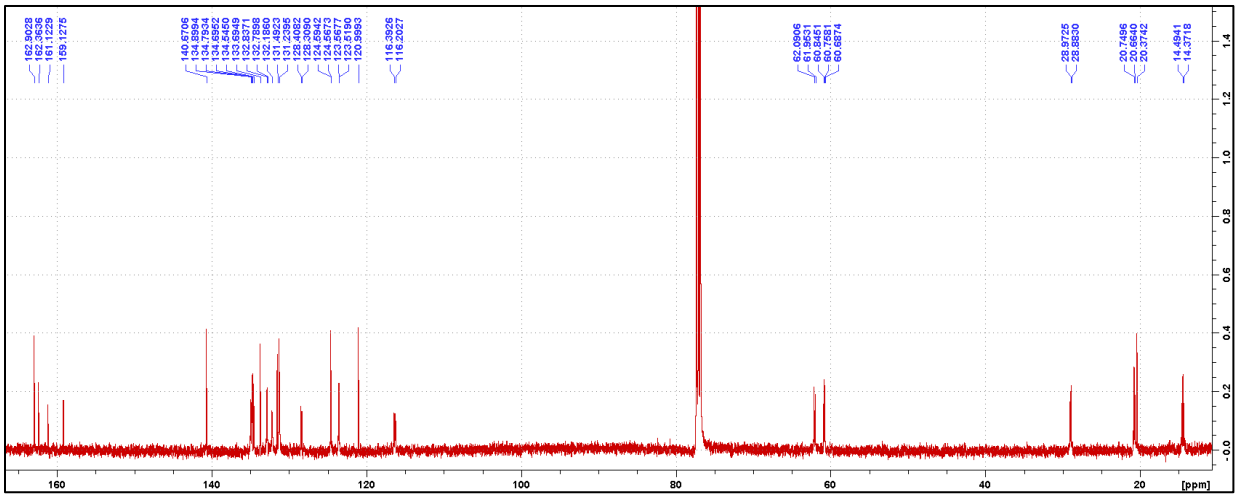

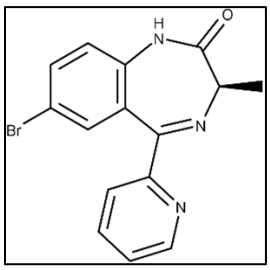

Synthesis of (R)-7-bromo-3-methyl-5-(pyridin-2-yl)-1,3-dihydro-2H-benzo[e][1,4]diazepin-2-one: 2-Aamino-5-bromophenylpyridin-2-yl methanone (10.05 g, 36.27 mmol) was added to anhydrous toluene (117 mL), followed by the addition of trifluoroacetic acid (5.55 mL, 72.53 mmol) dropwise over a period of 10 min, and the mixture was allowed to stir at room temperature for 30 min. (R)-4-methyloxazolidine-2,5-dione (5.01 g, 43.52 mmol) was added portion wise and

the reaction was heated to 50 °C for 18 h. After the majority of the starting material had been consumed by TLC (50% EtOAc:Hex), triethylamine (10.62, 76.16 mmol) was added dropwise over a period of 15 min at which point fuming was observed in the reaction. The reaction was then heated to 80 °C for 3 h at which point disappearance of the intermediate was observed via TLC (50% EtOAc:Hex). Upon cooling to room temperature, the solvent was removed under reduced pressure and the residue was dissolved in ethyl acetate (250 mL). The organic layer was washed with 5% aqueous sodium bicarbonate (250 mL), followed by 10% aqueous NaCl (250 mL). The organic layer was then dried with $MgSO_4$ and the solvent was removed under reduced pressure. The residue was stripped with 10% EtOAc:Heptane (50 mL, 2x) followed by a trituration in 10% EtOAc:Heptane (150 mL) at 60 °C for 4 h. The product was collected by filtration to yield a yellow solid (7.49 g, 62.5%): ^{1}H NMR (500 MHz, $CDCl_3$) δ 8.64-8.63 (m, 1H), 8.17 (s, 1H), 8.07-8.06 (d, *J* = 7.92 Hz, 1H), 7.85-7.82 (dt, *J* = 3.244, 1.71 Hz, 1H), 7.62-7.60 (dd, *J* = 3.62, 2.26 Hz, 1H), 7.56-7.55 (d, *J* = 2.22 Hz, 1H), 7.40-7.37 (m, 1H), 7.02-7.01 (d, *J* = 8.62 Hz, 1H), 3.87-3.85 (q, *J* = 6.47 Hz, 1H), 1.79-1.77 (d, *J* = 6.48 Hz, 3H); ^{13}C NMR (126 MHz, $CDCl_3$) δ 171.77, 166.37, 156.04, 148.93, 137.19, 136.86, 134.60, 134.01, 128.40, 124.67, 124.06, 122.67, 116.23, 59.00, 16.92.

Figure 326: ^{1}H spectra of (R)-7-bromo-3-methyl-5- (pyridin-2-yl) -1,3-dihydro-2H-benzo [e] [1,4] diazepin-2-one:

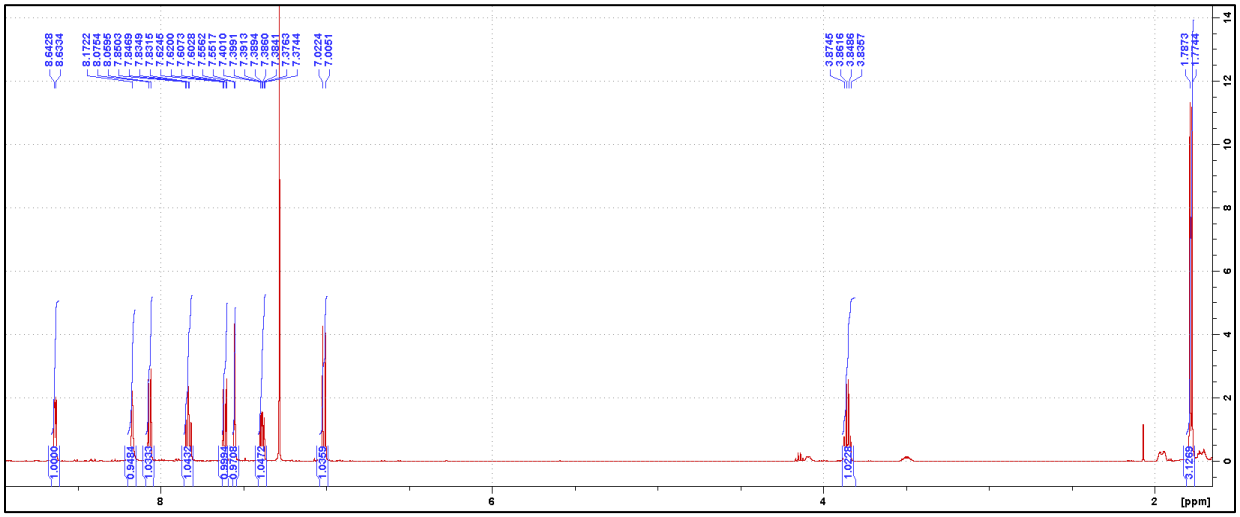

Figure 327: ^{13}C spectra of (R)-7-bromo-3-methyl-5- (pyridin-2-yl) -1,3-dihydro-2H-benzo [e] [1,4] diazepin-2-one:

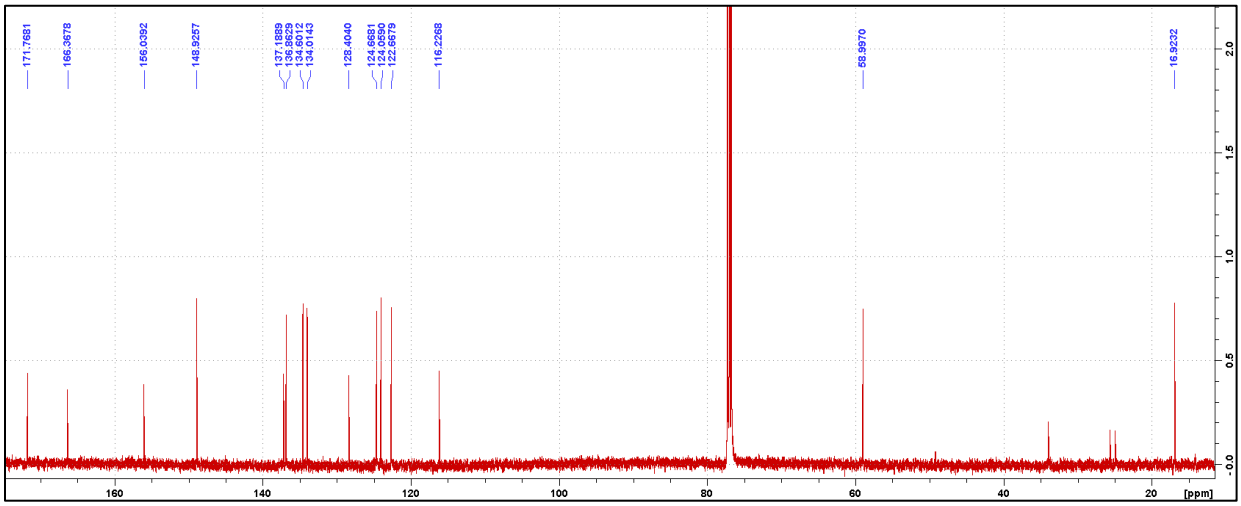

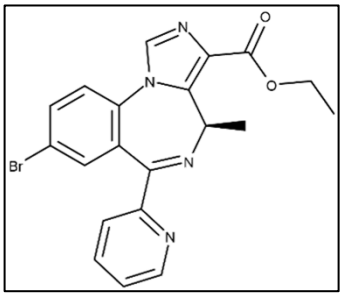

Synthesis of ethyl (R)-8-bromo-4-methyl-6-(pyridin-2-yl)-4H-benzo[f]imidazo[1,5-a] [1,4] diazepine-3-carboxylate: A three stopper RB flask was purged with nitrogen and vacuum 3 times. (R)-7-bromo-3-methyl-5- (pyridin-2-yl) -1,3-dihydro-2H-benzo [e] [1,4] diazepin-2-one (588.0 mg, 1.78 mmol) was dissolved in anhydrous tetrahydrofuran (5.5 mL) and added to the reaction flask. The mixture was cooled to -20 °C using a dry ice/IPA bath. A solution of 1M potassium tert-butoxide in anhydrous tetrahydrofuran (2.32 mL) was added dropwise over the course of 10 min, at which time the reaction color turned to a deep orange. Upon completion of the addition, the mixture was allowed to stir at -20 °C for 40 min. Diethyl chlorophosphate (0.36 mL, 2.49 mmol) was added dropwise over the course of 5 min while maintaining a temperature of -20 °C. After 3.5 h, no more conversion was observed via TLC (100% EtOAc) and ethyl isocyanoacetate (0.25 mL, 2.3 mmol) was added dropwise over the course of 5 min followed by the addition of a solution of 1M potassium tert-butoxide in anhydrous tetrahydrofuran (2.32 mL) at -20°C. The reaction was then warmed to room temperature and stirred overnight at which point all of the intermediate had been consumed via TLC (100% EtOAc). The reaction was then quenched with 5% aqueous sodium bicarbonate (25 mL), and the product was extracted with ethyl acetate (25 mL). The organic layer was washed with 10% aqueous sodium bicarbonate (25 mL) followed by 20% aqueous NaCl (25 mL). The organic layer was then dried with $MgSO_4$ and then concentrated under reduced pressure. The residue was loaded onto a precolumn with chloroform and separated by Biotage: 40-100% ethyl acetate in hexanes (15 CV) followed by 100% ethyl acetate (15 CV). The desired product was obtained as an off-white solid (372.5 g, 49.2%): ^{1}H NMR (500 MHz, $CDCl_3$) δ 8.49-8.48 (m, 1H), 7.94-7.93 (d, *J* = 7.90 Hz, 1H), 7.79 (s, 1H), 7.75-7.71 (dt, *J* = 3.41, 1.53 Hz, 1H), 7.65-7.63 (dd, *J* = 3.57, 2.13 Hz, 1H),

7.40-7.39 (d, *J* = 2.10 Hz, 1H), 7.38-7.37 (d, *J* = 8.59 Hz, 1H), 7.30-7.27 (m, 1H), 6.64-6.60 (q, *J* = 7.35 Hz, 1H), 4.36-4.28 (m, 2H), 2.08-2.07 (d, *J* = 6.72 Hz, 0.5H), 1.35-1.32 (t, *J* = 7.13 Hz, 1H), 1.21-1.19 (d, *J* = 7.36 Hz, 1H); ^{13}C NMR (126 MHz, $CDCl_3$) δ 164.56, 163.01, 157.25, 148.56, 141.64, 136.95, 134.96, 134.94, 134.73, 129.39, 124.71, 124.03, 123.85, 120.34, 60.77, 49.84, 14.58, 14.42.

Figure 328: ^{1}H spectra of (R)-8-bromo-4-methyl-6-(pyridin-2-yl)-4H-benzo[f]imidazo[1,5-a][1,4] diazepine-3-carboxylate:

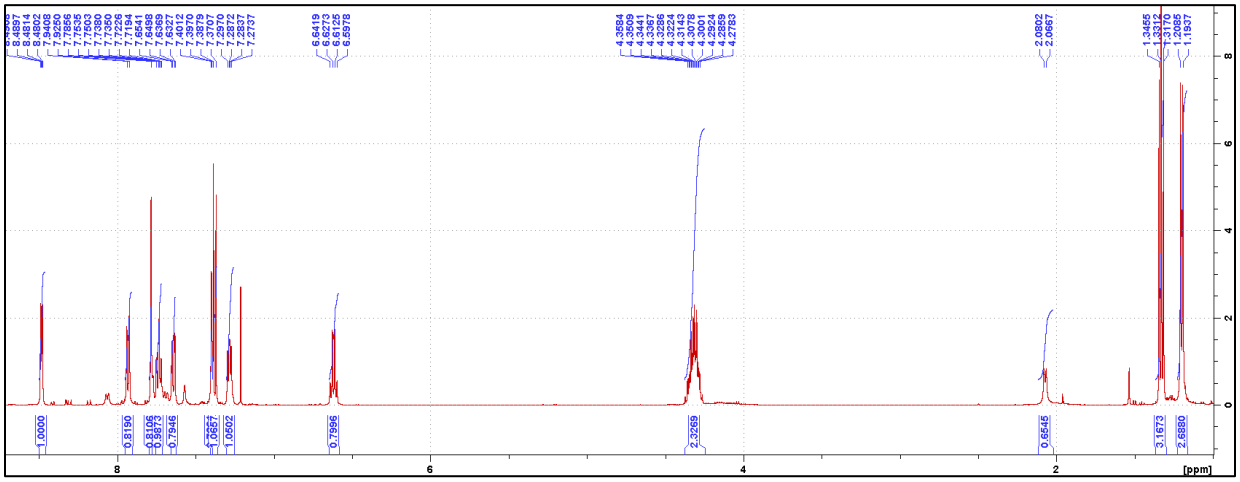

Figure 329: ^{13}C spectra of (R)-8-bromo-4-methyl-6-(pyridin-2-yl)-4H-benzo[f]imidazo[1,5-a][1,4] diazepine-3-carboxylate:

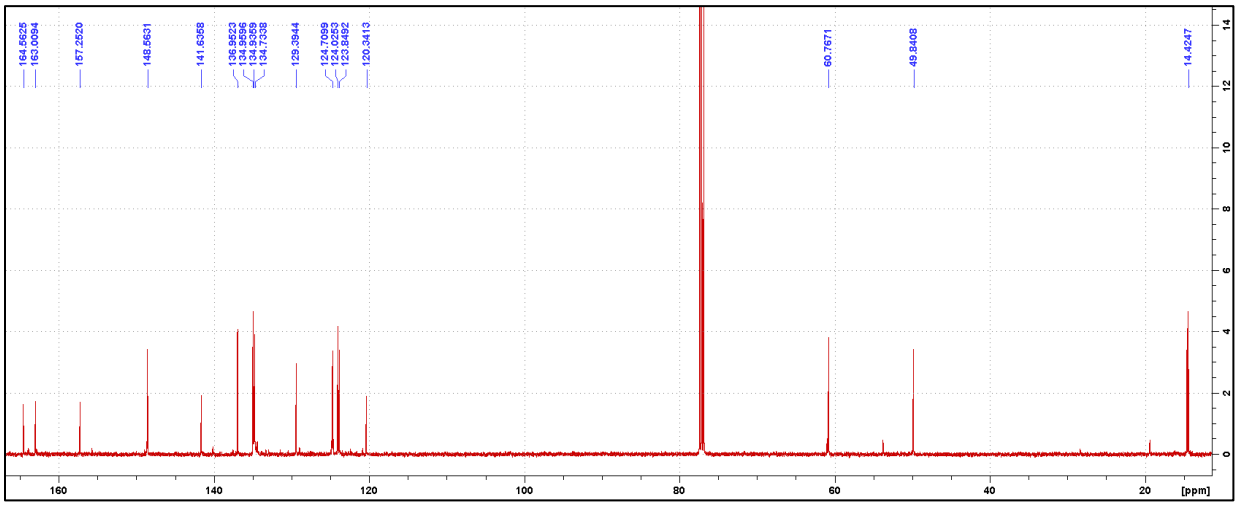

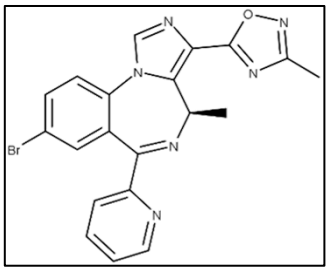

Synthesis of (R)-5- (8-bromo-4-methyl-6- (pyridin-2-yl) -4H-benzo [f] imidazo [1,5-a] [1,4] diazepin-3-yl) -3-methyl-1,2,4- oxadiazole: (E)-N'-hydroxyacetimidamide (438 mg, 5.91 mol) was dissolved in anhydrous THF (4 mL). Enough oven dried 3Å molecular sieves were added to fill approximately ¼ of the flask. NaH (60% dispersion in mineral oil, 65 mg, 1.63 mmol) was added portion wise, and the mixture was allowed to stir at RT for 1 h. In a separate flask, ethyl (R)-8-bromo-4-methyl-6-(pyridin-2-yl)-4H-benzo[f]imidazo[1,5-a] [1,4] diazepine-3-carboxylate (628.5 mg, 1.48 mol) was mixed in anhydrous THF (9.4 mL). The oxime solution was then added dropwise over the course of 15 min. The reaction was then allowed to stir at RT until full consumption of the starting material was observed via TLC (100% EtOAc). Full consumption was observed in 2 h. Once complete, the reaction was quenched with aqueous 10% $NaHCO_3$ (25 mL) and the mixture was extracted with EtOAc (3 x 25 mL). The organic fractions were pooled and washed with brine (75 mL) before being dried with anhydrous $MgSO_4$. The organic layer was concentrated to dryness and the crude material was loaded onto a precolumn with chloroform and separated by Biotage: 50-100% ethyl acetate in hexanes (15 CV) followed by 100% ethyl acetate (25 CV). The desired product was obtained as an off-white solid (411.9 mg, 64.0%): ^{1}H NMR (500 MHz, $CDCl_3$) δ 8.50-8.49 (d, *J* = 4.3 Hz, 1H), 7.96-7.94 (d, *J* = 7.9 Hz, 1H), 7.91 (s, 1H), 7.76-7.73 (m, 1H), 7.70-7.67 (dd, *J* = 3.57, 2.13 Hz, 1H), 7.43-7.42 (m, 2H), 7.31-7.29 (m, 1H), 6.66-6.62 (q, *J* = 7.31 Hz, 1H), 2.39 (s, 3H), 1.28-1.27 (d, *J* = 7.32 Hz, 3H); ^{13}C NMR (126 MHz, $CDCl_3$) δ 170.80, 167.45, 164.75, 157.18, 148.74, 139.21, 136.99, 136.37, 135.70, 135.18, 134.96, 134.89, 134.71, 129.44, 124.92, 124.81, 124.55, 124.06, 123.77, 120.60, 50.00, 14.70, 11.68.

Figure 330: ^{1}H spectra of (R)-5- (8-bromo-4-methyl-6- (pyridin-2-yl) -4H-benzo [f] imidazo [1,5-a] [1,4] diazepin-3-yl) -3-methyl-1,2,4- oxadiazole:

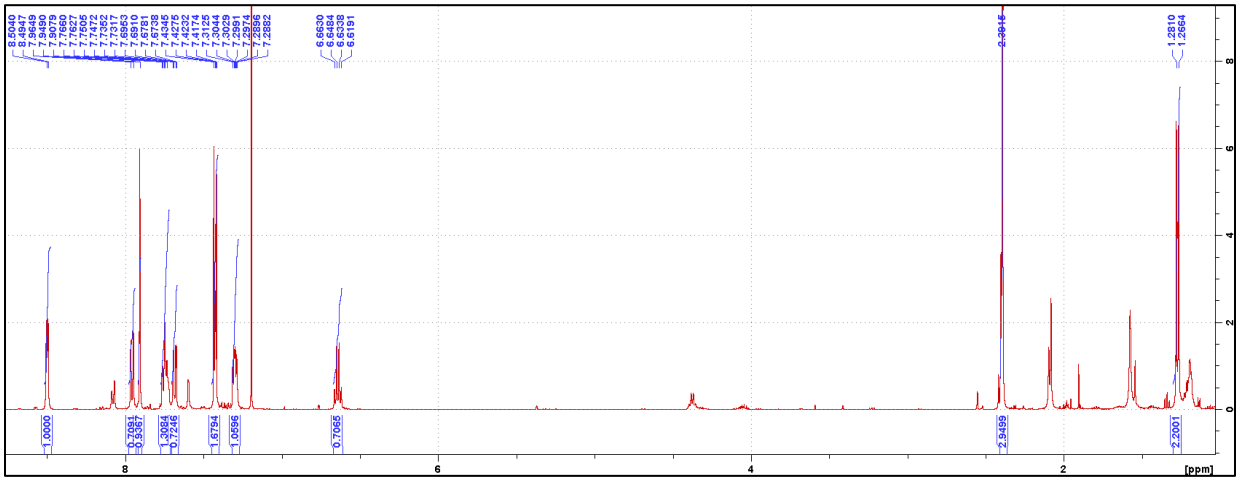

Figure 331: ^{13}C spectra of (R)-5- (8-bromo-4-methyl-6- (pyridin-2-yl) -4H-benzo [f] imidazo [1,5-a] [1,4] diazepin-3-yl) -3-methyl-1,2,4- oxadiazole:

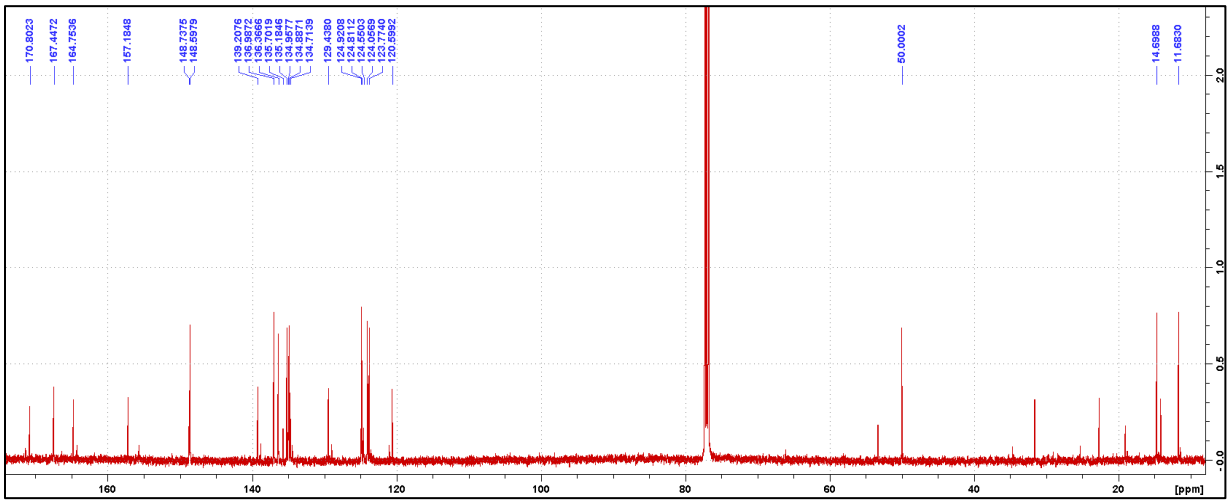

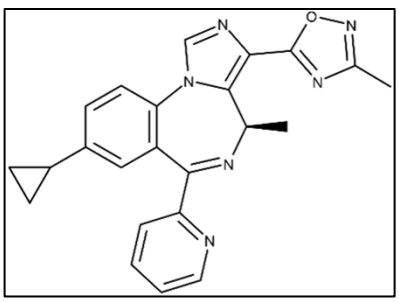

Synthesis of GL-III-64: Toluene (8.3 mL) and H_2O (1.2 mL) were degassed with nitrogen before the addition of (R)-5- (8-bromo-4-methyl-6- (pyridin-2-yl) -4H-benzo [f] imidazo [1,5-a] [1,4] diazepin-3-yl) -3-methyl-1,2,4- oxadiazole (411.9 mg, 0.95

mmol). Cyclopropane boronic acid was added (406 mg, 4.73 mol), followed by the addition of potassium phosphate tribasic (864 mg, 4.07 mmol), $Pd(OAc)_2$ (42.5 mg, 0.189 mmol), and tri(o-tolyl)phosphine (115 mg, 0.379 mmol). The reaction was then heated to 100 °C for 3 h at which point full consumption of the starting material was confirmed via mass spectrometry. The reaction was then cooled to RT before the addition of H_2O (25 mL) and the mixture was extracted with EtOAc (3 x 25 mL). The organic fractions were pooled and washed with brine (75 mL) before being dried over anhydrous $MgSO_4$. The organic layer was then concentrated to dryness before the crude material was loaded onto a precolumn with chloroform and separated by Biotage: 30-100% ethyl acetate in hexanes (20 CV) followed by 100% ethyl acetate (15 CV). The desired product was obtained as an off-white solid (173.8 mg, 46.3%): ^{1}H NMR (500 MHz, $CDCl_3$) δ 8.50-8.49 (m, 1H), 8.02-8.00 (m, 0.25H), 7.89-7.88 (m, 1.75H), 7.74-7.71 (m, 1H), 7.42-7.41 (d, *J* = 8.33 Hz, 1H), 7.28-7.26 (m, 1H), 7.19-7.18 (m, 1H), 7.07 (m, 0.25H), 6.93-6.92 (d, *J* = 1.62 Hz, 0.75H), 6.63-6.59 (q, *J* = 7.27 Hz, 0.75H), 4.38-4.34 (q, *J* = 6.85 Hz, 0.25H), 2.37 (s, 3H), 2.09-2.07 (d, *J* = 6.91 Hz, 0.8H), 1.82-1.80 (m, 1H), 1.25-1.24 (d, *J* = 7.30 Hz, 2.2H), 0.95-0.93 (m, 2H), 0.59 (m, 2H); ^{13}C NMR (126 MHz, $CDCl_3$) δ 170.05, 166.34, 165.33, 157.01, 147.66, 142.34, 138.26, 135.76, 135.40, 134.75, 132.08, 128.63, 128.17, 128.14, 127.86, 126.55, 123.57, 123.44, 123.33, 123.12, 121.77, 121.07, 48.96, 14.14, 13.46, 10.65, 8.89, 8.82.

Figure 332: ^{1}H spectra of GL-III-64:

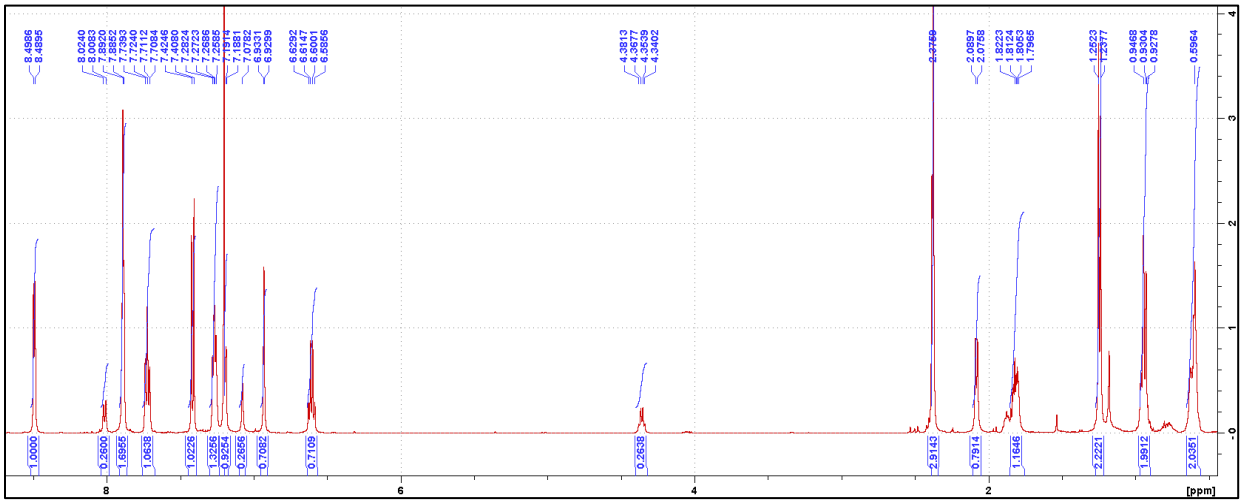

Figure 333: ^{13}C spectra of GL-III-64:

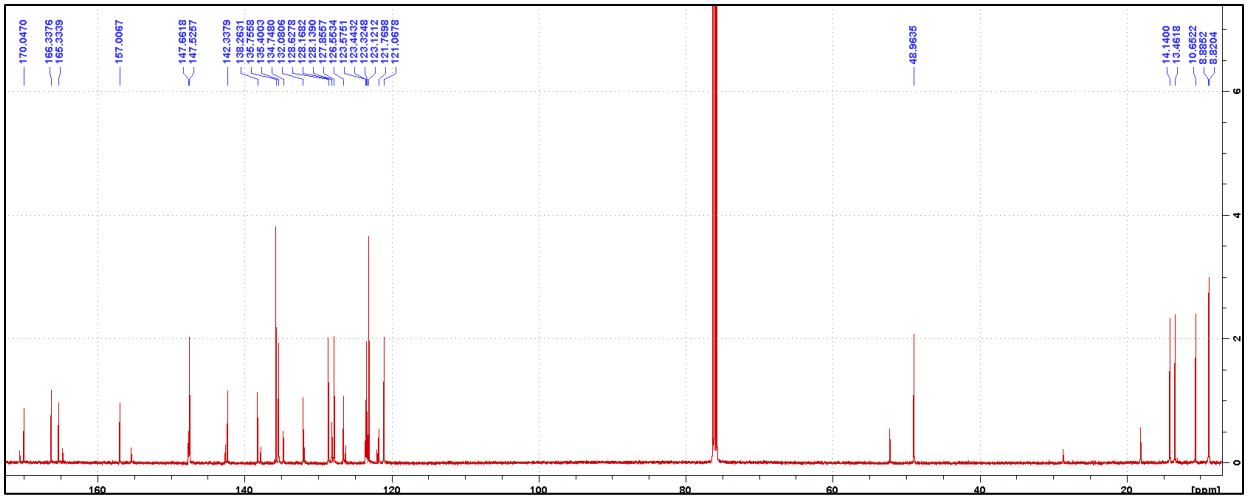

Figure 334: DAW-II-20 TSPO binding dose response curve:

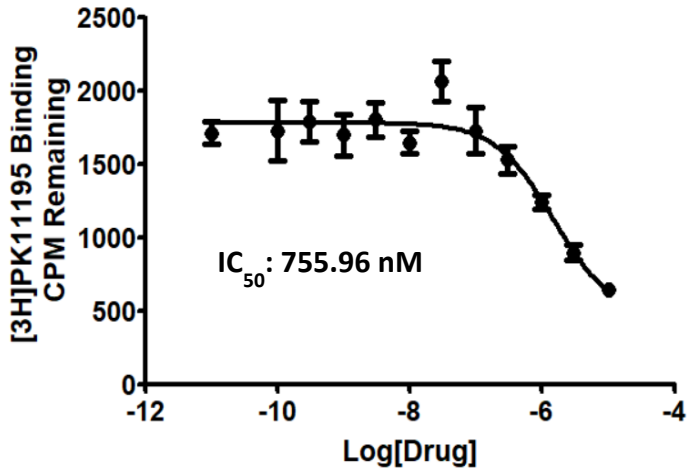

Figure 335: DAW-II-80 TSPO binding dose response curve:

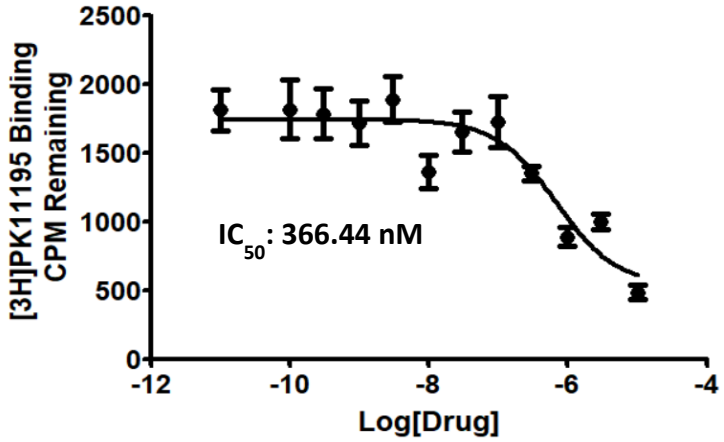

Figure 336: (S)-DAW-II-20 TSPO binding dose response curve:

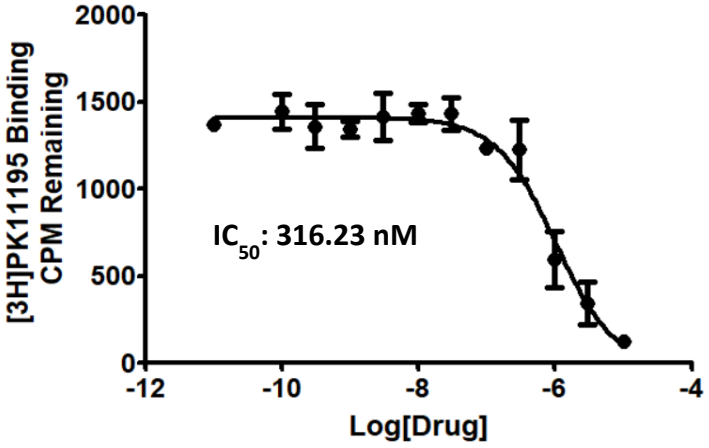

Figure 337: (R)-DAW-II-20 TSPO binding dose response curve:

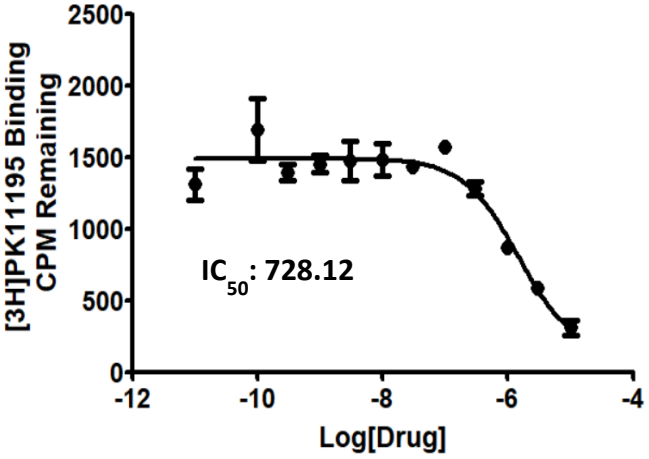

Figure 338: GL-III-64 TSPO binding dose response curve:

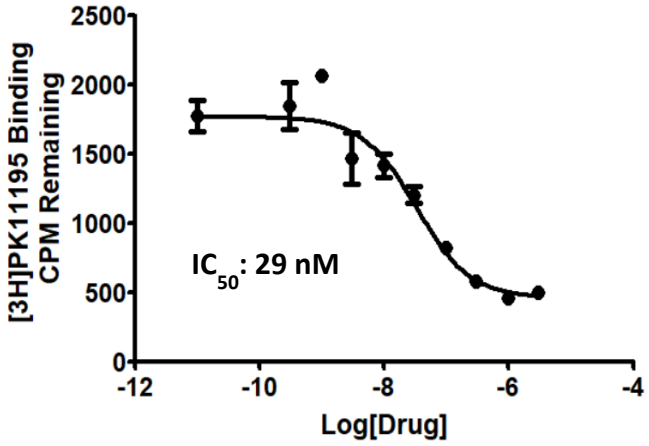

2.9.4 Conclusion

The TSPO receptor represents a promising target for several new drugs, some of which may be benzodiazepines. We have determined from a large library of benzodiazepines particular functional groups that increase the binding affinity to the TSPO receptor. A nitrogen in the 2' position as seen in GL-III-64 likely plays a very important role in receptor binding. As shown for DAW-II-20 and DAW-II-80, an isopropyl or cyclopropane group substituent attached to 7-membered ring are groups which assist in binding. Furthermore, we have shown that the S orientation of these functionalities has far superior binding than that of the R orientation. While an ethyl ester has shown to have good binding, this type of group could poses a challenge for drug development in respect to metabolism by esterases. We have shown that oxadiazole rings maintain strong TSPO binding while also having the ability to better control metabolism. Various groups could be attached to the oxadiazole rings of which we have only tested a few. MOE could likely be optimized to predict some of the best functionalities that could be added to the oxadiazole ring. Lastly, the bromine and cyclopropane ring in the 7-positon both have shown to yield strong TSPO

binding, however it may be possible to modify this group in such a way that additional hydrogen bond interactions are picked up from nearby amino acid residues in the TSPO binding pocket. These modifications may include an amide with a tail of various lengths and potential ether or alcohol for hydrogen bonding. MOE could likely again be optimized to predict the best groups for this position. Furthermore, beginning with an aryl bromide, this group could likely easily be modified with various transition metal catalyzed reactions. Overall, we have made progress in designing a benzodiazepine TSPO ligand that has the potential for a low nanomolar binding affinity.

PART 3: IMPROVED 2-PYRIDYL REDUCTIVE HOMOCOUPLING REACTION USING BIORENEWABLE SOLVENT CYRENE™ (DIHYDROLEVOGLUCOSENONE)

3.1 Introduction

Non-toxic and renewable solvents are very attractive to produce small molecules commercially and in the research laboratory. Greener alternatives to dimethylformamide (DMF), a commonly used polar aprotic organic solvent appreciated for its ability to dissolve organic compounds while being water soluble has led to the discovery of alternatives such as Cyrene™ (dihydrolevoglucosenone).[217] Cyrene™ is a bio-based solvent that is derived from a two-step process beginning with cellulose.[218] The cost of this solvent is comparable with DMF, but it can be anticipated that the price will decline with further demand. An important advantage is that Cyrene™ is non-toxic and biodegradable.[219] Menschutkin reactions and fluorinations have been carried out in Cyrene™ achieving better reaction rates than standard aprotic polar solvents.[217] Interestingly, the viscosity of Cyrene™ allowed for great improvements in the process of graphene dispersion.[220] Other reactions have been reported using Cyrene™ as a solvent for example peptide coupling reactions using HATU,[221] an amide forming reaction with acid chlorides,[222] reactions that formed urea products,[223] N-alkylations,[224] SNAr reactions,[224] and aldimine reactions.[224] Some transition metalcatalyzed reactions in Cyrene™ have been reported. These include a Suzuki–Miyarua reaction[225] and a Sonogashira and Cacchi-type annulation reaction.[226] Importantly, the application of Cyrene™ signicantly increases the sustainability of the production of chemicals and materials.

Herein, we report the use of Cyrene™ and Cyrene™ solvent blends to produce substituted 2,2′-bipyridines via a reductive homocoupling reaction (Scheme 10).

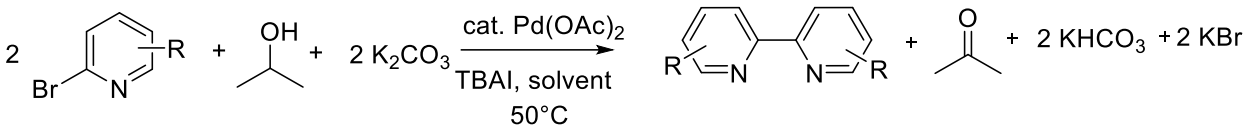

Scheme 10: Reductive homocoupling using isopropanol as reductant.

Starting from aryl halides, this reaction is usually catalyzed by palladium in the presence of another metal or a compound that is oxidized in the process.[227] Only a limited number of palladium-catalyzed reductive homocoupling reactions using non-toxic alcohols as reductants have been reported for the conversion of iodo- and bromopyridines. Zeng et al. reported the use of 3-pentanol as solvent using 3 mol% $Pd(dppf)Cl_2$ and 7.5 equivalent of CaF as base.[228] The reaction proceeded at 100 °C for bromo- and iodobenzene as well as 2-iodo and 2-bromopyridine. The use of 1,4-butanediol as solvent was reported by Huang et al. in conjunction with 0.5 mol% $Pd(OAc)_2$, 1.1 equivalent of cesium carbonate at 75 °C proceeding for a wide range of substituted aryl iodides, iodopyridines, and iodothiophenes.[229] The reaction times varied between 2 to 24 h and resulted in yields between 39–95%. Other green synthetic approaches for homocoupling and Ullmann reactions have been reported.[230] This includes several reports using water as solvent. Gadda et al. introduced a homocoupling of aryl iodides using microwave irradiation with 4.8 mol% of Pd/C at 150 °C.[231] The conversion for 2-iodopyridine was 47%. Other catalysts introduced included amphiphilic Pd carbon spheres giving conversions between 44–53% with a catalyst loading of 0.5% at 90 °C.[232] This work was followed by others, reporting Pd and Au nanosphere catalysts resulting in higher biaryl yields with the use of aryl bromides[233] and aryl chlorides[234] using high temperatures and in some instances long reaction times.[230] Other approaches include the use of

aryl boronic acids in combination with copper(I)chloride, a water extract of pomegranate ash (WEPA) and ethanol at room temperature[235] or Pd catalyzed reductive homocouplings with water extracted papaya bark ash and tobacco using ethanol or DMF as cosolvents.[236] These reports cited many other green approaches for the homocoupling of aryl boronic acids, which are usually synthesized from aryl halides. Recently, the application of a recyclable glycerol-based deep eutectic solvent was reported for the homocoupling of (hetero)aryl chlorides at 80 °C within 12 hours.[237]

3.2 Experimental Methods

3.2.1 Materials

All reagents and solvents[238] were obtained from Sigma-Aldrich Co. LLC, unless otherwise noted, and used as received.

3.2.2 Analytical Procedure

100 mL aliquots were taken from the reaction at the desired time points and added to a Pasteur pipette packed with cotton and 300 mg of Celite 545. The Celite was washed with 1 mL of dichloromethane. 25 mL of the collected filtrate was added to 1 mL of HPLC grade methanol and analyzed by HPLC (Shimadzu Nexera series) with a Photo Diode Array detector (PDA, Shimadzu SPD-M30A) and a single quadrupole mass analyzer (LCMS 2020, Shimadzu, Kyoto, Japan). 0.1% formic acid in methanol and 0.1% formic acid in water was used as the mobile phase. Analytes were separated using a Restek Pinnacle-C18 (4.6 mm × 50 mm, 5 mm particle size) column with gradient elution at a flow rate of 0.5 mL min^{-1}. The time program of mobile phase

was 20% to 100% over 20 min followed by 3 min at 100%. The column was equilibrated to 20% methanol in water for each injection. Data was acquired by PDA having a range of 190–700 nm but using a wavelength of 264 nm for quantification. Interface temperature, desolvation line temperature and heat block temperatures were 350 °C, 250 °C, and 400 °C, respectively. Nebulizing gas flow was 1.5 L min−1 and drying gas flow was 13 L min^{-1}. Relative reaction conversion percentage was determined by the ratio of peak area of starting material to product.

3.2.3 Standard Procedure

To a 20 mL Radley reaction tube was added 12 mL of solvent. The solvent was degassed by bubbling nitrogen through the solvent for 15 min. 2-Bromo-5-(trifluoromethyl)pyridine (compound 69) (0.75 g, 3.32 mmol) was added, followed by the addition of $Pd(OAc)_2$ (112.5 mg, 0.5 mmol, 15 mol%), tetrabutylammonium iodide (1.50 g, 4.06 mmol), and potassium carbonate (0.75 g, 5.43 mmol). The reaction tube was capped and heated to 50 °C. The desired temperature was reached within 15 min. After 30 min isopropyl alcohol (0.56 mL, 7.32 mmol) was added via syringe and the reaction was stirred for the desired amount of time. Aliquots were taken at the desired time points. Upon completion of the reaction by TLC (30% EtOAc in hexanes) the reaction mixture was filtered through Celite and washed with 15 mL Cyrene™/GVL. The mixture was extracted with heptane (25 mL, 6x). The fractions were combined and washed with water (150 mL) to remove any residual solvent. The organic layer was dried with $MgSO_4$ and concentrated to dryness to yield up to 95% of 5,5′-bis(trifluoromethyl)-2,2′-bipyridine (compound 70) as a white solid (99% purity). ^{1}H NMR (500 MHz, $CDCl_3$) δ 8.97 (m, 2H), 8.64–8.62 (m, 2H), 8.11–8.09 (m, 2H); ^{13}C NMR (126 MHz, CDCl3) δ 157.68, 146.30 (q, $^3J_{CF}$ = 4.05 Hz), 134.29 (q, $^3J_{CF}$ = 3.49

Hz), 127.14 (q, $^{2}J_{CF}$ = 33.02 Hz), 123.50 (q, $^{1}J_{CF}$ = 272.29 Hz), 121.24; ^{19}F NMR (471 MHz, CDCl3) δ −62.53.

Figure 339: ^{1}H Spectra of 5,5′-bis(trifluoromethyl)-2,2′-bipyridine (compound 70) isolated from the reaction with Cryene™/GVL:

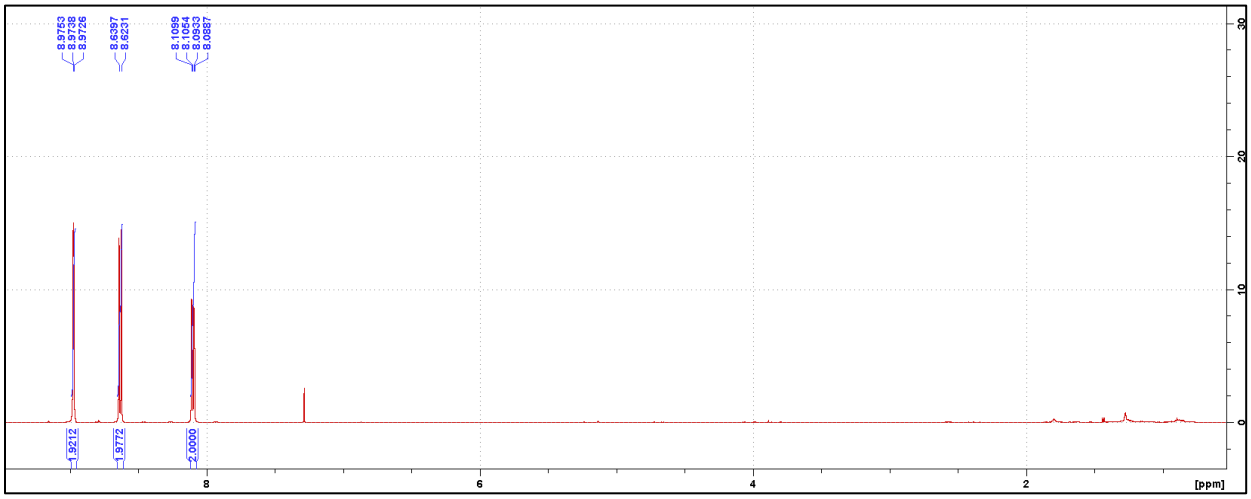

Figure 340: ^{13}C Spectra of 5,5′-bis(trifluoromethyl)-2,2′-bipyridine (compound 70) isolated from the reaction with Cryene™/GVL:

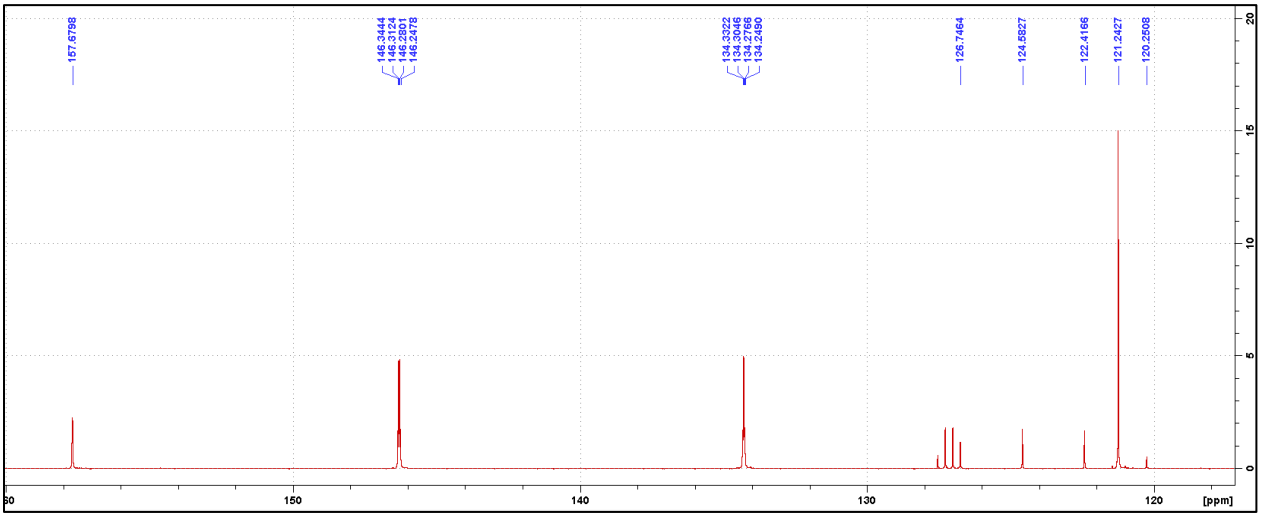

Figure 341: ^{19}F Spectra of 5,5′-bis(trifluoromethyl)-2,2′-bipyridine (compound 70) isolated from the reaction with Cyrene™/GVL:

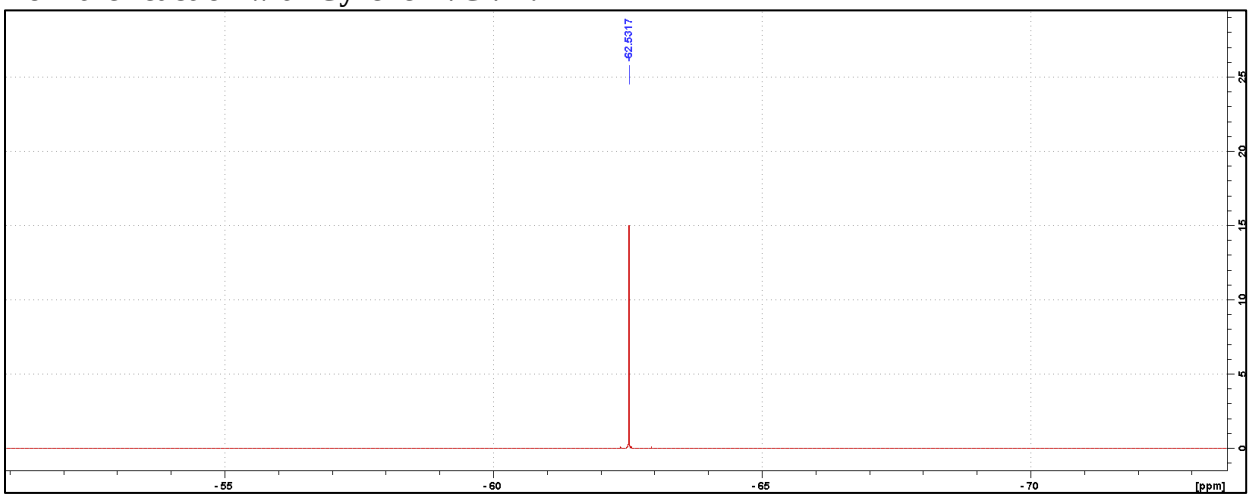

3.3 Results and Discussion

The initial reductive homocoupling of 2-bromo-5- (trifluoromethyl)pyridine was carried out with 15 mol% Pd(OAc)2, 1.2 equivalents of tetrabutylammonium iodide (TBAI), 1.6 equivalents of potassium carbonate, and 2.2 equivalents of isopropanol (IPA) in different solvents at 50°C (Table 4).

Reactions with commonly used solvents were conducted with Cyrene™, DMF, acetonitrile (ACN), γ-valerolactone (GVL), 2-methyltetrahydrofuran (2-MeTHF), N-methylpyrrolidone (NMP), 1-butanol, dimethoxyethane (DME), and water. For details see the standard analytical procedure. Cyrene™ was by far the best solvent for this reaction with a conversion of 98% after 24 h. DMF, which has shown to be a reproductive toxin,[239] resulted in a slow reaction achieving 53% in that same time period. Similar conversions were observed with ACN, which is not considered a green solvent, and GVL. GVL is a green solvent that has recently become useful as an alternative to DMF and NMP.[240] We also tested 2-MeTHF, a green solvent made from furfural,

which in turn can be isolated from biomass by distillation under acidic conditions.[241] The homocoupling reaction in 2-MeTHF showed 23% conversion after 24 h. The homocoupling in 1-butanol and DME after 24 h reached a conversion of 11% and 7%, respectively. The starting materials were not soluble in water thus, no conversion was observed.

Table 4: Reductive homocoupling of 2-bromo-5-(trifluoromethyl)pyridine in different solvents

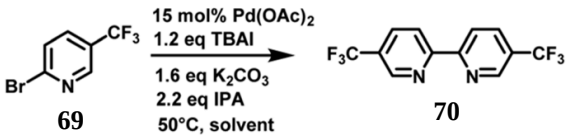

69 70

Solvent	Conversion[a] after 24 h (%)	cEF (complete *E* factor) (kg kg^{-1})	DOZN score
Cyrene™	98	49.5	8
Dimethylformamide (DMF)	53	76.4	21
Acetonitrile (ACN)	59	61.0	18
γ-Valerolactone (GVL)	53	82.0	15
2-Methyltetrahydrofuran	23	166.4	32
N-Methylpyrrolidone	16	270.3	39
1-Butanol	11	337.9	40
Dimethoxyethane (DME)	7	554.6	43
Water	0	∞	—

[a] Reductive homocoupling of 2-bromo-5-(trifluoromethyl)pyridine. All reactions were conducted in 12 mL of indicated solvent (276 mM) at 50 °C. Aliquots were taken at the desired time points and analyzed by reverse phase HPLC at 264 nm using a C18 column. Reaction conversion percentage was determined by the ratio of peak area of starting material to product.

We calculated the complete *E* factor (cEF) for these solvents.[242] The production of 5,5′-bis(trifluoromethyl)-2,2′-bipyridine in Cyrene™ with an cEF of 49.5 kg kg^{-1} still falls into the category of comparable processes to synthesize fine chemicals (5–50 kg kg^{-1}). Other solvents generate more waste per product due to the lower conversion. These cEF might even be higher due to incomplete reaction that can complicate product purification and might require additional amounts of solvent. In addition, we used the DOZN™ quantitative scoring online analysis to evaluated the different solvents for this reaction.[243] In addition to the mass analysis, this green chemistry tool takes into account safety, hazards, energy efficiency, renewability, and pollution. The aggregate DOZN™ scores (see calculations below) depend on the atom economy and are therefore following the trend of the cEF. However, the conversion of starting material is identical

for solvents GVL and DMF but the DOZN™ scores are different (15 vs. 21, Table 1) because GVL is a renewable solvent, non-toxic and safer to use.

Next, we compared Cyrene™ and commercially available Cyrene™ blends that consisted of 50% GVL in Cyrene™ and 20% 2-MeTHF in Cyrene™ (Figure. 342).

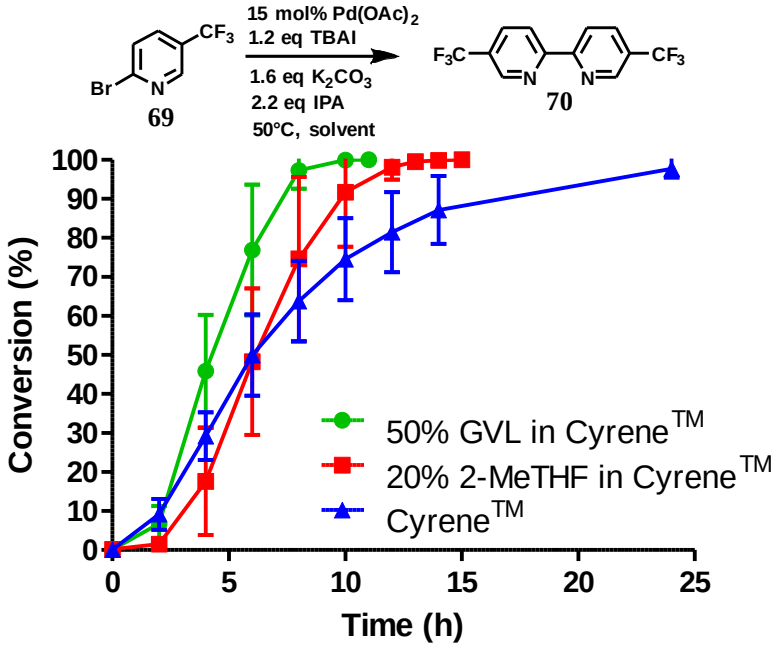

Figure 342: Reductive homocoupling of 2-bromo-5-(trifluoromethyl)pyridine. All reactions were conducted in 12 mL of indicated solvent (276 mM) at 50°C. Aliquots were taken at the desired time points and analyzed by reverse phase HPLC at 264 nm using a C18 column. Reaction conversion percentage was determined by the ratio of peak area of starting material to product.

Three independent trials for each solvent type were conducted. Cyrene™ itself significantly improved the rate of reaction. In contrast to DMF, the reaction reached full conversion after 24 h. Interestingly, Cyrene™ blends with GVL and 2-MeTHF further accelerated the homocoupling of 2-bromo-5′-(trifluoromethyl)pyridine. For some trials with Cyrene™/2-MeTHF, 100% conversion was observed after 10 h and for some trials with Cyrene™/GVL the reaction was complete within 8 h. All reactions were slow during the first 2 h and accelerated considerably after that. For solvents that did not contain Cyrene™, the initial reaction rate was significantly slower. The isolated yields for reactions carried out in Cyrene™ and Cyrene™ blends were up to 95%. Also, simple extraction with heptane provided pure 5,5′-bis(trifluoromethyl)-2,2′-

bipyridine as product (99% pure by HPLC). Other homocoupling reactions e.g. using solvent pentanol reported the formation of almost 20% of pyridine as dehalogenation product.[244] For these reactions further purification was employed such as recrystallization or column chromatography, which required a significant volume of solvents. In the case of column chromatography using hexanes and ethyl acetate, azeotropes are obtained that prevent recycling by simple distillation.[245] Heptane used for the extraction of 5,5′-bis(trifluoromethyl)-2,2′-bipyridine was reused as extractant after the evaporation to improve the sustainability of the reaction. We were not able to recover Cyrene™ or Cyrene™ blends because of their high boiling points.

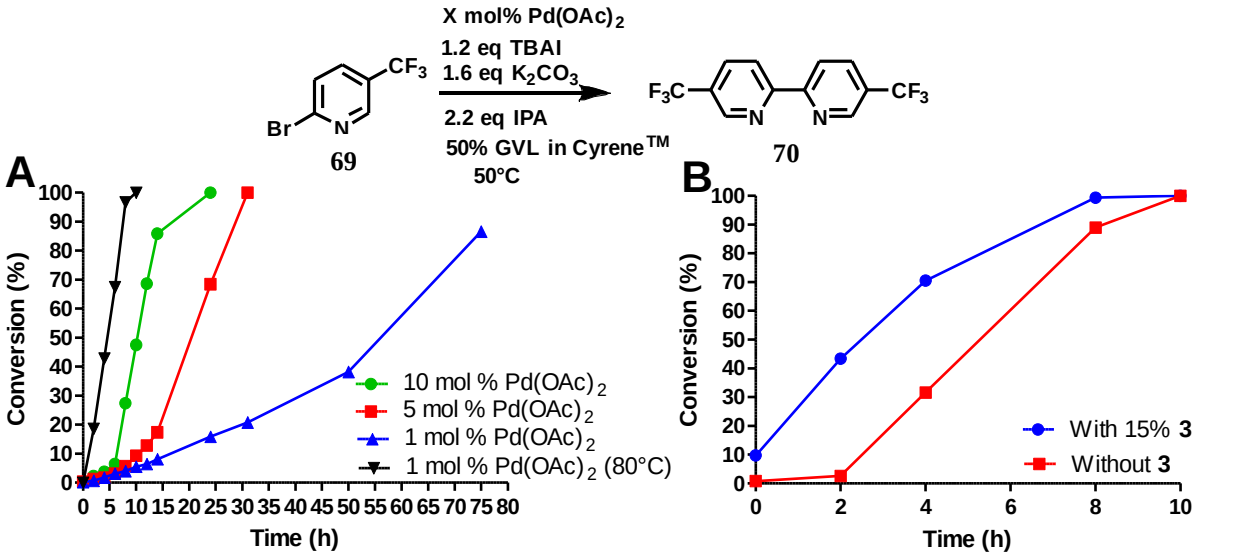

Figure 343: (A) Reductive homocoupling of 1 in the presence of 1, 5, and 10 mol% of $Pd(OAc)_2$; (B) reductive homocoupling of 1 in the presence of 15 mol% of $Pd(OAc)_2$ with and without the addition of 10% of 5,5′-bis(trifluoromethyl)-2,2′-bipyridine. All reactions were conducted with 12 mL of indicated solvent. Aliquots were taken at the desired time points and analyzed by reverse phase HPLC at 264 nm using a C18 column. Reaction conversion percentage was determined by the ratio of peak area of starting material to product.

Due to the high cost of $Pd(OAc)_2$ and relatively high catalyst loading (15 mol%), we examined the effect of lower catalyst loading in respect to conversion (Fig. 343A). The standard procedure using 15 mol% palladium acetate at 50°C afforded full conversion using the Cyrene™/GVL blend in proximately 8 h. Using 10 mol% $Pd(OAc)_2$, the reaction reached full

conversion at 24 h. 27.4% conversion was observed at 8 h. The use of 5 mol% $Pd(OAc)_2$ resulted in full conversion at 31 h. 5.7% conversion was observed at 8 h. The homocoupling reaction employing 1 mol% $Pd(OAc)_2$ reached 87% conversion after 75 h. 6.4% conversion was observed at 12 h. The increase of the reaction temperature to 80°C accelerated the reaction rate significantly achieving full conversion within 10 h. Thus, a lower catalyst loading could be employed but required a higher reaction temperature to reach completion in a reasonable amount of time. At 50°C, a pronounced slow onset of the reaction was observed, possibly due to low solubility or slow formation of the catalytic species. 2,2′-Bipyridines have been widely used as ligands for palladium-catalyzed reactions[246] and therefore we explored the addition of product 70 at the start of the reaction (Figure. 343B). We observed a faster onset of the reaction with the addition of 70 than without. The graph begins with 10% conversion because compound 70 is also the corresponding

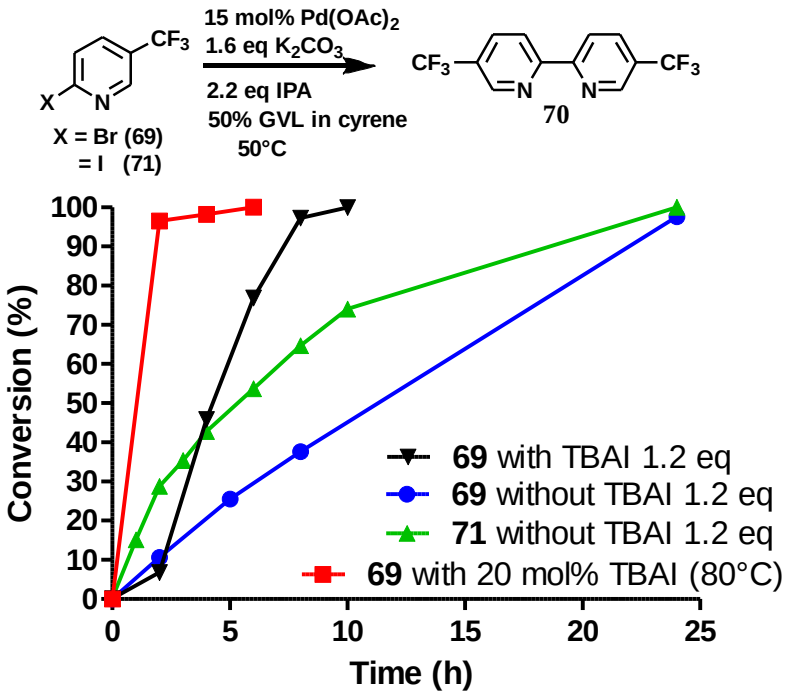

Figure 344: Reductive homocoupling of 69 and 71 in the presence and absence of TBAI. All reactions were conducted with 12 mL of 50% GVL in Cyrene™ (276 mM). Aliquots were taken at the desired time points and analyzed by reverse phase HPLC at 264 nm using a C18 column. Reaction conversion percentage was determined by the ratio of peak area of starting material to product.

product. Overall, we found that the reaction with the addition of 70 serving as palladium ligand was two hours faster than the reaction without.

To investigate the role of TBAI, which was added to assist in an assumed Finkelstein type reaction (bromo-iodo exchange reaction), we carried out the homocoupling of 2-bromo-5-(trifluoromethyl)pyridine (69) without TBAI using the Cyrene™/ GVL blend as solvent (Fig. 344).

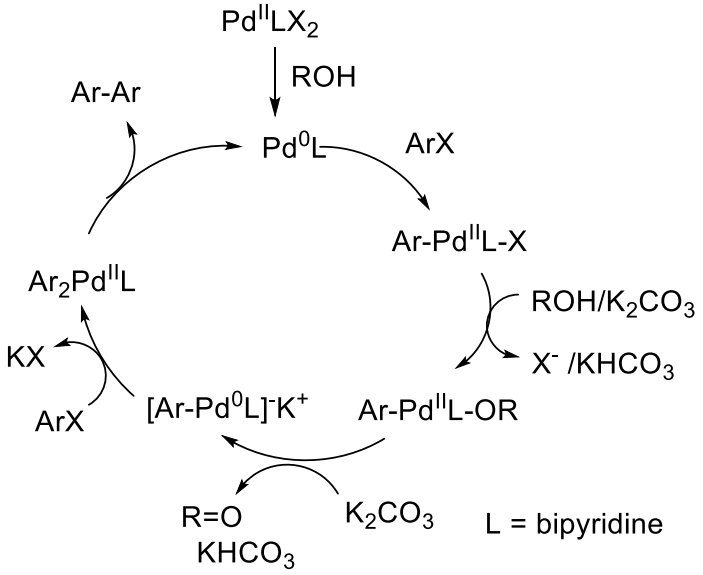

Scheme 11: Proposed catalytic cycle of the palladium-catalyzed reductive homocoupling.

In the absence of TBAI, the homocoupling of 1 was slower than with TBAI. A conversion of 97% was achieved after 24 h instead of 8 h with TBAI. Thus, TBAI significantly accelerated the rate of the reaction. Assuming that TBAI will form 2-iodo-5-(trifluoromethyl)pyridine (2) from 1 in situ, we investigated 2 in the absence of TBAI. During the beginning of the reaction, the conversion of 2 was substantially faster but slowed down after three hours. Full conversion of 2 was observed after 24 h. Thus, it can be concluded that substituted 2-bromopyridines in the presence of TBAI react faster than substituted 2-iodopyridines. During the reaction of 2-bromo-5-(trifluoromethyl)pyridine with TBAI, iodide is generated (Scheme 11). Thus, it can be

hypothesized that sub-stoichiometric amounts of TBAI are sufficient to accelerate this reaction. Indeed, we observed that 20 mol% of TBAI at an elevated temperature of 80 °C is sufficient to support 97% conversion of 2-bromo-5-(trifluoromethyl)pyridine within 2 h and full conversion in 6 h.

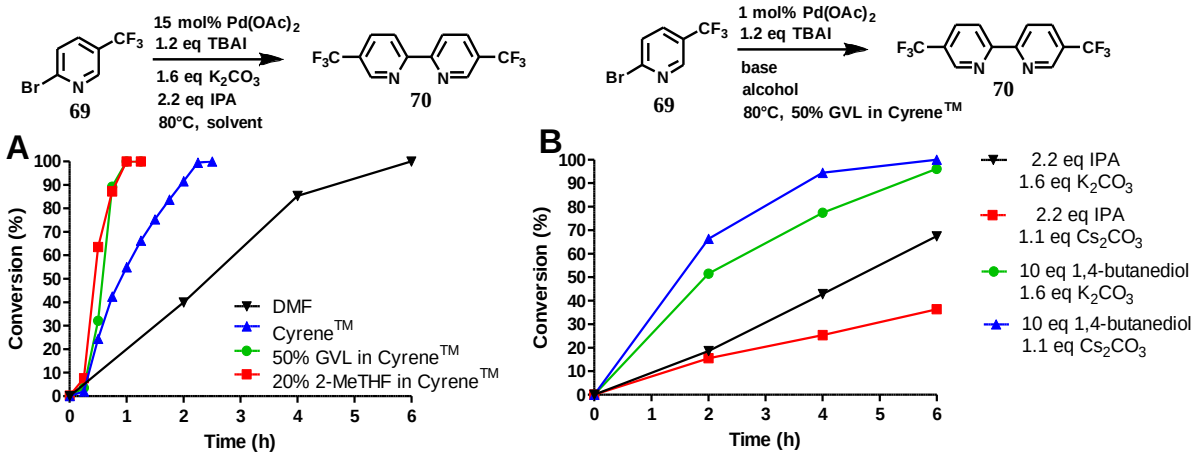

Figure 345: Reductive homocoupling at 80°C. All reactions were conducted in 12 mL of indicated solvent (276 mM). (A) Investigation of Cyrene™ and Cyrene™ solvent blends; (B) investigation of different alcohols and bases. Aliquots were taken at the desired time points and analyzed by reverse phase HPLC at 264 nm using a C18 column. Reaction conversion percentage was determined by the ratio of peak area of starting material to product.

Next, we investigated the conversion of this homocoupling reaction for Cyrene™ and Cyrene™ blends at 80 °C (Figure. 345A). For the homocoupling reaction carried out in DMF, we observed a significantly faster reaction with complete conversion within 6 h. In comparison, at 50 °C, the conversion in DMF was 3% after 5 h. Similar temperature-dependent accelerations of conversion were observed for Cyrene™ and Cyrene™ blends. For Cyrene™, full conversion was observed after 150 min. For the homocoupling carried out in GVL/Cyrene™ and 2-MeTHF/ Cyrene™, full conversion was observed after 60 min. All reactions showed very little conversion during the first 15 min of the reaction. Wilson et al. reported that Cyrene™ is stable in the presence of potassium carbonate at 25°C, whereas at 50 °C and 100 °C the formation of an aldol product was observed.[226] We did observe the formation of the Cyrene™ aldol product by thin liquid

chromatography and nuclear magnetic resonance, but this side product did not influence the conversion or yield of the reaction.

Huang et al. reported a yield of 59% for homocoupling product of 2-iodopyridine using 0.5% of $Pd(OAc)_2$, 1.1 equivalents of cesium carbonate, 1,4-butanediol as solvent at 75 °C after 24 h.[229] Using 2-bromo-5-(trifluoromethyl)pyridine under standard reaction conditions with 1 mol% of $Pd(OAc)_2$ at 80°C, we achieved a yield of 95% after 10 h at 80°C. However, we investigated a different base and alcohol (Figure. 345B). The change from potassium carbonate (1.6 eq.) to cesium carbonate (1.1 eq.) reduced the reaction rate. Secondly, we substituted isopropanol (2.2 eq.) for 1,4-butanediol (10 eq.) and kept potassium carbonate as base. This combination significantly increased the reaction rate and completion of conversion was observed after 6 h instead of 10 h. When cesium carbonate (1.1 eq.) was used in conjunction with 1,4-butanediol, the reaction rate appeared to increase even more, however, this change might not be statistically different if repeated multiple times. Huang et al. proposed that 1,4-butanediol might coordinate as bidentate ligand to palladium and therefore increase the stability of the catalytic species. Although we have no evidence to support this, we concluded that 1,4-butanediol (10 eq.) is superior to isopropanol (2.2 eq.) for our reaction and that potassium carbonate can still be used as a cheap base.

As reported by Hassan et al.,[247] the preparation of biaryls via a reductive homocoupling using aryl bromides in DMF with K_2CO_3 or Et_3N as base and the addition of IPA at 115°C is possible. Therefore, we investigated different substrates with the Cyrene™/GVL blend in the presence of 15 mol% $Pd(OAc)_2$, TBAI (1.2 eq.), and IPA (2.2 eq.) at 50°C (Table 5).

In the case of bromobenzene, we did not observe any conversion (Table 5, entry 1). This result supported our observation that the formation of a bipyridine product is useful to accelerate the homocoupling under these conditions. Next, we investigated 2-bromopyridine (Table 5, entry 2). 81.3% conversion was observed after 48 h. At 8 h, 3.3% conversion was observed, whereas 2-bromo-5′-(trifluoromethyl)pyridine was fully converted at that time point. Thus, the electron withdrawing character of the CF_3 not only accelerated the initial formation of compound 70 in contrast to 2-bromopyridine, but also resulted in a faster reaction with the completion within 8 h. Bipyridine ligands are most effective with the position of the nitrogens in the 2,2′ position. This enables bidentate coordination of palladium. To investigate this fact, 3- and 4-bromopyridine were employed under the same reaction conditions (Table 5, entries 3 and 4). Both substrates exhibited no conversion. Next, we investigated different substituents in the 5-position. For the electron donating methyl group, we observed 6.4% conversion of 2-bromo-5-methylpyridine over a period of 48 h (Table 5, entry 5). The methoxy group in para position is predominantly electron donating (resonance) and has less inductive electron withdrawing character.[248] For 2-bromo-4-methoxypyridine, we observed a conversion of 31.3% after 48 h (Table 5, entry 6). Interestingly, the conversion after 24 h was 10.4% but tripled for the next 24 h reaching 31.3% conversion. 2-Bromo-4-chloropyridine converted very quickly during the first 8 h (64.9%) (Table 5, entry 7). However, the reaction rate slowed and reached only 84.5% after 48 h. Esters are electron withdrawing groups and were well tolerated in this homocoupling reaction. Methyl 6-bromopyridine-3-carboxylate was a good substrate for this reaction resulting in full conversion after 48 h (Table 5, entry 8). Also in this case, very little conversion was observed during the first 8 h. The strong electron withdrawing properties of 2-bromo-4-cyanopyridine resulted in a rapid homocoupling reaction with full conversation after 12 h (Table 5, entry 9). Thus overall, the

relationship between reaction rate and substitution followed Hammett defined sigma values. Moving the CF_3 group to the 6 position reduced the reaction rate and resulted in 90% conversion for 2-bromo-6-(trifluoromethyl)pyridine after 48 h (Table 5, entry 10). In contrast, 2-bromo-4-

Table 5: Reaction progress of reductive homocoupling reactions with various substrates.[a]

		Conversion (%)				
Entry	Starting material	4 h	8 h	12 h	24 h	48 h
1	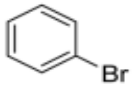	0.0	0.0	0.0	0.0	0.0
2	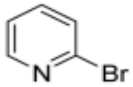	0.0	3.3	23.7	60.9	81.3
3	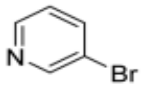	0.0	0.0	0.0	0.0	0.0
4	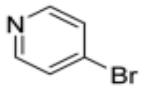	0.0	0.0	0.0	0.0	0.0
5	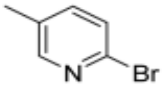	0.0	0.0	0.0	2.0	6.4
6	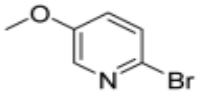	0.0	0.0	0.6	10.4	31.3
7	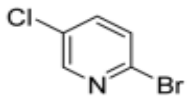	20.3	64.9	72.7	81.4	84.5
8	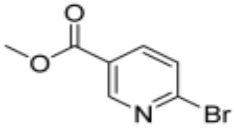	0.0	5.6	37.3	97.2	100
9	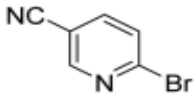	35.5	76.1	100	100	100
10	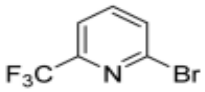	5.5	11.4	16.0	33.6	90.0
11	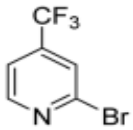	31.7	87.8	100	100	100
12	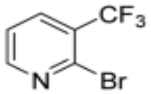	0.0	0.0	<1	<1	<1

[a] All reactions were carried out with 15 mol% $Pd(OAc)_2$, 1.2 equiv. of TBAI, 1.6 equiv. of K_2CO_3, and 2.2 equiv. of IPA in 50% GVL in Cyrene™ at 50 °C.

(trifluoromethyl) pyridine was converted almost as quickly as compound 69, reaching full conversion after 12 h. Although the position of the CF_3 group is closer to the bromine for both substrates in comparison to compound 69, the pyridine nitrogen is counteracting the electron withdrawing effect CF_3 group for entry 10. Probably due to steric effects, 2- bromo-3-(trifluoromethyl)pyridine was not converted under these reaction conditions (Table 2, entry 12). We also employed 2-bromopyridine-5-carbaldehyde but found a very complex mixture of products due to the described formation of aldol products with Cyrene™ (data not shown).[249]

We used the DOZN™ quantitative scoring analysis to evaluate 12 principles of green chemistry for the optimized process using GVL/Cyrene™ at 50°C for a 12 h reaction time and compared it with the reaction with DMF (see calculations below). The principal analysis showed score differences in the use of less hazardous materials (100.00 vs. 22.29), design of safer chemicals (1.19 vs. 0.62) and safer solvents and auxiliaries (42.62 vs. 10.03). Especially the long reaction time in DMF and lower yield resulted in a high score for design of energy efficiency (96.79 vs. 17.33) and inherently safer chemistry of accident prevention (100.00 vs. 17.89). The renewable aspect of Cyrene™ further reduced the score for the use of renewable feedstocks from 100.00 to 7.91. Thus, the overall score for the homocoupling in DMF was 456.98 vs. 87.18 for the reaction in 50% GVL/Cyrene™. The aggregate score was reduced from 38 to 7 resulting in a total improvement of 82%.

It can be concluded that the 50% GVL/Cyrene™ blend is superior to Cyrene™ and more importantly performed better than other commonly used polar aprotic solvents for the palladium catalyzed reductive homocoupling with isopropanol. It has been reported that the presence of isopropanol is important for the reduction of Pd^{II} to Pd^0,[228] which in turn undergoes an oxidative

addition of compound 69 (ArX) (Scheme 11). The bipyridine product/ligand formed during the reaction is likely to stabilize the palladium complex and improves solubility of the catalytic species. The formation of reduced aryl compounds by a dehalogenation side reaction has been reported at higher temperature.[247] For our reaction conditions, this side reaction was not observed. In contrast, coordination of isopropanol in the presence of potassium carbonate enabled the formation of a Pd^0 –Ar complex and formation of acetone. A second oxidative addition of 1 (ArX) afforded the diarylpalladium complex as proposed by Jutand and Mosleh,[250] which resulted in the formation of the aryl–aryl bond and regenerates Pd^0 for the next catalytic cycle. We demonstrated that the addition of 2,2′-bipyridine 70 as a ligand enabled a rapid homocoupling reaction right from the start of the reaction. The addition of compound 70 might improve the conversion of substrates summarized in Table 5, however, additional purification is necessary to separate the products from compound 70. An application of a water-soluble 2,2′-bipyridine ligand that is also soluble in the GVL/Cyrene™ blend might overcome this purification challenge. Furthermore, we demonstrated that the reaction is significantly faster at 80°C and that 1 mol% of $Pd(OAc)_2$ can be used. This higher temperature might have enabled full conversion of substrates summarized in Table 5. Huang et al. reported that the homocoupling in 1,4-butanediol is significantly faster than in isopropanol and that cesium carbonate is superior to potassium carbonate.[229] We confirmed this fact using 10 equivalents of 1,4- butanediol and 1.1 equivalents of cesium carbonate for the reaction in 50% GVL/Cyrene™. Although the greenness of the reaction was significantly improved with the use of bio-renewable and non-toxic solvent Cyrene™ in addition to a shorter reaction time and lower reaction temperature, there are aspects that can be invested to further improve this reaction. This includes further reduction of the catalyst loading and reaction temperature by using an optimized palladium ligand. The recycling of Cyrene™ could be another

improvement, which is often accomplished in industry with a wide variety of solvents. Finally, the ability to generate pure product without column chromatography is an important step to reduce the use of problematic solvents.

Figure 346: DOZN™ scoring for DMF reaction (top), DOZN™ principle scores for DMF reaction (bottom):

Product	
Product Name	6,6'-bis(trifluoromethyl)-2,2'-bipyridine (DMF)
Mass	0.76 g
Product Number	L512346
Product Brand	SIAL

Reaction Conditions								
Step Number(s)	Name of Synthesis Step	Time	Pressure Input Method	Pressure	Pressure Score	Temperatur	Temperat	Temperature Score
1	homocoupling	50.0 hr	General Conditions		No mention of va	Exact Value	50.0 C	

Co-Products		
Step Number(s)	Co-Product Name	Mass
1	acetone	0.52 g
2	Potassium bicarbonate	0.75 g
3	potassium bromide	0.5 g

Materials									
Step Number(s)	Brand	Material Number	Name	Mass	Is Waste(Y/N)	Waste Seve	Derivative	Renewable (Y	Solvent (Y/N)	B Score
1	SIAL	661120	2-bromo-5â-(trifluoromethyl)pyridine	0.75 g	No			No	No	
2	SIAL	319937	dimethylformamide	12.0 g	No			No	Yes	1
3	SIAL	426288	Tetrabutylammonium bromide	1.5 g	No			No	No	1
4	SIAL	720070	Palladium acetate	0.112 g	No			No	No	1
5	SIAL	209619	potassium carbonate	0.75 g	No			No	No	1
6	SIAL	190764	isopropanol	0.56 g	No			Yes	No	1

Process	
B score of Parent Compound	1
Parent product mass for B score	0.96 g
Catalytic Steps	1
Synthesis Steps	1
Pollution Monitoring (Y/N)	Yes
Synthesis steps with monitoring	1
Monitoring Rigor	1.0

Principle	Score
1.Prevention	0.00
2.Atom Economy	12.07
3.Less Hazardous Chemical Synthesis	103.35
4.Designing Safer Chemicals	5.78
5.Safer Solvents and Auxillaries	19.62
6.Design for Energy Efficiency	1031.05
7.Use of Renewable Feedstocks	19.88
8.Reduce Derivatives	0.00
9.Catalysis	0.50
10.Design for Degradation	2.26
11.Real-time analysis for Pollution Prevention	0.00
12.Inherently Safer Chemistry for Accident Prevention	57.05

	Breakdown
Improved Resource Use	5.41
Increased Energy Efficiency	1031.05
Reduced Human and Environmental Hazards	37.61
Overall	1074.07
Aggregate	21.0

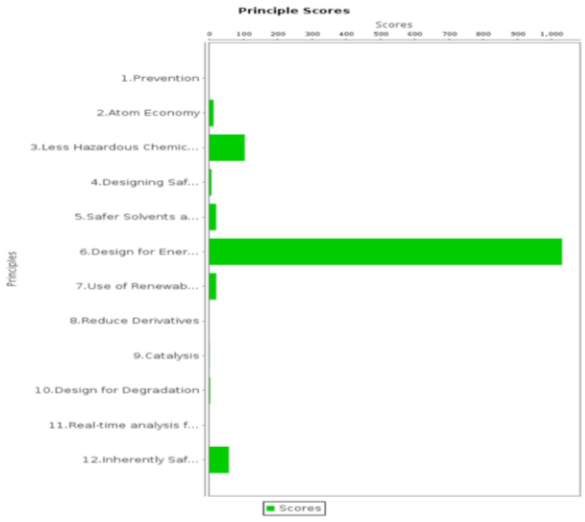

Figure 347: DOZN™ scoring for 50% GVL/Cyrene™ reaction (TOP), DOZN™ principle scores for 50% GVL/Cyrene™ reaction:

Product	
Product Name	6,6'-bis(trifluoromethyl)-2,2'-bipyridine (cyrene)
Mass	0.96 g
Product Number	L512346
Product Brand	SIAL

Reaction Conditions								
Step Number(s)	Name of Synthesis Step	Time	Pressure Input Method	Pressure	Pressure Sco	Temperature In	Temperatur	Temperature Score
1	homocoupling	8.0 hr	General Conditions		No mention d	Exact Value	50.0 C	

Co-Products		
Step Number(s)	Co-Product Name	Mass
1	acetone	0.52 g
2	Potassium bicarbonate	0.75 g
3	potassium bromide	0.5 g

Materials												
Step Number(s)	Brand	Material Number	Name	Mass	Is Waste(Y/N)	Waste Severity	Derivative (Y	Renewable (Y/N)	Solvent (Y/N)	B Score	Used As	Reaction Conditions
1	SIAL	661120	2-bromo-5ā-(trifluoromethyl)pyridine	0.75 g	No			No	No		Reactant	homocoupling;
2	SIAL	920207	Cyrene	12.0 g	No			Yes	Yes	1	Auxiliary	homocoupling;
3	SIAL	426288	Tetrabutylammonium bromide	1.5 g	No			No	No	2	Auxiliary	homocoupling;
4	SIAL	720070	Palladium acetate	0.112 g	No			No	No	1	Recovered	homocoupling;
5	SIAL	209619	potassium carbonate	0.75 g	No			No	No	1	Reactant	homocoupling;
6	SIAL	190764	isopropanol	0.56 g	No			Yes	No	1	Reactant	homocoupling;

Process	
B score of Parent Compound	1
Parent product mass for B score	0.96 g
Catalytic Steps	1
Synthesis Steps	1
Pollution Monitoring (Y/N)	Yes
Synthesis steps with monitoring	1
Monitoring Rigor	5.0

Principle	Score
1.Prevention	0.00
2.Atom Economy	10.44
3.Less Hazardous Chemical Synthesis	29.75
4.Designing Safer Chemicals	2.72
5.Safer Solvents and Auxiliaries	13.27
6.Design for Energy Efficiency	130.60
7.Use of Renewable Feedstocks	3.24
8.Reduce Derivatives	0.00
9.Catalysis	0.50
10.Design for Degradation	2.10
11.Real-time analysis for Pollution Prevention	0.00
12.Inherently Safer Chemistry for Accident Prevention	19.18

	Breakdown
Improved Resource Use	2.36
Increased Energy Efficiency	130.60
Reduced Human and Environmental Hazards	13.40
Overall	146.37
Aggregate	3.0

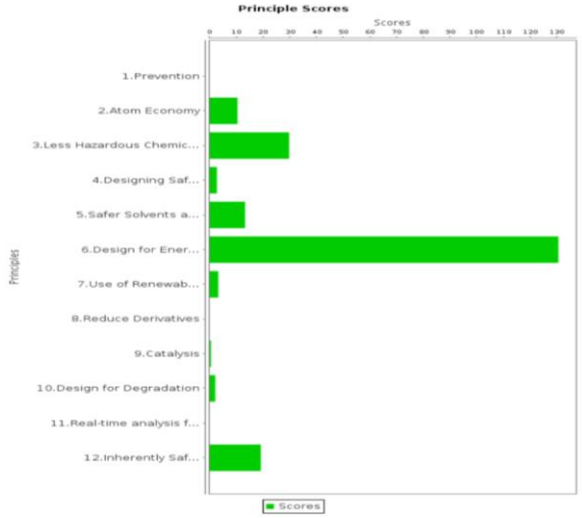

References:

(1) Orlov, I.; Rochel, N.; Moras, D.; Klaholz, B. P. Structure of the full human RXR/VDR nuclear receptor heterodimer complex with its DR3 target DNA. *The EMBO journal* **2012**, *31* (2), 291-300. DOI: 10.1038/emboj.2011.445 From NLM.

(2) Siegel, G. J., Basic neurochemistry : molecular, cellular, and medical aspects. 6th ed.; Lippincott Williams & Wilkins: Philadelphia, 1999; p xxi, 1183.

(3) Zhu, S.; Noviello, C. M.; Teng, J.; Walsh, R. M., Jr.; Kim, J. J.; Hibbs, R. E., Structure of a human synaptic GABAA receptor. Nature 2018, 559 (7712), 67-72.

(4) Tan, K. R.; Rudolph, U.; Luscher, C., Hooked on benzodiazepines: GABAA receptor subtypes and addiction. Trends in neurosciences 2011, 34 (4), 188-97.

(5) Shaffer, P. L.; Gewirth, D. T. Structural analysis of RXR-VDR interactions on DR3 DNA. *The Journal of steroid biochemistry and molecular biology* **2004**, *89-90* (1-5), 215-219. DOI: 10.1016/j.jsbmb.2004.03.084 From NLM.

(6) Yu, O. B.; Arnold, L. A. Calcitroic Acid-A Review. *ACS Chem Biol* **2016**, *11* (10), 2665-2672. DOI: 10.1021/acschembio.6b00569.

(7) Esvelt, R. P.; Schnoes, H. K.; DeLuca, H. F., Isolation and characterization of 1.alpha.-hydroxy-23-carboxytetranorvitamin D: a major metabolite of 1,25-dihydroxyvitamin D3. Biochemistry 1979, 18 (18), 3977-3983.

(8) Onisko, B. L.; Esvelt, R. P.; Schnoes, H. K.; DeLuca, H. F., Metabolites of 1 alpha, 25-dihydroxyvitamin D3 in rat bile. Biochemistry 1980, 19 (17), 4124-30.

(9) Pike, W. S., N. K., In Vitamin D, 2005; Vol. 2nd Ed.

(10) Rosenfeld, L. Vitamine--vitamin. The early years of discovery. *Clin Chem* **1997**, *43* (4), 680-685.

(11) Hopkins, F. G. Feeding experiments illustrating the importance of accessory factors in normal dietaries. *J Physiol* **1912**, *44* (5-6), 425-460. DOI: 10.1113/jphysiol.1912.sp001524.

(12) Funk, C. On the chemical nature of the substance which cures polyneuritis in birds induced by a diet of polished rice. *J Physiol* **1911**, *43* (5), 395-400. DOI: 10.1113/jphysiol.1911.sp001481.

(13) Nutrition classics from The Journal of Biological Chemistry 15:167-175, 1913. The necessity of certain lipins in the diet during growth. By E. V. McCollum and Marguerite Davis. *Nutr Rev* **1973**, *31* (9), 280-281. DOI: 10.1111/j.1753-4887.1973.tb07065.x.

(14) Luce, E. M. The Influence of Diet and Sunlight upon the Growth-promoting and Anti-rachitic Properties of the Milk afforded by a Cow. *Biochem J* **1924**, *18* (3-4), 716-739. DOI: 10.1042/bj0180716.

(15) Friedman, A. A brief history of rickets. *Pediatr Nephrol* **2020**, *35* (10), 1835-1841. DOI: 10.1007/s00467-019-04366-9.

(16) DeLuca, H. F. Vitamin D: Historical Overview. *Vitam Horm* **2016**, *100*, 1-20. DOI: 10.1016/bs.vh.2015.11.001.

(17) Chick, D. H. Study of rickets in Vienna 1919-1922. *Med Hist* **1976**, *20* (1), 41-51. DOI: 10.1017/s0025727300021785.

(18) Vieth, R. Why "Vitamin D" is not a hormone, and not a synonym for 1,25-dihydroxy-vitamin D, its analogs or deltanoids. *J Steroid Biochem Mol Biol* **2004**, *89-90* (1-5), 571-573. DOI: 10.1016/j.jsbmb.2004.03.037.

(19) Blunt, J. W.; Tanaka, Y.; DeLuca, H. F. Biological activity of 25-hydroxycholecalciferol, a metabolite of vitamin D3. *Proc Natl Acad Sci U S A* **1968**, *61* (4), 1503-1506. DOI: 10.1073/pnas.61.4.1503.

(20) Holick, M. F.; Schnoes, H. K.; DeLuca, H. F.; Suda, T.; Cousins, R. J. Isolation and identification of 1,25-dihydroxycholecalciferol. A metabolite of vitamin D active in intestine. *Biochemistry* **1971**, *10* (14), 2799-2804. DOI: 10.1021/bi00790a023.

(21) Pike, J. W.; Meyer, M. B.; Lee, S. M.; Onal, M.; Benkusky, N. A. The vitamin D receptor: contemporary genomic approaches reveal new basic and translational insights. *J Clin Invest* **2017**, *127* (4), 1146-1154. DOI: 10.1172/JCI88887.

(22) Brumbaugh, P. F.; Haussler, M. R. 1Alpha,25-dihydroxyvitamin D3 receptor: competitive binding of vitamin D analogs. *Life Sci* **1973**, *13* (12), 1737-1746. DOI: 10.1016/0024-3205(73)90120-3.

(23) Rochel, N.; Wurtz, J. M.; Mitschler, A.; Klaholz, B.; Moras, D. The crystal structure of the nuclear receptor for vitamin D bound to its natural ligand. *Mol Cell* **2000**, *5* (1), 173-179. DOI: 10.1016/s1097-2765(00)80413-x.

(24) Warnmark, A.; Treuter, E.; Wright, A. P.; Gustafsson, J. A. Activation functions 1 and 2 of nuclear receptors: molecular strategies for transcriptional activation. *Mol Endocrinol* **2003**, *17* (10), 1901-1909. DOI: 10.1210/me.2002-0384.

(25) Kumar, R.; Thompson, E. B. The structure of the nuclear hormone receptors. *Steroids* **1999**, *64* (5), 310-319. DOI: 10.1016/s0039-128x(99)00014-8.

(26) Blanco, J. C.; Wang, I. M.; Tsai, S. Y.; Tsai, M. J.; O'Malley, B. W.; Jurutka, P. W.; Haussler, M. R.; Ozato, K. Transcription factor TFIIB and the vitamin D receptor cooperatively activate

ligand-dependent transcription. *Proc Natl Acad Sci U S A* **1995**, *92* (5), 1535-1539. DOI: 10.1073/pnas.92.5.1535.

(27) Umesono, K.; Murakami, K. K.; Thompson, C. C.; Evans, R. M. Direct repeats as selective response elements for the thyroid hormone, retinoic acid, and vitamin D3 receptors. *Cell* **1991**, *65* (7), 1255-1266. DOI: 10.1016/0092-8674(91)90020-y.

(28) Bikle, D. D. Vitamin D: Production, Metabolism and Mechanisms of Action. In *Endotext*, Feingold, K. R., Anawalt, B., Blackman, M. R., Boyce, A., Chrousos, G., Corpas, E., de Herder, W. W., Dhatariya, K., Dungan, K., Hofland, J., et al. Eds.; 2000.

(29) Mangelsdorf, D. J.; Thummel, C.; Beato, M.; Herrlich, P.; Schutz, G.; Umesono, K.; Blumberg, B.; Kastner, P.; Mark, M.; Chambon, P.; et al. The nuclear receptor superfamily: the second decade. *Cell* **1995**, *83* (6), 835-839. DOI: 10.1016/0092-8674(95)90199-x.

(30) Chalk, K. J.; Kodicek, E. The association of 14C-labelled vitamin D2 with rat serum proteins. *Biochem J* **1961**, *79* (1), 1-7. DOI: 10.1042/bj0790001.

(31) McDonnell, D. P.; Mangelsdorf, D. J.; Pike, J. W.; Haussler, M. R.; O'Malley, B. W. Molecular cloning of complementary DNA encoding the avian receptor for vitamin D. *Science* **1987**, *235* (4793), 1214-1217. DOI: 10.1126/science.3029866.

(32) Callow, R. K.; Kodicek, E.; Thompson, G. A. Metabolism of tritiated vitamin D. *Proc R Soc Lond B Biol Sci* **1966**, *164* (994), 1-20. DOI: 10.1098/rspb.1966.0010.

(33) Bell, P. A.; Kodicek, E. Investigations on metabolites of vitamin D in rat bile. Separation and partial identification of a major metabolite. *Biochem J* **1969**, *115* (4), 663-669. DOI: 10.1042/bj1150663.

(34) Tsai, H. C.; Wong, R. G.; Norman, A. W. Studies on calciferol metabolism. IV. Subcellular localization of 1,25-dihydroxy-vitamin D 3 in intestinal mucosa and correlation with increased calcium transport. *J Biol Chem* **1972**, *247* (17), 5511-5519.

(35) Onisko, B. L.; Esvelt, R. P.; Schnoes, H. K.; DeLuca, H. F. Metabolites of 1 alpha, 25-dihydroxyvitamin D3 in rat bile. *Biochemistry* **1980**, *19* (17), 4124-4130. DOI: 10.1021/bi00558a034.

(36) Esvelt, R. P.; De Luca, H. F. Calcitroic acid: biological activity and tissue distribution studies. *Arch Biochem Biophys* **1981**, *206* (2), 403-413. DOI: 10.1016/0003-9861(81)90107-7.

(37) Holick, M. F.; Schnoes, H. K.; DeLuca, H. F.; Gray, R. W.; Boyle, I. T.; Suda, T. Isolation and identification of 24,25-dihydroxycholecalciferol, a metabolite of vitamin D made in the kidney. *Biochemistry* **1972**, *11* (23), 4251-4255. DOI: 10.1021/bi00773a009.

(38) Knutson, J. C.; DeLuca, H. F. 25-Hydroxyvitamin D3-24-hydroxylase. Subcellular location and properties. *Biochemistry* **1974**, *13* (7), 1543-1548. DOI: 10.1021/bi00704a034.

(39) Ohyama, Y.; Noshiro, M.; Okuda, K. Cloning and expression of cDNA encoding 25-hydroxyvitamin D3 24-hydroxylase. *FEBS Lett* **1991**, *278* (2), 195-198. DOI: 10.1016/0014-5793(91)80115-j.

(40) Jones, G.; Kung, M.; Kano, K. The isolation and identification of two new metabolites of 25-hydroxyvitamin D3 produced in the kidney. *J Biol Chem* **1983**, *258* (21), 12920-12928.

(41) Makin, G.; Lohnes, D.; Byford, V.; Ray, R.; Jones, G. Target cell metabolism of 1,25-dihydroxyvitamin D3 to calcitroic acid. Evidence for a pathway in kidney and bone involving 24-oxidation. *Biochem J* **1989**, *262* (1), 173-180. DOI: 10.1042/bj2620173.

(42) Sakaki, T.; Sawada, N.; Komai, K.; Shiozawa, S.; Yamada, S.; Yamamoto, K.; Ohyama, Y.; Inouye, K. Dual metabolic pathway of 25-hydroxyvitamin D3 catalyzed by human CYP24. *Eur J Biochem* **2000**, *267* (20), 6158-6165. DOI: 10.1046/j.1432-1327.2000.01680.x.

(43) Reddy, G. S.; Omdahl, J. L.; Robinson, M.; Wang, G.; Palmore, G. T.; Vicchio, D.; Yergey, A. L.; Tserng, K. Y.; Uskokovic, M. R. 23-carboxy-24,25,26,27-tetranorvitamin D3 (calcioic acid) and 24-carboxy-25,26,27-trinorvitamin D3 (cholacalcioic acid): end products of 25-hydroxyvitamin D3 metabolism in rat kidney through C-24 oxidation pathway. *Arch Biochem Biophys* **2006**, *455* (1), 18-30. DOI: 10.1016/j.abb.2006.08.021.

(44) Tachibana, Y.; Tsuji, M. Study on the metabolites of 1alpha,25-dihydroxyvitamin D4. *Steroids* **2001**, *66* (2), 93-97. DOI: 10.1016/s0039-128x(00)00208-7.

(45) Sakaki, T.; Kagawa, N.; Yamamoto, K.; Inouye, K. Metabolism of vitamin D3 by cytochromes P450. *Front Biosci* **2005**, *10*, 119-134. DOI: 10.2741/1514.

(46) Tang, E. K. Y.; Tieu, E. W.; Tuckey, R. C. Expression of human CYP27B1 in Escherichia coli and characterization in phospholipid vesicles. *FEBS J* **2012**, *279* (19), 3749-3761. DOI: 10.1111/j.1742-4658.2012.08736.x.

(47) Steenbock, H.; Black, A. Fat-soluble vitamins. XVII. The induction of growthpromoting and calcifying properties in a ration by exposure to ultraviolet light. *J. Biol. Chem.* **1924**, *61*, 405-422.

(48) Askew, F. A.; Bourdillon, R. B.; Bruce, H. M.; Jenkins, R. G. C.; Webster, T. A. The Distillation of Vitamin D. *Proc. R. Soc.* **1930**, *B107*, 76-90.

(49) Chalk, K. J.; Kodicek, E. The association of 14C-labelled vitamin D2 with rat serum proteins. *Biochem. J.* **1961**, *79*, 1-7.

(50) Blunt, J. W.; DeLuca, H. F.; Schnoes, H. K. 25-hydroxycholecalciferol. A biologically active metabolite of vitamin D3. *Biochemistry* **1968**, *7* (10), 3317-3322. DOI: 10.1021/bi00850a001.

(51) Brumbaugh, P. F.; Haussler, M. R. 1Alpha,25-dihydroxyvitamin D3 receptor: competitive binding of vitamin D analogs. *Life Sci.* **1973**, *13* (12), 1737-1746.

(52) Wang, Y. J.; Zhu, J. G.; DeLuca, H. F. Where is the vitamin D receptor? *Archives of Biochemistry and Biophysics* **2012**, *523* (1), 123-133. DOI: 10.1016/j.abb.2012.04.001.

(53) Huhtakangas, J. A.; Olivera, C. J.; Bishop, J. E.; Zanello, L. P.; Norman, A. W. The vitamin D receptor is present in caveolae-enriched plasma membranes and binds 1 alpha,25(OH)(2)-vitamin D-3 in vivo and in vitro. *Molecular Endocrinology* **2004**, *18* (11), 2660-2671. DOI: 10.1210/me.2004-0116.

(54) Orlov, I.; Rochel, N.; Moras, D.; Klaholz, B. P. Structure of the full human RXR/VDR nuclear receptor heterodimer complex with its DR3 target DNA. *Embo Journal* **2012**, *31* (2), 291-300. DOI: 10.1038/emboj.2011.445.

(55) Haussler, M. R.; Jurutka, P. W.; Mizwicki, M.; Norman, A. W. Vitamin D receptor (VDR)-mediated actions of 1 alpha,25(OH)(2)vitarnin D-3: Genomic and non-genomic mechanisms. *Best Pract Res Cl En* **2011**, *25* (4), 543-559. DOI: 10.1016/j.beem.2011.05.010.

(56) White, J. H.; Salehi-Tabar, R.; Dimitrow, V.; Bouttier, M. Diverse mechanism of transcriptional regulation by the vitamin D receptor. In *Vitamin D*, 4 ed.; Feldman, D. Ed.; Vol. 1; Elsevier, 2018; pp 175-187.

(57) Nurminen, V.; Neme, A.; Seuter, S.; Carlberg, C. The impact of the vitamin D-modulated epigenome on VDR target gene regulation. *Biochimica et biophysica acta* **2018**, *1861* (8), 697-705. DOI: 10.1016/j.bbagrm.2018.05.006.

(58) Plonska-Ocypa, K.; Grzywacz, P.; Sicinski, R. R.; Plum, L. A.; DeLuca, H. F. Synthesis and biological evaluation of a des-C,D-analog of 2-methylene-19-nor-1alpha,25-(OH)2D3. *J. Steroid Biochem. Mol. Biol.* **2007**, *103* (3-5), 298-304. DOI: 10.1016/j.jsbmb.2006.12.015.

(59) Mottershead, D. G.; Polly, P.; Lyons, R. J.; Sutherland, R. L.; Watts, C. K. High activity, soluble, bacterially expressed human vitamin D receptor and its ligand binding domain. *J. Cell. Biochem.* **1996**, *61* (3), 325-337. DOI: 10.1002/(SICI)1097-4644(19960601)61:3%3C325::AID-JCB1%3E3.0.CO;2-V.

(60) Molnar, F.; Sigueiro, R.; Sato, Y.; Araujo, C.; Schuster, I.; Antony, P.; Peluso, J.; Muller, C.; Mourino, A.; Moras, D.; et al. 1alpha,25(OH)2-3-epi-vitamin D3, a natural physiological metabolite of vitamin D3: its synthesis, biological activity and crystal structure with its receptor. *PLoS One* **2011**, *6* (3), e18124. DOI: 10.1371/journal.pone.0018124.

(61) Monkawa, T.; Yoshida, T.; Wakino, S.; Shinki, T.; Anazawa, H.; Deluca, H. F.; Suda, T.; Hayashi, M.; Saruta, T. Molecular cloning of cDNA and genomic DNA for human 25-hydroxyvitamin D3 1 alpha-hydroxylase. *Biochem Biophys Res Commun* **1997**, *239* (2), 527-533. DOI: 10.1006/bbrc.1997.7508. Takeyama, K.; Kitanaka, S.; Sato, T.; Kobori, M.; Yanagisawa, J.; Kato, S. 25-Hydroxyvitamin D3 1alpha-hydroxylase and vitamin D synthesis. *Science* **1997**, *277* (5333), 1827-1830. DOI: 10.1126/science.277.5333.1827. St-Arnaud, R.; Messerlian, S.; Moir, J. M.; Omdahl, J. L.; Glorieux, F. H. The 25-hydroxyvitamin D 1-alpha-hydroxylase gene maps to the pseudovitamin D-deficiency rickets (PDDR) disease locus. *J Bone Miner Res* **1997**, *12* (10), 1552-1559. DOI: 10.1359/jbmr.1997.12.10.1552. Zehnder, D.; Bland, R.; Williams, M. C.; McNinch, R. W.; Howie, A. J.; Stewart, P. M.; Hewison, M. Extrarenal expression of 25-hydroxyvitamin d(3)-1 alpha-hydroxylase. *J Clin Endocrinol Metab* **2001**, *86* (2), 888-894. DOI: 10.1210/jcem.86.2.7220.

(62) Norman, A. W.; Bouillon, R.; Farach-Carson, M. C.; Bishop, J. E.; Zhou, L. X.; Nemere, I.; Zhao, J.; Muralidharan, K. R.; Okamura, W. H. Demonstration that 1 beta,25-dihydroxyvitamin D3 is an antagonist of the nongenomic but not genomic biological responses and biological profile

of the three A-ring diastereomers of 1 alpha,25-dihydroxyvitamin D3. *J Biol Chem* **1993**, *268* (27), 20022-20030.

(63) Bischof, M. G.; Siu-Caldera, M. L.; Weiskopf, A.; Vouros, P.; Cross, H. S.; Peterlik, M.; Reddy, G. S. Differentiation-related pathways of 1 alpha,25-dihydroxycholecalciferol metabolism in human colon adenocarcinoma-derived Caco-2 cells: production of 1 alpha,25-dihydroxy-3epi-cholecalciferol. *Exp Cell Res* **1998**, *241* (1), 194-201. DOI: 10.1006/excr.1998.4044.

(64) Paaren, H. E.; Schoenen, H. K.; DeLuca, H. F. Synthesis of 1β-hydroxyvitamin D3 and 1β,25-dihydroxyvitamin D3. *Chem Comm* **1977**, *23*, 890-892.

(65) Pauwels, S.; Jans, I.; Billen, J.; Heijboer, A.; Verstuyf, A.; Carmeliet, G.; Mathieu, C.; Maestro, M.; Waelkens, E.; Evenepoel, P.; et al. 1beta,25-Dihydroxyvitamin D3: A new vitamin D metabolite in human serum. *J Steroid Biochem Mol Biol* **2017**, *173*, 341-348. DOI: 10.1016/j.jsbmb.2017.02.004.

(66) Wecksler, W. R.; Norman, A. W. Studies on the mode of action of calciferol XXV. 1 alpha,25-dihydroxy-5,6-trans-vitamin D3, the 5E-isomer of 1 alpha,25-dihydroxyvitamin D3. *Steroids* **1980**, *35* (4), 419-425. DOI: 10.1016/0039-128x(80)90142-7.

(67) Kobayashi, T.; Moriuchi, S.; Shimura, F.; Katsui, G. Synthesis and biological activity of 5,6-trans-vitamin D3 in anephric rats. *J Nutr Sci Vitaminol (Tokyo)* **1976**, *22* (4), 299-306. DOI: 10.3177/jnsv.22.299.

(68) VanAlstyne, E. M.; Norman, A. W.; Okamura, W. H. 7,8-Cis Geometric Isomers of the Steroid Hormone 1a,25-Dihydroxyvitamin D. *J Am Chem Soc* **1994**, *116*, 6207-6216.

(69) Maynard, D. F.; Trankle, W. G.; Norman, A. W.; Okamura, W. H. 14-epi stereoisomers of 25-hydroxy- and 1 alpha,25-dihydroxyvitamin D3: synthesis, isomerization to previtamins, and biological studies. *J Med Chem* **1994**, *37* (15), 2387-2393. DOI: 10.1021/jm00041a017.

(70) Kurek-Tyrlik, A.; Michalak, K.; Wicha, J. Synthesis of 17-epi-calcitriol from a common androstane derivative, involving the ring B photochemical opening and the intermediate triene ozonolysis. *J Org Chem* **2005**, *70* (21), 8513-8521. DOI: 10.1021/jo051357u.

(71) Michalak, K.; Wicha, J. Total synthesis of a CD-ring: side-chain building block for preparing 17-epi-calcitriol derivatives from the Hajos-Parrish dione. *J Org Chem* **2011**, *76* (16), 6906-6911. DOI: 10.1021/jo201083w.

(72) Binderup, L.; Latini, S.; Binderup, E.; Bretting, C.; Calverley, M.; Hansen, K. 20-epi-vitamin D3 analogues: a novel class of potent regulators of cell growth and immune responses. *Biochem Pharmacol* **1991**, *42* (8), 1569-1575. DOI: 10.1016/0006-2952(91)90426-6.

(73) Zhou, X.; Zhu, G. D.; Van Haver, D.; Vandewalle, M.; De Clercq, P. J.; Verstuyf, A.; Bouillon, R. Synthesis, biological activity, and conformational analysis of four seco-D-15,19-bisnor-1alpha,25-dihydroxyvitamin D analogues, diastereomeric at C17 and C20. *J Med Chem* **1999**, *42* (18), 3539-3556. DOI: 10.1021/jm980736v.

(74) Bischoff-Ferrari, H. A.; Giovannucci, E.; Willett, W. C.; Dietrich, T.; Dawson-Hughes, B. Estimation of optimal serum concentrations of 25-hydroxyvitamin D for multiple health outcomes. *Am J Clin Nutr* **2006**, *84* (1), 18-28. DOI: 10.1093/ajcn/84.1.18.

(75) Procsal, D. A.; Okamura, W. H.; Norman, A. W. Structural requirements for the interaction of 1 alpha, 25-(OH) 2- vitiamin D3 with its chick interestinal receptor system. *J Biol Chem* **1975**, *250* (21), 8382-8388.

(76) Perlman, K. L.; Sicinski, R. R.; Schnoes, H. K.; DeLuca, H. F. 1α,25-dihydroxy-19-nor-vitamin D3, a novel vitamin D-related compound with potential therapeutic activity. *Tetrahedron Lett.* **1990**, *31* (13), 1823-1824.

(77) Bouillon, R.; Sarandeses, L. A.; Allewaert, K.; Zhao, J.; Mascarenas, J. L.; Mourino, A.; Vrielynck, S.; de Clercq, P.; Vandewalle, M. Biologic activity of dihydroxylated 19-nor-(pre)vitamin D3. *J Bone Miner Res* **1993**, *8* (8), 1009-1015. DOI: 10.1002/jbmr.5650080815.

(78) Sicinski, R. R.; Perlman, K. L.; Prahl, J.; Smith, C.; DeLuca, H. F. Synthesis and biological activity of 1 alpha, 25-dihydroxy-18-norvitamin D3 and 1 alpha, 25-dihydroxy-18,19-dinorvitamin D3. *J Med Chem* **1996**, *39* (22), 4497-4506. DOI: 10.1021/jm950745t.

(79) Kubodera, N.; Miyamoto, K.; Matsumoto, M.; Kawanishi, T.; Ohkawa, H.; Mori, T. Synthetic studies of vitamin D analogues. X. Synthesis and biological activities of 1 alpha,25-dihydroxy-21-norvitamin D3. *Chem Pharm Bull (Tokyo)* **1992**, *40* (3), 648-651. DOI: 10.1248/cpb.40.648.

(80) Ostrem, V. K.; Lau, W. F.; Lee, S. H.; Perlman, K.; Prahl, J.; Schnoes, H. K.; DeLuca, H. F. Induction of monocytic differentiation of HL-60 cells by 1,25-dihydroxyvitamin D analogs. *J Biol Chem* **1987**, *262* (29), 14164-14171.

(81) Sakamaki, Y.; Inaba, Y.; Yoshimoto, N.; Yamamoto, K. Potent antagonist for the vitamin D receptor: vitamin D analogues with simple side chain structure. *J. Med. Chem.* **2010**, *53* (15), 5813-5826. DOI: 10.1021/jm100649d.

(82) Haussler, M. R.; Zerwekh, J. E.; Hesse, R. H.; Rizzardo, E.; Pechet, M. M. Biological activity of 1alpha-hydroxycholecalciferol, a synthetic analog of the hormonal form of vitamin D3. *Proc Natl Acad Sci U S A* **1973**, *70* (8), 2248-2252. DOI: 10.1073/pnas.70.8.2248. Holick, M. F.; Semmler, E. J.; Schnoes, H. K.; DeLuca, H. F. 1 -Hydroxy derivative of vitamin D 3 : a highly potent analog of 1 ,25-dihydroxyvitamin D 3. *Science* **1973**, *180* (4082), 190-191. DOI: 10.1126/science.180.4082.190.

(83) Verstuyf, A.; Verlinden, L.; van Etten, E.; Shi, L.; Wu, Y.; D'Halleweyn, C.; Van Haver, D.; Zhu, G. D.; Chen, Y. J.; Zhou, X.; et al. Biological activity of CD-ring modified 1alpha,25-

dihydroxyvitamin D analogues: C-ring and five-membered D-ring analogues. *J Bone Miner Res* **2000**, *15* (2), 237-252. DOI: 10.1359/jbmr.2000.15.2.237.

(84) Kutner, A.; Zhao, H.; Fitak, H.; Chodyn, M.; Halkes, S. J.; Wilson, S. R.; Van Del Velde, J.-P. New pharmaceutically active compounds. 1995.

(85) Kakuda, S.; Okada, K.; Eguchi, H.; Takenouchi, K.; Hakamata, W.; Kurihara, M.; Takimoto-Kamimura, M. Structure of the ligand-binding domain of rat VDR in complex with the nonsecosteroidal vitamin D3 analogue YR301. *Acta Crystallogr. Sect. F Struct. Biol. Cryst. Commun.* **2008**, *64* (Pt 11), 970-973. DOI: 10.1107/S1744309108026754.

(86) Boehm, M. F.; Fitzgerald, P.; Zou, A.; Elgort, M. G.; Bischoff, E. D.; Mere, L.; Mais, D. E.; Bissonnette, R. P.; Heyman, R. A.; Nadzan, A. M.; et al. Novel nonsecosteroidal vitamin D mimics exert VDR-modulating activities with less calcium mobilization than 1,25-dihydroxyvitamin D3. *Chem. Biol.* **1999**, *6* (5), 265-275. DOI: 10.1016/S1074-5521(99)80072-6.

(87) Hakamata, W.; Sato, Y.; Okuda, H.; Honzawa, S.; Saito, N.; Kishimoto, S.; Yamashita, A.; Sugiura, T.; Kittaka, A.; Kurihara, M. (2S,2'R)-analogue of LG190178 is a major active isomer. *Bioorg. Med. Chem. Lett.* **2008**, *18* (1), 120-123. DOI: 10.1016/j.bmcl.2007.11.007.

(88) Kashiwagi, H.; Ono, Y.; Ohta, M.; Morikami, K.; Takahashi, T. Systematic SAR study of the side chain of nonsecosteroidal vitamin D(3) analogs. *Bioorg. Med. Chem.* **2012**, *20* (14), 4495-4506. DOI: 10.1016/j.bmc.2012.05.023.

(89) Kashiwagi, H.; Ohta, M.; Ono, Y.; Morikami, K.; Itoh, S.; Sato, H.; Takahashi, T. Effects of fluorines on nonsecosteroidal vitamin D receptor agonists. *Bioorg. Med. Chem.* **2013**, *21* (3), 712-721. DOI: 10.1016/j.bmc.2012.11.029.

(90) Ge, Z.; Hao, M.; Xu, M.; Su, Z.; Kang, Z.; Xue, L.; Zhang, C. Novel nonsecosteroidal VDR ligands with phenyl-pyrrolyl pentane skeleton for cancer therapy. *Eur. J. Med. Chem.* **2016**, *107*, 48-62. DOI: 10.1016/j.ejmech.2015.10.042.

(91) Taniguchi, K.; Katagiri, K.; Kashiwagi, H.; Harada, S.; Sugimoto, Y.; Shimizu, Y.; Arakawa, H.; Ito, T.; Yamazaki, M.; Watanabe, T.; et al. A novel nonsecosteroidal VDR agonist (CH5036249) exhibits efficacy in a spontaneous benign prostatic hyperplasia beagle model. *J. Steroid Biochem. Mol. Biol.* **2010**, *121* (1-2), 204-207. DOI: 10.1016/j.jsbmb.2010.03.043.

(92) Fujii, S.; Masuno, H.; Taoda, Y.; Kano, A.; Wongmayura, A.; Nakabayashi, M.; Ito, N.; Shimizu, M.; Kawachi, E.; Hirano, T.; et al. Boron cluster-based development of potent nonsecosteroidal vitamin D receptor ligands: direct observation of hydrophobic interaction between protein surface and carborane. *J. Am. Chem. Soc.* **2011**, *133* (51), 20933-20941. DOI: 10.1021/ja208797n.

(93) Fujii, S.; Kano, A.; Masuno, H.; Songkram, C.; Kawachi, E.; Hirano, T.; Tanatani, A.; Kagechika, H. Design and synthesis of tetraol derivatives of 1,12-dicarba-closo-dodecaborane as non-secosteroidal vitamin D analogs. *Bioorg. Med. Chem. Lett.* **2014**, *24* (18), 4515-4519. DOI: 10.1016/j.bmcl.2014.07.075.

(94) Perakyla, M.; Malinen, M.; Herzig, K. H.; Carlberg, C. Gene regulatory potential of nonsteroidal vitamin D receptor ligands. *Mol. Endocrinol.* **2005**, *19* (8), 2060-2073. DOI: 10.1210/me.2004-0417.

(95) Ciesielski, F.; Sato, Y.; Chebaro, Y.; Moras, D.; Dejaegere, A.; Rochel, N. Structural basis for the accommodation of bis- and tris-aromatic derivatives in vitamin D nuclear receptor. *J. Med. Chem.* **2012**, *55* (19), 8440-8449. DOI: 10.1021/jm300858s.

(96) Gogoi, P.; Seoane, S.; Sigueiro, R.; Guiberteau, T.; Maestro, M. A.; Perez-Fernandez, R.; Rochel, N.; Mourino, A. Aromatic-Based Design of Highly Active and Noncalcemic Vitamin D Receptor Agonists. *J. Med. Chem.* **2018**, *61* (11), 4928-4937. DOI: 10.1021/acs.jmedchem.8b00337.

(97) Chen, F.; Su, Q.; Torrent, M.; Wei, N.; Peekhaus, N.; Mcmasters, D.; Fisher, J. L.; Glantschnig, H.; Hodor, P.; Flores, O.; et al. Identification and characterization of a novel nonsecosteroidal vitamin D receptor ligand. *DrugDev. Res.* **2007**, *68* (2), 51-60.

(98) Haussler, M. R.; Haussler, C. A.; Bartik, L.; Whitfield, G. K.; Hsieh, J. C.; Slater, S.; Jurutka, P. W. Vitamin D receptor: molecular signaling and actions of nutritional ligands in disease prevention. *Nutr. Rev.* **2008**, *66* (10 Suppl 2), S98-112. DOI: 10.1111/j.1753-4887.2008.00093.x.

(99) Makishima, M.; Lu, T. T.; Xie, W.; Whitfield, G. K.; Domoto, H.; Evans, R. M.; al, e. Vitamin D receptor as an intestinal bile acid sensor. *Science* **2002**, *296*, 1313-1316.

(100) Adachi, R.; Honma, Y.; Masuno, H.; Kawana, K.; Shimomura, I.; Yamada, S.; Makishima, M. Selective activation of vitamin D receptor by lithocholic acid acetate, a bile acid derivative. *J. Lipid Res.* **2005**, *46* (1), 46-57. DOI: 10.1194/jlr.M400294-JLR200.

(101) Ishizawa, M.; Matsunawa, M.; Adachi, R.; Uno, S.; Ikeda, K.; Masuno, H.; Shimizu, M.; Iwasaki, K.; Yamada, S.; Makishima, M. Lithocholic acid derivatives act as selective vitamin D receptor modulators without inducing hypercalcemia. *J. Lipid Res.* **2008**, *49* (4), 763-772. DOI: 10.1194/jlr.M700293-JLR200.

(102) Masuno, H.; Kazui, Y.; Tanatani, A.; Fujii, S.; Kawachi, E.; Ikura, T.; Ito, N.; Yamamoto, K.; Kagechika, H. Development of novel lithocholic acid derivatives as vitamin D receptor agonists. *Bioorg. Med. Chem.* **2019**, *27* (16), 3674-3681. DOI: 10.1016/j.bmc.2019.07.003.

(103) Arichi, N.; Fujiwara, S.; Ishizawa, M.; Makishima, M.; Hua, D. H.; Yamada, K. I.; Yamaoka, Y.; Takasu, K. Synthesis and biological evaluation of steroidal derivatives bearing a small ring as vitamin D receptor agonists. *Bioorg. Med. Chem. Lett.* **2017**, *27* (15), 3408-3411. DOI: 10.1016/j.bmcl.2017.05.089.

(104) Norman, A. W.; Manchand, P. S.; Uskokovic, M. R.; Okamura, W. H.; Takeuchi, J. A.; Bishop, J. E.; Hisatake, J. I.; Koeffler, H. P.; Peleg, S. Characterization of a novel analogue of 1alpha,25(OH)(2)-vitamin D(3) with two side chains: interaction with its nuclear receptor and cellular actions. *J. Med. Chem.* **2000**, *43* (14), 2719-2730. DOI: 10.1021/jm0000160.

(105) Mizwicki, M. T.; Keidel, D.; Bula, C. M.; Bishop, J. E.; Zanello, L. P.; Wurtz, J. M.; Moras, D.; Norman, A. W. Identification of an alternative ligand-binding pocket in the nuclear vitamin D receptor and its functional importance in 1alpha,25(OH)2-vitamin D3 signaling. *Proc. Natl. Acad. Sci. U. S. A.* **2004**, *101* (35), 12876-12881. DOI: 10.1073/pnas.0403606101.

(106) Ciesielski, F.; Rochel, N.; Moras, D. Adaptability of the Vitamin D nuclear receptor to the synthetic ligand Gemini: remodelling the LBP with one side chain rotation. *J. Steroid Biochem. Mol. Biol.* **2007**, *103* (3-5), 235-242. DOI: 10.1016/j.jsbmb.2006.12.003.

(107) Huet, T.; Maehr, H.; Lee, H. J.; Uskokovic, M. R.; Suh, N.; Moras, D.; Rochel, N. Structure-function study of gemini derivatives with two different side chains at C-20, Gemini-0072 and Gemini-0097. *Medchemcomm* **2011**, *2* (5), 424-429. DOI: 10.1039/C1MD00059D.

(108) Teske, K. A.; Yu, O.; Arnold, L. A. Inhibitors for the Vitamin D Receptor-Coregulator Interaction. *Vitam. Horm.* **2016**, *100*, 45-82. DOI: 10.1016/bs.vh.2015.10.002.

(109) Ishizuka, S.; Yamaguchi, H.; Yamada, S.; Nakayama, K.; Takayama, H. Stereochemistry of 25-hydroxyvitamin D3-26,23-lactone and 1 alpha, 25-dihydroxyvitamin D3-26,23-lactone in rat serum. *FEBS Lett.* **1981**, *134* (2), 207-211. DOI: 10.1016/0014-5793(81)80603-5.

(110) Miura, D.; Manabe, K.; Ozono, K.; Saito, M.; Gao, Q.; Norman, A. W.; Ishizuka, S. Antagonistic action of novel 1alpha,25-dihydroxyvitamin D3-26, 23-lactone analogs on differentiation of human leukemia cells (HL-60) induced by 1alpha,25-dihydroxyvitamin D3. *J Biol Chem* **1999**, *274* (23), 16392-16399.

(111) Kakuda, S.; Ishizuka, S.; Eguchi, H.; Mizwicki, M. T.; Norman, A. W.; Takimoto-Kamimura, M. Structural basis of the histidine-mediated vitamin D receptor agonistic and antagonistic mechanisms of (23S)-25-dehydro-1alpha-hydroxyvitamin D3-26,23-lactone. *Acta crystallographica. Section D, Biological crystallography* **2010**, *66* (Pt 8), 918-926. DOI: 10.1107/S0907444910020810.

(112) Saito, N.; Saito, H.; Anzai, M.; Yoshida, A.; Fujishima, T.; Takenouchi, K.; Miura, D.; Ishizuka, S.; Takayama, H.; Kittaka, A. Dramatic enhancement of antagonistic activity on vitamin D receptor: a double functionalization of 1alpha-hydroxyvitamin D3 26,23-lactones. *Org. Lett.* **2003**, *5* (25), 4859-4862. DOI: 10.1021/ol035922w.

(113) Saito, N.; Matsunaga, T.; Saito, H.; Anzai, M.; Takenouchi, K.; Miura, D.; Namekawa, J.; Ishizuka, S.; Kittaka, A. Further synthetic and biological studies on vitamin D hormone antagonists based on C24-alkylation and C2alpha-functionalization of 25-dehydro-1alpha-hydroxyvitamin D(3)-26,23-lactones. *J. Med. Chem.* **2006**, *49* (24), 7063-7075. DOI: 10.1021/jm060797q.

(114) Bury, Y.; Steinmeyer, A.; Carlberg, C. Structure activity relationship of carboxylic ester antagonists of the vitamin D(3) receptor. *Mol. Pharmacol.* **2000**, *58* (5), 1067-1074. DOI: 10.1124/mol.58.5.1067.

(115) Zugel, U.; Steinmeyer, A.; Giesen, C.; Asadullah, K. A novel immunosuppressive 1alpha,25-dihydroxyvitamin D3 analog with reduced hypercalcemic activity. *J Invest Dermatol* **2002**, *119* (6), 1434-1442. DOI: 10.1046/j.1523-1747.2002.19623.x.

(116) Kato, Y.; Nakano, Y.; Sano, H.; Tanatani, A.; Kobayashi, H.; Shimazawa, R.; Koshino, H.; Hashimoto, Y.; Nagasawa, K. Synthesis of 1alpha,25-dihydroxyvitamin D3-26,23-lactams (DLAMs), a novel series of 1 alpha,25-dihydroxyvitamin D3 antagonist. *Bioorg. Med. Chem. Lett.* **2004**, *14* (10), 2579-2583. DOI: 10.1016/j.bmcl.2004.02.076.

(117) Nakano, Y.; Kato, Y.; Imai, K.; Ochiai, E.; Namekawa, J.; Ishizuka, S.; Takenouchi, K.; Tanatani, A.; Hashimoto, Y.; Nagasawa, K. Practical synthesis and evaluation of the biological activities of 1 alpha,25-dihydroxyvitamin D-3 antagonists, 1 alpha,25-dihydroxyvitamin D-3-26,23-lactams. Designed on the basis of the helix 12-folding inhibition hypothesis. *Journal of Medicinal Chemistry* **2006**, *49* (8), 2398-2406. DOI: Doi 10.1021/Jm050738x.

(118) Cho, K.; Uneuchi, F.; Kato-Nakamura, Y.; Namekawa, J.; Ishizuka, S.; Takenouchi, K.; Nagasawa, K. Structure-activity relationship studies on vitamin D lactam derivatives as vitamin D receptor antagonist. *Bioorg. Med. Chem. Lett.* **2008**, *18* (15), 4287-4290. DOI: 10.1016/j.bmcl.2008.06.095.

(119) Lamblin, M.; Spingarn, R.; Wang, T. T.; Burger, M. C.; Dabbas, B.; Moitessier, N.; White, J. H.; Gleason, J. L. An o-aminoanilide analogue of 1alpha,25-dihydroxyvitamin D(3) functions as a strong vitamin D receptor antagonist. *J Med Chem* **2010**, *53* (20), 7461-7465, Research Support, Non-U.S. Gov't. DOI: 10.1021/jm1007159.

(120) Inaba, Y.; Yamamoto, K.; Yoshimoto, N.; Matsunawa, M.; Uno, S.; Yamada, S.; Makishima, M. Vitamin D3 derivatives with adamantane or lactone ring side chains are cell type-selective vitamin D receptor modulators. *Mol. Pharmacol.* **2007**, *71* (5), 1298-1311. DOI: 10.1124/mol.106.032318.

(121) Igarashi, M.; Yoshimoto, N.; Yamamoto, K.; Shimizu, M.; Ishizawa, M.; Makishima, M.; DeLuca, H. F.; Yamada, S. Identification of a highly potent vitamin D receptor antagonist: (25S)-

26-adamantyl-25-hydroxy-2-methylene-22,23-didehydro-19,27-dinor-20-epi-vita min D3 (ADMI3). *Arch. Biochem. Biophys.* **2007**, *460* (2), 240-253. DOI: 10.1016/j.abb.2006.11.026.

(122) Kudo, T.; Ishizawa, M.; Maekawa, K.; Nakabayashi, M.; Watarai, Y.; Uchida, H.; Tokiwa, H.; Ikura, T.; Ito, N.; Makishima, M.; et al. Combination of triple bond and adamantane ring on the vitamin D side chain produced partial agonists for vitamin D receptor. *J. Med. Chem.* **2014**, *57* (10), 4073-4087. DOI: 10.1021/jm401989c.

(123) Watarai, Y.; Ishizawa, M.; Ikura, T.; Zacconi, F. C.; Uno, S.; Ito, N.; Mourino, A.; Tokiwa, H.; Makishima, M.; Yamada, S. Synthesis, Biological Activities, and X-ray Crystal Structural Analysis of 25-Hydroxy-25(or 26)-adamantyl-17-[20(22),23-diynyl]-21-norvitamin D Compounds. *J. Med. Chem.* **2015**, *58* (24), 9510-9521. DOI: 10.1021/acs.jmedchem.5b00792.

(124) Inaba, Y.; Yoshimoto, N.; Sakamaki, Y.; Nakabayashi, M.; Ikura, T.; Tamamura, H.; Ito, N.; Shimizu, M.; Yamamoto, K. A new class of vitamin D analogues that induce structural rearrangement of the ligand-binding pocket of the receptor. *J. Med. Chem.* **2009**, *52* (5), 1438-1449. DOI: 10.1021/jm8014348.

(125) Anami, Y.; Sakamaki, Y.; Itoh, T.; Inaba, Y.; Nakabayashi, M.; Ikura, T.; Ito, N.; Yamamoto, K. Fine tuning of agonistic/antagonistic activity for vitamin D receptor by 22-alkyl chain length of ligands: 22S-Hexyl compound unexpectedly restored agonistic activity. *Bioorg. Med. Chem.* **2015**, *23* (22), 7274-7281. DOI: 10.1016/j.bmc.2015.10.026.

(126) Yamamoto, K.; Inaba, Y.; Yoshimoto, N.; Choi, M.; DeLuca, H. F.; Yamada, S. 22-Alkyl-20-epi-1alpha,25-dihydroxyvitamin D3 compounds of superagonistic activity: syntheses, biological activities and interaction with the receptor. *J. Med. Chem.* **2007**, *50* (5), 932-939. DOI: 10.1021/jm060889f.

(127) Nandhikonda, P.; Yasgar, A.; Baranowski, A. M.; Sidhu, P. S.; McCallum, M. M.; Pawlak, A. J.; Teske, K.; Feleke, B.; Yuan, N. Y.; Kevin, C.; et al. Peroxisome proliferation-activated receptor delta agonist GW0742 interacts weakly with multiple nuclear receptors, including the vitamin D receptor. *Biochemistry-Us* **2013**, *52* (24), 4193-4203, Research Support, N.I.H., Extramural

Research Support, Non-U.S. Gov't. DOI: 10.1021/bi400321p.

(128) Teske, K.; Nandhikonda, P.; Bogart, J. W.; Feleke, B.; Sidhu, P.; Yuan, N.; Preston, J.; Goy, R.; Arnold, L. A. Modulation of Transcription mediated by the Vitamin D Receptor and the Peroxisome Proliferator-Activated Receptor delta in the presence of GW0742 analogs. *J Biomol Res Ther* **2014**, *3* (1). DOI: 10.4172/2167-7956.1000111.

(129) Teske, K. A.; Rai, G.; Nandhikonda, P.; Sidhu, P. S.; Feleke, B.; Simeonov, A.; Yasgar, A.; Jadhav, A.; Maloney, D. J.; Arnold, L. A. Parallel Chemistry Approach to Identify Novel Nuclear Receptor Ligands Based on the GW0742 Scaffold. *ACS Comb Sci* **2017**, *19* (10), 646-656. DOI: 10.1021/acscombsci.7b00066.

(130) Teske, K. A.; Bogart, J. W.; Arnold, L. A. Novel VDR antagonists based on the GW0742 scaffold. *Bioorg. Med. Chem. Lett.* **2018**, *28* (3), 351-354. DOI: 10.1016/j.bmcl.2017.12.041.

(131) Teske, K.; Nandhikonda, P.; Bogart, J. W.; Feleke, B.; Sidhu, P.; Yuan, N.; Preston, J.; Goy, R.; Han, L.; Silvaggi, N. R.; et al. Identification of Vdr Antagonists among Nuclear Receptor Ligands Using Virtual Screening. *Nucl Receptor Res* **2014**, *1*. DOI: 10.11131/2014/101076.

(132) Teske, K. A.; Bogart, J. W.; Sanchez, L. M.; Yu, O. B.; Preston, J. V.; Cook, J. M.; Silvaggi, N. R.; Bikle, D. D.; Arnold, L. A. Synthesis and evaluation of vitamin D receptor-mediated activities of cholesterol and vitamin D metabolites. *Eur J Med Chem* **2016**, *109*, 238-246. DOI: 10.1016/j.ejmech.2016.01.002.

(133) Hector F. DeLuca, H. K. S., Robert P. Esvelt Processes for preparing calcitroic acid and esters thereof. 1981.

(134) Esvelt, R. P.; Fivizzani, M. A.; Paaren, H. E.; Schnoes, H. K.; DeLuca, H. F., Synthesis of calcitroic acid, a metabolite of 1.alpha.,25-dihydroxycholecalciferol. The Journal of Organic Chemistry 1981, 46 (2), 456-458.

(135) de Costa, B. R.; Makk, N.; Midgley, J. M.; Modi, N. T.; Watt, R. A.; Whalley, W. B., Unsaturated steroids. Part 12. Synthesis of 1α,3β-dihydroxy-24-nor-9,10-secochola-5,7,10(19)trien-23-oic (calcitroic) acid and of the cholic-and 25-homocholic acid analogues. Journal of the Chemical Society, Perkin Transactions 1 1985, (0), 1331-1336.

(136) Calverley, M. J., The Seleno-Acetal Route to Side-Chain Modified 1-Alpha-Hydroxy-Vitamin-D Analogs - Stereoselective Synthesis of the New 22z Isomer of Mc903 (Calcipotriol). Synlett 1990, 1990, 157−159.

(137) Meyer, D.; Rentsch, L.; Marti, R., Efficient and scalable total synthesis of calcitroic acid and its 13C-labeled derivative. RSC Advances 2014, 4 (61), 32327-32334.

(138) Posner, G. H.; Lee, J. K.; White, M. C.; Hutchings, R. H.; Dai, H.; Kachinski, J. L.; Dolan, P.; Kensler, T. W., Antiproliferative Hybrid Analogs of the Hormone 1alpha,25-Dihydroxyvitamin D(3): Design, Synthesis, and Preliminary Biological Evaluation. J Org Chem 1997, 62 (10), 3299-3314.

(139) Cooper, J. R.; Bloom, F. E.; Roth, R. H., The biochemical basis of neuropharmacology. 8th ed.; Oxford University Press: Oxford ; New York, 2003; p vii, 405 p.

(140) Spiering, M. J., The discovery of GABA in the brain. The Journal of biological chemistry 2018, 293 (49), 19159-19160.

(141) Roberts, E.; Frankel, S., gamma-Aminobutyric acid in brain: its formation from glutamic acid. The Journal of biological chemistry 1950, 187 (1), 55-63.

(142) Florey, E., An inhibitory and an excitatory factor of mammalian central nervous system, and their action of a single sensory neuron. Archives internationales de physiologie 1954, 62 (1), 33-53.

(143) Florey, E.; Mc, L. H., The effects of factor I and of gamma-aminobutyric acid on smooth muscle preparations. The Journal of physiology 1959, 145 (1), 66-76.

(144) Edwards, D. H.; Heitler, W. J.; Krasne, F. B., Fifty years of a command neuron: the neurobiology of escape behavior in the crayfish. Trends in neurosciences 1999, 22 (4), 153-61.

(145) Hayashi, T., Inhibition and excitation due to gamma-aminobutyric acid in the central nervous system. Nature 1958, 182 (4642), 1076-7.

(146) Krnjevic, K.; Schwartz, S., The action of gamma-aminobutyric acid on cortical neurones. Experimental brain research 1967, 3 (4), 320-36.

(147) Fenalti, G.; Law, R. H.; Buckle, A. M.; Langendorf, C.; Tuck, K.; Rosado, C. J.; Faux, N. G.; Mahmood, K.; Hampe, C. S.; Banga, J. P.; Wilce, M.; Schmidberger, J.; Rossjohn, J.; El-Kabbani, O.; Pike, R. N.; Smith, A. I.; Mackay, I. R.; Rowley, M. J.; Whisstock, J. C., GABA production by glutamic acid decarboxylase is regulated by a dynamic catalytic loop. Nature structural & molecular biology 2007, 14 (4), 280-6.

(148) Jin, X. T.; Galvan, A.; Wichmann, T.; Smith, Y., Localization and Function of GABA Transporters GAT-1 and GAT-3 in the Basal Ganglia. Frontiers in systems neuroscience 2011, 5, 63.

(149) Olsen, R. W., Tobin, A. J., Molecular biology of GABAA receptors. FASEB journal : official publication of the Federation of American Societies for Experimental Biology 1990, 4, 1469-1480.

(150) Bowery, N. G.; Smart, T. G., GABA and glycine as neurotransmitters: a brief history. British journal of pharmacology 2006, 147 Suppl 1, S109-19.

(151) Schofield, P. R.; Darlison, M. G.; Fujita, N.; Burt, D. R.; Stephenson, F. A.; Rodriguez, H.; Rhee, L. M.; Ramachandran, J.; Reale, V.; Glencorse, T. A.; et al., Sequence and functional expression of the GABA A receptor shows a ligand-gated receptor super-family. Nature 1987, 328 (6127), 221-7.

(152) Miller, P. S.; Aricescu, A. R., Crystal structure of a human GABAA receptor. Nature 2014, 512 (7514), 270-5.

(153) Richter, L.; de Graaf, C.; Sieghart, W.; Varagic, Z.; Morzinger, M.; de Esch, I. J.; Ecker, G. F.; Ernst, M., Diazepam-bound GABAA receptor models identify new benzodiazepine binding-site ligands. Nature chemical biology 2012, 8 (5), 455-64.

(154) Olsen, R. W.; Sieghart, W., GABA A receptors: subtypes provide diversity of function and pharmacology. Neuropharmacology 2009, 56 (1), 141-8.

(155) Sieghart, W., Structure and pharmacology of gamma-aminobutyric acidA receptor subtypes. Pharmacological reviews 1995, 47 (2), 181-234.

(156) Sternbach, L. H., The benzodiazepine story. Journal of medicinal chemistry 1979, 22 (1), 1-7.

(157) Fuentes, A. V.; Pineda, M. D.; Venkata, K. C. N., Comprehension of Top 200 Prescribed Drugs in the US as a Resource for Pharmacy Teaching, Training and Practice. Pharmacy 2018, 6 (2).

(158) Clayton, T.; Chen, J. L.; Ernst, M.; Richter, L.; Cromer, B. A.; Morton, C. J.; Ng, H.; Kaczorowski, C. C.; Helmstetter, F. J.; Furtmuller, R.; Ecker, G.; Parker, M. W.; Sieghart, W.; Cook, J. M., An updated unified pharmacophore model of the benzodiazepine binding site on

gamma-aminobutyric acid(a) receptors: correlation with comparative models. Current medicinal chemistry 2007, 14 (26), 2755-75.

(159) Prevot, T. D.; Li, G.; Vidojevic, A.; Misquitta, K. A.; Fee, C.; Santrac, A.; Knutson, D. E.; Stephen, M. R.; Kodali, R.; Zahn, N. M.; Arnold, L. A.; Scholze, P.; Fisher, J. L.; Markovic, B. D.; Banasr, M.; Cook, J. M.; Savic, M.; Sibille, E., Novel Benzodiazepine-Like Ligands with Various Anxiolytic, Antidepressant, or Pro-Cognitive Profiles. Molecular neuropsychiatry 2019, 5 (2), 84-97.

(160) Gill, K. M.; Lodge, D. J.; Cook, J. M.; Aras, S.; Grace, A. A., A novel alpha5GABA(A)R-positive allosteric modulator reverses hyperactivation of the dopamine system in the MAM model of schizophrenia. Neuropsychopharmacology : official publication of the American College of Neuropsychopharmacology 2011, 36 (9), 1903-11.

(161) Lewter, L. A.; Fisher, J. L.; Siemian, J. N.; Methuku, K. R.; Poe, M. M.; Cook, J. M.; Li, J. X., Antinociceptive Effects of a Novel alpha2/alpha3-Subtype Selective GABAA Receptor Positive Allosteric Modulator. ACS chemical neuroscience 2017, 8 (6), 1305-1312.

(162) Forkuo, G. S.; Nieman, A. N.; Yuan, N. Y.; Kodali, R.; Yu, O. B.; Zahn, N. M.; Jahan, R.; Li, G.; Stephen, M. R.; Guthrie, M. L.; Poe, M. M.; Hartzler, B. D.; Harris, T. W.; Yocum, G. T.; Emala, C. W.; Steeber, D. A.; Stafford, D. C.; Cook, J. M.; Arnold, L. A., Alleviation of Multiple Asthmatic Pathologic Features with Orally Available and Subtype Selective GABAA Receptor Modulators. Molecular pharmaceutics 2017, 14 (6), 2088-2098.

(163) Whitwam, J. G.; Amrein, R., Pharmacology of flumazenil. Acta anaesthesiologica Scandinavica. Supplementum 1995, 108, 3-14.

(164) Hadingham, K. L.; Garrett, E. M.; Wafford, K. A.; Bain, C.; Heavens, R. P.; Sirinathsinghji, D. J.; Whiting, P. J., Cloning of cDNAs encoding the human gamma-aminobutyric acid type A

receptor alpha 6 subunit and characterization of the pharmacology of alpha 6-containing receptors. Molecular pharmacology 1996, 49 (2), 253-9.

(165) Olsen, R. W., GABAA receptor: Positive and negative allosteric modulators. Neuropharmacology 2018, 136 (Pt A), 10-22.

(166) Hanchar, H. J.; Chutsrinopkun, P.; Meera, P.; Supavilai, P.; Sieghart, W.; Wallner, M.; Olsen, R. W., Ethanol potently and competitively inhibits binding of the alcohol antagonist Ro15-4513 to alpha4/6beta3delta GABAA receptors. Proceedings of the National Academy of Sciences of the United States of America 2006, 103 (22), 8546-51.

(167) Uhlen, M.; Fagerberg, L.; Hallstrom, B. M.; Lindskog, C.; Oksvold, P.; Mardinoglu, A.; Sivertsson, A.; Kampf, C.; Sjostedt, E.; Asplund, A.; Olsson, I.; Edlund, K.; Lundberg, E.; Navani, S.; Szigyarto, C. A.; Odeberg, J.; Djureinovic, D.; Takanen, J. O.; Hober, S.; Alm, T.; Edqvist, P. H.; Berling, H.; Tegel, H.; Mulder, J.; Rockberg, J.; Nilsson, P.; Schwenk, J. M.; Hamsten, M.; von Feilitzen, K.; Forsberg, M.; Persson, L.; Johansson, F.; Zwahlen, M.; von Heijne, G.; Nielsen, J.; Ponten, F., Proteomics. Tissue-based map of the human proteome. Science 2015, 347 (6220), 1260419.

(168) Uhlen, M.; Zhang, C.; Lee, S.; Sjostedt, E.; Fagerberg, L.; Bidkhori, G.; Benfeitas, R.; Arif, M.; Liu, Z.; Edfors, F.; Sanli, K.; von Feilitzen, K.; Oksvold, P.; Lundberg, E.; Hober, S.; Nilsson, P.; Mattsson, J.; Schwenk, J. M.; Brunnstrom, H.; Glimelius, B.; Sjoblom, T.; Edqvist, P. H.; Djureinovic, D.; Micke, P.; Lindskog, C.; Mardinoglu, A.; Ponten, F., A pathology atlas of the human cancer transcriptome. Science 2017, 357 (6352).

(169) Thul, P. J.; Akesson, L.; Wiking, M.; Mahdessian, D.; Geladaki, A.; Ait Blal, H.; Alm, T.; Asplund, A.; Bjork, L.; Breckels, L. M.; Backstrom, A.; Danielsson, F.; Fagerberg, L.; Fall, J.; Gatto, L.; Gnann, C.; Hober, S.; Hjelmare, M.; Johansson, F.; Lee, S.; Lindskog, C.; Mulder, J.;

Mulvey, C. M.; Nilsson, P.; Oksvold, P.; Rockberg, J.; Schutten, R.; Schwenk, J. M.; Sivertsson, A.; Sjostedt, E.; Skogs, M.; Stadler, C.; Sullivan, D. P.; Tegel, H.; Winsnes, C.; Zhang, C.; Zwahlen, M.; Mardinoglu, A.; Ponten, F.; von Feilitzen, K.; Lilley, K. S.; Uhlen, M.; Lundberg, E., A subcellular map of the human proteome. Science 2017, 356 (6340).

(170) https://www.cdc.gov/asthma/most_recent_national_asthma_data.htm.

(171) Reddel, H. K.; Bateman, E. D.; Becker, A.; Boulet, L. P.; Cruz, A. A.; Drazen, J. M.; Haahtela, T.; Hurd, S. S.; Inoue, H.; de Jongste, J. C.; et al. A summary of the new GINA strategy: a roadmap to asthma control. Eur. Respir. J. 2015, 46, 622−639.

(172) Cevhertas, L.; Ogulur, I.; Maurer, D. J.; Burla, D.; Ding, M.; Jansen, K.; Koch, J.; Liu, C.; Ma, S.; Mitamura, Y.; et al. Advances and recent developments in asthma in 2020. Allergy 2020, 75, 3124−3146.

(173) Cloutier, M. M.; Baptist, A. P.; Blake, K. V.; Brooks, E. G.; Bryant-Stephens, T.; DiMango, E.; Dixon, A. E.; Elward, K. S.; Hartert, T.; Krishnan, J. A.; et al. 2020 Focused Updates to the Asthma Management Guidelines: A Report from the National Asthma Education and Prevention Program Coordinating Committee Expert Panel Working Group. J. Allergy Clin. Immunol. 2020, 146, 1217− 1270.

(174) Sieghart, W.; Savic, M. M. International Union of Basic and Clinical Pharmacology. CVI: GABAA Receptor Subtype- and Function-selective Ligands: Key Issues in Translation to Humans. Pharmacol. Rev. 2018, 70, 836−878.

(175) Camoretti-Mercado, B.; Lockey, R. F. Airway smooth muscle pathophysiology in asthma. J. Allergy Clin. Immunol. 2021, 147, 1983− 1995.

(176) Bhandage, A. K.; Barragan, A. GABAergic signaling by cells of the immune system: more the rule than the exception. Cell. Mol. Life Sci. 2021, 78, 5667−5679.

(177) Forkuo, G. S.; Guthrie, M. L.; Yuan, N. Y.; Nieman, A. N.; Kodali, R.; Jahan, R.; Stephen, M. R.; Yocum, G. T.; Treven, M.; Poe, M. M.; et al. Development of GABAA Receptor Subtype-Selective Imidazobenzodiazepines as Novel Asthma Treatments. Mol. Pharmaceutics 2016, 13, 2026−2038.

(178) Jahan, R.; Stephen, M. R.; Forkuo, G. S.; Kodali, R.; Guthrie, M. L.; Nieman, A. N.; Yuan, N. Y.; Zahn, N. M.; Poe, M. M.; Li, G.; et al. Optimization of substituted imidazobenzodiazepines as novel asthma treatments. Eur. J. Med. Chem. 2017, 126, 550−560.

(179) Forkuo, G. S.; Nieman, A. N.; Kodali, R.; Zahn, N. M.; Li, G. G.; Roni, M. S. R.; Stephen, M. R.; Harris, T. W.; Jahan, R.; Guthrie, M. L.; et al. A Novel Orally Available Asthma Drug Candidate That Reduces Smooth Muscle Constriction and Inflammation by Targeting GABA(A) Receptors in the Lung. Mol. Pharmaceutics 2018, 15, 1766−1777.

(180) Forkuo, G. S.; Nieman, A. N.; Yuan, N. Y.; Kodali, R.; Yu, O. B.; Zahn, N. M.; Jahan, R.; Li, G.; Stephen, M. R.; Guthrie, M. L.; et al. Alleviation of Multiple Asthmatic Pathologic Features with Orally Available and Subtype Selective GABA(A) Receptor Modulators. Mol. Pharmaceutics 2017, 14, 2088−2098.

(181) Zahn, N. M.; Mikulsky, B. N.; Roni, M. S. R.; Yocum, G. T.; Mian, M. Y.; Knutson, D. E.; Cook, J. M.; Emala, C. W.; Stafford, D. C.; Arnold, L. A. Nebulized MIDD0301 Reduces Airway Hyperresponsiveness in Moderate and Severe Murine Asthma Models. ACS Pharmacol. Transl. Sci. 2020, 3, 1381−1390.

(182) Gallos, G.; Yim, P.; Chang, S.; Zhang, Y.; Xu, D. B.; Cook, J. M.; Gerthoffer, W. T.; Emala, C. W. Targeting the restricted alpha subunit repertoire of airway smooth muscle GABA(A) receptors augments airway smooth muscle relaxation. Am. J. Physiol.: Lung Cell. Mol. Physiol. 2012, 302, L248−L256.

(183) Yocum, G. T.; Turner, D. L.; Danielsson, J.; Barajas, M. B.; Zhang, Y.; Xu, D. B.; Harrison, N. L.; Homanics, G. E.; Farber, D. L.; Emala, C. W. GABA(A) receptor alpha(4)-subunit knockout enhances lung inflammation and airway reactivity in a murine asthma model. Am. J. Physiol.: Lung Cell. Mol. Physiol. 2017, 313, L406−L415.

(184) Yocum, G. T.; Perez-Zoghbi, J. F.; Danielsson, J.; Kuforiji, A. S.; Zhang, Y.; Li, G.; Rashid Roni, M. S.; Kodali, R.; Stafford, D. C.; Arnold, L. A.; et al. A novel GABA(A) receptor ligand MIDD0301 with limited blood-brain barrier penetration relaxes airway smooth muscle ex vivo and in vivo. Am. J. Physiol. Lung Cell Mol. Physiol. 2019, 316, L385−L390.

(185) Zahn, N. M.; Huber, A. T.; Mikulsky, B. N.; Stepanski, M. E.; Kehoe, A. S.; Li, G.; Schussman, M.; Rashid Roni, M. S.; Kodali, R.; Cook, J. M.; et al. MIDD0301 − A first-in-class anti-inflammatory asthma drug targets GABA(A) receptors without causing systemic immune suppression. Basic Clin. Pharmacol. Toxicol. 2019, 125, 75− 84.

(186) Roni, M. S. R.; Zahn, N. M.; Mikulsky, B. N.; Webb, D. A.; Mian, M. Y.; Knutson, D. E.; Guthrie, M. L.; Cook, J. M.; Stafford, D. C.; Arnold, L. A. Identification and Quantification of MIDD0301 Metabolites. Curr. Drug Metab. 2021, 22, 1114−1123.

(187) Roni, M. S. R.; Zahn, N. M.; Yocum, G. T.; Webb, D. A.; Mian, M. Y.; Meyer, M. J.; Tylek, A. S.; Cook, J. M.; Emala, C. W.; Stafford, D. C.; et al. Comparative pharmacodynamic and pharmacokinetic study of MIDD0301 and its (S) enantiomer. Drug Dev. Res. 2022, 83, 979−992.

(188) Knutson, D. E.; Roni, M. S. R.; Mian, M. Y.; Cook, J. M.; Stafford, D. C.; Arnold, L. A. Improved Scale-up Synthesis and Purification of Clinical Asthma Candidate MIDD0301. Org. Process Res. Dev. 2020, 24, 1467−1476.

(189) Daly, W. H.; Poche, D. The Preparation of N-Carboxyanhydrides of Alpha-Amino-Acids Using Bis(Trichloromethyl)Carbonate. Tetrahedron Lett. 1988, 29, 5859−5862.

(190) Kramer, J. R.; Deming, T. J. General Method for Purification of alpha-Amino acid-N-carboxyanhydrides Using Flash Chromatography. Biomacromolecules 2010, 11, 3668−3672.

(191) Roni, M. S. R.; Li, G.; Mikulsky, B. N.; Knutson, D. E.; Mian, M. Y.; Zahn, N. M.; Cook, J. M.; Stafford, D. C.; Arnold, L. A. The Effects of pH on the Structure and Bioavailability of Imidazobenzodiazepine-3-Carboxylate MIDD0301. Mol. Pharmaceutics 2020, 17, 1182−1192.

(192) Li, G.; Stephen, M. R.; Kodali, R.; Zahn, N. M.; Poe, M. M.; Tiruveedhula, V. V. N. P. B.; Huber, A. T.; Schussman, M. K.; Qualmann, K.; Panhans, C. M.; et al. Synthesis of chiral GABA(A) receptor subtype selective ligands as potential agents to treat schizophrenia as well as depression. ARKIVOC 2018, 2018, 158−182. (24) Kansy, M.; Senner, F.; Gubernator, K. Physicochemical high throughput screening: parallel artificial membrane permeation assay in the description of passive absorption processes. J. Med. Chem. 1998, 41, 1007−1010.

(193) Kansy, M.; Senner, F.; Gubernator, K. Physicochemical high throughput screening: parallel artificial membrane permeation assay in the description of passive absorption processes. J. Med. Chem. 1998, 41, 1007−1010.

(194) Besnard, J.; Ruda, G. F.; Setola, V.; Abecassis, K.; Rodriguiz, R. M.; Huang, X. P.; Norval, S.; Sassano, M. F.; Shin, A. I.; Webster, L. A.; et al. Automated design of ligands to polypharmacological profiles. Nature 2012, 492, 215−220.

(195) Liu, J.; Chen, T.; Norris, T.; Knappenberger, K.; Huston, J.; Wood, M.; Bostwick, R. A high-throughput functional assay for characterization of gamma-aminobutyric acid(A) channel modulators using cryopreserved transiently transfected cells. Assay Drug Dev. Technol. 2008, 6, 781−786.

(196) Chuang, S. H.; Reddy, D. S. Genetic and Molecular Regulation of Extrasynaptic GABA-A Receptors in the Brain: Therapeutic Insights for Epilepsy. J. Pharmacol. Exp. Ther. 2018, 364, 180−197.

(197) Masiulis, S.; Desai, R.; Uchanski, T.; Serna Martin, I.; Laverty, D.; Karia, D.; Malinauskas, T.; Zivanov, J.; Pardon, E.; Kotecha, A.; et al. GABAA receptor signalling mechanisms revealed by structural pharmacology. Nature 2019, 565, 454−459.

(198) Zahn, N. M.; Roni, M. S. R.; Yocum, G. T.; Meyer, M. J.; Webb, D. A.; Mian, M. Y.; Cook, J. M.; Stafford, D. C.; Emala, C. W.; Arnold, L. A. Development of Inhaled GABA(A) Receptor Modulators to Improve Function in Bronchoconstrictive Disorders. ACS Pharmacol. Transl. 2022, 5, 80−88.

(199) Fischer, B. D.; Schlitt, R. J.; Hamade, B. Z.; Rehman, S.; Ernst, M.; Poe, M. M.; Li, G.; Kodali, R.; Arnold, L. A.; Cook, J. M. Pharmacological and antihyperalgesic properties of the novel alpha2/ 3 preferring GABA(A) receptor ligand MP-III-024. Brain Res. Bull. 2017, 131, 62−69.

(200) Forkuo, G. S.; Nieman, A. N.; Kodali, R.; Zahn, N. M.; Li, G.; Rashid Roni, M. S.; Stephen, M. R.; Harris, T. W.; Jahan, R.; Guthrie, M. L.; Yu, O. B.; Fisher, J. L.; Yocum, G. T.; Emala, C. W.; Steeber, D. A.; Stafford, D. C.; Cook, J. M.; Arnold, L. A., A Novel Orally Available Asthma Drug Candidate That Reduces Smooth Muscle Constriction and Inflammation by Targeting GABAA Receptors in the Lung. Mol Pharm 2018, 15 (5), 1766-1777.

(201) Zahn, N. M.; Huber, A. T.; Mikulsky, B. N.; Stepanski, M. E.; Kehoe, A. S.; Li, G.; Schussman, M.; Rashid Roni, M. S.; Kodali, R.; Cook, J. M.; Stafford, D. C.; Steeber, D. A.; Arnold, L. A., MIDD0301 - A first-in-class anti-inflammatory asthma drug targets GABAA

receptors without causing systemic immune suppression. Basic Clin Pharmacol Toxicol 2019, 125 (1), 75-84.

(202) Knutson, D. E.; Roni, R.; Mian, Y.; Cook, J. M.; Stafford, D. C.; Arnold, L. A. Improved scale-up synthesis and purification of clinical asthma candidate MIDD0301. *Org Process Res Dev* **2020**, *24* (8), 1467-1476. DOI: 10.1021/acs.oprd.0c00200.

(203) Nieman, A. N.; Li, G.; Zahn, N. M.; Mian, M. Y.; Mikulsky, B. N.; Hoffman, D. A.; Wilcox, T. M.; Kehoe, A. S.; Luecke, I. W.; Poe, M. M.; et al. Targeting Nitric Oxide Production in Microglia with Novel Imidazodiazepines for Nonsedative Pain Treatment. *ACS Chem Neurosci* **2020**, *11* (13), 2019-2030. DOI: 10.1021/acschemneuro.0c00324.

(204) Sharmin, D.; Mian, M. Y.; Marcotte, M.; Prevot, T. D.; Sibille, E.; Witkin, J. M.; Cook, J. M. Synthesis and Receptor Binding Studies of alpha5 GABA(A)R Selective Novel Imidazodiazepines Targeted for Psychiatric and Cognitive Disorders. *Molecules* **2023**, *28* (12). DOI: 10.3390/molecules28124771.

(205) Gudasheva, T. A.; Deeva, O. A.; Pantileev, A. S.; Mokrov, G. V.; Rybina, I. V.; Yarkova, M. A.; Seredenin, S. B. The New Dipeptide TSPO Ligands: Design, Synthesis and Structure-Anxiolytic Activity Relationship. *Molecules* **2020**, *25* (21). DOI: 10.3390/molecules25215132.

(206) Lacapère, J.J.; Duma, L.; Finet, S.; Kassiou, M.; Papadopoulos, V. Insight into the structural features of TSPO: Implications for drug development. Trends Pharmacol. Sci. 2020, 41, 110–122.

(207) Papadopoulos, V.; Aghazadeh, Y.; Fan, J.; Campioli, E.; Zirkin, B.; Midzak, A. Translocator protein-mediated pharmacology of cholesterol transport and steroidogenesis. Mole. Cell. Endocrinol. 2015, 408, 90–98.

(208) Kim, T.; Pae, A.N. Translocator protein (TSPO) ligands for the diagnosis or treatment of neurodegenerative diseases: A patent review (2010–2015; part 1). Expert Opin. Ther. Patents 2016, 26, 1325–1351.

(209) Kim, T.; Pae, A.N. Translocator protein (TSPO) ligands for the diagnosis or treatment of neurodegenerative diseases: A patent review (2010–2015; part 2). Expert Opin. Ther. Patents 2016, 26, 1353–1366.

(210) Da Settimo, F.; Simorini, F.; Taliani, S.; La Motta, C.; Marini, A.M.; Salerno, S.; Da Pozzo, E. Anxiolytic-like effects of N, N-dialkyl-2-phenylindol-3-ylglyoxylamides by modulation of translocator protein promoting neurosteroid biosynthesis. J. Med. Chem. 2008, 51, 5798–5806.

(211) Kita, A.; Kohayakawa, H.; Kinoshita, T.; Ochi, Y.; Nakamichi, K.; Kurumiya, S.; Oka, M. Antianxiety and antidepressant-like effects of AC-5216, a novel mitochondrial benzodiazepine receptor ligand. Br. J. Pharmacol. 2004, 142, 1059–1072.

(212) Gudasheva, T.A.; Voronina, T.A.; Ostrovskaya, R.U.; Zaitseva, N.I.; Bondarenko, N.A.; Briling, V.K.; Seredenin, S.B. Design of N-acylprolyltyrosine “tripeptoid” analogues of neurotensin as potential atypical antipsychotic agents. J. Med. Chem. 1998, 41, 284–290.

(213) Gudasheva, T.A. Theoretical grounds and technologies for dipeptide drug development. Russ. Chem. Bull. 2015, 64, 2012–2021.

(214) Gudasheva, T.A.; Voronina, T.A.; Ostrovskaya, R.U.; Rozantsev, G.G.; Vasilevich, N.I.; Trofimov, S.S.; Kravchenko, E.V.; Skoldinov, A.P.; Seredenin, S.B. Synthesis and antiamnesic activity of a series of N-acylprolyl-containing dipeptides. Euro J. Med. Chem. 1996, 31, 151–157.

(215) Seredenin, S.B.; Voronina, T.A.; Gudasheva, T.A.; Ostrovskaya, R.U.; Rozantsev, G.G.; Skoldinov, A.P.; Trofimov, S.S.; Halikas, J.; Garibova, T.L. Biologically Active n-

Acylprolydipeptides Having Antiamnestic, Antihypoxic and Anorexigenic Effects. U.S. Patent No. 5,439,930, 8 August 1995.

(216) Rupprecht, Rainer, et al. "Translocator protein (18 kDa)(TSPO) as a therapeutic target for neurological and psychiatric disorders." Nature reviews Drug discovery 9.12 (2010): 971-988.

(217) Sherwood, J.; De bruyn, M.; Constantinou, A.; Moity, L.; McElroy, C. R.; Farmer, T. J.; Duncan, T.; Raverty, W.; Hunt, A. J.; Clark, J. H. Dihydrolevoglucosenone (Cyrene) as a bio-based alternative for dipolar aprotic solvents. *Chem Commun (Camb)* **2014**, *50* (68), 9650-9652. DOI: 10.1039/c4cc04133j.

(218) Camp, J. E. Bio-available Solvent Cyrene: Synthesis, Derivatization, and Applications. *ChemSusChem* **2018**, *11* (18), 3048-3055. DOI: 10.1002/cssc.201801420.

(219) S. L. Waaijers-van der Loop, Z. Dang, R. E. Rorije and N. Janssen, 2018, https://www.rivm.nl/sites/default/les/2019-02/Screening%20van20potenti%C3%ABle%20polair%20aprotische%20oplosmiddelen.pdf.

(220) Pan, K.; Fan, Y.; Leng, T.; Li, J.; Xin, Z.; Zhang, J.; Hao, L.; Gallop, J.; Novoselov, K. S.; Hu, Z. Sustainable production of highly conductive multilayer graphene ink for wireless connectivity and IoT applications. *Nat Commun* **2018**, *9* (1), 5197. DOI: 10.1038/s41467-018-07632-w.

(221) Wilson, K. L.; Murray, J.; Jamieson, C.; Watson, A. J. B. Cyrene as a bio-based solvent for HATU mediated amide coupling. *Org Biomol Chem* **2018**, *16* (16), 2851-2854. DOI: 10.1039/c8ob00653a.

(222) Bousfield, Thomas W., et al. "Synthesis of amides from acid chlorides and amines in the bio-based solvent Cyrene™." Green Chemistry 21.13 (2019): 3675-3681.

(223) Mistry, Liam, et al. "Synthesis of ureas in the bio-alternative solvent Cyrene." Green Chemistry 19.9 (2017): 2123-2128.

(224) Sullivan, Caren, et al. "Cyrene™ blends: a greener solvent system for organic syntheses." Green chemistry 24.18 (2022): 7184-7193.

(225) Wilson, Kirsty L., et al. "Cyrene as a bio-based solvent for the Suzuki–Miyaura cross-coupling." Synlett 29.05 (2018): 650-654.

(226) Wilson, Kirsty L., et al. "Scope and limitations of a DMF bio-alternative within Sonogashira cross-coupling and Cacchi-type annulation." Beilstein journal of organic chemistry 12.1 (2016): 2005-2011.

(227) Vasconcelos, Stanley NS, et al. "Synthesis of symmetrical biaryl compounds by homocoupling reaction." Tetrahedron 75.13 (2019): 1865-1959.

(228) Zeng, Minfeng, et al. "Palladium-catalyzed reductive homocoupling of aromatic halides and oxidation of alcohols." The Journal of Organic Chemistry 75.8 (2010): 2556-2563.

(229) Huang, Ye, Lijie Liu, and Wenhua Feng. "Facile palladium–catalyzed homocoupling of aryl halides using 1, 4-butanediol as solvent, reductant and O, O-ligand." ChemistrySelect 1.3 (2016): 630-634.

(230) Akhtar, Rabia, et al. "Recent green synthetic approaches toward Ullmann reaction: A review." Chemical Papers 76.12 (2022): 7275-7293.

(231) Gaedda, Thomas M., Yuji Kawanishi, and Akira Miyazawa. "Microwave-assisted Ullmann-type coupling reactions in alkaline water." Synthetic Communications 42.9 (2012): 1259-1267.

(232) Kamal, Ahmed, et al. "Water mediated Heck and Ullmann couplings by supported palladium nanoparticles: importance of surface polarity of the carbon spheres." Green chemistry 14.9 (2012): 2513-2522.

(233) Feiz, Afsaneh, et al. "The β-cyclodextrin decorated with palladium nanoparticles without pretreatment: An efficient heterogeneous catalyst for biaryls synthesis." Applied Organometallic Chemistry 32.12 (2018): e4608. Karimi, Babak, Hossein Barzegar, and Hojatollah Vali. "Au–Pd bimetallic nanoparticles supported on a high nitrogen-rich ordered mesoporous carbon as an efficient catalyst for room temperature Ullmann coupling of aryl chlorides in aqueous media." Chemical Communications 54.52 (2018): 7155-7158.

(234) Zhang, Leilei, et al. "Efficient and durable Au alloyed Pd single-atom catalyst for the Ullmann reaction of aryl chlorides in water." ACS Catalysis 4.5 (2014): 1546-1553.

(235) Lakshmidevi, Jangam, et al. "A quick and low E-factor waste valorization procedure for CuCl-catalyzed oxidative self-coupling of (hetero) arylboronic acid in pomegranate peel ash extract." Green Chemistry Letters and Reviews 15.3 (2022): 529-536.

(236) Lakshmidevi, Jangam, et al. "WEPA: a bio-derived medium for added base, π-acid and ligand free Ullmann coupling of aryl halides using Pd (OAc) 2." Chemical Communications 54.87 (2018): 12333-12336.

(237) Paparella, Andrea Nicola, et al. "A Glycerol-Based Deep Eutectic Solvent as Natural Medium and Organic Reductant for Homocoupling of (Hetero) Aryl Chlorides: a Green Route to 2, 2'-Bipyridine and Biaryl Scaffolds." ChemistrySelect 7.37 (2022): e202203438.

(238) Cyrene™ and Cyrene™ blends are commercially available at https://www.sigmaaldrich.com. Cyrene™: 807796. Cyrene™/g-Valerolactone blend (50/50, w/w): 920207. Cyrene™/2-MeTHF blend (80/20, w/w): 920193.

(239) Fei, Cai-feng, et al. "Exposure of mouse oocytes to N, N-dimethylformamide impairs mitochondrial functions and reduces oocyte quality." Environmental Toxicology 37.7 (2022): 1563-1574.

(240) Valentini, Federica, et al. "γ-Valerolactone (GVL) as a green and efficient dipolar aprotic reaction medium." Current Opinion in Green and Sustainable Chemistry 36 (2022): 100634.

(241) Alcantara, Andres R., and Pablo D. de Maria. "Recent advances on the use of 2-methyltetrahydrofuran (2-MeTHF) in biotransformations." Current Green Chemistry 5.2 (2018): 86-103.

(242) Sheldon, Roger A. "The E factor 25 years on: the rise of green chemistry and sustainability." Green Chemistry 19.1 (2017): 18-43.

(243) Sharma, Pankaj, et al. "DOZNTM 2.0: A quantitative green chemistry evaluator for a sustainable future." Journal of Organometallic Chemistry 970 (2022): 122367.

(244) Zeng, M.; Du, Y.; Shao, L.; Qi, C.; Zhang, X. M. Palladium-catalyzed reductive homocoupling of aromatic halides and oxidation of alcohols. *J Org Chem* **2010**, *75* (8), 2556-2563. DOI: 10.1021/jo100089d.

(245) Drueckhammer, Dale G., et al. "Acetone–heptane as a solvent system for combining chromatography on silica gel with solvent recycling." ACS Sustainable Chemistry & Engineering 1.1 (2013): 87-90.

(246) Hapke, Marko, Lars Brandt, and Arne Lützen. "Versatile tools in the construction of substituted 2, 2′-bipyridines—cross-coupling reactions with tin, zinc and boron compounds." Chemical Society Reviews 37.12 (2008): 2782-2797.

(247) Hassan, Jwanro, et al. "Catalytic alternative of the Ullmann reaction." Tetrahedron 54.45 (1998): 13793-13804.

(248) Ritchie, Calvin D., and William F. Sager. "An examination of structure-reactivity relationships." Prog. phys. org. Chem 2 (1964): 323-400.

(249) Hughes, Liam, et al. "Development of pharmaceutically relevant bio-based intermediates though aldol condensation and Claisen–Schmidt reactions of dihydrolevoglucosenone (Cyrene®)." Green Chemistry 20.19 (2018): 4423-4427.

(250) Jutand, Anny, and Adil Mosleh. "Nickel-and palladium-catalyzed homocoupling of aryl triflates. scope, limitation, and mechanistic aspects." The Journal of Organic Chemistry 62.2 (1997): 261-274.

Curriculum vitae

Daniel A Webb

Skills:

- Organic synthesis: milligram to hundred-gram scale reactions.
- Ability to perform reactions under inert atmosphere: catalysis, organometallic reagents, light sensitive reactions, oxygen sensitive reactions.
- Strong knowledge of medicinal chemistry: generation of structure activity relationship studies.
- Experience performing molecular modeling using Molecular Operating Environment (MOE).
- Proficient in programs such as: Lab solutions, Topspin, MestReNova, Molecular Operating Environment, ChemDraw, SciFinder-N.
- Ability to perform cell-based assays: CellTiter-Glo, HEK-293 cell culture.
- Analytical chemistry experience: NMR, single quadrupole LCMS, chiral separation by LC.
- Dedicated, detail oriented with a strong work ethic.
- Proficient Laboratory skills and experience.
- Professional, receptive, and effective communicator.
- Ability to adapt to various work environments.
- Strong time management skills.
- Self-motivated with ability to meet strict deadlines.

Research Experience:

Toward the Development of a Novel Orally-Available Asthma Treatment Targeting GABAA Receptors in the Lungs Jun 2020 – Present

- Optimized the synthesis for various lead compounds including metabolites.
- Worked on milligram scale to hundreds of grams.
- Worded safely with highly hazardous chemicals.
- Performed pre-clinical characterization of compounds.
- Understanding of medicinal chemistry and drug discovery and development.
- Presented scientific results frequently at local and national meetings.

Improved 2-Pyridyl Reductive Homocoupling Reaction Using Biorenewable Solvent Cyrene™ (Dihydrolevoglucosenone)

- Conducted extensive reaction optimization to improve yields and reaction parameters.
- Understanding of sustainable chemistry.
- Worked closely with Millipore Sigma during the course of the program.
- Presented results at monthly meetings.

An Investigation into Calcitroic Acid and its Phase II Conjugates Sep 2019 – February 2021

- Worked though and optimized the synthesis of calcitroic acid (12 step synthesis).
- Understanding of the use of protecting groups.
- Synthesis of drug metabolites (sulfates, glucuronic acid and glucose metabolites).

Towards the Synthesis of an Intrinsic Fluorescent Ligand for The Vitamin D Receptor Sep 2018 – May 2019

- Understanding of fluorescence properties of a compound and how to measure them.
- Worked with light sensitive compounds.
- Worked on a 1-10 milligram scale.

Work Experience:

Graduate Research Assistant, University of Wisconsin Milwaukee, Milwaukee, Aug 2019-Present

- Performed organic synthesis and detained analysis of novel compounds.
- Undertook nine independent synthesis projects with synthetic routes ranging from 2-12 steps.

- Synthesized greater than 40 novel compounds that were fully characterized and evaluated.

Graduate Teaching Assistant, University of Wisconsin Milwaukee, Milwaukee, Aug 2019-Present

- Provided instruction to undergraduate students in a laboratory setting.
- Aided students learning in and out of the classroom by providing additional resources.
- Maintained a safe and well-organized laboratory.

Graduate Student Intern, Millipore Sigma, Milwaukee, Jan 2022-Aug-2022

- Investigation into increased reaction efficiency using the bio-renewable solvent Cyrene.
- Conducted numerous reactions with monitoring at regular intervals to determine reaction progress.
- Provided regular updates to the research team.
- Provided in-depth written documentation of all collected data and procedures.

Patent Review Consultant, UWM Research Foundation, Milwaukee, Nov 2021-Present

- Performed background art searched to ensure the novel aspects of perspective inventions.
- Provided in-depth written documentation of all findings.

Graduate Student Intern, Millipore Sigma, Sheboygan Falls, Jun 2021-Aug 2021

- Developed a scalable synthetic approach to make a protected lysine molecule.
- Provided weekly updates on the progress of the project.
- Provided in-depth written documentation of all the collected data and procedures.

Part-time Associate Scientist, Pantherics Inc., Milwaukee (UWM), June 2021-Present

- Generated hundreds of grams of a drug candidate for *in-vivo* studies (mouse, rat, dog).
- Generated salt formulations of new API.

Research Assistant at the Milwaukee Institute for Drug Discovery, Milwaukee (UWM), Aug 2023-Present

- Synthesized different molecules for academic and industry collaborators.
- Prepared certificated of analysis for all final products.

Publications:

1. **Daniel A. Webb**, Michelle J. Meyer, Kayode M. Medubi, Anika S. Tylek, Gene T. Yocum, M.S. Rashid Roni, Nicolas M. Zahn, Sarah A. Swartwout, Ahmad K. Masoud, Charles W. Emala, Douglas C. Stafford, and Leggy A. Arnold; "Design, Synthesis, and Biological Evaluation of Novel Spiro Imidazobenzodiazepines to Identify Improved Inhaled Bronchodilators" Journal of Medicinal Chemistry 2023 66 (14), 9853-9865. DOI: 10.1021/acs.jmedchem.3c00647
2. **Daniel A. Webb**, Zeid Alsudani, Guolin Xu, Peng Gaob and Leggy A. Arnold; "Improved 2-pyridyl reductive homocoupling reaction using biorenewable solvent Cyrene™ (dihydrolevoglucosenone)" RSC Sustain., 2023, Advance Article. DOI: 10.1039/D3SU00005B
3. **Daniel A. Webb**, Maija Lee and Leggy A. Arnold "Modulating Vitamin D Receptor–Coregulator Binding with Small Molecules" in Vitamin D, Volume 2: Health, Disease and Therapeutics, David Feldman, Ed.; Academic Press, Fifth Edition, 2022 (in press)
4. Jose F. Perez-Zoghbi, Dannah Rae Sajorda, **Daniel A. Webb**, Leggy A. Arnold, Charles W. Emala, Gene T. Yocum "Imidazobenzodiazepine PI320 Relaxes Mouse Peripheral Airways by Inhibiting Calcium Mobilization" American Journal of Respiratory Cell And Molecular Biology, 2022 67 (4). DOI: https://doi.org/10.1165/rcmb.2022-0084OC
5. Tania R. Mutchie, **Daniel A. Webb**, Elliot S. Di Milo and Leggy A. Arnold. (2021). Strategies for the Design of Vitamin D Receptor Ligands. In: Badr, M.Z. (eds) Nuclear Receptors. Springer, Cham. https://doi.org/10.1007/978-3-030-78315-0_8
6. Olivia B. Yu, **Daniel A. Webb**, Elliot S. Di Milo, Tania R. Mutchie, Kelly A. Teske, Taosheng Chen, Wenwei Lin, Carole Peluso-Iltis, Natacha Rochel, Moritz Helmstadter, Daniel Merk, Leggy A. Arnold; "Biological Evaluation and Synthesis of Calcitroic Acid" Bioorganic Chemistry 116 (2021) 105310. DOI: https://doi.org/10.1016/j.bioorg.2021.105310
7. M.S. Rashid Roni, Nicolas M. Zahn, Gene T. Yocum, **Daniel A. Webb**, Md Yeunus Mian, Michelle J. Meyer, Anika S. Tylek, James M. Cook, Charles W. Emala, Douglas C. Stafford and Leggy A. Arnold* "Comparative Pharmacodynamic and Pharmacokinetic Study of MIDD0301 and its (S) Enantiomer" Drug Development Research, 2022, 1-14. DOI: https://doi.org/10.1002/ddr.21926

8. Nicholas M. Zahn, M.S. Rashid Roni, Gene T. Yocum, Michelle Meyer, **Daniel A. Webb**, Md Yeunus Mian, James M. Cook, Charles W. Emala, Douglas C. Stafford, Leggy A. Arnold* "Development of Inhaled GABAA Receptor Modulators to Improve Airway Function in Bronchoconstrictive Disorders" ACS Pharmacology & Translational Science, 2022, 5, 80-88. DOI: https://doi.org/10.1021/acsptsci.1c00238
9. M.S. Rashid Roni, Nicolas M. Zahn, Brandon N. Mikulsky, **Daniel Webb**, Md Yeunus Mian, Daniel E. Knutson, Margaret Guthrie, James M. Cook, Douglas C. Stafford and Leggy A. Arnold* "Identification and Quantification of MIDD0301 Metabolites" Current Drug Metabolism, 2021, 22, 1114-1123. DOI: 10.2174/1389200222666211202093841

Patents:

1. Arnold, A.; Stafford, D.; **Webb, D**.; Meyer, M. GABA(A) Receptor Modulators and Methods to Control Smooth Muscle Contraction and Inflammation. 020871-0008-US01, 2022

Awards and Recognition:

- George Sosnovsky Award for Excellence in Graduate Research
- H.C. Brown Lectures in Organic Chemistry Poster Award Winner
- 1st place: Graduate poster UWM Department of Chemistry & Biochemistry Annual Research Symposium, April 2023
- 1st place: Graduate Poster UWM Department of Chemistry & Biochemistry Annual Research Symposium, April 2022
- 1st place: 2021 ACS Milwaukee Fall Poster Session, October 2021
- 3rd place: Biohealth Communications Competition, October 2021
- Distinguished Dissertator Fellowship, Fall 2022 – Spring 2023
- Graduate Student Travel Award, UWM Department of Chemistry & Biochemistry, Fall 2022
- UWM Chancellors Award. Every semester appointed as a teaching assistant
- ACS 2019 Undergraduate Award in Analytical Chemistry

Presentations:

1. **Daniel A. Webb**, et. al.; 2023 Chemistry & Biochemistry Research Symposium & Awards Day: "Synthesis, Biological Evaluation, and Molecular Modeling of Novel Imidazobenzodiazepines to Identify Lead Compounds for the Oral Treatment of Asthma" April 28, 2023
2. **Daniel A. Webb**, et. al.; 2023 Chemistry & Biochemistry Research Symposium & Awards Day: "CyreneTM (dihydrolevoglucosenone) as Green Solvent to Improve the Efficiency of a Reductive Homocoupling Reaction with Substituted Pyridines" April 28, 2023
3. **Daniel A. Webb**, et. al.; Herbert C. Brown Lectures in Organic Chemistry 2023, Purdue University, IN: "Synthesis, Biological Evaluation, and Molecular Modeling of Novel Imidazobenzodiazepines to Identify Lead Compounds for the Oral Treatment of Asthma" April 14, 2023
4. **Daniel A. Webb**, et. al.; Spring 2023 ACS National Meeting and Exposition, Indianapolis, IN: Synthesis, Biological Evaluation, and Molecular Modeling of Novel Imidazobenzodiazepines to Identify Lead Compounds for the Oral Treatment of Asthma" March 26, 2023
5. **Daniel A. Webb**, et. al.; Spring 2023 ACS National Meeting and Exposition, Indianapolis, IN: "CyreneTM (dihydrolevoglucosenone) as Green Solvent to Improve the Efficiency of a Reductive Homocoupling Reaction with Substituted Pyridines" March 26, 2023
6. **Daniel A. Webb**, et. al.; MIDD Symposium: "Evaluation of Novel Benzodiazepines for the Potential Oral Treatment of Asthma", February 17, 2023
7. **Daniel A. Webb**, et. al.; MIDD Symposium: "Docking and Computational Studies of Novel Disubstituted Imidazobenzodiazepines" February 17, 2023
8. **Daniel A. Webb**, et. al.; Milwaukee Analytical Chemistry Conference: "Determination of Solubility and Permeability for Novel Imidazobenzodiazepines with Potential Application as an Orally Available Asthma Medication" August 29, 2022

9. **Daniel A. Webb**, et. al.; Fall 2022 ACS National Meeting and Exposition, Chicago, IL: "Synthesis and Evaluation of Disubstituted Imidazodiazepines Using a Novel Synthetic Strategy to Generate Compounds with Potential Application as an Orally Available Asthma Medication" August 21, 2022
10. **Daniel A. Webb**, et. al.; 2022 Chemistry & Biochemistry Research Symposium & Awards Day: "Synthesis and Evaluation of Disubstituted Imidazodiazepines Using a Novel Synthetic Strategy to Generate Compounds with Potential Application as an Orally Available Asthma Medication" April 22, 2022
11. **Daniel A. Webb**, et. al.; 2022 MIDD Symposium: "Development of a Novel Synthetic Strategy That Enables the Generation of Disubstituted Imidazodiazepines with Potential Application as Orally Available Asthma Medication", January 18, 2022
12. **Daniel A. Webb**, et. al.; 46th Annual UW-System Chem Faculties Meeting: "Development of a Novel Synthetic Strategy That Enables the Generation of Disubstituted Imidazodiazepines with Potential Application as Orally Available Asthma Medication" November 4, 2021
13. **Daniel A. Webb**, et. al.; 2021 ACS Milwaukee Fall Poster Session: "Development of a Novel Synthetic Strategy That Enables the Generation of Disubstituted Imidazodiazepines with Potential Application as Orally Available Asthma Medication" October 27, 2021
14. **Daniel A. Webb**, et. al.; Biohealth Communication Competition at 2021 Biohealth Summit: "Structure Activity Relationship of Oral Asthma Drug Candidate" October 7, 2021
15. **Daniel A. Webb**, et. al.; 2021 Chemistry & Biochemistry Research Symposium & Awards Day: "Synthesis of MIDD0301 Phase II Metabolites and Application of Amino Acid N-Carboxy Anhydrides to Generate New MIDD0301 Analogs" April 23, 2021
16. **Daniel A. Webb**, et. al.; 2019 undergraduate research symposium: "Towards the Synthesis of an Intrinsic Fluorescent Ligand for The Vitamin D Receptor" April 5, 2019
17. **Daniel A. Webb**, et. al.; Chemistry & Biochemistry Research Symposium & Awards Day 2019: "Towards the Synthesis of an Intrinsic Fluorescent Ligand for The Vitamin D Receptor" April 26, 2019
18. **Daniel A. Webb**, et. al.; Chem 584, Advanced Chemistry Lab II: "Determination and Identification of Halogen Exchange Progress by FTIR and NMR" May 14, 2019

Education:

Current:

Student at University of Wisconsin-Milwaukee – September 2019-Present
Pursuing a Ph.D. in Medicinal Organic Chemistry
Expected graduation: December 2023

Past:

University of Wisconsin-Milwaukee – September 2015-May 2019
Bachelor's of Science in Chemistry